AXONOPATHY IN NEURODEGENERATIVE DISEASE

EDITED BY: Samuel D. Crish, Robert W. Burgess, Denise M. Inman, Christine M. Dengler-Crish, Jason R. Richardson and Brett Schofield

PUBLISHED IN: Frontiers in Neuroscience

frontiers Research Topics

frontiers

ISSN 1664-8714
ISBN 978-2-88945-680-2
DOI 10.3389/978-2-88945-680-2

About Frontiers

Frontiers is more than just an open-access publisher of scholarly articles: it is a pioneering approach to the world of academia, radically improving the way scholarly research is managed. The grand vision of Frontiers is a world where all people have an equal opportunity to seek, share and generate knowledge. Frontiers provides immediate and permanent online open access to all its publications, but this alone is not enough to realize our grand goals.

Frontiers Journal Series

The Frontiers Journal Series is a multi-tier and interdisciplinary set of open-access, online journals, promising a paradigm shift from the current review, selection and dissemination processes in academic publishing. All Frontiers journals are driven by researchers for researchers; therefore, they constitute a service to the scholarly community. At the same time, the Frontiers Journal Series operates on a revolutionary invention, the tiered publishing system, initially addressing specific communities of scholars, and gradually climbing up to broader public understanding, thus serving the interests of the lay society, too.

Dedication to Quality

Each Frontiers article is a landmark of the highest quality, thanks to genuinely collaborative interactions between authors and review editors, who include some of the world's best academicians. Research must be certified by peers before entering a stream of knowledge that may eventually reach the public - and shape society; therefore, Frontiers only applies the most rigorous and unbiased reviews.
Frontiers revolutionizes research publishing by freely delivering the most outstanding research, evaluated with no bias from both the academic and social point of view. By applying the most advanced information technologies, Frontiers is catapulting scholarly publishing into a new generation.

What are Frontiers Research Topics?

Frontiers Research Topics are very popular trademarks of the Frontiers Journals Series: they are collections of at least ten articles, all centered on a particular subject. With their unique mix of varied contributions from Original Research to Review Articles, Frontiers Research Topics unify the most influential researchers, the latest key findings and historical advances in a hot research area! Find out more on how to host your own Frontiers Research Topic or contribute to one as an author by contacting the Frontiers Editorial Office: researchtopics@frontiersin.org

AXONOPATHY IN NEURODEGENERATIVE DISEASE

Topic Editors:
Samuel D. Crish, Northeast Ohio Medical University, United States
Robert W. Burgess, The Jackson Laboratory, United States
Denise M. Inman, Northeast Ohio Medical University, United States
Christine M. Dengler-Crish, Northeast Ohio Medical University, United States
Jason R. Richardson, Florida International University, United States
Brett Schofield, Northeast Ohio Medical University, United States

Axons are the major output processes of neurons, responsible for transmitting information to other neurons and tissues throughout the body. The 150,000+ kilometers of axons make up half of the brain's volume and require a large amount of energy. Normal axon function is the product of a massive number of intra- and extra-cellular mechanisms working in concert. Perhaps not surprisingly, the axon is a site of vulnerability during normal aging and in disease states, although this has only been recently appreciated. Axonopathy, broadly defined as functional or structural defects in the axon or its terminal, is common across a wide range of neurodegenerative conditions, including amyotrophic lateral sclerosis, Huntington's, Parkinson's, and Alzheimer's diseases, glaucoma, and as a result of neurotoxin exposure or drug treatment.

This Research Topic assembles a series of original research papers, reviews, and commentaries that will illustrate both the commonalities and important differences across neurodegenerative disorders. Though this collection cannot address all aspects of this topic, it is our hope that these manuscripts will educate other scientists and inspire new investigations into axon dysfunction and degeneration.

Citation: Crish, S. D., Burgess, R. W., Inman, D. M., Dengler-Crish, C. M., Richardson, J. R., Schofield, B., eds (2019). Axonopathy in Neurodegenerative Disease. Lausanne: Frontiers Media. doi: 10.3389/978-2-88945-680-2

Table of Contents

frontiers in Neuroscience

EDITORIAL
published: 23 October 2018
doi: 10.3389/fnins.2018.00769

Editorial: Axonopathy in Neurodegenerative Disease

Robert W. Burgess[1]* *and Samuel D. Crish*[2]

[1] The Jackson Laboratory, Bar Harbor, ME, United States, [2] Department of Pharmaceutical Sciences, Northeast Ohio Medical University, Rootstown, OH, United States

Keywords: axon degeneration, neuropathy, glaucoma, mitochondrial dysfuncion, chemotherapy induced neuropathy

The Editorial on the Research Topic

Axonopathy in Neurodegenerative Disease

Within the study of neurodegenerative diseases, axonopathy is increasingly recognized as a major contributor to the disease manifestation, and in some cases, the key pathogenic driver. Neurons, with their highly specialized anatomy, must maintain both dendritic arbors and long axon processes. The loss of the axon effectively disconnects the neuron from its postsynaptic partners, eliminating its function in neural circuitry. The loss of the axon may be an early symptom of more extensive degeneration and neuron loss to follow. This has been suggested for diseases such as amyotrophic lateral sclerosis (ALS), where changes in the distal terminal of motor neurons presage their eventual death (Fischer et al., 2004). In other cases, such as inherited peripheral neuropathies, the loss of the axon is the primary feature of the disease, with sensory and motor deficits manifesting in the distal extremities innervated by the longest neuronal projections (Cavanagh, 1964).

Many aspects of cell biology converge in maintaining axons and in their degeneration. Their length requires an elaborate cytoskeleton and transport machinery. Functioning mitochondria are required to meet local energy demands, again necessitating mitochondrial transport, fusion, fission, and possibly local translation of mitochondrial components to keep up with organelle and protein turnover (Misgeld and Schwarz, 2017). Finally, axons are also often intimately associated with myelinating glial cells, creating a mutually dependent functional unit to maintain axonal conduction and integrity. This Research Topic of Frontiers in Neuroscience is devoted to these issues of axon cell biology and the disorders that result from dysfunction in these processes. Many of the papers included in this Research Topic arose from presentations and discussions held at the 6th Molecular Mechanisms of Axon Degeneration conference, hosted at The Jackson Laboratory in Bar Harbor, Maine, in September of 2016. Additional contributions expand the scope of this Research Topic, particularly into areas related to degeneration of the optic nerve, relevant to glaucoma and other central neurodegenerations.

The review article by Stassart et al. provides an excellent summary of axon and glial cell biology and anatomy and how this interdependent relationship changes with disease (Stassart et al.). Similarly, axons and glial cells develop in concert, and undergo age-related changes that may predispose or even precipitate neurodegenerative diseases. The review by Salvadores et al. examines the impact of aging on the anatomy and function of axons (Salvadores et al.). Proper function of the axon depends on a well-order cytoskeleton. Cytoskeletal abnormalities are common to axon-centric diseases and toxic neuropathies, with specific chronic conditions such as tauopathies directly impacting axonal proteins. The review by Kneynsberg et al. examines the mechanisms by which tau, a microtubule associated protein, contributes to axon degeneration and disease (Kneynsberg et al.).

Another area of axonopathy research that has received a great deal of attention recently is chemotherapy-induced peripheral neuropathy (CIPN), a common side-effect of cancer treatment

OPEN ACCESS

Edited and reviewed by:
Vittorio Maglione, Istituto Neurologico Mediterraneo (IRCCS), Italy

***Correspondence:**
Robert W. Burgess
robert.burgess@jax.org

Specialty section:
This article was submitted to Neurodegeneration, a section of the journal Frontiers in Neuroscience

Received: *19 September 2018*
Accepted: *03 October 2018*
Published: *23 October 2018*

Citation:
Burgess RW and Crish SD (2018) Editorial: Axonopathy in Neurodegenerative Disease. Front. Neurosci. 12:769. doi: 10.3389/fnins.2018.00769

that decreases patient quality-of-life and is a major factor limiting drug dosage (Argyriou et al., 2014). This is a major concern clinically, but these drugs also provide tools for understanding axon degeneration and the normal cellular functions that are required to maintain healthy axons. The review by Fukuda et al. examines the cellular mechanisms underlying CIPN, which extend well beyond the impact of these drugs on the microtubule cytoskeleton (Fukuda et al.).

Axon degeneration is an active process, and this is most clearly demonstrated in Wallerian degeneration, which involves the fragmentation and disintegration of an axon distal to the site of an injury. Genetic studies have identified a spontaneous gain-of-function mouse mutation, Wallerian Degeneration Slowed (*WLD*^{s}), as well as recessive loss-of-function mutations in *Sarm1* as mutations that protect against Wallerian degeneration (Mack et al., 2001; Osterloh et al., 2012). Both *WLD*^{s} and loss of *Sarm1* lead to increased NAD^{+} levels locally in the axon, which in turn protects axons from degeneration. The therapeutic potential of this pathway is demonstrated in the original research article by Williams et al. which shows that nicotinamide and *WLD*^{s} act in concert to prevent retinal ganglion cell axon loss in glaucoma (Williams et al.).

Like NAD^{+} levels, local ATP and Ca^{++} homeostasis in axons depends on healthy mitochondria, which traffic through, and are localized in axons. Mutations affecting mitochondrial fusion, fission, and metabolism lead to an assortment of axonal defects and are also important in regeneration. The original research article by Knowlton et al. describes the relationship between mitochondrial function and the capacity for axon regeneration in *C. elegans* (Knowlton et al.). The review by Inman et al. examines how metabolic vulnerability specifically in axons and myelinating glial cells can contribute to axon loss in glaucoma (Inman and Harun-Or-Rashid). In contrast to metabolic issues, the original research article by Rogers et al. suggests that impaired mitophagy in nerve terminals contributes to the die-back neuropathy of motor neurons seen in mouse models of ALS (Rogers et al.). The need to maintain healthy mitochondria far from the cell body is a recurring theme in many neurodegenerative diseases. This is one argument favoring local protein synthesis in axons, which remains a controversial topic in neurobiology. The state of this question is addressed in the review by Spaulding and Burgess, including recent *in vivo* profiling studies of ribosome-associated mRNAs isolated from axons of the adult mouse visual system that indicate robust levels of translation, particularly of mitochondrial components (Spaulding and Burgess).

Axonopathy is often considered in the context of peripheral motor and sensory neurons, given their length, the presence of diseases that specifically affect these systems, and their sensitivity to challenges such as chemotherapy drugs or metabolic disorders such as diabetes. However, these characteristics are not limited to the peripheral nervous system. Many of the papers in this research topic focus on glaucoma, a neuropathy affecting axons of the optic nerve, one of the few central nervous system components outside of the brain and spinal cord. Glaucoma shares commonalities with other central neurodegenerations such as Alzheimer's, Parkinson's, and Huntington's diseases, often exhibiting comorbidity with those conditions, as well as exhibiting similar mechanisms with these and other axonopathies (Conforti et al., 2007).

Stresses such as hypoxia and oxidative stress arising from vascular dysfunction contribute to the pathogenesis of glaucoma, as described in the original research article by Chidlow et al. As in the degenerating brain, neuroinflammation plays a sizable role in glaucomatous neurodegeneration. One of this topic's original research articles, the loss of the pleiotropic cytokine IL-6 is shown to protect axons in glaucoma (Echevarria et al.). The mechanism underlying this protection remains unclear, but changes in axonal transport appear to be separated from changes in axon integrity, possibly separating these features in this model. Another original research article shows that more conventional inflammatory pathways may also contribute to glaucoma (Lambert et al.). Treatment with the synthetic steroid HE3286 reduced axonopathy in a rodent microbead occlusion model of glaucoma, possibly through its proposed targets of MAPK/ERK/NFκb signaling. The recurring mechanisms of axonal transport and cytoskeletal abnormalities are also in play in the axonopathy of glaucoma, as shown in the original research articles by Breen et al. and Wilson et al. Finally, the differential sensitivity of neurons to degeneration is a common yet puzzling feature of a variety of diseases and neurotoxic conditions. The review by Vidal-Sanz et al. describes the differential responses of different retinal ganglion cell populations in animal models exhibiting either ocular hypertension or optic nerve injury (Vidal-Sanz et al.). Together, these papers highlight the parallels of glaucoma and other diseases in which axonopathy is a key pathophysiological sequela.

Although the mechanisms that lead to axon degeneration may be shared across a range of diseases, they encompass a wide range of biological processes including cytoskeleton, transport, metabolism, translation, and inflammation. Perhaps this reflects the number of things that normally have to go correctly to actually preserve an axon, which in turn, could explain why axonopathy is often the harbinger of degeneration. Defining these processes is a challenge and predicts that there will not be a single "magic bullet" to correct all axonopathies, but the rapidly increasing depth of our knowledge concerning the functions required to maintain an axon will ultimately help in understanding how to prevent degeneration or even to promote regeneration in these diseases in the future.

AUTHOR CONTRIBUTIONS

All authors listed have made a substantial, direct and intellectual contribution to the work, and approved it for publication.

ACKNOWLEDGMENTS

We would like to thank all the authors of the research topic for their contributions, as well as, our co-editors, Drs. Inman, Richardson, Schofield, and Dengler-Crish. We would also like to thank the National Institutes of Health for the conference grant that supported the 6th Molecular Mechanisms of Axon Degeneration meeting (R13 NS098725).

REFERENCES

Argyriou, A. A., Kyritsis, A. P., Makatsoris, T., and Kalofonos, H. P. (2014). Chemotherapy-induced peripheral neuropathy in adults: a comprehensive update of the literature. *Cancer Manag. Res.* 6, 135–147. doi: 10.2147/CMAR.S44261

Cavanagh, J. B. (1964). The significance of the "dying back" process in experimental and human neurological disease. *Int. Rev. Exp. Pathol.* 3, 219–267.

Conforti, L., Adalbert, R., and Coleman, M. P. (2007). Neuronal death: where does the end begin? *Trends Neurosci.* 30, 159–166. doi: 10.1016/j.tins.2007.02.004

Fischer, L. R., Culver, D. G., Tennant, P., Davis, A. A., Wang, M., Castellano-Sanchez, A., et al. (2004). Amyotrophic lateral sclerosis is a distal axonopathy: evidence in mice and man. *Exp. Neurol.* 185, 232–240. doi: 10.1016/j.expneurol.2003.10.004

Mack, T. G., Reiner, M., Beirowski, B., Mi, W., Emanuelli, M., Wagner, D., et al. (2001). Wallerian degeneration of injured axons and synapses is delayed by a Ube4b/Nmnat chimeric gene. *Nat. Neurosci.* 4, 1199–1206. doi: 10.1038/nn770

Misgeld, T., and Schwarz, T. L. (2017). Mitostasis in neurons: maintaining mitochondria in an extended cellular architecture. *Neuron* 96, 651–666. doi: 10.1016/j.neuron.2017.09.055

Osterloh, J. M., Yang, J., Rooney, T. M., Fox, A. N., Adalbert, R., Powell, E. H., et al. (2012). dSarm/Sarm1 is required for activation of an injury-induced axon death pathway. *Science* 337, 481–484. doi: 10.1126/science.1223899

Conflict of Interest Statement: The authors declare that the research was conducted in the absence of any commercial or financial relationships that could be construed as a potential conflict of interest.

frontiers in Neuroscience

REVIEW
published: 11 July 2018
doi: 10.3389/fnins.2018.00467

The Axon-Myelin Unit in Development and Degenerative Disease

Ruth M. Stassart[1,2], *Wiebke Möbius*[1], *Klaus-Armin Nave*[1]* *and Julia M. Edgar*[1,3]*

[1] Department of Neurogenetics, Max-Planck-Institute of Experimental Medicine, Göttingen, Germany, [2] Department of Neuropathology, University Medical Center Leipzig, Leipzig, Germany, [3] Institute of Infection, Immunity and Inflammation, College of Medical Veterinary and Life Sciences, University of Glasgow, Glasgow, United Kingdom

Axons are electrically excitable, cable-like neuronal processes that relay information between neurons within the nervous system and between neurons and peripheral target tissues. In the central and peripheral nervous systems, most axons over a critical diameter are enwrapped by myelin, which reduces internodal membrane capacitance and facilitates rapid conduction of electrical impulses. The spirally wrapped myelin sheath, which is an evolutionary specialisation of vertebrates, is produced by oligodendrocytes and Schwann cells; in most mammals myelination occurs during postnatal development and after axons have established connection with their targets. Myelin covers the vast majority of the axonal surface, influencing the axon's physical shape, the localisation of molecules on its membrane and the composition of the extracellular fluid (in the periaxonal space) that immerses it. Moreover, myelinating cells play a fundamental role in axonal support, at least in part by providing metabolic substrates to the underlying axon to fuel its energy requirements. The unique architecture of the myelinated axon, which is crucial to its function as a conduit over long distances, renders it particularly susceptible to injury and confers specific survival and maintenance requirements. In this review we will describe the normal morphology, ultrastructure and function of myelinated axons, and discuss how these change following disease, injury or experimental perturbation, with a particular focus on the role the myelinating cell plays in shaping and supporting the axon.

Keywords: oligodendrocyte, Schwann cell, cytoskeleton, axonal transport, energy, neuroinflammation, morphology

OPEN ACCESS

Edited by:
Robert W. Burgess,
Jackson Laboratory, United States

Reviewed by:
John Svaren,
University of Wisconsin-Madison, United States
Andrea Loreto,
University of Cambridge, United Kingdom

***Correspondence:**
Klaus-Armin Nave
nave@em.mpg.de
Julia M. Edgar
edgar@em.mpg.de;
julia.edgar@glasgow.ac.uk

Specialty section:
This article was submitted to Neurodegeneration, a section of the journal Frontiers in Neuroscience

Received: *27 February 2018*
Accepted: *19 June 2018*
Published: *11 July 2018*

Citation:
Stassart RM, Möbius W, Nave K-A and Edgar JM (2018) The Axon-Myelin Unit in Development and Degenerative Disease. Front. Neurosci. 12:467. doi: 10.3389/fnins.2018.00467

INTRODUCTION

Neurons are highly polarized cells, with a long axon and shorter dendrites. Axons, which are the focus of this review, are unique among cellular processes, being capable of transmitting electrical impulses (spiking) and occupying, in many cases, an inordinately disproportionate amount of the neuron's volume. The axon's electrical excitability stems from the fact that **axolemma** (bolded terms are defined in **Table 1**) is rich in voltage-gated ion channels and ion pumps (Dumenieu et al., 2017). Extrapolation to humans, of serially reconstructed EM data from the highly branched basal cholinergic neurons of the forebrain in mice, suggests that single neurons can have a total axon length of 100 m (Wu et al., 2014). This extraordinary cellular asymmetry is initiated during early development when neuronal polarisation is established (Schelski and Bradke, 2017). All subsequent growth and maintenance of the axon is enabled by bidirectional axonal transport comprising molecular motors and microtubule tracks that convey materials between the cell body and the axon

TABLE 1 | Definitions.

Axolemma	**The axon's plasma membrane**
Axoplasm	The axon's cytoplasm
Compact myelin	Concentric layers around the axon of double-layered oligodendroglial or Schwann cell plasma membrane, closely apposed at both intracellular and extracellular surfaces. See **Figures 1A,B**.
g-ratio	A measure of myelin sheath thickness, defined as the ratio of the diameter of the fiber (axon plus myelin) to the diameter of the axon alone, which is always smaller than 1. It is calculated by measuring the circumference of each on nerve cross-sections, and converting areas to diameters, assuming the circumferences are circular.
Internode	Refers to the myelinated segment of the axon; adjacent internodes are separated by a node of Ranvier. **Figure 1D**
Juxtaparanode	The internodal region closest to the paranode, which harbors fast voltage-gated potassium channels. **Figure 1D**
Node of Ranvier	Short non-myelinated axonal region that serves the generation of action potentials; morphologically a gap flanked by myelinated "internodes." Nodes are usually ∼1 μm in length and rich in voltage gated sodium channels. **Figure 1D**
Non-compact myelin	The part of the myelinating cell process where membranes do not compact. Consists largely of tubing around the periphery of the process as well as transient openings of previously compacted myelin in some CNS fibers, and Schmidt-Lanterman incisures in the PNS. See **Figures 1**, **3**, **4**. Also referred to as "myelinic channels."
Paranode	The regions at either end of the internode where the non-compacted, paranodal loops of the myelin sheath about the axon **Figure 1D**
Septate junction	Intercellular junctions found in invertebrate epithelial cells that appear ladder-like by electron microscopy.
Spheroid	An abnormal focal swelling of the axon; mainly observed in the CNS. Often the axonal cytoskeletal elements are disorganized and axonal organelles are enriched, as observed by electron microscopy. Spheroids can also be visualized by light microscopy using respective antigen markers such as amyloid precursor protein (APP), when its transport along the axon is impaired.

terminus. In electron micrographs, axons are easily distinguished from other cellular processes because of their unique cytoskeletal organization and, often, because they are surrounded by a myelin sheath (**Figure 1**).

ORGANISATION AND MORPHOLOGY OF MYELINATED FIBRES

The Ultrastructure of the Myelinated Axon

Recent advances in imaging modalities and in image processing have contributed enormously to our understanding of the three-dimensional composition of fibre tracts. For example, electron microscopic volume imaging, including electron tomography of fine ultrastructural details; focussed ion beam-scanning electron microscopy (FIB-SEM); and serial block-face imaging (SBF) of larger volumes, provide an increasingly complete picture of the axon-myelin unit and its neighbouring cells [see for example, Snaidero et al. (2014)].

This is not to detract from the fact that conventional transmission electron microscopy (EM) has been instrumental in elucidating the relationship between the axon and its myelin sheath as well as the subcellular components of each, in normal versus pathological or experimental conditions (reviewed in Boullerne, 2016). Nonetheless, EM requires expertise and caution in tissue preparation and image interpretation. Conventional processing of tissue samples involving chemical fixation in aqueous solution, dehydration and plastic embedding, can generate considerable artefacts; mitochondria and the lipid-rich **compact myelin** being particularly susceptible to inadequate fixation. Consequently, "changes" in either must be interpreted in relation to control material handled in parallel. Cryopreparation, combining high-pressure-freezing and freeze-substitution (HPF-FS), has become a commonplace alternative (Möbius et al., 2016) and whilst less easily obtained, cryopreparations generate useful reference samples for myelin and axon phenotypes that might otherwise be masked by artefacts of conventional preparation, in particular those caused by tissue shrinkage associated with dehydration.

Electron microscopy combined with state-of-the-art fluorescence super resolution imaging have illuminated ultrastructural details of the axonal cytoskeleton. In the adult, the axonal cytoskeleton comprises actin filaments, microtubules with microtubule associated proteins, and neurofilaments. Briefly, actin filaments, which have been observed recently in axons using fluorescence super-resolution imaging, are arranged as bundles along the axon and as periodically spaced rings underneath the axolemma, likely providing elasticity and stability, respectively (reviewed by Kevenaar and Hoogenraad, 2015; Papandreou and Leterrier, 2018). Neurofilaments and microtubules are about 100 μm long in mature axons. They are aligned with the axon's long axis and can be distinguished in electron micrographs of its cross section, being 90–100 and 230–260 Å in diameter, respectively (Peters and Vaughn, 1967; **Figure 1**). Neurofilament heavy, medium and light chain triplets, in combination with α-internexin in the CNS or peripherin in the PNS, fashion a semi-rigid structure, providing temporary docking sites for vesicular organelles and integrating the membrane cytoskeleton and transmembrane adhesion molecules with the axon's interior (reviewed in Kirkcaldie and Dwyer, 2017; Yuan et al., 2017). Microtubules, which are uniformly orientated with the plus-end distally (reviewed in Rao and Baas, 2018), act as scaffolds for axonal transport (Kapitein and Hoogenraad, 2011; see Axonal transport). Cross-bridging proteins, such as spectrin, bullous pemphigoid antigen, plectin and microtubule associated proteins link neurofilaments, microtubules and actin (reviewed in Yuan et al., 2017). At the **node of Ranvier** microtubules are more abundant and neurofilaments less highly phosphorylated and more closely spaced compared to the **internode,** consistent

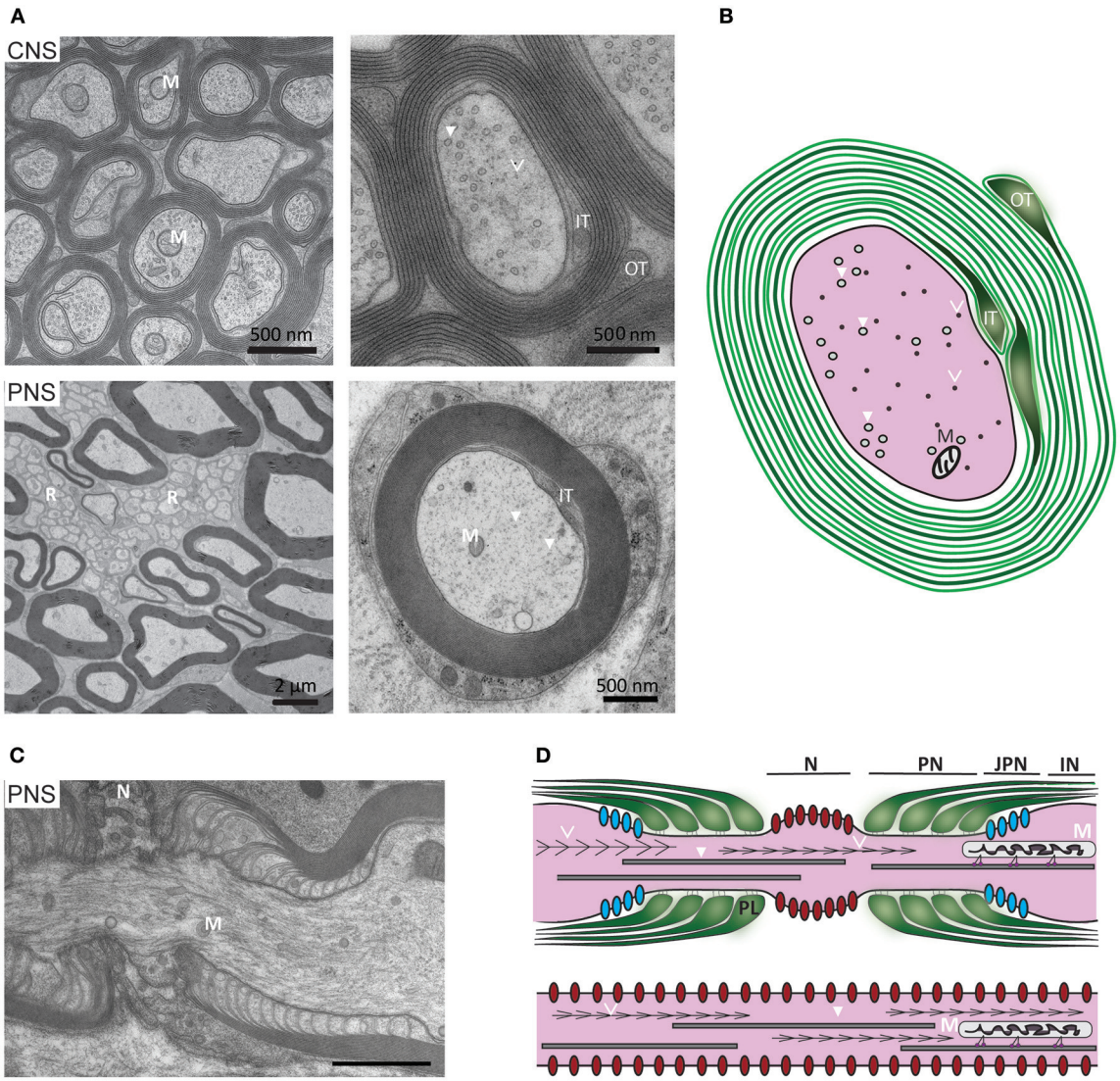

FIGURE 1 | Ultrastructure of myelinated axons in the CNS and PNS. (**A**, upper) In the CNS, myelinated axons are densely packed within white matter (here: mouse optic nerve) and the myelin sheaths of neighboring fibers often directly touch. At high magnification axonal cytoskeletal elements are visible: microtubules (arrows) and neurofilaments (arrowheads). As indicated in the schematic, mitochondria are closely associated with microtubules (M, mitochondria; IT, inner tongue; OT, outer tongue). (**A**, lower) In the PNS, the Schwann cell plasma membrane is covered with a basal lamina and the myelinated fibers are separated by connective tissue. Small caliber axons are not myelinated, but organized in so-called Remak bundles (R) formed by non-myelinating Schwann cells. At high magnification, mitochondria and cytoskeletal elements can be observed. **(B)** Schematic representation of a myelinated CNS fiber: The plasma membrane of the myelinating glial cell is depicted in green. The major dense line (depicted in grey) results from the apposition of the cytoplasmic surfaces of the plasma membrane. **(C)** Electron micrograph of a PNS node of Ranvier and (**D**, upper) schematic representation of the elements of a node: paranodal loops of the myelin sheath (green), Nav1.6 channels (red), Kv1 channels (blue), neurofilaments (arrowheads), microtubules (open arrowheads), mitochondria (M), which are transported along microtubules. N, node; PN, paranode; JPN, juxta paranode; IN, internode. (**D**, lower) Schematic representation of non-myelinated axon with uniform distribution of Nav1.6 channels along the axolemma.

with a nodal narrowing of the axon's diameter (**Figure 1**) that is particularly pronounced in the PNS (Reles and Friede, 1991).

The **axoplasm** also contains membrane-bound organelles; mitochondria being the most obvious in electron micrographs of the healthy axon. They are typically 0.1–0.3 µm in diameter, up to 10 µm in length, and oriented parallel to the axon's long-axis. In contrast to the PNS, they are not enriched at the **node of Ranvier** or **paranode** in CNS axons (Edgar et al., 2008) where they occupy a constant fraction (1.5%) of the volume of axons >0.7 µm diameter (Perge et al., 2009), suggesting energy requirements are linearly related to axonal size. Axons also contain synaptic vesicle precursors and dense core vesicles, autophagosomes, signalling endosomes, late endosomes and lysosomes, amyloid precursor protein, BDNF vesicles, smooth endoplasmic reticulum and the machinery for localised protein synthesis (reviewed in Maday et al., 2014; Lopez-Leal et al., 2016; Spaulding and Burgess, 2017;

Wu et al., 2017), which usually only become apparent following injury and regeneration (Lampert, 1967; Tsukita and Ishikawa, 1980; Court et al., 2011; **Figure 2**).

The myelin sheath comprises concentric wraps of the myelinating cell process around the axon, such that the lateral edges of the outermost layer abut the straddling **nodes of Ranvier**, and successively inner layers terminate increasingly distally from the node (depicted in **Figures 1C,D**). In **compact myelin**, an ∼2 nm space (the intraperiod space) exists between the extracellular surfaces of the wrapping glial cell process whilst its intracellular surfaces are effectively fused (forming the major dense line). Together, the major dense lines and the intraperiod spaces give compact myelin its characteristic ultrastructural appearance (**Figure 3A**). In mature CNS myelin, a single channel of cytoplasm remains around the perimeter of the glial cell process, and live imaging of Lucifer yellow filled oligodendrocytes in *ex vivo* spinal cord slices suggests that additional transient openings are present through the compact myelin (Velumian et al., 2011). Together, these cytoplasm-filled spaces constitute the non-compact myelin or "myelinic channel" system. In the PNS, this includes Schmidt-Lanterman incisures (SLI), which connect the Schwann cell abaxonal cytoplasm with the periaxonal cytoplasm (Ghabriel and Allt, 1981).

The myelinic channel, which we suggest plays an important role in glial-mediated axonal maintenance (see Mechanisms of injury: axonal pathology caused by oligodenroglial defects), is best understood if the myelin sheath is "virtually unwrapped" (**Figure 3B**). It provides continuity between the cell soma and the distal-most part of the myelin sheath at the glial-axonal junction (Ransom et al., 1991), and contains septin filaments (Buser et al., 2009; Patzig et al., 2016), microtubules, vesicles (the last two illustrated in **Figure 3C**) and multivesicular bodies. Ion channels, glutamate receptors and metabolic transporters (e.g., monocarboxylate transporter 1) are located on its adaxonal surface (Rinholm et al., 2011; Lee et al., 2012b; Nijland et al., 2014; Domenech-Estevez et al., 2015; Saab et al., 2016). The myelin sheath is separated from the **axolemma** by the periaxonal space, an ∼15 nm wide space (Peters, 1966) filled with extracellular fluid that reaches it through a spiralling pathway between the paranodal loops (reviewed in Rosenbluth, 2009). Taken together, the myelin sheath comprises a tightly wrapped double-layered cell process that is connected to its cell body via a system of fluid-filled channels.

The Myelination of Axons Was Critical in the Evolution of Higher Species

In the vertebrate central nervous system (CNS), myelinated axons define white matter tracts, including the corpus callosum, optic nerves, and spinal cord dorsal and ventral columns, which together account for ∼40% of CNS volume in humans (Morell, 1984); a higher proportion than in other species, reflecting the fact that "connectional elaboration" (= the expansion of neuronal connectivity) was key in human brain evolution (Schoenemann et al., 2005). In the peripheral nervous system (PNS), myelinated axon bundles constitute peripheral nerves, such as the sciatic nerve and the sural nerve, which link the CNS to peripheral targets. The optic nerve, being a CNS white matter tract, is erroneously named. One of the key differences between CNS and PNS axons is that in the adult, the former do not regenerate after injury.

The evolution of a rapidly functioning, yet complex nervous system was the prerequisite for development of cognitive function in higher vertebrate species. Acceleration of nerve conduction velocity can be achieved through two basic mechanisms (Hartline and Colman, 2007a). Expansion of axonal caliber, whilst effective in invertebrates with only a few nerve fibers, such as the giant axon of the squid, and the Mauthner axon in lower vertebrates, is not viable in higher vertebrates with large number of axons and consequent space restrictions. Here, glial cells adapted to insulate the axon with a multi-lamellar, concentrically wrapped membrane, termed the myelin sheath (Hartline and Colman, 2007; Nave and Werner, 2014). In vertebrates, myelin emerged first in cartilaginous fish and is functionally homologous with, but morphologically distinct from, myelin-like glial ensheathments in annelids and crustacea, (Hartline and Colman, 2007; Zalc et al., 2008). Non-myelinating axon-ensheathing cells exist in virtually all nervous systems (Schweigreiter et al., 2006).

In adult vertebrate CNS, axons larger than the ∼0.2 μm diameter "threshold" for myelination (Lee et al., 2012a; Goebbels et al., 2017) are surrounded by **compact myelin**, which is produced by oligodendrocytes. Oligodendrocyte precursors (OPCs), being present throughout life, can restore myelin sheaths following demyelination (Zawadzka et al., 2010) and potentially contribute to myelin turnover (Xiao et al., 2016). In the PNS, Schwann cells myelinate axons above a threshold size of ∼1 μm diameter (Voyvodic, 1989), whilst non-myelinating Schwann cells ensheath multiple small calibre axons within so-called "Remak bundles".

Myelinated Axons and Associated Cells Constitute CNS White Matter and PNS Nerves

Within a tract or nerve, axons are packed densely and (in general) aligned in parallel. This arrangement admits the application of diffusion tensor imaging, a magnetic resonance technique used in larger brains to map fibre tracts and identify white matter changes. Axonal densities vary from one tract to another depending largely on axonal diameter and myelination status; for example, from ∼70 to ∼380 axons per 100 μm^2 in cross-sections of the hippocampal commissure and basal telencephalic commissures of the adult rhesus monkey (LaMantia and Rakic, 1990). Estimates suggest that in mice, the optic nerve and corpus callosum respectively, contain ∼50,000 (Edgar et al., 2010) and 300,000 (Tomasch and Macmillan, 1957) axons in total; in humans the corresponding values are ∼1 and ∼800 million (Koppel and Innocenti, 1983; Mikelberg et al., 1989).

Fibre tracts comprise other important cellular elements including microglia or macrophages, which provide immune surveillance in the CNS and PNS, respectively (Perry and Gordon, 1988; Klein and Martini, 2016), and astrocytes in the CNS, the processes of which often surround axons (Luse, 1956).

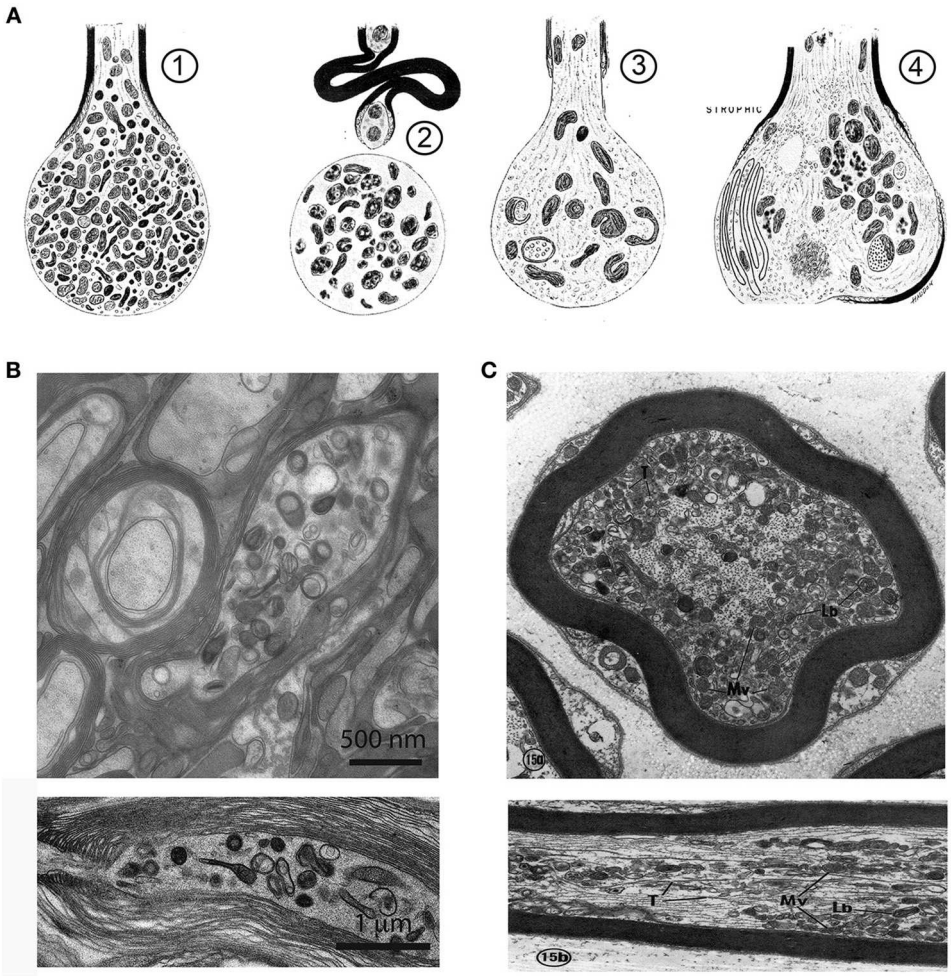

FIGURE 2 | Axonal organelle accumulations after traumatic injury or interruption of axonal transport. **(A)** Early description of axonal pathology after traumatic spinal cord injury in the rat, based on electron microscopic observations. (1) After transection the axonal stump swells and accumulates mitochondria, vesicles and dense bodies. (2) In a degenerative stage the organelles disintegrate. (3) A regenerative axon is characterized by a growth cone with multiple organelles. (4) A dystrophic axonal enlargement, caused by demyelinating disease or vitamin E deficiency is characterized by abundant filaments and organelles such as mitochondria, dense bodies, layered membrane loops, and cytoplasmic dense material. Reproduced from Lampert (1967), with permission. **(B)** Electron micrographs of focal swellings and organelle accumulations in CNS axons (upper: cross section, lower: longitudinal section), here derived from white matter of adult *Plp1* null mice**.** Note that organelle accumulations are predominantly located in the juxtaparanodal region (lower). **(C)** Electron micrographs of axonal changes in the PNS after interruption of axonal transport in the mouse saphenous nerve by cooling. At the distal side of the transport block, retrogradely transported axonal elements accumulate along the internode. These are, among others, multivesicular bodies (Mv), lamellated bodies (Lb) which intermingle with microtubules (T), and neurofilaments (Upper: cross section, Lower: longitudinal section). Reproduced from Tsukita and Ishikawa (1980) with permission.

Blood vessels, which perfuse fibre tracts, are lined by endothelial cells and associated with pericytes, smooth muscle cells and fibroblast-like cells. In humans, but not rodents, a number of neuronal cell bodies reside in the CNS white matter (Suarez-Sola et al., 2009).

Axonal Dimensions

Neurons have a single axon and these vary greatly in length as well as in ramification, as indicated before (Wu et al., 2014; Economo et al., 2016). In larger animals, axons of projection neurons can reach many meters in length (Wu et al., 2014; Wedel, 2018). This is particularly remarkable considering mammalian axons are $<20\,\mu m$ in diameter and their neuronal cell bodies are only some tens of microns across. In both the CNS and PNS, a range of diameters exists within and between tracts/nerves such that axons of a given length can differ in diameter ∼100-fold and thus 10,000-fold by volume. Measured diameters range from <0.1 to $>10\,\mu m$ in the CNS and from ∼0.1 to $\sim 20\,\mu m$ in the PNS, in mice (reviewed in Susuki, 2010; Edgar and Griffiths, 2013). Individual PNS nerves generally contain a wide range of axonal diameters and whilst this is also the case in the spinal cord lateral and ventral (anterior in human) columns, some CNS tracts, such as the corpus callosum, optic nerve and spinal cord dorsal (posterior in human) columns, contain predominantly

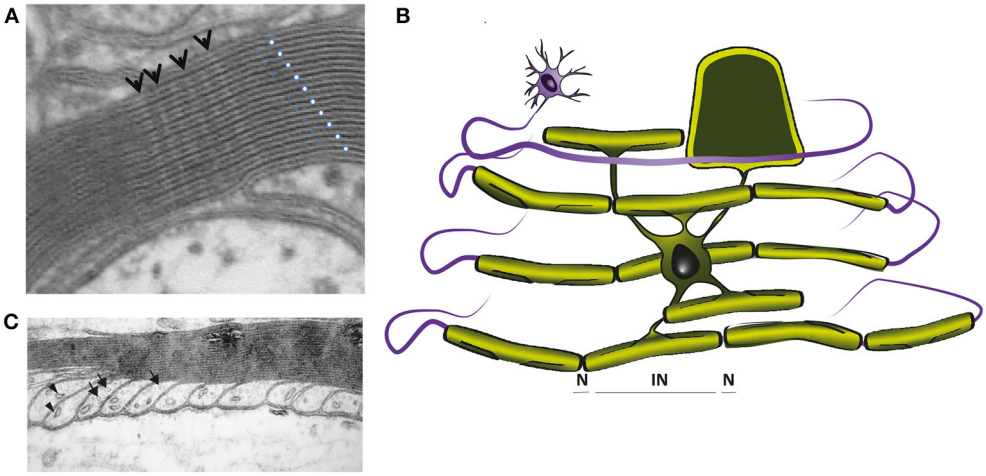

FIGURE 3 | (A) Electron micrograph showing the multilayered myelin sheath of a CNS axon in cross section. Note the regular periodicity of compact myelin, which is composed of the major dense line, reflecting the fused intracellular glial surfaces (white dots), and the 2 nm wide intraperiod space between the extracellular surfaces of adjacent wraps (blue dots). Arrows point to radial components. **(B)** In mature CNS, a single cytoplasmic channel is present around the perimeter of the glial cell process (light green), which is best understood, if the myelin is virtually unwrapped (schematically demonstrated for one internodal segment). The cytoplasmic channel connects the glial cell soma with the most distal part of the myelin sheath and contains organelles and cytoskeletal elements, as shown in **C**. **(C)** Electron micrograph of CNS paranodal loops, abutting the axon. These contain microtubules (arrows) and vesicles (arrowheads). (**A,C** were reproduced from Edgar and Griffiths, 2013, in Diffusion MRI, From Quantitative Measurement to *in vivo* Neuroanatomy; published by Elsevier).

small diameter axons. Physically, the most critical determinant of the calibre of a mature axon is the phosphorylation status of its medium neurofilaments (NFM; see The axonal cytoskeleton; reviewed by Kirkcaldie and Dwyer, 2017).

What is the reason for the range of diameters? Although conduction velocity increases with axonal diameter, the outcome is likely inconsequential in shorter axons and it has been speculated that information rate, which is dependent on firing rate, and consequently with axonal volume and energy use, is the crucial determinant of axonal diameter; with evolutionary pressure toward thin diameters due to space and energy constraints (Perge et al., 2012). Nonetheless, axonal diameter is not absolutely constant along the axon's length. In addition to consistent narrowing at the **node** and **paranode** (see The axonal cytoskeleton), the diameter of an individual axon fluctuates over its length (Perge et al., 2012) probably as a transient response to the movement of ions (Trigo and Smith, 2015).

Axon Initial Segment

The axon initial segment (AIS) is a specialized, non-myelinated region at the very proximal end of the myelinated axon at which action potentials are initiated. At the AIS, the **axolemma** is densely populated with ion channels including Nav channels and neuronal KCNQ potassium channels (reviewed in Dumenieu et al., 2017). Thus, over its 10–60 μm length, the AIS is similar in several respects to the **node of Ranvier**, including cytoskeletal arrangements. The AIS of mature CNS neurons helps maintain neuronal polarisation by acting as a selective sieve that restricts the movement of proteins from the somatodendritic compartment into the axon (Franssen et al., 2015).

Components of Nodal/Paranodal Specialisations (CNS/PNS)

Distal to the AIS and at both ends of a myelin sheath (**Figures 1C,D**, **3B**), the paranodal loops (part of the myelinic channel system) tightly appose the axon and the two are tethered by **septate**-like junctions, formed by Neurofascin 155 on the glial side and Contactin and Caspr on the axonal side (Charles et al., 2002). The node of Ranvier is the small amyelinated space between the outermost paranodal loops of adjacent myelin sheaths, whilst the juxtaparanode lies between the innermost paranodal loop and the internode proper (**Figures 1C,D**). In both the adult CNS and PNS, Nav1.6 Na^+ channels are located at the **node of Ranvier** and Kv1.1, Kv1.2 K^+ channels are localised to the **juxtaparanodal** region; although others are also present (Dumenieu et al., 2017). Various anchoring molecules including β IV spectrin and Ankyrin G as well as the paranodal-axonal transverse bands (forming **septate**-like junctions) restricts electrical activity to the nodal compartment and hinder lateral diffusion of these and other axonal membrane proteins (Rosenbluth, 2009). For detailed reviews see Rasband and Peles (2015) and Dumenieu et al. (2017). A recent study suggests that adjustment of node of Ranvier length might represent a rapid and energy-efficient mechanism for tuning the arrival time of information to its target, by altering conduction speed (Arancibia-Carcamo et al., 2017).

Although CNS and PNS nodal/paranodal structures are similar in several respects, important morphological differences include the covering of the nodal space. In the PNS, Schwann cells form the basal lamina that bridges the node, and Schwann cell microvilli contact the nodal area. In the CNS, some nodes are

covered by perinodal astrocytes or OPC processes (reviewed in Rasband and Peles, 2015).

AXO-GLIAL SIGNALLING, AXONAL MAINTENANCE, AND ENERGY METABOLISM

Cell Autonomous and Bi-Directional Signalling Regulate Axon and Myelin Dimensions

Distal to the AIS, the axon and the cells that myelinate it form a "symbiotic" unit. Each one uses both cell autonomous and bi-directional signaling mechanisms to initiate myelination and finely tune nodal and internodal (see Components of nodal/paranodal specialisations) dimensions to ensure the timely arrival of action potentials at the nerve terminus (Rushton, 1951; Stanford, 1987). Several recent studies have provided mechanistic insight to the molecular and cyto-architectural changes that take place in the myelinating cell during axonal engagement and wrapping, and this literature has been extensively reviewed elsewhere (Bauer et al., 2009; Snaidero and Simons, 2014; Hughes and Appel, 2016; Tricaud, 2017).

In the CNS, a neuronal "switch", the PI3K–AKT1–mTOR pathway, may be sufficient to trigger radial axonal growth, recruitment of OPCs and progressive myelination, as suggested from the phenotype of PTEN-deficient granule cell neurons and their (ectopically) myelinated parallel fiber axons (Goebbels et al., 2017). The wrapping of the oligodendrocyte process around the axon (the final number of wraps determines the thickness of the myelin sheath) and the extension of myelin along its length (determining internodal length) are intrinsically determined by glia growth, but modulated by the diameter of the axon they wrap (Bechler et al., 2015). Recently it was suggested that axons effect precise regulation of myelin formation by dictating the targeting of mRNAs to specific subcellular locations within the myelinating cell. Indeed, localised protein synthesis in OPCs is triggered by axonal action potentials (Wake et al., 2011). Correspondingly, electrically active axons are preferentially myelinated and neural activity probably also promotes myelin plasticity in the adult (reviewed in Almeida and Lyons, 2017; Bechler et al., 2018). Thus, whereas myelination is largely driven intrinsically in oligodendrocytes (Lee et al., 2012a), it can be modulated by extrinsic factors including electrical activity of axons, acting via oligodendroglial calcium transients (Baraban et al., 2018; Krasnow et al., 2018), the glutamatergic stimulation of glucose uptake (Saab et al., 2016) and other extracellular signalling molecules (Lundgaard et al., 2013; Emery and Lu, 2015).

Notably, axonal ensheathment, radial myelin growth and myelin elongation are controlled by different mechanisms in the PNS. Prior to myelination, Schwann cells separate single axons into a stable one-to-one relationship in a process called "axonal sorting". The established axon-myelin unit then grows in size, reaching up to 1 mm or more in internodal length (Hildebrand et al., 1994). Recently, a role for the Hippo pathway and YAP/TAZ in the integration of mechanical signals and myelination emerged in Schwann cells and has been linked to longitudinal myelin growth during development (Fernando et al., 2016; Poitelon et al., 2016). The **g-ratio**, which is a measure of the relationship between axonal diameter and myelin sheath thickness, is relatively constant for CNS and PNS axons of all diameters (Donaldson and Hoke, 1905). In the PNS, a threshold level of neuregulin on axons is required for myelin initiation and the total level of neuregulin on the axon's surface dictates the thickness of the myelin sheath (Michailov et al., 2004; Taveggia et al., 2005). Neuregulin1 downstream signaling involves PI3K/AKT and MEK/ERK pathway activation, both of which have been shown to be crucial for myelination in the PNS (Taveggia, 2016). In addition to the essential role of neuregulin1 for Schwann cell development and myelination, numerous other extrinsic and intrinsic signaling cues have been shown to regulate myelin sheath formation in the PNS, including ADAM secretases, Notch signaling and Nectin proteins (Pereira et al., 2012; Monk et al., 2015; Taveggia, 2016).

Reciprocally, oligodendrocytes and Schwann cells contribute to axonal outcomes such as the initial clustering and maintenance of sodium and potassium channels at the **node of Ranvier** and **juxtaparanode**, respectively (see Components of nodal/paranodal specialisations and **Figure 1**). Myelin also locally increases axonal calibre by modulating axonal neurofilament transport, as demonstrated by dynamic imaging *in vitro* (Uchida et al., 2013; Monsma et al., 2014), and phosphorylation and spacing (see The axonal cytoskeleton; Yuan et al., 2017), as evidenced by electron microscopic analysis of myelin-deficient *shiverer* mutant mice; although the responsible signalling mechanisms are not well understood. A stabilizing effect of mature myelin on the neuronal cytoskeleton is mediated in part by the myelin associated glycoprotein (MAG) which requires two axonal receptor families: sialoglycans (particularly the gangliosides GD1a and GT1b) and members of the Nogo receptor (NgR) family (Yin et al., 1998). Myelin and/or myelinating cells also influence the density of axonal mitochondria, such that non-myelinated axons and the axon initial segment (AIS) have a higher density of mitochondria than myelinated **internodes** (Bristow et al., 2002; Andrews et al., 2006).

Axonal Transport

Following the establishment of nodal/paranodal specialisations, nodal ion channels turn over slowly and are replenished by motor protein driven transport (Zhang et al., 2012). Neurons, being extremely polarised, are very dependent upon intracellular transport for the delivery and removal of proteins and organelles. ATP-dependent motor proteins utilise microtubules to transport these cargoes. Members of the extended kinesin superfamily, including kinesin-1, kinesin-2, and kinesin-3, transport their cargoes anterogradely (i.e., towards the microtubule plus-end) whilst dynein-1, in complex with its activator dynactin, is responsible for most retrograde (microtubule minus–end directed) transport. Until relatively recently, the movement of cargoes in myelinated axons *in vivo* was inferred from biochemical studies using radioactive tracers to label newly synthesised proteins, or from live imaging of cargoes in non-myelinated axons in culture, reviewed in Brauckmann (2004). Recently however, live imaging of the movement of mitochondria, peroxisomes or signalling endosomes in

myelinated axons *in vivo*, has been achieved (Sorbara et al., 2014; Sleigh et al., 2017).

Classically, axonal transport is divided into "fast" and "slow" according to the bulk speeds of cargo movement. For example, vesicles and mitochondria move fast at a rate of $\sim$1 μm s^{-1}, whereas cytoskeletal components translocate slowly at speeds of $\sim$1 mm per day; the difference being due to longer intermittent "stationery" phases of the cytoskeletal elements (Roy et al., 2000; Wang et al., 2000; Wang and Brown, 2002). Axonal transport is a highly regulated process, which is still poorly understood; motor proteins must recognise and bind specific cargoes, deliver these to the appropriate sites (e.g., the **node of Ranvier**, synapse, **internode**), change directions at axonal branch points, and offload cargo according to need. Regulation occurs, at least in part, through organelle-associated scaffolding proteins that bind to regulatory proteins, including kinases and GTPases, (reviewed in Fu and Holzbaur, 2014). Not surprisingly, transport is susceptible to perturbation following changes to motors, their regulators (Morfini et al., 2009), tracks, fuel supply and/or cargoes themselves, and manifests as organelle filled axonal swellings, neurofilament-filled swellings, thinning of the axon and/or axonal degeneration. Of note, demyelinating conditions were shown to impact anterograde axonal transport in the PNS (De Waegh et al., 1992), but the analysis of specific oligodendrocyte defects later revealed that the modulation of fast and slow transport in the CNS might be a glial function independent of myelin (Kirkpatrick et al., 2001; Edgar et al., 2004).

Energy Use and Supply

Axonal transport is an energy-dependent process that contributes to the brain's total energy consumption. The human brain, which occupies $\sim$2% of the body's mass, consumes $\sim$20% of its resting energy production (reviewed in Engl and Attwell, 2015) and white matter is estimated to consume around one third of the energy of grey matter (Sokoloff et al., 1977). A large proportion of the white matter's energy consumption is used by neurons to pump out sodium ions using energy-dependent Na^+-K^+-ATPases on the internodal axolemma, (reviewed in Engl and Attwell, 2015). In axons, the turnover of actin and microtubules (Engl et al., 2017), the phosphorylation of neurofilaments and the movement of cargo-bearing motor proteins (see Axonal transport) represent additional energy-consuming functions.

Molecular motors utilise 1 molecule of ATP per 8 nm step (reviewed in Maday et al., 2014). However, dyneins are less efficient than kinesins because they take more backward steps. It has been estimated that a single vesicle traversing a 1 m long human motor neuron from neuromuscular junction back to the soma or vice versa would require a minimum of 7.5×10^8 ATP or $\sim 1.25 \times 10^8$ ATP molecules, respectively (Maday et al., 2014). At an average rate of 1 μm s^{-1}, this represents 7.5×10^2 or 1.25×10^2 ATP s^{-1}. Based on 2 motile organelles per 10 μm axonal length (the maximum length of an axonal mitochondrion), 50% moving anterogradely and 50% moving retrogradely, transport would utilise $\sim 8.75 \times 10^7$ ATP s^{-1} per 1 m long axon. This equates to $\sim 6.29 \times 10^{-5}$ g of glucose per 24 h for a human sciatic nerve containing 1,000,000 axons. Importantly, these calculations are based on a very rough approximation of organelle numbers from our own electron microscopy images; assume only 1–2 motors simultaneously hydrolysing ATP per organelle; and no "tug-of-war" or "switch" events (Maday et al., 2014). In comparison, an estimated 1.54×10^9 molecules of ATP s^{-1} per cortical neuron in the rodent brain is used in action potential generation and propagation (Attwell and Laughlin, 2001).

Whilst glucose is the main substrate for feeding the TCA cycle and for ATP production in the nervous system (Hui et al., 2017), it has been demonstrated experimentally, *ex vivo* and *in vivo*, that pyruvate or lactate can sustain neuronal function, even over several hours of high level activity (Brown et al., 2001; Wyss et al., 2011; Trevisiol et al., 2017). What are the implications? Pyruvate and lactate are the 3-carbon products of glycolysis; lactate classically being generated from pyruvate to maintain NAD^+, and thus sustain glycolysis when oxygen levels are low. However, some cells synthesise most of their ATP by glycolysis even when oxygen is plentiful (Vander Heiden et al., 2009), especially in situations where cell growth is involved, such as development or cancer. Nonetheless, glycolysis yields only 2 molecules of ATP per 6-carbon glucose molecule and it is thought that most mammalian cells depend additionally on oxidative phosphorylation (OXPHOS; yielding $\sim$36 molecules of ATP per glucose) to meet their energy requirements. Indeed, neurons fail to survive if OXPHOS is prevented genetically (Fukui et al., 2007; Funfschilling et al., 2012). Therefore the observation that astrocytes and post-myelination oligodendrocytes could survive as completely "glycolytic" cells (Funfschilling et al., 2012; Supplie et al., 2017) came as a surprise; although the suggestion that astrocytes (which can store glucose as glycogen) supply lactate to neurons to support their synaptic functions metabolically and when glucose supplies are low, is well-established (reviewed in Barros and Weber, 2018). More recently we proposed that glycolytic oligodendrocytes could similarly fuel ATP synthesis in axonal mitochondria with lactate (Funfschilling et al., 2012). Indeed, the monocarboxylate transporters MCT-1 and MCT-2 (which transport monocarboxylates including pyruvate and lactate) are appropriately located on the adaxonal glial cell membrane and on the axolemma, respectively (summarised schematically in **Figure 4D**, Funfschilling et al., 2012), and normal levels of MCT-1 in oligodendrocytes are required to maintain axonal integrity in the CNS (Lee et al., 2012b).

Why would myelinating glia act as local fuelling stations for axonal mitochondria? Possible answers are that axons require much more energy than glia and that the barrier-like properties of the myelin sheath, which play such an important role in axonal insulation, likely hamper axonal glucose uptake from the extracellular space (Nave, 2010b).

If indeed glucose is prevented from reaching the myelinated axon, then the ATP to fuel axonal energy requirements should come from the oxidative phosphorylation of glial cell glycolysis products. However, a 2013 study in *Drosophila* larvae reported that the glycolytic enzyme glyceraldehyde-3-phosphate dehydrogenase (GAPDH) is localised to axonal transport vesicles (via a huntingtin-dependent mechanism), and that vesicular transport is supported by glycolytic ATP generation (Zala

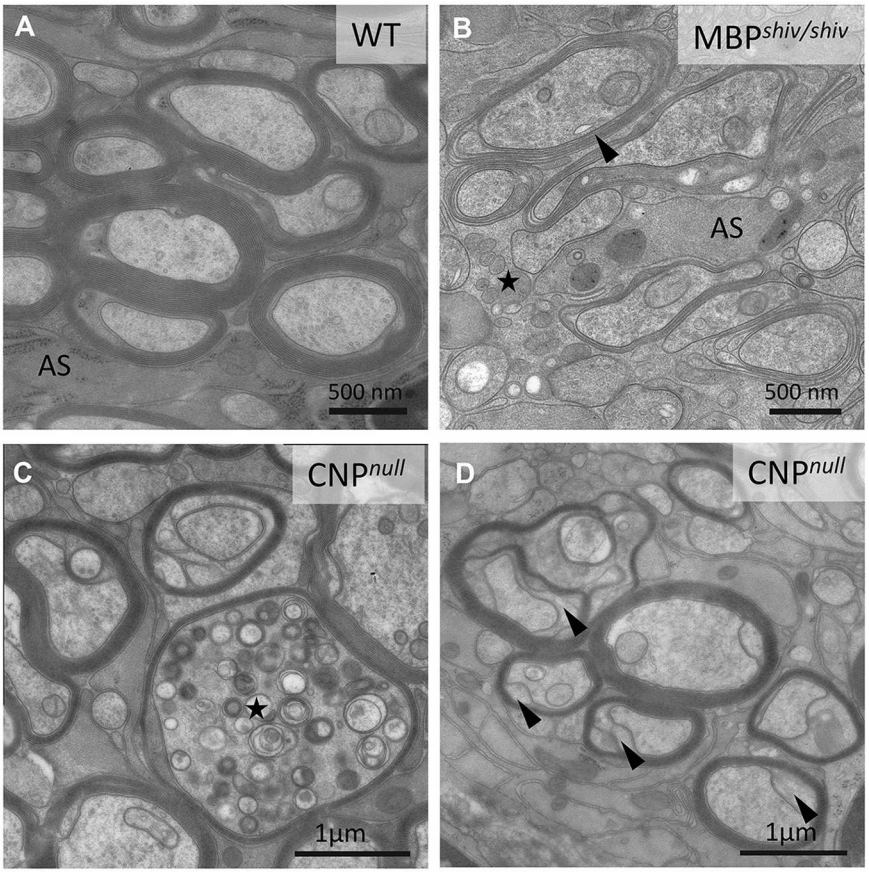

FIGURE 4 | Morphological characteristics of white matter in mouse "myelin mutants". **(A)** Normal myelinated optic nerve axons. **(B)** In the *shiverer* mouse, oligodendrocytes lacking myelin basic protein (MBP) are not able to form compact myelin, though a few loose myelin-like wraps are observed. Note the increased oligodendrocytic processes (asterisk). AS: Astrocyte process. **(C,D)** In contrast, the CNP^{null} mouse produces compact myelin but develops pronounced axonal swellings (asterisks in **C**) and enlarged inner tongues (arrowheads in **D**).

et al., 2013). Subsequently, the same authors found that a mouse forebrain fraction enriched in neuronally-derived motile vesicles was associated with 8 of 10 glycolytic enzymes and could synthesise ATP *in vitro* when appropriate substrates were added (Hinckelmann et al., 2016). These data suggest that, in some neurons, the transport of vesicles can be autonomous in terms of ATP synthesis. However, subsequent studies in *Drosophila*, using cell-specific gene silencing (Volkenhoff et al., 2015), confirmed also the principle of division of labour between neurons (requiring OXPHOS but no glycolysis) and glycolytic glial cells (requiring glycolysis but not OXPHOS) and revealed a remarkable evolutionary conservation of metabolic support.

GENERAL PATHOLOGY AND MECHANISMS OF AXONAL INJURY

The unique architectural features and metabolic requirements of myelinated fibers make their axons particularly susceptible to injury from a range of diverse causes; including physical trauma, oxygen and glucose deprivation, inflammation and the consequence of gene mutations. Axonal degeneration is also an early feature of classical neurodegenerative diseases associated with characteristic pathologies of neuronal somata, such as Alzheimer's.

Axonal injury, with or without frank axonal transection can (but does not inevitably) lead to neuronal dysfunction, depending amongst other things, on the site of injury relative to axonal branch points. Clinical signs and symptoms thus reflect both the white matter tract affected and the location of injury within the tract, as observed in spinal cord injury. Below we summarize what we have learned about general mechanisms of axonal injury and degeneration from human and animal studies, but note that the mechanisms described are not necessarily distinct. For example, dying back axonopathies can also involve Wallerian-like mechanisms (Coleman, 2005).

Mechanisms of Injury: Wallerian Degeneration

Wallerian degeneration (WD) was described over 150 years ago by August Waller (1850), and represents the degeneration of the axon distal to injury and the subsequent clearance of axonal debris. Classically, WD is induced by physical axotomy (nerve

cut) of a fiber tract, as for example in spinal cord injury and peripheral nerve trauma, but genetic evidence shows that a Wallerian-like mechanism also occurs in response to other forms of axonal injury such as "dying back" degeneration in peripheral neuropathies, and potentially in CNS axonal dystrophies in humans, as suggested from studies in mouse models (reviewed in Coleman, 2005; Conforti et al., 2014). Notably, although the rates of WD in PNS and CNS are similar, the clearance of debris by resident microglia in the CNS can take months to years, compared with a few days in the PNS (Perry et al., 1987; and reviewed in Vargas and Barres, 2007). In the PNS, Schwann cells contribute to the removal of myelin debris via a form of selective autophagy (Gomez-Sanchez et al., 2015; Jang et al., 2016). Efficient debris removal constitutes a prerequisite for subsequent regeneration in both the PNS and CNS and the failure of axonal regeneration after injury in the CNS has been linked to the presence of myelin-associated inhibitors of axonal regrowth at the injury site (reviewed in Vargas and Barres, 2007).

WD involves the remarkable process of active subcellular self-destruction. It is tightly regulated; involving a first latent phase (around 1.5–2 days post-axotomy in rodents) in which axons remain morphologically and metabolically intact and a second phase involving final breakdown of structural proteins and axonal fragmentation (reviewed in Gerdts et al., 2016). This second step is accompanied by reactive glial changes and immune cell activation (Beuche and Friede, 1984; Scheidt and Friede, 1987). In the PNS, these changes, especially the injury-response of Schwann cells, are the prerequisite of successful repair (Arthur-Farraj et al., 2012).

The Wallerian degeneration slow (*Wlds*) mouse was discovered serendipitously ∼30 years ago (Perry et al., 1990) yet, despite the plethora of studies aimed at elucidating it, the mechanism of delayed axonal degeneration is still not fully understood (reviewed in Gerdts et al., 2016). The *Wlds* mutation comprises a tandem triplication resulting in the fusion of two genes (Coleman et al., 1998), the product of which is a novel chimeric protein composed of the NAD^+ biosynthetic enzyme nicotinamide mononucleotide adenylyltransferase (NMNAT1) and a fragment of the ubiquitin ligase, Ube4b (Mack et al., 2001). NMNAT1 activity and a short N-terminal sequence are together required for the Wallerian degeneration slow effect (Avery et al., 2009; Conforti et al., 2009); most likely the extraneous NMNAT1 compensates for another NMNAT enzyme (NMNAT2) in the distal axon. NMNAT2 traffics anterogradely from the cell body into the distal axon, thus its depletion after injury (being unable to reach the axon distal to the injury and having a short half-life) is thought to initiate axonal self-destruction (Gilley and Coleman, 2010). Of note, a genetic knockout of *Nmnat2* is embryonic lethal, however, the phenotype is rescued *in vivo* upon generation of a double knockout of *Nmnat2* and *Sarm1* (Gilley et al., 2015) resulting in a normal, healthy lifespan (Gilley et al., 2017). Together, these observations led to the hypothesis that axonal depletion of NMNAT2 activates the intracellular, pro-degenerating protein SARM1 either (i) by increasing levels of NMN (the substrate for NMNAT, Di et al., 2015, 2017) and/or (ii) by decreasing NAD^+ in a feed-forward mechanism (Gerdts et al., 2015; Sasaki et al., 2016), initiating axonal self-destruction (Osterloh et al., 2012; Gerdts et al., 2015). Of note, SARM1 has recently shown to possess an intrinsic NAD^+ cleavage activity, which promotes axonal NAD^+ depletion and subsequent axonal degeneration (Essuman et al., 2017). A complex interplay with other signaling cascades such as MAPK and JNK also contribute to the initiation phase (for more extensive reviews, see Conforti et al., 2014; Gerdts et al., 2016). For instance, the DLK/MAP3K12 gene has been shown to promote axonal degeneration downstream of jun kinase signaling (Miller et al., 2009; Yang et al., 2015). Moreover, MAPK signaling has been implicated in the turnover of NMNAT2, with MAPK limiting axonal NMNAT2 levels, thereby promoting axonal breakdown (Walker et al., 2017). The transition between this early phase and the subsequent "execution phase" is thought to mark the point at which axons become committed to degenerate (Conforti et al., 2014). It is now established that increased intra-axonal calcium together with calpain (a calcium-dependent protease) activation is crucial in the execution phase, leading to, amongst other things, neurofilament proteolysis and destabilization of microtubules (Zhai et al., 2003; Conforti et al., 2014; Loreto et al., 2015; Gerdts et al., 2016). Nonetheless, inhibition of calpain activation does not fully prevent the latter, indicating that additional Ca^{2+}-dependent mechanisms contribute (Conforti et al., 2014). Notably, other mechanisms and organelles are likely to be involved. Indeed, overexpression of the mitochondrial NMNAT3 isoform protects axons from Wallerian degeneration (Yahata et al., 2009), and swelling and accumulation of axonal mitochondria at the paranodes represent early axonal changes in injury and disease models (for example, see Spencer and Schaumberg, 1977a; Edgar et al., 2004, and reviewed in Groh and Martini, 2017).

Mechanisms of Injury: Dying Back Axonopathy

Dying back axonopathy is a neuropathological feature of a heterogenous group of toxic injuries and genetic defects, and generally involves long axons of the peripheral nerves and spinal cord. It is seen, for example, in Charcot-Marie-Tooth neuropathy, hereditary spastic paraplegia, giant axonal neuropathy (GAN), adrenomyeloneuropathy (AMN) and organophosphorus compound-induced delayed neurotoxicity (OPIDN). The last **three** have not been extensively reviewed elsewhere and are described briefly in **Box1**–**3**. The geometry of the susceptible axonal populations and the limitations of histological evaluation probably contributed to the misconception that, in contrast to WD, degeneration in the dying back disorders progresses retrogradely from the axonal terminus. Rather, it is likely that degeneration appears retrogradely progressing because at the level of the whole tract (comprising many axons), it is most prevalent distally (see Figure 1 of Coleman, 2005). Indeed, early ultrastructural studies on hexacarbone induced neurotoxicity in rats, demonstrated that although a retrograde temporal spread of axonal swellings occurred, axonal degeneration was not initiated at the axon terminal nor spread centripetally along individual fibers (Spencer and Schaumberg, 1977a,b). Nevertheless, axonal

BOX 1 | Organophosphorus (OP) compound-induced delayed neurotoxicity.

OPIDN is an example of a pure axonal dying back neuropathy with a chemically induced degeneration of long, large-diameter sensorimotor axons in spinal cord and peripheral nerves, resulting in sensory loss and paralysis. In humans and susceptible animals, causes include occupational and accidental exposures to OP compounds (Smith and Spalding, 1959). Indeed, "Jake leg palsy", is attributed to consumption of tri-ortho-cresyl phosphate (TOCP)-adulterated Jamaican ginger extract during the Prohibition-era in the United States. Mechanistically, OP compounds inhibit serine esterases, including neuropathy target esterase (NTE), by organophosphorylation of the active site (Makhaeva et al., 2013). Support for a role of this enzyme and its biochemical cascade in the molecular pathogenesis of OPIDN came from identification of mutations in NTE in autosomal recessive motor neuron degeneration (NTE-MND; Rainier et al., 2008). Nonetheless, the mechanisms linking exposure to a neuropathic OP compound and the onset of OPIDN shortly after, are still poorly understood.

BOX 2 | Giant axonal neuropathy.

Giant axonal neuropathy (GAN; OMIM 256850) is an interesting example of a genetically-determined progressive axonopathy that, like OPIDN, affects both sensory and motor nerves in the PNS and CNS. GAN is a rare autosomal-recessive neurodegenerative disorder caused by mutations in the GAN gene (Bomont et al., 2000), which encodes gigaxonin, a BTB-KELCH family member. GAN is characterized histologically by large axonal swellings filled with axonal intermediate filament (IF). Using dorsal root ganglia cultures, Israeli et al. (2016) demonstrated that gigaxonin is required for ubiquitin-proteasomal degradation of neuronal intermediate filaments (IF) and that IF accumulation impairs mitochondrial movement leading to metabolic and oxidative stress, implicating axonal energy insufficiency in this disorder. Symptom onset usually occurs in childhood and most patients die in the second or third decade (reviewed in Kang et al., 2016).

BOX 3 | Adrenomyeloneuropathy (AMN).

Adrenomyeloneuropathy (AMN) is caused by mutations in the X-linked gene for adenosine triphosphate binding cassette transporter (ABCD1) (Mosser et al., 1993). This peroxisomal membrane protein is required for the import of very long-chain acyl CoA esters into peroxisomes for fatty acid β oxidation (van Roermund et al., 2008). Symptom onset usually occurs in the 3rd decade and can present with or without cerebral involvement (see below). Neurological symptoms include a progressive ataxic gait and spastic paraparesis and most probably reflect the degeneration of long spinal cord axons (Pujol et al., 2002). AMN is modelled in Abcd1 mutant mice, but the molecular mechanisms that link oligodendrocyte dysfunctions in β-oxidation to axonal degeneration remain to be established. A role of lipid-derived inflammatory mediators has been proposed (Kassmann and Nave, 2008; Ruiz et al., 2015) for both AMN and the allelic disorder X-linked adrenoleukodystrophy (X-ALD), a rapidly progressive inflammatory demyelinating disorder with onset in childhood or early adolescence (Kemp et al., 2012).

degeneration in these diseases seems length-dependent, pointing to a particular vulnerability of the long axons, possibly related to metabolic dysfunction or transport defects.

Mechanisms of Injury: Focal Axonal Degeneration and Inflammation-Induced Axonal Dysfunction

Inflammation is a primary event in multiple sclerosis (MS), neuromyelitis optica (NMO) and Guillane-Barré syndrome (GBS; a peripheral neuropathy). GBS is characterised, based on electrophysiological assessment, as primarily "demyelinating" or "axonal" and is triggered by a wide range of preceding infections, notably Campylobacter. Recent work suggests that the acute peripheral neuropathy triggered by Zika virus infection (Cao-Lormeau et al., 2016) might also be due to a GBS-like autoimmune response (see **Box 4**). MS, which is the best known inflammatory demyelinating disorder of the CNS, involves progressive axonal degeneration. Indeed, axonal and/or neuronal degeneration likely account for permanent neurological disability in secondary progressive MS. The causes of axonal injury in MS are still not known, and possibly include loss of trophic/metabolic support from oligodendrocytes, direct T-cell mediated injury, and energy insufficiency caused by soluble inflammatory factors (reviewed in Franklin et al., 2012).

Experimental evidence for inflammation-induced axonal dysfunction came from the widely used animal model of MS, "experimental autoimmune encephalomyelitis" (EAE). EAE is an induced autoimmune reaction against (usually) CNS myelin components, such as myelin oligodendrocyte glycoprotein (MOG). As a tool for understanding axonal injury in human MS, EAE models have important limitations, not least that EAE is a CD4 +ve T cell mediated pathology, whereas the aetiology of MS more likely involves CD8 +ve T cells, though it is still not known and may be heterogeneous in nature (Trapp and Nave, 2008; Stys et al., 2012).

In MOG-induced EAE, Nikic et al. (2011) demonstrated axonal changes they termed "focal axonal degeneration" (FAD). Using live imaging *in vivo*, they showed that FAD, which begins with focal axonal swelling, either progressed to axonal fragmentation or resolved. Similarly, in a mouse model of Pelizaeus Merzbacher disease (PMD), defined by a primary oligodendropathy, focal axonal swellings can occur on otherwise intact (non-transected) myelinated axons (Edgar et al., 2010; see Mechanisms of injury: axonal pathology downstream of oligodendroglial defects), raising the possibility of a temporal window for therapeutic intervention. FAD can be initiated by high levels of reactive oxygen and reactive nitrogen species (ROS and RNS) alone, implicating macrophages in its evolution in EAE, and likely also in MS, where morphologically similar changes can be observed in acute lesions (Nikic et al., 2011).

This raises the question whether axons undergoing the early pre-fragmentation stage of FAD can support electrical conduction. Certainly, nitric oxide can block neural conduction in rat spinal roots (Redford et al., 1997) and axonal depolarisation and neurological signs correlate with axonal mitochondrial

BOX 4 | Zika virus infection.

Zika virus is a neurotropic arbovirus of the family Flaviviridae that recently received considerable attention due to its links to microcephaly and, less sensationally, to GBS (Cao-Lormeau et al., 2016). In Ifnar1 knockout mouse spinal cord and dorsal root ganglia-derived cultures (Cumberworth et al., 2017) as well as in a patient who died of Zika-GBS (Dirlikov et al., 2018), PNS neurons and Schwann cells appear rather refractory to infection. However, infection of dorsal root ganglia neurons in Ifnar1 knockout mice in vivo was reported recently (Oh et al., 2017). Differences in the experimental studies may be due to viral strain-specific effects, although dissimilarity in glycosylation of the viral coat protein, related to the cell type in which the virus was propagated pre-administration, is an another confounding factor (Alain Kohl, personal communication). In contrast, CNS glia are highly susceptible in vitro, consistent with white matter pathology in pre-term and newborn infants with congenital Zika virus infection (Chimelli et al., 2017). Whether Zika-GBS has an autoimmune etiology (Uncini et al., 2017) or is due to a direct viral neuropathogenic mechanism remains to be determined.

dysfunction and precede demyelination, in mice with MOG EAE (Sadeghian et al., 2016), supporting the suggestion that neuroinflammation *per se* can contribute to neurological dysfunction in MS and other neuroinflammatory disorders. Mechanistically, this is likely related to axonal energy deficits, as nitric oxide and reactive oxygen species can damage mitochondrial respiratory chain complexes (reviewed in Smith and Lassmann, 2002). Indeed, a deficiency in complex IV function in axons (Mahad et al., 2009) and neuronal cell bodies (reviewed in Campbell and Mahad, 2018) in MS has been reported, although the causes and consequences in the disease context are as yet unproven.

Evidence for a role for the adaptive immune system in axonal injury originated from the analysis of mouse models of genetically determined CNS and PNS disorders with secondary immune reactions. Here, a role for T-lymphocytes in secondary axonal injury was demonstrated.by crossbreeding V(D)J recombination activation (*Rag1*) knockout mice, which lack mature T and B lymphocytes, to a model of the leukodystrophy PMD, caused by overexpression of the proteolipid *PLP1* gene (see Mechanisms of injury: axonal pathology downstream of oligodendroglial defects), in which axonal changes were reduced when lymphocytes were depleted. Similar observations were made in heterozygous myelin protein zero *(Mpz)* knockout and homozygous gap junction protein b (*Gjb1*) knockout mice; models of progressive demyelinating forms of the inherited peripheral neuropathies, Charcot Marie Tooth disease (CMT; Kobsar et al., 2003 and reviewed in Groh and Martini, 2017). Mechanistically, early localised axonal changes in these mutants seem to be exacerbated by T cells "attacking" the paranodal myelin (reviewed in Groh and Martini, 2017). Nonetheless, immune cells protect myelin and axons in *Mpz* deficient mice, a genetic model of a severe dysmyelinating peripheral neuropathy, Dejerine–Sottas syndrome (DSS; Berghoff et al., 2005). Hence, the role of the adaptive immune system seems to be dependent on disease-specific mechanisms, probably including myelin integrity and the response of the innate immune system (Berghoff et al., 2005).

Mechanisms of Injury: Axonal Pathology Caused by Oligodendroglial Defects

In humans, mutations in the *PLP1* gene including null, point and duplication/triplication changes, cause allelic leukodystrophies with a broad range of clinical severity, from spastic paraplegia type 2 (SPG2) to the connatal forms of PMD. All of these diseases were first identified by and later successfully modelled in *Plp1* mutant and *Plp1* overexpressing mice (Nave and Griffiths, 2004; Gruenenfelder et al., 2011). PLP and its isoform DM20 are expressed in oligodendrocytes and located in the compact myelin. The view that the survival of myelinated CNS axons is linked to the performance of surrounding glial cells initially emerged from studies of *Plp1* knockout mouse models (Griffiths et al., 1998).

However, defects in myelin biosynthesis and maintenance do not inevitably lead to axonal degeneration. For example, in the spontaneously occurring Long-Evans shaker (*les*) rat and the *shiverer* mouse, which both lack a functional myelin basic protein (*Mbp)* gene (Roach et al., 1985; O'Connor et al., 1999), CNS axons are severely de- or dysmyelinated (**Figures 4A,B**), but degenerative axonal changes are lacking (Rosenbluth, 1980; Griffiths et al., 1998; Edgar et al., 2004; Smith et al., 2013), presumably owing to unimpaired communication between axons and engulfing oligodendroglial processes (summarised in **Figure 5**). Nevertheless, *shiverer* axons do have a reduced calibre and retain an "immature" cytoskeleton (Brady et al., 1999; Kirkpatrick et al., 2001). Thus, *shiverer* elucidates the profound influence the myelinating oligodendrocyte exerts on the axonal cytoskeleton and on radial axonal growth (see Cell autonomous and bi-directional signalling regulate axonal and glial dimensions). Of note, the PNS of *shiverer* mice is fully myelinated (Privat et al., 1979; Kirschner and Ganser, 1980), possibly due to overlapping functions of MBP with myelin protein zero (MPZ) and peripheral myelin protein 2 (PMP2) in peripheral myelin (Martini et al., 1995).

De- and dysmyelination are associated with the (re)distribution of sodium channels along the axolemma, thus maintaining axonal conduction (Utzschneider et al., 1993; Waxman et al., 2004). However, the resultant non-saltatory action potential propagation increases energy consumption, and accordingly, increased numbers of mitochondria have been observed in *shiverer* axons (Andrews et al., 2006) and in human MS tissue (Zambonin et al., 2011).

In contrast to *shiverer*, mice deficient in PLP or CNP (2′,3′-cyclic nucleotide 3′-phosphodiesterase) synthesise normal amounts of myelin, but develop a pronounced axonal pathology (**Figures 2B**, **4C,D**). Taking advantage of the X-linked nature of the *Plp1* gene and female heterozygotes harbouring a mosaic of wild type and PLP-deficient myelin (the latter with subtle defects in compaction), we demonstrated that secondary axonal changes, such as organelle-filled focal swellings, are localised to the internodes formed by the PLP-deficient myelin (Edgar et al., 2004). This demonstrates that oligodendroglial support of axonal integrity is a very local function. Late

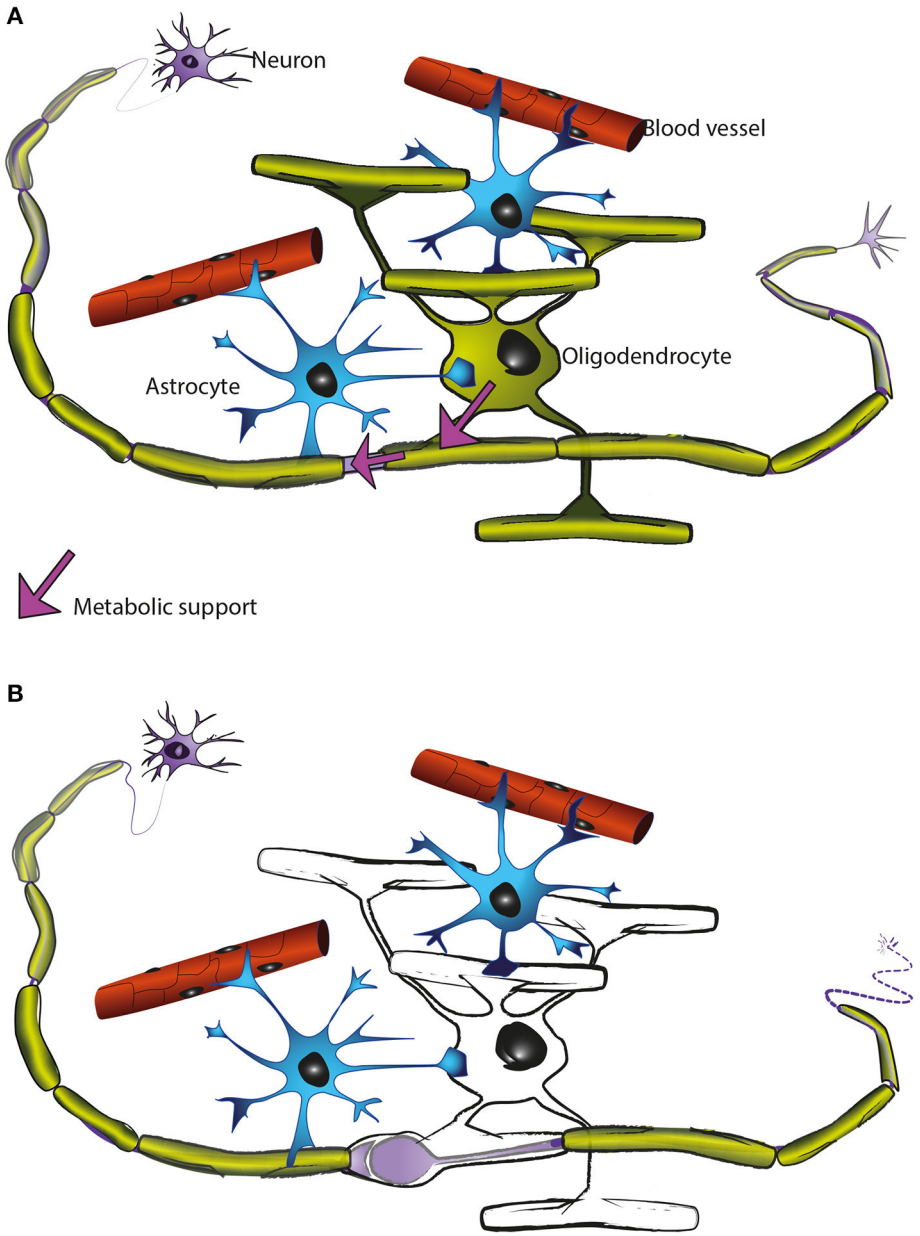

FIGURE 5 | Oligodendrocytes support axons. **(A)** In the CNS, oligodendrocytes (green) provide axons with the insulating myelin sheath (green: myelinated internodes). Moreover, oligodendrocytes support axonal integrity and function independent of myelination *per se* (for details see main text). Astrocytes (blue) not only contact blood vessels but additionally interact with axons and oligodendrocytes and contribute to brain homeostasis. Oligodendrocyte precursor cells (not illustrated) are also present in the mature CNS and are the main cellular source for new oligodendrocytes after injury and in remyelination. **(B)** Oligodendrocyte dysfunction leads to a perturbed axon-glia interaction which ultimately impairs axonal health. As the myelinic channel system is likely acting as a route by which oligodendrocytes supply metabolites to the myelinated axons, any perturbation of this system could potentially impact axonal integrity, resulting for example in focal axonal swelling and distal axonal degeneration.

onset length-dependent axonal degeneration in this mutant is likely a consequence of these early focal changes and organelle transport stasis (Edgar et al., 2004). That the axonal changes are secondary to the glial-cell defect was confirmed by cell transplantation experiments (Edgar et al., 2004) and using a novel oligodendroglia specific *Plp1* gene knockout model (Lüders et al., 2017). Axon degeneration is also the cause of progressive spasticity in the corresponding human *PLP1* null patients with SPG2 (Garbern et al., 2002); belonging to the family of disorders termed the hereditary spastic paraplegias. In mice, the absence of PLP from myelin causes a secondary loss of SIRT2, a nicotinamide adenine dinucleotide

(NAD)-dependent deacetylase, which is normally abundant in myelinic channels (Werner et al., 2007). The function of SIRT2 in myelin is not understood, but as a sensor of the NAD/NADH ratio in the myelin compartment, its activity is likely regulated by oligodendrocyte glycolysis and the generation of lactate.

Similarly, *Cnp1* knockout mice (Lappe-Siefke et al., 2003), lacking a membrane-associated protein of non-compacted myelin, are fully myelinated but focal axonal swellings and degeneration of axons are observed simultaneously, commencing after postnatal day 5 (P5), in all investigated white matter tracts (Edgar et al., 2009). The encoded 2′,3′-cyclic nucleotide phosphodiesterase (CNP) most likely not serving as an enzyme, interacts with actin to antagonise MBP in myelin membrane compaction (Snaidero et al., 2017). Thus, abnormal MBP-dependent closures of the myelinic channels likely result in the observed swellings at the inner tongue, that are predicted to perturb axon-glia communication (Lappe-Siefke et al., 2003; Edgar et al., 2009; Snaidero et al., 2017).

These and other observations have led us to hypothesise that the myelinic channel system is crucial to the function of the oligodendrocyte in axonal support, likely acting as the route through which the oligodendrocyte supplies metabolites to the myelinated axon and delivers membrane proteins to the adaxonal myelin surface (**Figure 5**).

In the *Plp1* transgenic line #72 (Readhead et al., 1994), axonal swellings and axonal transport defects correlate with active demyelination and microglial/macrophage activation in the optic nerve. In contrast, completely demyelinated axons remain intact, suggesting injured myelin and/or neuroinflammation is relatively more detrimental than the absence of myelin *per se* (Edgar et al., 2010). Indeed, axonal injury can occur beneath "not-yet" demyelinated axons in inflammatory demyelinating models (Nikic et al., 2011; Pohl et al., 2011; Oluich et al., 2012). This supports our suggestion that axons shielded from nutrients in the extracellular milieu, are susceptible to injury if even minor damage to myelinic channels leaves oligodendrocytes unable to fuel the axon's energy requirements.

Further evidence for a role of oligodendrocytes in axonal support comes from mice lacking the *Pex5* gene (encoding the peroxisomal biogenesis factor and targeting signal type-I receptor) in myelinating glia. In this model, the absence of oligodendroglial peroxisomes does not interfere with myelination but underlies a progressive clinical phenotype caused by subcortical demyelination, inflammation and widespread axonal degeneration (Kassmann et al., 2007).

Primary oligodendrocyte death also elicits axonal changes. The diphtheria-toxin mediated ablation of oligodendrocytes in mice leads to secondary focal axonal changes and a reduction in axonal densities (Ghosh et al., 2011; Pohl et al., 2011; Oluich et al., 2012). The significant temporal delay between oligodendrocyte cell death and axonal demise can probably be explained by the initial preservation of myelin sheaths, including their content of glycolytic enzymes and metabolite transporters (Saab et al., 2016). Axonal changes in this model are independent of the adaptive immune system, as evidenced by crossbreeding to *Rag1* deficient mice (Pohl et al., 2011), however a late-onset secondary T cell response with fatal demyelination has been reported (Traka et al., 2016).

Mechanisms of Injury: Axonal Pathology Caused by Schwann Cell Defects

Peripheral neuropathies are a heterogeneous group of diseases and result from inflammatory, toxic and metabolic conditions in addition to genetic defects. The last are referred to as Charcot-Marie-Tooth diseases (CMT) and can be subdivided into forms that primarily affect the Schwann cells (CMT type 1) or the axon (CMT type 2). Evidence for axonal support by Schwann cells emerged from murine mutants and transgenics for the peripheral myelin protein (*Pmp22*) gene (encoding the peripheral myelin protein of 22kDA; PMP22), which model CMT1A. A *Pmp22* point mutation defines the *Trembler* mouse (Suter et al., 1992), which is characterized by hypomyelination, demyelination, reduced axonal calibre, axonal cytoskeletal changes, and alterations in slow axonal transport (De Waegh and Brady, 1990; Kirkpatrick and Brady, 1994). Schwann cell–axon interactions are perturbed at paranodal glial-axonal junctions in *Trembler* (Robertson et al., 1997) and associated with a redistribution of axonal ion channels (Rosenbluth and Bobrowski-Khoury, 2014). Interestingly, nerve graft experiments demonstrated that axonal changes are spatially restricted to segments myelinated by "mutant" Schwann cells (De Waegh et al., 1992). Transgenic overexpression of *Pmp22* also induces dys- and demyelination and, in this case, a slowly progressive, distally pronounced, axonal loss (Sereda et al., 1996; Fledrich et al., 2014), providing a bona fide model of human Charcot-Marie-Tooth disease type 1A (CMT1A). In contrast to PMP22 overexpression in CMT1A disease, a heterozygous deletion of the *PMP22* gene causes hereditary neuropathy with liability to pressure palsies (HNPP) (Nicholson et al., 1994; Adlkofer et al., 1995; Li et al., 2007). HNPP is characterized by focal hypermyelination of peripheral nerves, and the application of mechanical compression induces a conduction block in affected patients as well as in respective animal models (Adlkofer et al., 1995; Li et al., 2007; Bai et al., 2010). Consistent with this, other CMT forms with increased myelin outfoldings, such as CMT4B, demonstrate a reduced nerve conduction velocity as well as a decreased compound muscle action potential (Previtali et al., 2007; Ng et al., 2013). However, the precise molecular mechanisms of disease progression and functional failure in CMT diseases remain only partially understood, and it is most likely that all human dysmyelinating neuropathies share a defect of Schwann cell-axon communication that is ultimately responsible for axonal conduction blocks, degeneration and a progressive clinical phenotype (Nave et al., 2007).

The role of the "mutant" glial cell versus altered myelin in PMP22-related axonal changes could not be uncoupled in these demyelinating models. Rather, it was the observation that axonal changes occur on axons with relatively (*Mag* and *Plp1*

knockout mice) or completely (*Cnp1* knockout mice) normal-appearing compact myelin that provided evidence that glial cells, independent of myelin, support axonal health (Nave, 2010a; and see Mechanisms of injury: axonal pathology caused by oligodenroglial defects). Mice lacking the myelin-associated glycoprotein (*Mag*) gene, assemble CNS and PNS myelin that harbours very minor morphological changes at the inner wrap, but have reduced axon calibre associated with altered neurofilament spacing and phosphorylation in the PNS (Yin et al., 1998; Pan et al., 2005). A progressive degenerative response including paranodal myelin tomaculi and axonal loss subsequently ensues (Yin et al., 1998; Pan et al., 2005).

Just as oligodendrocytes likely provide metabolic support for axons (see Energy supply and use), so there is evidence that Schwann cells play a similar role in the PNS. Beirowski et al. (2014) demonstrated that knocking out the gene encoding the ubiquitously expressed liver kinase B1 (LKB1), specifically in adult Schwann cells, did not affect myelin morphology but led to axonal loss, most specifically of small sensory axons in Remak bundles (C fibres). LKB1 is a key regulator of energy homeostasis, suggesting axonal degeneration in this model could pertain to axonal energy insufficiency; however the phenotype is complex and its interpretation is not straightforward. More recently, using mice lacking the nutrient sensing protein O-GlcNAc transferase (OGT) in Schwann cells, the same group demonstrated that Schwann cell OGT is required for the maintenance of normal myelin and to prevent axonal loss (Kim et al., 2016). Notably, mice lacking the myelin protein Periaxin (a model for DSS), which is O-GlcNAcyated, develop a very similar phenotype (Gillespie et al., 2000; Court et al., 2004) to the conditional OGT knockout mice (Kim et al., 2016). Recently, using the compound action potential as a readout of *ex-vivo* sciatic nerve function, Rich and Brown (2018) provided evidence that non-myelinated C fibres and myelinated A fibres in the same sciatic nerve preparation, have distinct metabolic profiles. The authors showed that when fructose is supplied as the sole energy source, C fibres can utilise it directly whereas A fibres benefit through receipt of lactate from Schwann cells. Together, these data are compatible with the hypothesis that myelinating cells provide metabolic support to axons encased in compact myelin, to abrogate the consequences of their being sequestered from extracellular glucose (Nave, 2010b).

CONCLUSIONS AND IMPLICATIONS FOR HUMAN DISEASES

In summary, we have provided an overview of the unique physical and functional properties of (myelinated) axons, with an emphasis on how these might contribute to the axon's vulnerability to injury in a variety of diseases and traumas. In particular, its relative isolation (in terms of distance) from its cell body, dependence on long-distance axonal transport, and high energy demands resulting largely from "spiking", probably all render axons susceptible to injury from a variety of insults.

In some cases, such as SPG10, which is due to a mutation in *KIF5A* (encoding a motor protein of axonal transport), the reason why axons are vulnerable seems evident. However, the particular susceptibility of motor neuron axons in some complex disorders such as familial amyotrophic lateral sclerosis (fALS), in which the mutated gene (*SOD1*; superoxide dismutase 1) is expressed in all neural cell types, remains an enigma; although multiple mechanisms have been implicated.

In MS, a "high grade" inflammatory demyelinating disorder, axonal injury probably also entails multiple mechanisms (see Mechanisms of injury: Focal axonal degeneration and inflammation-induced axonal dysfunction) and many aspects remain poorly understood, including the direct role for lymphocytes themselves. In classical axonal and demyelinating GBS, which also fall into this category, antibody-mediated complement activation and downstream calpain-dependent proteolysis is now generally considered the most likely effector of axonal demise (Willison et al., 2016). In the "low grade" inflammatory disorder AMN, axonal degeneration happens in a length dependent fashion (**Box 2**), but as in fALS, the mutated *ABCD1* gene is expressed in virtually all cell types and the underlying reasons for the axonal phenotype remain poorly understood. Insight into the effectors of this and other genetically-determined length-dependent axonopathies might come from understanding how axons are injured in the neurotoxic disorders like OPIDN (**Box 1**). With respect to axonopathies secondary to mutations in genes whose products are expressed in oligodendrocytes and/or Schwann cells, there is increasing evidence that axonal degeneration reflects a failure of the myelinating cell to provide metabolic support to the axon. Indeed axonal energy insufficiency might represent a common pathway in multiple neurodegenerative disorders; either due to failure of metabolic support from neighbouring glia; to ischemia as in stroke; or as a consequence of failure of OXPHOS due to nitric oxide (and potentially other factors) mediated injury to axonal mitochondria (summarised in **Figure 5B**).

Intriguingly, in rat and mouse models of axonopathies, the obvious restriction imposed on the physical length of axons compared to humans and larger species, does not reduce their susceptibility to "length-dependent degeneration", as for example in mouse models of SPG2 and CMT. Thus, actual physical length is not the defining factor. Rather, length-dependent degeneration in rodents is compatible with energy insufficiency being causally related to axonal demise, because presumably, energy provision is proportionally less in these small species, rendering their "long" axons just as susceptible as in larger species consuming a much greater calorie load.

Finally, axonal degeneration and/or dysfunction might not be the only axonally-related factors that contribute to neurological symptoms. Recently, we and others demonstrated reduced axonal calibre in mouse models of two complex neuropsychological disorders (Rett and Angelman syndromes; **Box 5**), which could potentially contribute to symptoms. Thus a variety of

BOX 5 | Rett and Angelman syndromes.

Rett and Angelman syndromes comprise part of the spectrum of neurologic disorders previously considered associated with autism (Jedele, 2007). Both present, after a short period of normal development, with global developmental delay, severe speech and communication deficits, progressive microcephaly, seizures, autistic behavior and a characteristic movement disorder. Angelman syndrome is due to loss of function of the maternally inherited ubiquitin protein ligase E3A (UBE3A) allele, while Rett syndrome is due in the majority of cases to loss of function mutation in the X-linked methyl-CpG- binding protein 2 (MECP2) gene. Remarkably, clinical features occur in the absence of evident neurodegeneration, and activation of a silenced Mecp2 allele, even with a radically truncated MeCP2 protein, in adult mice reverses neurological and morphological changes, suggesting MeCP2 might be required for maintenance of neuronal function, rather than for normal development (Guy et al., 2007; Tillotson et al., 2017). Female mice heterozygous for a Mecp2 null allele develop normally but subsequently exhibit a stiff, uncoordinated gait, tremor, breathing difficulties and hindlimb clasping. Although there is no evidence of axonal degeneration in the PNS of adult *Mecp2*$^{+/-}$ mice, the mean diameter of sciatic nerve axons is significantly reduced and myelin is slightly thinner than normal (Bahey et al., 2017). Similarly, in a mouse model of Angelman syndrome, reduced axonal diameter and white matter abnormalities underlie impaired brain growth and microcephaly (Judson et al., 2017). Similar subtle morphological changes could, in principle, contribute to the neurological signs in Rett and Angelman syndromes.

axonal changes, from reduced calibre, through mitochondrial dysfunction and focal swelling to transection, can probably all contribute to neurological symptoms in neurodegenerative diseases or injuries with primary or secondary involvement of axons.

AUTHOR CONTRIBUTIONS

JE and RS wrote the review and provided images. JE planned and edited the review. K-AN was involved in planning, writing and finally edited the manuscript. WM contributed electron micrographs and figure legends.

ACKNOWLEDGMENTS

The authors thank Dr Stuart Cobb and Professors David Attwell and Michael Coleman for helpful discussion. Work in our labs is funded by the Multiple Sclerosis Society UK (Ref 038) and European Union's Horizon 2020 research and innovation programme under ZikaPLAN grant agreement No 734584 (JE); DFG (SPP 1757) and the European Research Council (MyeliNANO) (K-AN); ERA-NET for Research Programs on Rare Diseases E-RARE-3 (01GM1605) and the German network on Charcot-Marie-Tooth Disease (CMT-NET, 01GM1511C) (RS).

REFERENCES

Adlkofer, K., Martini, R., Aguzzi, A., Zielasek, J., Toyka, K. V., and Suter, U. (1995). Hypermyelination and demyelinating peripheral neuropathy in Pmp22-deficient mice. *Nat. Genet.* 11, 274–280. doi: 10.1038/ng1195-274

Almeida, R. G., and Lyons, D. A. (2017). On myelinated axon plasticity and neuronal circuit formation and function. *J. Neurosci.* 37, 10023–10034. doi: 10.1523/JNEUROSCI.3185-16.2017

Andrews, H. E., White, K., Thomson, C. E., Edgar, J. M., Bates, D., Griffiths, I. R., et al. (2006). Increased axonal mitochondrial activity as an adaptation to myelin deficiency in the shiverer mouse. *J. Neurosci. Res.* 83, 1533–1539. doi: 10.1002/jnr.20842

Arancibia-Carcamo, I. L., Ford, M. C., Cossell, L., Ishida, K., Tohyama, K., and Attwell, D. (2017). Node of Ranvier length as a potential regulator of myelinated axon conduction speed. *Elife* 6:e23329. doi: 10.7554/eLife.23329

Arthur-Farraj, P. J., Latouche, M., Wilton, D. K., Quintes, S., Chabrol, E., Banerjee, A., et al. (2012). c-Jun reprograms Schwann cells of injured nerves to generate a repair cell essential for regeneration. *Neuron* 75, 633–647. doi: 10.1016/j.neuron.2012.06.021

Attwell, D., and Laughlin, S. B. (2001). An energy budget for signaling in the grey matter of the brain. *J. Cereb. Blood Flow Metab.* 21, 1133–1145. doi: 10.1097/00004647-200110000-00001

Avery, M. A., Sheehan, A. E., Kerr, K. S., Wang, J., and Freeman, M. R. (2009). WldS requires Nmnat1 enzymatic activity and N16-VCP interactions to suppress Wallerian degeneration. *J. Cell Biol.* 184, 501–513. doi: 10.1083/jcb.200808042

Bahey, N. G., Gadalla, K. K. E., McGonigal, R., Bailey, M. E. S., Edgar, J. M., and Cobb, S. R. (2017). Reduced axonal diameter of peripheral nerve fibers in a mouse model of Rett syndrome. *Neuroscience* 358, 261–268. doi: 10.1016/j.neuroscience.2017.06.061

Bai, Y., Zhang, X., Katona, I., Saporta, M. A., Shy, M. E., O'Malley, H. A., et al. (2010). Conduction block in PMP22 deficiency. *J Neurosci.* 30, 600–608. doi: 10.1523/JNEUROSCI.4264-09.2010

Baraban, M., Koudelka, S., and Lyons, D. A. (2018). Ca (2+) activity signatures of myelin sheath formation and growth *in vivo*. *Nat. Neurosci.* 21, 19–23. doi: 10.1038/s41593-017-0040-x

Barros, L. F., and Weber, B. (2018). CrossTalk proposal: an important astrocyte-to-neuron lactate shuttle couples neuronal activity to glucose utilisation in the brain. *J. Physiol.* 596, 347–350. doi: 10.1113/JP274944

Bauer, N. G., Richter-Landsberg, C., and Ffrench-Constant, C. (2009). Role of the oligodendroglial cytoskeleton in differentiation and myelination. *Glia* 57, 1691–1705. doi: 10.1002/glia.20885

Bechler, M. E., Byrne, L., and ffrench-Constant, C. (2015). CNS myelin sheath lengths are an intrinsic property of oligodendrocytes. *Curr. Biol.* 25, 2411–2416. doi: 10.1016/j.cub.2015.07.056

Bechler, M. E., Swire, M., and ffrench-Constant, C. (2018). Intrinsic and adaptive myelination-A sequential mechanism for smart wiring in the brain. *Dev. Neurobiol.* 78, 68–79. doi: 10.1002/dneu.22518

Beirowski, B., Babetto, E., Golden, J. P., Chen, Y. J., Yang, K., Gross, R. W., et al. (2014). Metabolic regulator LKB1 is crucial for Schwann cell-mediated axon maintenance. *Nat. Neurosci.* 17, 1351–1361. doi: 10.1038/nn.3809

Berghoff, M., Samsam, M., Muller, M., Kobsar, I., Toyka, K. V., Kiefer, R., et al. (2005). Neuroprotective effect of the immune system in a mouse model of severe dysmyelinating hereditary neuropathy: enhanced axonal degeneration following disruption of the RAG-1 gene. *Mol. Cell. Neurosci.* 28, 118–127. doi: 10.1016/j.mcn.2004.09.001

Beuche, W., and Friede, R. L. (1984). The role of non-resident cells in Wallerian degeneration. *J. Neurocytol.* 13, 767–796. doi: 10.1007/BF01148493

Bomont, P., Cavalier, L., Blondeau, F., Ben Hamida, C., Belal, S., Tazir, M., et al. (2000). The gene encoding gigaxonin, a new member of the cytoskeletal BTB/kelch repeat family, is mutated in giant axonal neuropathy. *Nat. Genet.* 26, 370–374. doi: 10.1038/81701

Boullerne, A. I. (2016). The history of myelin. *Exp. Neurol.* 283, 431–445. doi: 10.1016/j.expneurol.2016.06.005

Brady, S. T., Witt, A. S., Kirkpatrick, L. L., De Waegh, S. M., Readhead, C., Tu, P. H., et al. (1999). Formation of compact myelin is required for maturation of the axonal cytoskeleton. *J. Neurosci.* 19, 7278–7288. doi: 10.1523/JNEUROSCI.19-17-07278.1999

Brauckmann, S. (2004). The virtue of being too early: Paul A. Weiss, and 'axonal transport'. *Hist. Philos. Life Sci.* 26, 333–353. Available online at: https://www.jstor.org/stable/23333720

Bristow, E. A., Griffiths, P. G., Andrews, R. M., Johnson, M. A., and Turnbull, D. M. (2002). The distribution of mitochondrial activity in relation to optic nerve structure. *Arch. Ophthalmol.* 120, 791–796. doi: 10.1001/archopht.120.6.791

Brown, A. M., Wender, R., and Ransom, B. R. (2001). Metabolic substrates other than glucose support axon function in central white matter. *J. Neurosci. Res.* 66, 839–843. doi: 10.1002/jnr.10081

Buser, A. M., Erne, B., Werner, H. B., Nave, K. A., and Schaeren-Wiemers, N. (2009). The septin cytoskeleton in myelinating glia. *Mol. Cell. Neurosci.* 40, 156–166. doi: 10.1016/j.mcn.2008.10.002

Campbell, G., and Mahad, D. (2018). Mitochondrial dysfunction and axon degeneration in progressive multiple sclerosis. *FEBS Lett.* 17: 1873–3468 doi: 10.1002/1873-3468.13013

Cao-Lormeau, V. M., Blake, A., Mons, S., Lastere, S., Roche, C., Vanhomwegen, J., et al. (2016). Guillain-Barre Syndrome outbreak associated with Zika virus infection in French Polynesia: a case-control study. *Lancet* 9, 1531–1539. doi: 10.1016/S0140-6736(16)00562-6

Charles, P., Tait, S., Faivre-Sarrailh, C., Barbin, G., Gunn-Moore, F., Denisenko-Nehrbass, N., et al. (2002). Neurofascin is a glial receptor for the paranodin/Caspr-contactin axonal complex at the axoglial junction. *Curr. Biol.* 12, 217–220. doi: 10.1016/S0960-9822(01)00680-7

Chimelli, L., Melo, A. S. O., Avvad-Portari, E., Wiley, C. A., Camacho, A. H. S., Lopes, V. S., et al. (2017). The spectrum of neuropathological changes associated with congenital Zika virus infection. *Acta Neuropathol.* 133, 983–999. doi: 10.1007/s00401-017-1699-5

Coleman, M. (2005). Axon degeneration mechanisms: commonality amid diversity. *Nat. Rev. Neurosci.* 6, 889–898. doi: 10.1038/nrn1788

Coleman, M. P., Conforti, L., Buckmaster, E. A., Tarlton, A., Ewing, R. M., Brown, M. C., et al. (1998). An 85-kb tandem triplication in the slow Wallerian degeneration (*Wld*^{s}) mouse. *Proc. Natl. Acad. Sci. U.S.A.* 95, 9985–9990. doi: 10.1073/pnas.95.17.9985

Conforti, L., Gilley, J., and Coleman, M. P. (2014). Wallerian degeneration: an emerging axon death pathway linking injury and disease. *Nat. Rev. Neurosci.* 15, 394–409. doi: 10.1038/nrn3680

Conforti, L., Wilbrey, A., Morreale, G., Janeckova, L., Beirowski, B., Adalbert, R., et al. (2009). WldS protein requires Nmnat activity and a short N-terminal sequence to protect axons in mice. *J. Cell Biol.* 184, 491–500. doi: 10.1083/jcb.200807175

Court, F. A., Midha, R., Cisterna, B. A., Grochmal, J., Shakhbazau, A., Hendriks, W. T., et al. (2011). Morphological evidence for a transport of ribosomes from Schwann cells to regenerating axons. *Glia* 59, 1529–1539. doi: 10.1002/glia.21196

Court, F. A., Sherman, D. L., Pratt, T., Garry, E. M., Ribchester, R. R., Cottrell, D. F. Fleetwood-Walker, S. M., et al. (2004). Restricted growth of Schwann cells lacking Cajal bands slows conduction in myelinated nerves. *Nature* 431, 191–195. doi: 10.1038/nature02841

Cumberworth, S. L., Barrie, J. A., Cunningham, M. E., de Figueiredo, D. P. G., Schultz, V., Wilder-Smith, A. J., et al. (2017). Zika virus tropism and interactions in myelinating neural cell cultures: CNS cells and myelin are preferentially affected. *Acta Neuropathol. Commun.* 5:50. doi: 10.1186/s40478-017-0450-8

De Waegh, S. M., and Brady, S. T. (1990). Altered slow axonal transport and regeneration in a myelin-deficient mutant mouse: the trembler as an *in vivo* model for Schwann cell-axon interactions. *J. Neurosci.* 10, 1855–1865. doi: 10.1523/JNEUROSCI.10-06-01855.1990

De Waegh, S. M., Lee, V. M. Y., and Brady, S. T. (1992). Local modulation of neurofilament phosphorylation, axonal caliber, and slow axonal transport by myelinating Schwann cells. *Cell* 68, 451–463. doi: 10.1016/0092-8674(92)90183-D

Di, S. M., Loreto, A., Orsomando, G., Mori, V., Zamporlini, F., Hulse, R. P., et al. (2017). NMN Deamidase delays wallerian degeneration and rescues axonal defects caused by NMNAT2 deficiency *in vivo*. *Curr. Biol.* 27, 784–794. doi: 10.1016/j.cub.2017.01.070

Di, S. M., Nascimento-Ferreira, I., Orsomando,G., Mori,V.,Gilley,J., Brown, R., et al. (2015). A rise in NAD precursor nicotinamide mononucleotide (NMN) after injury promotes axon degeneration. *Cell Death Differ.* 22, 731–742. doi: 10.1038/cdd.2014.164

Dirlikov, E., Torres, J. V., Martines, R. B., Reagan-Steiner, S., Perez, G. V., Rivera, A., et al. (2018). Postmortem Findings in Patient with Guillain-Barre Syndrome and Zika Virus Infection. *Emerging Infect. Dis.* 24, 114–117. doi: 10.3201/eid2401.171331

Domenech-Estevez, E., Baloui, H., Repond, C., Rosafio, K., Medard, J. J., Tricaud, N., et al. (2015). Distribution of monocarboxylate transporters in the peripheral nervous system suggests putative roles in lactate shuttling and myelination. *J. Neurosci.* 35, 4151–4156. doi: 10.1523/JNEUROSCI.3534-14.2015

Donaldson, H. H., and Hoke, G. W. (1905). On the areas of the axis cylinder and medullary sheath as seen in cross sections of the spinal nerves of vertebrates. *J. Comp. Neurol.* 15, 1–16. doi: 10.1002/cne.920150102

Dumenieu, M., Oule, M., Kreutz, M. R., and Lopez-Rojas, J. (2017). The segregated expression of voltage-gated potassium and sodium channels in neuronal membranes: functional implications and regulatory mechanisms. *Front. Cell. Neurosci.* 11:115. doi: 10.3389/fncel.2017.00115

Economo, M. N., Clack, N. G., Lavis, L. D., Gerfen, C. R., Svoboda, K., Myers, E. W., et al. (2016). A platform for brain-wide imaging and reconstruction of individual neurons. *Elife* 5:e10566. doi: 10.7554/eLife.10566

Edgar, J. M., and Griffiths, I. R. (2013). "White matter structure: a microscopist's view," in *Diffusion MRI,* eds H. Johansen-Berg and T. E. J.Behrens (London: Elsevier), 127–149.

Edgar, J. M., McCulloch, M. C., Montague, P., Brown, A. M., Thilemann, S., Pratola, L., et al. (2010). Demyelination and axonal preservation in a transgenic mouse model of Pelizaeus-Merzbacher disease. *EMBO Mol. Med.* 2, 42–50. doi: 10.1002/emmm.200900057

Edgar, J. M., McCulloch, M. C., Thomson, C. E., and Griffiths, I. R. (2008). Distribution of mitochondria along small-diameter myelinated central nervous system axons. *J. Neurosci. Res.* 86, 2250–2257. doi: 10.1002/jnr.21672

Edgar, J. M., McLaughlin, M., Werner, H. B., McCulloch, M. C., Barrie, J. A., Brown, A., et al. (2009). Early ultrastructural defects of axons and axon-glia junctions in mice lacking expression of Cnp1. *Glia* 57, 1815–1824. doi: 10.1002/glia.20893

Edgar, J. M., McLaughlin, M., Yool, D., Zhang, S. C., Fowler, J., Montague, P., et al. (2004). Oligodendroglial modulation of fast axonal transport in a mouse model of hereditary spastic paraplegia. *J. Cell Biol.* 166, 121–131. doi: 10.1083/jcb.200312012

Emery, B., and Lu, Q. R. (2015). Transcriptional and epigenetic regulation of oligodendrocyte development and myelination in the central nervous system. *Cold Spring Harb. Perspect. Biol.* 7:a020461. doi: 10.1101/cshperspect.a020461

Engl, E., and Attwell, D. (2015). Non-signalling energy use in the brain. *J. Physiol. (Lond).* 593, 3417–3429. doi: 10.1113/jphysiol.2014.282517

Engl, E., Jolivet, R., Hall, C. N., and Attwell, D. (2017). Non-signalling energy use in the developing rat brain. *J. Cereb. Blood Flow Metab.* 37, 951–966. doi: 10.1177/0271678X16648710

Essuman, K., Summers, D. W., Sasaki, Y., Mao, X., DiAntonio, A., and Milbrandt, J. (2017). The SARM1 Toll/Interleukin-1 Receptor Domain Possesses Intrinsic NAD(+) cleavage activity that promotes pathological axonal degeneration. *Neuron* 93, 1334–1343. doi: 10.1016/j.neuron.2017.02.022

Fernando, R. N., Cotter, L., Perrin-Tricaud, C., Berthelot, J., Bartolami, S., Pereira, J. A., et al. (2016). Optimal myelin elongation relies on YAP activation by axonal growth and inhibition by Crb3/Hippo pathway. *Nat. Commun.* 7:12186. doi: 10.1038/ncomms12186

Fledrich, R., Stassart, R. M., Klink, A., Rasch, L. M., Prukop, T., Haag, L., et al. (2014). Soluble neuregulin-1 modulates disease pathogenesis in rodent models of Charcot-Marie-Tooth disease 1A. *Nat. Med.* 20, 1055–1061. doi: 10.1038/nm.3664

Franklin, R. J., ffrench-Constant, C., Edgar, J. M., and Smith, K. J. (2012). Neuroprotection and repair in multiple sclerosis. *Nat. Rev. Neurol.* 8, 624–634. doi: 10.1038/nrneurol.2012.200

Franssen, E. H., Zhao, R. R., Koseki, H., Kanamarlapudi, V., Hoogenraad, C. C., Eva, R., et al. (2015). Exclusion of integrins from CNS axons is regulated by Arf6 activation and the AIS. *J. Neurosci.* 35, 8359–8375. doi: 10.1523/JNEUROSCI.2850-14.2015

Fu, M. M., and Holzbaur, E. L. (2014). Integrated regulation of motor-driven organelle transport by scaffolding proteins. *Trends Cell Biol.* 24, 564–574. doi: 10.1016/j.tcb.2014.05.002

Fukui, H., Diaz, F., Garcia, S., and Moraes, C. T. (2007). Cytochrome c oxidase deficiency in neurons decreases both oxidative stress and amyloid formation in a mouse model of Alzheimer's disease. *Proc. Natl. Acad. Sci. U.S.A.* 104, 14163–14168. doi: 10.1073/pnas.0705738104

Funfschilling, U., Supplie, L. M., Mahad, D., Boretius, S., Saab, A. S., Edgar, J., et al. (2012). Glycolytic oligodendrocytes maintain myelin and long-term axonal integrity. *Nature* 485, 517–521. doi: 10.1038/nature11007

Garbern, J., Yool, D. A., Moore, G. J., Wilds, I., Faulk, M., Klugmann, M., et al. (2002). Patients lacking the major CNS myelin protein, proteolipid protein 1, develop length-dependent axonal degeneration in the absence of demyelination and inflammation. *Brain* 125, 551–561. doi: 10.1093/brain/awf043

Gerdts, J., Brace, E. J., Sasaki, Y., DiAntonio, A., and Milbrandt, J. (2015). SARM1 activation triggers axon degeneration locally via NAD(+) destruction. *Science* 348, 453–457. doi: 10.1126/science.1258366

Gerdts, J., Summers, D. W., Milbrandt, J., and DiAntonio, A. (2016). Axon self-destruction: new links among SARM1, MAPKs, and NAD+ metabolism. *Neuron* 89, 449–460. doi: 10.1016/j.neuron.2015.12.023

Ghabriel, M. N., and Allt, G. (1981). Incisures of schmidt-lanterman. *Prog. Neurobiol.* 17, 25–58. doi: 10.1016/0301-0082(81)90003-4

Ghosh, A., Manrique-Hoyos, N., Voigt, A., Schulz, J. B., Kreutzfeldt, M., Merkler, D., et al. (2011). Targeted ablation of oligodendrocytes triggers axonal damage. *PLoS ONE* 6:e22735. doi: 10.1371/journal.pone.0022735

Gillespie, C. S., Sherman, D. L., Fleetwood-Walker, S. M., Cottrell, D. F., Tait, S., Garry, E. M., et al. (2000). Peripheral demyelination and neuropathic pain behavior in periaxin-deficient mice. *Neuron* 26, 523–531. doi: 10.1016/S0896-6273(00)81184-8

Gilley, J., and Coleman, M. P. (2010). Endogenous Nmnat2 is an essential survival factor for maintenance of healthy axons. *PLoS Biol.* 8:e1000300. doi: 10.1371/journal.pbio.1000300

Gilley, J., Orsomando, G., Nascimento-Ferreira, I., and Coleman, M. P. (2015). Absence of SARM1 rescues development and survival of NMNAT2-deficient axons. *Cell Rep.* 10, 1974–1981. doi: 10.1016/j.celrep.2015.02.060

Gilley, J., Ribchester, R. R., and Coleman, M. P. (2017). Sarm1 Deletion, but Not Wld(S), Confers Lifelong Rescue in a Mouse Model of Severe Axonopathy. *Cell Rep.* 21, 10–16. doi: 10.1016/j.celrep.2017.09.027

Goebbels, S., Wieser, G. L., Pieper, A., Spitzer, S., Weege, B., Yan, K., et al. (2017). A neuronal PI(3,4,5)P3-dependent program of oligodendrocyte precursor recruitment and myelination. *Nat. Neurosci.* 20, 10–15. doi: 10.1038/nn.4425

Gomez-Sanchez, J. A., Carty, L., Iruarrizaga-Lejarreta, M., Palomo-Irigoyen, M., Varela-Rey, M., Griffith, M., et al. (2015). Schwann cell autophagy, myelinophagy, initiates myelin clearance from injured nerves. *J. Cell Biol.* 210, 153–168. doi: 10.1083/jcb.201503019

Griffiths, I. R., Klugmann, M., Anderson, T. J., Yool, D., Thomson, C. E., Schwab, M. H., et al. (1998). Axonal swellings and degeneration in mice lacking the major proteolipid of myelin. *Science* 280, 1610–1613. doi: 10.1126/science.280.5369.1610

Groh, J., and Martini, R. (2017). Neuroinflammation as modifier of genetically caused neurological disorders of the central nervous system: understanding pathogenesis and chances for treatment. *Glia* 65, 1407–1422. doi: 10.1002/glia.23162

Gruenenfelder, F. I., Thomson, G., Penderis, J., and Edgar, J. M. (2011). Axon-glial interaction in the CNS: what we have learned from mouse models of Pelizaeus-Merzbacher disease. *J. Anat.* 219, 33–43. doi: 10.1111/j.1469-7580.2011.01363.x

Guy, J., Gan, J., Selfridge, J., Cobb, S., and Bird, A. (2007). Reversal of neurological defects in a mouse model of Rett syndrome. *Science* 315, 1143–1147. doi: 10.1126/science.1138389

Hartline, D. K., and Colman, D. R. (2007). Rapid conduction and the evolution of giant axons and myelinated fibers. *Curr. Biol.* 17, 29–35. doi: 10.1016/j.cub.2006.11.042

Hildebrand, C., Bowe, C. M., and Remahl, I. N. (1994). Myelination and myelin sheath remodelling in normal and pathological PNS nerve fibres. *Prog. Neurobiol.* 43, 85–141. doi: 10.1016/0301-0082(94)90010-8

Hinckelmann, M. V., Virlogeux, A., Niehage, C., Poujol, C., Choquet, D., Hoflack, B., et al. (2016). Self-propelling vesicles define glycolysis as the minimal energy machinery for neuronal transport. *Nat. Commun.* 7:13233. doi: 10.1038/ncomms13233

Hughes, E. G., and Appel, B. (2016). The cell biology of CNS myelination. *Curr. Opin. Neurobiol.* 39, 93–100. doi: 10.1016/j.conb.2016.04.013

Hui, S., Ghergurovich, J. M., Morscher, R. J., Jang, C., Teng, X., Lu, W., et al. (2017). Glucose feeds the TCA cycle via circulating lactate. *Nature* 551, 115–118. doi: 10.1038/nature24057

Israeli, E., Dryanovski, D. I., Schumacker, P. T., Chandel, N. S., Singer, J. D., Julien, J. P., et al. (2016). Intermediate filament aggregates cause mitochondrial dysmotility and increase energy demands in giant axonal neuropathy. *Hum. Mol. Genet.* 25, 2143–2157. doi: 10.1093/hmg/ddw081

Jang, S. Y., Shin, Y. K., Park, S. Y., Park, J. Y., Lee, H. J., Yoo, Y. H., et al. (2016). Autophagic myelin destruction by Schwann cells during Wallerian degeneration and segmental demyelination. *Glia* 64, 730–742. doi: 10.1002/glia.22957

Jedele, K. B. (2007). The overlapping spectrum of rett and angelman syndromes: a clinical review. *Semin. Pediatr. Neurol.* 14, 108–117. doi: 10.1016/j.spen.2007.07.002

Judson, M. C., Burette, A. C., Thaxton, C. L., Pribisko, A. L., Shen, M. D., Rumple, A. M., et al. (2017). Decreased axon caliber underlies loss of fiber tract integrity, disproportional reductions in white matter volume, and microcephaly in angelman syndrome model mice. *J. Neurosci.* 37, 7347–7361. doi: 10.1523/JNEUROSCI.0037-17.2017

Kang, J. J., Liu, I. Y., Wang, M. B., and Srivatsan, E. S. (2016). A review of gigaxonin mutations in giant axonal neuropathy (GAN) and cancer. *Hum. Genet.* 135, 675–84. doi: 10.1007/s00439-016-1659-5

Kapitein, L. C., and Hoogenraad, C. C. (2011). Which way to go? Cytoskeletal organization and polarized transport in neurons. *Mol. Cell Neurosci.* 46, 9–20. doi: 10.1016/j.mcn.2010.08.015

Kassmann, C. M., and Nave, K. A. (2008). Oligodendroglial impact on axonal function and survival - a hypothesis. *Curr. Opin. Neurol.* 21, 235–241 doi: 10.1097/WCO.0b013e328300c71f

Kassmann, C. M., Lappe-Siefke, C., Baes, M., Brugger, B., Mildner, A., Werner, H. B., et al. (2007). Axonal loss and neuroinflammation caused by peroxisome-deficient oligodendrocytes. *Nat. Genet.* 39, 969–976. doi: 10.1038/ng2070

Kemp, S., Berger, J., and Aubourg, P. (2012). X-linked adrenoleukodystrophy: clinical, metabolic, genetic and pathophysiological aspects. *Biochim. Biophys. Acta* 1822, 1465–1474 doi: 10.1016/j.bbadis.2012.03.012

Kevenaar, J. T., and Hoogenraad, C. C. (2015). The axonal cytoskeleton: from organization to function. *Front. Mol. Neurosci.* 8:44. doi: 10.3389/fnmol.2015.00044

Kim, S., Maynard, J. C., Sasaki, Y., Strickland, A., Sherman, D. L., Brophy, P. J., et al. (2016). Schwann cell O-GlcNAc glycosylation is required for myelin maintenance and axon integrity. *J. Neurosci.* 36, 9633–9646. doi: 10.1523/JNEUROSCI.1235-16.2016

Kirkcaldie, M. T. K., and Dwyer, S. T. (2017). The third wave: intermediate filaments in the maturing nervous system. *Mol. Cell. Neurosci.*. 84, 68–76 doi: 10.1016/j.mcn.2017.05.010

Kirkpatrick, L. L., and Brady, S. T. (1994). Modulation of the axonal microtubule cytoskeleton by myelinating Schwann cells. *J. Neurosci.* 14, 7440–7450. doi: 10.1523/JNEUROSCI.14-12-07440.1994

Kirkpatrick, L. L., Witt, A. S., Payne, H. R., Shine, H. D., and Brady, S. T. (2001). Changes in microtubule stability and density in myelin-deficient shiverer mouse CNS axons. *J. Neurosci.* 21, 2288–2297. doi: 10.1523/JNEUROSCI.21-07-02288.2001

Kirschner, D. A., and Ganser, A. L. (1980). Compact myelin exists in the absence of basic protein in the shiverer mutant mouse. *Nature* 283, 207–210. doi: 10.1038/283207a0

Klein, D., and Martini, R. (2016). Myelin and macrophages in the PNS: an intimate relationship in trauma and disease. *Brain Res.* 1641, 130–138. doi: 10.1016/j.brainres.2015.11.033

Kobsar, I., Berghoff, M., Samsam, M., Wessig, C., Mäurer, M., Toyka, K. V., et al. (2003). Preserved myelin integrity and reduced axonopathy in GJB132-deficient mice lacking the recombination activating gene-1. *Brain* 126, 804–813. doi: 10.1093/brain/awg072

Koppel, H., and Innocenti, G. M. (1983). Is there a genuine exuberancy of callosal projections in development? A quantitative electron microscopic study in the cat. *Neurosci. Lett.* 41, 33–40. doi: 10.1016/0304-3940(83)90219-7

Krasnow, A. M., Ford, M. C., Valdivia, L. E., Wilson, S. W., and Attwell, D. (2018). Regulation of developing myelin sheath elongation by oligodendrocyte calcium transients *in vivo*. *Nat. Neurosci.* 21, 24–28. doi: 10.1038/s41593-017-0031-y

LaMantia, A. S., and Rakic, P. (1990). Cytological and quantitative characteristics of four cerebral commissures in the rhesus monkey. *J. Comp. Neurol.* 291, 520–537. doi: 10.1002/cne.902910404

Lampert, P. W. (1967). A comparative electron microscopic study of reactive, degenerating, regenerating and dystrophic axons. *J. Neuropath. Exp. Neurol* 26, 345–368. doi: 10.1097/00005072-196707000-00001

Lappe-Siefke, C., Goebbels, S., Gravel, M., Nicksch, E., Lee, J., Braun, P. E., et al. (2003). Disruption of the *CNP* gene uncouples oligodendroglial functions in axonal support and myelination. *Nat. Genet.* 33, 366–374. doi: 10.1038/ng1095

Lee, S., Leach, M. K., Redmond, S. A., Chong, S. Y., Mellon, S. H., Tuck, S. J., et al. (2012a). A culture system to study oligodendrocyte myelination processes using engineered nanofibers. *Nat. Methods* 9, 917–922. doi: 10.1038/nmeth.2105

Lee, Y., Morrison, B. M., Li, Y., Lengacher, S., Farah, M. H., Hoffman, P. N., et al. (2012b). Oligodendroglia metabolically support axons and contribute to neurodegeneration. *Nature* 487, 443–448. doi: 10.1038/nature11314

Li, J., Ghandour, K., Radovanovic, D., Shy, R. R., Krajewski, K. M., Shy, M. E., et al. (2007). Stoichiometric alteration of PMP22 protein determines the phenotype of hereditary neuropathy with liability to pressure palsies. *Arch. Neurol.* 64, 974–978. doi: 10.1001/archneur.64.7.974

Lopez-Leal, R., Alvarez, J., and Court, F. A. (2016). Origin of axonal proteins: is the axon-schwann cell unit a functional syncytium? *Cytoskeleton (Hoboken)* 73, 629–639. doi: 10.1002/cm.21319

Loreto, A., Di, S. M., Gering, M., and Conforti, L. (2015). Wallerian degeneration is executed by an NMN-SARM1-dependent late Ca(2+) influx but only modestly influenced by Mitochondria. *Cell Rep.* 13, 2539–2552. doi: 10.1016/j.celrep.2015.11.032

Lüders, K. A., Patzig, J., Simons, M., Nave, K. A., and Werner, H. B. (2017). Genetic dissection of oligodendroglial and neuronal Plp1 function in a novel mouse model of spastic paraplegia type 2. *Glia* 65, 1762–1776. doi: 10.1002/glia.23193

Lundgaard, I., Luzhynskaya, A., Stockley, J. H., Wang, Z., Evans, K. A., Swire, M., et al. (2013). Neuregulin and BDNF induce a switch to NMDA receptor-dependent myelination by oligodendrocytes. *PLoS Biol.* 11:e1001743. doi: 10.1371/journal.pbio.1001743

Luse, S. A. (1956). Electron microscopic observations of the central nervous system. *J. Biophys. Biochem. Cytol.* 2, 531–542. doi: 10.1083/jcb.2.5.531

Mack, T. G. A., Reiner, M., Beirowski, B., Mi, W. Q., Emanuelli, M., Wagner, D., et al. (2001). Wallerian degeneration of injured axons and synapses is delayed by a *Ube4b/Nmnat* chimeric gene. *Nat. Neurosci.* 4, 1199–1206. doi: 10.1038/nn770

Maday, S., Twelvetrees, A. E., Moughamian, A. J., and Holzbaur, E. L. (2014). Axonal transport: cargo-specific mechanisms of motility and regulation. *Neuron* 84, 292–309. doi: 10.1016/j.neuron.2014.10.019

Mahad, D. J., Ziabreva, I., Campbell, G., Lax, N., White, K., Hanson, P. S., et al. (2009). Mitochondrial changes within axons in multiple sclerosis. *Brain* 132, 1161–1174. doi: 10.1093/brain/awp046

Makhaeva, G. F., Radchenko, E. V., Palyulin, V. A., Rudakova, E. V., Aksinenko, A. Y., Sokolov, V. B., et al. (2013). Organophosphorus compound esterase profiles as predictors of therapeutic and toxic effects. *Chem. Biol. Interact.* 203, 231–237. doi: 10.1016/j.cbi.2012.10.012

Martini, R., Mohajeri, M. H., Kasper, S., Giese, K. P., and Schachner, M. (1995). Mice doubly deficient in the genes for MPZ and myelin basic protein show that both proteins contribute to the formation of the major dense line in peripheral nerve myelin. *J. Neurosci.* 15, 4488–4495. doi: 10.1523/JNEUROSCI.15-06-04488.1995

Michailov, G. V., Sereda, M. W., Brinkmann, B. G., Fischer, T. M., Haug, B., Birchmeier, C., et al. (2004). Axonal Neuregulin-1 regulates myelin sheath thickness. *Science* 304, 700–703. doi: 10.1126/science.1095862

Mikelberg, F. S., Drance, S. M., Schulzer, M., Yidegiligne, H. M., and Weis, M. M. (1989). The normal human optic nerve. Axon count and axon diameter distribution. *Ophthalmology* 96, 1325–1328. doi: 10.1016/S0161-6420(89)32718-7

Miller, B. R., Press, C., Daniels, R. W., Sasaki, Y., Milbrandt, J., and DiAntonio, A. (2009). A dual leucine kinase-dependent axon self-destruction program promotes Wallerian degeneration. *Nat. Neurosci.* 12, 387–389. doi: 10.1038/nn.2290

Möbius, W., Nave, K. A., and Werner, H. B. (2016). Electron microscopy of myelin: structure preservation by high-pressure freezing. *Brain Res.* 1641, 92–100. doi: 10.1016/j.brainres.2016.02.027

Monk, K. R., Feltri, M. L., and Taveggia, C. (2015). New insights on Schwann cell development. *Glia* 63, 1376–1393. doi: 10.1002/glia.22852

Monsma, P. C., Li, Y., Fenn, J. D., Jung, P., and Brown, A. (2014). Local regulation of neurofilament transport by myelinating cells. *J. Neurosci.* 34, 2979–2988. doi: 10.1523/JNEUROSCI.4502-13.2014

Morell, P. (1984). *Myelin*. Plenum Press: New York, NY; London.

Morfini, G. A., Burns, M., Binder, L. I., Kanaan, N. M., LaPointe, N., Bosco, D. A., et al. (2009). Axonal transport defects in neurodegenerative diseases. *J. Neurosci.* 29, 12776–12786. doi: 10.1523/JNEUROSCI.3463-09.2009

Mosser, J., Douar, A. M., Sarde, C. O., Kioschis, P., Feil, R., Moser, H., et al. (1993). Putative X-linked adrenoleukodystrophy gene shares unexpected homology with ABC transporters. *Nature* 361, 726–730. doi: 10.1038/361726a0

Nave, K. A. (2010a). Myelination and support of axonal integrity by glia. *Nature* 468, 244–252. doi: 10.1038/nature09614

Nave, K. A. (2010b). Myelination and the trophic support of long axons. *Nat. Rev. Neurosci.* 11, 275–283. doi: 10.1038/nrn2797

Nave, K. A., and Werner, H. B. (2014). Myelination of the nervous system: mechanisms and functions. *Annu. Rev. Cell Dev. Biol.* 30, 503–533. doi: 10.1146/annurev-cellbio-100913-013101

Nave, K. A., Sereda, M. W., and Ehrenreich, H. (2007). Mechanisms of disease: inherited demyelinating neuropathies–from basic to clinical research. *Nat. Clin. Pract. Neurol.* 3, 453–464. doi: 10.1038/ncpneuro0583

Nave, K.-A., and Griffiths, I. R. (2004). "Models of Pelizaeus-Merzbacher disease," in *Myelin Biology and Disorders*, eds R. A. Lazzarini, J. W. Griffin, H. Lassmann, K.-A. Nave, R. H. Miller, B. D. Trapp (Amsterdam: Elsevier), 1125–1142.

Ng, A. A., Logan, A. M., Schmidt, E. J., and Robinson, F. L. (2013). The CMT4B disease-causing phosphatases Mtmr2 and Mtmr13 localize to the Schwann cell cytoplasm and endomembrane compartments, where they depend upon each other to achieve wild-type levels of protein expression. *Hum. Mol. Genet.* 22, 1493–1506. doi: 10.1093/hmg/dds562

Nicholson, G. A., Valentijn, L. J., Cherryson, A. K., Kennerson, M. L., Bragg, T. L., DeKroon, R. M., et al. (1994). A frame shift mutation in the PMP22 gene in hereditary neuropathy with liability to pressure palsies. *Nat. Genet.* 6, 263–266. doi: 10.1038/ng0394-263

Nijland, P. G., Michailidou, I., Witte, M. E., Mizee, M. R., van der Pol, S. M., Van Het Hof, B., et al. (2014). Cellular distribution of glucose and monocarboxylate transporters in human brain white matter and multiple sclerosis lesions. *Glia* 62, 1125–1141. doi: 10.1002/glia.22667

Nikic, I., Merkler, D., Sorbara, C., Brinkoetter, M., Kreutzfeldt, M., Bareyre, F. M., et al. (2011). A reversible form of axon damage in experimental autoimmune encephalomyelitis and multiple sclerosis. *Nat. Med.* 17, 495–499. doi: 10.1038/nm.2324

O'Connor, L. T., Goetz, B. D., Kwiecien, J. M., Delaney, K. H., Fletch, A. L., and Duncan, I. D. (1999). Insertion of a retrotransposon in mbp disrupts mRNA splicing and myelination in a new mutant rat. *J. Neurosci.* 19, 3404–3413. doi: 10.1523/JNEUROSCI.19-09-03404.1999

Oh, Y., Zhang, F., Wang, Y., Lee, E. M., Choi, I. Y., Lim, H., et al. (2017). Zika virus directly infects peripheral neurons and induces cell death. *Nat. Neurosci.* 20, 1209–1212. doi: 10.1038/nn.4612

Oluich, L. J., Stratton, J. A., Xing, Y. L., Ng, S. W., Cate, H. S., Sah, P., et al. (2012). Targeted ablation of oligodendrocytes induces axonal pathology independent of overt demyelination. *J. Neurosci.* 32, 8317–8330. doi: 10.1523/JNEUROSCI.1053-12.2012

Osterloh, J. M., Yang, J., Rooney, T. M., Fox, A. N., Adalbert, R., Powell, E. H. et al. (2012). dSarm/Sarm1 is required for activation of an injury-induced axon death pathway. *Science* 337, 481–484. doi: 10.1126/science.1223899

Pan, B., Fromholt, S. E., Hess, E. J., Crawford, T. O., Griffin, J. W., Sheikh, K. A., et al. (2005). Myelin-associated glycoprotein and complementary axonal ligands, gangliosides, mediate axon stability in the CNS and PNS: neuropathology and behavioral deficits in single- and double-null mice. *Exp. Neurol.* 195, 208–217. doi: 10.1016/j.expneurol.2005.04.017

Papandreou, M. J., and Leterrier, C. (2018). The functional architecture of axonal actin. *Mol. Cell. Neurosci.* 18, 30041–30042 doi: 10.1016/j.mcn.2018.05.003

Patzig, J., Erwig, M. S., Tenzer, S., Kusch, K., Dibaj, P., Mobius, W., et al. (2016). Septin/anillin filaments scaffold central nervous system myelin to accelerate nerve conduction. *Elife* 5:17119. doi: 10.7554/eLife.17119

Pereira, J. A., Lebrun-Julien, F., and Suter, U. (2012). Molecular mechanisms regulating myelination in the peripheral nervous system. *Trends Neurosci.* 35, 123–134. doi: 10.1016/j.tins.2011.11.006

Perge, J. A., Koch, K., Miller, R., Sterling, P., and Balasubramanian, V. (2009). How the optic nerve allocates space, energy capacity, and information. *J. Neurosci.* 29, 7917–7928. doi: 10.1523/JNEUROSCI.5200-08.2009

Perge, J. A., Niven, J. E., Mugnaini, E., Balasubramanian, V., and Sterling, P. (2012). Why do axons differ in caliber? *J. Neurosci.* 32, 626–638. doi: 10.1523/JNEUROSCI.4254-11.2012

Perry, V. H., and Gordon, S. (1988). Macrophages and microglia in the nervous system. *Trends Neurosci.* 11, 273–277. doi: 10.1016/0166-2236(88)90110-5

Perry, V. H., Brown, M. C., and Gordon, S. (1987). The macrophage response to central and peripheral nerve injury. A possible role for macrophages in regeneration. *J. Exp. Med.* 165, 1218–1223.

Perry, V. H., Brown, M. C., and Lunn, E. R. (1990). Very slow retrograde and Wallerian degeneration in the CNS of C57BL/Ola mice. *Eur. J. Neurosci.* 3, 103–105.

Peters, A. (1966). The node of Ranvier in the central nervous system. *Quart. J. Exp. Physiol.* 51, 229–236. doi: 10.1113/expphysiol.1966.sp001852

Peters, A., and Vaughn, J. E. (1967). Microtubules and filaments in the axons and astrocytes of early postnatal rat optic nerves. *J. Cell Biol.* 32, 113–119. doi: 10.1083/jcb.32.1.113

Pohl, H. B., Porcheri, C., Mueggler, T., Bachmann, L. C., Martino, G., Riethmacher, D., et al. (2011). Genetically induced adult oligodendrocyte cell death is associated with poor myelin clearance, reduced remyelination, and axonal damage. *J. Neurosci.* 31, 1069–1080. doi: 10.1523/JNEUROSCI.5035-10.2011

Poitelon, Y., Lopez-Anido, C., Catignas, K., Berti, C., Palmisano, M., Williamson, C., et al. (2016). YAP and TAZ control peripheral myelination and the expression of laminin receptors in Schwann cells. *Nat. Neurosci.* 19, 879–887. doi: 10.1038/nn.4316

Previtali, S. C., Quattrini, A., and Bolino, A. (2007). Charcot-Marie-Tooth type 4B demyelinating neuropathy: deciphering the role of MTMR phosphatases. *Expert Rev. Mol. Med.* 9, 1–16. doi: 10.1017/S1462399407000439

Privat, A., Jacque, C., Bourre, J. M., Dupouey, P., and Baumann, N. (1979). Absence of the major dense line in myelin of the mutant mouse shiverer. *Neurosci. Lett.* 12, 107–112. doi: 10.1016/0304-3940(79)91489-7

Pujol, A., Hindelang, C., Callizot, N., Bartsch, U., Schachner, M., and Mandel, J. L. (2002). Late onset neurological phenotype of the X-ALD gene inactivation in mice: a mousemodel for adrenomyeloneuropathy. *Hum. Mol. Genet.* 11, 499–505. doi: 10.1093/hmg/11.5.499

Rainier, S., Bui, M., Mark, E., Thomas, D., Tokarz, D., Ming, L., et al. (2008). Neuropathy target esterase gene mutations cause motor neuron disease. *Am. J. Hum. Genet.* 82, 780–785. doi: 10.1016/j.ajhg.2007.12.018

Ransom, B. R., Butt, A. M., and Black, J. A. (1991). Ultrastructural identification of HRP-injected oligodendrocytes in the intact rat optic nerve. *Glia* 4, 37–45. doi: 10.1002/glia.440040105

Rao, A. N., and Baas, P. W. (2018). Polarity sorting of microtubules in the axon. *Trends Neurosci.* 41, 77–88. doi: 10.1016/j.tins.2017.11.002

Rasband, M. N., and Peles, E. (2015). The nodes of ranvier: molecular assembly and maintenance. *Cold Spring Harb. Perspect. Biol.* 8:a020495. doi: 10.1101/cshperspect.a020495

Readhead, C., Schneider, A., Griffiths, I. R., and Nave, K.-A. (1994). Premature arrest of myelin formation in transgenic mice with increased proteolipid protein gene dosage. *Neuron* 12, 583–595. doi: 10.1016/0896-6273(94)90214-3

Redford, E. J., Kapoor, R., and Smith, K. J. (1997). Nitric oxide donors reversibly block axonal conduction: demyelinated axons are especially susceptible. *Brain* 120, 2149–2157. doi: 10.1093/brain/120.12.2149

Reles, A., and Friede, R. L. (1991). Axonal cytoskeleton at the nodes of Ranvier. *J. Neurocytol.* 20, 450–458. doi: 10.1007/BF01252273

Rich, L. R., and Brown, A. M. (2018). Fibre sub-type specific conduction reveals metabolic function in mouse sciatic nerve. *J. Physiol.* 596, 1795–1812. doi: 10.1113/JP275680

Rinholm, J. E., Hamilton, N. B., Kessaris, N., Richardson, W. D., Bergersen, L. H., and Attwell, D. (2011). Regulation of oligodendrocyte development and myelination by glucose and lactate. *J. Neurosci.* 31, 538–548. doi: 10.1523/JNEUROSCI.3516-10.2011

Roach, A., Takahashi, N., Pravtcheva, D., Ruddle, F., and Hood, L. (1985). Chromosomal mapping of mouse myelin basic protein gene and structure and transcription of the partially deleted gene in shiverer mutant mice. *Cell* 42, 149–155. doi: 10.1016/S0092-8674(85)80110-0

Robertson, A. M., King, R. H. M., Muddle, J. R., and Thomas, P. K. (1997). Abnormal Schwann cell axon interactions in the Trembler-J mouse. *J. Anat.* 190, 423–432. doi: 10.1046/j.1469-7580.1997.19030423.x

Rosenbluth, J. (1980). Central myelin in the mouse mutant shiverer. *J. Comp. Neurol.* 194, 639–648. doi: 10.1002/cne.901940310

Rosenbluth, J. (2009). Multiple functions of the paranodal junction of myelinated nerve fibers. *J. Neurosci. Res.* 87, 3250–3258 doi: 10.1002/jnr.22013

Rosenbluth, J., and Bobrowski-Khoury, N. (2014). Paranodal dysmyelination in peripheral nerves of Trembler mice. *J. Neurosci. Res.* 92, 476–485. doi: 10.1002/jnr.23326

Roy, S., Coffee, P., Smith, G., Liem, R. K. H., Brady, S. T., and Black, M. M. (2000). Neurofilaments are transported rapidly but intermittently in axons: implications for slow axonal transport. *J. Neurosci.* 20, 6849–6861. doi: 10.1523/JNEUROSCI.20-18-06849.2000

Ruiz, M., Jové, M., Schlüter, A., Casasnovas, C., Villarroya, F., Guilera, C., et al. (2015). Altered glycolipid and glycerophospholipid signaling drive inflammatory cascades in adrenomyeloneuropathy. *Hum. Mol. Genet.* 24, 6861–6876. doi: 10.1093/hmg/ddv375

Rushton, W. A. (1951). A theory of the effects of fibre size in medullated nerve. *J. Physiol. (Lond).* 115, 101–122. doi: 10.1113/jphysiol.1951.sp004655

Saab, A. S., Tzvetavona, I. D., Trevisiol, A., Baltan, S., Dibaj, P., Kusch, K., et al. (2016). Oligodendroglial NMDA receptors regulate glucose import and axonal energy metabolism. *Neuron* 91, 119–132. doi: 10.1016/j.neuron.2016.05.016

Sadeghian, M., Mastrolia, V., Rezaei, H. A., Mosley, A., Mullali, G., Schiza, D., et al. (2016). Mitochondrial dysfunction is an important cause of neurological deficits in an inflammatory model of multiple sclerosis. *Sci. Rep.* 6:33249. doi: 10.1038/srep33249

Sasaki, Y., Nakagawa, T., Mao, X., DiAntonio, A., and Milbrandt, J. (2016). NMNAT1 inhibits axon degeneration via blockade of SARM1-mediated NAD(+) depletion. *Elife* 5:19749. doi: 10.7554/eLife.19749

Scheidt, P., and Friede, R. L. (1987). Myelin phagocytosis in Wallerian degeneration. Properties of millipore chambers and immunocytochemical identification of cell populations. *Acta Neuropath. (Berl.)* 75, 77–84. doi: 10.1007/BF00686796

Schelski, M., and Bradke, F. (2017). Neuronal polarization: from spatiotemporal signaling to cytoskeletal dynamics. *Mol. Cell. Neurosci.* 84, 11–28. doi: 10.1016/j.mcn.2017.03.008

Schoenemann, P. T., Sheehan, M. J., and Glotzer, L. D. (2005). Prefrontal white matter volume is disproportionately larger in humans than in other primates. *Nat. Neurosci.* 8, 242–252. doi: 10.1038/nn1394

Schweigreiter, R., Roots, B. I., Bandtlow, C. E., and Gould, R. M. (2006). Understanding myelination through studying its evolution. *Int. Rev. Neurobiol.* 73, 219–273. doi: 10.1016/S0074-7742(06)73007-0

Sereda, M., Griffiths, I. R., Pühlhofer, A., Stewart, H., Rossner, M. J., Zimmermann, F., et al. (1996). A transgenic rat model of Charcot-Marie-Tooth disease. *Neuron* 16, 1049–1060. doi: 10.1016/S0896-6273(00)80128-2

Sleigh, J. N., Vagnoni, A., Twelvetrees, A. E., and Schiavo, G. (2017). Methodological advances in imaging intravital axonal transport. *F1000Res* 6:200. doi: 10.12688/f1000research.10433.1

Smith, C. M., Cooksey, E., and Duncan, I. D. (2013). Myelin loss does not lead to axonal degeneration in a long-lived model of chronic demyelination. *J. Neurosci.* 33, 2718–2727. doi: 10.1523/JNEUROSCI.4627-12.2013

Smith, H. V., and Spalding, J. M. (1959). Outbreak of paralysis in Morocco due to ortho-cresyl phosphate poisoning. *Lancet* 2, 1019–1021. doi: 10.1016/S0140-6736(59)91486-2

Smith, K. J., and Lassmann, H. (2002). The role of nitric oxide in multiple sclerosis. *Lancet Neurol.* 1, 232–241. doi: 10.1016/S1474-4422(02)00102-3

Snaidero, N., and Simons, M. (2014). Myelination at a glance. *J. Cell Sci.* 127, 2999–3004. doi: 10.1242/jcs.151043

Snaidero, N., Mobius, W., Czopka, T., Hekking, L. H., Mathisen, C., Verkleij, D., et al. (2014). Myelin membrane wrapping of CNS axons by PI(3,4,5)P3-dependent polarized growth at the inner tongue. *Cell* 156, 277–290. doi: 10.1016/j.cell.2013.11.044

Snaidero, N., Velte, C., Myllykoski, M., Raasakka, A., Ignatev, A., Werner, H. B., et al. (2017). Antagonistic Functions of MBP and CNP Establish Cytosolic Channels in CNS Myelin. *Cell Rep.* 18, 314–323. doi: 10.1016/j.celrep.2016.12.053

Sokoloff, L., Reivich, M., Kennedy, C., Des Rosiers, M. H., Patlak, C. S., Pettigrew, K. D., et al. (1977). The [14C]deoxyglucose method for the measurement of local cerebral glucose utilization: theory, procedure, and normal values in the conscious and anesthetized albino rat. *J. Neurochem.* 28, 897–916. doi: 10.1111/j.1471-4159.1977.tb10649.x

Sorbara, C. D., Wagner, N. E., Ladwig, A., Nikic, I., Merkler, D., Kleele, T., et al. (2014). Pervasive axonal transport deficits in multiple sclerosis models. *Neuron* 84, 1183–1190. doi: 10.1016/j.neuron.2014.11.006

Spaulding, E. L., and Burgess, R. W. (2017). Accumulating evidence for axonal translation in neuronal homeostasis. *Front. Neurosci.* 11:312. doi: 10.3389/fnins.2017.00312

Spencer, P. S., and Schaumberg, H. H. (1977a). Ultrastructural studies of the dying-back process. III. The evolution of experimental peripheral giant axonal degeneration. *J. Neuropath. Exp. Neurol.* 36, 276–299.

Spencer, P. S., and Schaumberg, H. H. (1977b). Ultrastructural studies of the dying-back process. IV. Differential vulnerability of PNS and CNS fibers in experimental central-peripheral distal axonopathies. *J. Neuropath. Exp. Neurol.* 36, 300–320.

Stanford, L. R. (1987). Conduction velocity variations minimize conduction time differences among retinal ganglion cell axons. *Science* 238, 358–360. doi: 10.1126/science.3659918

Stys, P. K., Zamponi, G. W., and van, M. J., Geurts, J. J. (2012). Will the real multiple sclerosis please stand up? *Nat. Rev. Neurosci.* 13, 507–514. doi: 10.1038/nrn3275

Suarez-Sola, M. L., Gonzalez-Delgado, F. J., Pueyo-Morlans, M., Medina-Bolivar, O. C., Hernandez-Acosta, N. C., Gonzalez-Gomez, M., et al. (2009). Neurons in the white matter of the adult human neocortex. *Front. Neuroanat.* 3:7. doi: 10.3389/neuro.05.007.2009

Supplie, L. M., Duking, T., Campbell, G., Diaz, F., Moraes, C. T., Gotz, M., et al. (2017). Respiration-deficient astrocytes survive as glycolytic cells *in vivo*. *J. Neurosci.* 37, 4231–4242. doi: 10.1523/JNEUROSCI.0756-16.2017

Susuki, K. (2010). Myelin: a specialized membrane for cell communication. *Nat. Educ.* 3:59.

Suter, U., Welcher, A. A., Özcelik, T., Snipes, G. J., Kosaras, B., Francke, U., et al. (1992). *Trembler* mouse carries a point mutation in a myelin gene. *Nature* 356, 241–244. doi: 10.1038/356241a0

Taveggia, C. (2016). Schwann cells-axon interaction in myelination. *Curr. Opin. Neurobiol.* 39, 24–29. doi: 10.1016/j.conb.2016.03.006

Taveggia, C., Zanazzi, G., Petrylak, A., Yano, H., Rosenbluth, J., Einheber, S., et al. (2005). Neuregulin-1 type III determines the ensheathment fate of axons. *Neuron* 47, 681–694. doi: 10.1016/j.neuron.2005.08.017

Tillotson, R., Selfridge, J., Koerner, M. V., Gadalla, K. K. E., Guy, J., De, S. D., et al. (2017). Radically truncated MeCP2 rescues Rett syndrome-like neurological defects. *Nature* 550, 398–401. doi: 10.1038/nature24058

Tomasch, J., and Macmillan, A. (1957). The number of fibers in the corpus callosum of the white mouse. *J. Comp. Neurol.* 107, 165–168. doi: 10.1002/cne.901070107

Traka, M., Podojil, J. R., McCarthy, D. P., Miller, S. D., and Popko, B. (2016). Oligodendrocyte death results in immune-mediated CNS demyelination. *Nat. Neurosci.* 19, 65–74. doi: 10.1038/nn.4193

Trapp, B. D., and Nave, K. A. (2008). Multiple sclerosis: an immune or neurodegenerative disorder? *Annu. Rev. Neurosci.* 31, 247–269. doi: 10.1146/annurev.neuro.30.051606.094313

Trevisiol, A., Saab, A. S., Winkler, U., Marx, G., Imamura, H., Mobius, W., et al. (2017). Monitoring ATP dynamics in electrically active white matter tracts. *Elife* 6:24241. doi: 10.7554/eLife.24241

Tricaud, N. (2017). Myelinating schwann cell polarity and mechanically-driven myelin sheath elongation. *Front. Cell. Neurosci.* 11:414. doi: 10.3389/fncel.2017.00414

Trigo, D., and Smith, K. J. (2015). Axonal morphological changes following impulse activity in mouse peripheral nerve *in vivo*: the return pathway for sodium ions. *J. Physiol. (Lond).* 593, 987–1002. doi: 10.1113/jphysiol.2014.279331

Tsukita, S., and Ishikawa, H. (1980). The movement of membranous organelles in axons. Electron microscopic identification of antergradely and retrogradely transported organelles. *J. Cell Biol.* 84, 513–530.

Uchida, A., Colakoglu, G., Wang, L., Monsma, P. C., and Brown, A. (2013). Severing and end-to-end annealing of neurofilaments in neurons. *Proc. Natl. Acad. Sci. U.S.A.* 110, E2696–E2705. doi: 10.1073/pnas.1221835110

Uncini, A., Gonzalez-Bravo, D. C., Acosta-Ampudia, Y. Y., Ojeda, E. C., Rodriguez, Y., Monsalve, D. M., et al. (2017). Clinical and nerve conduction features in Guillain-Barre syndrome associated with Zika virus infection in Cucuta, Colombia. *Eur. J. Neurol.* 25, 644–650. doi: 10.1111/ene.13552

Utzschneider, D. A., Thio, C., Sontheimer, H., Ritchie, J. M., Waxman, S. G., and Kocsis, J. D. (1993). Action potential conduction and sodium channel content in the optic nerve of the myelin-deficient rat. *Proc. Biol. Sci.* 254, 245–250. doi: 10.1098/rspb.1993.0153

van Roermund, C. W., Visser, W. F., Ijlst, L., van Cruchten, A., Boek, M., Kulik, W., et al. (2008). The human peroxisomal ABC half transporter ALDP functions as a homodimer and accepts acyl-CoA esters. *FASEB J.* 22, 4201–4208. doi: 10.1096/fj.08-110866

Vander Heiden, M. G., Cantley, L. C., and Thompson, C. B. (2009). Understanding the Warburg effect: the metabolic requirements of cell proliferation. *Science* 324, 1029–1033. doi: 10.1126/science.1160809

Vargas, M. E., and Barres, B. A. (2007). Why is Wallerian degeneration in the CNS so slow? *Annu. Rev. Neurosci.* 30, 153–179. doi: 10.1146/annurev.neuro.30.051606.094354

Velumian, A. A., Samoilova, M., and Fehlings, M. G. (2011). Visualization of cytoplasmic diffusion within living myelin sheaths of CNS white matter axons using microinjection of the fluorescent dye Lucifer Yellow. *Neuroimage* 56, 27–34. doi: 10.1016/j.neuroimage.2010.11.022

Volkenhoff, A., Weiler, A., Letzel, M., Stehling, M., Klambt, C., and Schirmeier, S. (2015). Glial glycolysis is essential for neuronal survival in Drosophila. *Cell Metab.* 22, 437–447. doi: 10.1016/j.cmet.2015.07.006

Voyvodic, J. T. (1989). Target size regulates calibre and myelination of sympathetic axons. *Nature* 342, 430–433. doi: 10.1038/342430a0

Wake, H., Lee, P. R., and Fields, R. D. (2011). Control of local protein synthesis and initial events in myelination by action potentials. *Science* 333, 1647–1651. doi: 10.1126/science.1206998

Walker, L. J., Summers, D. W., Sasaki, Y., Brace, E. J., Milbrandt, J., and DiAntonio, A. (2017). MAPK signaling promotes axonal degeneration by speeding the turnover of the axonal maintenance factor *NMNAT*2. Elife 6:22540. doi: 10.7554/eLife.22540

Waller, J. (1850). Experiments on the section of the glossopharyngeal and hypoglossal nerves of the frog, and observations of the alterations produced thereby in the structure of their primitive fibres. *Phil. Trans. R Soc. Lond.* 140, 423–429. doi: 10.1098/rstl.1850.0021

Wang, L., and Brown, A. (2002). Rapid movement of microtubules in axons. *Curr. Biol.* 12, 1496–1501. doi: 10.1016/S0960-9822(02)01078-3

Wang, L., Ho, C. L., Sun, D., Liem, R. K., and Brown, A. (2000). Rapid movement of axonal neurofilaments interrupted by prolonged pauses. *Nat. Cell. Biol.* 2, 137–141. doi: 10.1038/35004008

Waxman, S. G., Craner, M. J., and Black, J. A. (2004). Na^+ channel expression along axons in multiple sclerosis and its models. *TiPS* 25, 584–591. doi: 10.1016/j.tips.2004.09.001

Wedel, M. J. (2018). A monument of inefficiency: the presumed course of the recurrent laryngeal nerve in sauropod dinosaurs. *Acta Palaeontol. Polonica* 57, 251–256. doi: 10.4202/app.2011.0019

Werner, H. B., Kuhlmann, K., Shen, S., Uecker, M., Schardt, A., Dimova, K., et al. (2007). Proteolipid protein is required for transport of sirtuin 2 into CNS Myelin. *J. Neurosci.* 27, 7717–7730. doi: 10.1523/JNEUROSCI.1254-07.2007

Willison, H. J., Jacobs, B. C., and van Doorn, P. A. (2016). Guillain-Barre syndrome. *Lancet* 388, 717–727. doi: 10.1016/S0140-6736(16)00339-1

Wu, H., Williams, J., and Nathans, J. (2014). Complete morphologies of basal forebrain cholinergic neurons in the mouse. *Elife* 3:e02444. doi: 10.7554/eLife.02444

Wu, Y., Whiteus, C., Xu, C. S., Hayworth, K. J., Weinberg, R. J., Hess, H. F., et al. (2017). Contacts between the endoplasmic reticulum and other membranes in neurons. *Proc. Natl. Acad. Sci. U.S.A.* 114, 4859–4867. doi: 10.1073/pnas.1701078114

Wyss, M. T., Jolivet, R., Buck, A., Magistretti, P. J., and Weber, B. (2011). *In vivo* evidence for lactate as a neuronal energy source. *J. Neurosci.* 31, 7477–7485. doi: 10.1523/JNEUROSCI.0415-11.2011

Xiao, L., Ohayon, D., McKenzie, I. A., Sinclair-Wilson, A., Wright, J. L., Fudge, A. D., et al. (2016). Rapid production of new oligodendrocytes is required in the earliest stages of motor-skill learning. *Nat. Neurosci.* 19, 1210–1217. doi: 10.1038/nn.4351

Yahata, N., Yuasa, S., and Araki, T. (2009). Nicotinamide mononucleotide adenylyltransferase expression in mitochondrial matrix delays Wallerian degeneration. *J. Neurosci.* 29, 6276–6284. doi: 10.1523/JNEUROSCI.4304-08.2009

Yang, J., Wu, Z., Renier, N., Simon, D. J., Uryu, K., Park, D. S., et al. (2015). Pathological axonal death through a MAPK cascade that triggers a local energy deficit. *Cell* 160, 161–176. doi: 10.1016/j.cell.2014.11.053

Yin, X. H., Crawford, T. O., Griffin, J. W., Tu, P. H., Lee, V. M., Li, C. M., et al. (1998). Myelin-associated glycoprotein is a myelin signal that modulates the caliber of myelinated axons. *J. Neurosci.* 18, 1953–1962. doi: 10.1523/JNEUROSCI.18-06-01953.1998

Yuan, A., Rao, M. V., Veeranna, and Nixon, R. A. (2017). Neurofilaments and Neurofilament Proteins in Health and Disease. *Cold Spring Harb. Perspect Biol.* 9:18309. doi: 10.1101/cshperspect.a018309

Zala, D., Hinckelmann, M. V., Yu, H., Lyra da Cunha, M. M., Liot, G., Cordelieres, F. P., et al. (2013). Vesicular glycolysis provides on-board energy for fast axonal transport. *Cell* 152, 479–491. doi: 10.1016/j.cell.2012.12.029

Zalc, B., Goujet, D., and Colman, D. (2008). The origin of the myelination program in vertebrates. *Curr. Biol.* 18, R511–R512. doi: 10.1016/j.cub.2008.04.010

Zambonin, J. L., Zhao, C., Ohno, N., Campbell, G. R., Engeham, S., Ziabreva, I., et al. (2011). Increased mitochondrial content in remyelinated axons: implications for multiple sclerosis. *Brain* 134, 1901–1913. doi: 10.1093/brain/awr110

Zawadzka, M., Rivers, L. E., Fancy, S. P., Zhao, C., Tripathi, R., Jamen, F., et al. (2010). CNS-resident glial progenitor/stem cells produce Schwann cells as well as oligodendrocytes during repair of CNS demyelination. *Cell Stem Cell* 6, 578–590. doi: 10.1016/j.stem.2010.04.002

Zhai, Q., Wang, J., Kim, A., Liu, Q., Watts, R., Hoopfer, E., et al. (2003). Involvement of the ubiquitin-proteasome system in the early stages of wallerian degeneration. *Neuron* 39, 217–225. doi: 10.1016/S0896-6273(03)00429-X

Zhang, Y., Bekku, Y., Dzhashiashvili, Y., Armenti, S., Meng, X., Sasaki, Y., et al. (2012). Assembly and maintenance of nodes of ranvier rely on distinct sources of proteins and targeting mechanisms. *Neuron* 73, 92–107. doi: 10.1016/j.neuron.2011.10.016

Conflict of Interest Statement: The authors declare that the research was conducted in the absence of any commercial or financial relationships that could be construed as a potential conflict of interest.

frontiers in Neuroscience

REVIEW
published: 04 September 2017
doi: 10.3389/fnins.2017.00451

Axonal Degeneration during Aging and Its Functional Role in Neurodegenerative Disorders

Natalia Salvadores[1,2], *Mario Sanhueza*[1,2], *Patricio Manque*[1] *and Felipe A. Court*[1,2]*

[1] Center for Integrative Biology, Faculty of Sciences, Universidad Mayor, Santiago, Chile, [2] Fondap Geroscience Center for Brain Health and Metabolism, Santiago, Chile

Aging constitutes the main risk factor for the development of neurodegenerative diseases. This represents a major health issue worldwide that is only expected to escalate due to the ever-increasing life expectancy of the population. Interestingly, axonal degeneration, which occurs at early stages of neurodegenerative disorders (ND) such as Alzheimer's disease, Amyotrophic lateral sclerosis, and Parkinson's disease, also takes place as a consequence of normal aging. Moreover, the alteration of several cellular processes such as proteostasis, response to cellular stress and mitochondrial homeostasis, which have been described to occur in the aging brain, can also contribute to axonal pathology. Compelling evidence indicate that the degeneration of axons precedes clinical symptoms in NDs and occurs before cell body loss, constituting an early event in the pathological process and providing a potential therapeutic target to treat neurodegeneration before neuronal cell death. Although, normal aging and the development of neurodegeneration are two processes that are closely linked, the molecular basis of the switch that triggers the transition from healthy aging to neurodegeneration remains unrevealed. In this review we discuss the potential role of axonal degeneration in this transition and provide a detailed overview of the literature and current advances in the molecular understanding of the cellular changes that occur during aging that promote axonal degeneration and then discuss this in the context of ND.

Keywords: axonal degeneration, aging, neurodegeneration, disease models, axonopathy

OPEN ACCESS

Edited by:
Samuel David Crish, Northeast Ohio Medical University, United States

Reviewed by:
Alba Di Pardo, Centre for Neurogenetics and Rare Diseases, Italy
Sabine Gilch, University of Calgary, Canada

***Correspondence:**
Felipe A. Court
felipe.court@umayor.cl

Specialty section:
This article was submitted to Neurodegeneration, a section of the journal Frontiers in Neuroscience

Received: *07 June 2017*
Accepted: *25 July 2017*
Published: *04 September 2017*

Citation:
Salvadores N, Sanhueza M, Manque P and Court FA (2017) Axonal Degeneration during Aging and Its Functional Role in Neurodegenerative Disorders. Front. Neurosci. 11:451. doi: 10.3389/fnins.2017.00451

INTRODUCTION

Neurodegeneration during Aging

The aging process is part of life and as such, it cannot be circumvented. However, much effort is currently devoted to understand the molecular changes that occur during aging and cause pathologies, in an attempt of being able to modify them to have the possibility of living a healthier aging.

The effects of aging on the brain are multiple and importantly, age constitutes the main risk factor for the development of neurodegenerative disorders (NDs) such as Alzheimer's disease (AD), Parkinson's disease (PD), and amyotrophic lateral sclerosis (ALS), which are characterized by progressive neuronal death and loss of specific neuronal populations. Considering the constant increase in life expectancy, NDs are nowadays an important problem for the society and our efforts to understand the mechanisms underlying these disorders has not been sufficient to provide a definitive help to the millions of patients worldwide.

For a better comprehension of the molecular and cellular changes that occur during aging, seven pillars of aging were defined, which are common processes involved in most chronic disorders that take place in an aging organism. These seven pillars are proteostasis, adaptation to stress, inflammation, stem cells and regeneration, epigenetics, metabolism, and macromolecular damage (Kennedy et al., 2014). Notably, changes in these cellular events are common to most NDs, suggesting that similar mechanisms might at least partially explain different age-related diseases. Even though NDs share phenotypic commonalities such as protein aggregation, cellular stress responses, and failure in RNA metabolism, it is still not clear why heterogeneous responses to similar genetic and environmental stimuli take place in different neuronal populations. Understanding the molecular basis of these pillars of aging and the timeframe in which they are activated could help us to tackle pre-symptomatically NDs and avoid irreversible cellular changes.

Axonal degeneration, which occurs at early stages of NDs, also takes place as a consequence of normal aging. Indeed, many cellular processes that are altered with advanced age have shown to contribute to axonal pathology. Importantly, the degeneration of axons represents an early event during the development of NDs, preceding both cell death and the onset of clinical symptoms, which has important therapeutic implications. Although, the molecular basis of the transition that makes an individual to develop neurodegeneration with advanced age is currently unknown, increasing evidence support the potential role of axonal degeneration in this transition, which is the focus of this review. An outline of the mechanisms associated to axonal degeneration is presented below, followed by a detailed overview of the literature and current advances in the molecular understanding of the cellular changes that occur during aging and its relationship with axonal degeneration.

Axonal Degeneration Overview

The process of axonal degeneration is an essential developmental event that consists in the selective destruction of axons (Schuldiner and Yaron, 2014). Moreover, axonal degeneration also occurs as a consequence of aging and represents a feature of NDs, constituting an important contributor to neuronal dysfunction (Neukomm and Freeman, 2014). Notably, the evidence indicates that axonal degeneration is an early event in NDs, taking place previous to neuronal cell death (Deckwerth and Johnson, 1994; Adalbert and Coleman, 2013).

Axonal degeneration is an evolutionary conserved process that can be activated by different stimuli including mechanical damage, axonal transport defects or by drugs used for chemotherapy. Although, the exact molecular and cellular pathways by which axonal degeneration occurs remain to be fully clarified, key contributing factors have been identified in the last decade and crucial findings have contributed to elucidate the mechanisms involved. Important clues have been obtained by studying Wallerian degeneration (WD), which correspond to degeneration of isolated axon after their mechanical transection. Furthermore, studies in the mouse strain Wld^S, which presents delayed axonal degeneration after injury, has been crucial to understand the mechanisms associated to axonal degeneration, and its functional relevance in NDs (Mack et al., 2001). After nerve transection, desomatized wild type axons undergo three phases: a latent phase, axonal fragmentation and axonal disintegration. The latent phase stills poorly understood but it is known that axons remain apparently normal for 1–2 days in mice after nerve injury (Court and Coleman, 2012), and can still conduct action potential (Moldovan et al., 2009). In the last stage, all the structures inside the axon are degraded. Disintegration of axonal cytoskeleton is followed by myelin degradation and macrophage infiltration that clear cell debris (Coleman, 2005).

Genetic analysis of the Wld^S mice unveiled that this natural mutation corresponds to a neomorphic one, that overexpresses a chimeric protein formed by fusion of the N-terminus of the E4 ubiquitin ligase Ube4b with the complete sequence of nicotinamide mono nucleotide adenylyltransferase 1 (Nmnat1; Coleman and Freeman, 2010). Axonal protection observed by up-regulating Nmnat1 is linked to mitochondrial metabolism (Avery et al., 2009; Fang et al., 2012), and the main mechanism does not seem to be the enzymatic production of NAD by Nmnat1 but most likely the action of downstream targets of this protein (Sorci et al., 2007; Coleman and Freeman, 2010). Recently, a loss-of-function mutation in the Sterile alpha and Toll/interleukin receptor (TIR) motif-containing protein 1 (Sarm1) was found, which cell-autonomously suppresses WD, confirming that this process is indeed an active program (Osterloh et al., 2012). SARM1 is a conserved mediator of WD, acting through the dimerization of the TIR domain to rapidly deplete NAD^+ in injured axons to trigger degeneration (Gerdts et al., 2015; Summers et al., 2016; Essuman et al., 2017). This mechanism explains NMNAT1 suppression of WD as this protein blocks the injury-induced NAD^+ consumption caused by SARM1, a mechanism that seems to be more important than the altered NAD^+ production caused by NMNAT1 (Sasaki et al., 2016). These findings open the possibility to identify novel molecules actively involved in the process that could lead ultimately to a deeper characterization and novel therapeutic targets for neurodegeneration.

We have demonstrated that mitochondrial dysfunction is a key process associated to axonal degeneration (Barrientos et al., 2011). The degeneration of axons was shown to be associated to the formation of the mitochondrial permeability transition pore (mPTP) between the inner and outer mitochondrial membrane. mPTP formation triggers the mitochondrial permeability transition (mPT), which leads to an increase in axonal reactive oxygen species (ROS) followed by intra-axonal calcium release (Calixto et al., 2012; Villegas et al., 2014). Interestingly, blocking mPTP either pharmacologically or genetically, by removal of the mPTP component Cyclophilin D (CypD), significantly delays axonal degeneration (Barrientos et al., 2011). Notably, formation of the mPTP has been linked to the pathogenesis of NDs including AD (Du et al., 2008), PD (Martin et al., 2014), and ALS (Martin et al., 2009) and has been suggested as a potential therapeutic target for these diseases.

Increasing evidence suggest that axonal degeneration occurs before cell body loss and notably, previous to the onset of clinical symptoms in different models of age-related diseases including ALS (Dadon-Nachum et al., 2010), PD (Tagliaferro and

Burke, 2016), and AD (Adalbert and Coleman, 2013). Hence, the understanding of the molecular and cellular mechanisms underlying this potentially reversible phase is critical for the development of therapeutic strategies aimed at the prevention and intervention of these disorders. Multiple molecular and cellular changes that occur during the process of aging can contribute to the accumulation of axonal damage, which is a prominent histopathological feature of the aging brain. Importantly, these cellular changes are common to almost all NDs, suggesting that similar mechanisms participate in the onset and development of these disorders. In the following section, we discuss how each of these changes contribute to the alteration of axonal integrity.

MOLECULAR MECHANISMS INVOLVED IN AGING AND THEIR RELATIONSHIP WITH AXONAL DEGENERATION

The urgency to extend healthspan, the period of healthy life preceding the development of age-related chronic diseases, has been recently highlighted. From this perspective, the field of Geroscience has invested increasing efforts to understand the mechanisms that underlie lifespan alteration, linking aging, and chronic diseases with the final aim of developing therapies for age-associated diseases (Kennedy et al., 2014). In this section we will review latest findings on each of the seven pillars of aging (**Figure 1**) with the aim of understanding whether they are related to axonal degeneration and how this event can be shifting healthy aging toward pathological aging with prevalence of chronic and neurodegenerative diseases.

Adaptation to Stress

In response to harmful stimuli, protective mechanisms that trigger adaptive responses can be activated to maintain cell homeostasis. If such noxious stimuli persist, programmed cell death is usually activated to eliminate damaged cells (Fulda et al., 2010). Whether cells react by triggering protective or destructive pathways depends on different factors including the nature and extent of the stress. Cells can respond to harmful stimuli in a number of ways and these adaptive responses include, among others, antioxidant defense mechanisms, the unfolded protein response (UPR), the heat-shock response and the DNA damage response (Fulda et al., 2010). As an example, it has been shown that following hypoxic injury, activation of the hypoxia inducible factor 1 (HIF-1) induces the expression of several genes that can promote cell survival and tissue adaptation by increasing blood supply and oxygen delivery to the injured tissue (Majmundar et al., 2010).

Compelling evidence indicate that the capability to induce an effective response following environmental and cellular injury decreases with the progression of aging. Hence, as organisms age, along with a general deterioration of cellular function, there is a decline in the stress responses that promote homeostatic repair. Examples of this diminished capability to compensate the altered cellular homeostasis include diminished

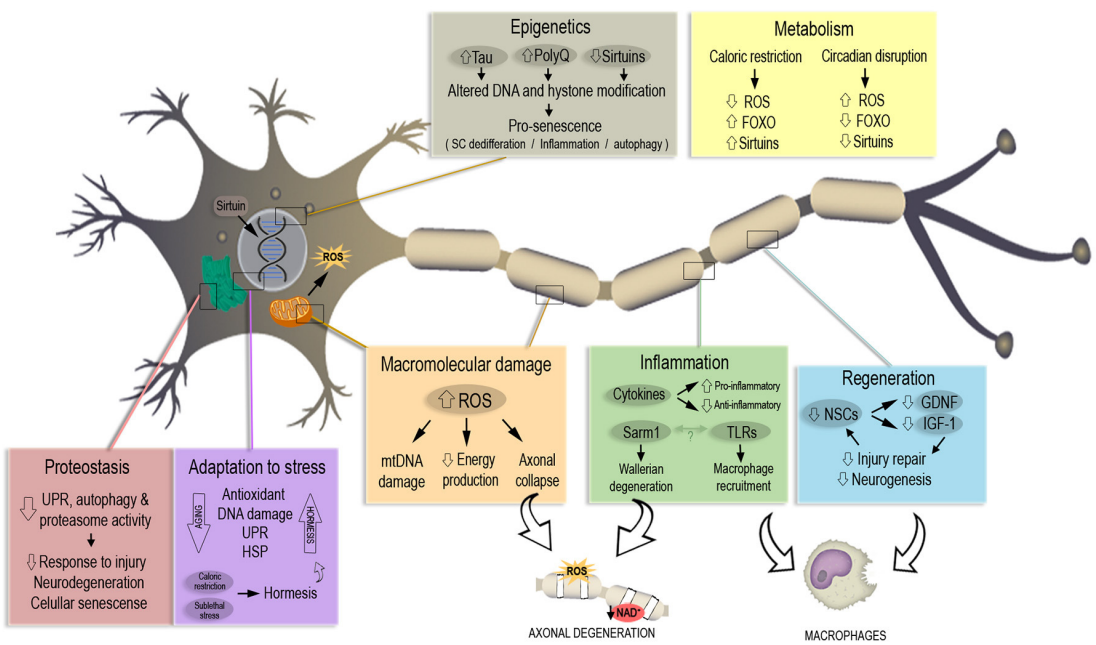

FIGURE 1 | The seven pillars of aging in the context of neuronal and axonal degeneration. Each pillar associated to the aging process is represented in a colored box. Most relevant pathways and molecules misregulated during aging are highlighted in each box, altogether with the consequences in neuronal senescence and axonal degeneration. A misregulated response to macromolecular damage and inflammation lead to increased ROS and a decrease in available NAD^+, triggering axonal degeneration. Aging also decreases the number of neuronal stem cells (NSCs) and their regenerative capability. Caloric restriction works in a protective way against aging with a mechanism opposite to the one observed with the age-linked disruption of circadian rhythm. Altered DNA modification and repair trigger pro-senescence phenotypes that lead to neuronal death, same phenotype induced by decrease of response to stress stimuli and oxidative damage.

HIF-1 activity (Majmundar et al., 2010), decreased heat shock response (Fargnoli et al., 1990) and altered response against DNA damage (Druzhyna et al., 2008). Notably, the concept of hormesis has emerged in the context of homeostasis, associated to a phenomenon in which an organism that has been subjected to sub-lethal stress such as caloric restriction, can engage signaling pathways that increase the neuronal capabilities of stress resistance against oxidative stress, mitochondrial disruption, protein misfolding, and DNA damage, thus reducing physiological decline and leading to life span extension (Mattson, 2008). By instance, studies performed in different models including mice (Miller et al., 2017), monkeys (Mattison et al., 2017), and humans (Prehn et al., 2016) have demonstrated that dietary energy restriction can protect against brain degeneration, promote cognitive improvement and increase life span (discussed in more detail in Section Metabolism).

Importantly, studies aimed at determine the effect of caloric restriction in NDs have shown positive outcomes using models of AD (Wu et al., 2008), PD (Maswood et al., 2004), and Huntington disease (HD; Duan et al., 2003). Several mechanisms have been demonstrated to contribute to this protective stress response and includes the Ca^{2+}–cyclic AMP response element-binding protein (CREB) pathway, the sirtuin–forkhead box O (FOXO) pathway and the nuclear regulatory factor 2 (NRF2)–antioxidant response element (ARE) pathway (Mattson, 2008; Stranahan and Mattson, 2012). Similarly, the experimental activation of other adaptive pathways, with the purpose of testing their potential therapeutic benefit for different NDs, has been recently investigated. In this line, the role of UPR activation, which is a main player of the proteostasis network, in the development of NDs such as AD (Duran-Aniotz et al., 2017) and PD (Valdes et al., 2014) has revealed interesting results. Recent evidence has shown an important link between the UPR and axonal degeneration and will be discussed in detail in the following section. Additionally, autophagy constitutes an essential component of the adaptive response to cell stress that helps to maintain cellular homeostasis and quality control. This mechanism is essential to regulate the axonal proteome and maintain axonal homeostasis by eliminating damaged organelles and protein aggregates (Komatsu et al., 2007; Maday and Holzbaur, 2014). However, the experimental induction of autophagy can result in protective or harmful effects to axons, which appears to depend on the context of the experimental setting. Indeed, there are reports demonstrating detrimental effects of autophagy activation on axonal integrity (Park et al., 2008; Kim et al., 2009; Liu et al., 2010; Cheng et al., 2011; Wakatsuki et al., 2017), while other studies have shown a protective effect (Komatsu et al., 2007; Launay et al., 2014; He et al., 2016). Despite the opposed outcomes, these studies strongly suggest that autophagy represent an important process involved in axonal maintenance and degeneration.

Proteostasis

The maintenance of protein homeostasis (referred to as proteostasis), which involve the correct synthesis, folding, trafficking, secretion, and degradation of proteins, relies on a network of different mechanisms and pathways that include the UPR, the heat-shock response, the autophagy pathway, the ubiquitin–proteasome system, chaperones and the endoplasmic reticulum (ER)-associated degradation machinery (ERAD). This cellular machinery maintains the equilibrium of the proteome and prevents the accumulation of misfolded proteins (Labbadia and Morimoto, 2015).

Compelling evidence has demonstrated a decline in the homeostatic capacity of the proteostasis network with increasing age. By instance, several studies have demonstrated that the levels of chaperones are markedly decreased with age in different organs including the brain (Paz Gavilán et al., 2006; Hussain and Ramaiah, 2007; Naidoo et al., 2008; Walther et al., 2015). Chaperoning activity can also be influenced by age-related changes such as energy failure due to mitochondrial damage, which affect the function of ATP-dependent chaperones (Brehme et al., 2014). Additionally, a number of studies have demonstrated aging-associated defects on autophagy (Cuervo and Dice, 2000; Lipinski et al., 2010; Rubinsztein et al., 2011) and proteasome activity (Bulteau et al., 2002; Ferrington, 2005; Dasuri et al., 2009; Keller et al., 2015), which contribute to the decline of brain proteostasis. Notably, there is evidence indicating that either manipulating the proteostasis network or preventing its deterioration, can induce a slowdown in the aging progression in different animal models (Ruan et al., 2002; Henis-Korenblit et al., 2010; Kruegel et al., 2011; Vilchez et al., 2012; Owusu-Ansah et al., 2013; Labunskyy et al., 2014). As an example, overexpression of the mitochondrial heat shock protein 22 leads to increased lifespan in *Drosophila* (Morrow, 2004). Another study showed that activation of autophagy by overexpression of Atg5 was able to extend the lifespan of mice (Pyo et al., 2013). Similarly, enhancement and activation of the 20S proteasome in *Caenorhabditis elegans*, resulted in life span extension (Chondrogianni et al., 2015).

A common feature of aging and NDs is the misfolding and accumulation of protein aggregates in the brain, a slow process that initiates decades before clinical symptoms manifest. The exact cause that leads to protein aggregation in the brain is unknown, although deregulation of protein homeostasis through perturbation of the ER has been shown to be involved (Martínez et al., 2017). The build-up of misfolded proteins at the ER, a condition known as ER stress, triggers the UPR signaling pathway in order to restore proteostasis and promote cell survival (Sidrauski and Walter, 1997; Harding et al., 1999; Haze et al., 1999). Disruption of this adaptive pathway has been associated with advanced age and it has emerged as a key contributor to the pathogenesis of NDs such as AD (Cissé et al., 2010, 2016; Li et al., 2013), prion disease (Moreno et al., 2012, 2013), ALS (Hetz et al., 2009), PD (Imai et al., 2001; Cooper et al., 2006; Valdes et al., 2014), and HD (Vidal et al., 2012; Zuleta et al., 2012).

Recent evidence indicates that activation of ER stress plays a critical role in the neuronal response to axonal injury in both peripheral and CNSs (Smith and Mallucci, 2016). Indeed, numerous studies have shown activation of the UPR upon axonal damage in different type of cells including Schwann cells (Mantuano et al., 2011), motoneurons (Penas et al., 2011), retinal ganglion cells (Hu et al., 2012), and in sensory neurons of the dorsal root ganglia (Ying et al., 2015). Interestingly,

pharmacological and genetic manipulation of components of the UPR pathway has shown to induce cognitive improvement and motor recovery in disease and nervous system injury models, respectively (Li et al., 2013; Valenzuela et al., 2016). By instance, studies from our group have demonstrated a protective role of the transcription factor X-Box-binding protein 1 (XBP1), a major regulator of the UPR, following nervous system damage. After spinal cord injury, XBP1-deficient mice presented significant impairment of locomotor recovery when compared with control mice. Notably, local administration of active XBP1 by gene therapy to the injured area enhanced locomotor recovery (Valenzuela et al., 2012). Looking at the functional role of the UPR in locomotor recovery following peripheral nerve injury, our group demonstrated that genetic ablation of Xbp1 induced a delay in locomotor recovery after injury. Conversely, overexpression of XBP1s in transgenic mice and local XBP1s gene transfer to neurons of wild-type mice, increased axonal regeneration and locomotor recovery (Oñate et al., 2016). Additionally, the protective effects of XBP1 activation on neuronal death, following axonal injury, were shown in a model of optic nerve crush. Axotomy triggered transient activation of the inositol-requiring enzyme 1α (IRE1α)/XBP1 pathway, and overexpression of the transcription factor strongly protected neurons from apoptosis (Hu et al., 2012). In a more recent study, using mouse models of traumatic optic nerve injury and glaucoma, the same group demonstrated that inhibition of eukaryotic translation initiation factor 2α-C/EBP homologous protein and XBP1 activation synergistically protect retinal ganglion cell axons and preserve visual function (Yang et al., 2016). Together, this evidence highlights the important role of the UPR signaling pathway in the processes of axonal degeneration and regeneration.

Inflammation

Even though activation of immune responses and inflammatory processes are consistently linked to aging (Chung H. Y. et al., 2009), it has been difficult to define the role of inflammation in neurodegeneration (Ransohoff, 2016). Inflammation corresponds to the protective response by which immune cells react in a balanced way against unexpected cells or debris (Karin and Clevers, 2016). For example, inflammation constitutes a primary response against pathogenic microorganisms in the intestinal epithelium. Metabolic changes observed in aging cells (DNA damage, loss of proteostasis, stress signals) affect the immune response against pathogens in the intestine and it is likely the cause why elderly individuals are more susceptible to infectious diseases and changes in health and lifespan (Ayyaz and Jasper, 2013). Another metabolic change that occurs in aging cells is the redox imbalance, which can be caused by weakness of the anti-oxidative defense system that cannot cope with the increased production of reactive species (Chung H. Y. et al., 2009). Notably, the increased lifespan observed with the anti-oxidant action of caloric restriction is associated to the modulation of pro-inflammatory signals such as NF-kB, TNF-α, and interleukins (Kim et al., 2002; Zou et al., 2004). Importantly, aging is associated with abnormal inflammatory responses in the brain, where the levels of pro-inflammatory cytokines are elevated, and the anti-inflammatory ones are reduced (Ye and Johnson, 1999; Sierra et al., 2007; Cribbs et al., 2012).

The nervous system is able to generate immune responses, and most of these processes are commanded by microglia and dendritic cells (Carson et al., 2006). Macrophages dominate sites of CNS injury where they promote both injury and repair. These cells are classified into the proinflammatory, neurotoxic M1 cells, and the M2 cells, which promote axon growth and remyelination (Kigerl et al., 2009). Morphologically, inflammation in the CNS is characterized by a different shaped microglia, which looks hypertrophic after an acute damage, or dystrophic after aging and neurodegeneration (Ransohoff, 2016). On the other hand, following injury to the nervous system, an important event is the inflammatory response associated to WD. In this process, glial cells fragment axons, isolate and convert myelin into lipid droplets even before the arrival of macrophages (Stoll et al., 1989). Then, the levels of cytokines and chemokines such as TNF-α and IL-1 are upregulated, leading to macrophage recruitment (Gillen et al., 1998; Liefner et al., 2000).

Multiple sclerosis (MS) is perhaps the most classic neurodegenerative disease associated to inflammation. MS is an autoimmune disease triggered by $CD4^+$ T helper lymphocytes and characterized by demyelination scattered throughout the CNS (Lucchinetti and Bruck, 2004). Mitochondria plays an important role in the pathomechanism of MS, affecting the normal relation between axons and glia through several defects including Ca^{2+} imbalance caused by excessive proinflammatory cytokines, deregulation of oxidative stress, impaired energy production and mitochondrial autophagy (Patergnani et al., 2017). These processes are in part mediated by the formation of the mPTP, which interestingly, has been strongly linked to axonal degeneration (Barrientos et al., 2011; Villegas et al., 2014). In fact, blocking mPTP formation has been proposed as a therapy for MS, with different compounds being currently tested in clinical trials (Su et al., 2012; Shirani et al., 2016).

Another interesting connection between inflammation, aging and axonal degeneration was made after the discovery that SARM1 is required for the degeneration of axons (Osterloh et al., 2012). Sarm1 is a pro-degenerative molecule that works after injury to trigger degeneration through a loss of NAD^+, which is mediated by its TIR domain (Gerdts et al., 2015; Summers et al., 2016; Essuman et al., 2017). A crucial aspect of the mechanism is that Sarm1 cell-autonomously triggers axonal degeneration, a surprising finding considering the role of this molecule in immune responses (Carty et al., 2006). Sarm1, Myd88, and Trif are adaptor molecules for Toll-like receptors, and as they are expressed in neurons, they are able to produce cytokines in response to pathogen infection (Chen et al., 2011; Lin et al., 2014). Interestingly, Sarm1 is not expressed in glial cells (Lin et al., 2014) and it is evolutionarily distinct from other proteins carrying TIR domains (Malapati et al., 2017), suggesting that its complete role is not yet fully understood. Sarm1 colocalizes with mitochondria (Panneerselvam et al., 2012) and regulates cell death after glucose and oxygen deprivation, recruiting JNK3 to the mitochondria (Kim et al., 2007; Mukherjee et al., 2013). Also, this protein was found in a genome-wide screening as an activator of PMK-1, a *C. elegans* p38-related kinase involved in

stress-induced detoxification, oxidative stress and aging (Crook-McMahon et al., 2014). Notably, over a decade ago Sarm1 was proposed as a candidate gene implicated in the onset of hereditary inflammatory diseases, after analyzing family-based human linkage disequilibrium studies (Mink and Csiszar, 2005). Recently, mice lacking the Sarm1 protein showed resistance to distal axonal degeneration in a model of chemotherapy induced peripheral neuropathy (Turkiew et al., 2017). These studies, altogether with the recent characterization of the TIR domain, open novel opportunities to use Sarm1 as a target for therapeutic approaches for neuropathies.

Stem Cells and Regeneration

Regeneration of tissues after injury requires in most cases, the presence of functional stem cells, the population of cells able to self-renew and the primal source of differentiated cell types. As all cells, Stem cells can be target of damaging mechanisms that can affect their function, decrease their viability and ultimately, compromise their ability to produce new cell lines. The damage received by stem cells is the basis of one of the most accepted theories of aging, which suggests that aging at the organism level is caused by exhaustion of stem-cell populations and the loss of regenerative responses after damage (Ruzankina et al., 2007). Several age-associated processes have been linked to the affected function of stem cells, including telomere shortening (Ferron et al., 2009), cellular senescence (Molofsky et al., 2006), and other interconnected pillars of aging such as epigenetic (Sun et al., 2014), metabolism (Deng et al., 2015), and proteostasis (Fredriksson et al., 2012).

In the nervous system, neural stem cells (NSCs) are responsible for neurogenesis and neuron replenishment within limited areas of the CNS. Many approaches have been tested to use NSCs injection in specific regions of the brain as a therapeutic intervention for NDs. By instance NSCs injected into the subiculum or hippocampus of two different transgenic AD mouse models decreased Aβ pathology and improved synaptic deficits (Blurton-Jones et al., 2014). Similar results were obtained in the P301S-tau model, where injection of NSCs that differentiated into astrocytes, increased glial-derived neurotrophic factor (GDNF) production and led to neuroprotection (Hampton et al., 2010). In contrast, it has been more difficult to observe an improvement in PD after injection of NSCs in the substantia nigra (Lindvall, 2013), and in HD after injection of NSCs in the striatum (Cicchetti et al., 2009). However, just as in AD, the increased production of neurotrophins such as IGF-1 and GDNF could be key to reach an improvement in motor and cognitive response in both diseases. Therefore, transplantation of NSCs that stimulate neurotrophin production appears to be a promising therapeutic intervention for NDs (Marsh and Blurton-Jones, 2017).

NSCs have been also used to improve axonal regeneration in the peripheral nervous system (PNS) after injury or nerve transection. WD in axons is a required initial step for regeneration (Martin et al., 2010) and after axonal damage, Schwann cells switch from a myelinating to a phagocytic phenotype and recruit macrophages to initiate the regenerative process (Fairbairn et al., 2015). Following sciatic nerve injury in rats, injection of NSCs transfected with two recombinant vectors containing either brain-derived neurotrophic factor (BDNF) gene or GDNF gene increased myelination and induced functional recovery (Fu et al., 2011). Similarly, a silicon conduit filled with NSCs and NGF connecting a sciatic nerve injury was used to increase axon myelination and induce functional recovery in rats (Xu et al., 2012). It will be interesting to follow the next clinical trials using stem cells and specially, how they manage the current difficulties in the translation to patients, including heterogeneity of lines and techniques (Marsh and Blurton-Jones, 2017).

Epigenetics

The fact that individuals with similar genetic backgrounds can age very differently constitutes an intriguing situation. Epigenetics involve the understanding of the mechanisms that allow individual cells to translate their genome differentially under functional and stable conditions in a multicellular organism (Schwartzman and Tanay, 2015). These mechanisms include DNA methylation, histone modification and chromatin accessibility, and they provide a different level of control for the genetic expression in each cell of the organism harboring the same genetic information at the DNA level. DNA methylation occurs at the 5′ position of a cytosine, preferentially when it is followed by a guanine (CpG context) and it is a major and dynamic mechanism for differential gene expression between tissues and cell-type differentiation (Boyd-Kirkup et al., 2013). On the other hand, histone modification through methylation, phosphorylation, acetylation and ubiquitylation, is another dynamic way to control gene expression, regulating the balance between the accessible euchromatin and the compacted heterochromatin, and with this, the facilitated transcription of specific DNA regions.

Both DNA methylation and histone modification have been linked to aging, supporting one of the original theories of aging: the increased difficulty of cells to express genes with aging due to changes in the DNA, especially the ones related to more relevant pathways for aged cells such as autophagy (Madeo et al., 2015). The modification of histones is a process affected by age. For instance, the protective effect of Sirtuins and Polycomb proteins through deacetylation and methylation respectively, is lost in old cells triggering the upregulation of NFkB and pro-senescence genes like p16 (Rando and Chang, 2012). Decreased levels of methylation were found in inflammatory genes such as TNF and iNOS when DNA from old blood cells was sequenced (Gowers et al., 2011). Also, hypermethylation was found in CpG islands of promoter regions of DNA from aged cells (Christensen et al., 2009), in DNA-binding factor genes in human brain (Hernandez et al., 2011) and in genes associated to development and differentiation such as FGF17, FZD1, and FZD7 (Salpea et al., 2012).

Epigenetic events in the context of neurodegeneration and axonal degeneration are less described than in aging, in part because studying epigenetic changes in the brain is particularly difficult. Cell heterogeneity and different functional states of neuronal populations makes epigenetics studies in the brain harder than other tissues (Maze et al., 2014). The microtubule-associated protein tau, a main player in AD pathomechanism, triggers heterochromatin relaxation in

transgenic flies and AD patients in a mechanism mediated by oxidative stress and DNA damage (Frost et al., 2014). DNA remodeling increases the transcription of genes normally silent as compared to control transcriptional profiles, suggesting that this epigenetic effect may work as a potential therapeutic target for AD. Similar clues have been found in the study of HD, another neurodegenerative disease caused by the expansion of CAG repeats coding for glutamine (PolyQ) in the huntingtin gene. PolyQ expansions in this gene have been linked to DNA remodeling and histone modifications (Steffan et al., 2001; Sadri-Vakili et al., 2007), changes in DNA methylation and transcription of key neuronal-specific genes (Ng et al., 2013; Wood, 2013), and alteration of ncRNAs (Johnson et al., 2008; Lee et al., 2011). Expansions in C9orf72, the gene that is most commonly linked to ALS, include CpG islands that are hypermethylated in tissue from ALS patients (Xi et al., 2015), and altered histone methylation pattern causes reduction on the C9orf72 mRNA expression in the patient's brain (Belzil et al., 2014).

As explained above, WD after axonal injury is associated to dedifferentiation and proliferation of Schwann cells. Proliferation is regulated through an epigenetic effect of the histone demethylase Jmjd3, which after injury activates the Ink4a/Arf locus to switch off proliferation and trigger the senescence program (Gomez-Sanchez et al., 2013). The high plasticity observed in Schwann cells could also play an important role in the events leading to neurodegeneration. Current research efforts are focusing on trying to properly define the link between disease-linked mutations and the temporality of epigenetic effects. Hopefully, that connection could be used as a potential biomarker to determine pre-clinically the progression of neurodegenerative disorders.

Metabolism

In this section, we will focus on two topics that, even though are connected to previously described mechanisms, can still provide novel views to understand the connection between aging and degenerative mechanisms in the neuron. These topics are nutrigenomics or the effect of the food and nutrients on gene expression (Grayson, 2010), and the regulation of circadian clocks and sleep patterns (Musiek and Holtzman, 2016).

Nowadays, the relevance of specific and personalized diets, with the aim of improving the quality and extension of life, is getting common. However, the beneficial outcome of specific types of food or a reduction on caloric intake, not only applies to lifespan extension (Madeo et al., 2015) but also has been associated to axonal degeneration (Speakman and Mitchell, 2011). Caloric restriction extends lifespan through different mechanisms that include increased autophagy and activation of mTOR and FOXO (Galluzzi et al., 2014), reduction of mitochondrial ROS production (Ash and Merry, 2011), mitochondrial biogenesis via upregulation of PGC-1a (Nisoli et al., 2005) and activity of Sirtuins (Jasper, 2013). Sirtuins are deacetylases that catalyze the consumption of NAD^+, and are required for lifespan extension after supplementing nicotinic acid (a source of NAD^+). Sirtuins have been extensively studied with contrasting results. In flies and worms, Sirt1 was linked with extension of lifespan (Rogina and Helfand, 2004; Viswanathan et al., 2005), a discovery that was later challenged (Burnett et al., 2011).

Not that well-studied, at least in a direct way, is the effect of caloric restriction on axonal degeneration. Previous studies performed by our group using a genetic *mec-4d C. elegans* model of axonal degeneration and a mouse model of acute injury, demonstrated that caloric restricted diet and systemic antioxidant treatment protected both models from axonal degeneration, which was associated with decreased oxidative damage. Moreover, downregulation of the Insulin/IGF-1-like signaling (IIS) pathway protected neurodegeneration in a DAF-16/FOXO–dependent manner (Calixto et al., 2012). As mentioned above, FOXO is an important player in lifespan extension acting as an effector of the stress-response JNK pathway, both antagonizing IIS and working together with the TOR pathway as a molecular switch between growth promotion and lifespan extension according to nutrient availability (Wang et al., 2005). Importantly, a phase 2 trial based on dietary restriction proved to be successful against metabolic syndrome through reducing glucose and circulating IGF-1 (Wei et al., 2017). Using another variation of dietary restriction (intermittent fasting), improvements in motor performance were observed in a mouse model of neuropathic pain (Madorsky et al., 2009) and in a spinal cord injury mouse model (Jeong et al., 2011), further supporting the effect of caloric restriction in neuronal health. Notably, SIRT2 was also linked to axonal degeneration (Araki et al., 2004) and WD (Suzuki and Koike, 2007) in a mechanism that involves tubulin deacetylation and a delay on axonal degeneration. However, the potential role of SIRT2 and NAD^+/NADH balance in WD was discarded in *Drosophila*, as downregulation of this enzyme did not induce spontaneous degeneration and did not suppress the ability of Wld^S to slow axonal degeneration *in vivo* (Avery et al., 2009).

In addition, emerging evidence indicate that a ketogenic diet, which consists of high fat, adequate protein and low carbohydrate intake, can improve motor and cognitive performance in NDs. By instance, administration of ketogenic diet to transgenic ALS mice resulted in higher motor neuron survival and an in motor function improvement when compared to control mice (Zhao et al., 2006). Another study performed by the same group in transgenic ALS mice fed with caprylic triglyceride showed protection from spinal cord motor neuron loss and improved motor performance (Zhao et al., 2012). Similar positive results have been obtained in AD models. For example, the toxic effects of Aβ on hippocampal neurons were prevented by addition of β-hydroxybutyrate to cell cultures (Kashiwaya et al., 2000). Moreover, studies performed in transgenic mouse models of AD fed with ketogenic diet showed decreased levels of Aβ aggregates and tau pathology in the brain (Van der Auwera et al., 2005; Kashiwaya et al., 2013). The effects of ketogenic diet on PD have also been investigated. Administration of β-hydroxybutyrate to mice treated with MPTP protected from neurodegeneration and motor impairment (Tieu et al., 2003). Similarly, PD pathology induced by 6-hydroxydopamine in rats was attenuated when a ketogenic diet was administered (Cheng et al., 2009).

Another process that links metabolism with aging and neurodegeneration is the circadian clock. Sleep problems and

circadian malfunctions are known consequences of aging and NDs and they are also hallmarks of early stages of NDs (Musiek and Holtzman, 2016). In humans, the control of the circadian rhythm is based on the interaction of CLOCK with ARNTL, a protein found in high levels at the beginning of the day. This complex activates PER and CRY, which is upregulated at night and blocks the CLOCK-ARNTL complex at the start of the night cycle. When CRY levels decrease in the morning, the original complex forms again and re-starts the day cycle 24 h later (Videnovic et al., 2014). This process occurs mostly in neurons from the suprachiasmatic nucleus (SCN), the peacemaker of our body, and the activity of these neurons controls up to 10% of the human genome. Furthermore, degeneration of this group of neurons causes sleep and circadian disruption, which leads to increase in ROS production (Koh et al., 2006; Wang et al., 2012), inflammation (Prolo et al., 2005), proteostasis alterations (Stratmann et al., 2012), and neurodegeneration (Holth et al., 2017). Genzer et al. linked the circadian changes with the levels of BDNF, the most abundant neurotrophin in the brain that causes neurodegeneration when its levels are low. When mice were fed a high fat diet, circadian levels of brain and liver BDNF were altered, mTOR was downregulated and AMPK was activated, which could link circadian clock with obesity and neurodegeneration (Genzer et al., 2016). In *Drosophila*, downregulation of other two modifiers of circadian clock, Spag and Dbt, causes upregulation of the caspase Dronc which cleaves tau and increases neurodegeneration in a model of tauopathy (Means et al., 2015). As in the case of caloric restriction, circadian rhythm is also regulated by Sirtuins and FOXO. Notably, SIRT1 is a master regulator of the circadian clock, activating the key components CLOCK and ARNTL. As the organism ages, SIRT1 decreases in the SCN failing to properly control the circadian clock (Chang and Guarente, 2014). Supporting this mechanism, NAD^+ levels also follow a rhythm regulated by the circadian levels of NAMPT (nicotinamide phosphoribosyltransferase), an important step in NAD^+ metabolism (Nakahata et al., 2009). Even though there is no solid connection yet between circadian rhythm and axonal degeneration, it would be interesting to further explore the mentioned components of circadian regulation and NAD^+ levels on axonal degeneration and its connection to neurodegenerative conditions.

Macromolecular Damage

Several external sources and internal metabolic processes generate as by-product free radicals (FR) such as ROS (Lipsky and King, 2015). For a long time the generation of FR has been linked to aging (Harman, 1956), and the theory that senescence is associated with the accumulation of oxidative damage to macromolecules caused by ROS has been focus of intense research. Damage of organic molecules by FR affects different processes such as proteostasis and response to stress, and importantly puts the mitochondria in a central stage of the aging process. Mitochondria is the largest ROS generator, and in conditions of excessive ROS production, damage to key mitochondrial proteins and DNA occurs, leading to mitochondrial dysfunction, decreased energy production and overall senescence of the cell (Richardson and Schadt, 2014). It has been proposed that with increasing age, the low demand of energy produced by mitochondria due to sedentary lifestyle induces metabolic changes that lead to altered reductants/oxidants ratio. This change triggers a shift favoring an oxidized redox state leading to macromolecular damage (Brewer, 2010). However, whether macromolecular damage caused by oxidative stress constitutes the cause or the consequence of aging and ND-related mechanisms remains yet unclear.

The effect of oxidative damage on macromolecules has been extensively studied in relation to NDs. For example, In the case of ALS, the first genetic link to the disease was made with the discovery of mutations in superoxide dismutase SOD1, an enzyme that catalyzes the conversion of the toxic O_2^- anions into O_2 and H_2O_2 (Rosen et al., 1993). Oxidative damage in the mitochondria was immediately linked to the disease and further studies aimed at testing potential pharmacological targets in SOD1 transgenic models revealed modest beneficial outcomes (Julien and Kriz, 2006). Furthermore, these studies have been unsuccessfully translated into humans (Ludolph et al., 2009). TDP43 and FUS, other 2 ALS-causative genes, are involved in the prevention or repair of transcription-associated DNA damage, as their depletion increases DNA damage (Hill et al., 2016). Similarly, increased DNA damage is observed in iPSC-derived neurons with expansions in the C9orf72 gene. These cells also show mitochondrial dysfunction and increased oxidative stress (Lopez-Gonzalez et al., 2016). In addition, mitochondrial dysfunction and oxidative macromolecular damage are prominent features of AD. Using primary neuronal cultures from 3xTg-AD mice, Gosh et al. demonstrated an early, reversible oxidized redox state compared to wild-type neurons. This oxidized state preceded an age-related increase in ROS levels and macromolecular ROS damage (Ghosh et al., 2012). Moreover, a proteomic study performed in early AD subjects revealed that lipid peroxidation is an early event in the progression of AD (Reed et al., 2009). Looking at the impact of oxidative damage on the pathology displayed by the AD transgenic model Tg2576, a recent study showed that ROS constitute a key contributor to the development of cerebral amyloid angiopathy, vasomotor dysfunction and microhemorrhage (Han et al., 2015). Similarly, loss of glutathione and increased oxidative DNA and protein damage were observed in an *in vitro* model of PD, where inhibition of mitochondrial complex I by rotenone, induced the typical features of PD including aggregation of α-synuclein (Sherer et al., 2002).

Axonal integrity, which as previously discussed is altered at initial stages of NDs, can be disrupted as consequence of oxidative damage to axonal macromolecules. An *in vitro* study performed in myelin purified from rats showed that myelin-associated protein and lipids are highly vulnerable to oxidative damage (Bongarzone et al., 1995). A recent study in aged wild-type mice demonstrated that motor nerve dysfunction triggered by axonal and myelin damage was associated with a decline in antioxidant defense mechanisms, which led to oxidative protein and lipid damage (Hamilton et al., 2016). Additionally, a number of studies have shown that oxidative damage to axonal components can trigger defects in transport across the axon (Roediger and Armati, 2003; Sharma et al., 2010), which is an

early feature of NDs (De Vos et al., 2007; Chu et al., 2012; Sadleir et al., 2016).

AXONAL DEGENERATION AT EARLY STAGES OF AGE-RELATED NEURODEGENERATIVE CONDITIONS

As reviewed above, many of the changes at the molecular and cellular level that occur during the aging process may have an impact on the integrity of axons. Importantly, the evidence indicates that axonal degeneration constitutes an early phase in the process of neurodegeneration that is shared by different age-related neurological diseases (Dadon-Nachum et al., 2010; Adalbert and Coleman, 2013; Tagliaferro and Burke, 2016). In this section we will examine the association of specific NDs with the pillars of aging and evidence implicating axonal degeneration in their pathophysiology. We will focus specifically on AD, PD, and ALS, which constitute the most common age-related NDs. A summary of this information is presented in **Tables 1, 2**.

Alzheimer's Disease

AD is a progressive neurodegenerative disorder and constitutes the most frequent form of dementia in the elderly population (Alzheimer's Association, 2016). Although several risk factors have been associated with the pathophysiology of sporadic AD, aging being the most important one, its exact cause remains unrevealed. However, compelling evidence indicate that Aβ dyshomeostasis constitutes a key event involved in the etiopathogenesis of AD, which promotes the accumulation of the protein and further development of all the neuropathological and clinical features of the disease (Selkoe and Hardy, 2016).

As discussed above, perturbation of the proteostasis network leading to the accumulation of protein aggregates is a normal feature of aging, and there is increasing evidence showing that this also occurs in AD (Hoozemans et al., 2005, 2009; Peng et al., 2016; Duran-Aniotz et al., 2017). Hence, it is possible that deterioration of the cellular function as a consequence of aging leads to the imbalance of Aβ production and degradation, triggering the abnormal accumulation of the peptide, reaching toxic levels. Indeed, although Aβ deposition in the brain constitutes the main pathological feature of AD, this process also occurs during normal aging. Histopathological analyses have revealed that in the cases where Aβ deposition is present in brain tissue from non-demented individuals, the amyloid structures are not associated with abnormal neuronal processes, synapse loss, and cognitive alterations as occur in AD brain tissue (Serrano-Pozo et al., 2011), suggesting that degeneration of axons and dendrites (also referred to as neurites) constitutes a key event involved in the Aβ-related mechanisms that participate in the transition from normal aging to dementia. Moreover, neurons affected in AD follow a dying-back pattern of degeneration, where axonal disruption and synaptic loss precede neuronal cell death and manifest in early stages of the disease (Serrano-Pozo et al., 2011; Adalbert and Coleman, 2013).

Although Aβ-related axonal and dendritic dystrophy is an early histopathological observation in postmortem AD brains (Knowles et al., 1999; Nelson et al., 2012) and in animal models of AD (Mucke et al., 2000), whether Aβ deposition is the cause of axonal and dendritic degeneration or constitutes a consequence of an underlying neurodegenerative process remains currently unknown and there is evidence demonstrating that both possibilities may occur. Traumatic brain injury (TBI) is one of the main environmental risk factors for the development of AD (Alzheimer's Association, 2016). Diffuse axonal injury represents a typical consequence of TBI, where disruption of the cytoskeleton results in swollen axons, altered axonal transport, and mitochondrial dysfunction (Choe, 2016). Intra-axonal upregulation of the amyloid precursor protein (APP) and increased processing of the protein resulting in diffuse Aβ plaque deposition occurs quickly after TBI and notably, studies in long-term survivors have revealed that axonal degeneration persists and mature Aβ plaques and tau pathology develops, which is associated with cognitive impairment (Johnson et al., 2011). These studies suggest that Aβ accumulation occurs due to the disruption of axonal integrity following injury. Hence, it is possible that the axonal damage that occurs as a consequence of aging, could also contribute to the accumulation of Aβ. In a recent study, looking at the mechanisms of dystrophic neurite formation in AD, Sadleir and colleagues were able to show that exposure of cultured neurons to Aβ oligomers caused microtubule depolymerization leading to altered axonal trafficking (Sadleir et al., 2016). The results were confirmed in brain tissue from both AD patients and transgenic mice, where they observed that dystrophic neurites in the close proximity to Aβ plaques contained low microtubule density, accumulation of autophagic intermediates and increased β-site APP cleaving enzyme (BACE1) and APP levels, which caused enhanced generation of Aβ (Sadleir et al., 2016).

Extensive research focusing on the mechanisms underlying Aβ neurotoxicity has been undertaken and as a result, its association with numerous pathogenic pathways has been suggested. Among the pathways activated by Aβ, most of them are implicated in the process of axonal degeneration, including oxidative stress (Behl et al., 1994; Hensley et al., 1994; Butterfield et al., 2013), mitochondrial dysfunction (Devi, 2006; Wang et al., 2009; Kerr et al., 2017), and abnormal calcium signaling (Mattson et al., 1992; Furukawa et al., 1996; Demuro et al., 2005; Meyer-Luehmann et al., 2008). To date, AD drug development has been based primarily on the amyloid hypothesis, and the majority of randomized controlled trials have been designed to target this protein. However, the overall outcomes have been dramatic, with a 99.6% failure rate for approval (Cummings et al., 2014). Nevertheless, the trails have arguably been conducted late and when there is extensive pathology and degeneration. As mentioned above, axonal degeneration represents an early event during the progression of AD, hence, unveiling the exact mechanisms that trigger the degeneration of axons represent a promising step in the field of AD drug development.

Parkinson's Disease

PD is the most common motor-related ND. The precise cause of the disease remains largely unknown; although it is thought that PD is the result of a combination of genetic and environmental

TABLE 1 | Association of AD, PD and ALS with the pillars of aging.

	Alzheimer's disease	Parkinson's disease	Amyotrophic lateral sclerosis
Proteostasis	IRE1 signaling activation (Duran-Aniotz et al., 2017) Rescue by inhibition of ER acetylation (Peng et al., 2016) Elevated UPR markers (Hoozemans et al., 2005)	Altered autophagy (Li et al., 2017) Proteostasis alterations in stem cells (Chung et al., 2013) ATF6α protection (Egawa et al., 2011)	Decreased foldases and chaperones (Filareti et al., 2017) Mitochondrial UPR ERα activation (Riar et al., 2017) Rescue by XBP1 deficiency (Hetz et al., 2009)
Inflammation	Protection by TNF inhibition (MacPherson et al., 2017) Aβ-associated microglia hyperreactivity (Yin et al., 2017) Role of variant TREM2 (Jonsson et al., 2013)	The role of IL1 (Pott Godoy et al., 2008) Microglial activation (Gerhard et al., 2006) TNFα overexpressed (Mogi et al., 1994)	Inflammation and necroptosis (Ito et al., 2016) Glial activation (Alshikho et al., 2016) Decreased levels of α-1-antitrypsin (Wormser et al., 2016)
Stem cells and regeneration	APP binding to clathrin decreased in NSC (Poulsen et al., 2017) Altered neurogenesis (Unger et al., 2016) Altered stem cell proliferation and neurogenesis (Wu et al., 2016)	α synuclein-induced alteration of neurogenesis (Desplats et al., 2012) Impaired generation of neural precursor cells (Höglinger et al., 2004)	Protective effect of NSC on number and function of motor neurons in SOD1 rats (Xu et al., 2009)
Adaptation to stress	Role of DNA repair factor BRCA1 (Suberbielle et al., 2015) Role of EphB2 depletion (Cissé et al., 2010) Altered glutathione metabolism (Liu et al., 2004)	Altered DNA damage repair (Sepe et al., 2016) Role of XBP1 (Valdes et al., 2014) Altered antioxidant response (Sofic et al., 1992)	Protection by XBP1 deficiency (Hetz et al., 2009) DNA repair dysfunction (Kikuchi et al., 2002) Dysfunction of heat shock response (Chen et al., 2016)
Epigenetics	Role of DNA hydroxymethylation (Zhao et al., 2017) Decreased methylation of CREB regulated transcription coactivator 1 gene (Mendioroz, 2016) DNA methylation near TREM2 (Smith et al., 2016)	α-synuclein involved in histone methylation (Sugeno et al., 2016) Epigenetic deregulation in iPSC-derived dopaminergic neurons (Fernandez-Santiago et al., 2015) Decreased methylation of α-synuclein gene (Jowaed et al., 2010)	Different methylomes in T-cell and monocytes (Lam et al., 2016) Role for cytosine demethylation (Esanov et al., 2016) Rescue by C9orf72 hypermethylation (Liu et al., 2015)
Metabolism	Glucose metabolism (Chiotis et al., 2017) Fatty acid metabolism (Snowden et al., 2017) Metabolites of ornithine (Inoue et al., 2013)	Altered fat distribution (Bernhardt et al., 2016) Changes in glucose metabolism (Dunn et al., 2014) Iron metabolism is altered (Logroscino et al., 1997)	Mitochondrial bioenergetics (Ladd et al., 2017) Astrocyte metabolism (Madji Hounoum et al., 2017) Mutations in transcription-associated DNA damage repair proteins (Hill et al., 2016)
Macro molecular damage	Redox changes (Ghosh et al., 2012) Oxidative DNA damage in leukocytes (Migliore et al., 2005) Peroxynitrite involved in oxidative damage (Smith et al., 1997)	Lipid peroxidation (Mythri et al., 2011) Peripheral protein oxidation (Saito et al., 2009) Mitochondrial impairment and oxidative damage (Sherer et al., 2002)	SOD gene mutations (Rosen et al., 1993) Mutations in iPSC-derived neurons linked with oxidative stress (Lopez-Gonzalez et al., 2016)

risk factors (Pires et al., 2017). Due to the strong association between mutations in α-synuclein gene and the development of familial PD, a central focus of PD research has been the misfolding and deposition of this protein (Gao et al., 2008; Imaizumi et al., 2012; Gonzalez-Horta, 2015; Wang and Hay, 2015).

Recent evidence indicate that the degeneration of axons of dopaminergic neurons constitute an early event in PD development. Thus, axonal degeneration plays a critical yet unclear role in this disease. Following the observation that degeneration of the distal axons of the cardiac sympathetic nerve precedes loss of cell bodies in PD patients (Orimo et al., 2005), Orimo and colleagues focused on the involvement of α-synuclein on the degeneration of axons and the timing of this process and demonstrated that the pathology commence at the distal axon and continues in a retrograde fashion (Orimo et al., 2008). Additional evidence supporting these findings includes *in vitro* studies of primary neurons exposed to α-synuclein fibrils, where recruitment of endogenous α-synuclein to form insoluble aggregates was observed. Interestingly, the pathology was initially observed in axons and was associated to neuronal dysfunction, propagating proximally to the soma leading to neuronal cell death (Volpicelli-Daley et al., 2011). Moreover, studies in a transgenic mouse model expressing a mutant form of α-synuclein revealed striatal dopaminergic axonal disruption, while the integrity of cell bodies of dopaminergic neurons

TABLE 2 | Evidence for axonal degeneration in the pathophysiology of AD, PD and ALS.

Disease	Evidence for axonal degeneration in NDs	References
Alzheimer's disease	Axonal pathology triggered by Aβ precedes cell body death	Adalbert et al., 2009
	Axonal leakage, swollen axons, and varicosities are associated with Aβ plaques and hyperphosphorylated tau in AD brains	Xiao et al., 2011
	Autophagic vesicles are linked with axonal pathology in transgenic AD mice	Sanchez-Varo et al., 2011
	Microtubule-stabilizing agent Epothilone D reduces axonal dysfunction un a mouse model of tau	Zhang et al., 2012
	Aβ oligomers cause microtubule depolymerization leading to altered axonal trafficking	Sadleir et al., 2016
Parkinson's disease	Alterations in axonal transport associated with α-synuclein mutations *in vitro*	Saha, 2004
	Degeneration of axons precedes loss of cell bodies in PD patients	Orimo et al., 2005
	Transgenic α-synuclein mouse model shows striatal dopaminergic axonal, but not cell body, disruption	Tofaris, 2006
	α-synuclein is linked with axonal degeneration which iniciates at the distal axon and continues retrograde	Orimo et al., 2008
	α-synuclein rat model shows altered axonal transport	Chung C. Y. et al., 2009
	Transgenic LRRK2 mouse model shows dopaminergic axonal, but not cell body, disruption	Li et al., 2009
	Axonal pathology triggered by α-synuclein propagates later to the soma is associated with neuronal dysfunction	Volpicelli-Daley et al., 2011
	Early decline in axonal transport associated with α-synuclein aggregation in PD patients	Chu et al., 2012
	Autophagy is involved in axonal pathology and associated with α-synuclein and LRRK2 proteins	Friedman et al., 2012
Amyotrophic lateral sclerosis	Axonal pathology starts at the distal axon and continues in a "dying back" pattern in the innervated muscle fibers	Fischer et al., 2004
	SARM1 gene mutations are linked with ALS development	Fogh et al., 2014
	Defects in axonal transport constitute a typical feature in Drosophila models of ALS	Baldwin et al., 2016
	Axonal degeneration is mediated by necroptosis and inflammation in ALS	Ito et al., 2016
	Potassium channel abnormalities are linked to axon degeneration in ALS mouse model	Maglemose et al., 2017
	ALS-related mutations change the subcellular expression and localization of RNAs within neuronal axon	Rotem et al., 2017

was maintained (Tofaris, 2006). Similarly, characterization of a transgenic mouse model that expresses mutant leucine-rich repeat kinase 2 (LRRK2), the single most common cause of inherited PD, showed a significant alteration of axonal integrity, however, no loss of dopaminergic neurons was observed (Li et al., 2009).

Based on the evidence indicating that axons are the first site of degenerative change and are compromised before cell soma, Chu and colleagues used human PD tissue to investigate axonal transport in the initial stages of PD. The group demonstrated an early decline in axonal transport motor proteins, which occurred before the alteration of dopaminergic phenotypic markers and was associated with α-synuclein aggregation (Chu et al., 2012). This result is in line with previous studies demonstrating alterations in axonal transport associated with α-synuclein mutations *in vitro* (Saha, 2004) and *in vivo* (Chung C. Y. et al., 2009). Looking at the mechanisms of axonal degeneration in PD, a study performed in an autophagy-deficient mouse model revealed that deletion of the autophagy gene Atg7 triggered early dendritic and axonal dystrophy, which was associated with enhanced levels of endogenous α-synuclein and LRRK2 proteins. This study suggests that alterations in autophagy might be involved in the pathogenesis of sporadic PD and linked with axonal degeneration (Friedman et al., 2012).

A workshop presenting the state-of-the-art of axonal pathology research in PD was recently carried out and a summary of the current knowledge on the field was published (Kurowska et al., 2016). The view of axonal degeneration as an early process in the development of PD is discussed and the importance of finding early diagnostic markers, as well as targeting axonal degeneration as a preventive measure are highlighted.

Amyotrophic Lateral Sclerosis

ALS is a progressive adult-onset disorder, characterized by the selective death of upper and lower motor neurons leading to paralysis and muscle atrophy. About 10% of ALS cases have a genetic cause, and many different forms of the disease are the result of different genetic mutations (Al-Chalabi et al., 2016). Currently, the cause of the sporadic form of the disease remains unknown (Pasinelli and Brown, 2006).

An important component of the neuronal dysfunction in ALS is the degeneration of axons (Ferraiuolo et al., 2011). The disease initiates at the distal motor axons and continues in a "dying back" pattern, with denervation and reinnervation taking place in the innervated muscle fibers at early stages (Fischer et al., 2004). Evidence suggest that in ALS, axonal damage takes place before loss of cell bodies and the onset of clinical symptoms, which appear only after a large proportion of motor units are lost (Dadon-Nachum et al., 2010). Interestingly, the Wld^S mouse model shows delayed axon degeneration in some peripheral neuropathies. However, it has not been successful

on improving the symptoms and axonal pathology present in SOD1 mutant rodent models of ALS (Vande Velde et al., 2004; Fischer et al., 2005). Nonetheless, by performing a genome-wide association meta-analysis, Fogh et al. identified the SARM1 locus as spot for three SNPs linked to patients with ALS (Fogh et al., 2014).

Several studies have shown impaired axonal transport in ALS, which has been demonstrated to constitute an early event during the progression of the disease (Williamson and Cleveland, 1999; Murakami et al., 2001; De Vos et al., 2007). By instance, altered mitochondrial transport through the axon was demonstrated in two different SOD1 mutant mouse models of ALS (Magrané et al., 2014). Furthermore, mutations in the RNA-binding protein TDP-43 can cause ALS and interestingly, it was recently demonstrated that this protein functions as an mRNA transporter across the axonal cytoskeleton and that mutations in this protein leading to ALS, alter this transport function (Alami et al., 2014). Notably, genetic studies performed in families with ALS revealed mutations in the genes encoding the transporter proteins dynactin (Puls et al., 2003) and tubulin (Smith et al., 2014) which lead to reduced binding of the mutant protein to microtubules and decreased repolymerization capability respectively.

As discussed previously, sirtuins are an important link between aging and neurodegeneration. In ALS, altered sirtuin levels have been observed in both transgenic mouse models (Han et al., 2012) and patients tissue (Körner et al., 2013). Moreover, in *Drosophila,* Sirtuin1 was described as a suppressor of neurodegeneration in the ALS model DVAP-P58S (Sanhueza et al., 2015). Sirtuin 1 protection from axonal degeneration is regulated by Nmnat1, the protein overexpressed in the WldS model (Araki et al., 2004). Furthermore, resveratrol, a polyphenol that exhibits beneficial effects in NDs, protects against WD by activating Sirtuin 1 through dissociation from its inhibitor DBC1 (Calliari et al., 2014). There is evidence indicating that the metabolites obtained from NADH play a crucial role on the effect of Sirtuins (Jasper, 2013), and considering that these metabolites, especially nicotinamide mononucleotide (NMN), are crucial in the axonal degenerative process (Di Stefano et al., 2017), it seems plausible that sirtuins and NAD^+ metabolism might play a central role on the ALS pathomechanism, even as a potential therapeutic target for the disease (Pasinetti et al., 2013; Tang, 2016).

As mentioned previously, different gene mutations can lead to several forms of ALS. Together, the evidence presented above suggests that axonal degeneration plays a key role in ALS pathophysiology and that common mechanisms involved in axonal pathology can contribute to the development of the different forms of ALS, which will benefit the search for potential therapies to tackle them before the disease is already declared and irreversible.

Huntington's Disease and Other Pathologies

HD is a disease that in contrast to the previously described ones, it is the most common monogenic neurological disease. HD is caused by the expansion of the gene codifying for the huntingtin protein. The mutant version carries long polyglutamine sequences encoded by repeated CAG. In HD patients, expression of mutant Htt affects neurons in the striatum and cortex, triggering neuronal dysfunction and apoptosis. Neuronal death causes motor and cognitive impairment, leading to death of patients 18 years after the onset of motor problems (Bates et al., 2015).

Abnormal splicing and formation of amino-terminal Htt fragments are consequences in which the translation of mutant huntingtin causes toxicity in the disease. Htt fragments aggregate in the nucleus and sequester other proteins disrupting the proteostasis network. Interestingly, Htt fragments also affect mitochondrial function and cellular trafficking, leading to axonal dysfunction and degeneration. Even though experimental evidence demonstrate that axonal degeneration is an early event in HD (Li and Conforti, 2013), its temporal relation with cell loss and disease symptoms is not completely understood. It has been determined in mouse models of HD and human patients that callosal axons degenerate long before the onset of motor symptoms (Gatto et al., 2015). This phenotype was worsened with age and suggests a dying-back pattern of degeneration in HD (Gatto et al., 2015). Early signs of axonal aggregates were also described in striatal axonal projections to the globus pallidus and the substantia nigra of mice expressing full-length mutant huntingtin. Neuropil aggregates were associated with degenerated mitochondria and with defects on protein transport (Li et al., 2001). Importantly, a different study determined that the axonal swellings were formed age-dependently and were independent of inclusions in the soma, suggesting that axon degeneration precedes death of other neuronal compartments in a model of HD (Marangoni et al., 2014). Mechanistically, axonal pathology in an HD mouse model shares molecular pathways with a model of axonal injury, as proteomic screens identified proteins with similar expression levels in both models (Wishart et al., 2012). Transport failure and the associated axonal dysfunction therefore appear as central causes of early HD symptoms.

There are other age-related NDs where axonal dysfunction plays a central role, including glaucoma (Weinreb et al., 2016), progressive supranuclear palsy (Lopez et al., 2016), and vascular dementia (Elahi and Miller, 2017). They share commonalities with the disorders already covered here, and importantly, some of the overlapping symptoms in patients can be caused by accumulation of axonal dysfunction with age, regardless the specific causative gene of each disorder.

CONCLUDING REMARKS

Why some individuals develop neurodegeneration and associated cognitive decline with advanced age, while others are able to preserve the cognitive function, has been the focus of intense research in recent years. However, the exact age-related molecular and cellular changes that trigger this

susceptibility to neurodegeneration remain to be established. Here, we revised the evidence that support the potential role of axonal degeneration in this transition. As discussed in this review, many molecular and cellular changes that occur as organisms age may contribute to the deterioration of axons. Notably, increasing evidence in recent years has raised the awareness of axonal pathology as an early, common contributor to the pathomechanism of different age-related neurological diseases. This pathological overlapping shared by NDs represents an important focus of research not only for the impact in our current understanding of the etiology of this diseases, but also for the drug development field as it might provide potential targets for future therapeutic and, most importantly, preventative strategies aimed at limiting axonal and therefore neuronal degeneration in NDs.

AUTHOR CONTRIBUTIONS

NS, MS planned, researched and wrote the manuscript. PM, FC edited and helped in the planning of the manuscript.

FUNDING

This work was supported by Center for Integrative Biology, Universidad Mayor de Chile, FONDECYT-1150766, Geroscience Center for Brain Health and Metabolism (FONDAP-15150012), FONDECYT Postdoctoral fellowship N° 3170577 (MS), Ring Initiative ACT1109, and Canada-Israel Health Research initiative, jointly Funded by the Canadian Institutes of Health Research, the Israel Science Foundation, the International Development Research Centre, Canada and the Azrieli Foundation, Canada.

REFERENCES

Adalbert, R., and Coleman, M. P. (2013). Review: axon pathology in age-related neurodegenerative disorders. *Neuropathol. Appl. Neurobiol.* 39, 90–108. doi: 10.1111/j.1365-2990.2012.01308.x

Adalbert, R., Nogradi, A., Babetto, E., Janeckova, L., Walker, S. A., Kerschensteiner, M., et al. (2009). Severely dystrophic axons at amyloid plaques remain continuous and connected to viable cell bodies. *Brain* 132, 402–416. doi: 10.1093/brain/awn312

Alami, N. H., Smith, R. B., Carrasco, M. A., Williams, L. A., Winborn, C. S., Han, S. S. W., et al. (2014). Axonal transport of TDP-43 mRNA granules is impaired by ALS-causing mutations. *Neuron* 81, 536–543. doi: 10.1016/j.neuron.2013.12.018

Al-Chalabi, A., van den Berg, L. H., and Veldink, J. (2016). Gene discovery in amyotrophic lateral sclerosis: implications for clinical management. *Nat. Rev. Neurol.* 13, 96–104. doi: 10.1038/nrneurol.2016.182

Alshikho, M. J., Zürcher, N. R., Loggia, M. L., Cernasov, P., Chonde, D. B., Izquierdo Garcia, D., et al. (2016). Glial activation colocalizes with structural abnormalities in amyotrophic lateral sclerosis. *Neurology* 87, 2554–2561. doi: 10.1212/WNL.0000000000003427

Alzheimer's Association (2016). 2016 Alzheimer's disease facts and figures. *Alzheimers Dement.* 12, 459–509. doi: 10.1016/j.jalz.2016.03.001

Araki, T., Sasaki, Y., and Milbrandt, J. (2004). Increased nuclear NAD biosynthesis and SIRT1 activation prevent axonal degeneration. *Science* 305, 1010–1013. doi: 10.1126/science.1098014

Ash, C. E., and Merry, B. J. (2011). The molecular basis by which dietary restricted feeding reduces mitochondrial reactive oxygen species generation. *Mech. Ageing Dev.* 132, 43–54. doi: 10.1016/j.mad.2010.12.001

Avery, M. A., Sheehan, A. E., Kerr, K. S., Wang, J., and Freeman, M. R. (2009). Wld Srequires Nmnat1 enzymatic activity and N16–VCP interactions to suppress Wallerian degeneration. *J. Cell Biol.* 184, 501–513. doi: 10.1083/jcb.200808042

Ayyaz, A., and Jasper, H. (2013). Intestinal inflammation and stem cell homeostasis in aging *Drosophila melanogaster*. *Front. Cell. Infect. Microbiol.* 3:98. doi: 10.3389/fcimb.2013.00098

Baldwin, K. R., Godena, V. K., Hewitt, V. L., and Whitworth, A. J. (2016). Axonal transport defects are a common phenotype in Drosophila models of ALS. *Hum. Mol. Genet.* 15, 2378–2392. doi: 10.1093/hmg/ddw105

Barrientos, S. A., Martinez, N. W., Yoo, S., Jara, J. S., Zamorano, S., Hetz, C., et al. (2011). Axonal degeneration is mediated by the mitochondrial permeability transition pore. *J. Neurosci.* 31, 966–978. doi: 10.1523/JNEUROSCI.4065-10.2011

Bates, G. P., Dorsey, R., Gusella, J. F., Hayden, M. R., Kay, C., Leavitt, B. R., et al. (2015). Huntington disease. *Nat. Rev. Dis. Primers* 26, 15005–15021. doi: 10.1038/nrdp.2015.5

Behl, C., Davis, J. B., Lesley, R., and Schubert, D. (1994). Hydrogen peroxide mediates amyloid beta protein toxicity. *Cell* 77, 817–827. doi: 10.1016/0092-8674(94)90131-7

Belzil, V. V., Bauer, P. O., Gendron, T. F., Murray, M. E., Dickson, D., and Petrucelli, L. (2014). Characterization of DNA hypermethylation in the cerebellum of c9FTD/ALS patients. *Brain Res.* 1584, 15–21. doi: 10.1016/j.brainres.2014.02.015

Bernhardt, D., Muller, H.-P., Ludolph, A. C., Dupuis, L., and Kassubek, J. (2016). Body fat distribution in Parkinson's disease: an MRI-based body fat quantification study. *Parkinsonism Relat. Disord.* 33, 84–89. doi: 10.1016/j.parkreldis.2016.09.016

Blurton-Jones, M., Spencer, B., Michael, S., Castello, N. A., Agazaryan, A. A., Davis, J. L., et al. (2014). Neural stem cells genetically-modified to express neprilysin reduce pathology in Alzheimer transgenic models. *Stem Cell Res. Ther.* 5:46. doi: 10.1186/scrt440

Bongarzone, E. R., Pasquini, J. M., and Soto, E. F. (1995). Oxidative damage to proteins and lipids of CNS myelin produced by *in vitro* generated reactive oxygen species. *J. Neurosci. Res.* 41, 213–221. doi: 10.1002/jnr.490410209

Boyd-Kirkup, J. D., Green, C. D., Wu, G., Wang, D., and Han, J.-D. J. (2013). Epigenomics and the regulation of aging. *Epigenomics* 5, 205–227. doi: 10.2217/epi.13.5

Brehme, M., Voisine, C., Rolland, T., Wachi, S., Soper, J. H., Zhu, Y., et al. (2014). A chaperome subnetwork safeguards proteostasis in aging and neurodegenerative disease. *Cell Rep.* 9, 1135–1150. doi: 10.1016/j.celrep.2014.09.042

Brewer, G. J. (2010). Epigenetic oxidative redox shift (EORS) theory of aging unifies the free radical and insulin signaling theories. *Exp. Gerontol.* 45, 173–179. doi: 10.1016/j.exger.2009.11.007

Bulteau, A.-L., Szweda, L. I., and Friguet, B. (2002). Age-dependent declines in proteasome activity in the heart. *Arch. Biochem. Biophys.* 397, 298–304. doi: 10.1006/abbi.2001.2663

Burnett, C., Valentini, S., Cabreiro, F., Goss, M., Somogyvári, M., Piper, M. D., et al. (2011). Absence of effects of Sir2 overexpression on lifespan in *C. elegans* and Drosophila. *Nature* 477, 482–485. doi: 10.1038/nature10296

Butterfield, D. A., Swomley, A. M., and Sultana, R. (2013). Amyloid β-peptide (1–42)-induced oxidative stress in Alzheimer Disease: importance in disease pathogenesis and progression. *Antioxid. Redox Signal.* 19, 823–835. doi: 10.1089/ars.2012.5027

Calixto, A., Jara, J. S., and Court, F. A. (2012). Diapause formation and downregulation of insulin-like signaling via DAF-16/FOXO delays axonal degeneration and neuronal loss. *PLoS Genet.* 8:e1003141. doi: 10.1371/journal.pgen.1003141

Calliari, A., Bobba, N., Escande, C., and Chini, E. N. (2014). Resveratrol delays Wallerian degeneration in a NAD^+ and DBC1 dependent manner. *Exp. Neurol.* 251, 91–100. doi: 10.1016/j.expneurol.2013.11.013

Carson, M. J., Doose, J. M., Melchior, B., Schmid, C. D., and Ploix, C. C. (2006). CNS immune privilege: hiding in plain sight. *Immunol. Rev.* 213, 48–65. doi: 10.1111/j.1600-065X.2006.00441.x

Carty, M., Goodbody, R., Schroder, M., Stack, J., Moynagh, P. N., and Bowie, A. G. (2006). The human adaptor SARM negatively regulates adaptor protein TRIF-dependent Toll-like receptor signaling. *Nat. Immunol.* 7, 1074–1081. doi: 10.1038/ni1382

Chang, H.-C., and Guarente, L. (2014). SIRT1 and other sirtuins in metabolism. *Trends Endocrinol. Metab.* 25, 138–145. doi: 10.1016/j.tem.2013.12.001

Chen, C.-Y., Lin, C.-W., Chang, C.-Y., Jiang, S.-T., and Hsueh, Y.-P. (2011). Sarm1, a negative regulator of innate immunity, interacts with syndecan-2 and regulates neuronal morphology. *J. Cell Biol.* 193, 769–784. doi: 10.1083/jcb.201008050

Chen, L., Nye, D. M., Stone, M. C., Weiner, A. T., Gheres, K. W., Xiong, X., et al. (2016). Mitochondria and caspases tune nmnat-mediated stabilization to promote axon regeneration. *PLoS Genet.* 12:e1006503. doi: 10.1371/journal.pgen.1006503

Cheng, B., Yang, X., An, L., Gao, B., Liu, X., and Liu, S. (2009). Ketogenic diet protects dopaminergic neurons against 6-OHDA neurotoxicity via up-regulating glutathione in a rat model of Parkinson's disease. *Brain Res.* 1286, 25–31. doi: 10.1016/j.brainres.2009.06.060

Cheng, H. C., Kim, S. R., Oo, T. F., Kareva, T., Yarygina, O., Rzhetskaya, M., et al. (2011). Akt suppresses retrograde degeneration of dopaminergic axons by inhibition of macroautophagy. *J. Neurosci.* 31, 2125–2135. doi: 10.1523/JNEUROSCI.5519-10.2011

Chiotis, K., Saint-Aubert, L., Rodriguez-Vieitez, E., Leuzy, A., Almkvist, O., Savitcheva, I., et al. (2017). Longitudinal changes of tau PET imaging in relation to hypometabolism in prodromal and Alzheimer's disease dementia. *Mol. Psychiatry*. doi: 10.1038/mp.2017.108. [Epub ahead of print].

Choe, M. C. (2016). The pathophysiology of concussion. *Curr. Pain Headache Rep.* 20:42. doi: 10.1007/s11916-016-0573-9

Chondrogianni, N., Georgila, K., Kourtis, N., Tavernarakis, N., and Gonos, E. S. (2015). 20S proteasome activation promotes life span extension and resistance to proteotoxicity in *Caenorhabditis elegans*. *FASEB J.* 29, 611–622. doi: 10.1096/fj.14-252189

Christensen, B. C., Houseman, E. A., Marsit, C. J., Zheng, S., Wrensch, M. R., Wiemels, J. L., et al. (2009). Aging and environmental exposures alter tissue-specific DNA methylation dependent upon CpG island context. *PLoS Genet.* 5:e1000602. doi: 10.1371/journal.pgen.1000602

Chu, Y., Morfini, G. A., Langhamer, L. B., He, Y., Brady, S. T., and Kordower, J. H. (2012). Alterations in axonal transport motor proteins in sporadic and experimental Parkinson's disease. *Brain* 135, 2058–2073. doi: 10.1093/brain/aws133

Chung, C. Y., Khurana, V., Auluck, P. K., Tardiff, D. F., Mazzulli, J. R., Soldner, F., et al. (2013). Identification and rescue of α-synuclein toxicity in Parkinson patient-derived neurons. *Science* 342, 983–987. doi: 10.1126/science.1245296

Chung, C. Y., Koprich, J. B., Siddiqi, H., and Isacson, O. (2009). Dynamic changes in presynaptic and axonal transport proteins combined with striatal neuroinflammation precede dopaminergic neuronal loss in a rat model of AAV -synucleinopathy. *J. Neurosci.* 29, 3365–3373. doi: 10.1523/JNEUROSCI.5427-08.2009

Chung, H. Y., Cesari, M., Anton, S., Marzetti, E., Giovannini, S., Seo, A. Y., et al. (2009). Molecular inflammation: underpinnings of aging and age-related diseases. *Ageing Res. Rev.* 8, 18–30. doi: 10.1016/j.arr.2008.07.002

Cicchetti, F., Saporta, S., Hauser, R. A., Parent, M., Saint-Pierre, M., Sanberg, P. R., et al. (2009). Neural transplants in patients with Huntington's disease undergo disease-like neuronal degeneration. *Proc. Natl. Acad. Sci. U.S.A.* 106, 12483–12488. doi: 10.1073/pnas.0904239106

Cissé, M., Duplan, E., Lorivel, T., Dunys, J., Bauer, C., Meckler, X., et al. (2016). The transcription factor XBP1s restores hippocampal synaptic plasticity and memory by control of the Kalirin-7 pathway in Alzheimer model. *Mol. Psychiatry*. 11:385. doi: 10.1038/mp.2016.152

Cissé, M., Halabisky, B., Harris, J., Devidze, N., Dubal, D. B., Sun, B., et al. (2010). Reversing EphB2 depletion rescues cognitive functions in Alzheimer model. *Nature* 469, 47–52. doi: 10.1038/nature09635

Coleman, M. (2005). Axon degeneration mechanisms: commonality amid diversity. *Nat. Rev. Neurosci.* 6, 889–898. doi: 10.1038/nrn1788

Coleman, M. P., and Freeman, M. R. (2010). Wallerian Degeneration, Wld, S., and Nmnat. *Annu. Rev. Neurosci.* 33, 245–267. doi: 10.1146/annurev-neuro-060909-153248

Cooper, A. A., Gitler, A. D., Cashikar, A., Haynes, C. M., Hill, K. J., Bhullar, B., et al. (2006). Alpha-synuclein blocks ER-golgi traffic and Rab1 rescues neuron loss in Parkinson's Models. *Science* 313, 324–328. doi: 10.1126/science.1129462

Court, F. A., and Coleman, M. P. (2012). Mitochondria as a central sensor for axonal degenerative stimuli. *Trends Neurosci.* 35, 364–372. doi: 10.1016/j.tins.2012.04.001

Cribbs, D. H., Berchtold, N. C., Perreau, V., Coleman, P. D., Rogers, J., Tenner, A. J., et al. (2012). Extensive innate immune gene activation accompanies brain aging, increasing vulnerability to cognitive decline and neurodegeneration: a microarray study. *J. Neuroinflammation* 9:179. doi: 10.1186/1742-2094-9-179

Crook-McMahon, H. M., Oláhová, M., Button, E. L., Winter, J. J., and Veal, E. A. (2014). Genome-wide screening identifies new genes required for stress-induced phase 2 detoxification gene expression in animals. *BMC Biol.* 12:64. doi: 10.1186/s12915-014-0064-6

Cuervo, A. M., and Dice, J. F. (2000). Age-related decline in chaperone-mediated autophagy. *J. Biol. Chem.* 275, 31505–31513. doi: 10.1074/jbc.M002102200

Cummings, J. L., Morstorf, T., and Zhong, K. (2014). Alzheimer's disease drug-development pipeline: few candidates, frequent failures. *Alzheimers Res. Ther.* 6:37. doi: 10.1186/alzrt269

Dadon-Nachum, M., Melamed, E., and Offen, D. (2010). The "Dying-Back" phenomenon of motor neurons in ALS. *J. Mol. Neurosci.* 43, 470–477. doi: 10.1007/s12031-010-9467-1

Dasuri, K., Zhang, L., Ebenezer, P., Liu, Y., Fernandez-Kim, S. O., and Keller, J. N. (2009). Aging and dietary restriction alter proteasome biogenesis and composition in the brain and liver. *Mech. Ageing Dev.* 130, 777–783. doi: 10.1016/j.mad.2009.10.003

De Vos, K. J., Chapman, A. L., Tennant, M. E., Manser, C., Tudor, E. L., Lau, K. F., et al. (2007). Familial amyotrophic lateral sclerosis-linked SOD1 mutants perturb fast axonal transport to reduce axonal mitochondria content. *Hum. Mol. Genet.* 16, 2720–2728. doi: 10.1093/hmg/ddm226

Deckwerth, T. L., and Johnson, E. M. (1994). Neurites can remain viable after destruction of the neuronal soma by programmed cell death (Apoptosis). *Dev. Biol.* 165, 63–72. doi: 10.1006/dbio.1994.1234

Demuro, A., Mina, E., Kayed, R., Milton, S. C., Parker, I., and Glabe, C. G. (2005). Calcium dysregulation and membrane disruption as a ubiquitous neurotoxic mechanism of soluble amyloid oligomers. *J. Biol. Chem.* 280, 17294–17300. doi: 10.1074/jbc.M500997200

Deng, H., Gerencser, A. A., and Jasper, H. (2015). Signal integration by Ca^{2+} regulates intestinal stem-cell activity. *Nature* 528, 212–217. doi: 10.1038/nature16170

Desplats, P., Spencer, B., Crews, L., Pathel, P., Morvinski-Friedmann, D., Kosberg, K., et al. (2012). α-synuclein induces alterations in adult neurogenesis in parkinson disease models via p53-mediated repression of notch1. *J. Biol. Chem.* 287, 31691–31702. doi: 10.1074/jbc.M112.354522

Devi, L. (2006). Accumulation of amyloid precursor protein in the mitochondrial import channels of human Alzheimer's Disease brain is associated with mitochondrial dysfunction. *J. Neurosci.* 26, 9057–9068. doi: 10.1523/JNEUROSCI.1469-06.2006

Di Stefano, M., Loreto, A., Orsomando, G., Mori, V., Zamporlini, F., Hulse, R. P., et al. (2017). NMN deamidase delays wallerian degeneration and rescues axonal defects caused by NMNAT2 deficiency *in vivo*. *Curr. Biol.* 27, 784–794. doi: 10.1016/j.cub.2017.01.070

Druzhyna, N. M., Wilson, G. L., and LeDoux, S. P. (2008). Mitochondrial DNA repair in aging and disease. *Mech. Ageing Dev.* 129, 383–390. doi: 10.1016/j.mad.2008.03.002

Du, H., Guo, L., Fang, F., Chen, D., Sosunov, A. A., McKhann, G. M., et al. (2008). Cyclophilin D deficiency attenuates mitochondrial and neuronal perturbation and ameliorates learning and memory in Alzheimer's disease. *Nat. Med.* 14, 1097–1105. doi: 10.1038/nm.1868

Duan, W., Guo, Z., Jiang, H., Ware, M., Li, X.-J., and Mattson, M. P. (2003). Dietary restriction normalizes glucose metabolism and BDNF levels, slows disease progression, and increases survival in huntingtin mutant mice. *Proc. Natl. Acad. Sci. U.S.A.* 100, 2911–2916. doi: 10.1073/pnas.0536856100

Dunn, L., Allen, G. F., Mamais, A., Ling, H., Li, A., Duberley, K. E., et al. (2014). Dysregulation of glucose metabolism is an early event in sporadic Parkinson's disease. *Neurobiol. Aging* 35, 1111–1115. doi: 10.1016/j.neurobiolaging.2013.11.001

Duran-Aniotz, C., Cornejo, V. H., Espinoza, S., Ardiles, Á. O., Medinas, D. B., Salazar, C., et al. (2017). IRE1 signaling exacerbates Alzheimer's disease pathogenesis. *Acta Neuropathol.* doi: 10.1007/s00401-017-1694-x. [Epub ahead of print].

Egawa, N., Yamamoto, K., Inoue, H., Hikawa, R., Nishi, K., Mori, K., et al. (2011). The endoplasmic reticulum stress sensor, ATF6, protects against neurotoxin-induced dopaminergic neuronal death. *J. Biol. Chem.* 286, 7947–7957. doi: 10.1074/jbc.M110.156430

Elahi, F. M., and Miller, B. L. (2017). A clinicopathological approach to the diagnosis of dementia. *Nat. Rev. Neurol.* 13, 457–476. doi: 10.1038/nrneurol.2017.96

Esanov, R., Belle, K. C., van Blitterswijk, M., Belzil, V. V., Rademakers, R., Dickson, D. W., et al. (2016). C9orf72 promoter hypermethylation is reduced while hydroxymethylation is acquired during reprogramming of ALS patient cells. *Exp. Neurol.* 277, 171–177. doi: 10.1016/j.expneurol.2015.12.022

Essuman, K., Summers, D. W., Sasaki, Y., Mao, X., DiAntonio, A., and Milbrandt, J. (2017). The SARM1 toll/interleukin-1 receptor domain possesses intrinsic NAD+ cleavage activity that promotes pathological axonal degeneration. *Neuron* 93, 1334.e5–1343.e5. doi: 10.1016/j.neuron.2017.02.022

Fairbairn, N. G., Meppelink, A. M., Ng-Glazier, J., Randolph, M. A., and Winograd, J. M. (2015). Augmenting peripheral nerve regeneration using stem cells: A review of current opinion. *World J. Stem Cells* 7, 11–26. doi: 10.4252/wjsc.v7.i1.11

Fang, Y., Soares, L., Teng, X., Geary, M., and Bonini, N. M. (2012). A novel Drosophila model of nerve injury reveals an essential role of nmnat in maintaining axonal integrity. *Curr. Biol.* 22, 590–595. doi: 10.1016/j.cub.2012.01.065

Fargnoli, J., Kunisada, T., Fornace, A. J., Schneider, E. L., and Holbrook, N. J. (1990). Decreased expression of heat shock protein 70 mRNA and protein after heat treatment in cells of aged rats. *Proc. Natl. Acad. Sci. U.S.A.* 87, 846–850. doi: 10.1073/pnas.87.2.846

Fernandez-Santiago, R., Carballo-Carbajal, I., Castellano, G., Torrent, R., Richaud, Y., Sanchez-Danes, A., et al. (2015). Aberrant epigenome in iPSC-derived dopaminergic neurons from Parkinson's disease patients. *EMBO Mol. Med.* 7, 1529–1546. doi: 10.15252/emmm.201505439

Ferraiuolo, L., Kirby, J., Grierson, A. J., Sendtner, M., and Shaw, P. J. (2011). Molecular pathways of motor neuron injury in amyotrophic lateral sclerosis. *Nat. Rev. Neurol.* 7, 616–630. doi: 10.1038/nrneurol.2011.152

Ferrington, D. A. (2005). Altered proteasome structure, function, and oxidation in aged muscle. *FASEB J.* 19, 644–646. doi: 10.1096/fj.04-2578fje

Ferron, S. R., Marques-Torrejon, M. A., Mira, H., Flores, I., Taylor, K., Blasco, M. A., et al. (2009). Telomere shortening in neural stem cells disrupts neuronal differentiation and neuritogenesis. *J. Neurosci.* 29, 14394–14407. doi: 10.1523/JNEUROSCI.3836-09.2009

Filareti, M., Luotti, S., Pasetto, L., Pignataro, M., Paolella, K., Messina, P., et al. (2017). Decreased levels of foldase and chaperone proteins are associated with an early-onset amyotrophic lateral sclerosis. *Front. Mol. Neurosci.* 10:99. doi: 10.3389/fnmol.2017.00099

Fischer, L. R., Culver, D. G., Davis, A. A., Tennant, P., Wang, M., Coleman, M., et al. (2005). The WldS gene modestly prolongs survival in the SOD1G93A fALS mouse. *Neurobiol. Dis.* 19, 293–300. doi: 10.1016/j.nbd.2005.01.008

Fischer, L. R., Culver, D. G., Tennant, P., Davis, A. A., Wang, M., Castellano-Sanchez, A., et al. (2004). Amyotrophic lateral sclerosis is a distal axonopathy: evidence in mice and man. *Exp. Neurol.* 185, 232–240. doi: 10.1016/j.expneurol.2003.10.004

Fogh, I., Ratti, A., Gellera, C., Lin, K., Tiloca, C., Moskvina, V., et al. (2014). A genome-wide association meta-analysis identifies a novel locus at 17q11.2 associated with sporadic amyotrophic lateral sclerosis. *Hum. Mol. Genet.* 23, 2220–2231. doi: 10.1093/hmg/ddt587

Fredriksson, Å., Johansson Krogh, E., Hernebring, M., Pettersson, E., Javadi, A., Almstedt, A., et al. (2012). Effects of aging and reproduction on protein quality control in soma and gametes of *Drosophila melanogaster*. *Aging Cell* 11, 634–643. doi: 10.1111/j.1474-9726.2012.00823.x

Friedman, L. G., Lachenmayer, M. L., Wang, J., He, L., Poulose, S. M., Komatsu, M., et al. (2012). Disrupted autophagy leads to dopaminergic axon and dendrite degeneration and promotes presynaptic accumulation of α-synuclein and LRRK2 in the brain. *J. Neurosci.* 32, 7585–7593. doi: 10.1523/JNEUROSCI.5809-11.2012

Frost, B., Hemberg, M., Lewis, J., and Feany, M. B. (2014). Tau promotes neurodegeneration through global chromatin relaxation. *Nat. Neurosci.* 17, 357–366. doi: 10.1038/nn.3639

Fu, K.-Y., Dai, L.-G., Chiu, I.-M., Chen, J.-R., and Hsu, S.-H. (2011). Sciatic nerve regeneration by microporous nerve conduits seeded with glial cell line-derived neurotrophic factor or brain-derived neurotrophic factor gene transfected neural stem cells. *Artif. Organs* 35, 363–372. doi: 10.1111/j.1525-1594.2010.01105.x

Fulda, S., Gorman, A. M., Hori, O., and Samali, A. (2010). Cellular stress responses: cell survival and cell death. *Int. J. Cell Biol.* 2010, 1–23. doi: 10.1155/2010/214074

Furukawa, K., Barger, S. W., Blalock, E. M., and Mattson, M. P. (1996). Activation of K channels and suppression of neuronal activity by secreted β-amyloid-precursor protein. *Nature* 379, 74–78. doi: 10.1038/379074a0

Galluzzi, L., Pietrocola, F., Levine, B., and Kroemer, G. (2014). Metabolic control of autophagy. *Cell* 159, 1263–1276. doi: 10.1016/j.cell.2014.11.006

Gao, H. M., Kotzbauer, P. T., Uryu, K., Leight, S., Trojanowski, J. Q., and Lee, V. M. Y. (2008). Neuroinflammation and oxidation/nitration of alpha-synuclein linked to dopaminergic neurodegeneration. *J. Neurosci.* 28, 7687–7698. doi: 10.1523/JNEUROSCI.0143-07.2008

Gatto, R. G., Chu, Y., Ye, A. Q., Price, S. D., Tavassoli, E., Buenaventura, A., et al. (2015). Analysis of YFP(J16)-R6/2 reporter mice and postmortem brains reveals early pathology and increased vulnerability of callosal axons in Huntington's disease. *Hum. Mol. Genet.* 24, 5285–5298. doi: 10.1093/hmg/ddv248

Genzer, Y., Dadon, M., Burg, C., Chapnik, N., and Froy, O. (2016). Effect of dietary fat and the circadian clock on the expression of brain-derived neurotrophic factor (BDNF). *Mol. Cell. Endocrinol.* 430, 49–55. doi: 10.1016/j.mce.2016.04.015

Gerdts, J., Brace, E. J., Sasaki, Y., DiAntonio, A., and Milbrandt, J. (2015). SARM1 activation triggers axon degeneration locally via NAD^+ destruction. *Science* 348, 453–457. doi: 10.1126/science.1258366

Gerhard, A., Pavese, N., Hotton, G., Turkheimer, F., Es, M., Hammers, A., et al. (2006). *In vivo* imaging of microglial activation with [11C](R)-PK11195 PET in idiopathic Parkinson's disease. *Neurobiol. Dis.* 21, 404–412. doi: 10.1016/j.nbd.2005.08.002

Ghosh, D., LeVault, K. R., Barnett, A. J., and Brewer, G. J. (2012). A reversible early oxidized redox state that precedes macromolecular ros damage in aging nontransgenic and 3xTg-AD mouse neurons. *J. Neurosci.* 32, 5821–5832. doi: 10.1523/JNEUROSCI.6192-11.2012

Gillen, C., Jander, S., and Stoll, G. (1998). Sequential expression of mRNA for proinflammatory cytokines and interleukin-10 in the rat peripheral nervous system: comparison between immune-mediated demyelination and wallerian degeneration. *J. Neurosci. Res.* 51, 489–496. doi: 10.1002/(SICI)1097-4547(19980215)51:4<489::AID-JNR8>3.0.CO;2-8

Gomez-Sanchez, J. A., Gomis-Coloma, C., Morenilla-Palao, C., Peiro, G., Serra, E., Serrano, M., et al. (2013). Epigenetic induction of the Ink4a/Arf locus prevents Schwann cell overproliferation during nerve regeneration and after tumorigenic challenge. *Brain* 136, 2262–2278. doi: 10.1093/brain/awt130

Gonzalez-Horta, A. (2015). The interaction of alpha-synuclein with membranes and its implication in Parkinson's Disease: a literature review. *Nat. Prod. Commun.* 10, 1775–1778.

Gowers, I. R., Walters, K., Kiss-Toth, E., Read, R. C., Duff, G. W., and Wilson, A. G. (2011). Age-related loss of CpG methylation in the tumour necrosis factor promoter. *Cytokine* 56, 792–797. doi: 10.1016/j.cyto.2011.09.009

Grayson, M. (2010). Nutrigenomics. *Nature* 468:S1. doi: 10.1038/468S1a

Hamilton, R., Walsh, M., Singh, R., Rodriguez, K., Gao, X., Rahman, M. M., et al. (2016). Oxidative damage to myelin proteins accompanies peripheral nerve motor dysfunction in aging C57BL/6 male mice. *J. Neurol. Sci.* 370, 47–52. doi: 10.1016/j.jns.2016.09.021

Hampton, D. W., Webber, D. J., Bilican, B., Goedert, M., Spillantini, M. G., and Chandran, S. (2010). Cell-mediated neuroprotection in

a mouse model of human tauopathy. *J. Neurosc.* 30, 9973–9983. doi: 10.1523/JNEUROSCI.0834-10.2010

Han, B. H., Zhou, M.-L., Johnson, A. W., Singh, I., Liao, F., Vellimana, A. K., et al. (2015). Contribution of reactive oxygen species to cerebral amyloid angiopathy, vasomotor dysfunction, and microhemorrhage in aged Tg2576 mice. *Proc. Natl. Acad. Sci. U.S.A.* 112, E881–E890. doi: 10.1073/pnas.1414930112

Han, S., Choi, J.-R., Soon Shin, K., and Kang, S. J. (2012). Resveratrol upregulated heat shock proteins and extended the survival of G93A-SOD1 mice. *Brain Res.* 1483, 112–117. doi: 10.1016/j.brainres.2012.09.022

Harding, H. P., Zhang, Y., and Ron, D. (1999). Protein translation and folding are coupled by an endoplasmic-reticulum-resident kinase. *Nature* 397, 271–274. doi: 10.1038/16729

Harman, D. (1956). Aging: a theory based on free radical and radiation chemistry. *J. Gerontol.* 11, 298–300. doi: 10.1093/geronj/11.3.298

Haze, K., Yoshida, H., Yanagi, H., Yura, T., and Mori, K. (1999). Mammalian transcription factor ATF6 is synthesized as a transmembrane protein and activated by proteolysis in response to endoplasmic reticulum stress. *Mol. Biol. Cell* 10, 3787–3799. doi: 10.1091/mbc.10.11.3787

He, M., Ding, Y., Chu, C., Tang, J., Xiao, Q., and Luo, Z.-G. (2016). Autophagy induction stabilizes microtubules and promotes axon regeneration after spinal cord injury. *Proc. Natl. Acad. Sci. U.S.A.* 113, 11324–11329. doi: 10.1073/pnas.1611282113

Henis-Korenblit, S., Zhang, P., Hansen, M., McCormick, M., Lee, S.-J., Cary, M., et al. (2010). Insulin/IGF-1 signaling mutants reprogram ER stress response regulators to promote longevity. *Proc. Natl. Acad. Sci. U.S.A.* 107, 9730–9735. doi: 10.1073/pnas.1002575107

Hensley, K., Carney, J. M., Mattson, M. P., Aksenova, M., Harris, M., Wu, J. F., et al. (1994). A model for beta-amyloid aggregation and neurotoxicity based on free radical generation by the peptide: relevance to Alzheimer disease. *Proc. Natl. Acad. Sci. U.S.A.* 91, 3270–3274. doi: 10.1073/pnas.91.8.3270

Hernandez, D. G., Nalls, M. A., Gibbs, J. R., Arepalli, S., van der Brug, M., Chong, S., et al. (2011). Distinct DNA methylation changes highly correlated with chronological age in the human brain. *Hum. Mol. Genet.* 20, 1164–1172. doi: 10.1093/hmg/ddq561

Hetz, C., Thielen, P., Matus, S., Nassif, M., Court, F., Kiffin, R., et al. (2009). XBP-1 deficiency in the nervous system protects against amyotrophic lateral sclerosis by increasing autophagy. *Genes Dev.* 23, 2294–2306. doi: 10.1101/gad.1830709

Hill, S. J., Mordes, D. A., Cameron, L. A., Neuberg, D. S., Landini, S., Eggan, K., et al. (2016). Two familial ALS proteins function in prevention/repair of transcription-associated DNA damage. *Proc. Natl. Acad. Sci. U.S.A.* 113, E7701–E7709. doi: 10.1073/pnas.1611673113

Höglinger, G. U., Rizk, P., Muriel, M. P., Duyckaerts, C., Oertel, W. H., Caille, I., et al. (2004). Dopamine depletion impairs precursor cell proliferation in Parkinson disease. *Nat. Neurosci.* 7, 726–735. doi: 10.1038/nn1265

Holth, J. K., Patel, T. K., and Holtzman, D. M. (2017). Sleep in Alzheimer's Disease–beyond amyloid. *Neurobiol. Sleep Circadian Rhythms* 2, 4–14. doi: 10.1016/j.nbscr.2016.08.002

Hoozemans, J. J. M., van Haastert, E. S., Nijholt, D. A. T., Rozemuller, A. J. M., Eikelenboom, P., and Scheper, W. (2009). The unfolded protein response is activated in pretangle neurons in Alzheimer's disease hippocampus. *Am. J. Pathol.* 174, 1241–1251. doi: 10.2353/ajpath.2009.080814

Hoozemans, J. J. M., Veerhuis, R., Van Haastert, E. S., Rozemuller, J. M., Baas, F., Eikelenboom, P., et al. (2005). The unfolded protein response is activated in Alzheimer's disease. *Acta Neuropathol.* 110, 165–172. doi: 10.1007/s00401-005-1038-0

Hu, Y., Park, K. K., Yang, L., Wei, X., Yang, Q., Cho, K.-S., et al. (2012). Differential effects of unfolded protein response pathways on axon injury-induced death of retinal ganglion cells. *Neuron* 73, 445–452. doi: 10.1016/j.neuron.2011.11.026

Hussain, S. G., and Ramaiah, K. V. A. (2007). Reduced eIF2α phosphorylation and increased proapoptotic proteins in aging. *Biochem. Biophys. Res. Commun.* 355, 365–370. doi: 10.1016/j.bbrc.2007.01.156

Imai, Y., Soda, M., Inoue, H., Hattori, N., Mizuno, Y., and Takahashi, R. (2001). An unfolded putative transmembrane polypeptide, which can lead to endoplasmic reticulum stress, is a substrate of Parkin. *Cell* 105, 891–902. doi: 10.1016/S0092-8674(01)00407-X

Imaizumi, Y., Okada, Y., Akamatsu, W., Koike, M., Kuzumaki, N., Hayakawa, H., et al. (2012). Mitochondrial dysfunction associated with increased oxidative stress and alpha-synuclein accumulation in PARK2 iPSC-derived neurons and postmortem brain tissue. *Mol. Brain* 5:35. doi: 10.1186/1756-6606-5-35

Inoue, K., Tsutsui, H., Akatsu, H., Hashizume, Y., Matsukawa, N., Yamamoto, T., et al. (2013). Metabolic profiling of Alzheimer's disease brains. *Sci. Rep.* 3, 795–799. doi: 10.1038/srep02364

Ito, Y., Ofengeim, D., Najafov, A., Das, S., Saberi, S., Li, Y., et al. (2016). RIPK1 mediates axonal degeneration by promoting inflammation and necroptosis in ALS. *Science* 353, 603–608. doi: 10.1126/science.aaf6803

Jasper, H. (2013). Sirtuins: longevity focuses on NAD. *Nat. Chem. Biol.* 9, 666–667. doi: 10.1038/nchembio.1369

Jeong, M.-A., Plunet, W., Streijger, F., Lee, J. H. T., Plemel, J. R., Park, S., et al. (2011). Intermittent fasting improves functional recovery after rat thoracic contusion spinal cord injury. *J. Neurotrauma* 28, 479–492. doi: 10.1089/neu.2010.1609

Johnson, R., Zuccato, C., Belyaev, N. D., Guest, D. J., Cattaneo, E., and Buckley, N. J. (2008). A microRNA-based gene dysregulation pathway in Huntington's disease. *Neurobiol. Dis.* 29, 438–445. doi: 10.1016/j.nbd.2007.11.001

Johnson, V. E., Stewart, W., and Smith, D. H. (2011). Widespread tau and amyloid-beta pathology many years after a single traumatic brain injury in humans. *Brain Pathol.* 22, 142–149. doi: 10.1111/j.1750-3639.2011.00513.x

Jonsson, T., Stefansson, H., Steinberg, S., Jonsdottir, I., Jonsson, P. V., Snaedal, J., et al. (2013). Variant of TREM2 associated with the risk of Alzheimer's disease. *N. Engl. J. Med.* 368, 107–116. doi: 10.1056/NEJMoa1211103

Jowaed, A., Schmitt, I., Kaut, O., and Wullner, U. (2010). Methylation regulates alpha-synuclein expression and is decreased in parkinson"s disease patients" brains. *J. Neurosci.* 30, 6355–6359. doi: 10.1523/JNEUROSCI.6119-09.2010

Julien, J.-P., and Kriz, J. (2006). Transgenic mouse models of amyotrophic lateral sclerosis. *Biochim. Biophys. Acta Mol. Basis Dis.* 1762, 1013–1024. doi: 10.1016/j.bbadis.2006.03.006

Karin, M., and Clevers, H. (2016). Reparative inflammation takes charge of tissue regeneration. *Nature* 529, 307–315. doi: 10.1038/nature17039

Kashiwaya, Y., Bergman, C., Lee, J.-H., Wan, R., King, M. T., Mughal, M. R., et al. (2013). A ketone ester diet exhibits anxiolytic and cognition-sparing properties, and lessens amyloid and tau pathologies in a mouse model of Alzheimer's disease. *Neurobiol. Aging* 34, 1530–1539. doi: 10.1016/j.neurobiolaging.2012.11.023

Kashiwaya, Y., Takeshima, T., Mori, N., Nakashima, K., Clarke, K., and Veech, R. L. (2000). D-beta-hydroxybutyrate protects neurons in models of Alzheimer's and Parkinson's disease. *Proc. Natl. Acad. Sci. U.S.A.* 97, 5440–5444. doi: 10.1073/pnas.97.10.5440

Keller, L., Lincoln, B., Albasi, S., Frendo, N., Freund, R., and Keller, L. (2015). Drosophila neuronal injury follows a temporal sequence of cellular events leading to degeneration at the neuromuscular junction. *J. Exp. Neurosci.* 9(Suppl. 2), 1–9. doi: 10.4137/JEN.S25516

Kennedy, B. K., Berger, S. L., Brunet, A., Campisi, J., Cuervo, A. M., Epel, E. S., et al. (2014). Geroscience: linking aging to chronic disease. *Cell* 159, 709–713. doi: 10.1016/j.cell.2014.10.039

Kerr, J. S., Adriaanse, B. A., Greig, N. H., Mattson, M. P., Cader, M. Z., Bohr, V. A., et al. (2017). Mitophagy and Alzheimer's Disease: cellular and molecular mechanisms. *Trends Neurosci.* 40, 151–166. doi: 10.1016/j.tins.2017.01.002

Kigerl, K. A., Gensel, J. C., Ankeny, D. P., Alexander, J. K., Donnelly, D. J., and Popovich, P. G. (2009). Identification of two distinct macrophage subsets with divergent effects causing either neurotoxicity or regeneration in the injured mouse spinal cord. *J. Neurosci.* 29, 13435–13444. doi: 10.1523/JNEUROSCI.3257-09.2009

Kikuchi, H., Furuta, A., Nishioka, K.-I., Suzuki, S., Nakabeppu, Y., and Iwaki, T. (2002). Impairment of mitochondrial DNA repair enzymes against accumulation of 8-oxo-guanine in the spinal motor neurons of amyotrophic lateral sclerosis. *Acta Neuropathol.* 103, 408–414. doi: 10.1007/s00401-001-0480-x

Kim, H. J., Jung, K. J., Yu, B. P., Cho, C. G., Choi, J. S., and Chung, H. Y. (2002). Modulation of redox-sensitive transcription factors by calorie restriction during aging. *Mech. Ageing Dev.* 123, 1589–1595. doi: 10.1016/S0047-6374(02)00094-5

Kim, S. R., Kareva, T., Yarygina, O., Kholodilov, N., and Burke, R. E. (2009). AAV transduction of dopamine neurons with constitutively active Rheb protects from neurodegeneration and mediates axon regrowth. *Mol. Ther.* 20, 275–286. doi: 10.1038/mt.2011.213

Kim, Y., Zhou, P., Qian, L., Chuang, J.-Z., Lee, J., Li, C., et al. (2007). MyD88-5 links mitochondria, microtubules, and JNK3 in neurons and regulates neuronal survival. *J. Exp. Med.* 204, 2063–2074. doi: 10.1084/jem.20070868

Knowles, R. B., Wyart, C., Buldyrev, S. V., Cruz, L., Urbanc, B., Hasselmo, M. E., et al. (1999). Plaque-induced neurite abnormalities: implications for disruption of neural networks in Alzheimer's disease. *Proc. Natl. Acad. Sci. U.S.A.* 96, 5274–5279. doi: 10.1073/pnas.96.9.5274

Koh, K., Evans, J. M., Hendricks, J. C., and Sehgal, A. (2006). A Drosophila model for age-associated changes in sleep:wake cycles. *Proc. Natl. Acad. Sci. U.S.A.* 103, 13843–13847. doi: 10.1073/pnas.0605903103

Komatsu, M., Wang, Q. J., Holstein, G. R., Victor L Friedrich, J., Iwata, J.-I., Kominami, E., et al. (2007). Essential role for autophagy protein Atg7 in the maintenance of axonal homeostasis and the prevention of axonal degeneration. *Proc. Natl. Acad. Sci. U.S.A.* 104, 14489–14494. doi: 10.1073/pnas.0701311104

Körner, S., Böselt, S., Thau, N., Rath, K. J., Dengler, R., and Petri, S. (2013). Differential sirtuin expression patterns in amyotrophic lateral sclerosis (ALS) postmortem tissue: neuroprotective or neurotoxic properties of sirtuins in ALS? *Neurodegener. Dis.* 11, 141–152. doi: 10.1159/000338048

Kruegel, U., Robison, B., Dange, T., Kahlert, G., Delaney, J. R., Kotireddy, S., et al. (2011). Elevated proteasome capacity extends replicative lifespan in *Saccharomyces cerevisiae*. *PLoS Genet.* 7:e1002253. doi: 10.1371/journal.pgen.1002253

Kurowska, Z., Kordower, J. H., Stoessl, A. J., Burke, R. E., Brundin, P., Yue, Z., et al. (2016). Is axonal degeneration a key early event in Parkinson's Disease? *J. Parkinsons Dis.* 6, 703–707. doi: 10.3233/JPD-160881

Labbadia, J., and Morimoto, R. I. (2015). The biology of proteostasis in aging and disease. *Annu. Rev. Biochem.* 84, 435–464. doi: 10.1146/annurev-biochem-060614-033955

Labunskyy, V. M., Gerashchenko, M. V., Delaney, J. R., Kaya, A., Kennedy, B. K., Kaeberlein, M., et al. (2014). Lifespan extension conferred by endoplasmic reticulum secretory pathway deficiency requires induction of the unfolded protein response. *PLoS Genet.* 10:e1004019. doi: 10.1371/journal.pgen.1004019

Ladd, A. C., Brohawn, D. G., Thomas, R. R., Keeney, P. M., Berr, S. S., Khan, S. M., et al. (2017). RNA-seq analyses reveal that cervical spinal cords and anterior motor neurons from amyotrophic lateral sclerosis subjects show reduced expression of mitochondrial DNA-encoded respiratory genes, and rhTFAM may correct this respiratory deficiency. *Brain Res.* 1667, 74–83. doi: 10.1016/j.brainres.2017.05.010

Lam, L., Chin, L., Halder, R. C., Sagong, B., Famenini, S., Sayre, J., et al. (2016). Epigenetic changes in T-cell and monocyte signatures and production of neurotoxic cytokines in ALS patients. *FASEB J.* 30, 3461–3473. doi: 10.1096/fj.201600259RR

Launay, N., Aguado, C., Fourcade, S., Ruiz, M., Grau, L., Riera, J., et al. (2014). Autophagy induction halts axonal degeneration in a mouse model of X-adrenoleukodystrophy. *Acta Neuropathol.* 129, 399–415. doi: 10.1007/s00401-014-1378-8

Lee, S.-T., Chu, K., Im, W.-S., Yoon, H.-J., Im, J.-Y., Park, J.-E., et al. (2011). Altered microRNA regulation in Huntington's disease models. *Exp. Neurol.* 227, 172–179. doi: 10.1016/j.expneurol.2010.10.012

Li, H., Li, S. H., Yu, Z. X., Shelbourne, P., and Li, X. J. (2001). Huntingtin aggregate-associated axonal degeneration is an early pathological event in Huntington's disease mice. *J. Neurosci.* 21, 8473–8481.

Li, J.-Y., and Conforti, L. (2013). Axonopathy in Huntington's disease. *Exp. Neurol.* 246, 62–71. doi: 10.1016/j.expneurol.2012.08.010

Li, L.-S., Lu, Y.-L., Nie, J., Xu, Y.-Y., Zhang, W., Yang, W.-J., et al. (2017). Dendrobium nobileLindl alkaloid, a novel autophagy inducer, protects against axonal degeneration induced by Aβ 25-35in hippocampus neurons *in vitro*. *CNS Neurosci. Ther.* 23, 329–340. doi: 10.1111/cns.12678

Li, S., Yang, L., Selzer, M. E., and Hu, Y. (2013). Neuronal endoplasmic reticulum stress in axon injury and neurodegeneration. *Ann. Neurol.* 74, 768–777. doi: 10.1002/ana.24005

Li, Y., Liu, W., Oo, T. F., Wang, L., Tang, Y., Jackson-Lewis, V., et al. (2009). Mutant LRRK2R1441G BAC transgenic mice recapitulate cardinal features of Parkinson's disease. *Nat. Neurosci.* 12, 826–828. doi: 10.1038/nn.2349

Liefner, M., Siebert, H., Sachse, T., Michel, U., Kollias, G., and Brück, W. (2000). The role of TNF-alpha during Wallerian degeneration. *J. Neuroimmunol.* 108, 147–152. doi: 10.1016/S0165-5728(00)00262-9

Lin, C.-W., Liu, H.-Y., Chen, C.-Y., and Hsueh, Y.-P. (2014). Neuronally-expressed Sarm1 regulates expression of inflammatory and antiviral cytokines in brains. *Innate Immun.* 20, 161–172. doi: 10.1177/1753425913485877

Lindvall, O. (2013). Developing dopaminergic cell therapy for Parkinson's disease–give up or move forward? *Mov. Disord.* 28, 268–273. doi: 10.1002/mds.25378

Lipinski, M. M., Zheng, B., Lu, T., Yan, Z., Py, B. F., Ng, A., et al. (2010). Genome-wide analysis reveals mechanisms modulating autophagy in normal brain aging and in Alzheimer's disease. *Proc. Natl. Acad. Sci. U.S.A.* 107, 14164–14169. doi: 10.1073/pnas.1009485107

Lipsky, M. S., and King, M. (2015). Biological theories of aging. *Dis. Mon.* 61, 460–466. doi: 10.1016/j.disamonth.2015.09.005

Liu, H., Wang, H., Shenvi, S., Hagen, T. M., and Liu, R. M. (2004). Glutathione metabolism during aging and in Alzheimer Disease. *Ann. N. Y. Acad. Sci.* 1019, 346–349. doi: 10.1196/annals.1297.059

Liu, K., Lu, Y., Lee, J. K., Samara, R., Willenberg, R., Sears-Kraxberger, I., et al. (2010). PTEN deletion enhances the regenerative ability of adult corticospinal neurons. *Nat. Neurosci.* 13, 1075–1081. doi: 10.1038/nn.2603

Liu, L., Zhang, K., Sandoval, H., Yamamoto, S., Jaiswal, M., Sanz, E., et al. (2015). Glial lipid droplets and ROS induced by mitochondrial defects promote neurodegeneration. *Cell* 160, 177–190. doi: 10.1016/j.cell.2014.12.019

Logroscino, G., Marder, K., Graziano, J., Freyer, G., Slavkovich, V., LoIacono, N., et al. (1997). Altered systemic iron metabolism in Parkinson's disease. *Neurology* 49, 714–717. doi: 10.1212/WNL.49.3.714

Lopez, G., Bayulkem, K., and Hallett, M. (2016). Progressive supranuclear palsy (PSP): Richardson syndrome and other PSP variants. *Acta Neurol. Scand.* 134, 242–249. doi: 10.1111/ane.12546

Lopez-Gonzalez, R., Lu, Y., Gendron, T. F., Karydas, A., Tran, H., Yang, D., et al. (2016). Poly(GR) in C9ORF72-related ALS/FTD compromises mitochondrial function and increases oxidative stress and DNA damage in iPSC-derived motor neurons. *Neuron* 92, 383–391. doi: 10.1016/j.neuron.2016.09.015

Lucchinetti, C., and Bruck, W. (2004). The pathology of primary progressive multiple sclerosis. *Mult. Scler.* 10(Suppl. 1), S23–S30. doi: 10.1191/1352458504ms1027oa

Ludolph, A. C., Bendotti, C., Blaugrund, E., Hengerer, B., Löffler, J. P., Martin, J., et al. (2009). Guidelines for the preclinical *in vivo* evaluation of pharmacological active drugs for ALS/MND: report on the 142nd ENMC international workshop. *Amyotroph. Lateral Scler.* 8, 217–223. doi: 10.1080/17482960701292837

Mack, T. G. A., Reiner, M., Beirowski, B., Mi, W., Emanuelli, M., Wagner, D., et al. (2001). Wallerian degeneration of injured axons and synapses is delayed by a Ube4b/Nmnat chimeric gene. *Nat. Neurosci.* 4, 1199–1206. doi: 10.1038/nn770

MacPherson, K. P., Sompol, P., Kannarkat, G. T., Chang, J., Sniffen, L., Wildner, M. E., et al. (2017). Peripheral administration of the soluble TNF inhibitor XPro1595 modifies brain immune cell profiles, decreases beta-amyloid plaque load, and rescues impaired long-term potentiation in 5xFAD mice. *Neurobiol. Dis.* 10, 81–95. doi: 10.1016/j.nbd.2017.02.010

Maday, S., and Holzbaur, E. L. F. (2014). Autophagosome biogenesis in primary neurons follows an ordered and spatially regulated pathway. *Dev. Cell* 30, 71–85. doi: 10.1016/j.devcel.2014.06.001

Madeo, F., Zimmermann, A., Maiuri, M. C., and Kroemer, G. (2015). Essential role for autophagy in life span extension. *J. Clin. Invest.* 125, 85–93. doi: 10.1172/JCI73946

Madji Hounoum, B., Mavel, S., Coque, E., Patin, F., Vourc'h, P., Marouillat, S., et al. (2017). Wildtype motoneurons, ALS-Linked SOD1 mutation and glutamate profoundly modify astrocyte metabolism and lactate shuttling. *Glia* 65, 592–605. doi: 10.1002/glia.23114

Madorsky, I., Opalach, K., Waber, A., Verrier, J. D., Solmo, C., Foster, T., et al. (2009). Intermittent fasting alleviates the neuropathic phenotype in a mouse model of Charcot-Marie-Tooth disease. *Neurobiol. Dis.* 34, 146–154. doi: 10.1016/j.nbd.2009.01.002

Maglemose, R., Hedegaard, A., Lehnhoff, J., Dimintiyanova, K. P., Moldovan, M., Grøndahl, L., et al. (2017). Potassium channel abnormalities are consistent with early axon degeneration of motor axons in the G127X SOD1 mouse model of amyotrophic lateral sclerosis. *Exp. Neurol.* 292, 154–167. doi: 10.1016/j.expneurol.2017.03.008

Magrané, J., Cortez, C., Gan, W.-B., and Manfredi, G. (2014). Abnormal mitochondrial transport and morphology are common pathological

denominators in SOD1 and TDP43 ALS mouse models. *Hum. Mol. Genet.* 23, 1413–1424. doi: 10.1093/hmg/ddt528

Majmundar, A. J., Wong, W. J., and Simon, M. C. (2010). Hypoxia-inducible factors and the response to hypoxic stress. *Mol. Cell* 40, 294–309. doi: 10.1016/j.molcel.2010.09.022

Malapati, H., Millen, S. M., and, J., Buchser, W. (2017). The axon degeneration gene SARM1 is evolutionarily distinct from other TIR domain-containing proteins. *Mol. Genet. Genomics* 292, 909–922. doi: 10.1007/s00438-017-1320-6

Mantuano, E., Henry, K., Yamauchi, T., Hiramatsu, N., Yamauchi, K., Orita, S., et al. (2011). The unfolded protein response is a major mechanism by which LRP1 regulates schwann cell survival after injury. *J. Neurosci.* 31, 13376–13385. doi: 10.1523/JNEUROSCI.2850-11.2011

Marangoni, M., Adalbert, R., Janeckova, L., Patrick, J., Kohli, J., Coleman, M. P., et al. (2014). Age-related axonal swellings precede other neuropathological hallmarks in a knock-in mouse model of Huntington's disease. *Neurobiol. Aging* 35, 2382–2393. doi: 10.1016/j.neurobiolaging.2014.04.024

Marsh, S. E., and Blurton-Jones, M. (2017). Neural stem cell therapy for neurodegenerative disorders: the role of neurotrophic support. *Neurochem. Int.* 106, 94–100. doi: 10.1016/j.neuint.2017.02.006

Martin, L. J., Gertz, B., Pan, Y., Price, A. C., Molkentin, J. D., and Chang, Q. (2009). The mitochondrial permeability transition pore in motor neurons: involvement in the pathobiology of ALS mice. *Exp. Neurol.* 218, 333–346. doi: 10.1016/j.expneurol.2009.02.015

Martin, L. J., Semenkow, S., Hanaford, A., and Wong, M. (2014). The mitochondrial permeability transition pore regulates Parkinson's disease development in mutant α-synuclein transgenic mice. *Neurobiol. Aging* 35, 1132–1152. doi: 10.1016/j.neurobiolaging.2013.11.008

Martin, S. M., O'Brien, G. S., Portera-Cailliau, C., and Sagasti, A. (2010). Wallerian degeneration of zebrafish trigeminal axons in the skin is required for regeneration and developmental pruning. *Development* 137, 3985–3994. doi: 10.1242/dev.053611

Martínez, G., Duran-Aniotz, C., Cabral-Miranda, F., Vivar, J. P., and Hetz, C. (2017). Endoplasmic reticulum proteostasis impairment in aging. *Aging Cell* 9, e1003433–e1003439. doi: 10.1111/acel.12599

Maswood, N., Young, J., Tilmont, E., Zhang, Z., Gash, D. M., Gerhardt, G. A., et al. (2004). Caloric restriction increases neurotrophic factor levels and attenuates neurochemical and behavioral deficits in a primate model of Parkinson's disease. *Proc. Natl. Acad. Sci. U.S.A.* 101, 18171–18176. doi: 10.1073/pnas.0405831102

Mattison, J. A., Colman, R. J., Beasley, T. M., Allison, D. B., Kemnitz, J. W., Roth, G. S., et al. (2017). Caloric restriction improves health and survival of rhesus monkeys. *Nat. Commun.* 8, 1–12. doi: 10.1038/ncomms14063

Mattson, M. P. (2008). Hormesis defined. *Ageing Res. Rev.* 7, 1–7. doi: 10.1016/j.arr.2007.08.007

Mattson, M. P., Cheng, B., Davis, D., Bryant, K., Lieberburg, I., and Rydel, R. E. (1992). beta-Amyloid peptides destabilize calcium homeostasis and render human cortical neurons vulnerable to excitotoxicity. *J. Neurosci.* 12, 376–389.

Maze, I., Shen, L., Zhang, B., Garcia, B. A., Shao, N., Mitchell, A., et al. (2014). Analytical tools and current challenges in the modern era of neuroepigenomics. *Nat. Neurosci.* 17, 1476–1490. doi: 10.1038/nn.3816

Means, J. C., Venkatesan, A., Gerdes, B., Fan, J.-Y., Bjes, E. S., and Price, J. L. (2015). Drosophila spaghetti and doubletime link the circadian clock and light to caspases, apoptosis and tauopathy. *PLoS Genet.* 11, e1005171–e1005124. doi: 10.1371/journal.pgen.1005171

Mendioroz, M., Celarain, N., Altuna, M., de Gordoa, J. S.-R., Zelaya, M. V., Roldán, M., et al. (2016). CRTC1 gene is differentially methylated in the human hippocampus in Alzheimer's disease. *Alzheimers Res. Ther.* 8:15. doi: 10.1186/s13195-016-0183-0

Meyer-Luehmann, M., Spires-Jones, T. L., Prada, C., Garcia-Alloza, M., de Calignon, A., Rozkalne, A., et al. (2008). Rapid appearance and local toxicity of amyloid-β plaques in a mouse model of Alzheimer's disease. *Nature* 451, 720–724. doi: 10.1038/nature06616

Migliore, L., Fontana, I., Trippi, F., Colognato, R., Coppedè, F., Tognoni, G., et al. (2005). Oxidative DNA damage in peripheral leukocytes of mild cognitive impairment and AD patients. *Neurobiol. Aging* 26, 567–573. doi: 10.1016/j.neurobiolaging.2004.07.016

Miller, K. N., Burhans, M. S., Clark, J. P., Howell, P. R., Polewski, M. A., DeMuth, T. M., et al. (2017). Aging and caloric restriction impact adipose tissue, adiponectin, and circulating lipids. *Aging Cell* 16, 497–507. doi: 10.1111/acel.12575

Mink, M., and Csiszar, K. (2005). *SARM1:* a candidate gene in the onset of hereditary infectious/inflammatory diseases. *Clin. Immunol.* 115, 333–334. doi: 10.1016/j.clim.2005.03.002

Mogi, M., Harada, M., Riederer, P., Narabayashi, H., Fujita, K., and Nagatsu, T. (1994). Tumor necrosis factor-α (TNF-α) increases both in the brain and in the cerebrospinal fluid from parkinsonian patients. *Neurosci. Lett.* 165, 208–210. doi: 10.1016/0304-3940(94)90746-3

Moldovan, M., Alvarez, S., and Krarup, C. (2009). Motor axon excitability during Wallerian degeneration. *Brain* 132, 511–523. doi: 10.1093/brain/awn332

Molofsky, A. V., Slutsky, S. G., Joseph, N. M., He, S., Pardal, R., Krishnamurthy, J., et al. (2006). Increasing p16INK4a expression decreases forebrain progenitors and neurogenesis during ageing. *Nature* 443, 448–452. doi: 10.1038/nature05091

Moreno, J. A., Halliday, M., Molloy, C., Radford, H., Verity, N., Axten, J. M., et al. (2013). Oral treatment targeting the unfolded protein response prevents neurodegeneration and clinical disease in prion-infected mice. *Sci. Transl. Med.* 5, 206ra138–206ra138. doi: 10.1126/scitranslmed.3006767

Moreno, J. A., Radford, H., Peretti, D., Steinert, J. R., Verity, N., Martin, M. G., et al. (2012). Sustained translational repression by eIF2α-P mediates prion neurodegeneration. *Nature* 354, 707–714. doi: 10.1038/nature11058

Morrow, G. (2004). Overexpression of the small mitochondrial Hsp22 extends Drosophila life span and increases resistance to oxidative stress. *FASEB J.* 18, 598–599. doi: 10.1096/fj.03-0860fje

Mucke, L., Masliah, E., Yu, G. Q., Mallory, M., Rockenstein, E. M., Tatsuno, G., et al. (2000). High-level neuronal expression of abeta 1-42 in wild-type human amyloid protein precursor transgenic mice: synaptotoxicity without plaque formation. *J. Neurosci.* 20, 4050–4058.

Mukherjee, P., Woods, T. A., Moore, R. A., and Peterson, K. E. (2013). Activation of the innate signaling molecule MAVS by bunyavirus infection upregulates the adaptor protein SARM1, leading to neuronal death. *Immunity* 38, 705–716. doi: 10.1016/j.immuni.2013.02.013

Murakami, T., Warita, H., Hayashi, T., Sato, K., Manabe, Y., Mizuno, S., et al. (2001). A novel SOD1 gene mutation in familial ALS with low penetrance in females. *J. Neurol. Sci.* 189, 45–47. doi: 10.1016/S0022-510X(01)00558-5

Musiek, E. S., and Holtzman, D. M. (2016). Mechanisms linking circadian clocks, sleep, and neurodegeneration. *Science* 354, 1004–1008. doi: 10.1126/science.aah4968

Mythri, R. B., Venkateshappa, C., Harish, G., Mahadevan, A., Muthane, U. B., Yasha, T. C., et al. (2011). Evaluation of markers of oxidative stress, antioxidant function and astrocytic proliferation in the striatum and Frontal cortex of Parkinson's Disease brains. *Neurochem. Res.* 36, 1452–1463. doi: 10.1007/s11064-011-0471-9

Naidoo, N., Ferber, M., Master, M., Zhu, Y., and Pack, A. I. (2008). Aging impairs the unfolded protein response to sleep deprivation and leads to proapoptotic signaling. *J. Neurosci.* 28, 6539–6548. doi: 10.1523/JNEUROSCI.5685-07.2008

Nakahata, Y., Sahar, S., Astarita, G., Kaluzova, M., and Sassone-Corsi, P. (2009). Circadian control of the NAD^+ salvage pathway by CLOCK-SIRT1. *Science* 324, 654–657. doi: 10.1126/science.1170803

Nelson, P. T., Alafuzoff, I., Bigio, E. H., Bouras, C., Braak, H., Cairns, N. J., et al. (2012). Correlation of Alzheimer Disease neuropathologic changes with cognitive status: a review of the literature. *J. Neuropathol. Exp. Neurol.* 71, 362–381. doi: 10.1097/NEN.0b013e31825018f7

Neukomm, L. J., and Freeman, M. R. (2014). Diverse cellular and molecular modes of axon degeneration. *Trends Cell Biol.* 24, 515–523. doi: 10.1016/j.tcb.2014.04.003

Ng, C. W., Yildirim, F., Yap, Y. S., Dalin, S., Matthews, B. J., Velez, P. J., et al. (2013). Extensive changes in DNA methylation are associated with expression of mutant huntingtin. *Proc. Natl. Acad. Sci. U.S.A.* 110, 2354–2359. doi: 10.1073/pnas.1221292110

Nisoli, E., Tonello, C., Cardile, A., Cozzi, V., Bracale, R., Tedesco, L., et al. (2005). Calorie restriction promotes mitochondrial biogenesis by inducing the expression of eNOS. *Science* 310, 314–317. doi: 10.1126/science.1117728

Oñate, M., Catenaccio, A., Martínez, G., Armentano, D., Parsons, G., Kerr, B., et al. (2016). Activation of the unfolded protein response promotes

axonal regeneration after peripheral nerve injury. *Sci. Rep.* 6:21709. doi: 10.1038/srep21709

Orimo, S., Amino, T., Itoh, Y., Takahashi, A., Kojo, T., Uchihara, T., et al. (2005). Cardiac sympathetic denervation precedes neuronal loss in the sympathetic ganglia in Lewy body disease. *Acta Neuropathol.* 109, 583–588. doi: 10.1007/s00401-005-0995-7

Orimo, S., Uchihara, T., Nakamura, A., Mori, F., Kakita, A., Wakabayashi, K., et al. (2008). Axonal α-synuclein aggregates herald centripetal degeneration of cardiac sympathetic nerve in Parkinson's disease. *Brain* 131, 642–650. doi: 10.1093/brain/awm302

Osterloh, J. M., Yang, J., Rooney, T. M., Fox, A. N., Adalbert, R., Powell, E. H., et al. (2012). dSarm/Sarm1 is required for activation of an injury-induced axon death pathway. *Science* 337, 481–484. doi: 10.1126/science.1223899

Owusu-Ansah, E., Song, W., and Perrimon, N. (2013). Muscle mitohormesis promotes longevity via systemic repression of insulin signaling. *Cell* 155, 699–712. doi: 10.1016/j.cell.2013.09.021

Panneerselvam, P., Singh, L. P., Ho, B., Chen, J., and Ding, J. L. (2012). Targeting of pro-apoptotic TLR adaptor SARM to mitochondria: definition of the critical region and residues in the signal sequence. *Biochem. J.* 442, 263–271. doi: 10.1042/BJ20111653

Park, K. K., Liu, K., Hu, Y., Smith, P. D., Wang, C., Cai, B., et al. (2008). Promoting axon regeneration in the adult CNS by modulation of the PTEN/mTOR pathway. *Science* 322, 963–966. doi: 10.1126/science.1161566

Pasinelli, P., and Brown, R. H. (2006). Molecular biology of amyotrophic lateral sclerosis: insights from genetics. *Nat. Rev. Neurosci.* 7, 710–723. doi: 10.1038/nrn1971

Pasinetti, G. M., Bilski, A. E., and Zhao, W. (2013). Sirtuins as therapeutic targets of ALS. *Cell Res.* 23, 1073–1074. doi: 10.1038/cr.2013.94

Patergnani, S., Fossati, V., Bonora, M., Giorgi, C., Marchi, S., Missiroli, S., et al. (2017). Mitochondria in multiple sclerosis: molecular mechanisms of pathogenesis. *Int. Rev. Cell Mol. Biol.* 328, 49–103. doi: 10.1016/bs.ircmb.2016.08.003

Paz Gavilán, M., Vela, J., Castaño, A., Ramos, B., del Río, J. C., Vitorica, J., et al. (2006). Cellular environment facilitates protein accumulation in aged rat hippocampus. *Neurobiol. Aging* 27, 973–982. doi: 10.1016/j.neurobiolaging.2005.05.010

Penas, C., Font-Nieves, M., Forés, J., Petegnief, V., Planas, A., Navarro, X., et al. (2011). Autophagy, and BiP level decrease are early key events in retrograde degeneration of motoneurons. *Cell Death Differ.* 18, 1617–1627. doi: 10.1038/cdd.2011.24

Peng, Y., Kim, M. J., Hullinger, R., O'Riordan, K. J., Burger, C., Pehar, M., et al. (2016). Improved proteostasis in the secretory pathway rescues Alzheimer's disease in the mouse. *Brain* 139, 937–952. doi: 10.1093/brain/awv385

Pires, A. O., Teixeira, F. G., Mendes-Pinheiro, B., Serra, S. C., Sousa, N., and Salgado, A. J. (2017). Old and new challenges in parkinson's disease therapeutics. *Prog. Neurobiol.* doi: 10.1016/j.pneurobio.2017.04.006. [Epub ahead of print].

Pott Godoy, M. C., Tarelli, R., Ferrari, C. C., Sarchi, M. I., and Pitossi, F. J. (2008). Central and systemic IL-1 exacerbates neurodegeneration and motor symptoms in a model of Parkinson's disease. *Brain* 131, 1880–1894. doi: 10.1093/brain/awn101

Poulsen, E. T., Iannuzzi, F., Rasmussen, H. F., Maier, T. J., Enghild, J. J., Jørgensen, A. L., et al. (2017). An aberrant phosphorylation of amyloid precursor protein tyrosine regulates its trafficking and the binding to the clathrin endocytic complex in neural stem cells of Alzheimer's Disease Patients. *Front. Mol. Neurosci.* 10:59. doi: 10.3389/fnmol.2017.00059

Prehn, K., Jumpertz von Schwartzenberg, R., Mai, K., Zeitz, U., Witte, A. V., Hampel, D., et al. (2016). Caloric restriction in older adults—differential effects of weight loss and reduced weight on brain structure and function. *Cereb. Cortex* 27, 1765–1778. doi: 10.1093/cercor/bhw008

Prolo, L. M., Takahashi, J. S., and Herzog, E. D. (2005). Circadian rhythm generation and entrainment in astrocytes. *J. Neurosci.* 25, 404–408. doi: 10.1523/JNEUROSCI.4133-04.2005

Puls, I., Jonnakuty, C., LaMonte, B. H., Holzbaur, E. L. F., Tokito, M., Mann, E., et al. (2003). Mutant dynactin in motor neuron disease. *Nat. Genet.* 33, 455–456. doi: 10.1038/ng1123

Pyo, J.-O., Yoo, S.-M., Ahn, H.-H., Nah, J., Hong, S.-H., Kam, T.-I., et al. (2013). Overexpression of Atg5 in mice activates autophagy and extends lifespan. *Nat Commun.* 4:2300. doi: 10.1038/ncomms3300

Rando, T. A., and Chang, H. Y. (2012). Aging, rejuvenation, and epigenetic reprogramming: resetting the aging clock. *Cell* 148, 46–57. doi: 10.1016/j.cell.2012.01.003

Ransohoff, R. M. (2016). How neuroinflammation contributes to neurodegeneration. *Science* 353, 777–783. doi: 10.1126/science.aag2590

Reed, T. T., Pierce, W. M., Markesbery, W. R., and Butterfield, D. A. (2009). Proteomic identification of HNE-bound proteins in early Alzheimer disease: insights into the role of lipid peroxidation in the progression of AD. *Brain Res.* 1274, 66–76. doi: 10.1016/j.brainres.2009.04.009

Riar, A. K., Burstein, S. R., Palomo, G. M., Arreguin, A., Manfredi, G., and Germain, D. (2017). Sex specific activation of the ERα axis of the mitochondrial UPR (UPRmt) in the G93A-SOD1 mouse model of familial ALS. *Hum. Mol. Genet.* 26, 1318–1327. doi: 10.1093/hmg/ddx049

Richardson, A. G., and Schadt, E. E. (2014). The role of macromolecular damage in aging and age-related disease. *J. Gerontol. Ser. A Biol. Sci. Med. Sci.* 69, S28–S32. doi: 10.1093/gerona/glu056

Roediger, B., and Armati, P. J. (2003). Oxidative stress induces axonal beading in cultured human brain tissue. *Neurobiol. Dis.* 13, 222–229. doi: 10.1016/S0969-9961(03)00038-X

Rogina, B., and Helfand, S. L. (2004). Sir2 mediates longevity in the fly through a pathway related to calorie restriction. *Proc. Natl. Acad. Sci. U.S.A.* 101, 15998–16003. doi: 10.1073/pnas.0404184101

Rosen, D. R., Siddique, T., Patterson, D., Figlewicz, D. A., Sapp, P., Hentati, A., et al. (1993). Mutations in Cu/Zn superoxide dismutase gene are associated with familial amyotrophic lateral sclerosis. *Nature* 362, 59–62. doi: 10.1038/362059a0

Rotem, N., Magen, I., Ionescu, A., Gershoni-Emek, N., Altman, T., Costa, C. J., et al. (2017). ALS along the axons - expression of coding and noncoding RNA differs in axons of ALS models. *Sci. Rep.* 7:44500. doi: 10.1038/srep44500

Ruan, H., Tang, X. D., Chen, M.-L., Joiner, M.-L. A., Sun, G., Brot, N., et al. (2002). High-quality life extension by the enzyme peptide methionine sulfoxide reductase. *Proc. Natl. Acad. Sci. U.S.A.* 99, 2748–2753. doi: 10.1073/pnas.032671199

Rubinsztein, D. C., Mariño, G., and Kroemer, G. (2011). Autophagy and aging. *Cell* 146, 682–695. doi: 10.1016/j.cell.2011.07.030

Ruzankina, Y., Pinzon-Guzman, C., Asare, A., Ong, T., Pontano, L., Cotsarelis, G., et al. (2007). Deletion of the Developmentally essential gene ATR in Adult mice leads to age-related phenotypes and stem cell loss. *Cell Stem Cell* 1, 113–126. doi: 10.1016/j.stem.2007.03.002

Sadleir, K. R., Kandalepas, P. C., Buggia-Prévot, V., Nicholson, D. A., Thinakaran, G., and Vassar, R. (2016). Presynaptic dystrophic neurites surrounding amyloid plaques are sites of microtubule disruption, BACE1 elevation, and increased Aβ generation in Alzheimer's disease. *Acta Neuropathologica* 132, 235–256. doi: 10.1007/s00401-016-1558-9

Sadri-Vakili, G., Bouzou, B., Benn, C. L., Kim, M.-O., Chawla, P., Overland, R. P., et al. (2007). Histones associated with downregulated genes are hypo-acetylated in Huntington's disease models. *Hum. Mol. Genet.* 16, 1293–1306. doi: 10.1093/hmg/ddm078

Saha, A. R. (2004). Parkinson's disease α-synuclein mutations exhibit defective axonal transport in cultured neurons. *J. Cell. Sci.* 117, 1017–1024. doi: 10.1242/jcs.00967

Saito, Y., Hamakubo, T., Yoshida, Y., Ogawa, Y., Hara, Y., Fujimura, H., et al. (2009). Preparation and application of monoclonal antibodies against oxidized DJ-1. Significant elevation of oxidized DJ-1 in erythrocytes of early-stage Parkinson disease patients. *Neuroscience Lett.* 465, 1–5. doi: 10.1016/j.neulet.2009.08.074

Salpea, P., Russanova, V. R., Hirai, T. H., Sourlingas, T. G., Sekeri-Pataryas, K. E., Romero, R., et al. (2012). Postnatal development- and age-related changes in DNA-methylation patterns in the human genome. *Nucleic Acids Res.* 40, 6477–6494. doi: 10.1093/nar/gks312

Sanchez-Varo, R., Trujillo-Estrada, L., Sanchez-Mejias, E., Torres, M., Baglietto-Vargas, D., Moreno-Gonzalez, I., et al. (2011). Abnormal accumulation of autophagic vesicles correlates with axonal and synaptic pathology in young Alzheimer's mice hippocampus. *Acta Neuropathol.* 123, 53–70. doi: 10.1007/s00401-011-0896-x

Sanhueza, M., Chai, A., Smith, C., McCray, B. A., Simpson, T. I., Taylor, J. P., et al. (2015). Network analyses reveal novel aspects of ALS pathogenesis. *PLoS Genet.* 11:e1005107. doi: 10.1371/journal.pgen.1005107

Sasaki, Y., Nakagawa, T., Mao, X., DiAntonio, A., and Milbrandt, J. (2016). NMNAT1 inhibits axon degeneration via blockade of SARM1-mediated NAD^+ depletion. *Elife* 5:e19749. doi: 10.7554/eLife.19749

Schuldiner, O., and Yaron, A. (2014). Mechanisms of developmental neurite pruning. *Cell. Mol. Life Sci.* 72, 101–119. doi: 10.1007/s00018-014-1729-6

Schwartzman, O., and Tanay, A. (2015). Single-cell epigenomics: techniques and emerging applications. *Nat. Rev. Genet.* 16, 716–726. doi: 10.1038/nrg3980

Selkoe, D. J., and Hardy, J. (2016). The amyloid hypothesis of Alzheimer's disease at 25 years. *EMBO Mol Med.* 8, 595–608. doi: 10.15252/emmm.201606210

Sepe, S., Milanese, C., Gabriels, S., Derks, K. W. J., Payan-Gomez, C., van IJcken, W. F. J., et al. (2016). Inefficient DNA repair is an aging-related modifier of Parkinson's Disease. *Cell Rep.* 15, 1866–1875. doi: 10.1016/j.celrep.2016.04.071

Serrano-Pozo, A., Frosch, M. P., Masliah, E., and Hyman, B. T. (2011). Neuropathological ALTERATIONS in Alzheimer Disease. *Cold Spring Harb. Perspect. Med.* 1, a006189–a006189. doi: 10.1101/cshperspect.a006189

Sharma, R., Buras, E., Terashima, T., Serrano, F., Massaad, C. A., Hu, L., et al. (2010). Hyperglycemia induces oxidative stress and impairs axonal transport rates in mice. *PLoS ONE* 5:e13463. doi: 10.1371/journal.pone.0013463

Sherer, T. B., Betarbet, R., Stout, A. K., Lund, S., Baptista, M., Panov, A. V., et al. (2002). An *in vitro* model of Parkinson's disease: linking mitochondrial impairment to altered alpha-synuclein metabolism and oxidative damage. *J. Neurosci.* 22, 7006–7015.

Shirani, A., Okuda, D. T., and Stüve, O. (2016). Therapeutic advances and future prospects in progressive forms of multiple sclerosis. *Neurotherapeutics* 13, 58–69. doi: 10.1007/s13311-015-0409-z

Sidrauski, C., and Walter, P. (1997). The Transmembrane kinase Ire1p is a site-specific endonuclease that initiates mRNA splicing in the unfolded protein response. *Cell* 90, 1031–1039. doi: 10.1016/S0092-8674(00)80369-4

Sierra, A., Gottfried-Blackmore, A. C., McEwen, B. S., and Bulloch, K. (2007). Microglia derived from aging mice exhibit an altered inflammatory profile. *Glia* 55, 412–424. doi: 10.1002/glia.20468

Smith, A. R., Smith, R. G., Condliffe, D., Hannon, E., Schalkwyk, L., Mill, J., et al. (2016). Increased DNA methylation near TREM2 is consistently seen in the superior temporal gyrus in Alzheimer's disease brain. *Neurobiol. Aging* 47, 639.e7–639.e13. doi: 10.1016/j.neurobiolaging.2016.07.008

Smith, B. N., Ticozzi, N., Fallini, C., Gkazi, A. S., Topp, S., Kenna, K. P., et al. (2014). Exome-wide rare variant analysis identifies TUBA4A mutations associated with familial ALS. *Neuron* 84, 324–331. doi: 10.1016/j.neuron.2014.09.027

Smith, H. L., and Mallucci, G. R. (2016). The unfolded protein response: mechanisms and therapy of neurodegeneration. *Brain* 139, 2113–2121. doi: 10.1093/brain/aww101

Smith, M. A., Richey Harris, P. L., Sayre, L. M., Beckman, J. S., and Perry, G. (1997). Widespread peroxynitrite-mediated damage in Alzheimer's disease. *J. Neurosci.* 17, 2653–2657.

Snowden, S. G., Ebshiana, A. A., Hye, A., An, Y., Pletnikova, O., O'Brien, R., et al. (2017). Association between fatty acid metabolism in the brain and Alzheimer disease neuropathology and cognitive performance: a nontargeted metabolomic study. *PLoS Med.* 14, e1002266–e1002219. doi: 10.1371/journal.pmed.1002266

Sofic, E., Lange, K. W., Jellinger, K., and Riederer, P. (1992). Reduced and oxidized glutathione in the substantia nigra of patients with Parkinson's disease. *Neurosci. Lett.* 142, 128–130. doi: 10.1016/0304-3940(92)90355-B

Sorci, L., Cimadamore, F., Scotti, S., Petrelli, R., Cappellacci, L., Franchetti, P., et al. (2007). Initial-rate kinetics of human NMN-adenylyltransferases: substrate and metal ion specificity, inhibition by products and multisubstrate analogues, and isozyme contributions to NAD^+ biosynthesis. *Biochemistry* 46, 4912–4922. doi: 10.1021/bi6023379

Speakman, J. R., and Mitchell, S. E. (2011). Caloric restriction. *Mol. Aspects Med.* 32, 159–221. doi: 10.1016/j.mam.2011.07.001

Steffan, J. S., Bodai, L., Pallos, J., Poelman, M., McCampbell, A., Apostol, B. L., et al. (2001). Histone deacetylase inhibitors arrest polyglutamine-dependent neurodegeneration in Drosophila. *Nature* 413, 739–743. doi: 10.1038/35099568

Stoll, G., Trapp, B. D., and Griffin, J. W. (1989). Macrophage function during Wallerian degeneration of rat optic nerve: clearance of degenerating myelin and Ia expression. *J. Neurosci.* 9, 2327–2335.

Stranahan, A. M., and Mattson, M. P. (2012). Recruiting adaptive cellular stress responses for successful brain ageing. *Nat. Rev. Neurosci.* 13, 209–216. doi: 10.1038/nrn3151

Stratmann, M., Suter, D. M., Molina, N., Naef, F., and Schibler, U. (2012). Circadian Dbp transcription relies on highly dynamic BMAL1-CLOCK interaction with E boxes and requires the proteasome. *Mol. Cell* 48, 277–287. doi: 10.1016/j.molcel.2012.08.012

Su, K. G., Savino, C., Marracci, G., Chaudhary, P., Yu, X., Morris, B., et al. (2012). Genetic inactivation of the p66 isoform of ShcA is neuroprotective in a murine model of multiple sclerosis. *Eur. J. Neurosci.* 35, 562–571. doi: 10.1111/j.1460-9568.2011.07972.x

Suberbielle, E., Djukic, B., Evans, M., Kim, D. H., Taneja, P., Wang, X., et al. (2015). DNA repair factor BRCA1 depletion occurs in Alzheimer brains and impairs cognitive function in mice. *Nat. Commun.* 6, 8897. doi: 10.1038/ncomms9897

Sugeno, N., Jackel, S., Voigt, A., Wassouf, Z., Schulze-Hentrich, J., and Kahle, P. J. (2016). alpha-Synuclein enhances histone H3 lysine-9 dimethylation and H3K9me2-dependent transcriptional responses. *Sci. Rep.* 6:36328. doi: 10.1038/srep36328

Summers, D. W., Gibson, D. A., DiAntonio, A., and Milbrandt, J. (2016). SARM1-specific motifs in the TIR domain enable NAD^+ loss and regulate injury-induced SARM1 activation. *Proc. Natl. Acad. Sci. U.S.A.* 113, E6271–E6280. doi: 10.1073/pnas.1601506113

Sun, D., Luo, M., Jeong, M., Rodriguez, B., Xia, Z., Hannah, R., et al. (2014). Epigenomic profiling of young and aged HSCs reveals concerted changes during aging that reinforce self-renewal. *Stem Cell* 14, 673–688. doi: 10.1016/j.stem.2014.03.002

Suzuki, K., and Koike, T. (2007). Mammalian Sir2-related protein (SIRT) 2–mediated modulation of resistance to axonal degeneration in slow Wallerian degeneration mice: a crucial role of tubulin deacetylation. *Neuroscience* 147, 599–612. doi: 10.1016/j.neuroscience.2007.04.059

Tagliaferro, P., and Burke, R. E. (2016). Retrograde axonal degeneration in Parkinson Disease. *JPD* 6, 1–15. doi: 10.3233/JPD-150769

Tang, B. L. (2016). Could sirtuin activities modify ALS onset and progression? *Cell. Mol. Neurobiol.* 594, 78–14. doi: 10.1007/s10571-016-0452-2

Tieu, K., Perier, C., Caspersen, C., Teismann, P., Wu, D.-C., Yan, S.-D., et al. (2003). D-β-hydroxybutyrate rescues mitochondrial respiration and mitigates features of parkinson disease. *J. Clin. Invest.* 112, 892–901. doi: 10.1172/JCI200318797

Tofaris, G. K. (2006). Pathological changes in dopaminergic nerve cells of the substantia nigra and olfactory bulb in mice transgenic for truncated human-synuclein(1-120): implications for lewy body disorders. *J. Neurosci.* 26, 3942–3950. doi: 10.1523/JNEUROSCI.4965-05.2006

Turkiew, E., Falconer, D., Reed, N., and Hoke, A. (2017). Deletion of Sarm1 gene is neuroprotective in two models of peripheral neuropathy. *J. Peripher. Nerv. Syst.* doi: 10.1111/jns.12219. [Epub ahead of print].

Unger, M. S., Marschallinger, J., Kaindl, J., Höfling, C., Rossner, S., Heneka, M. T., et al. (2016). Early changes in hippocampal neurogenesis in transgenic mouse models for Alzheimer's Disease. *Mol. Neurobiol.* 53, 5796–5806. doi: 10.1007/s12035-016-0018-9

Valdes, P., Mercado, G., Vidal, R. L., Molina, C., Parsons, G., Court, F. A., et al. (2014). Control of dopaminergic neuron survival by the unfolded protein response transcription factor XBP1. *Proc. Natl. Acad. Sci. U.S.A.* 111, 6804–6809. doi: 10.1073/pnas.1321845111

Valenzuela, V., Collyer, E., Armentano, D., Parsons, G. B., Court, F. A., and Hetz, C. (2012). Activation of the unfolded protein response enhances motor recovery after spinal cord injury. *Cell Death Dis.* 3, 272–279. doi: 10.1038/cddis.2012.8

Valenzuela, V., Martínez, G., Duran-Aniotz, C., and Hetz, C. (2016). Gene therapy to target ER stress in brain diseases. *Brain Res.* 1648(Pt. B), 561–570. doi: 10.1016/j.brainres.2016.04.064

Van der Auwera, I., Wera, S., Van Leuven, F., and Henderson, S. T. (2005). Nutrition & metabolism. *Nutr. Metab.* 2, 28–28. doi: 10.1186/1743-7075-2-28

Vande Velde, C., Garcia, M. L., Yin, X., Trapp, B. D., and Cleveland, D. W. (2004). The neuroprotective factor Wlds does not attenuate mutant SOD1-mediated motor neuron disease. *Neuromol. Med.* 5, 193–203. doi: 10.1385/NMM:5:3:193

Vidal, R. L., Figueroa, A., Court, F. A., Thielen, P., Molina, C., Wirth, C., et al. (2012). Targeting the UPR transcription factor XBP1 protects against Huntington's disease through the regulation of FoxO1 and autophagy. *Hum. Mol. Genet.* 21, 2245–2262. doi: 10.1093/hmg/dds040

Videnovic, A., Lazar, A. S., Barker, R. A., and Overeem, S. (2014). "The clocks that time us"—circadian rhythms in neurodegenerative disorders. *Nat. Rev. Neurol.* 10, 683–693. doi: 10.1038/nrneurol.2014.206

Vilchez, D., Morantte, I., Liu, Z., Douglas, P. M., Merkwirth, C., and Ana, P. C., Rodrigues, et al. (2012). RPN-6 determines *C. elegans* longevity under proteotoxic stress conditions. *Nature* 489, 263–268. doi: 10.1038/nature11315

Villegas, R., Martinez, N. W., Lillo, J., Pihan, P., Hernandez, D., Twiss, J. L., et al. (2014). Calcium release from intra-axonal endoplasmic reticulum leads to axon degeneration through mitochondrial dysfunction. *J. Neurosci.* 34, 7179–7189. doi: 10.1523/JNEUROSCI.4784-13.2014

Viswanathan, M., Kim, S. K., Berdichevsky, A., and Guarente, L. (2005). A role for SIR-2.1 regulation of ER stress response genes in determining *C. elegans* life span. *Dev. Cell* 9, 605–615. doi: 10.1016/j.devcel.2005.09.017

Volpicelli-Daley, L. A., Luk, K. C., Patel, T. P., Tanik, S. A., Riddle, D. M., Stieber, A., et al. (2011). Exogenous α-synuclein fibrils induce lewy body pathology leading to synaptic dysfunction and neuron death. *Neuron* 72, 57–71. doi: 10.1016/j.neuron.2011.08.033

Wakatsuki, S., Tokunaga, S., Shibata, M., and Araki, T. (2017). GSK3B-mediated phosphorylation of MCL1 regulates axonal autophagy to promote Wallerian degeneration. *J. Cell Biol.* 216, 477–493. doi: 10.1083/jcb.201606020

Walther, D. M., Kasturi, P., Zheng, M., Pinkert, S., Vecchi, G., Ciryam, P., et al. (2015). Widespread proteome remodeling and aggregation in aging *C. elegans*. *Cell* 161, 919–932. doi: 10.1016/j.cell.2015.03.032

Wang, M. C., Bohmann, D., and Jasper, H. (2005). JNK extends life span and limits growth by antagonizing cellular and organism-wide responses to insulin signaling. *Cell* 121, 115–125. doi: 10.1016/j.cell.2005.02.030

Wang, T. A., Yu, Y. V., Govindaiah, G., Ye, X., Artinian, L., Coleman, T. P., et al. (2012). Circadian rhythm of redox state regulates excitability in suprachiasmatic nucleus neurons. *Science* 337, 839–842. doi: 10.1126/science.1222826

Wang, T., and Hay, J. C. (2015). Alpha-synuclein toxicity in the early secretory pathway: how it drives neurodegeneration in parkinsons disease. *Front. Neurosci.* 9:433. doi: 10.3389/fnins.2015.00433

Wang, X., Su, B., Lee, H. G., Li, X., Perry, G., Smith, M. A., et al. (2009). Impaired balance of mitochondrial fission and fusion in Alzheimer's Disease. *J. Neurosci.* 29, 9090–9103. doi: 10.1523/JNEUROSCI.1357-09.2009

Wei, M., Brandhorst, S., Shelehchi, M., Mirzaei, H., Cheng, C. W., Budniak, J., et al. (2017). Fasting-mimicking diet and markers/risk factors for aging, diabetes, cancer, and cardiovascular disease. *Sci. Transl. Med.* 9:eaai8700. doi: 10.1126/scitranslmed.aai8700

Weinreb, R. N., Leung, C. K. S., Crowston, J. G., Medeiros, F. A., Friedman, D. S., Wiggs, J. L., et al. (2016). Primary open-angle glaucoma. *Nat. Rev. Dis. Primers* 2, 16067–16019. doi: 10.1038/nrdp.2016.67

Williamson, T. L., and Cleveland, D. W. (1999). Slowing of axonal transport is a very early event in the toxicity of ALS-linked SOD1 mutants to motor neurons. *Nat. Neurosci.* 2, 50–56. doi: 10.1038/4553

Wishart, T. M., Rooney, T. M., Lamont, D. J., Wright, A. K., Morton, A. J., Jackson, M., et al. (2012). Combining comparative proteomics and molecular genetics uncovers regulators of synaptic and axonal stability and degeneration *in vivo*. *PLoS Genet.* 8:e1002936. doi: 10.1371/journal.pgen.1002936

Wood, H. (2013). Neurodegenerative disease: altered DNA methylation and RNA splicing could be key mechanisms in Huntington disease. *Nat. Rev. Neurol.* 9, 119–119. doi: 10.1038/nrneurol.2013.23

Wormser, U., Mandrioli, J., Vinceti, M., Fini, N., Sintov, A., Brodsky, B., et al. (2016). Reduced levels of alpha-1-antitrypsin in cerebrospinal fluid of amyotrophic lateral sclerosis patients: a novel approach for a potential treatment. *J. Neuroinflammation* 13:131. doi: 10.1186/s12974-016-0589-4

Wu, P., Shen, Q., Dong, S., Xu, Z., Tsien, J. Z., and Hu, Y. (2008). Calorie restriction ameliorates neurodegenerative phenotypes in forebrain-specific presenilin-1 and presenilin-2 double knockout mice. *Neurobiol. Aging* 29, 1502–1511. doi: 10.1016/j.neurobiolaging.2007.03.028

Wu, Y., Zhang, S., Xu, Q., Zou, H., Zhou, W., Cai, F., et al. (2016). Regulation of global gene expression and cell proliferation by APP. *Sci. Rep.* 6:22460. doi: 10.1038/srep22460

Xi, Z., Zhang, M., Bruni, A. C., Maletta, R. G., Colao, R., Fratta, P., et al. (2015). The C9orf72 repeat expansion itself is methylated in ALS and FTLD patients. *Acta Neuropathol.* 129, 715–727. doi: 10.1007/s00401-015-1401-8

Xiao, A.-W., He, J., Wang, Q., Luo, Y., Sun, Y., Zhou, Y.-P., et al. (2011). The origin and development of plaques and phosphorylated tau are associated with axonopathy in Alzheimer's disease. *Neurosci. Bull.* 27, 287–299. doi: 10.1007/s12264-011-1736-7

Xu, L., Ryugo, D. K., Pongstaporn, T., Johe, K., and Koliatsos, V. E. (2009). Human neural stem cell grafts in the spinal cord of SOD1 transgenic rats: differentiation and structural integration into the segmental motor circuitry. *J. Comp. Neurol.* 514, 297–309. doi: 10.1002/cne.22022

Xu, L., Zhou, S., Feng, G.-Y., Zhang, L.-P., Zhao, D.-M., Sun, Y., et al. (2012). Neural stem cells enhance nerve regeneration after sciatic nerve injury in rats. *Mol. Neurobiol.* 46, 265–274. doi: 10.1007/s12035-012-8292-7

Yang, L., Li, S., Miao, L., Huang, H., Liang, F., Teng, X., et al. (2016). Rescue of glaucomatous neurodegeneration by differentially modulating neuronal endoplasmic reticulum stress molecules. *J. Neurosci.* 36, 5891–5903. doi: 10.1523/JNEUROSCI.3709-15.2016

Ye, S. M., and Johnson, R. W. (1999). Increased interleukin-6 expression by microglia from brain of aged mice. *J. Neuroimmunol.* 93, 139–148. doi: 10.1016/S0165-5728(98)00217-3

Yin, Z., Raj, D., Saiepour, N., Van Dam, D., Brouwer, N., Holtman, I. R., et al. (2017). Immune hyperreactivity of Aβ plaque-associated microglia in Alzheimer's disease. *Neurobiol. Aging.* 55, 115–122. doi: 10.1016/j.neurobiolaging.2017.03.021

Ying, Z., Zhai, R., McLean, N. A., Johnston, J. M., Misra, V., and Verge, V. M. K. (2015). The unfolded protein response and cholesterol biosynthesis link luman/CREB3 to regenerative axon growth in sensory neurons. *J. Neurosci.* 35, 14557–14570. doi: 10.1523/JNEUROSCI.0012-15.2015

Zhang, B., Carroll, J., Trojanowski, J. Q., Yao, Y., Iba, M., Potuzak, J. S., et al. (2012). The microtubule-stabilizing agent, epothilone D, reduces axonal dysfunction, neurotoxicity, cognitive deficits, and Alzheimer-like pathology in an interventional study with aged tau transgenic mice. *J. Neurosci.* 32, 3601–3611. doi: 10.1523/JNEUROSCI.4922-11.2012

Zhao, J., Zhu, Y., Yang, J., Li, L., Wu, H., De Jager, P. L., et al. (2017). A genome-wide profiling of brain DNA hydroxymethylation in Alzheimer's disease. *Alzheimers Dement.* 13, 674–688. doi: 10.1016/j.jalz.2016.10.004

Zhao, W., Varghese, M., Vempati, P., Dzhun, A., Cheng, A., Wang, J., et al. (2012). Caprylic triglyceride as a novel therapeutic approach to effectively improve the performance and attenuate the symptoms due to the Motor neuron loss in ALS disease. *PLoS ONE* 7:e49191. doi: 10.1371/journal.pone.0049191

Zhao, Z., Lange, D. J., Voustianiouk, A., MacGrogan, D., Ho, L., Suh, J., et al. (2006). A ketogenic diet as a potential novel therapeutic intervention in amyotrophic lateral sclerosis. *BMC Neurosci.* 7:29. doi: 10.1186/1471-2202-7-29

Zou, Y., Jung, K. J., Kim, J. W., Yu, B. P., and Chung, H. Y. (2004). Alteration of soluble adhesion molecules during aging and their modulation by calorie restriction. *FASEB J.* 18, 320–322. doi: 10.1096/fj.03-0849fje

Zuleta, A., Vidal, R. L., Armentano, D., Parsons, G., and Hetz, C. (2012). AAV-mediated delivery of the transcription factor XBP1s into the striatum reduces mutant Huntingtin aggregation in a mouse model of Huntington's disease. *Biochem. Biophys. Res. Commun.* 420, 558–563. doi: 10.1016/j.bbrc.2012.03.033

Conflict of Interest Statement: The authors declare that the research was conducted in the absence of any commercial or financial relationships that could be construed as a potential conflict of interest.

frontiers in Neuroscience

REVIEW
published: 17 October 2017
doi: 10.3389/fnins.2017.00572

Axonal Degeneration in Tauopathies: Disease Relevance and Underlying Mechanisms

Andrew Kneynsberg[1,2], *Benjamin Combs*[2], *Kyle Christensen*[1,2], *Gerardo Morfini*[3*†] and *Nicholas M. Kanaan*[1,2,4*†]

[1] Neuroscience Program, Michigan State University, East Lansing, MI, United States, [2] Department of Translational Science and Molecular Medicine, College of Human Medicine, Michigan State University, Grand Rapids, MI, United States, [3] Department of Anatomy and Cell Biology, University of Illinois at Chicago, Chicago, IL, United States, [4] Hauenstein Neuroscience Center, Mercy Health Saint Mary's, Grand Rapids, MI, United States

OPEN ACCESS

Edited by:
Samuel David Crish,
Northeast Ohio Medical University,
United States

Reviewed by:
Gloria Lee,
University of Iowa, United States
Roland Brandt,
University of Osnabrück, Germany

***Correspondence:**
Nicholas M. Kanaan
nicholas.kanaan@hc.msu.edu
Gerardo Morfini
gmorfini@uic.edu

† Co-senior authors.

Specialty section:
This article was submitted to Neurodegeneration, a section of the journal Frontiers in Neuroscience

Received: 31 July 2017
Accepted: 29 September 2017
Published: 17 October 2017

Citation:
Kneynsberg A, Combs B, Christensen K, Morfini G and Kanaan NM (2017) Axonal Degeneration in Tauopathies: Disease Relevance and Underlying Mechanisms. Front. Neurosci. 11:572. doi: 10.3389/fnins.2017.00572

Tauopathies are a diverse group of diseases featuring progressive dying-back neurodegeneration of specific neuronal populations in association with accumulation of abnormal forms of the microtubule-associated protein tau. It is well-established that the clinical symptoms characteristic of tauopathies correlate with deficits in synaptic function and neuritic connectivity early in the course of disease, but mechanisms underlying these critical pathogenic events are not fully understood. Biochemical *in vitro* evidence fueled the widespread notion that microtubule stabilization represents tau's primary biological role and that the marked atrophy of neurites observed in tauopathies results from loss of microtubule stability. However, this notion contrasts with the mild phenotype associated with tau deletion. Instead, an analysis of cellular hallmarks common to different tauopathies, including aberrant patterns of protein phosphorylation and early degeneration of axons, suggests that alterations in kinase-based signaling pathways and deficits in axonal transport (AT) associated with such alterations contribute to the loss of neuronal connectivity triggered by pathogenic forms of tau. Here, we review a body of literature providing evidence that axonal pathology represents an early and common pathogenic event among human tauopathies. Observations of axonal degeneration in animal models of specific tauopathies are discussed and similarities to human disease highlighted. Finally, we discuss potential mechanistic pathways other than microtubule destabilization by which disease-related forms of tau may promote axonopathy.

Keywords: axonal transport, Alzheimer's disease (AD), chronic traumatic encephalopathy (CTE), pick's disease, progressive supranuclear palsy, corticobasal degeneration, neurodegeneration, animal models of tauopathies

INTRODUCTION

Proper brain function relies on appropriate connectivity between specific neuronal populations. An essential cellular process underlying such connectivity involves the generation and continued maintenance of molecular constituents within axons and dendrites (Conde and Caceres, 2009; Rasband, 2010). Maintenance of axons is particularly challenging in neurons because of their

large size and complex biochemical heterogeneity of discrete functional compartments (i.e., nodes of Ranvier and synapses) within this major neuronal subdomain (Morfini et al., 2001). The axonal cytoskeleton features a polarized microtubule organization, a characteristic that allows for bidirectional transport of membrane-bounded organelles (MBOs) to and from the neuronal soma (Baas et al., 2016). Specialized intracellular transport events include the regulated delivery of MBOs from the soma to the pre- and post-synaptic compartments, the removal of old materials from these compartments, and the maintenance of neurotrophic support, among many others (Morfini et al., 2001). Long distance MBO trafficking events, collectively referred to as axonal transport (AT), are mainly powered by the kinesin and dynein superfamily of microtubule-based molecular motors (Black, 2016; Morfini et al., 2016). To date, a large body of genetic and experimental evidence indicates that maintenance of the unique cytoarchitecture and connectivity of neurons depends on appropriate functionality of major AT components, including microtubules, molecular motors, and protein kinases involved in their regulation (Gibbs et al., 2015; Morfini et al., 2016). Accordingly, genetic mutations in specific molecular motor protein subunits are implicated as potential causative factors for various neurodegenerative diseases (Morfini et al., 2009; Kanaan et al., 2013; Brady and Morfini, 2017).

Tauopathies comprise a heterogeneous group of diseases, including Alzheimer's disease (AD), frontal temporal dementia with parkinsonism linked to chromosome 17 (FTDP-17), chronic traumatic encephalopathy (CTE), progressive supranuclear palsy (PSP), corticobasal degeneration (CBD), and Pick's disease (PiD) (Arendt et al., 2016). Being originally limited to observations derived from post-mortem brains at advanced disease stages, much of the past research on tauopathies focused on mechanisms linking aberrant accumulation of filamentous tau aggregates to cognitive decline and neuronal cell death. However, the recent development of animal models of tauopathies facilitated the identification of much earlier pathogenic events. Detailed pathological analysis of these models indicates that disease-specific symptoms coincide with reductions in synaptic function and neuronal connectivity that long precede the loss of neurons (Morfini et al., 2009). Collectively, the available evidence indicates that neurons affected in tauopathies follow a dying back pattern of degeneration (Higuchi et al., 2002; Kanaan et al., 2013; Brady and Morfini, 2017). Based on this knowledge, interventions focused on maintenance of neuronal connectivity, rather than prevention of cell death, may represent a more pressing therapeutic need for tauopathies (Cheng et al., 2010; Lingor et al., 2012). Identification of disease-relevant mechanisms linking tau to axonal and neuritic degeneration may provide specific molecular targets to improve neuronal connectivity in human tauopathies (Kanaan et al., 2013).

Abbreviations: PET, Positron emission tomography; DTI, Diffuse tensor imaging; MRI, Magnetic resonance imaging; AD, Alzheimer's disease; FTDP-17, Frontal temporal dementia with parkinsonism linked to chromosome 17; CTE, Chronic traumatic encephalopathy; PSP, Progressive supranuclear palsy; CBD, Corticobasal degeneration; PiD, Pick's disease.

EVIDENCE OF AXONOPATHY IN HUMAN TAUOPATHIES

Degenerating axons follow a stereotypical set of morphological changes, typically initiated by enlargement of areas known as swellings or spheroid bodies (Raff et al., 2002). Concomitantly, axons undergo thinning between spheroids, ultimately displaying a beaded appearance as dystrophy progresses. This thinning process continues until the axon becomes fragmented, and eventually degraded (Zhou et al., 1998). Accordingly, the extent of these progressive morphological changes can be used to evaluate axonal degeneration *in vivo* and *in vitro* (Gatto et al., 2015; Kneynsberg et al., 2016). Demyelination often accompanies this process, highlighting the interdependence among oligodendrocytes and their myelinated axon tract (Barres et al., 1993).

Distinctive clinical and neuropathological features of specific tauopathies including AD (reviewed in Masters et al., 2015); FTDP-17, (reviewed in Ghetti et al., 2015); PSP, (Williams and Lees, 2009); CBD, (reviewed in Kouri et al., 2011); PiD, (Mckhann et al., 2001); and CTE, (reviewed in Kiernan et al., 2015) are reviewed elsewhere. Below, we provide a concise review of independent studies in human brains, which collectively provide strong evidence supporting the contention that axonal pathology represents an early and critical pathogenic event common to multiple human tauopathies (**Table 1**).

Alzheimer's Disease (AD)

The strong focus on tau lesions in AD yielded a large body of data establishing axonal degeneration as a prominent neuropathological hallmark of this disease (Kanaan et al., 2013). Tau inclusions within dystrophic neurites, known as neuropil threads, are a robust neuropathological feature of AD brains that appear before neurofibrillary tangles (NFTs) form in neuronal somata (Kowall and Kosik, 1987; Ghoshal et al., 2002). Immunohistochemical evidence demonstrates that pathological forms of tau known to inhibit AT accumulate in neuropil threads, suggesting localized disruption of cellular processes critical for axonal maintenance in AD, including AT (Kanaan et al., 2011; Combs et al., 2016a). Observations of abnormal vesicle accumulations within dystrophic neurites of AD brains provide further support for this notion (Praprotnik et al., 1996; Dessi et al., 1997).

Consistent with AT deficits in AD, results from ultrastructural and immunohistochemical analyses of AD brains reveal a clear correlation between loss of synapses and the manifestation of cognitive deficits (Dekosky and Scheff, 1990; Terry et al., 1991). Highlighting the pathological relevance of these findings, brain imaging studies in living AD patients document significant atrophy of axon-rich white matter structures, suggesting that axonal degeneration represents a prominent feature of the disease. Brain regions affected in patients with mild cognitive impairment, a well-established prodromal AD stage, mainly include axonal projections in the perforant pathway and cortical regions (Stoub et al., 2006; Huang and Auchus, 2007), where axon demyelination also occurs (Sjobeck and Englund, 2003; Sjobeck et al., 2005; Ihara et al., 2010). In more advanced AD cases,

TABLE 1 | Features of axonopathy in human tauopathies.

Disease	Affected brain regions	Tau pathologies	Neuronal/ glial	Synapse loss	Signs of axonal degeneration	*In Vivo* imaging observations
Alzheimer's Disease	Entorhinal cortex, hippocampus, cortex	Neurofibrillary tangles, neuropil threads, neuritic plaques	Primarily neuronal	Yes	Dystrophic axons, axonal swelling, demyelination	Progressive loss of white matter in regions displaying tau pathology correlated with clinical presentation (PET and DTI)
Frontal Temporal Dementia with Parkinsonism Linked to Chromosome 17	Frontal and temporal cortices	Varies by case but can include neurofibrillary tangles and glial pathologies resembling sporadic tauopathies	Both	Yes	Dystrophic axons, axonal swelling, demyelination	White matter loss in symptomatic and asymptomatic carriers of FTDP-17 mutations (PET and DTI)
Chronic Traumatic Encephalopathy	Frontal and temporal cortices, hippocampus	Neurofibrillary tangles, astrocytic plaques, coiled bodies, neuritic threads	Both	Yes	Dystrophic axons, axonal injuries following head injury	White matter abnormalities observed in some athletes after mild traumatic brain injury (DTI)
Progressive Supranuclear Palsy	Basal ganglia, internal capsule, and thalamic fasciculus	Neurofibrillary tangles, globose tangles, tufted astrocytes, coiled bodies	Both	Yes	Dystrophic axons, axonal spheroids, demyelination	White matter loss corresponding to disease severity and symptomatic presentation (DTI)
Corticobasal Degeneration	Frontal and parietal cortices	Astrocytic plaques, coiled bodies, globose tangles, neuritic threads	Both	Yes	Dystrophic axons, swollen terminals, demyelination	White matter loss corresponding to clinical presentations (DTI and MRI)
Pick's Disease	Frontal, temporal, and parietal lobes; hippocampus	Pick bodies, neuropil threads, ramified astrocytes	Neuronal >glial	Yes	Varied thinning and thickening of axons, demyelination	Severe atrophy of cortical white matter (MRI)

white matter atrophy extends to the corpus callosum, where the degree of atrophy directly correlates with cognitive decline (Vermersch et al., 1996; Hampel et al., 1998). Diffuse tensor imaging (DTI) techniques quantitatively measure water diffusion within cellular structures to identify microstructural changes in white matter that may not be evident with other imaging techniques (Meerschaert et al., 2016). Significantly, results from DTI studies show alterations in specific axonal tracts connecting association cortices, while others involved with motor or visual functions are largely spared. Again, the extent to which these tracts are affected displays a close correlation with the degree of cognitive decline (Bozzali et al., 2002).

Frontotemporal Dementia with Parkinsonism Linked to Chromosome 17 (FTDP-17)

FTDP-17 represents a subgroup of inherited early-onset tauopathies resulting from mutations in the gene encoding tau. The discovery of FTDP-17 tau mutations demonstrated that tau dysfunction alone suffices to cause neuronal dysfunction and degeneration (Foster et al., 1997; Hutton et al., 1998), and axonal pathology is seen in FTDP-17 brains. Specifically, positron emission tomographic (PET) imaging studies in FTDP-17 patients show the accumulation of tau aggregates in white matter areas (Wszolek et al., 1992). Interestingly, brain imaging studies found white matter alterations in pre-symptomatic disease stages (Rohrer et al., 2010; Dopper et al., 2014). Similar to neuropil threads in AD, mutant tau aggregates localize within dystrophic axons of FTDP-17 brains (Delisle et al., 1999; Murrell et al., 1999; Lippa et al., 2000; Kouri et al., 2014). As discussed below, animal models of specific FTDP-17 variants largely recapitulate the axonopathy phenotype observed in affected human brains.

Chronic Traumatic Encephalopathy (CTE)

CTE is a neurodegenerative disease associated with repetitive subconcussive and mild traumatic brain injuries (reviewed in Blennow et al., 2016). Focal areas of neuronal and glial tau inclusions at the depths of cortical sulci and in perivascular regions are pathognomonic CTE lesions found in the frontal and temporal cortices, as well as the hippocampus (Mckee et al., 2012). Symptoms of diffuse axonal injuries, including axonal swellings, unregulated calcium influx, and cytoskeletal abnormalities are evident within the first 24 h after concussion and may persist for weeks (Blumbergs et al., 1994; Maxwell et al., 1995; Giza and Hovda, 2001). Tau-positive neuropil threads also are a prominent neuropathological feature of CTE and cognitive decline correlates with axonal atrophy in subcortical white matter (Tokuda et al., 1991; Kraus et al., 2007; Mckee et al., 2009). Pathological forms of tau, identified by conformation-dependent tau antibodies, were recently found to localize within axons of cortical white matter and neuropil threads in the cholinergic basal forebrain (Kanaan et al., 2016; Mufson et al., 2016). Using a PET tracer, protein aggregates, likely made up of tau, were identified within white matter tracts of former professional football players suspected of having CTE (Barrio et al., 2015). Membrane-associated proteins, including amyloid precursor protein, accumulate in axons after traumatic brain injuries, suggesting AT disruption may play a role in CTE

pathogenesis (Uryu et al., 2007). Additionally, a multitude of DTI studies have identified white matter changes in athletes at risk for concussions or repetitive subconcussive impacts from several sports, including boxing, football, soccer, ice hockey, as well as in veterans exposed to blast trauma (Zhang et al., 2003; Koerte et al., 2012a,b; McAllister et al., 2014; Petrie et al., 2014).

Progressive Supranuclear Palsy (PSP)

In PSP, tau aggregates are observed in both neurons (NFTs and globose tangles) and glial cells (tufted astrocytes and coiled bodies) (Pollock et al., 1986; Hauw et al., 1994). The presence of neuropil threads in PSP indicates the presence pathological tau in axons, particularly in the basal ganglia, internal capsule, and thalamic fasciculus (Hauw et al., 1990; Dickson, 1999). Additionally, axonal spheroids are found in subcortical white matter, the putamen, globus pallidus, and the subthalamic nucleus (Probst et al., 1988; Ahmed et al., 2008). Extending these findings, DTI studies in early PSP cases found evidence of white matter degeneration within the pons, substantia nigra, cerebellar peduncles, and corpus callosum and the degree of atrophy in some of these regions correlates to disease severity and onset of symptoms (Padovani et al., 2006; Knake et al., 2010; Whitwell et al., 2011; Zhang et al., 2016). Interestingly, PSP is characterized by abundant tau lesions termed coiled bodies within oligodendrocytes, the cells responsible for generating myelin sheaths in the central nervous system. Demyelination is particularly evident in white matter tracts of PSP-affected brains, directly correlating with tau burden in the superior cerebellar peduncle and red nucleus. These findings suggest that tau-induced oligodendrocyte dysfunction could indirectly contribute to the axonal degeneration phenotype observed in PSP (Ishizawa et al., 2000).

Corticobasal Degeneration (CBD)

The characteristic tau pathology of CBD includes astrocytic plaques, occasional coiled bodies, and neuronal globose inclusions that are primarily found in the frontal and parietal lobes of the cerebral cortex, the cerebellum, and substantia nigra (Rebeiz et al., 1968; Feany and Dickson, 1995). Neuropil thread pathology is prominent in cortical gray and white matter, the subthalamic nucleus, and the striatum of CBD brains (Ikeda et al., 1994; Dickson, 1999). MRI and DTI-based studies find significantly greater white matter abnormalities in CBD (Doi et al., 1999; Zhang et al., 2016). Additional studies identified pathological changes in specific hand sensorimotor fiber tracts in patients who manifested limb apraxia at early CBD stages (Borroni et al., 2008), furthering the linkage between axonal degeneration and specific symptomatic outcomes. The extensive astroglial lesions in CBD and other tauopathies suggest that pathological forms of tau may affect astrocyte-specific functions critical to neuronal health, including sustained trophic support (**Figure 1C**; Kahlson and Colodner, 2015).

Pick's Disease (PiD)

Pick's disease (PiD) is characterized by severe atrophy of the frontal, temporal, and parietal lobes. Cytoplasmic neuronal tau inclusions known as Pick bodies represent the major neuropathological hallmark of PiD, and these are typically found in the dentate gyrus of the hippocampus and frontal and temporal cortices (Pollock et al., 1986; Probst et al., 1996). MRI studies of Pick's disease cases document severe atrophy of cortical white matter (Wang et al., 2006; Yamakawa et al., 2006). Microscopic evaluation of post-mortem brain tissue reveals that axons surrounding the dendrites of neurons in the affected brain regions (e.g., polymorphic layer of the dentate gyrus) often display pathological tau, in addition, glial tau pathology is observed (Cochran et al., 1994; Probst et al., 1996). Neuritic threads and spheroids are observed in mossy fibers projecting to the dentate nucleus along with abnormal tau in cerebellar white matter and other axons in PiD brains (Probst et al., 1996; Braak et al., 1999). A marked loss of myelinated axons is observed in subcortical white matter (Dickson, 1998) as well as perforant pathway synaptic loss (Lippa, 2004). Accumulation of AT-related molecules in Pick bodies (e.g., kinesin and synpatophysin) suggests AT is impaired in PiD (Nakamura et al., 1994).

Collectively, results from ultrastructural, immunohistochemical, and brain imaging-based studies strongly implicate axonopathy and the consequent neural disconnection as a pathogenic component common to all tauopathies. Localization of pathological forms of tau within dystrophic axons in each tauopathy further suggests alterations in one or more cellular processes critical for axonal maintenance, including AT (Morfini et al., 2002a; Kanaan et al., 2013).

ANIMAL MODELS OF TAUOPATHIES

Models of tauopathy using the expression of specific tau variants include transgenic mice and viral vector-mediated gene delivery of tau-encoding cDNA constructs in rodent brains, among others (Ballatore et al., 2007; LaFerla and Green, 2012; Combs et al., 2016b). As discussed below, these animal models exhibit characteristics reminiscent of those seen in human tauopathies, further supporting a role of axonopathy in the disease process.

Several transgenic tauopathy models were produced over the years, which replicate selected cardinal features of human tauopathies (Gotz et al., 2007). The early animal models are based on expression of wild-type human 4R (Gotz et al., 1995) and 3R (Brion et al., 1999) tau variants and these mice show only mild phenotypes. However, tau transgenic mice with stronger gene promoters produce a clear neurodegenerative phenotype and many of these transgenic models (e.g., the T44 and ALZ17 lines) feature tau pathology mainly in the brainstem and spinal cord (Ishihara et al., 1999; Spittaels et al., 1999; Probst et al., 2000). Axonopathy in these models manifests in the form of axonal spheroids, axonal neurofilament- and tau-immunoreactive inclusions (Spittaels et al., 1999). Expanding on these early models, the 8c transgenic mouse line expresses a human tau gene cassette that produces all six human tau isoforms and these mice display signs of axonopathy including axonal swellings and spheroids, but do not develop NFTs (Duff et al., 2000). The 8c line was later crossed with a tau knockout line to produce mice that exclusively express human tau isoforms in the absence of endogenous mouse tau (Tucker

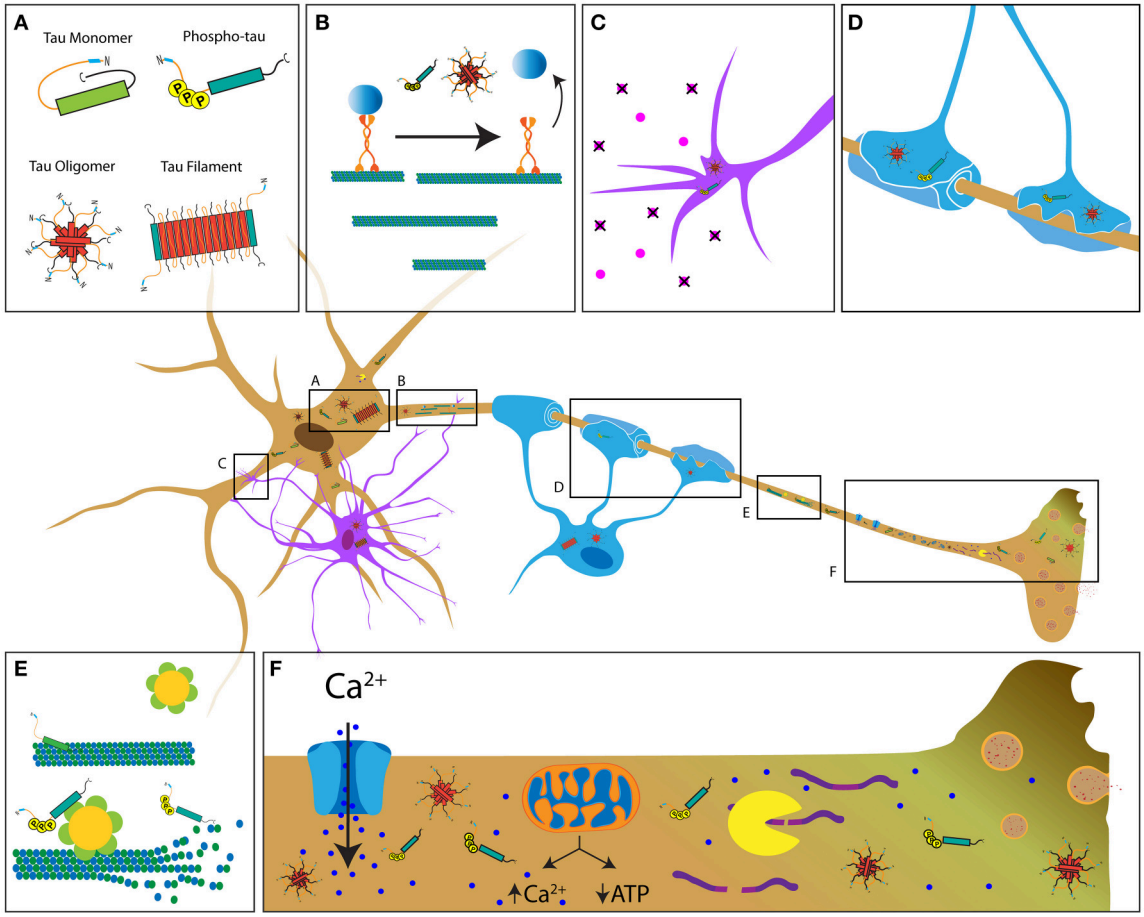

FIGURE 1 | Potential mechanisms contributing to tau-induced axonal degeneration in tauopathies. **(A)** Pathological forms of tau include phosphorylated tau, tau oligomers, and tau filaments, all of which feature increased exposure of the PAD (blue region of tau) (Kanaan et al., 2011). In contrast, this domain is hidden in soluble tau monomers, which feature a paperclip conformation (Jeganathan et al., 2008). Depending on the specific tauopathy, pathological tau is present in neurons (brown cell), astrocytes (purple cell, **C**) and oligodendrocytes (blue cell, **D**). **(B)** Pathological conformations of tau impair axonal transport through activation of a phosphotransferase-based signaling pathway that promotes detachment of transported cargoes from the motor protein conventional kinesin. **(C,D)** Accumulation of pathological tau may also interfere with cellular processes involved in trophic support by astrocytes and oligodendrocytes, ultimately resulting in axonal dysfunction and demyelination. **(E)** Disease-related modifications of tau (e.g., phosphorylation) that reduce its binding to microtubules may promote aberrant katanin-mediated microtubule severing. **(F)** Disease-related forms of tau can alter Ca^{2+} homeostasis through various mechanisms, including abnormal modulation of ion channel activity, the endoplasmic reticulum and/or mitochondrial Ca^{2+} buffering. Enhanced Ca^{2+} levels may in turn increase calpain activity, leading to abnormal cleavage of cytoskeletal proteins. Together, these mechanisms represent the multifaceted pathways by which tau that likely contributes to axonopathy.

et al., 2001). Interestingly, mice resulting from this cross show early accumulation of pathological tau within axons (e.g., CP13 positive phospho-tau), before such changes are detected in neuronal somata (Andorfer et al., 2003). Thus, overexpression of exogenous human tau alone suffices to cause axonopathy, which appears inconsistent with microtubule destabilization playing a role in tauopathies. Instead, these observations suggest that exogenous transgenic tau promotes a toxic gain of function that affects the maintenance of axons (Kanaan et al., 2011).

After the discovery of autosomal dominant tau mutations in FTDP-17 families (Hutton et al., 1998), several groups generated transgenic mice expressing FTDP-17-related mutant forms of tau. Unlike wild-type tau expressing models, these mice successfully recapitulate NFT-like inclusions typical of tauopathies (Lewis et al., 2000; Gotz et al., 2001; Allen et al., 2002). P301L tau remains the most commonly studied FTDP-17 mutation (Dumanchin et al., 1998; Hutton et al., 1998; Rizzu et al., 1999), and several transgenic mouse models are based on expression of this mutant form of tau. JNPL3 transgenic mice for example, feature expression of 4R/0N P301L tau under control of the mouse prion promoter (Lewis et al., 2000). Interestingly, these mice feature not only NFT-like and pre-tangle tau inclusions, but also axonal spheroids and degenerated myelinated axonal tracts, predominantly in the spinal cord (Lewis et al., 2000; Lin et al., 2003, 2005). In rTg4510 mice, the P301L tau transgene is downstream of a tetracycline operon-responsive element (TRE), and they express a tetracycline-controlled transactivator (tTA) that is under control of the Ca^{2+}-calmodulin kinase

II-α (CaMKIIα) promoter, which provides relatively selective expression of tau in forebrain neurons (Mayford et al., 1996; Santacruz et al., 2005; Spires et al., 2006). Accordingly, mutant tau expression can be suppressed through doxycycline treatment, thus providing spatial and temporal control of tau expression (Santacruz et al., 2005). Interestingly, signs of axonopathy in the rTg4510 model are comparable to those in JNPL3 mice, including swollen axons, NFT-like inclusions, myelin loss, and accumulation of mitochondria in swollen axons (Ludvigson et al., 2011). The rTgTauEC model uses a similar Tet-Off system as the rTg4510 model. However, tTA expression is controlled by the neuropsin promoter (de Calignon et al., 2012), which restricts mutant tau expression to a subset of entorhinal cortex (EC) neurons (Yasuda and Mayford, 2006). In this model, initial signs of axonopathy include strong Alz50 immunoreactivity [Alz50 is an antibody that recognizes a pathological tau conformation (Carmel et al., 1996)] within axonal terminals of the outer two-thirds molecular layer of the dentate gyrus, followed by age-dependent axonal degeneration and loss of hippocampal neurons (de Calignon et al., 2012). Microglia activation and astrogliosis is observed in rTgTauEC mice, suggesting that glial dysfunction might exacerbate axonopathy in this model. Additionally, the rTgTauEC model shows spread of pathological tau through interconnected neurons, suggesting transsynaptic release of misfolded or aggregated tau into the synaptic cleft and uptake by downstream neurons (de Calignon et al., 2012). Based on these observations, it is reasonable to posit that synaptic and axonal degeneration may not only be a primary source of neuronal disconnection, but also promote the release and spread of pathological tau species through synaptically connected networks (reviewed in Walsh and Selkoe, 2016).

Glial contributions to axonopathy are an active area of research, and models that selectively overexpress tau in glial cells are valuable models of tauopathies. One such model expresses 4R/1N P301L tau specifically in oligodendrocytes, achieved by controlling expression through the 2′,3′-cyclic nucleotide 3′ phosphodiesterase promoter. These mice displayed oligodendrocyte tau inclusions, AT deficits that preceded axonal degeneration, and deficits in myelination (Higuchi et al., 2005). This model highlights the importance of oligodendrocytes on axonal maintenance because tau inclusions appear to promote deficits in oligodendrocyte function that in turn indirectly contribute to axonopathy (**Figure 1D**; Chin and Goldman, 1996; Dickson et al., 1996).

Viral vector-mediated gene delivery facilitates the introduction of exogenous genes with extensive spatial and temporal control over its expression. In wild-type mice, injection of recombinant adeno-associated viral (rAAV) vectors encoding P301L tau into the EC (Siman et al., 2013, 2015) or the hippocampus (Jaworski et al., 2009, 2011) results in axonal degeneration. Injected mice display accumulation of tau phosphorylated at the AT8 epitope within synapses, degeneration of axons in the performant pathway and spread of P301L tau into the dentate gyrus (Siman et al., 2013). Similar to some transgenic tau models, rAAV-based tauopathy models also display reactive gliosis around degenerating axons, which may contribute to axonal pathology (Siman et al., 2013, 2015). Furthermore, injection of an rAAV vector encoding pseudophosphorylated AT8 tau in the EC led to early signs of axonopathy, including the development of spheroids and a swollen morphology (Combs et al., 2016b). Similarly, lentiviral vectors encoding wild-type or P301L tau induce markers of axonopathy when injected in the rat hippocampus, that includes a time-dependent increase in swollen, fragmented, and dystrophic axons, as well as microglial activation (Caillierez et al., 2013; Hebron et al., 2014).

Collectively, data from various animal models of tauopathy reveal axonal degeneration as a prominent pathological feature, and further suggest there is a contribution to this phenotype from glial cells. Based on their resemblance to this specific aspect of human tauopathies, these animal models may help define mechanisms and specific molecular components mediating the toxic effect of pathogenic tau on axonal maintenance and function.

PATHOGENIC MECHANISMS LINKING ABNORMAL TAU TO AXONOPATHY

The initial discovery of tau protein was based on biochemical procedures that revealed its ability to associate with purified microtubules and modulate their dynamic growth behavior *in vitro* (Weingarten et al., 1975; Cleveland et al., 1977a,b). These biochemical properties of tau quickly led to its designation as a microtubule-associated protein, and the suggestion that microtubule stabilization represents tau's primary functional role in neurons (Weingarten et al., 1975; Cleveland et al., 1977a,b). Several subsequent reports document various effects of tau on microtubule dynamics in cultured cell lines (reviewed in Feinstein and Wilson, 2005). By extension, microtubule destabilization resulting from loss of tau function is widely believed to represent a major mechanism underlying neuronal dysfunction and degeneration in human tauopathies (Guo et al., 2017). However, direct experimental evidence that tau is required for the maintenance of microtubule stability in cultured primary neurons or in neurons *in vivo* has yet to be provided.

Collectively, data from the available four transgenic tau knockout mouse lines (reviewed in Ke et al., 2012) reveal little to no effect on behavior, cognition, and neuropathology associated with germline removal of the tau gene (Harada et al., 1994; Dawson et al., 2001; Tucker et al., 2001; Fujio et al., 2007; Morris et al., 2011; van Hummel et al., 2016). These findings are inconsistent with a critical role for tau in sustaining microtubule stabilization *in vivo*. Furthermore, axonal development is normal in cultured primary neurons obtained from some tau knockout mice (Harada et al., 1994; Takei et al., 2000). Deleterious effects of removing tau documented so far are limited to mild behavioral and parkinsonian-like deficiencies with advancing age in a couple of mouse lines (Ikegami et al., 2000; Lei et al., 2014), alterations in microtubule density limited to small caliber cerebellar parallel fibers in one model (Harada et al., 1994), and delayed neurite development in cultured neurons from another (Dawson et al., 2001). Additional experiments using primary cultured neurons show that immunodepletion of axonal tau does not lead to appreciable

alterations in axonal microtubule content or dynamics (Tint et al., 1998); thus, extending findings from tau knockout mice. Tau-independent mechanisms for microtubule stabilization, including post-translational modifications of tubulin and the existence of additional microtubule-associated proteins, could explain the marginal impact of tau deletion on microtubule stability (Song and Brady, 2015; Matamoros and Baas, 2016).

Available experimental evidence suggests that tau performs functions other than microtubule stabilization in neurons. Numerous studies suggest a role for tau in multiple cellular processes and compartments, some of which may not include microtubule interactions. The functional repertoire of tau includes microtubule-actin cytoskeleton interactions (Selden and Pollard, 1986; Liu et al., 1999), regulation of AT (LaPointe et al., 2009; Kanaan et al., 2011), nuclear and nucleolar functions (Papasozomenos and Binder, 1987; Loomis et al., 1990; Sultan et al., 2011), end-binding protein regulation (Ramirez-Rios et al., 2016), cytoskeleton-plasma membrane interactions (Brandt et al., 1995), RNA-binding protein and stress granule regulation (Vanderweyde et al., 2016), as well as scaffolding of phosphotransferases (Lee et al., 1998; Liao et al., 1998; Ittner et al., 2010; Kanaan et al., 2013). Supporting this later role, a number of protein kinases and phosphatases reportedly interact with tau including PP1 (Liao et al., 1998), GSK3β (Sun et al., 2002), Cdk5 (Li et al., 2006), Fyn (Lee et al., 1998), and others (Liu et al., 2016). Together, these reports support a role for tau as a scaffolding protein that targets phosphotransferases to microtubules; thus, facilitating their interaction with specific microtubule-associated protein substrates (e.g., motor proteins) (reviewed in Morfini et al., 2002b; Kanaan et al., 2013). Experimental evidence also suggests such a role may extend to the dendritic compartment, where tau appears to regulate localization and activity of the tyrosine protein kinase Fyn (Xia et al., 2015; Lau et al., 2016). Collectively, the available evidence supports a broader functional repertoire for tau unrelated to microtubule stabilization, providing clues to the potential mechanisms by which pathogenic forms of tau may promote axonopathy (**Figure 1**).

The dependence of axons on proper anterograde and retrograde AT is evident because mutations in selected conventional kinesins or cytoplasmic dynein subunits suffice to promote dying-back degeneration of neurons (Morfini et al., 2009). Providing an explanation for the axonal degeneration phenotype observed in tauopathies, multiple independent studies documented deficits in AT triggered by pathogenic forms of tau, including oligomeric tau (Higuchi et al., 2005; Gotz et al., 2006; Cox et al., 2016; Swanson et al., 2017). Several mechanisms are proposed to mediate this toxic effect. The early observation that tau overexpression leads to alterations in intracellular trafficking of cellular organelles in cultured cell lines suggested that tau inhibits AT (Stamer et al., 2002). *In vitro* studies using purified components of the AT system further supported a model where tau would elicit this effect by competing with conventional kinesin heavy chain subunits for microtubule binding (Seitz et al., 2002; Mandelkow et al., 2003). However, studies in the squid axoplasm preparation reveal that even supraphysiological (i.e., ∼20-fold higher) levels of human tau monomers do not negatively impact AT (Morfini et al., 2007). Pulse chase studies *in vivo* extend the conclusions from squid axoplasm studies to mammalian neurons, showing normal AT rates in the optic nerve of tau-overexpressing mice (Yuan et al., 2008).

The highly dynamic nature of the interaction between tau and microtubules *in vitro* and *in situ* also appears inconsistent with the notion that tau physically blocks motor proteins (Samsonov et al., 2004; Janning et al., 2014; Stern et al., 2017). Recent work suggests that disease-related phosphorylation does not cause tau to fall off microtubules as the off-rate is unaffected by pseudophosphorylation at the PHF1 site (i.e., S396 and S404), but may reduce microtubule binding by decreasing the on-rate (Niewidok et al., 2016). The highly dynamic conformational flexibility of tau likely facilitates its interaction with a large repertoire of binding partners (Jeganathan et al., 2006; Uversky, 2015; Stern et al., 2017) (reviewed in Bakota et al., 2017). Further, tau's role as a scaffolding protein and the recruitment of phosphotransferases to the microtubule cytoskeleton associated with this function could in turn be subject to phosphoregulation.

The major motor proteins responsible for AT, conventional kinesin and cytoplasmic dynein, are regulated by specific protein kinases providing a novel mechanism linking pathological forms of tau to deficits in AT (Kanaan et al., 2013; Gibbs et al., 2015; Brady and Morfini, 2017). Unlike soluble tau monomers, tau aggregates inhibit anterograde AT in the isolated squid axoplasm when perfused at physiological levels (LaPointe et al., 2009). Remarkably, this effect is dependent upon amino acids 2–18 in the extreme amino terminus of tau, a motif termed the phosphatase-activating domain (PAD) (Kanaan et al., 2011). PAD is sufficient to activate protein phosphatase 1 (PP1) and GSK3 in a manner independent of microtubule binding (Kanaan et al., 2011). PP1 reportedly activates GSK3β by dephosphorylating the autoinhibitory residue (Ser 9), causing its activation (Morfini et al., 2004). Active GSK3 in turn phosphorylates kinesin light chain subunits of conventional kinesin, promoting release of transported cargoes from this motor protein (Morfini et al., 2002b). Systematic evaluation of the effects that numerous tau construct variants elicit on AT reveals that different pathological changes (e.g., mutations, aggregation, oligomerization and phosphorylation) promote increased PAD exposure (**Figure 1A**; Kanaan et al., 2012). Given the unique dependence of axons on sustained AT, these studies highlight a specific kinase-dependent mechanism by which pathological forms of tau may cause axonal dysfunction, further supporting a role of tau as a modulator of protein kinases involved in AT regulation (**Figure 1B**). More recent studies provide further support for this mechanism in mammalian neurons by showing that amyloid-β oligomer-mediated impairments in AT require both tau and specific phosphotransferases (Decker et al., 2010; Vossel et al., 2015). Additionally, phosphorylation of tau at specific epitopes modulates both its dynamic behavior and its effect on AT (Kanaan et al., 2012; Tiernan et al., 2016; Stern et al., 2017). For example, tyrosine 18 phosphorylation within PAD by non-receptor kinases blocks the inhibitory effect of pathogenic tau on anterograde AT (Kanaan et al., 2012). In contrast, phospho-mimicking residues within the proline-rich region and the C-terminus confer a toxic effect on anterograde AT upon wild

type tau monomers (Kanaan et al., 2011; Tiernan et al., 2016; Stern et al., 2017). Interestingly, tau-induced toxicity in cultured cortical astrocytes is associated with kinesin-dependent transport deficits (Yoshiyama et al., 2003), suggesting that tau may impair microtubule-dependent transport in glial cells as well.

In addition to the mechanisms above, mechanisms linking pathological tau to Ca^{2+} dysregulation may negatively impact axonal connectivity (**Figure 1F**). For example, injection of wild-type tau in the squid giant synapse promotes release of Ca^{2+} from the endoplasmic reticulum, leading to inhibition of synaptic vesicle exocytosis and synaptic transmission through a mechanism involving PAD exposure and GSK3 activation (**Figure 1F**; Moreno et al., 2016). Oligomeric tau is particularly toxic to synaptic function, causing impaired long-term potentiation (Fa et al., 2016) and long-term depression (Decker et al., 2015) in cultured neurons and mouse brain slice cultures, as well as memory deficits in living mice (Fa et al., 2016). Studies also show that tau oligomers can cause Ca^{2+} imbalance and cell death in induced pluripotent stem cells (Imamura et al., 2016), and tau may further increase Ca^{2+} levels by directly inhibiting plasma membrane Ca^{2+} ATPase (Berrocal et al., 2016). Besides the endoplasmic reticulum, mitochondria are a main source of Ca^{2+} buffering in cells (Werth and Thayer, 1994). Interestingly, P301L mutant tau reduces the number of axonal mitochondria (Rodriguez-Martin et al., 2016) and the N-terminal domain of tau may stimulate autophagic turnover of mitochondria in neurons (Amadoro et al., 2014). Reduced numbers and/or dysfunction of axonal mitochondria could in turn promote abnormal Ca^{2+} levels (reviewed in Eckert et al., 2014). Ultimately, pathogenic tau-mediated increases in Ca^{2+} levels may promote abnormal activation of calcium-activated proteases and proteolysis of critical cytoskeletal protein components (**Figure 1F**; Yin et al., 2016). Consistent with this notion, increased calpain activation occurs in AD and other tauopathy brains (Adamec et al., 2002), and inhibition of calcium activated protease reduces axonal degeneration in the P301L transgenic mouse model (Rao et al., 2014). Interestingly, studies suggest that microtubules devoid of tau are more vulnerable to degradation by the microtubule-severing protein katanin, providing another route by which abnormal tau modifications promote cytoskeletal degradation (**Figure 1E**; Qiang et al., 2006; Sudo and Baas, 2011). Collectively, these studies suggest various mechanism linking pathogenic forms of tau to axonal degeneration. A better understanding of these mechanisms may provide a broader set of tau-based therapeutic targets.

CONCLUSIONS

The landscape of tauopathies is marked by significant heterogeneity in clinical presentation, cellular topography, and neuropathological features. Despite this diversity, an examinations of human brains and animal models of tauopathies reveal axonopathy as a common feature of these diverse diseases (Hyman et al., 1990; Ahmed et al., 2008; Kovacs et al., 2008; Ling et al., 2015). A comprehensive analysis demonstrates that tau likely plays a central role in axonal dysfunction and degeneration and that disease-related modifications of tau contribute to axonopathy and synaptic dysfunction through multiple pathways including misregulation of phosphotransferase activities, AT deficits, disruption of Ca^{2+} homeostasis, altered glial function, and others (**Figure 1**). Developing and implementing therapeutic strategies based on preserving neuronal connectivity will require a continued deepening of our understanding of these mechanisms and the identification of specific molecular components linking pathological tau to axonopathy in the context of each tauopathy.

AUTHOR CONTRIBUTIONS

AK, BC, KC, GM, and NK all contributed equally with writing, editing and figure preparation for the manuscript.

FUNDING

This work was supported by the National Institute of Health grants AG044372 and NS082730 (NK), NS066942 and NS096642 (GM), the BrightFocus Foundation grant A2013364S (NK), the Jean P. Schultz Biomedical Research Endowment (NK), and the Secchia Family Foundation Research Fund (NK).

REFERENCES

Adamec, E., Mohan, P., Vonsattel, J. P., and Nixon, R. A. (2002). Calpain activation in neurodegenerative diseases: confocal immunofluorescence study with antibodies specifically recognizing the active form of calpain 2. *Acta Neuropathol.* 104, 92–104. doi: 10.1007/s00401-002-0528-6

Ahmed, Z., Josephs, K. A., Gonzalez, J., Delledonne, A., and Dickson, D. W. (2008). Clinical and neuropathologic features of progressive supranuclear palsy with severe pallido-nigro-luysial degeneration and axonal dystrophy. *Brain* 131, 460–472. doi: 10.1093/brain/awm301

Allen, B., Ingram, E., Takao, M., Smith, M. J., Jakes, R., Virdee, K., et al. (2002). Abundant tau filaments and nonapoptotic neurodegeneration in transgenic mice expressing human P301S tau protein. *J. Neurosci.* 22, 9340–9351.

Amadoro, G., Corsetti, V., Florenzano, F., Atlante, A., Ciotti, M. T., Mongiardi, M. P., et al. (2014). AD-linked, toxic NH2 human tau affects the quality control of mitochondria in neurons. *Neurobiol. Dis.* 62, 489–507. doi: 10.1016/j.nbd.2013.10.018

Andorfer, C., Kress, Y., Espinoza, M., De Silva, R., Tucker, K. L., Barde, Y. A., et al. (2003). Hyperphosphorylation and aggregation of tau in mice expressing normal human tau isoforms. *J. Neurochem.* 86, 582–590. doi: 10.1046/j.1471-4159.2003.01879.x

Arendt, T., Stieler, J. T., and Holzer, M. (2016). Tau and tauopathies. *Brain Res. Bull.* 126, 238–292. doi: 10.1016/j.brainresbull.2016.08.018

Baas, P. W., Rao, A. N., Matamoros, A. J., and Leo, L. (2016). Stability properties of neuronal microtubules. *Cytoskeleton (Hoboken)* 73, 442–460. doi: 10.1002/cm.21286

Bakota, L., Ussif, A., Jeserich, G., and Brandt, R. (2017). Systemic and network functions of the microtubule-associated protein tau: implications for tau-based therapies. *Mol. Cell. Neurosci.* 16, 30257–30263. doi: 10.1016/j.mcn.2017.03.003

Ballatore, C., Lee, V. M., and Trojanowski, J. Q. (2007). Tau-mediated neurodegeneration in Alzheimer's disease and related disorders. *Nat. Rev. Neurosci.* 8, 663–672. doi: 10.1038/nrn2194

Barres, B. A., Jacobson, M. D., Schmid, R., Sendtner, M., and Raff, M. C. (1993). Does oligodendrocyte survival depend on axons? *Curr. Biol.* 3, 489–497. doi: 10.1016/0960-9822(93)90039-Q

Barrio, J. R., Small, G. W., Wong, K. P., Huang, S. C., Liu, J., Merrill, D. A., et al. (2015). *In vivo* characterization of chronic traumatic encephalopathy using [F-18]FDDNP PET brain imaging. *Proc. Natl. Acad. Sci. U.S.A.* 112, E2039–E2047. doi: 10.1073/pnas.1409952112

Berrocal, M., Corbacho, I., Sepulveda, M. R., Gutierrez-Merino, C., and Mata, A. M. (2016). Phospholipids and calmodulin modulate the inhibition of PMCA activity by tau. *Biochim. Biophys. Acta* 1864, 1028–1035. doi: 10.1016/j.bbamcr.2016.10.023

Black, M. M. (2016). Axonal transport: the orderly motion of axonal structures. *Methods Cell Biol.* 131, 1–19. doi: 10.1016/bs.mcb.2015.06.001

Blennow, K., Brody, D. L., Kochanek, P. M., Levin, H., Mckee, A., Ribbers, G. M., et al. (2016). Traumatic brain injuries. *Nat. Rev. Dis. Primers* 2:16084. doi: 10.1038/nrdp.2016.84

Blumbergs, P. C., Scott, G., Manavis, J., Wainwright, H., Simpson, D. A., and Mclean, A. J. (1994). Staining of amyloid precursor protein to study axonal damage in mild head injury. *Lancet* 344, 1055–1056. doi: 10.1016/S0140-6736(94)91712-4

Borroni, B., Garibotto, V., Agosti, C., Brambati, S. M., Bellelli, G., Gasparotti, R., et al. (2008). White matter changes in corticobasal degeneration syndrome and correlation with limb apraxia. *Arch. Neurol.* 65, 796–801. doi: 10.1001/archneur.65.6.796

Bozzali, M., Falini, A., Franceschi, M., Cercignani, M., Zuffi, M., Scotti, G., et al. (2002). White matter damage in Alzheimer's disease assessed *in vivo* using diffusion tensor magnetic resonance imaging. *J. Neurol. Neurosurg. Psychiatr.* 72, 742–746. doi: 10.1136/jnnp.72.6.742

Braak, E., Arai, K., and Braak, H. (1999). Cerebellar involvement in Pick's disease: affliction of mossy fibers, monodendritic brush cells, and dentate projection neurons. *Exp. Neurol.* 159, 153–163. doi: 10.1006/exnr.1999.7131

Brady, S. T., and Morfini, G. A. (2017). Regulation of motor proteins, axonal transport deficits and adult-onset neurodegenerative diseases. *Neurobiol. Dis.* 105, 273–282. doi: 10.1016/j.nbd.2017.04.010

Brandt, R., Leger, J., and Lee, G. (1995). Interaction of tau with the neural plasma membrane mediated by tau's amino-terminal projection domain. *J. Cell Biol.* 131, 1327–1340. doi: 10.1083/jcb.131.5.1327

Brion, J. P., Tremp, G., and Octave, J. N. (1999). Transgenic expression of the shortest human tau affects its compartmentalization and its phosphorylation as in the pretangle stage of Alzheimer's disease. *Am. J. Pathol.* 154, 255–270. doi: 10.1016/S0002-9440(10)65272-8

Caillierez, R., Begard, S., Lecolle, K., Deramecourt, V., Zommer, N., Dujardin, S., et al. (2013). Lentiviral delivery of the human wild-type tau protein mediates a slow and progressive neurodegenerative tau pathology in the rat brain. *Mol. Ther.* 21, 1358–1368. doi: 10.1038/mt.2013.66

Carmel, G., Mager, E. M., Binder, L. I., and Kuret, J. (1996). The structural basis of monoclonal antibody Alz50's selectivity for Alzheimer's disease pathology. *J. Biol. Chem.* 271, 32789–32795. doi: 10.1074/jbc.271.51.32789

Cheng, H. C., Ulane, C. M., and Burke, R. E. (2010). Clinical progression in Parkinson disease and the neurobiology of axons. *Ann. Neurol.* 67, 715–725. doi: 10.1002/ana.21995

Chin, S. S., and Goldman, J. E. (1996). Glial inclusions in CNS degenerative diseases. *J. Neuropathol. Exp. Neurol.* 55, 499–508. doi: 10.1097/00005072-199605000-00001

Cleveland, D. W., Hwo, S. Y., and Kirschner, M. W. (1977a). Physical and chemical properties of purified tau factor and the role of tau in microtubule assembly. *J. Mol. Biol.* 116, 227–247. doi: 10.1016/0022-2836(77)90214-5

Cleveland, D. W., Hwo, S. Y., and Kirschner, M. W. (1977b). Purification of tau, a microtubule-associated protein that induces assembly of microtubules from purified tubulin. *J. Mol. Biol.* 116, 207–225. doi: 10.1016/0022-2836(77)90213-3

Cochran, E. J., Fox, J. H., and Mufson, E. J. (1994). Severe panencephalic Pick's disease with Alzheimer's disease-like neuropil threads and synaptophysin immunoreactivity. *Acta Neuropathol.* 88, 479–484. doi: 10.1007/BF00389503

Combs, B., Hamel, C., and Kanaan, N. M. (2016a). Pathological conformations involving the amino terminus of tau occur early in Alzheimer's disease and are differentially detected by monoclonal antibodies. *Neurobiol. Dis.* 94, 18–31. doi: 10.1016/j.nbd.2016.05.016

Combs, B., Kneynsberg, A., and Kanaan, N. M. (2016b). Gene therapy models of Alzheimer's disease and other dementias. *Methods Mol. Biol.* 1382, 339–366. doi: 10.1007/978-1-4939-3271-9_25

Conde, C., and Caceres, A. (2009). Microtubule assembly, organization and dynamics in axons and dendrites. *Nat. Rev. Neurosci.* 10, 319–332. doi: 10.1038/nrn2631

Cox, K., Combs, B., Abdelmesih, B., Morfini, G., Brady, S. T., and Kanaan, N. M. (2016). Analysis of isoform-specific tau aggregates suggests a common toxic mechanism involving similar pathological conformations and axonal transport inhibition. *Neurobiol. Aging* 47, 113–126. doi: 10.1016/j.neurobiolaging.2016.07.015

Dawson, H. N., Ferreira, A., Eyster, M. V., Ghoshal, N., Binder, L. I., and Vitek, M. P. (2001). Inhibition of neuronal maturation in primary hippocampal neurons from tau deficient mice. *J. Cell Sci.* 114, 1179–1187.

de Calignon, A., Polydoro, M., Suarez-Calvet, M., William, C., Adamowicz, D. H., Kopeikina, K. J., et al. (2012). Propagation of tau pathology in a model of early Alzheimer's disease. *Neuron* 73, 685–697. doi: 10.1016/j.neuron.2011.11.033

Decker, H., Lo, K. Y., Unger, S. M., Ferreira, S. T., and Silverman, M. A. (2010). Amyloid-beta peptide oligomers disrupt axonal transport through an NMDA receptor-dependent mechanism that is mediated by glycogen synthase kinase 3beta in primary cultured hippocampal neurons. *J. Neurosci.* 30, 9166–9171. doi: 10.1523/JNEUROSCI.1074-10.2010

Decker, J. M., Kruger, L., Sydow, A., Zhao, S., Frotscher, M., Mandelkow, E., et al. (2015). Pro-aggregant Tau impairs mossy fiber plasticity due to structural changes and Ca(++) dysregulation. *Acta Neuropathol. Commun.* 3, 23. doi: 10.1186/s40478-015-0193-3

Dekosky, S. T., and Scheff, S. W. (1990). Synapse loss in frontal cortex biopsies in Alzheimer's disease: correlation with cognitive severity. *Ann. Neurol.* 27, 457–464. doi: 10.1002/ana.410270502

Delisle, M. B., Murrell, J. R., Richardson, R., Trofatter, J. A., Rascol, O., Soulages, X., et al. (1999). A mutation at codon 279 (N279K) in exon 10 of the Tau gene causes a tauopathy with dementia and supranuclear palsy. *Acta Neuropathol.* 98, 62–77. doi: 10.1007/s004010051052

Dessi, F., Colle, M. A., Hauw, J. J., and Duyckaerts, C. (1997). Accumulation of SNAP-25 immunoreactive material in axons of Alzheimer's disease. *Neuroreport* 8, 3685–3689. doi: 10.1097/00001756-199712010-00006

Dickson, D. W. (1998). Pick's disease: a modern approach. *Brain Pathol.* 8, 339–354. doi: 10.1111/j.1750-3639.1998.tb00158.x

Dickson, D. W. (1999). Neuropathologic differentiation of progressive supranuclear palsy and corticobasal degeneration. *J. Neurol.* 246(Suppl. 2), II6–II15. doi: 10.1007/BF03161076

Dickson, D. W., Feany, M. B., Yen, S. H., Mattiace, L. A., and Davies, P. (1996). Cytoskeletal pathology in non-Alzheimer degenerative dementia: new lesions in diffuse Lewy body disease, Pick's disease, and corticobasal degeneration. *J. Neural Transm. Suppl.* 47, 31–46. doi: 10.1007/978-3-7091-6892-9_2

Doi, T., Iwasa, K., Makifuchi, T., and Takamori, M. (1999). White matter hyperintensities on MRI in a patient with corticobasal degeneration. *Acta Neurol. Scand.* 99, 199–201. doi: 10.1111/j.1600-0404.1999.tb07345.x

Dopper, E. G., Rombouts, S. A., Jiskoot, L. C., Den Heijer, T., De Graaf, J. R., De Koning, I., et al. (2014). Structural and functional brain connectivity in presymptomatic familial frontotemporal dementia. *Neurology* 83, e19–e26. doi: 10.1212/WNL.0000000000000583

Duff, K., Knight, H., Refolo, L. M., Sanders, S., Yu, X., Picciano, M., et al. (2000). Characterization of pathology in transgenic mice over-expressing human genomic and cDNA tau transgenes. *Neurobiol. Dis.* 7, 87–98. doi: 10.1006/nbdi.1999.0279

Dumanchin, C., Camuzat, A., Campion, D., Verpillat, P., Hannequin, D., Dubois, B., et al. (1998). Segregation of a missense mutation in the microtubule-associated protein tau gene with familial frontotemporal dementia and parkinsonism. *Hum. Mol. Genet.* 7, 1825–1829. doi: 10.1093/hmg/7.11.1825

Eckert, A., Nisbet, R., Grimm, A., and Gotz, J. (2014). March separate, strike together–role of phosphorylated TAU in mitochondrial dysfunction in Alzheimer's disease. *Biochim. Biophys. Acta* 1842, 1258–1266. doi: 10.1016/j.bbadis.2013.08.013

Fa, M., Puzzo, D., Piacentini, R., Staniszewski, A., Zhang, H., Baltrons, M. A., et al. (2016). Extracellular Tau oligomers produce an immediate impairment of LTP and memory. *Sci. Rep.* 6:19393. doi: 10.1038/srep19393

Feany, M. B., and Dickson, D. W. (1995). Widespread cytoskeletal pathology characterizes corticobasal degeneration. *Am. J. Pathol.* 146, 1388–1396.

Feinstein, S. C., and Wilson, L. (2005). Inability of tau to properly regulate neuronal microtubule dynamics: a loss-of-function mechanism by which tau might mediate neuronal cell death. *Biochim. Biophys. Acta* 1739, 268–279. doi: 10.1016/j.bbadis.2004.07.002

Foster, N. L., Wilhelmsen, K., Sima, A. A., Jones, M. Z., D'amato, C. J., and Gilman, S. (1997). Frontotemporal dementia and parkinsonism linked to chromosome 17: a consensus conference. Conference participants. *Ann. Neurol* 41, 706–715. doi: 10.1002/ana.410410606

Fujio, J., Hosono, H., Ishiguro, K., Ikegami, S., and Fujita, S. C. (2007). Tau phosphorylation in the mouse brain during aversive conditioning. *Neurochem. Int.* 51, 200–208. doi: 10.1016/j.neuint.2007.04.024

Gatto, R. G., Chu, Y., Ye, A. Q., Price, S. D., Tavassoli, E., Buenaventura, A., et al. (2015). Analysis of YFP(J16)-R6/2 reporter mice and postmortem brains reveals early pathology and increased vulnerability of callosal axons in Huntington's disease. *Hum. Mol. Genet.* 24, 5285–5298. doi: 10.1093/hmg/ddv248

Ghetti, B., Oblak, A. L., Boeve, B. F., Johnson, K. A., Dickerson, B. C., and Goedert, M. (2015). Invited review: frontotemporal dementia caused by microtubule-associated protein tau gene (MAPT) mutations: a chameleon for neuropathology and neuroimaging. *Neuropathol. Appl. Neurobiol.* 41, 24–46. doi: 10.1111/nan.12213

Ghoshal, N., Garcia-Sierra, F., Wuu, J., Leurgans, S., Bennett, D. A., Berry, R. W., et al. (2002). Tau conformational changes correspond to impairments of episodic memory in mild cognitive impairment and Alzheimer's disease. *Exp. Neurol.* 177, 475–493. doi: 10.1006/exnr.2002.8014

Gibbs, K. L., Greensmith, L., and Schiavo, G. (2015). Regulation of axonal transport by protein kinases. *Trends Biochem. Sci.* 40, 597–610. doi: 10.1016/j.tibs.2015.08.003

Giza, C. C., and Hovda, D. A. (2001). The Neurometabolic Cascade of Concussion. *J. Athl. Train.* 36, 228–235.

Gotz, J., Chen, F., Van Dorpe, J., and Nitsch, R. M. (2001). Formation of neurofibrillary tangles in P301l tau transgenic mice induced by Abeta 42 fibrils. *Science* 293, 1491–1495. doi: 10.1126/science.1062097

Gotz, J., Deters, N., Doldissen, A., Bokhari, L., Ke, Y., Wiesner, A., et al. (2007). A decade of tau transgenic animal models and beyond. *Brain Pathol.* 17, 91–103. doi: 10.1111/j.1750-3639.2007.00051.x

Gotz, J., Ittner, L. M., and Kins, S. (2006). Do axonal defects in tau and amyloid precursor protein transgenic animals model axonopathy in Alzheimer's disease? *J. Neurochem.* 98, 993–1006. doi: 10.1111/j.1471-4159.2006.03955.x

Gotz, J., Probst, A., Spillantini, M. G., Schafer, T., Jakes, R., Burki, K., et al. (1995). Somatodendritic localization and hyperphosphorylation of tau protein in transgenic mice expressing the longest human brain tau isoform. *EMBO J.* 14, 1304–1313.

Guo, T., Noble, W., and Hanger, D. P. (2017). Roles of tau protein in health and disease. *Acta Neuropathol.* 133, 665–704. doi: 10.1007/s00401-017-1707-9

Hampel, H., Teipel, S. J., Alexander, G. E., Horwitz, B., Teichberg, D., Schapiro, M. B., et al. (1998). Corpus callosum atrophy is a possible indicator of region- and cell type-specific neuronal degeneration in Alzheimer disease: a magnetic resonance imaging analysis. *Arch. Neurol.* 55, 193–198. doi: 10.1001/archneur.55.2.193

Harada, A., Oguchi, K., Okabe, S., Kuno, J., Terada, S., Ohshima, T., et al. (1994). Altered microtubule organization in small-calibre axons of mice lacking tau protein. *Nature* 369, 488–491. doi: 10.1038/369488a0

Hauw, J. J., Daniel, S. E., Dickson, D., Horoupian, D. S., Jellinger, K., Lantos, P. L., et al. (1994). Preliminary NINDS neuropathologic criteria for Steele-Richardson-Olszewski syndrome (progressive supranuclear palsy). *Neurology* 44, 2015–2019. doi: 10.1212/WNL.44.11.2015

Hauw, J. J., Verny, M., Delaere, P., Cervera, P., He, Y., and Duyckaerts, C. (1990). Constant neurofibrillary changes in the neocortex in progressive supranuclear palsy. Basic differences with Alzheimer's disease and aging. *Neurosci. Lett.* 119, 182–186. doi: 10.1016/0304-3940(90)90829-X

Hebron, M. L., Algarzae, N. K., Lonskaya, I., and Moussa, C. (2014). Fractalkine signaling and Tau hyper-phosphorylation are associated with autophagic alterations in lentiviral Tau and Abeta1-42 gene transfer models. *Exp. Neurol.* 251, 127–138. doi: 10.1016/j.expneurol.2013.01.009

Higuchi, M., Lee, V. M., and Trojanowski, J. Q. (2002). Tau and axonopathy in neurodegenerative disorders. *Neuromolecular Med.* 2, 131–150. doi: 10.1385/NMM:2:2:131

Higuchi, M., Zhang, B., Forman, M. S., Yoshiyama, Y., Trojanowski, J. Q., and Lee, V. M. (2005). Axonal degeneration induced by targeted expression of mutant human tau in oligodendrocytes of transgenic mice that model glial tauopathies. *J. Neurosci.* 25, 9434–9443. doi: 10.1523/JNEUROSCI.2691-05.2005

Huang, J., and Auchus, A. P. (2007). Diffusion tensor imaging of normal appearing white matter and its correlation with cognitive functioning in mild cognitive impairment and Alzheimer's disease. *Ann. N. Y. Acad. Sci.* 1097, 259–264. doi: 10.1196/annals.1379.021

Hutton, M., Lendon, C. L., Rizzu, P., Baker, M., Froelich, S., Houlden, H., et al. (1998). Association of missense and 5′-splice-site mutations in tau with the inherited dementia FTDP-17. *Nature* 393, 702–705. doi: 10.1038/31508

Hyman, B. T., Van Hoesen, G. W., and Damasio, A. R. (1990). Memory-related neural systems in Alzheimer's disease: an anatomic study. *Neurology* 40, 1721–1730. doi: 10.1212/WNL.40.11.1721

Ihara, M., Polvikoski, T. M., Hall, R., Slade, J. Y., Perry, R. H., Oakley, A. E., et al. (2010). Quantification of myelin loss in frontal lobe white matter in vascular dementia, Alzheimer's disease, and dementia with Lewy bodies. *Acta Neuropathol.* 119, 579–589. doi: 10.1007/s00401-009-0635-8

Ikeda, K., Akiyama, H., Haga, C., Kondo, H., Arima, K., and Oda, T. (1994). Argyrophilic thread-like structure in corticobasal degeneration and supranuclear palsy. *Neurosci. Lett.* 174, 157–159. doi: 10.1016/0304-3940(94)90010-8

Ikegami, S., Harada, A., and Hirokawa, N. (2000). Muscle weakness, hyperactivity, and impairment in fear conditioning in tau-deficient mice. *Neurosci. Lett.* 279, 129–132. doi: 10.1016/S0304-3940(99)00964-7

Imamura, K., Sahara, N., Kanaan, N. M., Tsukita, K., Kondo, T., Kutoku, Y., et al. (2016). Calcium dysregulation contributes to neurodegeneration in FTLD patient iPSC-derived neurons. *Sci. Rep.* 6:34904. doi: 10.1038/srep34904

Ishihara, T., Hong, M., Zhang, B., Nakagawa, Y., Lee, M. K., Trojanowski, J. Q., et al. (1999). Age-dependent emergence and progression of a tauopathy in transgenic mice overexpressing the shortest human tau isoform. *Neuron* 24, 751–762. doi: 10.1016/S0896-6273(00)81127-7

Ishizawa, K., Lin, W. L., Tiseo, P., Honer, W. G., Davies, P., and Dickson, D. W. (2000). A qualitative and quantitative study of grumose degeneration in progressive supranuclear palsy. *J. Neuropathol. Exp. Neurol.* 59, 513–524. doi: 10.1093/jnen/59.6.513

Ittner, L. M., Ke, Y. D., Delerue, F., Bi, M., Gladbach, A., Van Eersel, J., et al. (2010). Dendritic function of tau mediates amyloid-beta toxicity in Alzheimer's disease mouse models. *Cell* 142, 387–397. doi: 10.1016/j.cell.2010.06.036

Janning, D., Igaev, M., Sundermann, F., Bruhmann, J., Beutel, O., Heinisch, J. J., et al. (2014). Single-molecule tracking of tau reveals fast kiss-and-hop interaction with microtubules in living neurons. *Mol. Biol. Cell* 25, 3541–3551. doi: 10.1091/mbc.E14-06-1099

Jaworski, T., Dewachter, I., Lechat, B., Croes, S., Termont, A., Demedts, D., et al. (2009). AAV-tau mediates pyramidal neurodegeneration by cell-cycle re-entry without neurofibrillary tangle formation in wild-type mice. *PLoS ONE* 4:e7280. doi: 10.1371/journal.pone.0007280

Jaworski, T., Lechat, B., Demedts, D., Gielis, L., Devijver, H., Borghgraef, P., et al. (2011). Dendritic degeneration, neurovascular defects, and inflammation precede neuronal loss in a mouse model for tau-mediated neurodegeneration. *Am. J. Pathol.* 179, 2001–2015. doi: 10.1016/j.ajpath.2011.06.025

Jeganathan, S., Hascher, A., Chinnathambi, S., Biernat, J., Mandelkow, E. M., and Mandelkow, E. (2008). Proline-directed pseudo-phosphorylation at AT8 and PHF1 epitopes induces a compaction of the paperclip folding of Tau and generates a pathological (MC-1) conformation. *J. Biol. Chem.* 283, 32066–32076. doi: 10.1074/jbc.M805300200

Jeganathan, S., Von Bergen, M., Brutlach, H., Steinhoff, H. J., and Mandelkow, E. (2006). Global hairpin folding of tau in solution. *Biochemistry* 45, 2283–2293. doi: 10.1021/bi0521543

Kahlson, M. A., and Colodner, K. J. (2015). Glial Tau pathology in tauopathies: functional consequences. *J. Exp. Neurosci.* 9, 43–50. doi: 10.4137/JEN.S25515

Kanaan, N. M., Cox, K., Alvarez, V. E., Stein, T. D., Poncil, S., and Mckee, A. C. (2016). Characterization of early pathological tau conformations and phosphorylation in chronic traumatic encephalopathy. *J. Neuropathol. Exp. Neurol.* 75, 19–34. doi: 10.1093/jnen/nlv001

Kanaan, N. M., Morfini, G. A., Lapointe, N. E., Pigino, G. F., Patterson, K. R., Song, Y., et al. (2011). Pathogenic forms of tau inhibit kinesin-dependent axonal transport through a mechanism involving activation of axonal phosphotransferases. *J. Neurosci.* 31, 9858–9868. doi: 10.1523/JNEUROSCI.0560-11.2011

Kanaan, N. M., Morfini, G., Pigino, G., Lapointe, N. E., Andreadis, A., Song, Y., et al. (2012). Phosphorylation in the amino terminus of tau prevents inhibition of anterograde axonal transport. *Neurobiol. Aging* 33, 826 e815–830. doi: 10.1016/j.neurobiolaging.2011.06.006

Kanaan, N. M., Pigino, G. F., Brady, S. T., Lazarov, O., Binder, L. I., and Morfini, G. A. (2013). Axonal degeneration in Alzheimer's disease: when signaling abnormalities meet the axonal transport system. *Exp. Neurol.* 246, 44–53. doi: 10.1016/j.expneurol.2012.06.003

Ke, Y. D., Suchowerska, A. K., Van Der Hoven, J., De Silva, D. M., Wu, C. W., Van Eersel, J., et al. (2012). Lessons from tau-deficient mice. *Int. J. Alzheimers. Dis.* 2012:873270. doi: 10.1155/2012/873270

Kiernan, P. T., Montenigro, P. H., Solomon, T. M., and Mckee, A. C. (2015). Chronic traumatic encephalopathy: a neurodegenerative consequence of repetitive traumatic brain injury. *Semin. Neurol.* 35, 20–28. doi: 10.1055/s-0035-1545080

Knake, S., Belke, M., Menzler, K., Pilatus, U., Eggert, K. M., Oertel, W. H., et al. (2010). *In vivo* demonstration of microstructural brain pathology in progressive supranuclear palsy: a DTI study using TBSS. *Mov. Disord.* 25, 1232–1238. doi: 10.1002/mds.23054

Kneynsberg, A., Collier, T. J., Manfredsson, F. P., and Kanaan, N. M. (2016). Quantitative and semi-quantitative measurements of axonal degeneration in tissue and primary neuron cultures. *J. Neurosci. Methods* 266, 32–41. doi: 10.1016/j.jneumeth.2016.03.004

Koerte, I. K., Ertl-Wagner, B., Reiser, M., Zafonte, R., and Shenton, M. E. (2012a). White matter integrity in the brains of professional soccer players without a symptomatic concussion. *JAMA* 308, 1859–1861. doi: 10.1001/jama.2012.13735

Koerte, I. K., Kaufmann, D., Hartl, E., Bouix, S., Pasternak, O., Kubicki, M., et al. (2012b). A prospective study of physician-observed concussion during a varsity university hockey season: white matter integrity in ice hockey players. Part 3 of 4. *Neurosurg. Focus* 33, E3:1–7. doi: 10.3171/2012.10.FOCUS12303

Kouri, N., Carlomagno, Y., Baker, M., Liesinger, A. M., Caselli, R. J., Wszolek, Z. K., et al. (2014). Novel mutation in MAPT exon 13 (p.N410H) causes corticobasal degeneration. *Acta Neuropathol.* 127, 271–282. doi: 10.1007/s00401-013-1193-7

Kouri, N., Whitwell, J. L., Josephs, K. A., Rademakers, R., and Dickson, D. W. (2011). Corticobasal degeneration: a pathologically distinct 4R tauopathy. *Nat. Rev. Neurol.* 7, 263–272. doi: 10.1038/nrneurol.2011.43

Kovacs, G. G., Majtenyi, K., Spina, S., Murrell, J. R., Gelpi, E., Hoftberger, R., et al. (2008). White matter tauopathy with globular glial inclusions: a distinct sporadic frontotemporal lobar degeneration. *J. Neuropathol. Exp. Neurol.* 67, 963–975. doi: 10.1097/NEN.0b013e318187a80f

Kowall, N. W., and Kosik, K. S. (1987). Axonal disruption and aberrant localization of tau protein characterize the neuropil pathology of Alzheimer's disease. *Ann. Neurol.* 22, 639–643. doi: 10.1002/ana.410220514

Kraus, M. F., Susmaras, T., Caughlin, B. P., Walker, C. J., Sweeney, J. A., and Little, D. M. (2007). White matter integrity and cognition in chronic traumatic brain injury: a diffusion tensor imaging study. *Brain* 130, 2508–2519. doi: 10.1093/brain/awm216

LaFerla, F. M., and Green, K. N. (2012). Animal models of Alzheimer disease. *Cold Spring Harb. Perspect. Med.* 2:a006320. doi: 10.1101/cshperspect.a006320

LaPointe, N. E., Morfini, G., Pigino, G., Gaisina, I. N., Kozikowski, A. P., Binder, L. I., et al. (2009). The amino terminus of tau inhibits kinesin-dependent axonal transport: implications for filament toxicity. *J. Neurosci. Res.* 87, 440–451. doi: 10.1002/jnr.21850

Lau, D. H., Hogseth, M., Phillips, E. C., O'neill, M. J., Pooler, A. M., Noble, W., et al. (2016). Critical residues involved in tau binding to fyn: implications for tau phosphorylation in Alzheimer's disease. *Acta Neuropathol. Commun.* 4, 49. doi: 10.1186/s40478-016-0317-4

Lee, G., Newman, S. T., Gard, D. L., Band, H., and Panchamoorthy, G. (1998). Tau interacts with src-family non-receptor tyrosine kinases. *J Cell Sci.* 111(Pt 21), 3167–3177.

Lei, P., Ayton, S., Moon, S., Zhang, Q., Volitakis, I., Finkelstein, D. I., et al. (2014). Motor and cognitive deficits in aged tau knockout mice in two background strains. *Mol. Neurodegener.* 9:29. doi: 10.1186/1750-1326-9-29

Lewis, J., Mcgowan, E., Rockwood, J., Melrose, H., Nacharaju, P., Van Slegtenhorst, M., et al. (2000). Neurofibrillary tangles, amyotrophy and progressive motor disturbance in mice expressing mutant (P301L) tau protein. *Nat. Genet.* 25, 402–405. doi: 10.1038/78078

Li, T., Hawkes, C., Qureshi, H. Y., Kar, S., and Paudel, H. K. (2006). Cyclin-dependent protein kinase 5 primes microtubule-associated protein tau site-specifically for glycogen synthase kinase 3beta. *Biochemistry* 45, 3134–3145. doi: 10.1021/bi051635j

Liao, H., Li, Y., Brautigan, D. L., and Gundersen, G. G. (1998). Protein phosphatase 1 is targeted to microtubules by the microtubule-associated protein Tau. *J. Biol. Chem.* 273, 21901–21908. doi: 10.1074/jbc.273.34.21901

Lin, W. L., Lewis, J., Yen, S. H., Hutton, M., and Dickson, D. W. (2003). Ultrastructural neuronal pathology in transgenic mice expressing mutant (P301L) human tau. *J. Neurocytol.* 32, 1091–1105. doi: 10.1023/B:NEUR.0000021904.61387.95

Lin, W. L., Zehr, C., Lewis, J., Hutton, M., Yen, S. H., and Dickson, D. W. (2005). Progressive white matter pathology in the spinal cord of transgenic mice expressing mutant (P301L) human tau. *J. Neurocytol.* 34, 397–410. doi: 10.1007/s11068-006-8726-0

Ling, H., Hardy, J., and Zetterberg, H. (2015). Neurological consequences of traumatic brain injuries in sports. *Mol. Cell. Neurosci.* 66, 114–122. doi: 10.1016/j.mcn.2015.03.012

Lingor, P., Koch, J. C., Tonges, L., and Bahr, M. (2012). Axonal degeneration as a therapeutic target in the CNS. *Cell Tissue Res.* 349, 289–311. doi: 10.1007/s00441-012-1362-3

Lippa, C. F. (2004). Synaptophysin immunoreactivity in Pick's disease: comparison with Alzheimer's disease and dementia with Lewy bodies. *Am. J. Alzheimers. Dis. Other Demen.* 19, 341–344. doi: 10.1177/153331750401900606

Lippa, C. F., Zhukareva, V., Kawarai, T., Uryu, K., Shafiq, M., Nee, L. E., et al. (2000). Frontotemporal dementia with novel tau pathology and a Glu342Val tau mutation. *Ann. Neurol.* 48, 850–858. doi: 10.1002/1531-8249(200012)48:6<850::AID-ANA5>3.0.CO;2-V

Liu, C., Song, X., Nisbet, R., and Gotz, J. (2016). Co-immunoprecipitation with Tau Isoform-specific antibodies reveals distinct protein interactions and highlights a putative role for 2N tau in disease. *J. Biol. Chem.* 291, 8173–8188. doi: 10.1074/jbc.M115.641902

Liu, C. W., Lee, G., and Jay, D. G. (1999). Tau is required for neurite outgrowth and growth cone motility of chick sensory neurons. *Cell Motil. Cytoskeleton* 43, 232–242. doi: 10.1002/(SICI)1097-0169(1999)43:3<232::AID-CM6>3.0.CO;2-7

Loomis, P. A., Howard, T. H., Castleberry, R. P., and Binder, L. I. (1990). Identification of nuclear tau isoforms in human neuroblastoma cells. *Proc. Natl. Acad. Sci. U.S.A.* 87, 8422–8426. doi: 10.1073/pnas.87.21.8422

Ludvigson, A. E., Luebke, J. I., Lewis, J., and Peters, A. (2011). Structural abnormalities in the cortex of the rTg4510 mouse model of tauopathy: a light and electron microscopy study. *Brain Struct. Funct.* 216, 31–42. doi: 10.1007/s00429-010-0295-4

Mandelkow, E. M., Stamer, K., Vogel, R., Thies, E., and Mandelkow, E. (2003). Clogging of axons by tau, inhibition of axonal traffic and starvation of synapses. *Neurobiol. Aging* 24, 1079–1085. doi: 10.1016/j.neurobiolaging.2003.04.007

Masters, C. L., Bateman, R., Blennow, K., Rowe, C. C., Sperling, R. A., and Cummings, J. L. (2015). Alzheimer's disease. *Nat. Rev. Dis. Primers* 1:15056. doi: 10.1038/nrdp.2015.56

Matamoros, A. J., and Baas, P. W. (2016). Microtubules in health and degenerative disease of the nervous system. *Brain Res. Bull.* 126, 217–225. doi: 10.1016/j.brainresbull.2016.06.016

Maxwell, W. L., Mccreath, B. J., Graham, D. I., and Gennarelli, T. A. (1995). Cytochemical evidence for redistribution of membrane pump calcium-ATPase and ecto-Ca-ATPase activity, and calcium influx in myelinated nerve fibres of the optic nerve after stretch injury. *J. Neurocytol.* 24, 925–942. doi: 10.1007/BF01215643

Mayford, M., Bach, M. E., Huang, Y. Y., Wang, L., Hawkins, R. D., and Kandel, E. R. (1996). Control of memory formation through regulated expression of a CaMKII transgene. *Science* 274, 1678–1683. doi: 10.1126/science.274.5293.1678

McAllister, T. W., Ford, J. C., Flashman, L. A., Maerlender, A., Greenwald, R. M., Beckwith, J. G., et al. (2014). Effect of head impacts on diffusivity measures in a cohort of collegiate contact sport athletes. *Neurology* 82, 63–69. doi: 10.1212/01.wnl.0000438220.16190.42

Mckee, A. C., Cantu, R. C., Nowinski, C. J., Hedley-Whyte, E. T., Gavett, B. E., Budson, A. E., et al. (2009). Chronic traumatic encephalopathy in athletes: progressive tauopathy after repetitive head injury. *J. Neuropathol. Exp. Neurol.* 68, 709–735. doi: 10.1097/NEN.0b013e3181a9d503

Mckee, A. C., Stein, T. D., Nowinski, C. J., Stern, R. A., Daneshvar, D. H., Alvarez, V. E., et al. (2012). The spectrum of disease in chronic traumatic encephalopathy. *Brain* 136(Pt 1), 43–64. doi: 10.1093/brain/aws307

Mckhann, G. M., Albert, M. S., Grossman, M., Miller, B., Dickson, D., Trojanowski, J. Q., et al. (2001). Clinical and pathological diagnosis of frontotemporal dementia: report of the work group on frontotemporal dementia and pick's disease. *Arch. Neurol.* 58, 1803–1809. doi: 10.1001/archneur.58.11.1803

Meerschaert, M. M., Magin, R. L., and Ye, A. Q. (2016). Anisotropic fractional diffusion tensor imaging. *J. Vib. Control* 22, 2211–2221. doi: 10.1177/1077546314568696

Moreno, H., Morfini, G., Buitrago, L., Ujlaki, G., Choi, S., Yu, E., et al. (2016). Tau pathology-mediated presynaptic dysfunction. *Neuroscience* 325, 30–38. doi: 10.1016/j.neuroscience.2016.03.044

Morfini, G. A., Burns, M., Binder, L. I., Kanaan, N. M., Lapointe, N., Bosco, D. A., et al. (2009). Axonal transport defects in neurodegenerative diseases. *J. Neurosci.* 29, 12776–12786. doi: 10.1523/JNEUROSCI.3463-09.2009

Morfini, G., Pigino, G., Beffert, U., Busciglio, J., and Brady, S. T. (2002a). Fast axonal transport misregulation and Alzheimer's disease. *Neuromolecular Med.* 2, 89–99. doi: 10.1385/NMM:2:2:089

Morfini, G., Pigino, G., Mizuno, N., Kikkawa, M., and Brady, S. T. (2007). Tau binding to microtubules does not directly affect microtubule-based vesicle motility. *J. Neurosci. Res.* 85, 2620–2630. doi: 10.1002/jnr.21154

Morfini, G., Schmidt, N., Weissmann, C., Pigino, G., and Kins, S. (2016). Conventional kinesin: biochemical heterogeneity and functional implications in health and disease. *Brain Res. Bull.* 126, 347–353. doi: 10.1016/j.brainresbull.2016.06.009

Morfini, G., Szebenyi, G., Brown, H., Pant, H. C., Pigino, G., Deboer, S., et al. (2004). A novel CDK5-dependent pathway for regulating GSK3 activity and kinesin-driven motility in neurons. *EMBO J.* 23, 2235–2245. doi: 10.1038/sj.emboj.7600237

Morfini, G., Szebenyi, G., Elluru, R., Ratner, N., and Brady, S. T. (2002b). Glycogen synthase kinase 3 phosphorylates kinesin light chains and negatively regulates kinesin-based motility. *EMBO J.* 21, 281–293. doi: 10.1093/emboj/21.3.281

Morfini, G., Szebenyi, G., Richards, B., and Brady, S. T. (2001). Regulation of kinesin: implications for neuronal development. *Dev. Neurosci.* 23, 364–376. doi: 10.1159/000048720

Morris, M., Koyama, A., Masliah, E., and Mucke, L. (2011). Tau reduction does not prevent motor deficits in two mouse models of Parkinson's disease. *PLoS ONE* 6:e29257. doi: 10.1371/journal.pone.0029257

Mufson, E. J., Perez, S. E., Nadeem, M., Mahady, L., Kanaan, N. M., Abrahamson, E. E., et al. (2016). Progression of tau pathology within cholinergic nucleus basalis neurons in chronic traumatic encephalopathy: a chronic effects of neurotrauma consortium study. *Brain Inj.* 30, 1399–1413. doi: 10.1080/02699052.2016.1219058

Murrell, J. R., Spillantini, M. G., Zolo, P., Guazzelli, M., Smith, M. J., Hasegawa, M., et al. (1999). Tau gene mutation G389R causes a tauopathy with abundant pick body-like inclusions and axonal deposits. *J. Neuropathol. Exp. Neurol.* 58, 1207–1226. doi: 10.1097/00005072-199912000-00002

Nakamura, Y., Takeda, M., Yoshimi, K., Hattori, H., Hariguchi, S., Hashimoto, S., et al. (1994). Involvement of clathrin light chains in the pathology of Pick's disease; implication for impairment of axonal transport. *Neurosci. Lett.* 180, 25–28. doi: 10.1016/0304-3940(94)90905-9

Niewidok, B., Igaev, M., Sundermann, F., Janning, D., Bakota, L., and Brandt, R. (2016). Presence of a carboxy-terminal pseudorepeat and disease-like pseudohyperphosphorylation critically influence tau's interaction with microtubules in axon-like processes. *Mol. Biol. Cell* 27, 3537–3549. doi: 10.1091/mbc.E16-06-0402

Padovani, A., Borroni, B., Brambati, S. M., Agosti, C., Broli, M., Alonso, R., et al. (2006). Diffusion tensor imaging and voxel based morphometry study in early progressive supranuclear palsy. *J. Neurol. Neurosurg. Psychiatr.* 77, 457–463. doi: 10.1136/jnnp.2005.075713

Papasozomenos, S. C., and Binder, L. I. (1987). Phosphorylation determines two distinct species of Tau in the central nervous system. *Cell Motil. Cytoskeleton* 8, 210–226. doi: 10.1002/cm.970080303

Petrie, E. C., Cross, D. J., Yarnykh, V. L., Richards, T., Martin, N. M., Pagulayan, K., et al. (2014). Neuroimaging, behavioral, and psychological sequelae of repetitive combined blast/impact mild traumatic brain injury in Iraq and Afghanistan war veterans. *J. Neurotrauma* 31, 425–436. doi: 10.1089/neu.2013.2952

Pollock, N. J., Mirra, S. S., Binder, L. I., Hansen, L. A., and Wood, J. G. (1986). Filamentous aggregates in Pick's disease, progressive supranuclear palsy, and Alzheimer's disease share antigenic determinants with microtubule-associated protein, tau. *Lancet* 2:1211. doi: 10.1016/S0140-6736(86)92212-9

Praprotnik, D., Smith, M. A., Richey, P. L., Vinters, H. V., and Perry, G. (1996). Filament heterogeneity within the dystrophic neurites of senile plaques suggests blockage of fast axonal transport in Alzheimer's disease. *Acta Neuropathol.* 91, 226–235. doi: 10.1007/s004010050420

Probst, A., Gotz, J., Wiederhold, K. H., Tolnay, M., Mistl, C., Jaton, A. L., et al. (2000). Axonopathy and amyotrophy in mice transgenic for human four-repeat tau protein. *Acta Neuropathol.* 99, 469–481. doi: 10.1007/s004010051148

Probst, A., Langui, D., Lautenschlager, C., Ulrich, J., Brion, J. P., and Anderton, B. H. (1988). Progressive supranuclear palsy: extensive neuropil threads in addition to neurofibrillary tangles. Very similar antigenicity of subcortical neuronal pathology in progressive supranuclear palsy and Alzheimer's disease. *Acta Neuropathol.* 77, 61–68. doi: 10.1007/BF00688244

Probst, A., Tolnay, M., Langui, D., Goedert, M., and Spillantini, M. G. (1996). Pick's disease: hyperphosphorylated tau protein segregates to the somatoaxonal compartment. *Acta Neuropathol.* 92, 588–596. doi: 10.1007/s004010050565

Qiang, L., Yu, W., Andreadis, A., Luo, M., and Baas, P. W. (2006). Tau protects microtubules in the axon from severing by katanin. *J. Neurosci.* 26, 3120–3129. doi: 10.1523/JNEUROSCI.5392-05.2006

Raff, M. C., Whitmore, A. V., and Finn, J. T. (2002). Axonal self-destruction and neurodegeneration. *Science* 296, 868–871. doi: 10.1126/science.1068613

Ramirez-Rios, S., Denarier, E., Prezel, E., Vinit, A., Stoppin-Mellet, V., Devred, F., et al. (2016). Tau antagonizes end-binding protein tracking at microtubule ends through a phosphorylation-dependent mechanism. *Mol. Biol. Cell* 27, 2924–2934. doi: 10.1091/mbc.E16-01-0029

Rao, M. V., Mcbrayer, M. K., Campbell, J., Kumar, A., Hashim, A., Sershen, H., et al. (2014). Specific calpain inhibition by calpastatin prevents tauopathy and neurodegeneration and restores normal lifespan in tau P301L mice. *J. Neurosci.* 34, 9222–9234. doi: 10.1523/JNEUROSCI.1132-14.2014

Rasband, M. N. (2010). The axon initial segment and the maintenance of neuronal polarity. *Nat. Rev. Neurosci.* 11, 552–562. doi: 10.1038/nrn2852

Rebeiz, J. J., Kolodny, E. H., and Richardson, E. P. Jr. (1968). Corticodentatonigral degeneration with neuronal achromasia. *Arch. Neurol.* 18, 20–33. doi: 10.1001/archneur.1968.00470310034003

Rizzu, P., Van Swieten, J. C., Joosse, M., Hasegawa, M., Stevens, M., Tibben, A., et al. (1999). High prevalence of mutations in the microtubule-associated protein tau in a population study of frontotemporal dementia in the Netherlands. *Am. J. Hum. Genet.* 64, 414–421. doi: 10.1086/302256

Rodriguez-Martin, T., Pooler, A. M., Lau, D. H., Morotz, G. M., De Vos, K. J., Gilley, J., et al. (2016). Reduced number of axonal mitochondria and tau hypophosphorylation in mouse P301L tau knockin neurons. *Neurobiol. Dis.* 85, 1–10. doi: 10.1016/j.nbd.2015.10.007

Rohrer, J. D., Ridgway, G. R., Modat, M., Ourselin, S., Mead, S., Fox, N. C., et al. (2010). Distinct profiles of brain atrophy in frontotemporal lobar degeneration caused by progranulin and tau mutations. *Neuroimage* 53, 1070–1076. doi: 10.1016/j.neuroimage.2009.12.088

Samsonov, A., Yu, J. Z., Rasenick, M., and Popov, S. V. (2004). Tau interaction with microtubules *in vivo*. *J. Cell Sci.* 117, 6129–6141. doi: 10.1242/jcs.01531

Santacruz, K., Lewis, J., Spires, T., Paulson, J., Kotilinek, L., Ingelsson, M., et al. (2005). Tau suppression in a neurodegenerative mouse model improves memory function. *Science* 309, 476–481. doi: 10.1126/science.1113694

Seitz, A., Kojima, H., Oiwa, K., Mandelkow, E. M., Song, Y. H., and Mandelkow, E. (2002). Single-molecule investigation of the interference between kinesin, tau and MAP2c. *EMBO J.* 21, 4896–4905. doi: 10.1093/emboj/cdf503

Selden, S. C., and Pollard, T. D. (1986). Interaction of actin filaments with microtubules is mediated by microtubule-associated proteins and regulated by phosphorylation. *Ann. N. Y. Acad. Sci.* 466, 803–812. doi: 10.1111/j.1749-6632.1986.tb38464.x

Siman, R., Cocca, R., and Dong, Y. (2015). The mTOR inhibitor rapamycin mitigates perforant pathway neurodegeneration and synapse loss in a mouse model of early-stage alzheimer-type tauopathy. *PLoS ONE* 10:e0142340. doi: 10.1371/journal.pone.0142340

Siman, R., Lin, Y. G., Malthankar-Phatak, G., and Dong, Y. (2013). A rapid gene delivery-based mouse model for early-stage Alzheimer disease-type tauopathy. *J. Neuropathol. Exp. Neurol.* 72, 1062–1071. doi: 10.1097/NEN.0000000000000006

Sjobeck, M., and Englund, E. (2003). Glial levels determine severity of white matter disease in Alzheimer's disease: a neuropathological study of glial changes. *Neuropathol. Appl. Neurobiol.* 29, 159–169. doi: 10.1046/j.1365-2990.2003.00456.x

Sjobeck, M., Haglund, M., and Englund, E. (2005). Decreasing myelin density reflected increasing white matter pathology in Alzheimer's disease–a neuropathological study. *Int. J. Geriatr. Psychiatry* 20, 919–926. doi: 10.1002/gps.1384

Song, Y., and Brady, S. T. (2015). Post-translational modifications of tubulin: pathways to functional diversity of microtubules. *Trends Cell Biol.* 25, 125–136. doi: 10.1016/j.tcb.2014.10.004

Spires, T. L., Orne, J. D., Santacruz, K., Pitstick, R., Carlson, G. A., Ashe, K. H., et al. (2006). Region-specific dissociation of neuronal loss and neurofibrillary pathology in a mouse model of tauopathy. *Am. J. Pathol.* 168, 1598–1607. doi: 10.2353/ajpath.2006.050840

Spittaels, K., Van Den Haute, C., Van Dorpe, J., Bruynseels, K., Vandezande, K., Laenen, I., et al. (1999). Prominent axonopathy in the brain and spinal cord of transgenic mice overexpressing four-repeat human tau protein. *Am. J. Pathol.* 155, 2153–2165. doi: 10.1016/S0002-9440(10)65533-2

Stamer, K., Vogel, R., Thies, E., Mandelkow, E., and Mandelkow, E. M. (2002). Tau blocks traffic of organelles, neurofilaments, and APP vesicles in neurons and enhances oxidative stress. *J. Cell Biol.* 156, 1051–1063. doi: 10.1083/jcb.200108057

Stern, J. L., Lessard, D. V., Hoeprich, G. J., Morfini, G. A., and Berger, C. L. (2017). Phospho-regulation of tau modulates inhibition of kinesin-1 motility. *Mol. Biol. Cell.* 28, 1079–1087. doi: 10.1091/mbc.E16-10-0728

Stoub, T. R., Detoledo-Morrell, L., Stebbins, G. T., Leurgans, S., Bennett, D. A., and Shah, R. C. (2006). Hippocampal disconnection contributes to memory dysfunction in individuals at risk for Alzheimer's disease. *Proc. Natl. Acad. Sci. U.S.A.* 103, 10041–10045. doi: 10.1073/pnas.0603414103

Sudo, H., and Baas, P. W. (2011). Strategies for diminishing katanin-based loss of microtubules in tauopathic neurodegenerative diseases. *Hum. Mol. Genet.* 20, 763–778. doi: 10.1093/hmg/ddq521

Sultan, A., Nesslany, F., Violet, M., Begard, S., Loyens, A., Talahari, S., et al. (2011). Nuclear tau, a key player in neuronal DNA protection. *J. Biol. Chem.* 286, 4566–4575. doi: 10.1074/jbc.M110.199976

Sun, W., Qureshi, H. Y., Cafferty, P. W., Sobue, K., Agarwal-Mawal, A., Neufield, K. D., et al. (2002). Glycogen synthase kinase-3beta is complexed with tau protein in brain microtubules. *J. Biol. Chem.* 277, 11933–11940. doi: 10.1074/jbc.M107182200

Swanson, E., Breckenridge, L., Mcmahon, L., Som, S., Mcconnell, I., and Bloom, G. S. (2017). Extracellular tau oligomers induce invasion of endogenous tau into the somatodendritic compartment and axonal transport dysfunction. *J. Alzheimers. Dis.* 58, 803–820. doi: 10.3233/JAD-170168

Takei, Y., Teng, J., Harada, A., and Hirokawa, N. (2000). Defects in axonal elongation and neuronal migration in mice with disrupted tau and map1b genes. *J. Cell Biol.* 150, 989–1000. doi: 10.1083/jcb.150.5.989

Terry, R. D., Masliah, E., Salmon, D. P., Butters, N., Deteresa, R., Hill, R., et al. (1991). Physical basis of cognitive alterations in Alzheimer's disease: synapse loss is the major correlate of cognitive impairment. *Ann. Neurol.* 30, 572–580. doi: 10.1002/ana.410300410

Tiernan, C. T., Combs, B., Cox, K., Morfini, G., Brady, S. T., Counts, S. E., et al. (2016). Pseudophosphorylation of tau at S422 enhances SDS-stable dimer formation and impairs both anterograde and retrograde fast axonal transport. *Exp. Neurol.* 283, 318–329. doi: 10.1016/j.expneurol.2016.06.030

Tint, I., Slaughter, T., Fischer, I., and Black, M. M. (1998). Acute inactivation of tau has no effect on dynamics of microtubules in growing axons of cultured sympathetic neurons. *J. Neurosci.* 18, 8660–8673.

Tokuda, T., Ikeda, S., Yanagisawa, N., Ihara, Y., and Glenner, G. G. (1991). Re-examination of ex-boxers' brains using immunohistochemistry with antibodies to amyloid beta-protein and tau protein. *Acta Neuropathol.* 82, 280–285. doi: 10.1007/BF00308813

Tucker, K. L., Meyer, M., and Barde, Y. A. (2001). Neurotrophins are required for nerve growth during development. *Nat. Neurosci.* 4, 29–37. doi: 10.1038/82868

Uryu, K., Chen, X. H., Martinez, D., Browne, K. D., Johnson, V. E., Graham, D. I., et al. (2007). Multiple proteins implicated in neurodegenerative diseases accumulate in axons after brain trauma in humans. *Exp. Neurol.* 208, 185–192. doi: 10.1016/j.expneurol.2007.06.018

Uversky, V. N. (2015). Intrinsically disordered proteins and their (disordered) proteomes in neurodegenerative disorders. *Front. Aging Neurosci.* 7:18. doi: 10.3389/fnagi.2015.00018

Vanderweyde, T., Apicco, D. J., Youmans-Kidder, K., Ash, P. E., Cook, C., Lummertz Da Rocha, E., et al. (2016). Interaction of tau with the RNA-Binding Protein TIA1 regulates tau pathophysiology and toxicity. *Cell Rep.* 15, 1455–1466. doi: 10.1016/j.celrep.2016.04.045

van Hummel, A., Bi, M., Ippati, S., Van Der Hoven, J., Volkerling, A., Lee, W. S., et al. (2016). No overt deficits in aged tau-deficient C57Bl/6.Mapttm1(EGFP)Kit GFP knockin mice. *PLoS ONE* 11:e0163236. doi: 10.1371/journal.pone.0163236

Vermersch, P., Roche, J., Hamon, M., Daems-Monpeurt, C., Pruvo, J. P., Dewailly, P., et al. (1996). White matter magnetic resonance imaging hyperintensity in Alzheimer's disease: correlations with corpus callosum atrophy. *J. Neurol.* 243, 231–234. doi: 10.1007/BF00868519

Vossel, K. A., Xu, J. C., Fomenko, V., Miyamoto, T., Suberbielle, E., Knox, J. A., et al. (2015). Tau reduction prevents Abeta-induced axonal transport deficits by blocking activation of GSK3beta. *J. Cell Biol.* 209, 419–433. doi: 10.1083/jcb.201407065

Walsh, D. M., and Selkoe, D. J. (2016). A critical appraisal of the pathogenic protein spread hypothesis of neurodegeneration. *Nat. Rev. Neurosci.* 17, 251–260. doi: 10.1038/nrn.2016.13

Wang, L. N., Zhu, M. W., Feng, Y. Q., and Wang, J. H. (2006). Pick's disease with Pick bodies combined with progressive supranuclear palsy without tuft-shaped astrocytes: a clinical, neuroradiologic and pathological study of an autopsied case. *Neuropathology* 26, 222–230. doi: 10.1111/j.1440-1789.2006.00671.x

Weingarten, M. D., Lockwood, A. H., Hwo, S. Y., and Kirschner, M. W. (1975). A protein factor essential for microtubule assembly. *Proc. Natl. Acad. Sci. U.S.A.* 72, 1858–1862. doi: 10.1073/pnas.72.5.1858

Werth, J. L., and Thayer, S. A. (1994). Mitochondria buffer physiological calcium loads in cultured rat dorsal root ganglion neurons. *J. Neurosci.* 14, 348–356.

Whitwell, J. L., Master, A. V., Avula, R., Kantarci, K., Eggers, S. D., Edmonson, H. A., et al. (2011). Clinical correlates of white matter tract degeneration in progressive supranuclear palsy. *Arch. Neurol.* 68, 753–760. doi: 10.1001/archneurol.2011.107

Williams, D. R., and Lees, A. J. (2009). Progressive supranuclear palsy: clinicopathological concepts and diagnostic challenges. *Lancet Neurol.* 8, 270–279. doi: 10.1016/S1474-4422(09)70042-0

Wszolek, Z. K., Pfeiffer, R. F., Bhatt, M. H., Schelper, R. L., Cordes, M., Snow, B. J., et al. (1992). Rapidly progressive autosomal dominant parkinsonism and dementia with pallido-ponto-nigral degeneration. *Ann. Neurol.* 32, 312–320. doi: 10.1002/ana.410320303

Xia, D., Li, C., and Gotz, J. (2015). Pseudophosphorylation of Tau at distinct epitopes or the presence of the P301L mutation targets the microtubule-associated protein Tau to dendritic spines. *Biochim. Biophys. Acta* 1852, 913–924. doi: 10.1016/j.bbadis.2014.12.017

Yamakawa, K., Takanashi, M., Watanabe, M., Nakamura, N., Kobayashi, T., Hasegawa, M., et al. (2006). Pathological and biochemical studies on a case of Pick disease with severe white matter atrophy. *Neuropathology* 26, 586–591. doi: 10.1111/j.1440-1789.2006.00738.x

Yasuda, M., and Mayford, M. R. (2006). CaMKII activation in the entorhinal cortex disrupts previously encoded spatial memory. *Neuron* 50, 309–318. doi: 10.1016/j.neuron.2006.03.035

Yin, Y., Wang, Y., Gao, D., Ye, J., Wang, X., Fang, L., et al. (2016). Accumulation of human full-length tau induces degradation of nicotinic acetylcholine

receptor alpha4 via activating calpain-2. *Sci. Rep.* 6:27283. doi: 10.1038/srep 27283

Yoshiyama, Y., Zhang, B., Bruce, J., Trojanowski, J. Q., and Lee, V. M. (2003). Reduction of detyrosinated microtubules and Golgi fragmentation are linked to tau-induced degeneration in astrocytes. *J. Neurosci.* 23, 10662–10671.

Yuan, A., Kumar, A., Peterhoff, C., Duff, K., and Nixon, R. A. (2008). Axonal transport rates *in vivo* are unaffected by tau deletion or overexpression in mice. *J. Neurosci.* 28, 1682–1687. doi: 10.1523/JNEUROSCI.5242-07.2008

Zhang, L., Ravdin, L. D., Relkin, N., Zimmerman, R. D., Jordan, B., Lathan, W. E., et al. (2003). Increased diffusion in the brain of professional boxers: a preclinical sign of traumatic brain injury? *AJNR Am. J. Neuroradiol.* 24, 52–57.

Zhang, Y., Walter, R., Ng, P., Luong, P. N., Dutt, S., Heuer, H., et al. (2016). Progression of microstructural degeneration in progressive supranuclear palsy and corticobasal syndrome: a longitudinal diffusion tensor imaging study. *PLoS ONE* 11:e0157218. doi: 10.1371/journal.pone.0157218

Zhou, L., Miller, B. L., Mcdaniel, C. H., Kelly, L., Kim, O. J., and Miller, C. A. (1998). Frontotemporal dementia: neuropil spheroids and presynaptic terminal degeneration. *Ann. Neurol.* 44, 99–109. doi: 10.1002/ana.410440116

Conflict of Interest Statement: The authors declare that the research was conducted in the absence of any commercial or financial relationships that could be construed as a potential conflict of interest.

frontiers in Neuroscience

REVIEW
published: 31 August 2017
doi: 10.3389/fnins.2017.00481

A Mechanistic Understanding of Axon Degeneration in Chemotherapy-Induced Peripheral Neuropathy

Yusuke Fukuda[1,2†], *Yihang Li*[1,2†] *and Rosalind A. Segal*[1,2*]

[1] *Department of Neurobiology, Harvard Medical School, Boston, MA, United States,* [2] *Department of Cancer Biology, Dana-Farber Cancer Institute, Boston, MA, United States*

Chemotherapeutic agents cause many short and long term toxic side effects to peripheral nervous system (PNS) that drastically alter quality of life. Chemotherapy-induced peripheral neuropathy (CIPN) is a common and enduring disorder caused by several anti-neoplastic agents. CIPN typically presents with neuropathic pain, numbness of distal extremities, and/or oversensitivity to thermal or mechanical stimuli. This adverse side effect often requires a reduction in chemotherapy dosage or even discontinuation of treatment. Currently there are no effective treatment options for CIPN. While the underlying mechanisms for CIPN are not understood, current data identify a "dying back" axon degeneration of distal nerve endings as the major pathology in this disorder. Therefore, mechanistic understanding of axon degeneration will provide insights into the pathway and molecular players responsible for CIPN. Here, we review recent findings that expand our understanding of the pathogenesis of CIPN and discuss pathways that may be shared with the axonal degeneration that occurs during developmental axon pruning and during injury-induced Wallerian degeneration. These mechanistic insights provide new avenues for development of therapies to prevent or treat CIPN.

Keywords: axon, chemotherapy, CIPN, degeneration, DRG, neuropathy, sensory neuron, Wallerian

OPEN ACCESS

Edited by:
Robert W. Burgess, The Jackson Laboratory, United States

Reviewed by:
Sandra Rieger, Mount Desert Island Biological Laboratory, United States
Christian Gonzalez-Billault, Universidad de Chile, Chile

***Correspondence:**
Rosalind A. Segal
Rosalind_segal@dfci.harvard.edu

[†]*These authors have contributed equally to this work.*

Specialty section:
This article was submitted to Neurodegeneration, a section of the journal Frontiers in Neuroscience

Received: *23 May 2017*
Accepted: *14 August 2017*
Published: *31 August 2017*

Citation:
Fukuda Y, Li Y and Segal RA (2017) A Mechanistic Understanding of Axon Degeneration in Chemotherapy-Induced Peripheral Neuropathy. Front. Neurosci. 11:481. doi: 10.3389/fnins.2017.00481

INTRODUCTION

Cancer therapies result in multiple toxic side effects that limit the doses used and cause long-lasting damage to patients. Chemotherapy-induced peripheral neuropathy (CIPN) is a severe and long lasting side effect caused by diverse anticancer agents that damage sensory and/or motor nerves. Symptoms of CIPN include numbness, pain, burning, tingling, heat/cold hyperalgesia, and mechanical allodynia, as well as reduced motor function. CIPN commonly presents with a "Glove-and-Stocking" distribution with the most distal portions of the limb exhibiting the greatest deficits (Brewer et al., 2016). CIPN occurs in 30–70% of patients treated with specific categories of anticancer agents (Seretny et al., 2014). Symptoms usually begin after multiple doses of the chemotherapeutic agents, and progress as treatment continues. After the treatments cease, they can resolve in a short time period, or persist as a long-lasting sequela of cancer therapy.

Clinical assessment of CIPN is usually based on patient-derived questionnaires and physician-based grading scales such as the common toxicity criteria (CTC) scale. These evaluation methods suffer from subjectivity and inconsistency (Cavaletti et al., 2010; Brewer et al., 2016). More

objective evaluation methods have also been developed, such as quantitative sensory testing (QST), which measures the detection threshold for both mechanical and thermal sensory inputs. Nerve conduction studies (NCS), which assess both sensory and motor nerve action potential can also be used in patient assessment (Brewer et al., 2016), as decreased amplitude of sensory action potential are commonly observed in CIPN patients (Chaudhry et al., 1994; Park et al., 2013). Skin biopsy and quantitative assessment of intraepidermal nerve fiber (IENF) density provides a sensitive, objective and quantitative measurement of the small nerve fiber neuropathy commonly seen in CIPN (Periquet et al., 1999; Kroigard et al., 2014). However, these more objective measurements are not easily deployed in clinical assessments.

CHEMOTHERAPEUTIC DRUGS THAT CAUSE CIPN

Multiple anticancer drugs cause peripheral neuropathies; the most common are the taxanes, vinca alkaloids, platinum-based drugs, and protease inhibitors (Brewer et al., 2016; **Table 1**). Taxane agents (e.g., paclitaxel and docetaxel) exert their antimitotic effect by binding to polymerized tubulin within microtubules, and thereby preventing microtubule depolymerization (Jordan and Wilson, 2004). Vinca alkaloids (e.g., vincristine and vinblastine), another class of agents targeting microtubules, promote microtubule depolymerization and thereby disrupt mitotic spindles and cause cell cycle arrest (Jordan and Wilson, 2004; Kavallaris, 2010). As highly polarized dorsal root ganglion (DRG) sensory neurons require proper microtubule dynamics for axonal transport of mRNAs, proteins, mitochondria and other organelles, it is perhaps not surprising that these microtubule binding agents can cause degeneration of peripheral nerve fibers and symptoms of CIPN (Authier et al., 2000; Ja'afer et al., 2006; Gornstein and Schwarz, 2014; Geisler et al., 2016). As these two drugs with opposite effects on microtubule stability both can cause CIPN, it appears likely that diverse perturbations in microtubule dynamics may play a critical role instigating CIPN.

The platinum-based chemotherapeutics (e.g., cisplatin and oxaliplatin) exert their antineoplastic activity by forming interstrand DNA adduct (Suchankova et al., 2012), leading to cell cycle arrest (Johnstone et al., 2014). Patients treated with platinum agents exhibit predominantly sensory neuropathy (Addington and Freimer, 2016). It is not known whether this sensory neuropathy is due to damage of nuclear or mitochondrial DNA in DRG neurons or other cells, or reflects other actions of platinum-based compounds.

Proteasome inhibitors represent a novel class of anticancer drugs that result in protein accumulation and apoptosis (Adams, 2004). Bortezomib, an inhibitor of the 20S subunit of the proteasome, was the first proteasome inhibitor approved for clinical treatment of multiple myeloma (Curran and McKeage, 2009). Bortezomib induces a peripheral sensory neuropathy. As bortezomib exerts a microtubule stabilizing activity similar to paclitaxel in addition to proteasome inhibition (Poruchynsky et al., 2008), it is not clear whether the neuropathic effect reflects proteasome inhibition or microtubule changes.

TABLE 1 | Chemotherapeutic drugs implicated in CIPN.

Type of drug	Example	Mechanisms of drug action in treating cancer	Type of neuron affected
Platinum agents	Cisplatin Oxaliplatin	Bind to DNA, cell cycle arrest and apoptosis	Sensory
Taxane	Paclitaxel	Inhibit microtubule depolymerization, mitotic arrest	Sensory
Vinca alkaloid	Vincristine	Inhibit microtubule polymerization, mitotic arrest	Sensory, as well as motor and autonomic
Proteasome inhibitor	Bortezomib	Inhibit proteasome degradation, cycle arrest; enhance microtubule polymerization	Sensory

While other agents have been reported to cause neuropathy in some patients, the above chemotherapeutic agents represent the major drug categories currently responsible for CIPN. These agents have different mechanisms of action, and so it is not known whether they cause CIPN by a common pathway. Given the poor understanding of the disorder, it is not surprising that there are currently no effective treatments of CIPN, and that multiple clinical trials have had disappointing results. Among recent trials, duloxetine, an antidepressant therapy that inhibits serotonin and norepinephrine reuptake, was shown to have a small, but significant beneficial effect on CIPN (Smith et al., 2013). However, the other 14 out of 15 therapies tested failed to show beneficial effects on CIPN patients (Majithia et al., 2016). Thus, there is a clear need for greater understanding of CIPN to enable development and testing of new therapies. This review summarizes the up-to-date understanding of CIPN, discusses the known mechanisms of general axon degeneration and how this understanding provides insight into for future research into the pathogenesis of CIPN.

PRE-CLINICAL MODELS FOR STUDYING CIPN

Animal Models

To understand the biology of CIPN, a variety of preclinical models have been developed. Chemotherapy drugs are typically given to rodents (rats or mice) through intraperitoneal or intravenous injection, followed by behavioral, electrophysiological, or morphological analysis. These models enable a rigorous assessment of the neuropathological features consistently observed following chemotherapeutic treatment. A recent review (Hoke and Ray, 2014) provides a thorough overview of the current animal models used for CIPN study.

A "dying back" axon degeneration is a prototypical pathological feature of CIPN in patients, and this can be assessed both in patients and in rodent models by skin biopsy and measurement of IENF density (Authier et al., 2000). Both the number of innervating nerve fibers and the neuronal subtypes perturbed by chemotherapeutic agents can be readily and quantitatively assessed in animal models. Additional studies of sensory and motor nerve conduction including sensory and compound muscle action potentials and latency of evoked response can be carried out to assess CIPN in animal models. Several groups have reported decreased sciatic nerve fiber diameter in rats treated with various dosages of paclitaxel (Authier et al., 2000; Persohn et al., 2005; Arrieta et al., 2011), as well as decreased peripheral nerve conduction (Persohn et al., 2005); however motor function is not altered (Authier et al., 2000). Peripheral nerve fiber degeneration has also been reported in rats/mice treated with vincristine (Ja'afer et al., 2006; Geisler et al., 2016), bortezomib (Cavaletti et al., 2007; Carozzi et al., 2010; Meregalli et al., 2010) and cisplatin (Carozzi et al., 2010; Arrieta et al., 2011). Although sensory neurons represent the most common target of CIPN, damage to motor and autonomic neurons have also been reported (Mora et al., 2016).

Behavioral studies in rodent models of CIPN assess mechanical allodynia, mechanical hyperalgesia, and thermal hypo- and hyperalgesia following exposure to chemotherapeutic drugs. Mechanical allodynia, the over sensitization to touch, is assessed by applying a series of monofilaments, the Von Frey filaments, to the hind paw of the animal and the threshold of pressure applied that causes the animals to withdraw their paw is measured. To measure changes in responses to temperature, a hot or cold stimulus is applied by tail immersion or radiant heat, and the response as assessed by tail flick or paw withdrawal is quantified. It is not yet known which of these behaviors best reflects the clinical condition. Thermal hyperalgesia is commonly observed in rodent models of CIPN (Authier et al., 2000; Cata et al., 2008; Zheng et al., 2012), while mechanical hyperalgesia (Authier et al., 2000) and thermal allodynia (Arrieta et al., 2011) are also reported. Unfortunately, the behaviors observed are inconsistent among different research groups, which is likely due to the fact that current rodent models are not standardized for animal strain, age, sex, or drug dosing schedule (Hoke and Ray, 2014). The diverse methods of initiating and assessing CIPN in rodent models make it difficult to compare data across laboratories.

Non-mammalian models have also been reported, but are less commonly studied. Lisse and colleagues reported on a Zebrafish model, in which DRG axon degeneration and impaired twitching response were observed after a 4-day treatment with paclitaxel (Lisse et al., 2016). Several groups have also established *Drosophila* models to study the underlying mechanisms of CIPN. To establish these models, adult flies or larvae are fed with food that contains chemotherapeutic drugs. *Drosophila* larvae fed paclitaxel exhibited axonal swellings and axon loss in sensory neurons without alterations at the neuromuscular junction (Bhattacharya et al., 2012). In this *Drosophila* model, axon degeneration occurs without loss of the neuronal cell bodies. Interestingly, overexpression of NMNAT, a protective protein during axon injury, prevented this paclitaxel-induced axon degeneration. Cisplatin fed adult *Drosophila* exhibited enhanced neuronal apoptosis in the brain and displayed defective climbing behavior (Podratz et al., 2011b, 2013). These results are consistent with findings from rodent models and from people, suggesting that these non-mammalian systems can provide valuable models to study CIPN.

Tissue Culture Models

In addition to animal models, tissue culture preparations of rat and mouse DRG sensory neurons are used to study CIPN at a mechanistic level (Malgrange et al., 1994; Yang et al., 2009; Guo et al., 2017). While most studies have relied on embryonic tissue, a recent study by Gornstein et al. developed a DRG culture from adult mice to study paclitaxel-induced neuropathy (Gornstein and Schwarz, 2017). Recent methods for turning human adult cells into induced pluripotent stem cells (iPSCs) and reprogramming these cells to generate peripheral sensory neurons have enabled studies of CIPN on cultured human cells (Chambers et al., 2012; Wainger et al., 2015). A recent study analyzed the effects on different chemotherapy agents on neurite outgrowth using commercially available iPSC-derived neurons coupled with high content imaging analysis. Both paclitaxel and vincristine-treated neurons showed decreased neurite outgrowth without increased cell death, while cisplatin treatment induced cell death (Wheeler et al., 2015). Moreover, knocking down *TUBB2A*, a gene encoding a tubulin isoform that has previously been identified as the locus for a single nucleotide polymorphism associated with enhanced risk of CIPN (Leandro-Garcia et al., 2012), increased the sensitivity of iPSC-derived neurons to paclitaxel treatment (Wheeler et al., 2015). This result supports the hypothesis that disruption of microtubule dynamics may be one mechanism contributing to CIPN. These findings also suggest that human iPSC-induced neurons can provide a reliable and powerful *in vitro* human model for mechanistic and therapeutic studies of CIPN.

PATHOLOGY OF CIPN

The mechanism(s) whereby chemotherapies cause CIPN are not yet understood, nor is it clear whether distinct agents converge on a shared pathway to induce symptoms. While effects of chemotherapeutic agents on neurons, glial cells, and skin cells have each been suggested to initiate the neurological symptoms, studies in patients and in animal models implicate axonal degeneration as a common process in CIPN pathology. Specifically, chemotherapeutic agents either directly or indirectly trigger a "dying back" axon degeneration that proceeds in a distal-to-proximal manner. Potential mechanisms for initiating axon degeneration include defects in axon transport, altered mitochondrial function, or altered Ca^{+2} homeostasis (**Figure 1**).

CIPN and Axon Transport

Paclitaxel, vincristine, and bortezomib all affect microtubule dynamics by inhibiting the processes of tubulin depolymerization and polymerization (**Figure 1**). Paclitaxel causes retraction bulbs at the tips of sensory nerve axons, indicating axon

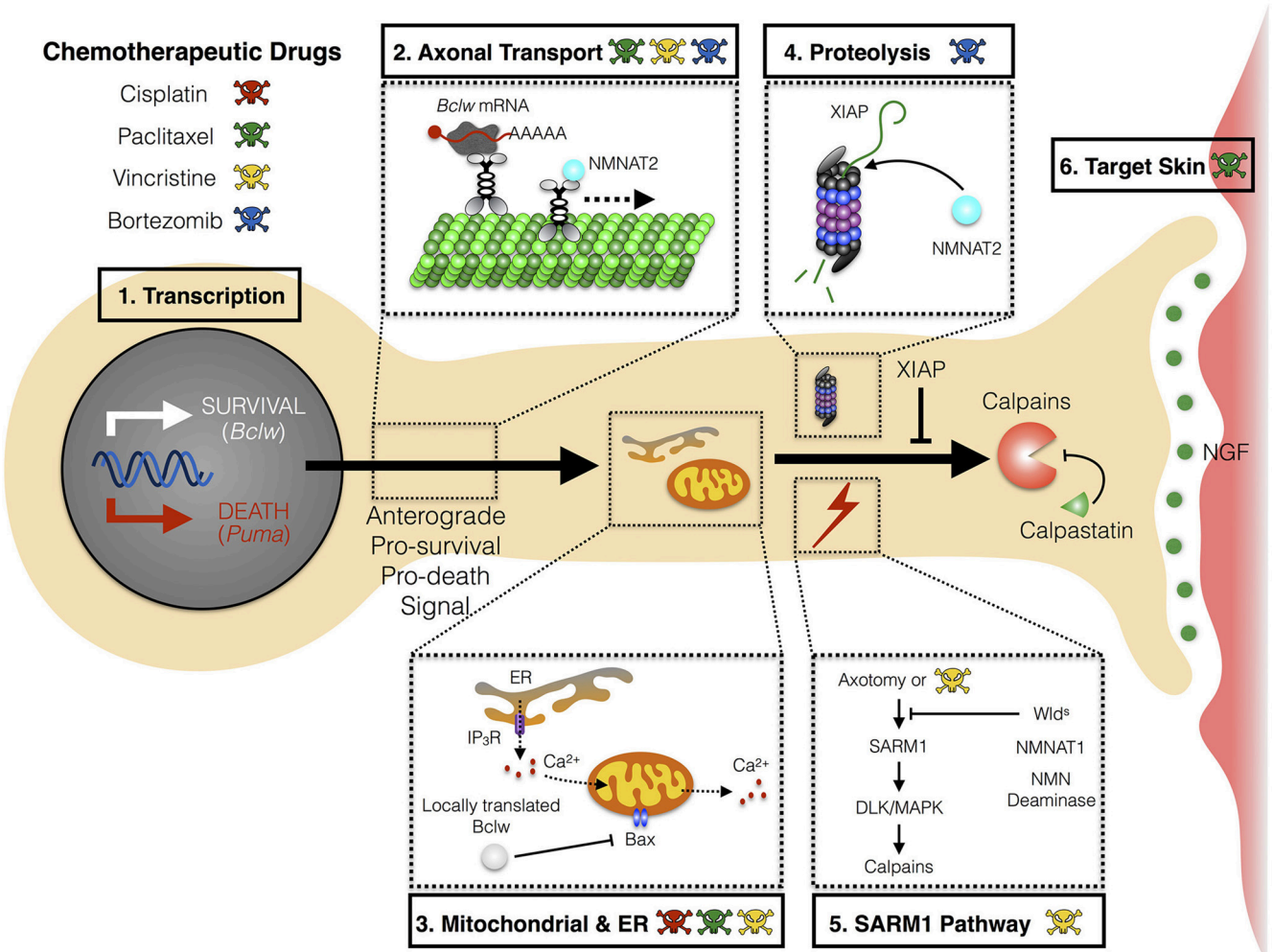

FIGURE 1 | Mechanism of axon degeneration and sites of action of chemotherapeutic drugs. Axon degeneration is determined by factors that can either enhance death and/or inhibit survival pathways. Key mechanisms that underlie this pathway are transcriptional programs, microtubule-dependent transport, local translation to modulate mitochondrial function, and proteolysis. Chemotherapeutic agents (illustrated by colored skull and cross bones) that are currently known to modulate these key mechanisms are depicted (see text for detail). **(1)** During developmental axon pruning, target-derived neurotrophins instruct transcription of key pro-survival genes (*Bclw*). Under neurotrophic deprivation, the function of pro-survival genes is overcome by induction of pro-death genes (*Puma*). **(2)** Key transcripts of neurotrophin-dependent retrograde response genes (*Bclw*) are transported in an anterograde manner by kinesin motor proteins toward distal axons. Cell soma-derived factors (NMNAT2) are also transported to axons to replenish axonal pools of proteins with fast turnover rate. **(3)** Local translation of Bclw and LaminB2 (not shown) modulates mitochondrial function to inhibit the caspase cascade. Mitochondrial and ER integrity is also critical for maintaining Ca^{2+} homeostasis to prevent activation of Ca^{2+}-dependent calpains. **(4)** Neurotrophic deprivation leads to degradation of XIAP, a key inhibitor of the caspase cascade. NMNAT2, a survival factor with a short half-life, is possibly degraded through the proteasome in axons. **(5)** Vincristine and axotomy activates SARM1 and DLK/MAPK signaling, leading to activation of calpains, the ultimate convergence point for executing axon degeneration. Expression of Wld^S, axonal NMNAT1, or NMN deaminase provides protection against vincristine or injury-induced degeneration. **(6)** Non neuron-autonomous effects from other cell types can potentially sensitize axons to degeneration during CIPN. Paclitaxel-induced neurotoxicity can mediate inflammatory response and epithelial damage to perturb skin homeostasis. Bclw, Bcl-2-like protein 2; Puma, p53 upregulated modulator of apoptosis; NMNAT, nicotinamide mononucleotide adenylyltransferase; ER, endoplasmic reticulum; IP_3R, inositol 1,4,5-triphosphate receptor; BAX, Bcl-2-like protein 4; XIAP, X-linked inhibitor of apoptosis protein; SARM1, sterile α-motif-containing and armadillo-motif-containing protein; DLK, dual leucine zipper kinase; MAPK, mitogen-activated protein kinase; Wld^S, Wallerian degeneration slow; NMN, nicotinamide mononucleotide; CIPN, chemotherapy-induced peripheral neuropathy.

degeneration (Gornstein and Schwarz, 2017). Epothilone B, a chemotherapy drug currently in clinical trials, is a structurally distinct compound that binds to the same site on tubulin as paclitaxel. Interestingly, DRG cultures treated with epothilone B showed a similar axon tip retraction as cultures treated with paclitaxel (Gornstein and Schwarz, 2017). This further indicates that altered microtubule dynamics contributes to taxane-induced axonopathy. As both anterograde and retrograde axonal transport rely on microtubule integrity and dynamics, CIPN drugs targeting microtubule are likely to result in altered axonal transport of essential cellular components. LaPointe and colleagues used an *in vitro* vesicle motility assay and

discovered that vincristine and paclitaxel inhibit anterograde axonal transport in axoplasm isolated from squid giant axons, and that vincristine inhibits retrograde transport as well (LaPointe et al., 2013). Additional studies in simple systems affirm that paclitaxel can reduce axonal transport (Theiss and Meller, 2000; Shemesh and Spira, 2010). In support of the possibility that impaired transport causes CIPN, a recent study demonstrated reductions in the levels of several axonal mRNAs in the distal nerves of mice treated with paclitaxel (Bobylev et al., 2015). In contrast, time lapse studies detected little change in mitochondria and late endosome/lysosome transport along microtubules following paclitaxel treatment (Gornstein and Schwarz, 2017). Thus, it is possible that paclitaxel causes defective mRNA transport, rather than a general disruption of microtubule-based motility.

Mitotoxicity in CIPN

Mitochondrial dysfunction is commonly observed in CIPN (**Figure 1**). Abnormal mitochondrial morphology including swelling, vacuolation, enlargement, and loss of cristae structure have been observed in peripheral nerve axons (Flatters and Bennett, 2006; Xiao et al., 2012; Zheng et al., 2012; Bobylev et al., 2017), but not in the surrounding Schwann cells (Xiao et al., 2012) in several CIPN animal models. Potential causes of altered mitochondria include paclitaxel-induced depletion of mRNAs encoding mitochondrial fission/fusion machinery in distal axons (Bobylev et al., 2015). Mitochondria dynamics may be altered in cisplatin-treated animals due to decreased level of mitochondrial fusion protein MFN2 in distal axon segments (Bobylev et al., 2017). Moreover, increased mitochondrial fragmentation, as well as decreased mitochondrial fission/fusion dynamics and motility, occur rapidly in vincristine-treated DRG cultures and precede axon degeneration (Berbusse et al., 2016). Platinum agents can also affect mitochondrial function through damaging mitochondrial DNA (mtDNA), and thereby impeding mtDNA replication and transcription (Podratz et al., 2011a). Thus, mitochondrial dysfunction may represent a common mechanism for axon degeneration in CIPN (**Figure 1**).

Ca^{2+} Homeostasis and Cation Channels

Ca^{2+} homeostasis is critical for neuronal and axonal health. Mitochondria and the endoplasmic reticulum (ER) both function as intracellular stores of Ca^{2+}, and paclitaxel treatment alters Ca^{2+} homeostasis, potentially by inducing Ca^{2+} release from the mitochondria (Kidd et al., 2002; **Figure 1**). An alternative mechanism for alterations in intracellular Ca^{2+} dynamics was presented by Boehmerle and colleagues, who reported that paclitaxel-induced Ca^{2+} oscillation reflects altered function of inositol 1,4,5-trisphosphate receptors (IP_3R) in the ER (Boehmerle et al., 2006; **Figure 1**). Indeed, chronic paclitaxel exposure leads to impaired phosphoinositide-mediated Ca^{2+} signaling in both neuroblastoma cell and DRG cultures (Boehmerle et al., 2007). Increased intracellular Ca^{2+} can activate the potent protease calpain, which directly triggers axon degeneration (Wang et al., 2012). Moreover, Ca^{2+} reducing drugs alleviate mechanical allodynia and hyperalgesia in paclitaxel and vincristine rat models (Siau and Bennett, 2006).

Chemotherapeutic agents may alter cation channels more generally. Recent studies showed that cisplatin, paclitaxel or bortezomib treatment result in increased expression of the non-selective cation channels, TRPV1 and TRPA1, in cultured DRG neurons (Ta et al., 2010; Hara et al., 2013; Quartu et al., 2014). As TRP channels are critical for pain signaling, alterations in these cation channels may be an important component of CIPN. Therefore, approaches that target Ca^{2+} homeostasis and/or cation channels provide potential future therapies.

Central Sensitization and CNS Glial Activation

While abundant data indicate that peripheral nerves and epidermal innervation are affected in CIPN, changes in the central nervous system (CNS) may also contribute to the disorder. Central sensitization may occur as a direct or indirect consequence of chemotherapeutic agents. Low concentrations of chemotherapeutic drugs, oxaliplatin, and paclitaxel, can be detected in the CNS after systemic dosing that produce hyperalgesia in rats (Huang et al., 2016). Paclitaxel can directly sensitize spinal neurons to TRPV1-mediated capsaicin response (Li et al., 2015), while oxaliplatin can increase expression and release of chemokine C-X3-C motif ligand 1 from spinal cord neurons (Huang et al., 2016). Thus, chemotherapeutic agents can possibly act directly on spinal neurons to mediate central sensitization.

The release of chemokines and cytokines from spinal neurons may further potentiate neuropathic pain by activating microglia and astrocytes. Paclitaxel can induce activation of astrocytes, and in some cases microglia, in the dorsal horn of the spinal cord (Zhang et al., 2012; Ruiz-Medina et al., 2013). Consistent with these effects, drugs that affect astrocytes and microglia, including cannabinoid agonists and minocycline, have been reported to alleviate mechanical allodynia in rats (Boyette-Davis et al., 2011; Burgos et al., 2012). Interestingly, some chemotherapeutics can also activate astrocytes and microglia in regions of the brain associated with chronic pain and nociceptive processing, as paclitaxel increases expression of GFAP in anterior cingulate cortex concurrent with behavioral evidence of thermal hyperalgesia (Masocha, 2015). Collectively, these evidences demonstrate a potential contribution of CNS sensitization and glial activation to the neuropathic pain that occurs in CIPN.

MECHANISTIC INSIGHTS INTO CIPN AND AXON DEGENERATION

The recent failures of multiple clinical trials for CIPN (Majithia et al., 2016) underscore the need to explore and address underlying molecular mechanisms more broadly. Since all the relevant chemotherapeutic agents, either directly or indirectly, trigger a "dying back" axon degeneration, a greater understanding of the biology of axon degeneration process *per-se* can identify major players and signaling pathways that can be targeted. Axon degeneration can be provoked by multiple stimuli in addition to chemotherapeutic agents. Axon pruning

during development and axotomy also entail axon degeneration. Here we will discuss what is currently known about the cellular pathways for axon degeneration in these contexts, to provide insights for addressing the molecular mechanisms of axon degeneration during CIPN.

Developmental Axon Pruning

Axon degeneration constitutes a necessary and healthy end result of pruning that allows plasticity of neuronal circuitry during development. The process of axon pruning has been studied in diverse species including mice, *Drosophila*, *C. elegans*, and zebrafish (Kage et al., 2005; Hayashi et al., 2009; Poulain and Chien, 2013; Yu and Schuldiner, 2014; Riccomagno and Kolodkin, 2015). Early in development, excess innervation can be observed in both the CNS and PNS. Subsequently, refinement of neuronal connectivity through axon pruning enables the establishment of the robust mature circuitry. Multiple signaling processes critical for axon pruning and refinement have been identified in studies of both central and peripheral neurons.

Repulsive axon guidance cues such as the semaphorins bind to pruning receptors and initiate local axon degeneration in the CNS. For example, in the hippocampus, stereotyped pruning of infrapyramidal bundle (IPB) is initiated by semaphorin3F expressed in interneurons in the stratum oriens, and is achieved by signaling complexes containing neuropilin-2 and plexin-A3 (Bagri et al., 2003). A similar role for semaphorin3F in axon pruning has been observed in corticospinal tract from layer 5 of the visual cortex (Low et al., 2008). In *Drosophila,* mushroom body (MB) γ neurons provide another system where stereotyped axon pruning occurs during development. Pruning of dorsal and medial axonal branches during metamorphosis requires signaling through a TGF-β receptor complex in MB γ neurons, and is initiated by myoglianin secreted from nearby glial cells (Awasaki et al., 2011). Although TGF-β signaling is essential for axon fragmentation, it is not sufficient. Thus, glial cells initiate the process of axon fragmentation in these cells but other factors are required to fully execute axon pruning. Similarly, chemotherapeutic agents acting directly on nearby glial cells may sensitize neurons subsequently undergo axon degeneration. Although paclitaxel has been shown to induce inflammatory responses and promote epithelial damage prior to the induction of axon degeneration (Lisse et al., 2016; Zhang et al., 2016), this model of sensitization has not yet been explored with other chemotherapeutic drugs.

Much of our understanding of developmental axon pruning is derived from studies of neurotrophins, nerve growth factor (NGF), brain-derived neurotrophic factor (BDNF) and neurotrophins 3 and 4 (NT3 and NT4), which are released in a limited amount by target tissues and promote axon and cell body survival (Harrington and Ginty, 2013). The role of neurotrophins in regulating axonal survival and degeneration is most widely studied in the PNS, particularly sympathetic and sensory neurons. Target-derived neurotrophins bind and activate tropomyosin receptor kinase (Trk) receptors in the innervating axon terminals. Endocytosis of the activated receptors results in signaling endosomes that are retrogradely trafficked along the axons. The signaling endosomes initiate instructive programs that promote both axonal and cell survival (Tasdemir-Yilmaz and Segal, 2016). Consequently, neurons that fail to receive neurotrophins lose their innervation, and may undergo apoptosis. This selection process of both axonal and cell degeneration is further enhanced by active signaling to eliminate axon processes. In superior cervical ganglion (SCG) sympathetic neurons, active signaling through the p75 neurotrophin receptor (p75NTR) can promote axon degeneration or even apoptosis (Singh et al., 2008). These examples provide evidence of overlap between cellular and axonal survival and death processes, and suggest that cumulative responses to pro-survival and pro-death signals may also play a role in the axon degeneration observed in CIPN.

Regulation of Axonal Survival during Development: Coordination of Transcription, Transport, Translation, and Proteolysis

Regulation occurs at multiple levels to determine whether axons will survive or degenerate, including nuclear transcription, axonal translation and protein activity (Tasdemir-Yilmaz and Segal, 2016). *In vitro* culture systems using compartmented culture platforms have proven to be valuable tools that recapitulate the spatially and fluidically isolated cell body and distal axon compartment observed *in vivo*, enabling mechanistic understanding of the multiple regulatory steps involved in determining and implementing axonal survival or degeneration.

In these compartmented systems, stimulation of axon terminals with target-derived neurotrophins promotes axon outgrowth and prevents both axon degeneration and cell body apoptosis. In contrast, neurotrophin stimulation of cell bodies prevents apoptosis, but does not prevent axon degeneration. Therefore, some of the retrograde response genes that are selectively transcribed in response to neurotrophin stimulation of axons and not by stimulation of cell bodies are likely to encode components needed for axonal survival. These transcriptional changes can be closely linked to events in the axon, as many newly transcribed mRNAs are transported to the distal axons, where they are translated into protein. For example, the Bcl2 family member, *Bclw* (aka *Bcl2l2*) is a retrograde response gene, and newly transcribed *Bclw* mRNA is transported to the axons, where it is locally translated and the resultant protein promotes axonal survival (Pazyra-Murphy et al., 2009; Courchesne et al., 2011; Cosker et al., 2013; **Figure 1**).

Recently, the RNA binding protein SFPQ was shown to bind multiple axonal transcripts including *Bclw* and *LaminB2* mRNAs (Cosker et al., 2016). While LaminB2 is predominantly a nuclear membrane protein, locally translated LaminB2 associates with axonal mitochondria and adjusts mitochondrial function (Yoon et al., 2012). SFPQ is needed for transport and axonal localization of *Bclw*, *LaminB2,* and others, and so functions to promote axonal survival and prevent axon degeneration (Cosker et al., 2016; Thomas-Jinu et al., 2017). Together these studies demonstrate that regulated transcription, axonal transport, and local translation work in concert to determine and implement axon survival pathways. Currently, there is no evidence for

chemotherapeutic agents affecting transcription of pro-survival genes or translation of axonal mRNAs. However, as this pathway is critical in axon survival, such studies represent an important direction for future research.

In addition to the neurotrophin-mediated axon survival pathways above, key transcriptional programs have recently been uncovered that actively promote axon degeneration during trophic deprivation. Simon et al. demonstrated that loss of neurotrophic support induces transcription of *Puma*, which encodes a pro-apoptotic BH3-only family protein Puma, through the DLK/MAPK signaling pathway (Simon et al., 2016; **Figure 1**). Maor-Nof et al. provided further mechanistic insight into this transcriptional program, demonstrating that the phosphatase Dusp16 functions to put a brake on the degenerative response by inhibiting *Puma* transcription (Maor-Nof et al., 2016). At present it is not clear whether the Puma protein subsequently functions in the cell bodies or in axons to trigger axon degeneration. In either case, it will be important to assess whether this pro-degenerative component contributes to the biology of CIPN.

A final step in executing axon degeneration involves proteolytic cleavage of axonal proteins by caspases and calpains. Initiator caspase-9 and the effector caspases-3 and -6 have all been implicated in axon degenerative cascades (Nikolaev et al., 2009; Schoenmann et al., 2010; Simon et al., 2012; Cusack et al., 2013; Unsain et al., 2013). Caspase-mediated degeneration is usually held in check by inhibitor of apoptosis protein (IAP) (**Figure 1**) (Potts et al., 2003; Cusack et al., 2013; Unsain et al., 2013). Calpains are Ca^{2+}-activated proteases that execute axonal degeneration by proteolysis of multiple cellular proteins. Calpastatin inhibits calpain activation during developmental pruning and so limits the extent of axon degeneration (Yang et al., 2013). Similarly, calpain-mediated proteolysis has been implicated as a convergent pathway that contributes to axon degeneration in CIPN (**Figure 1**). Mice treated with paclitaxel that are administered calpain inhibitors show reduced signs of axonal degeneration in sensory neurons and improved clinical measures of neuropathy (Wang et al., 2004) One of the targets of calpain during paclitaxel-induced peripheral neuropathy is neuronal calcium sensor-1 (NCS-1). NCS-1 binds to IP_3R to enhance intracellular calcium signaling. Paclitaxel disrupts IP_3R-mediated intracellular calcium signaling via NCS-1 degradation (Boehmerle et al., 2007). In the future, it will be important to identify other molecular downstream targets of calpain relevant to peripheral neuropathy. Nonetheless, these studies demonstrate calpain as a promising therapeutic target for CIPN.

Wallerian Degeneration

Axon degeneration due to traumatic injury represents another useful model for mechanistic studies of axon degeneration or survival. Following axotomy, an initial latent phase is followed by fragmentation of the cytoskeleton, destruction of organelles, and ultimately disintegration of axons distal to the severed site (Gerdts et al., 2016). This process of axon degeneration is referred to as Wallerian degeneration (WD). Much of the mechanistic understanding of WD derives from a spontaneous genetic mutation, Wallerian degeneration slow (*Wld*^{s}), which delays the process of WD. This mutation encodes a chimeric fusion protein of the N-terminal fragment of E4 ubiquitin ligase Ube4b and the enzyme nicotinamide mononucleotide adenylyltransferase 1 (NMNAT1; Conforti et al., 2000). The axonal protective effect of the mutant Wld^s depends on the NMNAT1 portion of the fusion protein, which synthesizes nicotinamide adenine dinucleotide (NAD^+) from nicotinamide mononucleotide (NMN; Araki et al., 2004). This protective role of Wld^s is conserved evolutionarily across diverse species (MacDonald et al., 2006; Martin et al., 2010).

Building on the exciting discovery that the Wld^s mutation slows the process of axon degeneration, multiple studies have addressed the roles of NMNAT enzymes in axonal survival. There are three mammalian NMNATs. Loss of function mutations in NMNAT2, but not the other NMNATs triggers Wallerian-like degeneration in undamaged axons (Gilley and Coleman, 2010; Gilley et al., 2013). As NMNAT2 is selectively expressed in axons and has a very short half-life, NMNAT activity in axons requires continued anterograde transport of this enzyme from the cell soma (**Figure 1**). Slowing the turnover of NMNAT2 can significantly delay injury-induced WD (Xiong et al., 2012; Babetto et al., 2013; Milde et al., 2013a,b). These studies on NMNAT2 highlight the essential role of axonal transport and proteasomal degradation in maintaining homeostatic protein content in axons. Disruption of either pathway can reduce any levels of critical axonal protein levels below a necessary threshold and so induce degeneration cascade. Therefore, chemotherapy-induced changes in axonal transport, translation and proteasomal degradation represent important avenues of investigation in future studies of CIPN.

Studies of axotomy have also identified SARM1, a scaffolding molecule, as a critical regulator of axonal degeneration. Loss of function of SARM1 significantly delays axon degeneration after injury, indicating that SARM1 functions as a pro-degeneration factor in WD (Osterloh et al., 2012; Gerdts et al., 2013). Depletion of SARM1 prevents the axon degeneration phenotype seen with NMNAT2 loss of function, indicating that these two components act in the same signaling cascade, with SARM1 downstream of NMNAT2 (Gilley et al., 2015). To understand the functions of SARM1 and NMNAT2, several investigations have analyzed the importance of NAD^+ vs. NMN and ATP, the product and the substrates of NMNAT2 enzymatic activity, respectively. It is not yet clear whether loss of NMNAT2 triggers axon degeneration as a result of NAD^+ deficiency, or accumulation of NMN, or other outcomes. Whether SARM1 alters NAD^+ or NMN to induce axon degeneration is an area of active investigation (Di Stefano et al., 2015, 2017; Gerdts et al., 2015; Sasaki et al., 2016; Essuman et al., 2017). One important consequence of SARM1 activation or of NMNAT2 loss is activation of DLK/MAPK signaling, which ultimately triggers calpain-mediated axon degeneration (Yang et al., 2013, 2015; **Figure 1**).

Calpain and many additional components implicated in axonal responses to injury are linked to CIPN. Initial evidence of these similarities came from studies demonstrating that Wld^s mutant neurons display resistance to vincristine-induced neuropathy (Wang et al., 2001). More recently, SARM1 knockout mice were shown to be resistant to vincristine in an *in vivo* model (Geisler et al., 2016). Essuman et al. demonstrated that SARM1

functions as a NAD^+-depleting enzyme and that the intrinsic NADase activity of SARM1 is required for vincristine-induced axon degeneration (Essuman et al., 2017). Additional evidence that the SARM1 pathway plays a critical role in CIPN includes data that expression of axonal NMNAT1 and constitutive expression of the NMN deaminase that consumes NMN, both protect against vincristine-induced peripheral neuropathy (Sasaki et al., 2009; Di Stefano et al., 2017). Therefore, inhibition of SARM1 enzymatic activity might be a useful therapeutic strategy in CIPN.

Human Variants

In addition to these models of development and axotomy, a final approach for identifying molecular cascades implicated in CIPN is to discover human variations that alter susceptibility to CIPN. The incidence of CIPN varies significantly from person to person. Increased age, diabetes, and previous neuropathy are known risk factors for CIPN. However, it is likely that genetic variations are also important for susceptibility. Several genome wide association studies (GWAS) have identified gene variants associated with increased vulnerability to CIPN. Single nucleotide polymorphisms of FGD4 and EPHA5 were significantly associated with susceptibility to paclitaxel-induced peripheral neuropathy in both European and African ancestral groups (Baldwin et al., 2012). FGD4 (FYVE, RhoGEF, and PH Domain Containing 4) is a Rho GTP/GDP exchange protein regulating actin cytoskeleton dynamics (Obaishi et al., 1998). Mutations of FGD4 in humans lead to autosomal recessive demyelinating Charcot-Marie-Tooth neuropathy (type 4H; De Sandre-Giovannoli et al., 2005; Delague et al., 2007; Stendel et al., 2007). The EPHA family is a group of tyrosine kinase receptors that bind to the Ephrin ligands. Eph/Ephrin signaling has been implicated in regulating axon outgrowth and guidance during development (Dickson, 2002; Egea and Klein, 2007). A recent study performed next generation sequencing on patients who developed significant neuropathy after paclitaxel, and identified variations of three related receptors, EPHA5/6/8, that correlated with susceptibility to paclitaxel-induced neuropathy (Apellaniz-Ruiz et al., 2017). Other CIPN associated genes identified by GWAS studies also play critical roles in neurite outgrowth and nerve development including FZD3 (Baldwin et al., 2012), TUBB2A (Leandro-Garcia et al., 2012), VAC14 (Hertz et al., 2016). These candidates may affect CIPN by directly affecting the cytoskeleton organization (TUBB2A, FGD4), by regulating intracellular trafficking (VAC14) or may function as signaling molecules regulating axon growth (EPHA, FZD3). Future verifications are required to confirm the involvement of these genes in CIPN pathology, and how these factors might contribute to the disorder.

CONCLUDING REMARKS

As summarized in this review, multiple chemotherapeutic agents that cause CIPN are directed against different molecular targets. Preclinical studies have generated several hypotheses to explain the pathogenesis of CIPN by these agents, including defective axon transport, mitotoxicity, and altered Ca^{2+} homeostasis. While each agent may initially affect the nervous system in a distinctive manner, the pathologies observed in CIPN converge to cause an axon degenerative process. Mechanistic studies of the phenotypically similar axon degeneration processes during developmental axon pruning or during injury-induced WD are likely to shed new light on the molecular basis of CIPN. Indeed, several signaling molecules on the SARM1, DLK/MAPK, and NMNAT pathways that protect axons from WD can also impact CIPN. Concurrently, human GWAS studies have identified pathways implicated in neurite outgrowth and/or axon maintenance that may be relevant for axon degeneration in CIPN. These findings suggest that axon degeneration is central to CIPN pathology. Enhanced understanding of the pathologic process of axon degeneration will be essential for developing an arsenal of effective therapies of CIPN.

AUTHOR CONTRIBUTIONS

All authors listed have made a substantial, direct, and intellectual contribution to the work, and approved it for publication.

ACKNOWLEDGMENTS

We thank members of the Segal lab for helpful discussions. Work in the Segal lab on CIPN has been funded by the Barr-Weaver Award, and NCI R01CA205255.

REFERENCES

Adams, J. (2004). The proteasome: a suitable antineoplastic target. *Nat. Rev. Cancer* 4, 349–360. doi: 10.1038/nrc1361

Addington, J., and Freimer, M. (2016). Chemotherapy-induced peripheral neuropathy: an update on the current understanding [version 1; referees: 2 approved]. *F1000Res.* 5:1466. doi: 10.12688/f1000research.8053.1

Apellaniz-Ruiz, M., Tejero, H., Inglada-Perez, L., Sanchez-Barroso, L., Gutierrez-Gutierrez, G., Calvo, I., et al. (2017). Targeted sequencing reveals low-frequency variants in epha genes as markers of paclitaxel-induced peripheral neuropathy. *Clin. Cancer Res.* 23, 1227–1235. doi: 10.1158/1078-0432.CCR-16-0694

Araki, T., Sasaki, Y., and Milbrandt, J. (2004). Increased nuclear NAD biosynthesis and SIRT1 activation prevent axonal degeneration. *Science* 305, 1010–1013. doi: 10.1126/science.1098014

Arrieta, O., Hernandez-Pedro, N., Fernandez-Gonzalez-Aragon, M. C., Saavedra-Perez, D., Campos-Parra, A. D., Rios-Trejo, M. A., et al. (2011). Retinoic acid reduces chemotherapy-induced neuropathy in an animal model and patients with lung cancer. *Neurology* 77, 987–995. doi: 10.1212/WNL.0b013e31822e045c

Authier, N., Gillet, J. P., Fialip, J., Eschalier, A., and Coudore, F. (2000). Description of a short-term Taxol-induced nociceptive neuropathy in rats. *Brain Res.* 887, 239–249. doi: 10.1016/S0006-8993(00)02910-3

Awasaki, T., Huang, Y., O'Connor, M. B., and Lee, T. (2011). Glia instruct developmental neuronal remodeling through TGF-beta signaling. *Nat. Neurosci.* 14, 821–823. doi: 10.1038/nn.2833

Babetto, E., Beirowski, B., Russler, E. V., Milbrandt, J., and DiAntonio, A. (2013). The Phr1 ubiquitin ligase promotes injury-induced axon self-destruction. *Cell Rep.* 3, 1422–1429. doi: 10.1016/j.celrep.2013.04.013

Bagri, A., Cheng, H. J., Yaron, A., Pleasure, S. J., and Tessier-Lavigne, M. (2003). Stereotyped pruning of long hippocampal axon branches triggered by retraction inducers of the semaphorin family. *Cell* 113, 285–299. doi: 10.1016/S0092-8674(03)00267-8

Baldwin, R. M., Owzar, K., Zembutsu, H., Chhibber, A., Kubo, M., Jiang, C., et al. (2012). A genome-wide association study identifies novel loci for paclitaxel-induced sensory peripheral neuropathy in CALGB 40101. *Clin. Cancer Res.* 18, 5099–5109. doi: 10.1158/1078-0432.CCR-12-1590

Berbusse, G. W., Woods, L. C., Vohra, B. P., and Naylor, K. (2016). Mitochondrial dynamics decrease prior to axon degeneration induced by vincristine and are partially rescued by overexpressed cytNmnat1. *Front. Cell. Neurosci.* 10:179. doi: 10.3389/fncel.2016.00179

Bhattacharya, M. R., Gerdts, J., Naylor, S. A., Royse, E. X., Ebstein, S. Y., Sasaki, Y., et al. (2012). A model of toxic neuropathy in Drosophila reveals a role for MORN4 in promoting axonal degeneration. *J. Neurosci.* 32, 5054–5061. doi: 10.1523/JNEUROSCI.4951-11.2012

Bobylev, I., Joshi, A. R., Barham, M., Neiss, W. F., and Lehmann, H. C. (2017). Depletion of mitofusin-2 causes mitochondrial damage in cisplatin-induced neuropathy. *Mol. Neurobiol.* doi: 10.1007/s12035-016-0364-7. [Epub ahead of print].

Bobylev, I., Joshi, A. R., Barham, M., Ritter, C., Neiss, W. F., Hoke, A., et al. (2015). Paclitaxel inhibits mRNA transport in axons. *Neurobiol. Dis.* 82, 321–331. doi: 10.1016/j.nbd.2015.07.006

Boehmerle, W., Splittgerber, U., Lazarus, M. B., McKenzie, K. M., Johnston, D. G., Austin, D. J., et al. (2006). Paclitaxel induces calcium oscillations via an inositol 1,4,5-trisphosphate receptor and neuronal calcium sensor 1-dependent mechanism. *Proc. Natl. Acad. Sci. U.S.A.* 103, 18356–18361. doi: 10.1073/pnas.0607240103

Boehmerle, W., Zhang, K., Sivula, M., Heidrich, F. M., Lee, Y., Jordt, S. E., et al. (2007). Chronic exposure to paclitaxel diminishes phosphoinositide signaling by calpain-mediated neuronal calcium sensor-1 degradation. *Proc. Natl. Acad. Sci. U.S.A.* 104, 11103–11108. doi: 10.1073/pnas.0701546104

Boyette-Davis, J., Xin, W., Zhang, H., and Dougherty, P. M. (2011). Intraepidermal nerve fiber loss corresponds to the development of taxol-induced hyperalgesia and can be prevented by treatment with minocycline. *Pain* 152, 308–313. doi: 10.1016/j.pain.2010.10.030

Brewer, J. R., Morrison, G., Dolan, M. E., and Fleming, G. F. (2016). Chemotherapy-induced peripheral neuropathy: current status and progress. *Gynecol. Oncol.* 140, 176–183. doi: 10.1016/j.ygyno.2015.11.011

Burgos, E., Gomez-Nicola, D., Pascual, D., Martin, M. I., Nieto-Sampedro, M., and Goicoechea, C. (2012). Cannabinoid agonist WIN 55,212-2 prevents the development of paclitaxel-induced peripheral neuropathy in rats. Possible involvement of spinal glial cells. *Eur. J. Pharmacol.* 682, 62–72. doi: 10.1016/j.ejphar.2012.02.008

Carozzi, V. A., Canta, A., Oggioni, N., Sala, B., Chiorazzi, A., Meregalli, C., et al. (2010). Neurophysiological and neuropathological characterization of new murine models of chemotherapy-induced chronic peripheral neuropathies. *Exp. Neurol.* 226, 301–309. doi: 10.1016/j.expneurol.2010.09.004

Cata, J. P., Weng, H. R., and Dougherty, P. M. (2008). Behavioral and electrophysiological studies in rats with cisplatin-induced chemoneuropathy. *Brain Res.* 1230, 91–98. doi: 10.1016/j.brainres.2008.07.022

Cavaletti, G., Frigeni, B., Lanzani, F., Mattavelli, L., Susani, E., Alberti, P., et al. (2010). Chemotherapy-Induced Peripheral Neurotoxicity assessment: a critical revision of the currently available tools. *Eur. J. Cancer* 46, 479–494. doi: 10.1016/j.ejca.2009.12.008

Cavaletti, G., Gilardini, A., Canta, A., Rigamonti, L., Rodriguez-Menendez, V., Ceresa, C., et al. (2007). Bortezomib-induced peripheral neurotoxicity: a neurophysiological and pathological study in the rat. *Exp. Neurol.* 204, 317–325. doi: 10.1016/j.expneurol.2006.11.010

Chambers, S. M., Qi, Y., Mica, Y., Lee, G., Zhang, X. J., Niu, L., et al. (2012). Combined small-molecule inhibition accelerates developmental timing and converts human pluripotent stem cells into nociceptors. *Nat. Biotechnol.* 30, 715–720. doi: 10.1038/nbt.2249

Chaudhry, V., Rowinsky, E. K., Sartorius, S. E., Donehower, R. C., and Cornblath, D. R. (1994). Peripheral neuropathy from taxol and cisplatin combination chemotherapy: clinical and electrophysiological studies. *Ann. Neurol.* 35, 304–311. doi: 10.1002/ana.410350310

Conforti, L., Tarlton, A., Mack, T. G., Mi, W., Buckmaster, E. A., Wagner, D., et al. (2000). A Ufd2/D4Cole1e chimeric protein and overexpression of Rbp7 in the slow Wallerian degeneration (WldS) mouse. *Proc. Natl. Acad. Sci. U.S.A.* 97, 11377–11382. doi: 10.1073/pnas.97.21.11377

Cosker, K. E., Fenstermacher, S. J., Pazyra-Murphy, M. F., Elliott, H. L., and Segal, R. A. (2016). The RNA-binding protein SFPQ orchestrates an RNA regulon to promote axon viability. *Nat. Neurosci.* 19, 690–696. doi: 10.1038/nn.4280

Cosker, K. E., Pazyra-Murphy, M. F., Fenstermacher, S. J., and Segal, R. A. (2013). Target-derived neurotrophins coordinate transcription and transport of bclw to prevent axonal degeneration. *J. Neurosci.* 33, 5195–5207. doi: 10.1523/JNEUROSCI.3862-12.2013

Courchesne, S. L., Karch, C., Pazyra-Murphy, M. F., and Segal, R. A. (2011). Sensory neuropathy attributable to loss of Bcl-w. *J. Neurosci.* 31, 1624–1634. doi: 10.1523/JNEUROSCI.3347-10.2011

Curran, M. P., and McKeage, K. (2009). Bortezomib: a review of its use in patients with multiple myeloma. *Drugs* 69, 859–888. doi: 10.2165/00003495-200969070-00006

Cusack, C. L., Swahari, V., Hampton Henley, W., Michael Ramsey, J., and Deshmukh, M. (2013). Distinct pathways mediate axon degeneration during apoptosis and axon-specific pruning. *Nat. Commun.* 4, 1876. doi: 10.1038/ncomms2910

De Sandre-Giovannoli, A., Delague, V., Hamadouche, T., Chaouch, M., Krahn, M., Boccaccio, I., et al. (2005). Homozygosity mapping of autosomal recessive demyelinating Charcot-Marie-Tooth neuropathy (CMT4H) to a novel locus on chromosome 12p11.21-q13.11. *J. Med. Genet.* 42, 260–265. doi: 10.1136/jmg.2004.024364

Delague, V., Jacquier, A., Hamadouche, T., Poitelon, Y., Baudot, C., Boccaccio, I., et al. (2007). Mutations in FGD4 encoding the Rho GDP/GTP exchange factor FRABIN cause autosomal recessive Charcot-Marie-Tooth type 4H. *Am. J. Hum. Genet.* 81, 1–16. doi: 10.1086/518428

Di Stefano, M., Loreto, A., Orsomando, G., Mori, V., Zamporlini, F., Hulse, R. P., et al. (2017). NMN deamidase delays wallerian degeneration and rescues axonal defects caused by NMNAT2 deficiency *in vivo*. *Curr. Biol.* 27, 784–794. doi: 10.1016/j.cub.2017.01.070

Di Stefano, M., Nascimento-Ferreira, I., Orsomando, G., Mori, V., Gilley, J., Brown, R., et al. (2015). A rise in NAD precursor nicotinamide mononucleotide (NMN) after injury promotes axon degeneration. *Cell Death Diff.* 22, 731–742. doi: 10.1038/cdd.2014.164

Dickson, B. J. (2002). Molecular mechanisms of axon guidance. *Science* 298, 1959–1964. doi: 10.1126/science.1072165

Egea, J., and Klein, R. (2007). Bidirectional Eph-ephrin signaling during axon guidance. *Trends Cell Biol.* 17, 230–238. doi: 10.1016/j.tcb.2007.03.004

Essuman, K., Summers, D. W., Sasaki, Y., Mao, X., DiAntonio, A., and Milbrandt, J. (2017). The SARM1 toll/interleukin-1 receptor domain possesses intrinsic NAD+ cleavage activity that promotes pathological axonal degeneration. *Neuron* 93, 1334.e5–1343.e5. doi: 10.1016/j.neuron.2017.02.022

Flatters, S. J., and Bennett, G. J. (2006). Studies of peripheral sensory nerves in paclitaxel-induced painful peripheral neuropathy: evidence for mitochondrial dysfunction. *Pain* 122, 245–257. doi: 10.1016/j.pain.2006.01.037

Geisler, S., Doan, R. A., Strickland, A., Huang, X., Milbrandt, J., and DiAntonio, A. (2016). Prevention of vincristine-induced peripheral neuropathy by genetic deletion of SARM1 in mice. *Brain* 139, 3092–3108. doi: 10.1093/brain/aww251

Gerdts, J., Brace, E.J., Sasaki, Y., DiAntonio, A., and Milbrandt, J. (2015). SARM1 activation triggers axon degeneration locally via NAD^+ destruction. *Science* 348, 453–457. doi: 10.1126/science.1258366

Gerdts, J., Summers, D. W., Milbrandt, J., and DiAntonio, A. (2016). Axon self-destruction: new links among SARM1, MAPKs, and NAD+ metabolism. *Neuron* 89, 449–460. doi: 10.1016/j.neuron.2015.12.023

Gerdts, J., Summers, D. W., Sasaki, Y., DiAntonio, A., and Milbrandt, J. (2013). Sarm1-mediated axon degeneration requires both SAM and TIR interactions. *J. Neurosci.* 33, 13569–13580. doi: 10.1523/JNEUROSCI.1197-13.2013

Gilley, J., Adalbert, R., Yu, G., and Coleman, M. P. (2013). Rescue of peripheral and CNS axon defects in mice lacking NMNAT2. *J. Neurosci.* 33, 13410–13424. doi: 10.1523/JNEUROSCI.1534-13.2013

Gilley, J., and Coleman, M. P. (2010). Endogenous Nmnat2 is an essential survival factor for maintenance of healthy axons. *PLoS Biol.* 8:e1000300. doi: 10.1371/journal.pbio.1000300

Gilley, J., Orsomando, G., Nascimento-Ferreira, I., and Coleman, M. P. (2015). Absence of SARM1 rescues development and survival of NMNAT2-deficient axons. *Cell Rep.* 10, 1974–1981. doi: 10.1016/j.celrep.2015.02.060

Gornstein, E. L., and Schwarz, T. L. (2017). Neurotoxic mechanisms of paclitaxel are local to the distal axon and independent of transport defects. *Exp. Neurol.* 288, 153–166. doi: 10.1016/j.expneurol.2016.11.015

Gornstein, E., and Schwarz, T. L. (2014). The paradox of paclitaxel neurotoxicity: mechanisms and unanswered questions. *Neuropharmacology* 76(Pt A), 175–183. doi: 10.1016/j.neuropharm.2013.08.016

Guo, L., Hamre, J. 3rd, Eldridge, S., Behrsing, H. P., Cutuli, F. M., Mussio, J., et al. (2017). Multiparametric image analysis of rat dorsal root ganglion cultures to evaluate peripheral neuropathy-inducing chemotherapeutics. *Toxicol. Sci.* 156, 275–288. doi: 10.1093/toxsci/kfw254

Hara, T., Chiba, T., Abe, K., Makabe, A., Ikeno, S., Kawakami, K., et al. (2013). Effect of paclitaxel on transient receptor potential vanilloid 1 in rat dorsal root ganglion. *Pain* 154, 882–889. doi: 10.1016/j.pain.2013.02.023

Harrington, A. W., and Ginty, D. D. (2013). Long-distance retrograde neurotrophic factor signalling in neurons. *Nat. Rev. Neurosci.* 14, 177–187. doi: 10.1038/nrn3253

Hayashi, Y., Hirotsu, T., Iwata, R., Kage-Nakadai, E., Kunitomo, H., Ishihara, T., et al. (2009). A trophic role for Wnt-Ror kinase signaling during developmental pruning in *Caenorhabditis elegans*. *Nat. Neurosci.* 12, 981–987. doi: 10.1038/nn.2347

Hertz, D. L., Owzar, K., Lessans, S., Wing, C., Jiang, C., Kelly, W. K., et al. (2016). Pharmacogenetic discovery in CALGB (Alliance) 90401 and mechanistic validation of a VAC14 Polymorphism that increases risk of docetaxel-induced neuropathy. *Clin. Cancer Res.* 22, 4890–4900. doi: 10.1158/1078-0432.CCR-15-2823

Hoke, A., and Ray, M. (2014). Rodent models of chemotherapy-induced peripheral neuropathy. *ILAR J.* 54, 273–281. doi: 10.1093/ilar/ilt053

Huang, Z. Z., Li, D., Ou-Yang, H. D., Liu, C. C., Liu, X. G., Ma, C., et al. (2016). Cerebrospinal fluid oxaliplatin contributes to the acute pain induced by systemic administration of oxaliplatin. *Anesthesiology* 124, 1109–1121. doi: 10.1097/ALN.0000000000001084

Ja'afer, F. M., Hamdan, F. B., and Mohammed, F. H. (2006). Vincristine-induced neuropathy in rat: electrophysiological and histological study. *Exp. Brain Res.* 173, 334–345. doi: 10.1007/s00221-006-0499-2

Johnstone, T. C., Park, G. Y., and Lippard, S. J. (2014). Understanding and improving platinum anticancer drugs–phenanthriplatin. *Anticancer Res.* 34, 471–476.

Jordan, M. A., and Wilson, L. (2004). Microtubules as a target for anticancer drugs. *Nat. Rev. Cancer* 4, 253–265. doi: 10.1038/nrc1317

Kage, E., Hayashi, Y., Takeuchi, H., Hirotsu, T., Kunitomo, H., Inoue, T., et al. (2005). MBR-1, a novel helix-turn-helix transcription factor, is required for pruning excessive neurites in *Caenorhabditis elegans*. *Curr. Biology: CB* 15, 1554–1559. doi: 10.1016/j.cub.2005.07.057

Kavallaris, M. (2010). Microtubules and resistance to tubulin-binding agents. *Nature reviews Cancer* 10, 194–204. doi: 10.1038/nrc2803

Kidd, J. F., Pilkington, M. F., Schell, M. J., Fogarty, K. E., Skepper, J. N., Taylor, C. W., et al. (2002). Paclitaxel affects cytosolic calcium signals by opening the mitochondrial permeability transition pore. *J. Biol. Chem.* 277, 6504–6510. doi: 10.1074/jbc.M106802200

Kroigard, T., Schroder, H. D., Qvortrup, C., Eckhoff, L., Pfeiffer, P., Gaist, D., et al. (2014). Characterization and diagnostic evaluation of chronic polyneuropathies induced by oxaliplatin and docetaxel comparing skin biopsy to quantitative sensory testing and nerve conduction studies. *Eur. J. Neurol.* 21, 623–629. doi: 10.1111/ene.12353

LaPointe, N. E., Morfini, G., Brady, S. T., Feinstein, S. C., Wilson, L., and Jordan, M. A. (2013). Effects of eribulin, vincristine, paclitaxel and ixabepilone on fast axonal transport and kinesin-1 driven microtubule gliding: implications for chemotherapy-induced peripheral neuropathy. *Neurotoxicology* 37, 231–239. doi: 10.1016/j.neuro.2013.05.008

Leandro-Garcia, L. J., Leskela, S., Jara, C., Green, H., Avall-Lundqvist, E., Wheeler, H. E., et al. (2012). Regulatory polymorphisms in beta-tubulin IIa are associated with paclitaxel-induced peripheral neuropathy. *Clin. Cancer Res.* 18, 4441–4448. doi: 10.1158/1078-0432.CCR-12-1221

Li, Y., Adamek, P., Zhang, H., Tatsui, C. E., Rhines, L. D., Mrozkova, P., et al. (2015). The cancer chemotherapeutic paclitaxel increases human and rodent sensory neuron responses to TRPV1 by activation of TLR4. *J. Neurosci.* 35, 13487–13500. doi: 10.1523/JNEUROSCI.1956-15.2015

Lisse, T. S., Middleton, L. J., Pellegrini, A. D., Martin, P. B., Spaulding, E. L., Lopes, O., et al. (2016). Paclitaxel-induced epithelial damage and ectopic MMP-13 expression promotes neurotoxicity in zebrafish. *Proc. Natl. Acad. Sci. U.S.A.* 113, E2189–2198. doi: 10.1073/pnas.1525096113

Low, L. K., Liu, X. B., Faulkner, R. L., Coble, J., and Cheng, H. J. (2008). Plexin signaling selectively regulates the stereotyped pruning of corticospinal axons from visual cortex. *Proc. Natl. Acad. Sci. U.S.A.* 105, 8136–8141. doi: 10.1073/pnas.0803849105

MacDonald, J. M., Beach, M. G., Porpiglia, E., Sheehan, A. E., Watts, R. J., and Freeman, M. R. (2006). The Drosophila cell corpse engulfment receptor Draper mediates glial clearance of severed axons. *Neuron* 50, 869–881. doi: 10.1016/j.neuron.2006.04.028

Majithia, N., Temkin, S. M., Ruddy, K. J., Beutler, A. S., Hershman, D. L., and Loprinzi, C. L. (2016). National Cancer Institute-supported chemotherapy-induced peripheral neuropathy trials: outcomes and lessons. *Support. Care Cancer* 24, 1439–1447. doi: 10.1007/s00520-015-3063-4

Malgrange, B., Delree, P., Rigo, J. M., Baron, H., and Moonen, G. (1994). Image analysis of neuritic regeneration by adult rat dorsal root ganglion neurons in culture: quantification of the neurotoxicity of anticancer agents and of its prevention by nerve growth factor or basic fibroblast growth factor but not brain-derived neurotrophic factor or neurotrophin-3. *J. Neurosci. Methods* 53, 111–122. doi: 10.1016/0165-0270(94)90151-1

Maor-Nof, M., Romi, E., Sar Shalom, H., Ulisse, V., Raanan, C., Nof, A., et al. (2016). Axonal degeneration is regulated by a transcriptional program that coordinates expression of pro- and anti-degenerative factors. *Neuron* 92, 991–1006. doi: 10.1016/j.neuron.2016.10.061

Martin, S. M., O'Brien, G. S., Portera-Cailliau, C., and Sagasti, A. (2010). Wallerian degeneration of zebrafish trigeminal axons in the skin is required for regeneration and developmental pruning. *Development* 137, 3985–3994. doi: 10.1242/dev.053611

Masocha, W. (2015). Astrocyte activation in the anterior cingulate cortex and altered glutamatergic gene expression during paclitaxel-induced neuropathic pain in mice. *PeerJ* 3:e1350. doi: 10.7717/peerj.1350

Meregalli, C., Canta, A., Carozzi, V. A., Chiorazzi, A., Oggioni, N., Gilardini, A., et al. (2010). Bortezomib-induced painful neuropathy in rats: a behavioral, neurophysiological and pathological study in rats. *Eur. J. Pain* 14, 343–350. doi: 10.1016/j.ejpain.2009.07.001

Milde, S., Fox, A. N., Freeman, M. R., and Coleman, M. P. (2013a). Deletions within its subcellular targeting domain enhance the axon protective capacity of Nmnat2 *in vivo*. *Sci. Rep.* 3:2567. doi: 10.1038/srep02567

Milde, S., Gilley, J., and Coleman, M. P. (2013b). Subcellular localization determines the stability and axon protective capacity of axon survival factor Nmnat2. *PLoS Biol.* 11:e1001539. doi: 10.1371/journal.pbio.1001539

Mora, E., Smith, E. M., Donohoe, C., and Hertz, D. L. (2016). Vincristine-induced peripheral neuropathy in pediatric cancer patients. *Am. J. Cancer Res.* 6, 2416–2430.

Nikolaev, A., McLaughlin, T., O'Leary, D. D., and Tessier-Lavigne, M. (2009). APP binds DR6 to trigger axon pruning and neuron death via distinct caspases. *Nature* 457, 981–989. doi: 10.1038/nature07767

Obaishi, H., Nakanishi, H., Mandai, K., Satoh, K., Satoh, A., Takahashi, K., et al. (1998). Frabin, a novel FGD1-related actin filament-binding protein capable of changing cell shape and activating c-Jun N-terminal kinase. *J. Biol. Chem.* 273, 18697–18700. doi: 10.1074/jbc.273.30.18697

Osterloh, J. M., Yang, J., Rooney, T. M., Fox, A. N., Adalbert, R., Powell, E. H., et al. (2012). dSarm/Sarm1 is required for activation of an injury-induced axon death pathway. *Science* 337, 481–484. doi: 10.1126/science.1223899

Park, S. B., Goldstein, D., Krishnan, A. V., Lin, C. S., Friedlander, M. L., Cassidy, J., et al. (2013). Chemotherapy-induced peripheral neurotoxicity: a critical analysis. *CA Cancer J. Clin.* 63, 419–437. doi: 10.3322/caac.21204

Pazyra-Murphy, M. F., Hans, A., Courchesne, S. L., Karch, C., Cosker, K. E., Heerssen, H. M., et al. (2009). A retrograde neuronal survival response: target-derived neurotrophins regulate MEF2D and bcl-w. *J. Neurosci.* 29, 6700–6709. doi: 10.1523/JNEUROSCI.0233-09.2009

Periquet, M. I., Novak, V., Collins, M. P., Nagaraja, H. N., Erdem, S., Nash, S. M., et al. (1999). Painful sensory neuropathy: prospective evaluation using skin biopsy. *Neurology* 53, 1641–1647. doi: 10.1212/WNL.53.8.1641

Persohn, E., Canta, A., Schoepfer, S., Traebert, M., Mueller, L., Gilardini, A., et al. (2005). Morphological and morphometric analysis of paclitaxel and docetaxel-induced peripheral neuropathy in rats. *Eur. J. Cancer* 41, 1460–1466. doi: 10.1016/j.ejca.2005.04.006

Podratz, J. L., Knight, A. M., Ta, L. E., Staff, N. P., Gass, J. M., Genelin, K., et al. (2011a). Cisplatin induced mitochondrial DNA damage in dorsal root ganglion neurons. *Neurobiol. Dis.* 41, 661–668. doi: 10.1016/j.nbd.2010.11.017

Podratz, J. L., Staff, N. P., Boesche, J. B., Giorno, N. J., Hainy, M. E., Herring, S. A., et al. (2013). An automated climbing apparatus to measure chemotherapy-induced neurotoxicity in Drosophila melanogaster. *Fly* 7, 187–192. doi: 10.4161/fly.24789

Podratz, J. L., Staff, N. P., Froemel, D., Wallner, A., Wabnig, F., Bieber, A. J., et al. (2011b). Drosophila melanogaster: a new model to study cisplatin-induced neurotoxicity. *Neurobiol. Dis.* 43, 330–337. doi: 10.1016/j.nbd.2011.03.022

Poruchynsky, M. S., Sackett, D. L., Robey, R. W., Ward, Y., Annunziata, C., and Fojo, T. (2008). Proteasome inhibitors increase tubulin polymerization and stabilization in tissue culture cells: a possible mechanism contributing to peripheral neuropathy and cellular toxicity following proteasome inhibition. *Cell Cycle* 7, 940–949. doi: 10.4161/cc.7.7.5625

Potts, P. R., Singh, S., Knezek, M., Thompson, C. B., and Deshmukh, M. (2003). Critical function of endogenous XIAP in regulating caspase activation during sympathetic neuronal apoptosis. *J. Cell Biol.* 163, 789–799. doi: 10.1083/jcb.200307130

Poulain, F. E., and Chien, C. B. (2013). Proteoglycan-mediated axon degeneration corrects pretarget topographic sorting errors. *Neuron* 78, 49–56. doi: 10.1016/j.neuron.2013.02.005

Quartu, M., Carozzi, V. A., Dorsey, S. G., Serra, M. P., Poddighe, L., Picci, C., et al. (2014). Bortezomib treatment produces nocifensive behavior and changes in the expression of TRPV1, CGRP, and substance P in the rat DRG, spinal cord, and sciatic nerve. *Biomed Res. Int.* 2014:1 80428. doi: 10.1155/2014/180428

Riccomagno, M. M., and Kolodkin, A. L. (2015). Sculpting neural circuits by axon and dendrite pruning. *Annu. Rev. Cell Dev. Biol.* 31, 779–805. doi: 10.1146/annurev-cellbio-100913-013038

Ruiz-Medina, J., Baulies, A., Bura, S. A., and Valverde, O. (2013). Paclitaxel-induced neuropathic pain is age dependent and devolves on glial response. *Eur. J. Pain* 17, 75–85. doi: 10.1002/j.1532-2149.2012.00172.x

Sasaki, Y., Nakagawa, T., Mao, X., DiAntonio, A., and Milbrandt, J. (2016). NMNAT1 inhibits axon degeneration via blockade of SARM1-mediated NAD^+ depletion. *eLife* 5:e19749. doi: 10.7554/eLife.19749

Sasaki, Y., Vohra, B. P., Baloh, R. H., and Milbrandt, J. (2009). Transgenic mice expressing the Nmnat1 protein manifest robust delay in axonal degeneration *in vivo*. *J. Neurosci.* 29, 6526–6534. doi: 10.1523/JNEUROSCI.1429-09.2009

Schoenmann, Z., Assa-Kunik, E., Tiomny, S., Minis, A., Haklai-Topper, L., Arama, E., et al. (2010). Axonal degeneration is regulated by the apoptotic machinery or a NAD+-sensitive pathway in insects and mammals. *J. Neurosci.* 30, 6375–6386. doi: 10.1523/JNEUROSCI.0922-10.2010

Seretny, M., Currie, G. L., Sena, E. S., Ramnarine, S., Grant, R., MacLeod, M. R., et al. (2014). Incidence, prevalence, and predictors of chemotherapy-induced peripheral neuropathy: a systematic review and meta-analysis. *Pain* 155, 2461–2470. doi: 10.1016/j.pain.2014.09.020

Shemesh, O. A., and Spira, M. E. (2010). Paclitaxel induces axonal microtubules polar reconfiguration and impaired organelle transport: implications for the pathogenesis of paclitaxel-induced polyneuropathy. *Acta Neuropathol.* 119, 235–248. doi: 10.1007/s00401-009-0586-0

Siau, C., and Bennett, G. J. (2006). Dysregulation of cellular calcium homeostasis in chemotherapy-evoked painful peripheral neuropathy. *Anesth. Analg.* 102, 1485–1490. doi: 10.1213/01.ane.0000204318.35194.ed

Simon, D. J., Pitts, J., Hertz, N. T., Yang, J., Yamagishi, Y., Olsen, O., et al. (2016). Axon degeneration gated by retrograde activation of somatic pro-apoptotic signaling. *Cell* 164, 1031–1045. doi: 10.1016/j.cell.2016.01.032

Simon, D. J., Weimer, R. M., McLaughlin, T., Kallop, D., Stanger, K., Yang, J., et al. (2012). A caspase cascade regulating developmental axon degeneration. *J. Neurosci.* 32, 17540–17553. doi: 10.1523/JNEUROSCI.3012-12.2012

Singh, K. K., Park, K. J., Hong, E. J., Kramer, B. M., Greenberg, M. E., Kaplan, D. R., et al. (2008). Developmental axon pruning mediated by BDNF-p75NTR-dependent axon degeneration. *Nat. Neurosci.* 11, 649–658. doi: 10.1038/nn.2114

Smith, E. M., Pang, H., Cirrincione, C., Fleishman, S., Paskett, E. D., Ahles, T., et al. (2013). Effect of duloxetine on pain, function, and quality of life among patients with chemotherapy-induced painful peripheral neuropathy: a randomized clinical trial. *JAMA* 309, 1359–1367. doi: 10.1001/jama.2013.2813

Stendel, C., Roos, A., Deconinck, T., Pereira, J., Castagner, F., Niemann, A., et al. (2007). Peripheral nerve demyelination caused by a mutant Rho GTPase guanine nucleotide exchange factor, frabin/FGD4. *Am. J. Hum. Genet.* 81, 158–164. doi: 10.1086/518770

Suchankova, T., Kubicek, K., Kasparkova, J., Brabec, V., and Kozelka, J. (2012). Platinum-DNA interstrand crosslinks: molecular determinants of bending and unwinding of the double helix. *J. Inorg. Biochem.* 108, 69–79. doi: 10.1016/j.jinorgbio.2011.09.025

Ta, L. E., Bieber, A. J., Carlton, S. M., Loprinzi, C. L., Low, P. A., and Windebank, A. J. (2010). Transient Receptor Potential Vanilloid 1 is essential for cisplatin-induced heat hyperalgesia in mice. *Mol. Pain* 6:15. doi: 10.1186/1744-8069-6-15

Tasdemir-Yilmaz, O. E., and Segal, R. A. (2016). There and back again: coordinated transcription, translation and transport in axonal survival and regeneration. *Curr. Opin. Neurobiol.* 39, 62–68. doi: 10.1016/j.conb.2016.04.006

Theiss, C., and Meller, K. (2000). Taxol impairs anterograde axonal transport of microinjected horseradish peroxidase in dorsal root ganglia neurons *in vitro*. *Cell Tissue Res.* 299, 213–224. doi: 10.1007/s004410050019

Thomas-Jinu, S., Gordon, P. M., Fielding, T., Taylor, R., Smith, B. N., Snowden, V., et al. (2017). Non-nuclear pool of splicing factor SFPQ regulates axonal transcripts required for normal motor development. *Neuron* 94, 322.e5–336.e5. doi: 10.1016/j.neuron.2017.03.026

Unsain, N., Higgins, J. M., Parker, K. N., Johnstone, A. D., and Barker, P. A. (2013). XIAP regulates caspase activity in degenerating axons. *Cell Rep.* 4, 751–763. doi: 10.1016/j.celrep.2013.07.015

Wainger, B. J., Buttermore, E. D., Oliveira, J. T., Mellin, C., Lee, S., Saber, W. A., et al. (2015). Modeling pain *in vitro* using nociceptor neurons reprogrammed from fibroblasts. *Nat. Neurosci.* 18, 17–24. doi: 10.1038/nn.3886

Wang, J. T., Medress, Z. A., and Barres, B. A. (2012). Axon degeneration: molecular mechanisms of a self-destruction pathway. *J. Cell Biol.* 196, 7–18. doi: 10.1083/jcb.201108111

Wang, M. S., Davis, A. A., Culver, D. G., Wang, Q., Powers, J. C., and Glass, J. D. (2004). Calpain inhibition protects against Taxol-induced sensory neuropathy. *Brain* 127, 671–679. doi: 10.1093/brain/awh078

Wang, M.-S., Wu, Y., Culver, D. G., and Glass, J. D. (2001). The gene for slow Wallerian degeneration (Wld^s) is also protective against vincristine neuropathy. *Neurobiol. Dis.* 8, 155–161. doi: 10.1006/nbdi.2000.0334

Wheeler, H. E., Wing, C., Delaney, S. M., Komatsu, M., and Dolan, M. E. (2015). Modeling chemotherapeutic neurotoxicity with human induced pluripotent stem cell-derived neuronal cells. *PLoS ONE* 10:e0118020. doi: 10.1371/journal.pone.0118020

Xiao, W. H., Zheng, H., and Bennett, G. J. (2012). Characterization of oxaliplatin-induced chronic painful peripheral neuropathy in the rat and comparison with the neuropathy induced by paclitaxel. *Neuroscience* 203, 194–206. doi: 10.1016/j.neuroscience.2011.12.023

Xiong, X., Hao, Y., Sun, K., Li, J., Li, X., Mishra, B., et al. (2012). The Highwire ubiquitin ligase promotes axonal degeneration by tuning levels of Nmnat protein. *PLoS Biol.* 10:e1001440. doi: 10.1371/journal.pbio.1001440

Yang, I. H., Siddique, R., Hosmane, S., Thakor, N., and Hoke, A. (2009). Compartmentalized microfluidic culture platform to study mechanism of paclitaxel-induced axonal degeneration. *Exp. Neurol.* 218, 124–128. doi: 10.1016/j.expneurol.2009.04.017

Yang, J., Weimer, R. M., Kallop, D., Olsen, O., Wu, Z., Renier, N., et al. (2013). Regulation of axon degeneration after injury and in development by the endogenous calpain inhibitor calpastatin. *Neuron* 80, 1175–1189. doi: 10.1016/j.neuron.2013.08.034

Yang, J., Wu, Z., Renier, N., Simon, D. J., Uryu, K., Park, D. S., et al. (2015). Pathological axonal death through a MAPK cascade that triggers a local energy deficit. *Cell* 160, 161–176. doi: 10.1016/j.cell.2014.11.053

Yoon, B. C., Jung, H., Dwivedy, A., O'Hare, C. M., Zivraj, K. H., and Holt, C. E. (2012). Local translation of extranuclear lamin B promotes axon maintenance. *Cell* 148, 752–764. doi: 10.1016/j.cell.2011.11.064

Yu, F., and Schuldiner, O. (2014). Axon and dendrite pruning in Drosophila. *Curr. Opin. Neurobiol.* 27, 192–198. doi: 10.1016/j.conb.2014.04.005

Zhang, H., Li, Y., de Carvalho-Barbosa, M., Kavelaars, A., Heijnen, C. J., Albrecht, P. J., et al. (2016). Dorsal root ganglion infiltration by macrophages contributes to paclitaxel chemotherapy-induced peripheral neuropathy. *J. Pain* 17, 775–786. doi: 10.1016/j.jpain.2016.02.011

Zhang, H., Yoon, S. Y., and Dougherty, P. M. (2012). Evidence that spinal astrocytes but not microglia contribute to the pathogenesis of Paclitaxel-induced painful neuropathy. *J. Pain* 13, 293–303. doi: 10.1016/j.jpain.2011.12.002

Zheng, H., Xiao, W. H., and Bennett, G. J. (2012). Mitotoxicity and bortezomib-induced chronic painful peripheral neuropathy. *Exp. Neurol.* 238, 225–234. doi: 10.1016/j.expneurol.2012.08.023

Conflict of Interest Statement: The authors declare that the research was conducted in the absence of any commercial or financial relationships that could be construed as a potential conflict of interest.

frontiers in Neuroscience

ORIGINAL RESEARCH
published: 25 April 2017
doi: 10.3389/fnins.2017.00232

Nicotinamide and WLD^S Act Together to Prevent Neurodegeneration in Glaucoma

*Pete A. Williams[1], Jeffrey M. Harder[1], Nicole E. Foxworth[1], Brynn H. Cardozo[1], Kelly E. Cochran[1] and Simon W. M. John[1,2]**

[1] The Jackson Laboratory, Howard Hughes Medical Institute, Bar Harbor, ME, USA, [2] Department of Ophthalmology, Tufts University of Medicine, Boston, MA, USA

Glaucoma is a complex neurodegenerative disease characterized by progressive visual dysfunction leading to vision loss. Retinal ganglion cells are the primary affected neuronal population, with a critical insult damaging their axons in the optic nerve head. This insult is typically secondary to harmfully high levels of intraocular pressure (IOP). We have previously determined that early mitochondrial abnormalities within retinal ganglion cells lead to neuronal dysfunction, with age-related declines in NAD (NAD^+ and NADH) rendering retinal ganglion cell mitochondria vulnerable to IOP-dependent stresses. The Wallerian degeneration slow allele, *Wld^S*, decreases the vulnerability of retinal ganglion cells in eyes with elevated IOP, but the exact mechanism(s) of protection from glaucoma are not determined. Here, we demonstrate that *Wld^S* increases retinal NAD levels. Coupled with nicotinamide administration (an NAD precursor), it robustly protects from glaucomatous neurodegeneration in a mouse model of glaucoma (94% of eyes having no glaucoma, more than *Wld^S* or nicotinamide alone). Importantly, nicotinamide and *Wld^S* protect somal, synaptic, and axonal compartments, prevent loss of anterograde axoplasmic transport, and protect from visual dysfunction as assessed by pattern electroretinogram. Boosting NAD production generally benefits major compartments of retinal ganglion cells, and may be of value in other complex, age-related, axonopathies where multiple neuronal compartments are ultimately affected.

Keywords: glaucoma, NAD^+, *Wld^S*, axon degeneration, retinal ganglion cell

OPEN ACCESS

Edited by:
Denise M. Inman, Northeast Ohio Medical University, USA

Reviewed by:
Wonkyu Ju, University of California, San Diego, USA
Bogdan Beirowski, Hunter James Kelly Research Institute, USA

***Correspondence:**
Simon W. M. John
simon.john@jax.org

Specialty section:
This article was submitted to Neurodegeneration, a section of the journal Frontiers in Neuroscience

Received: *03 February 2017*
Accepted: *07 April 2017*
Published: *25 April 2017*

Citation:
Williams PA, Harder JM, Foxworth NE, Cardozo BH, Cochran KE and John SWM (2017) Nicotinamide and WLD^S Act Together to Prevent Neurodegeneration in Glaucoma. Front. Neurosci. 11:232. doi: 10.3389/fnins.2017.00232

INTRODUCTION

Glaucoma is complex, multifactorial disease characterized by the progressive dysfunction and loss of retinal ganglion cells. Affecting 80 million people, glaucoma is a leading cause of vision loss worldwide (Quigley and Broman, 2006) and is one of the most common neurodegenerations. Major risk factors include increased intraocular pressure (IOP) and age. Degeneration of the retinal ganglion cell during glaucoma is a compartmentalized process, with differing mechanisms

Abbreviations: FDR, false discovery rate; GCL, ganglion cell layer; INL; inner nuclear layer; IPL, inner plexiform layer; IOP, intraocular pressure; mo, months of age; NAD, nicotinamide adenine dinucleotide; NAM, nicotinamide; NMN, nicotinamide mononucleotide; OCT, optimal cutting temperature; ON, overnight; RNA-seq, RNA-sequencing; RT, room temperature; *Wld^S*, Wallerian degeneration slow allele.

damaging distinct compartments (soma, axon, dendrite, and synapse; Whitmore et al., 2005). Genetic or pharmacological targeting of processes underlying compartmental damage only provides partial protection against glaucoma [e.g., inhibition of somal degeneration through genetic removal of *Bax* (Libby et al., 2005b) and preventing synapse elimination through the genetic or pharmacological inhibition of C1 (Williams et al., 2016)]. It is important to discover strategies that protect all neuronal cell compartments as this may allow additional cell survival and increased neuronal function. Therapies that target early dysfunction and protect multiple neuronal compartments are likely to be the most effective at preserving vision.

The DBA/2J (D2) mouse is a widely used model of glaucoma, which recapitulates the hallmark features of the human disease (Libby et al., 2005a; Nickells et al., 2012). In D2 mice in our colony, ocular hypertension occurs in the majority of eyes by 8–9 months of age (mo). Retinal ganglion cells are damaged as early as 9 mo with disrupted electrical activity (Porciatti, 2015), and dendritic and synaptic atrophy without detectable RGC loss or optic nerve degeneration (Williams et al., 2013, 2016). Optic nerve degeneration occurs from 10 mo onwards with local axonal dystrophy being an early event. To understand the earliest molecular changes that occur in glaucoma, we have used RNA-sequencing (RNA-seq) to analyze D2 retinal ganglion cells at different ages. This identified mitochondrial dysfunction and metabolite depletion (most notably reduction in total NAD [NAD(t); NAD^+ and NADH)] as a primary driver of early damage in glaucoma. Restoration of NAD, using a diet supplemented in nicotinamide (NAM; an NAD precursor), or through gene therapy (over expression of *Nmnat1*; coding an NAD producing enzyme), protects from glaucoma (Williams et al., 2017). Based on the presence of early glaucomatous damage in axons and synapses we hypothesize that targeting NAD-based treatments to these neuronal compartments will prove to be an even more effective treatment.

The Wallerian degeneration slow allele (*Wld^S*) is a chimera of *Ube4b* and *Nmnat1* producing a fusion protein, WLD^S (Mack et al., 2001). WLD^S protects from an array of neurodegenerations including glaucoma (Howell et al., 2007; Beirowski et al., 2008). WLD^S has NAD producing activity (Wang et al., 2005; Coleman and Freeman, 2010; Wu et al., 2011), and improves mitochondrial function and viability after injury (Avery et al., 2012; O'Donnell et al., 2013). Thus, WLD^S provides a promising option for combinational therapy with NAM.

In the present study, we show that WLD^S has a role in NAD(t) production in the retina, that both WLD^S and NAM protect synapses and axons in glaucoma, and that NAM supplementation further reduces the risk of severe glaucomatous optic nerve degeneration in *Wld^S* D2 eyes. Remarkably, this combination of enzyme and precursor is profoundly protective and prevents glaucoma in 94% of eyes. This combination may be of substantial benefit in other neurodegenerative models, especially where WLD^S alone may be less effective due to age or other causes of NAD depletion.

METHODS

Mouse Strains, Breeding, and Husbandry

Mice were housed and fed in a 14 h light/10 h dark cycle with food and water available *ad libitum*. All breeding and experimental procedures were undertaken in accordance with the Association for research for Vision and Ophthalmology Statement for the Use of Animals in Ophthalmic Research. The Institutional Biosafety Committee and the Animal Care and Use Committee at The Jackson Laboratory approved this study. DBA/2J (D2), DBA/2J-*Gpnmb^{R150X}* (D2-*Gpnmb$^+$*), and DBA/2J.Bola-*Wld^S*/Sj (D2.*Wld^S*) strains were utilized and have been described in detail elsewhere (Libby et al., 2005a; Howell et al., 2007). D2-*Gpnmb$^+$* mice do not develop high IOP or glaucomatous neurodegeneration. For aged glaucoma experiments D2 or D2.*Wld^S* mice were administered NAM in food and/or water starting at 6 mo (prophylactic, prior to high IOP). NAM (550 mg/kg/d; PanReac AppliChem) was dissolved in regular acid drinking water (350 ml) and changed once per week.

Differential Gene Expression and Pathway Analysis

RNA-sequencing datasets were utilized from publically available RNA-sequencing transcripts generated by our lab and published previously (Gene Expression Omnibus accession number GSE90654). Adjustment for multiple testing was performed using false discovery rate (FDR, q). Genes were considered to be significantly differentially expression at an FDR < 0.05. For pathway analysis, QIAGEN's Ingenuity Pathway Analysis (IPA, Qiagen) was used for network generation across genes that are significantly differentially expressed.

NAD^+/NADH Quantification

For NAD^+/NADH [NAD total; NAD(t)] quantification retinas were dissociated as previously described and measured following the manufacturer's instructions (Biovision). Results were calculated according to the standard curve generated by using standards from the kits. Final NAD(t) concentrations for each samples were normalized to total protein concentration measured by DC assay.

Clinical Phenotyping

In all experiments, the progression of the iris disease and IOP in mutant or drug-treated mice were compared to control D2 mice as previously described (John et al., 1998; Chang et al., 1999). Briefly, for IOP measurement, mice were anesthetized and securely placed on a surgical platform. A drop of PBS was placed on the cornea to prevent dehydration and the anterior chamber was cannulated using a pulled glass microneedle attached to a micromanipulator. IOP was recorded as outlined in John et al. (1997) and Savinova et al. (2001). In each experiment, iris disease and IOP were assessed. Iris disease was assessed at 2-month intervals starting at 6 months of age until experiment completion. Intraocular pressure was measured at 45-day intervals beginning at 8–9 mo until experiment completion.

Pattern Electroretinography (PERG)

PERG was recorded subcutaneously from the snout as previously reported (Chou et al., 2014). Briefly, patterned stimuli (gratings of 0.05 cycles/degree, 100% contrast) generated on LED panels were presented at each eye separately with slight different frequencies around 1 Hz. Waveforms were retrieved using an asynchronous averaging method. Mice were anesthetized using ketamine/xylazine (Savinova et al., 2001) and body temperature maintained at 37°C on a feedback-controlled heated stage monitored by rectal thermometer.

Optic Nerve Assessment and Grading of Glaucomatous Damage

The processing of optic nerves and staining with paraphenylenediamine (PPD) was as previously reported (Smith et al., 2002). PPD stains the myelin sheath of all axons but darkly stains the axoplasm of only damaged axons. It is well-established to provide a very sensitive measure of optic nerve damage. Briefly, intracranial portions of optic nerves were fixed in 4% PFA at RT for 48 h, processed and embedded in plastic. A segment of optic nerve from within a region up to 1 mm from the posterior surface of the sclera was sectioned (1 μm thick sections) and stained with PPD. Typically 30–50 sections are taken from each nerve. Multiple sections of each nerve were considered when determining damage level. Optic nerves were analyzed and determined to have one of three damage levels:

(1) No or early damage (NOE)—Less than 5% axons damaged and no gliosis. This level of damage is seen in age and sex matched non-glaucomatous mice and is not due to glaucoma. Although none of these eyes exhibit glaucomatous nerve damage, this damage level is called no or early glaucoma as some of these eyes have early molecular changes that precede neurodegeneration (Howell et al., 2011). These molecular changes can be detected by gene expression studies. Eyes with these early molecular changes but no degeneration are considered to have early glaucoma when discussing metabolic, mitochondrial and gene expression changes in this paper.
(2) Moderate damage (MOD)—average of 30% axon loss and early gliosis,
(3) Severe (SEV)—Greater than 50% axonal loss and damage with prominent gliosis.

Anterograde Axon Transport

Mice were anesthetized using ketamine/xylazine and intravitreally injected with 2 μl AF488 cholera toxin subunit B (1 mg/ml in PBS; ThermoFisher Scientific). After 72 h mice were anesthetized and euthanized via 4% PFA cardiac perfusion. Brains and eyes were post-fixed in 4% PFA for an additional 24 h, cryoprotected in 30% sucrose in PBS overnight (ON), OCT cryoembedded, and sectioned at 20 μm. AF488 was visualized using a Zeiss AxioObserver or Zeiss AxioImager.

Histology

For immunofluorescence staining, mice were euthanized, their eyes enucleated, and placed in 4% PFA overnight (ON). Retinas were dissected and flatmounted onto slides, permeabilized with 0.1% Triton-X for 15 mins, blocked with 2% BSA in PBS, and stained ON at RT in primary antibody. After primary antibody incubation, retinas were washed five times in PBS, stained for 4 h at RT with secondary antibody. Antibodies used are shown in **Table 1**. Slides were then washed a further five times with PBS, stained with DAPI for 15 mins, mounted with fluoromount, coverslipped, and sealed with nail-polish. For retinal sections, eyes were cryoprotected in 30% sucrose ON, frozen in OCT, and cryosectioned at 18 μm. Slides were warmed to room temperature and the procedure above was followed. For immunofluorescence quantification Z-stack images were Z-projected, the color channel with the secondary fluorophore cropped out, a region of interest placed around the IPL, and mean pixel intensity measured (as in Bosco et al., 2011; Williams et al., 2012, 2016, 2017; Samuel et al., 2014). Retinas were imaged using a Zeiss AxioObserver in one session with exposure limits set the same for all images. For Nissl staining frozen sections were warmed to room temperature, placed in 1:1 alcohol:chloroform ON, and rehydrated through serial alcohol gradient. Slides were washed once in distilled water and stained for 15 mins in 0.1% cresyl violet in distilled water before being differentiated in 95% alcohol, dehydrated in 100% alcohol, and cleared in xylene. Slides prepared as above. Nissl stained retinal sections were imaged using a Nikon Eclipse E200. All images were prepared using FIJI (ImageJ).

Statistical Analysis

The sample size (number of eyes, n) is shown in each figure legend. Graphing and statistical analysis was performed in R. *Student's t*-test was used for pairwise analysis in quantitative plots, *Fisher's exact* test was used for nerve grade comparisons. Error bars refer to standard error of the mean unless otherwise stated. $^*P < 0.05$, $^{**}P < 0.01$, $^{***}P < 0.001$.

RESULTS

RNA-Sequencing Implicates Early Axonal and Synaptic Dysfunction in Glaucoma

We have recently reported metabolic and mitochondrial dysfunction in retinal ganglion cells early in glaucoma. In the current study, we reexamined publicly available RNA-seq datasets generated by our lab (Williams et al., 2017). RNA-seq was performed on RNA from retinal ganglion cells from 9 month old D2 and D2-*Gpnmb*$^+$ eyes (a strain matched control that does not develop glaucoma). At this 9 mo time point, the majority of eyes have had ongoing high IOP, but degeneration of the optic nerve has not yet occurred. We used unsupervised

TABLE 1 | Antibodies used in this study.

Antibody	Concentration	Manufacturer	Catalog number
GAP-43	1:500	Abcam	Ab16053
RBPMS	1:500	Novus Biologicals	NBP2–20112
Synaptophysin	1:250	Synaptic Systems	101002
TOM20	1:250	Abcam	Ab78547

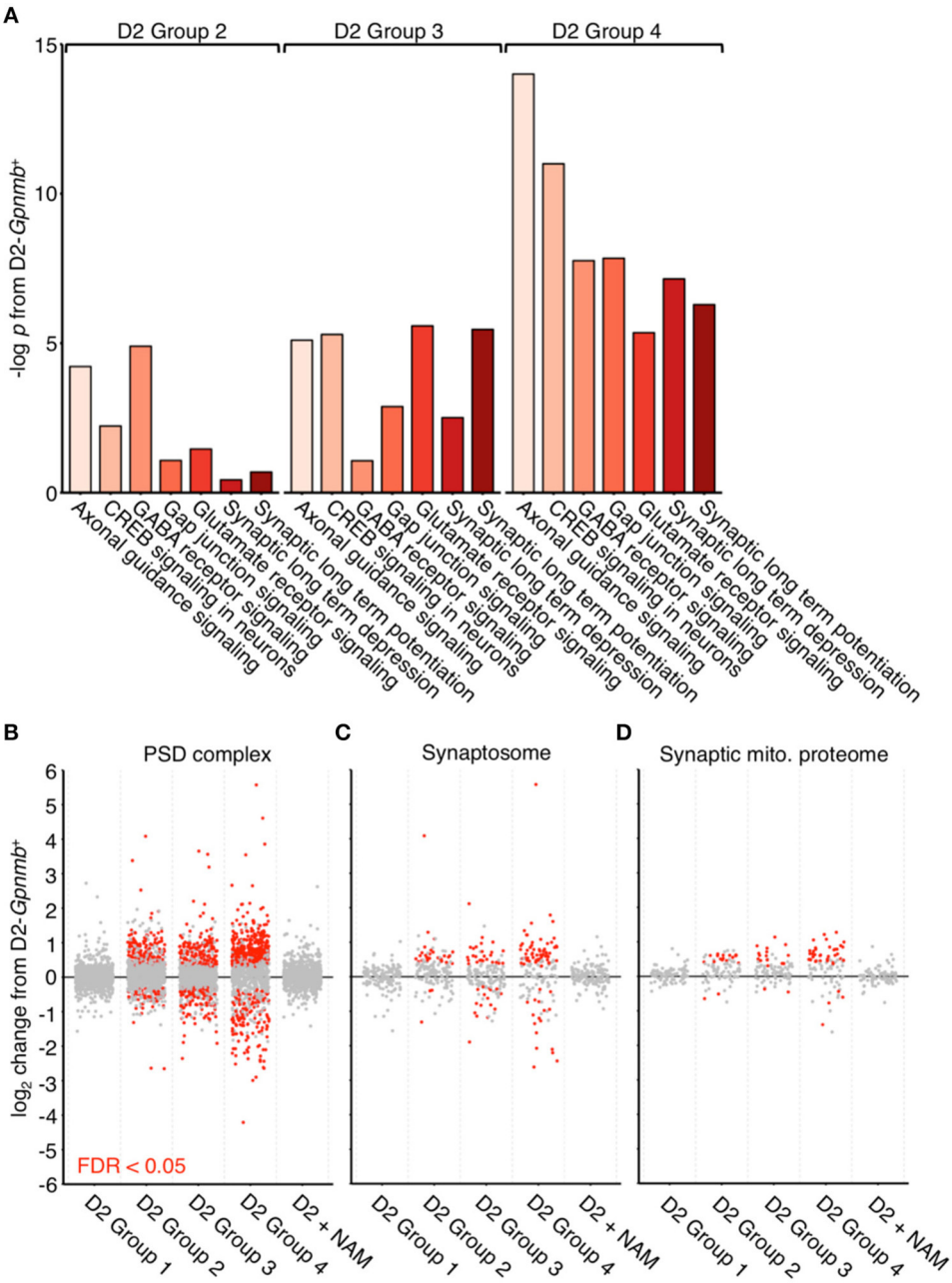

FIGURE 1 | Dysregulation of synaptic and axonal transcripts occurs early in glaucoma. (A) Ingenuity pathway analysis of RNA transcripts from retinal ganglion cells from 9 mo D2 eyes compared to no glaucoma, age-, and sex-matched D2-*Gpnmb*$^+$ controls. Pathway analysis identifies highly significant early transcriptomic changes to synaptic and axonal pathways, which become more enriched with increasing disease progression at a transcriptomic level (all samples came from mice with no glaucoma, thus these changes occur before detectable neurodegeneration). These pathways contain differentially expressed genes encoding multiple proteins that are known to be associated axon and synapse dysfunction or degeneration in other neurodegenerations. These include multiple members of the ephrin family of receptors (*Epha2*, *Epha4*, *Epha5*, *Epha6*, *Ephb2*, *Ephb3*, *Ephb4 Ephb6*; Chen et al., 2012), metabotropic glutamate receptors (*Grm3*, *Grm5*, *Grm6*, *Grm7*; Ribeiro et al., 2017), *Ryr3* (Balschun et al., 1999; Del Prete et al., 2014), and semaphorins (*Sema3a*, *Sema3b*, *Sema3d*, *Sema4a*, *Sema5a*, *Sema6a*, *Sema6c*, *Sema7a*; Shirvan et al., 2002; Good et al., 2004; Pasterkamp and Giger, 2009; Smith et al., 2015; Gutiérrez-Franco et al., 2016). There are no significantly enriched pathways in D2 Group 1 or D2 + NAM samples compared to controls. **(B–D)** Individual gene expression plots show gene sets representing proteins in the post-synaptic density **(B)**, the synaptosome **(C)**, and the synaptic mitochondrial proteome **(D)** as previously defined (Collins et al., 2006). Dots represent individual genes, gray, not differentially expressed; red, differentially expressed [at FDR (q) < 0.05 compared to D2-*Gpnmb*$^+$ control]. For all gene sets, number of differentially expressed genes increases with increased disease progression, this implies early transcriptomic dysfunction within synaptic compartments. These differentially expressed gene changes are absent from D2 Group 1 (i.e., no glaucoma at transcriptomic level), as well as from D2 + NAM samples, suggesting that NAM prevents early synaptic transcriptomic changes.

hierarchical clustering to generate novel clusters based on global gene expression patterns separating samples into four groups: D2 Group 1 (containing the subset of D2 samples that have not yet developed any glaucoma), and D2 Groups 2, 3, and 4 [all at early molecular stages of glaucoma with increasing group number reflecting increased glaucoma progression at a transcriptomic level (Williams et al., 2017)]. Here, we analyzed these groups paying particular attention to pathways that might give clues about damaging mechanisms insulting individual neuronal compartments, especially the axon and synapse, which are both directly insulted and undergo early damage. We discovered early transcriptional dysregulation of synaptic and axonal pathways that increased in significance with disease progression (**Figure 1A**). We noted significant enrichment of genes within pathways corresponding to "Axon guidance signaling" (gene families including ephrins and semaphorins that have roles in synapse formation, neuronal morphogenesis, and neuronal plasticity) and "CREB signaling in neurons" (gene families that are strongly implicated in neuronal survival and synaptic plasticity), as well as other synaptic pathways ("GABA receptor signaling", "Glutamate receptor signaling", "Synaptic long-term depression," and "Synaptic long-term potentiation"). Genes of interest are listed further in the figure legend for **Figure 1**.

Nicotinamide Supplementation Prevents Synapse Related Transcriptomic Changes

A diet supplemented in NAM potently inhibits mitochondrial dysfunction during glaucoma pathogenesis (Williams et al., 2017). Analyzing our RNA-seq dataset, we discovered that retinal ganglion cells from NAM treated mice (D2 + NAM) were robustly protected from the transcriptomic dysregulation of synaptic genes that was present in untreated D2s (**Figure 1B**). In addition, there were no enriched pathways in samples from NAM treated D2 mice compared to D2-*Gpnmb*$^+$ controls. Thus, NAM supplementation prevents the earliest transcriptomic changes relevant to synapses and axons in glaucoma.

WLD^S and NAM Increase Retinal NAD Levels and Prevent Mitochondrial Changes

WLD^S prevents axon and synapse degeneration in various models of disease. Due to its NMNAT activity, we

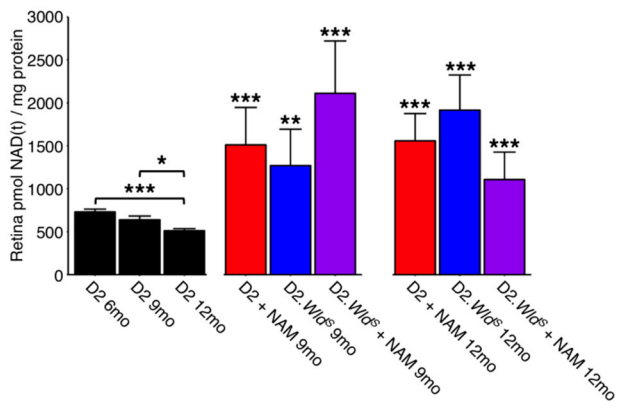

FIGURE 2 | NAM supplementation and/or WLD^S robustly restores NAD(t) levels through to 12 months. NAD(t) levels decrease with age in D2 retinas. The presence of the *Wld*^{S} allele or a diet supplemented in NAM robustly increases NAD(t) levels through to 12 months (a typical end-time in this model where the majority of eyes have severe glaucoma; $n = 22$/group). $^*P < 0.05$, $^{**}P < 0.01$, $^{***}P < 0.001$; *Student's t*-test compared to age-matched D2 retinas.

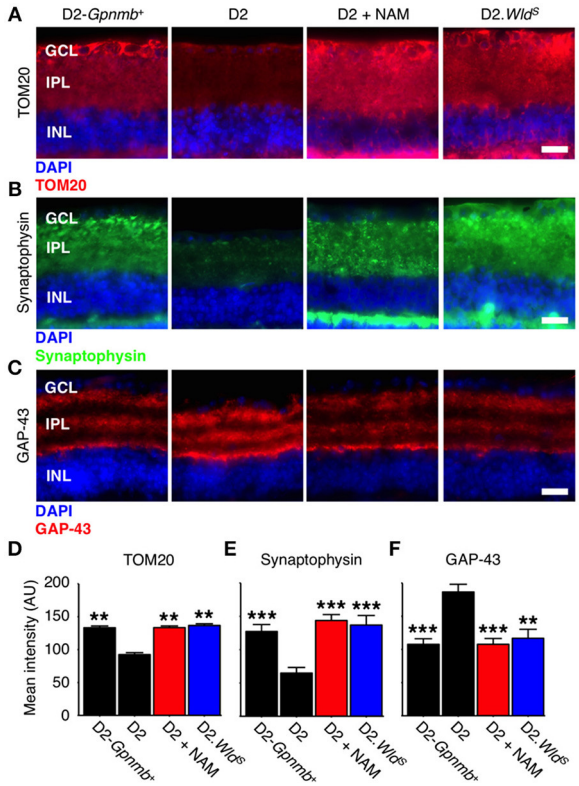

FIGURE 3 | NAM supplementation or WLD^S robustly protects from synapse elimination and neuronal stress. (A) Presence of the *Wld*^{S} allele or NAM prevents decreases in TOM20 staining (red). TOM20 is a central component of an essential complex responsible for recognition and translocation of mitochondrial preproteins (Neupert, 1997). We have previously demonstrated decreased mtRNA content in glaucomatous RGCs (Williams et al., 2017). These changes are correlated with a decrease TOM20 staining within the dendrite/synapses of D2 retinas. Retinas from NAM supplemented mice or mice carrying the *Wld*^{S} allele have TOM20 immunoreactivity levels similar to non-glaucomatous controls. 12 mo shown for all. Quantitative data are presented in **(D)**. **(B)** Retinal ganglion cell synapses elimination begins early in glaucoma and progresses to widespread synapse loss by 12 mo. Presence of the *Wld*^{S} allele or NAM protects retinal ganglion cell synapses (as assessed by synaptophysin staining, *green*), even at late time points when degeneration is almost complete in untreated D2 eyes. 12 mo shown for all. Quantitative data are presented in **(E)**. **(C)** GAP-43 levels increase in the retinal ganglion cell following axon injury at the proximal end of the axon (i.e., close to the optic nerve head; Doster et al., 1991). Presence of the *Wld*^{S} allele or NAM prevents increases in GAP-43 (red), reflecting dampened axon injury. Quantitative data are presented in **(F)**. Images are shown from representative samples corresponding to nerve grades at 12 mo. $n = 8$/group. $^{**}P < 0.01$, $^{***}P < 0.001$; *Student's t*-test compared to D2. Scale bars = 20 μm. GCL, ganglion cell layer; IPL, inner plexiform layer; INL, inner nuclear layer.

hypothesized that WLD^S would increase available levels of NAD(t), in the retina similar to NAM treatment. Thus, we performed NAD [NAD(t); NAD^+ and NADH)] assays on D2.*Wld*^{S} mice at two different ages, both pertinent to neurodegeneration in D2 glaucoma. WLD^S dramatically increased retinal NAD(t) levels throughout our experimental time points at 9 mo and at 12 mo (12 mo is a typical terminal time-point for this model, where a majority of eyes have severe neurodegeneration; **Figure 2**). Another effect of NAM treatment in glaucoma is to prevent mitochondrial changes (Williams et al., 2017). An early marker of mitochondrial change in glaucoma is a decrease in TOM20 immunoreactivity levels. Both NAM treatment and *Wld*^{S} prevented the decrease in mitochondrial TOM20 immunoreactivity levels observed in D2 glaucoma (**Figures 3A,D**).

WLD^S and NAM Protect from Synapse Elimination in Glaucoma

In D2 glaucoma there is a loss of synapses which is first evident (though mild) at 9 mo of age and progresses throughout the disease (Williams et al., 2016). We tested whether NAM or WLD^S could protect from synapse loss out to an end stage, late-time point in this glaucoma (12 months of age where the majority of eyes have severe neurodegeneration). NAM and WLD^S robustly protected against retinal ganglion cell synapse loss and neuronal stress in this model (**Figures 3B,C,E,F**).

WLD^S and NAM Robustly Protect from Axon Degeneration in Glaucoma

To test whether the levels of available enzyme and precursor (NAM) limited optic nerve protection in glaucoma, we administered NAM to D2.*Wld*^{S} mice (D2.*Wld*^{S} + NAM). D2.*Wld*^{S} + NAM mice had a profoundly decreased risk of developing glaucomatous neurodegeneration. NAM or WLD^S alone protected ~60–75% of optic nerves from degeneration, while combining NAM with WLD^S protected 94% (**Figures 4A,F**). Remarkably, this combined protection affords an ~12-fold decrease in risk of developing glaucomatous nerve damage. NAM and WLD^S robustly protected against retinal ganglion cell soma loss and retinal thinning (**Figures 4B,D,E**). Given this and along with the profound degree of optic nerve protection, the combinatorial treatment is much more effective overall. NAM and WLD^S protected anterograde axoplasmic

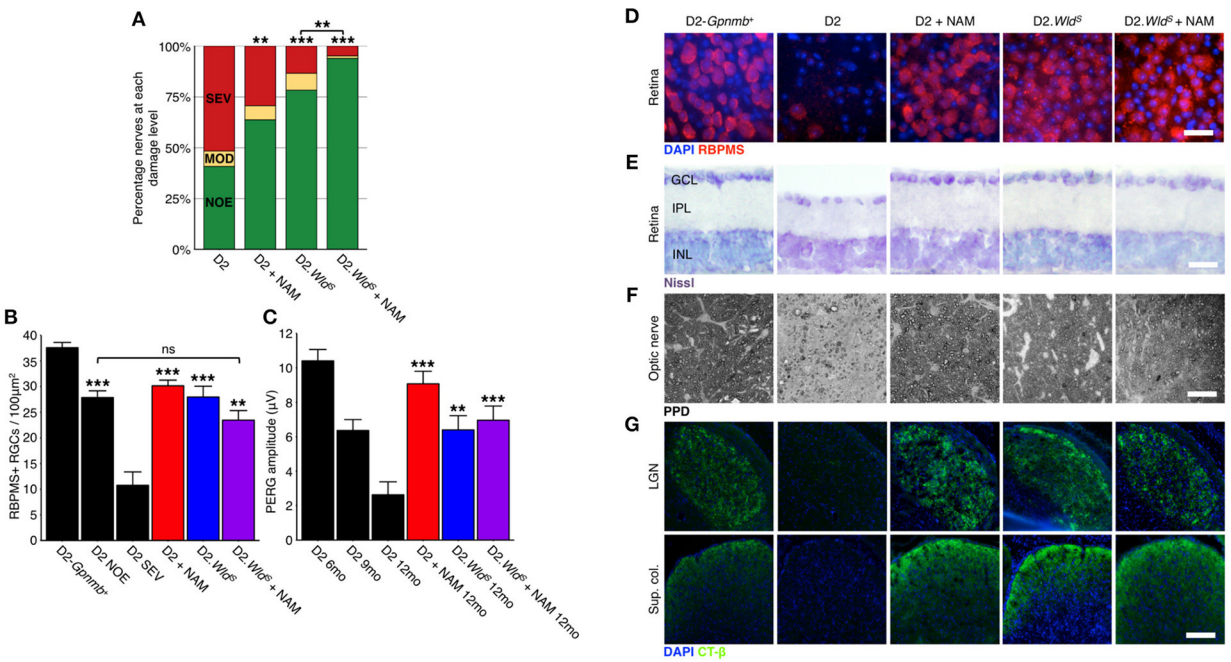

FIGURE 4 | NAM supplementation in combination with WLD^S robustly protects from glaucomatous neurodegeneration. (A) Presence of the *Wld*^{S} allele or NAM significantly protect D2 eyes from optic nerve degeneration as assessed by PPD staining (examples in **F**). Combination of the *Wld*^{S} allele and NAM significantly protects a greater proportion of optic nerves than either treatment alone (94% of eyes have no detectable glaucoma). Green, NOE; no or early glaucoma, yellow, MOD; moderate glaucoma, red, SEV; severe glaucoma. $n > 60$/group. **(B)** Presence of the *Wld*^{S} allele and/or NAM protects from retinal ganglion cell soma loss **(D)**, red, RBPMS, a specific marker of retinal ganglion cells, $n > 6$/group. The density drop between D2 NOE and D2-*Gpnmb*$^+$ is due to pressure induced stretching of the retina, inner plexiform layer thinning and nerve fiber layer thinning (examples in **E**). **(C)** Presence of the *Wld*^{S} allele or NAM significantly protect from a loss of visual function as assessed by pattern electroretinography (PERG, $n > 20$/group). PERG is a sensitive measure of retinal ganglion cell function, and thus the *Wld*^{S} allele and/or NAM protect even the earliest changes in glaucoma. $^{***}P < 0.001$ between 12 mo treatment groups and D2 12 mo. (**G**) Presence of the *Wld*^{S} allele and/or NAM protects retinal ganglion cells from axon loss. These axons terminate in key brain regions and have functional axoplasmic transport as assessed by CT-β labeling (*green*, $n = 10$/group). Retinal ganglion cell counts and axoplasmic transport images are from representative samples corresponding to NOE nerve grades at 12 mo. Representative images are shown in **D–G**. **(C,D)** $^{**}P < 0.01$, $^{***}P < 0.001$, ns, not significant. Scale bars = 20 µm **(D–F)**, 200 µm **(G)**. GCL, ganglion cell layer; IPL, inner plexiform layer; INL, inner nuclear layer.

transport to major retinal ganglion cell targets in the brain (**Figure 4G**), and electrophysiological function of retinal ganglion cells (as assessed by pattern electroretinography) to levels similar to controls (**Figure 4C**). Importantly, neither NAM nor WLD^S changed the clinical presentation of the disease (iris disease or increased IOP; **Figure 5**).

As individually protected eyes (NAM or WLD^S alone) are already indistinguishable from controls, a greater degree of protection is not expected within eyes for the combinatorial treatment (D2.*Wld*^{S} + NAM). However, as the combined treatment protects a significantly greater proportion of optic nerves as well as that other retinal ganglion cell parameters are also protected in eyes with protected nerves, these data indicate that in D2.*Wld*^{S} + NAM eyes retinal ganglion cells and axonal transport are protected in a greater percentage of eyes. Thus, the benefit of WLD^S + NAM is in that it fully prevents degeneration in all retinal ganglion cell compartments tested in the presence of elevated IOP in a greater percentage of eyes than either condition alone.

DISCUSSION

Neurons exist on a metabolic knife-edge primarily reliant on mitochondrial oxidative respiration and NAD dependent

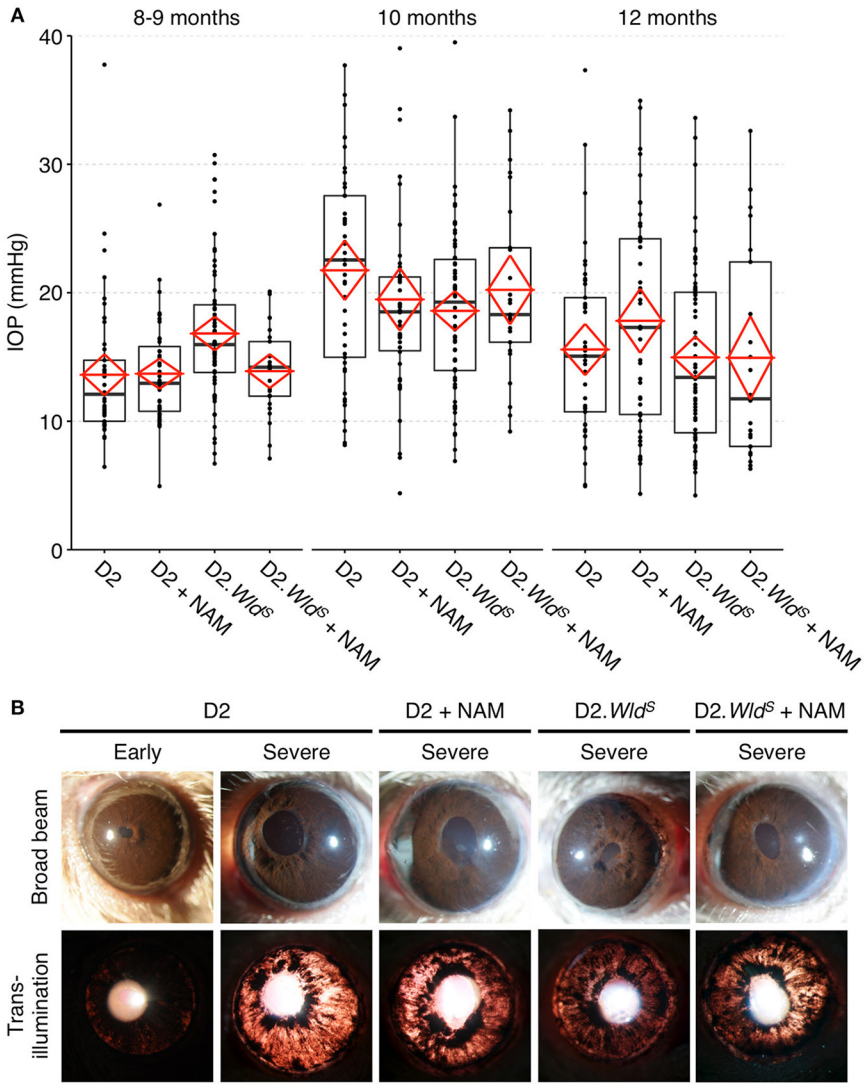

FIGURE 5 | Presence of the *Wld*^{S} allele or a diet supplemented in NAM do not change clinical disease progression/presentation in treated eyes. IOP profiles **(A)** and clinical presentation of iris disease **(B)**. IOP is not significantly different between cohorts within the same age-group. Iris disease (iris pigment dispersion resulting in asynchronous ocular hypertension) progressed at a similar rate and reached a severe state in all groups within the same time-frame. For boxplots, the upper and lower hinges represent the upper and lower quartiles. The centerline of each diamond (red) represents the mean, and the upper and lower diamond points represent 95% confidence intervals of the mean ($n > 45$ for 8–9 and 10 month groups, $n > 25$ for 12 month groups).

metabolism to meet energy demands. Our previous studies have demonstrated that NAD(t) depleting processes contribute to glaucoma (Williams et al., 2017). Here, we find that dietary supplementation of NAM (an NAD precursor) in combination with WLD^S protects D2 mice from glaucoma (preventing functional vision loss, retinal, and optic nerve damage). Importantly, the combination of WLD^S and NAM protects many more eyes (94% not developing glaucoma) than either treatment alone.

We previously determined that an age-dependent decline of NAD(t) renders retinal ganglion cells vulnerable to insults from elevated IOP, leading to subsequent glaucomatous degeneration (Williams et al., 2017). A diet supplemented with NAM boosts NAD(t) levels and reduces susceptibility to glaucoma. To better understand the effects of NAM and importance of NAD(t) levels, we studied the effects of NAM and an NAD-producing enzyme, WLD^S, on pre-degenerative changes in glaucoma. NAM treatment prevented synaptic and mitochondrial changes based on transcript and protein expression data. WLD^S is well-established to delay axon degeneration and provide variable, context-dependent protection of soma or synapses (Deckwerth and Johnson, 1994; Gillingwater et al., 2006; Beirowski et al., 2008). Here we show that WLD^S increases NAD(t) levels in the retina, and in addition to preventing optic nerve and soma degeneration, WLD^S prevents pre-degenerative changes in glaucoma (including synaptic loss, and a decrease in mitochondrial TOM20 levels) similar to NAM treatment.

As both NAM and WLD^S independently boost retinal NAD(t) levels and have similar protective effects in glaucoma, these data are consistent with WLD^S protecting retinal ganglion cells by increasing NAD(t) levels. They provide further support to the concept that maintaining NAD(t) levels is critical in enabling retinal ganglion cells to resist changes caused by glaucomatous insults. When presented in combination, D2.*Wld*^{S} and NAM act together to protect significantly more optic nerves from glaucoma than when tested alone. The combined treatment lowers the risk of developing glaucoma by ∼12-fold in this model. The combined treatment did not further increase NAD(t), however, possibly due to a physiological limit of NAD(t) production within the retina (the activity of NAMPT, the rate limiting enzyme in NAM salvage, may be limiting). Nevertheless, it remains possible that the combined treatment is more protective as it enhances the supply of NAD(t) without further increasing its steady state level (i.e., greater NAD flux). Alternatively NAM and WLD^S may act via different mechanisms. It is conceivable that NAM administration directly protects retinal mitochondria (possibly neuronal and non-neuronal) from dysfunction through its NAD dependent actions on the sirtuin family of enzymes while WLD^S protects axons. NAM may also protect by modulating DNA damage responses and/or vascular tone, due to its direct inhibitory effects on PARP and cyclic ADP ribose (Sethi et al., 1996; Geiger et al., 2000; Gibson and Kraus, 2012). WLD^S also has NAD independent roles in protecting axons (Zhai et al., 2006, 2008; Coleman and Freeman, 2010; Antenor-Dorsey and O'Malley, 2012; Kitay et al., 2013; O'Donnell et al., 2014). WLD^S has been shown to partially attenuate mitochondrial transport defects following axotomy (O'Donnell et al., 2013), and our TOM20 results may be in part due to increased mitochondrial motility following induction of elevated IOP. Further studies are required to fully elucidate the mechanism of NAM and WLD^S protection.

Our group has previously demonstrated that overexpression of murine *Nmnat1* also protects from glaucoma (Williams et al., 2017). A benefit of WLD^S over NMNAT1 alone is suggested to be the localization of WLD^S at the site of injury, likely the axon or synapse (Beirowski et al., 2009), whereas NMNAT1 is predominantly nuclear. Consistent with this hypothesis, strategies that drive misexpression of NMNAT1 outside of the nucleus result in robust axonal protection comparable to that of WLD^S (Sasaki et al., 2009). Here, we show that the combination of WLD^S and NAM is profoundly protective with 94% of treated eyes not developing glaucoma. Previously, we observed protection in only 84% of NAM + *Nmnat1* treated eyes (using the same NAM dose as the current study). With the caveats that its gene was inherited and not virally transduced (unlike *Nmnat1*) and *in vivo* NMNAT1 activity levels are difficult to compare, WLD^S may provide a more effective therapy (*Fisher's exact* test, $P < 0.01$, NAM + WLD^S vs. NAM + *Nmnat1*). However, future experiments are needed to definitively test this. The axonal protection conferred by the murine *Wld*^{S} allele is conserved across species, delaying axon degeneration in mice (Lunn et al., 1989), rats (Adalbert et al., 2005; Beirowski et al., 2008), zebrafish (O'Donnell et al., 2014), and flies (Hoopfer et al., 2006), as well as human neuronal cultures (Kitay et al., 2013). Although significant work is required before moving *Wld*^{S} into the clinic, based on these collective data there is definite promise for axon and synapse targeted treatments that manipulate molecules in the NAD pathway.

The combination of NAM and WLD^S offers a potent neuroprotective strategy for glaucoma, and is likely to benefit even patients that are refractory to IOP lowering treatments. Although glaucoma may be uniquely sensitive to WLD^S mediated protection, our current data raise the possibility of combining *Wld*^{S} (and/or *Nmnat1*) gene therapy with NAM administration in other neurodegenerative conditions. Such a combination has great potential to provide more effective protection than *Wld*^{S} alone. It is likely to be of especial value for age-related axonopathies. Importantly, this combination may even extend the protection beyond the axon to other neuronal compartments providing much-improved outcomes.

AUTHOR CONTRIBUTIONS

PW and JH: designed and performed experiments, wrote the manuscript; NF, BC, and KC: performed experiments; SJ: conceived experiments, wrote the manuscript.

FUNDING

The Jackson Laboratory Fellowships (PW, JH), NEI NIH (R01-EY11721) (SJ), the Barbara and Joseph Cohen foundation, the Partridge Foundation, and the Lano Family Foundation (SJ). SJ is an Investigator of HHMI.

ACKNOWLEDGMENTS

The authors would like to thank Electron Microscopy, Histolopathology, Gene Expression Services, and Computational Sciences at The Jackson Laboratory, G. Howell and R. Libby for discussion and experiment design, M. de Vries for assistance with organizing, and A. Bell for IOP measurements.

REFERENCES

Adalbert, R., Gillingwater, T. H., Haley, J. E., Bridge, K., Beirowski, B., Berek, L., et al. (2005). A rat model of slow Wallerian degeneration (Wld^S) with improved preservation of neuromuscular synapses. *Eur. J. Neurosci.* 21, 271–277. doi: 10.1111/j.1460-9568.2004.03833.x

Antenor-Dorsey, J. A., and O'Malley, K. L. (2012). Wld^S but not Nmnat1 protects dopaminergic neurites from MPP$^+$ neurotoxicity. *Mol. Neurodegener.* 7:5. doi: 10.1186/1750-1326-7-5

Avery, M. A., Rooney, T. M., Pandya, J. D., Wishart, T. M., Gillingwater, T. H., Geddes, J. W., et al. (2012). Wld^S prevents axon degeneration through increased mitochondrial flux and enhanced mitochondrial Ca^{2+} buffering. *Curr. Biol.* 22, 596–600. doi: 10.1016/j.cub.2012.02.043

Balschun, D., Wolfer, D. P., Bertocchini, F., Barone, V., Conti, A., Zuschratter, W., et al. (1999). Deletion of the ryanodine receptor type 3 (RyR3) impairs forms of synaptic plasticity and spatial learning. *EMBO J.* 18, 5264–5273. doi: 10.1093/emboj/18.19.5264

Beirowski, B., Babetto, E., Coleman, M. P., and Martin, K. R. (2008). The WldS gene delays axonal but not somatic degeneration in a rat glaucoma model. *Eur. J. Neurosci.* 28, 1166–1179. doi: 10.1111/j.1460-9568.2008.06426.x

Beirowski, B., Babetto, E., Gilley, J., Mazzola, F., Conforti, L., Janeckova, L., et al. (2009). Non-nuclear Wld(S) determines its neuroprotective efficacy for axons and synapses *in vivo*. *J. Neurosci.* 29, 653–668. doi: 10.1523/JNEUROSCI.3814-08.2009

Bosco, A., Steele, M. R., and Vetter, M. L. (2011). Early microglia activation in a mouse model of chronic glaucoma. *J. Comp. Neurol.* 519, 599–620. doi: 10.1002/cne.22516

Chang, B., Smith, R. S., Hawes, N. L., Anderson, M. G., Zabaleta, A., Savinova, O., et al. (1999). Interacting loci cause severe iris atrophy and glaucoma in DBA/2J mice. *Nat. Genet.* 21, 405–409. doi: 10.1038/7741

Chen, Y., Fu, A. K., and Ip, N. Y. (2012). Eph receptors at synapses: implications in neurodegenerative diseases. *Cell. Signal.* 24, 606–611. doi: 10.1016/j.cellsig.2011.11.016

Chou, T. H., Bohorquez, J., Toft-Nielsen, J., Ozdamar, O., and Porciatti, V. (2014). Robust mouse pattern electroretinograms derived simultaneously from each eye using a common snout electrode. *Invest. Ophthalmol. Vis. Sci.* 55, 2469–2475. doi: 10.1167/iovs.14-13943

Coleman, M. P., and Freeman, M. R. (2010). Wallerian degeneration, wld^s, and Nmnat. *Annu. Rev. Neurosci.* 33, 245–267. doi: 10.1146/annurev-neuro-060909-153248

Collins, M. O., Husi, H., Yu, L., Brandon, J. M., Anderson, C. N., Blackstock, W. P., et al. (2006). Molecular characterization and comparison of the components and multiprotein complexes in the postsynaptic proteome. *J. Neurochem.* 97 (Suppl. 1), 16–23. doi: 10.1111/j.1471-4159.2005.03507.x

Deckwerth, T. L., and Johnson, E. M. (1994). Neurites can remain viable after destruction of the neuronal soma by programmed cell death (apoptosis). *Dev. Biol.* 165, 63–72. doi: 10.1006/dbio.1994.1234

Del Prete, D., Checler, F., and Chami, M. (2014). Ryanodine receptors: physiological function and deregulation in Alzheimer disease. *Mol. Neurodegener.* 9:21. doi: 10.1186/1750-1326-9-21

Doster, S. K., Lozano, A. M., Aguayo, A. J., and Willard, M. B. (1991). Expression of the growth-associated protein GAP-43 in adult rat retinal ganglion cells following axon injury. *Neuron* 6, 635–647. doi: 10.1016/0896-6273(91)90066-9

Geiger, J., Zou, A. P., Campbell, W. B., and Li, P. L. (2000). Inhibition of cADP-ribose formation produces vasodilation in bovine coronary arteries. *Hypertension* 35, 397–402. doi: 10.1161/01.HYP.35.1.397

Gibson, B. A., and Kraus, W. L. (2012). New insights into the molecular and cellular functions of poly(ADP-ribose) and PARPs. *Nat. Rev. Mol. Cell Biol.* 13, 411–424. doi: 10.1038/nrm3376

Gillingwater, T. H., Ingham, C. A., Parry, K. E., Wright, A. K., Haley, J. E., Wishart, T. M., et al. (2006). Delayed synaptic degeneration in the CNS of Wld^S mice after cortical lesion. *Brain* 129, 1546–1556. doi: 10.1093/brain/awl101

Good, P. F., Alapat, D., Hsu, A., Chu, C., Perl, D., Wen, X., et al. (2004). A role for semaphorin 3A signaling in the degeneration of hippocampal neurons during Alzheimer's disease. *J. Neurochem.* 91, 716–736. doi: 10.1111/j.1471-4159.2004.02766.x

Gutiérrez-Franco, A., Costa, C., Eixarch, H., Castillo, M., Medina-Rodríguez, E. M., Bribián, A., et al. (2016). Differential expression of sema3A and sema7A in a murine model of multiple sclerosis: implications for a therapeutic design. *Clin. Immunol.* 163, 22–33. doi: 10.1016/j.clim.2015.12.005

Hoopfer, E. D., McLaughlin, T., Watts, R. J., Schuldiner, O., O'Leary, D. D., and Luo, L. (2006). Wld^S protection distinguishes axon degeneration following injury from naturally occurring developmental pruning. *Neuron* 50, 883–895. doi: 10.1016/j.neuron.2006.05.013

Howell, G. R., Libby, R. T., Jakobs, T. C., Smith, R. S., Phalan, F. C., Barter, J. W., et al. (2007). Axons of retinal ganglion cells are insulted in the optic nerve early in DBA/2J glaucoma. *J. Cell Biol.* 179, 1523–1537. doi: 10.1083/jcb.200706181

Howell, G. R., Macalinao, D. G., Sousa, G. L., Walden, M., Soto, I., Kneeland, S. C., et al. (2011). Molecular clustering identifies complement and endothelin induction as early events in a mouse model of glaucoma. *J. Clin. Invest.* 121, 1429–1444. doi: 10.1172/JCI44646

John, S. W., Hagaman, J. R., MacTaggart, T. E., Peng, L., and Smithes, O. (1997). Intraocular pressure in inbred mouse strains. *Invest. Ophthalmol. Vis. Sci.* 38, 249–253.

John, S. W., Smith, R. S., Savinova, O. V., Hawes, N. L., Chang, B., Turnbull, D., et al. (1998). Essential iris atrophy, pigment dispersion, and glaucoma in DBA/2J mice. *Invest. Ophthalmol. Vis. Sci.* 39, 951–962.

Kitay, B. M., McCormack, R., Wang, Y., Tsoulfas, P., and Zhai, R. G. (2013). Mislocalization of neuronal mitochondria reveals regulation of Wallerian degeneration and NMNAT/WLD(S)-mediated axon protection independent of axonal mitochondria. *Hum. Mol. Genet.* 22, 1601–1614. doi: 10.1093/hmg/ddt009

Libby, R. T., Anderson, M. G., Pang, I. H., Robinson, Z. H., Savinova, O. V., Cosma, I. M., et al. (2005a). Inherited glaucoma in DBA/2J mice: pertinent disease features for studying the neurodegeneration. *Vis. Neurosci.* 22, 637–648. doi: 10.1017/S0952523805225130

Libby, R. T., Li, Y., Savinova, O. V., Barter, J., Smith, R. S., Nickells, R. W., et al. (2005b). Susceptibility to neurodegeneration in a glaucoma is modified by Bax gene dosage. *PLoS Genet.* 1:e4. doi: 10.1371/journal.pgen.0010004

Lunn, E. R., Perry, V. H., Brown, M. C., Rosen, H., and Gordon, S. (1989). Absence of Wallerian degeneration does not hinder regeneration in peripheral nerve. *Eur. J. Neurosci.* 1, 27–33. doi: 10.1111/j.1460-9568.1989.tb00771.x

Mack, T. G., Reiner, M., Beirowski, B., Mi, W., Emanuelli, M., Wagner, D., et al. (2001). Wallerian degeneration of injured axons and synapses is delayed by a Ube4b/Nmnat chimeric gene. *Nat. Neurosci.* 4, 1199–1206. doi: 10.1038/nn770

Neupert, W. (1997). Protein import into mitochondria. *Annu. Rev. Biochem.* 66, 863–917. doi: 10.1146/annurev.biochem.66.1.863

Nickells, R. W., Howell, G. R., Soto, I., and John, S. W. (2012). Under pressure: cellular and molecular responses during glaucoma, a common neurodegeneration with axonopathy. *Annu. Rev. Neurosci.* 35, 153–179. doi: 10.1146/annurev.neuro.051508.135728

O'Donnell, K. C., Lulla, A., Stahl, M. C., Wheat, N. D., Bronstein, J. M., and Sagasti, A. (2014). Axon degeneration and PGC-1α-mediated protection in a zebrafish model of α-synuclein toxicity. *Dis. Model. Mech.* 7, 571–582. doi: 10.1242/dmm.013185

O'Donnell, K. C., Vargas, M. E., and Sagasti, A. (2013). Wld^s and PGC-1α regulate mitochondrial transport and oxidation state after axonal injury. *J. Neurosci.* 33, 14778–14790. doi: 10.1523/JNEUROSCI.1331-13.2013

Pasterkamp, R. J., and Giger, R. J. (2009). Semaphorin function in neural plasticity and disease. *Curr. Opin. Neurobiol.* 19, 263–274. doi: 10.1016/j.conb.2009.06.001

Porciatti, V. (2015). Electrophysiological assessment of retinal ganglion cell function. *Exp. Eye Res.* 141, 164–170. doi: 10.1016/j.exer.2015.05.008

Quigley, H. A., and Broman, A. T. (2006). The number of people with glaucoma worldwide in 2010 and 2020. *Br. J. Ophthalmol.* 90, 262–267. doi: 10.1136/bjo.2005.081224

Ribeiro, F. M., Vieira, L. B., Pires, R. G., Olmo, R. P., and Ferguson, S. S. (2017). Metabotropic glutamate receptors and neurodegenerative diseases. *Pharmacol. Res.* 115, 179–191. doi: 10.1016/j.phrs.2016.11.013

Samuel, M. A., Voinescu, P. E., Lilley, B. N., de Cabo, R., Foretz, M., Viollet, B., et al. (2014). LKB1 and AMPK regulate synaptic remodeling in old age. *Nat. Neurosci.* 17, 1190–1197. doi: 10.1038/nn.3772

Sasaki, Y., Vohra, B. P., Baloh, R. H., and Milbrandt, J. (2009). Transgenic mice expressing the Nmnat1 protein manifest robust delay in axonal degeneration *in vivo*. *J. Neurosci.* 29, 6526–6534. doi: 10.1523/JNEUROSCI.1429-09.2009

Savinova, O. V., Sugiyama, F., Martin, J. E., Tomarev, S. I., Paigen, B. J., Smith, R. S., et al. (2001). Intraocular pressure in genetically distinct mice: an update and strain survey. *BMC Genet.* 2:12. doi: 10.1186/1471-2156-2-12

Sethi, J. K., Empson, R. M., and Galione, A. (1996). Nicotinamide inhibits cyclic ADP-ribose-mediated calcium signalling in sea urchin eggs. *Biochem J.* 319(Pt 2), 613–617. doi: 10.1042/bj3190613

Shirvan, A., Kimron, M., Holdengreber, V., Ziv, I., Ben-Shaul, Y., Melamed, S., et al. (2002). Anti-semaphorin 3A antibodies rescue retinal ganglion cells from cell death following optic nerve axotomy. *J. Biol. Chem.* 277, 49799–49807. doi: 10.1074/jbc.M204793200

Smith, E. S., Jonason, A., Reilly, C., Veeraraghavan, J., Fisher, T., Doherty, M., et al. (2015). SEMA4D compromises blood-brain barrier, activates microglia, and inhibits remyelination in neurodegenerative disease. *Neurobiol. Dis.* 73, 254–268. doi: 10.1016/j.nbd.2014.10.008

Smith, R., John, S., Nishina, P., and Sundberg, J. (2002). *Systematic Evaluation of the Mouse Eye. Anatomy, Pathology and Biomethods*. Boca Raton, FL: CRC Press.

Wang, J., Zhai, Q., Chen, Y., Lin, E., Gu, W., McBurney, M. W., et al. (2005). A local mechanism mediates NAD-dependent protection of axon degeneration. *J. Cell Biol.* 170, 349–355. doi: 10.1083/jcb.200504028

Whitmore, A. V., Libby, R. T., and John, S. W. (2005). Glaucoma: thinking in new ways-a rôle for autonomous axonal self-destruction and other compartmentalised processes? *Prog. Retin. Eye Res.* 24, 639–662. doi: 10.1016/j.preteyeres.2005.04.004

Williams, P. A., Harder, J. M., Foxworth, N. E., Cochran, K. E., Philip, V. M., Porciatti, V., et al. (2017). Vitamin B3 modulates mitochondrial vulnerability and prevents glaucoma in aged mice. *Science* 355, 756–760. doi: 10.1126/science.aal0092

Williams, P. A., Howell, G. R., Barbay, J. M., Braine, C. E., Sousa, G. L., John, S. W., et al. (2013). Retinal ganglion cell dendritic atrophy in DBA/2J glaucoma. *PLoS ONE* 8:e72282. doi: 10.1371/journal.pone.0072282

Williams, P. A., Piechota, M., von Ruhland, C., Taylor, E., Morgan, J. E., and Votruba, M. (2012). Opa1 is essential for retinal ganglion cell synaptic architecture and connectivity. *Brain* 135, 493–505. doi: 10.1093/brain/awr330

Williams, P. A., Tribble, J. R., Pepper, K. W., Cross, S. D., Morgan, B. P., Morgan, J. E., et al. (2016). Inhibition of the classical pathway of the complement cascade prevents early dendritic and synaptic degeneration in glaucoma. *Mol. Neurodegener.* 11, 26. doi: 10.1186/s13024-016-0091-6

Wu, J., Zhang, F., Yan, M., Wu, D., Yu, Q., Zhang, Y., et al. (2011). WldS enhances insulin transcription and secretion via a SIRT1-dependent pathway and improves glucose homeostasis. *Diabetes* 60, 3197–3207. doi: 10.2337/db11-0232

Zhai, R. G., Cao, Y., Hiesinger, P. R., Zhou, Y., Mehta, S. Q., Schulze, K. L., et al. (2006). Drosophila NMNAT maintains neural integrity independent of its NAD synthesis activity. *PLoS Biol.* 4:e416. doi: 10.1371/journal.pbio.0040416

Zhai, R. G., Zhang, F., Hiesinger, P. R., Cao, Y., Haueter, C. M., and Bellen, H. J. (2008). NAD synthase NMNAT acts as a chaperone to protect against neurodegeneration. *Nature* 452, 887–891. doi: 10.1038/nature06721

Conflict of Interest Statement: The authors declare that the research was conducted in the absence of any commercial or financial relationships that could be construed as a potential conflict of interest.

frontiers in Neuroscience

ORIGINAL RESEARCH
published: 10 May 2017
doi: 10.3389/fnins.2017.00263

A Select Subset of Electron Transport Chain Genes Associated with Optic Atrophy Link Mitochondria to Axon Regeneration in *Caenorhabditis elegans*

Wendy M. Knowlton[1], *Thomas Hubert*[1], *Zilu Wu*[2], *Andrew D. Chisholm*[1] *and Yishi Jin*[1,2,3]*

[1] Section of Neurobiology, Division of Biological Sciences, University of California, San Diego, CA, USA, [2] Howard Hughes Medical Institute, University of California, San Diego, CA, USA, [3] Department of Cellular and Molecular Medicine, School of Medicine, University of California, San Diego, CA, USA

The role of mitochondria within injured neurons is an area of active interest since these organelles are vital for the production of cellular energy in the form of ATP. Using mechanosensory neurons of the nematode *Caenorhabditis elegans* to test regeneration after neuronal injury *in vivo*, we surveyed genes related to mitochondrial function for effects on axon regrowth after laser axotomy. Genes involved in mitochondrial transport, calcium uptake, mitophagy, or fission and fusion were largely dispensable for axon regrowth, with the exception of *eat-3/Opa1*. Surprisingly, many genes encoding components of the electron transport chain were dispensable for regrowth, except for the iron-sulfur proteins *gas-1*, *nduf-2.2*, *nduf-7*, and *isp-1*, and the putative oxidoreductase *rad-8*. In these mutants, axonal development was essentially normal and axons responded normally to injury by forming regenerative growth cones, but were impaired in subsequent axon extension. Overexpression of *nduf-2.2* or *isp-1* was sufficient to enhance regrowth, suggesting that mitochondrial function is rate-limiting in axon regeneration. Moreover, loss of function in *isp-1* reduced the enhanced regeneration caused by either a gain-of-function mutation in the calcium channel EGL-19 or overexpression of the MAP kinase DLK-1. While the cellular function of RAD-8 remains unclear, our genetic analyses place *rad-8* in the same pathway as other electron transport genes in axon regeneration. Unexpectedly, *rad-8* regrowth defects were suppressed by altered function in the ubiquinone biosynthesis gene *clk-1*. Furthermore, we found that inhibition of the mitochondrial unfolded protein response via deletion of *atfs-1* suppressed the defective regrowth in *nduf-2.2* mutants. Together, our data indicate that while axon regeneration is not significantly affected by general dysfunction of cellular respiration, it is sensitive to the proper functioning of a select subset of electron transport chain genes, or to the cellular adaptations used by neurons under conditions of injury.

Keywords: electron transport chain, growth cone, oxidoreductase *rad-8*, iron-sulfur protein, mitochondrial unfolded protein response

OPEN ACCESS

Edited by:
Robert W. Burgess,
The Jackson Laboratory, USA

Reviewed by:
Alejandra Rojas Alvarez,
Pontifical Catholic University of Chile, Chile
Kunihiro Matsumoto,
Nagoya University, Japan

***Correspondence:**
Yishi Jin
yijin@ucsd.edu

Specialty section:
This article was submitted to Neurodegeneration, a section of the journal Frontiers in Neuroscience

Received: *17 January 2017*
Accepted: *24 April 2017*
Published: *10 May 2017*

Citation:
Knowlton WM, Hubert T, Wu Z, Chisholm AD and Jin Y (2017) A Select Subset of Electron Transport Chain Genes Associated with Optic Atrophy Link Mitochondria to Axon Regeneration in Caenorhabditis elegans. Front. Neurosci. 11:263. doi: 10.3389/fnins.2017.00263

INTRODUCTION

Most neurons are intrinsically competent to regenerate their axonal processes after damage, although neurons of the adult mammalian central nervous system are generally unsuccessful in their regrowth attempts (He and Jin, 2016). Extensive studies in multiple model systems have revealed a complex set of intrinsic and extrinsic regulators of axon regeneration, and efforts are underway to understand these mechanisms with the aim of coaxing neurons into regrowing their connections and restoring neural function (Tedeschi and Bradke, 2016).

Successful axon regeneration is an intricate multistep process: The initial injury generates various cellular signals that must be detected, propagated, and interpreted by the neuron, and early responses include resealing the disrupted membrane and stabilizing damaged structures. Following this, the "repair" response involves preparing cellular structures for repair, initiating genetic growth/regrowth programs, synthesizing cellular components needed for regeneration and transporting them to the injury site, and the formation of pro-growth structures such as growth cones. Finally, for functional restoration of the neural circuit, regrowing axons must reach their targets, pathfinding successfully in the post-developmental environment while overcoming growth-inhibiting factors.

Using the nematode *Caenorhabditis elegans*, we and others have taken a genetic approach to identifying molecular mechanisms of axon regeneration, reviewed in Chisholm et al. (2016). The axons of *C. elegans* sensory and motor neurons respond to damage by forming growth cones at the severed axon stump followed by extending the axon and eventually reconnecting to targets (Yanik et al., 2004). As in other animals, axonal injury triggers an initial transient change in axonal calcium levels, the dynamics of which are important determinants of subsequent regrowth (Ghosh-Roy et al., 2010). A MAP kinase cascade involving the dual leucine-zipper kinase DLK-1 is essential and rate-limiting for early steps in regeneration, including growth cone formation (Hammarlund et al., 2009; Yan et al., 2009; Yan and Jin, 2012). DLK-1 activity is regulated by calcium and acts as a link between initial injury signals and subsequent cytoskeletal and transcriptional responses (Ghosh-Roy et al., 2012; Chen et al., 2015). In response to damage, the axonal microtubule cytoskeleton undergoes an intricate sequence of changes resulting in the formation of a regenerative growth cone between 4 and 6 h after axotomy (Ghosh-Roy et al., 2012; Chen et al., 2015). Subsequent axon extension over the next 48 h is characterized by erratic guidance, frequent branching and pruning, yet can result in functional reconnection with the original targets (Yanik et al., 2004; Ghosh-Roy et al., 2010).

In our previous screen of more than 650 genes with human homologs, two genes in the mitochondrial electron transport chain (ETC), *isp-1* and *nduf-2.2*, were found to be required for axon regeneration in peripheral lateral mechanosensory (PLM) neurons (Chen et al., 2011). The *isp-1* gene encodes the sole iron-sulfur protein in the ubiquinol-cytochrome c reductase complex, or Complex III, of the ETC (Feng et al., 2001). The *nduf-2.2* gene encodes one of seven iron-sulfur proteins in the NADH ubiquinone oxidoreductase complex, also known as ETC Complex I (Kayser et al., 2001). Loss of function in either gene had no obvious effect on neuronal development but significantly reduced PLM axon regeneration, suggesting that axon regrowth depends on mitochondrial ETC function.

To further explore the contribution of mitochondria to axon regrowth, we have conducted a targeted screen of viable mutants defective in mitochondrial regulation or function. From this screen we have identified two additional Complex I iron-sulfur protein genes, *gas-1* and *nduf-7*, as well as the putative ETC component *rad-8* as being required for effective regeneration. Interestingly, loss of function mutants of most ETC component-encoding genes as well as mutants in genes relating to mitochondrial transport, calcium uptake, mitophagy, or mitochondrial fission/fusion did not affect axon regrowth, with the exception of the mitochondrial inner membrane fusion-promoting gene *eat-3*. Most of the axon regeneration-defective mutants responded to injury by forming growth cones at a normal rate, but exhibited decreased axon regrowth. Overexpression of either *isp-1* or *nduf-2.2* in the nervous system was sufficient to enhance axon regrowth beyond that seen in controls. Genetic double mutant analysis suggested that mitochondria act downstream or in parallel to injury-related calcium or DLK-1 signals. Our genetic analyses support a role for *rad-8* in the mitochondrial ETC, and revealed an unexpected genetic interaction between *rad-8* and the demethoxyubiquinone dehydroxylase *clk-1*, which synthesizes ubiquinone for use in the ETC. Additionally, mutants of *atfs-1,* a transcription factor involved in the mitochondrial unfolded protein response, suppressed defective regrowth seen in the *nduf-2.2* mutant despite having normal axon regeneration levels on their own. Together our data reveal a role for mitochondrial function in the extension of regrowing axons after injury, although it may not be the proper functioning of the ETC *per se* that determines regeneration success, but rather the cellular adaptations in injured neurons.

MATERIALS AND METHODS

Genetics and Strains

C. elegans were cultured on nematode growth medium plates seeded with OP50 *E. coli* at 20°C for all experiments. Most strains contained P*mec-4*-GFP*(zdIs5)* for visualization of touch neurons, except those used for axotomy with the mito-GFP marker, which contained the P*mec-4-TagRFP(juIs252)* transgene. Mutants were obtained from Shohei Mitani's lab through the Japan National Bio-Resource Project, or from the *Caenorhabditis* Genetics Center, which is funded by NIH Office of Research Infrastructure Programs (P40 OD010440). All mutations were outcrossed at least twice to wild type. Alleles and strains used, as well as primer sequences for genotyping, are listed in **Table S1**.

Molecular Biology and Transgenes

For rescue and overexpression experiments, coding sequences were cloned from N2 wild type genomic DNA using primers listed in **Table S2** into the pCR8 backbone (Invitrogen) to create Gateway entry clones, which were then recombined into

Gateway destination vectors to generate expression plasmids. For the mitochondrial GFP marker, the N-terminal 29 amino acid mitochondrial targeting sequence of human COX8a was cloned upstream of GFP using Gibson Assembly (New England Biolabs) into pCR8 to generate a Gateway entry vector, and then recombined with tissue-specific Gateway destination vectors.

Transgenic arrays were generated following standard microinjection procedure (Mello et al., 1991), with expression plasmids at the concentrations listed in **Table S3**. RFP or mKate2 driven by promoters for AIY neurons (*ttx-3*), AFD neurons (*gcy-8*), or coelomocytes (*unc-122*) was used as visual markers for transgenic arrays. Most arrays were created in wild type worms and crossed into the mutant backgrounds using primers listed in **Table S4** to distinguish array sequences from genomic loci.

Laser Axotomy and Microscopy

Final larval stage worms (L4) were anesthetized in M9 buffer containing 0.1% phenoxypropanol and mounted on agar containing 0.03% phenoxypropanol. PLM femtosecond laser axotomy and regrowth quantitation were performed essentially as described (Wu et al., 2007). For the experiment using alternate anesthesia, 0.1% levamisole in M9 buffer was used at both time points, and the agar for mounting did not contain any drugs. Axon regrowth measurements were obtained from three-dimensional reconstructions of ∼1 μm sections using the Zeiss LSM Image Browser software, and any neurite >1 μm was included in the analysis. Strains were tested in at least two separate experiments and any sick animals or animals with regrowing axons fused to the severed neurite fragment were censored from the analysis.

For mitoGFP quantification, worms were mounted in phenoxypropanol as above and visualized at 63x using an LSM710 confocal microscope (Zeiss). For quantification of axonal mitochondrial density without injury, discrete axonal GFP puncta were quantified from 0 to 170 μm from the PLM cell body. For mitoGFP density measurements after injury, the number of discrete axonal GFP puncta were counted in the entire segment of the axon still attached to the cell body at both the time of injury (0 h) and 24 h later.

Statistical Analyses

Data are graphed as mean ± SEM using GraphPad Prism (version 5.01). All data were tested for statistical significance using unpaired Student's *t*-tests or *ANOVA* with Tukey's multiple comparison post-test in comparison to wild type animals tested on the same day. ns = $p > 0.05$, $^{*}p < 0.05$, $^{**}p < 0.01$, and $^{***}p < 0.001$. Numbers in graphs are the number of animals tested.

RESULTS

Regrowing PLM Axons Maintain Mitochondrial Density

Mitochondria in *C. elegans* neurons have been visualized using mito-GFP markers (Fatouros et al., 2012; Morsci et al., 2016), revealing that mitochondria form discrete puncta in axonal processes and more complex networks in cell bodies. We confirmed these observations using a pan-neuronally expressed mitochondrial reporter P*rgef-1*-mito-GFP(*juEx7517*) (**Figure S1A**) as well as a touch neuron specific marker P*mec-4*-mito-GFP(*juEx3328*) (**Figure S1B**). The density of mitochondrial puncta in the proximal PLM axon was approximately one per ten microns (**Figure S1C**), which is similar to that recently reported for *C. elegans* motor neurons (Han et al., 2016). Mitochondrial density in the distal axon of ALM neurons has been reported to increase during adult life (Morsci et al., 2016), yet we observed that the mitochondrial density in proximal PLM axons remains stable through the seventh day of adulthood (**Figure S1C**), suggesting that mitochondrial density may be differentially regulated between different neuron types, or even between distal and proximal parts of the same axon.

To examine whether mitochondrial distribution changes in response to axon injury we performed laser axotomy at the fourth larval stage, immediately before the final molt to adulthood. We observed an increase in the number of mitochondrial puncta in the proximal axon 24 h after injury (**Figures 1A,B**); however, this increase was proportional to axon regrowth such that the density of axonal mitochondria in the regrowing axon was maintained at pre-injury levels (**Figure 1C**). These observations suggest that the regrowing PLM axon maintains a constant mitochondrial density during regrowth, possibly by either increasing mitochondrial biogenesis or transport from the cell soma. Additionally, we noticed that mitochondria were generally not located at the regrowing tips of axons, but rather were variable distances away from the growth cone (**Figures 1B,D**). This is in contrast to a recent report wherein regrowing commissural axons of *C. elegans* motor neurons exhibit a marked increase in the density of mitochondrial puncta after injury as a result of increased cellular transport as well as localization of mitochondria to the growth cone (Han et al., 2016). These two studies in different neural subsets suggest that the density and localization of mitochondria after injury may be controlled in a cell type-specific manner. Regardless, the maintenance or increase of axonal mitochondrial density after injury (as opposed to decrease) in PLM neurons suggests that these organelles are important in axon regrowth. We therefore took a genetic approach to define which aspects of mitochondrial function might be relevant in axon regeneration.

A Survey of Mitochondria-Related Genes: Transport, Calcium Uptake, and Biogenesis

To learn how mitochondria contribute to axon regrowth, we surveyed genes whose orthologs are known to affect mitochondrial biogenesis, transport, or calcium uptake (**Table 1**). In addition, we performed a more extensive survey of genes involved in the electron transport chain (see next section; **Table 2**). As in our previous large-scale mutant screen (Chen et al., 2011), our analysis was confined to viable mutants; Because mitochondrial function is essential for viability (Tsang and Lemire, 2003), we exploited null mutants in non-essential genes or partial loss of function mutants in those genes that are essential to animal development and survival.

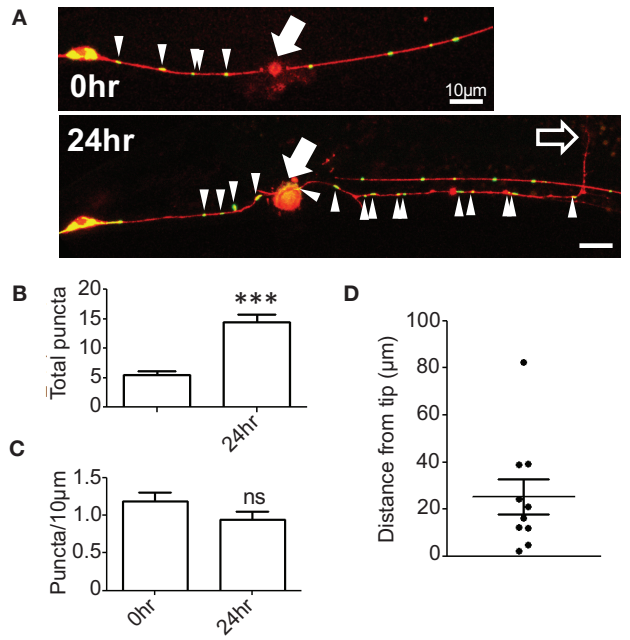

FIGURE 1 | Mitochondrial density is maintained in regenerating axons. **(A)** PLM axons were visualized with P*mec-4*-TagRFP(*juIs252*) and mitochondria with P*mec-4*-mitoGFP(*juEx3328*). Axons were severed ~50 μm from the cell body and the number of mitoGFP puncta and the length of the regrowing axon quantified 24 h post injury. **(B)** Quantification of total number of mitoGFP puncta in the portion of axon attached to the cell body (proximal axon) 24 h post injury. **(C)** Mitochondrial density was calculated as the total number of puncta divided by the length of the entire proximal axon, normalized to 10 μm. **(D)** Quantification of the distance between the regrowing axon tip or growth cone and the closest mitochondrial punctum. $n = 10$ animals tested, p-value from paired t-test: ns, not significant, $^{***}p < 0.001$. Filled arrows mark injury site, arrowheads indicate mitoGFP puncta in proximal axon, and unfilled arrow indicates tip of regrowing axon. Scale bars = 10 μm.

TABLE 1 | Mitochondrial pathways screened for axon regeneration.

Gene (allele)	Human ortholog	Pathway	Regrowth (% of WT)	*n*	*p*-value
miro-1(tm1966)	*RHOT1*	Transport	114.8 ± 7.8	22	0.1587
miro-2(tm2933)	*RHOT2*	Transport	110.7 ± 7.9	26	0.2907
trak-1(tm1572)	*TRAK1*	Transport	104.4 ± 3.3	22	0.7081
mcu-1(ju1154)	*MCU*	Calcium	82.96 ± 3.2	22	0.1174
emre-1(tm6230)	*SMDT1*	Calcium	92.09 ± 7.4	29	0.3975
pink-1(tm1779)	*PINK1*	Mitophagy	72.65 ± 5.8	26	**
pink-1(ok3538)	*PINK1*	Mitophagy	88.42 ± 3.8	28	0.2247
pdr-1(gk448)	*PARK2*	Mitophagy	110.7 ± 2.9	24	0.2895
pdr-1(tm395)	*PARK2*	Mitophagy	96.68 ± 2.9	23	0.7505
pdr-1(tm598)	*PARK2*	Mitophagy	95.15 ± 4.0	20	0.6758
drp-1(tm1108)	*DNM1L*	Fission	94.1 ± 4.0	23	0.3419
fis-1(tm1867)	*FIS1*	Fission	113. ± 6.6	22	0.1775
fis-1(tm2227)	*FIS1*	Fission	108.8 ± 7.3	21	0.4543
fis-2(gk363)	*FIS1*	Fission	107.9 ± 8.3	22	0.4745
fis-2(gk414)	*FIS1*	Fission	115.0 ± 6.4	41	0.0735
fis-2(tm1832)	*FIS1*	Fission	107.5 ± 8.5	28	0.4462
fzo-1(tm1133)	*MFN2*	Fusion	87.33 ± 5.4	19	0.074
eat-3(ad426)	*OPA1*	Fusion	62.02 ± 6.2	17	***
eat-3(tm1107)	*OPA1*	Fusion	70.27 ± 4.2	26	***

Human orthologs of C. elegans genes, as well as their mitochondrial pathway are listed. Regrowth is reported as mean percentage of wild type (WT) ± S.E.M., n = number of animals tested, and p-value from Student's t-test of mutant vs. same-day control, $^{**}p < 0.01$, $^{***}p < 0.001$.

We first focused on genes implicated in microtubule-dependent transport of mitochondria. The Miro and Trak/Milton protein families act as adaptors between mitochondria and microtubule-binding molecular motors and are required in other organisms for anterograde and retrograde transport of mitochondria in axons (Schwarz, 2013). The *C. elegans* genome contains two Miro family members *miro-1* and *miro-2* (Shen et al., 2016; Xu et al., 2016) and a single Trak/Milton family member *trak-1* (Mercer et al., 2009). *miro-1(tm1966)* null mutants appear superficially wild type, but have been shown to have increased longevity and reduced mitochondrial content (Shen et al., 2016), as well as altered mitochondrial morphology in the epidermis (Xu et al., 2016). *miro-2(tm2933)* null mutants are superficially wild type and have normal epidermal mitochondrial morphology (Xu et al., 2016). Single mutants in *miro-1* or *miro-2* displayed normal PLM axon regeneration, suggesting individual Miro genes are not required for regrowth. *trak-1(tm1572)* null mutants also displayed normal PLM axon regeneration. Together these data suggest that despite the observed increase in the number of mitochondrial puncta in the regrowing axons, and in contrast to the recently reported role for *miro-1* in motor axon regeneration (Han et al., 2016), individual transport adaptors are dispensable for PLM axon regeneration.

One of the initial signals of axonal damage is an increase of axonal calcium that spreads wave-like bi-directionally away from the site of injury (Ghosh-Roy et al., 2010). Injury-triggered calcium transients are also observed in *C. elegans* epidermal wound responses, where they trigger local mitochondrial calcium uptake and reactive oxygen species (ROS) production critical for wound repair (Xu and Chisholm, 2014). To test whether mitochondrial calcium pathways might be involved in axon repair or regeneration, we tested null mutations in the mitochondrial calcium uniporter (MCU) ortholog *mcu-1* and in the essential MCU regulator (EMRE) ortholog *emre-1,* required for coupling uniporter opening to calcium-sensing subunits (Sancak et al., 2013). These *mcu-1* and *emre-1* mutants displayed normal PLM axon regrowth, consistent with observations in *mcu-1* mutants in motor axon regrowth (Han et al., 2016), suggesting that mitochondrial calcium uptake is not a critical determinant of axon regeneration.

We next tested *C. elegans* homologs of genes involved in mitophagy, the breakdown of faulty mitochondria. In mammals and *Drosophila* the PINK1 serine/threonine kinase activates the ubiquitin-ligase activity of PARKIN/PDR-1, which marks mitochondria for degradation (Song et al., 2013). The *C. elegans* PINK1 ortholog *pink-1* and the Parkin/PDR1 ortholog *pdr-1* have been implicated in mitophagy and mitochondrial

TABLE 2 | Mitochondrial electron transport chain genes tested.

Gene (allele)	Human ortholog	ETC complex	Regrowth (% of WT)	*n*	*p*-value
gas-1(fc21)	*NDUFS2*	I	70.0 ± 6.0	25	***
nduf-2.2(ok437)	*NDUFS2*	I	41.7 ± 5.3	25	***
nduf-7(et19)	*NDUFS7*	I	67.5 ± 3.8	23	***
nuo-6(qm200)	*NDUFB4*	I	106.1 ± 6.2	24	0.4557
mev-1(kn1)	*SDHC*	II	94.0 ± 7.5	21	0.5693
sdha-2(tm1420)	*SDHA*	II	97.6 ± 6.0	22	0.8019
clk-1(e2519)	*COQ7*	Ubiquinone	91.1 ± 4.7	24	0.2637
clk-1(qm30)	*COQ7*	Ubiquinone	91.3 ± 4.5	29	0.212
rad-8(mn163)	*RTN4IP1*	II/III	51.5 ± 7.4	25	***
isp-1(qm150)	*UQCRFS1*	III	23.3 ± 3.9	27	***
ucr-2.3(ok3073)	*UQCRC2*	III	106.5 ± 5.9	30	0.4429
ucr-2.3(pk732)	*UQCRC2*	III	83.05 ± 5.5	27	0.0656
asg-2(ok3344)	*ATP5L*	ATP synthase	82.84 ± 5.6	26	0.0908
asg-2(tm1472)	*ATP5L*	ATP synthase	82.5 ± 6.2	21	0.1068

*Human orthologs of C. elegans electron transport chain genes and their complex association are listed. Regrowth is reported as mean percentage of wild type (WT) ± S.E.M., n = number of animals tested, and p-value from Student's t-test of mutant vs. same-day control, ***p < 0.001.*

biogenesis (Palikaras et al., 2015; Pickrell and Youle, 2015). We tested two *pink-1* deletions, both of which are presumed null mutants: *pink-1(tm1779)* (Samann et al., 2009) displayed significantly reduced axon regeneration, yet *pink-1(ok3538)* (Valenci et al., 2015) displayed normal axon regrowth. We note that the *tm1779* deletion also affects the inter-genic region of the operon that includes the 3′ untranslated region of the upstream F-box gene EEED8.10; *tm1779* may affect expression of the downstream gene(s), or *tm1779* strains may contain background mutations that we were unable to eliminate in outcrossing. Axon regrowth was normal in three independent alleles of the *PARKIN* homolog *pdr-1*, all of which are thought to cause strong loss of function at the protein level (Springer et al., 2005; Valenci et al., 2015). Together, we conclude that mitophagy-related genes are not required for axon regeneration.

Finally, we tested *C. elegans* genes implicated in mitochondrial fission and fusion (Mishra and Chan, 2014), namely *drp-1/DNM1L* and the *FIS1* homologs *fis-1* and *fis-2* for fission, and *fzo-1/MFN1* and *eat-3/OPA1* for fusion (**Table 1**). While *drp-1* null mutants have an abnormally fused mitochondrial network, the network in *fis-1* or *fis-2* null mutants is normal; FIS-1 and FIS-2 have been suggested to play a role in mitophagy-related mitochondrial fission rather than mitochondrial network maintenance (Breckenridge et al., 2008; Shen et al., 2014). When tested for axon regrowth after injury, all these fission-defective mutants displayed normal regrowth phenotypes (**Table 1**). We next examined a null allele of *fzo-1* and two loss-of-function alleles of *eat-3/Opa1*, orthologs of which mediate fusion of the outer and inner mitochondrial membranes, respectively (Breckenridge et al., 2008; Kanazawa et al., 2008; Rolland et al., 2009). Interestingly, *eat-3,* but not *fzo-1,* mutants displayed significantly reduced axon regrowth. As *fzo-1* and *eat-3* mutants exhibit comparably fragmented mitochondrial networks in other cell types (Breckenridge et al., 2008), the requirement for *eat-3* in regrowth may be independent of its role in mitochondrial fusion. The *eat-3* ortholog Opa1 functions in remodeling the cristae of the inner mitochondrial membrane, independent of its role in IMM fusion (Cogliati et al., 2013; Pernas and Scorrano, 2016). Since cristae house the electron transport chain, and our previous and current screen implicated ETC function in axon regrowth, we hypothesized that the requirement for *eat-3* in axon regrowth is indirect, via its effects on the ETC. However, mutants of *immt-1, immt-2, moma-1,* and *chch*-3, genes which have been implicated in cristae formation or maintenance (Mun et al., 2010; Head et al., 2011), all showed normal axon regrowth (**Figure S2**). Nevertheless, and in light of the two genes identified in the original screen belonging to the ETC, we next turned our attention to ETC genes and whether ETC function is critical for axon regrowth.

Select Components of the Electron Transport Chain Are Required for Axon Regeneration

Four multiprotein complexes (Complexes I–IV) work to metabolize products from the citric acid cycle in order to create an electrochemical gradient across the inner mitochondrial membrane, which in turn powers the ATP synthase (Complex V) that generates ATP to power cellular reactions (**Figure 2A**). While complete loss of function in mitochondrial electron transport is lethal (Tsang and Lemire, 2003), viable mutations in a number of *C. elegans* ETC components have been identified, many of which have been studied for their effects on animal lifespan (Munkacsy and Rea, 2014; Dancy et al., 2015). Besides the previously tested genes *nduf-2.2* and *isp-1,* we tested mutants in nine additional ETC components, some of which have been shown biochemically by others to display reduced ETC function (**Table 2**). Of the new mutants tested, only three had significantly reduced axon regrowth: the Complex I iron-sulfur protein-encoding genes *gas-1* and *nduf-7* and the putative mitochondrial oxidoreductase *rad-8* (**Figures 2B–G**).

We first extended our previous observations of impaired regrowth in *isp-1* and *nduf-2.2* mutants. The *isp-1(qm150)* allele is a point mutation that reduces Complex III function and lowers overall cellular respiration by 40% (Feng et al., 2001). Axon regrowth defects seen in this mutant were completely rescued by expression of wild type *isp-1* under the control of a pan-neuronal promoter (**Figure 3A**), suggesting a cell-autonomous requirement for ETC function in axon regrowth.

C. elegans encodes two orthologs of the NDUFS2 subunit of complex I: *nduf-2.2* and *gas-1* (Kayser et al., 2001). *gas-1* is ubiquitously expressed, whereas the expression pattern of *nduf-2.2* is undetermined (Kayser et al., 2004). The *nduf-2.2(ok437)* allele is a large deletion and likely null with unknown effects on mitochondrial metabolism, although mutants appear superficially wild type. In contrast, *gas-1(fc21)* partial loss of function mutants are small and slow-growing and display drastically reduced Complex I activity (Kayser et al., 1999,

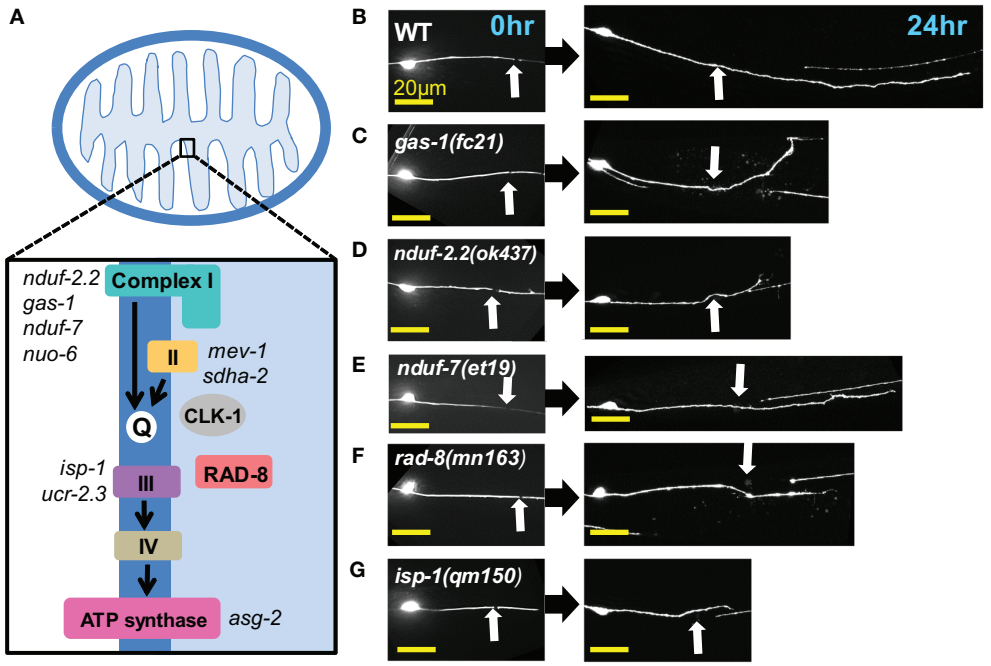

FIGURE 2 | Axon regeneration is reduced in a subset of electron transport chain gene mutants. (A) Diagram of the electron transport chain located on the inner mitochondrial membrane, with ETC genes tested indicated next to their complex. **(B–G)** Representative images of wild type (WT) and the five ETC mutants with significantly decreased axon regeneration 24 h after injury. Arrow indicates injury site. Scale bars = 20 µm.

2001). Consistent with previous observations, *nduf-2.2(ok437)* reduced regrowth by roughly 60%, and expression of wild type *nduf-2.2* under the control of a ubiquitously expressed promoter fully rescued axon regrowth phenotypes (**Figure 3B**). *gas-1(fc21)* mutants, which grow slowly and have a small body phenotype, also displayed a defect in PLM axon regrowth (**Table 2**), although not as severe as in *nduf-2.2* mutants. This suggests that defective axon regrowth is not the result of organismal growth rate and that *nduf-2.2* may play the predominant role in regrowing axons. As *gas-1(fc21)* was originally isolated based on hypersensitivity to anesthetics (Kayser et al., 1999), we tested its effects on axon regrowth using two independent immobilization agents, phenoxypropanol and levamisole, with comparable results (**Figure 3C**). Pan-neuronal expression of wild type *gas-1* was sufficient to rescue *gas-1(fc21)* axon regrowth defects to normal levels (**Figure 3D**). A recent report identified the *et19* partial loss-of-function allele of *nduf-7,* another Complex I iron-sulfur protein (Rauthan et al., 2015). *nduf-7(et19)* mutants are viable and healthy yet slightly slow-growing, and displayed defective axon regrowth (**Figure 2E**). Together, these data suggest the ETC Complex I iron-sulfur protein subunits are important for axon regeneration.

The above results on subunits of the ETC Complexes I and III are consistent with a general requirement for mitochondrial respiration and ATP synthesis in axon regrowth. Indeed, recent results showing a requirement for mitochondria in motor axon regrowth have been interpreted as reflecting the high energetic requirements in this process (Han et al., 2016). To further address the role of the ETC in axon regrowth we examined additional ETC components (**Table 2**). Unexpectedly, loss of function in most of these genes had no effect on PLM axon regeneration: In Complex I, we tested *nuo-6/NDUFB4*(*qm200),* which exhibits reduced Complex I activity and overall mitochondrial respiration, as well as impaired motor axon regrowth after injury (Yang and Hekimi, 2010b; Han et al., 2016). In Complex II we tested the *kn1* allele of *mev-1/SDHC*, which displays decreased Complex II function but normal ATP levels (Ishii et al., 1998). Also in Complex II, the *tm1420* allele of *sdha-2/SDHA*, has a 519 bp in-frame deletion in exon four, which removes most of the FAD-binding domain of the protein and thus likely rendering it unable to oxidize succinate. We tested two alleles of the Complex III core protein *ucr-2.3/UQCRC2*l: the *ok3073* allele is a 415 bp deletion and 4 bp insertion creating a premature stop codon; *pk732* is a point mutation in the insulinase domain (Butler et al., 2010). No viable alleles in genes encoding subunits of Complex IV were available. For the ATP synthase, we tested two deletion alleles of the γ-subunit homolog *asg-2/ATP5L*. We also tested *clk-1/COQ7*, which catalyzes the final step in the synthesis of ubiquinone, an essential electron carrier that shuttles electrons from Complexes I or II to Complex III (Felkai et al., 1999). *clk-1(e2519)* is a point mutation in the active site and is defective in conversion of 5-demethoxyubiquinone into ubiquinone, while the *clk-1(qm30)* deletion is a null (Ewbank et al., 1997; Miyadera et al., 2001; Branicky et al., 2006). Collectively, these mutants have varying

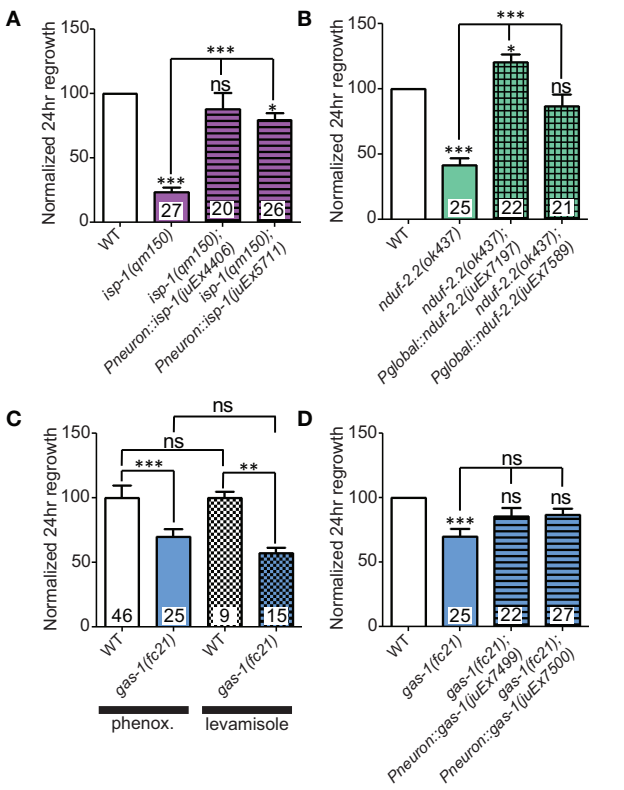

FIGURE 3 | Iron-sulfur proteins can be rescued with genomic sequences. Two independently-generated pan-neuronal or global transgenic arrays of wild type genomic sequences were able to rescue the mutants **(A)** *isp-1(qm150)* and **(B)** *nduf-2.2(ok437)*, respectively. **(C)** Testing *gas-1(fc21)* mutants using either 0.1% phenoxypropanol or 0.1% levamisole revealed that the impairments in regeneration in this mutant are independent of the immobilization method used. **(D)** Pan-neuronal transgenic arrays containing the wild type genomic sequence of *gas*-1 were able to partially restore axon regrowth in *gas-1(fc21)* mutants. Lower tier *p*-values calculated by Student's *t*-test vs. same-day control and upper tier *p*-values calculated by *ANOVA* with Tukey's multiple comparison post-test across mutant strains: ns, not significant, $^{*}p < 0.05$, $^{**}p < 0.01$ $^{***}p < 0.001$.

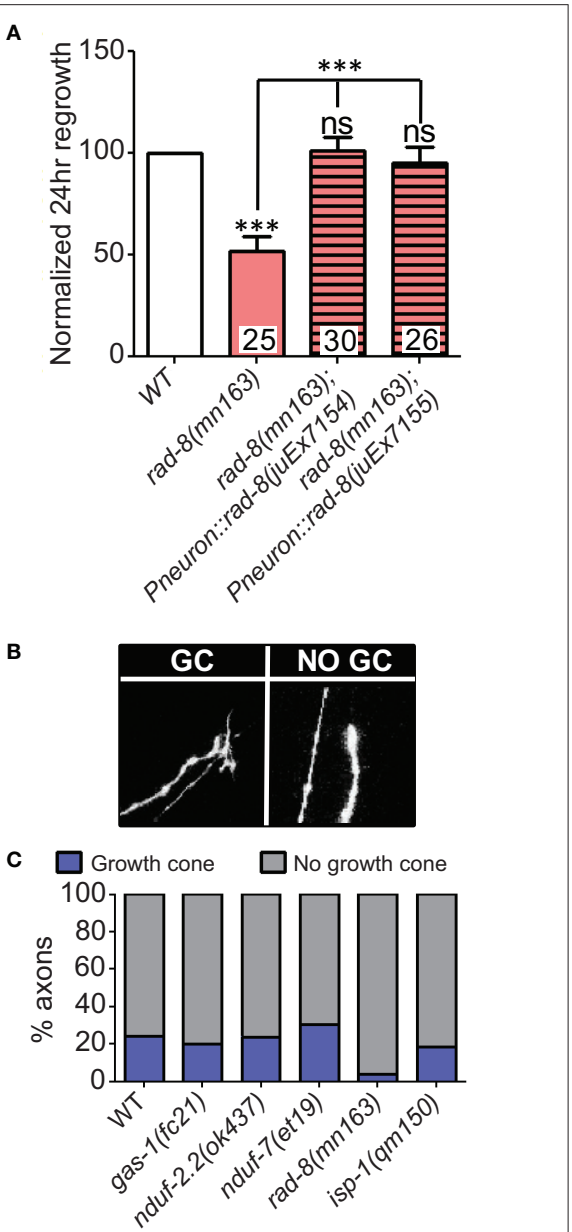

FIGURE 4 | *rad*-8 mutants can be rescued with genomic sequence and exhibit fewer growth cones. (A) Wild type genomic sequence of *rad-8* expressed pan-neuronally can rescue *rad-8(mn163)* axon regeneration to normal levels. **(B)** Examples of regrowing axon terminals with (left) or without (right) growth cones. **(C)** Proportions of ETC mutant animals with axons terminating with (blue) or without (gray) growth cones at 24 h post-injury, with only *rad-8* mutants showing fewer growth cones than wild type. Lower tier *p*-values calculated by Student's *t*-test vs. same-day control and upper tier *p*-values calculated by *ANOVA* with Tukey's multiple comparison post-test across mutant strains: ns, not significant, $^{***}p < 0.001$.

effects on ETC function and ATP production (Dancy et al., 2015), yet all had largely normal axon regeneration 24 h after axotomy, contradicting our hypothesis that the ETC is required for axon regeneration (**Table 2**).

Among the additional ETC components tested, only *rad-8* mutants displayed defective regrowth (**Figure 2F**, **Table 2**). *rad-8* encodes a putative mitochondrial oxidoreductase, and the *mn163* mutation results in a premature stop codon and is a presumed null allele. This mutant has decreased electron transfer from Complex II to Complex III (Fujii et al., 2011), but normal ATP levels (Braeckman et al., 2000); the precise role of RAD-8 in electron transport is unclear. Pan-neuronal expression of wild type *rad-8* was sufficient to rescue *rad-8* axon regrowth defects (**Figure 4A**). Unlike *isp-1* and other ETC mutants, regrowing PLM axons in *rad-8(mn163)* displayed a reduced frequency of growth cones 24 h after injury (4 vs. 20% in wild type; **Figures 4B,C**).

Overall, since many of the ETC mutants have normal axon regrowth, our data suggest that PLM axon regeneration is not

simply dependent on ATP generation by the entire ETC, but rather on the function of specific subset of ETC components. The relationship between dysfunction of a small group of ETC components and overall mitochondrial metabolism is complex, thus it may be that these genes have a special function within the ETC, or that their loss or mutation leads to cellular adaptations which inhibit axon regrowth (see below).

Mitochondrial ETC Genes Are Required for Axon Extension and Act Downstream or in Parallel to Injury Signals

To get a deeper understanding of the regeneration defects in the affected ETC mutants, we next asked whether mitochondria are required for early responses such as formation of growth cones at the tip of the regrowing axon. Defective axon regrowth 24 h after injury could result from the failure of a number of steps in regrowth, from initial injury detection and signal propagation to growth cone formation and axon extension. These five ETC mutants with defective axon regrowth had a normal frequency of growth cone formation at 6 h after injury (**Figure 5A**). Furthermore, by this time point, regrowing wild type axons had extended nearly 20 μm, whereas the ETC mutants consistently displayed reduced axon extension (**Figure 5B**). Altogether these data suggest that the ETC genes are not required in injury detection and growth cone formation, rather they likely function in the extension phase of axon regeneration.

Elevated calcium influx after injury with a gain-of-function mutation in the voltage gated calcium channel EGL-19 or elevated injury signaling by overexpression of *dlk-1* each enhance axon regrowth beyond wild type levels (Ghosh-Roy et al., 2010; Yan and Jin, 2012). To test whether the ETC functions downstream of the initial injury signaling, we performed double mutant analyses between *isp-1(qm150)* mutants and either *egl-19(gf)* or DLK-1 overexpressing animals. Double mutants of *isp-1(qm150)* and the *egl-19(ad695)* mutant were strongly defective in regrowth, although not as strongly as *isp-1(qm150)* alone (**Figure 5C**). Similarly, *isp-1(qm150)* was almost fully epistatic to the effects of *dlk-1* overexpression. We conclude that the role of mitochondria in axon regeneration lies downstream of initial injury signals and that boosting these early events cannot bypass the requirement for mitochondria in later axon extension. The partial epistasis of *isp-1* with *egl-19(gf)* is consistent with multiple pathways acting downstream of injury signals.

Overexpression of *nduf-2.2* or *isp-1* Can Enhance Axon Regeneration

During the above rescue experiments, we noticed that animals expressing one of the *nduf-2.2* transgenic arrays displayed axon regrowth significantly higher than wild type, even in the *nduf-2.2(ok437)* background (**Figure 3B**). We explored

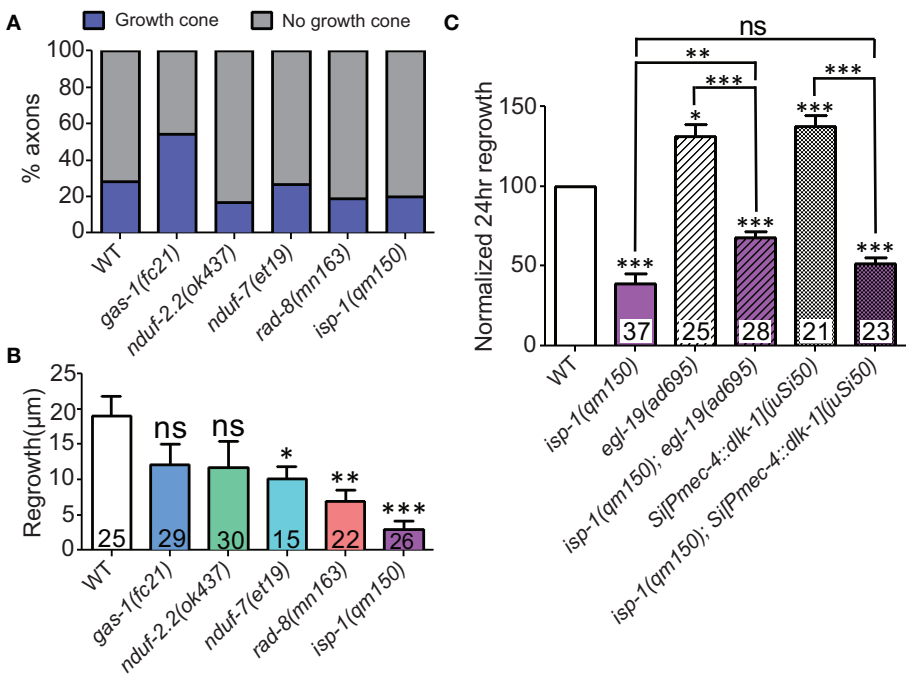

FIGURE 5 | ETC genes affect axon extension, downstream of early injury signaling. (A) The proportions of ETC mutant animals with axons terminating with (blue) or without (gray) growth cones at 6 h post-injury are largely normal, suggesting that all mutants can respond to injury by forming growth structures. **(B)** Measuring axon length at 6 h post-injury reveals deficits in the ETC mutants, indicating defects in axon extension. **(C)** The *isp-1(qm150)* mutation can partially or fully block the enhanced regeneration phenotypes of either *egl-19(gf)* or two extra copies of *dlk-1* in mechanosensory neurons, respectively. Colored bars in **(C)** indicate presence of *qm150* mutant allele. Lower tier *p*-values calculated by Student's *t*-test vs. same-day control and upper tier *p*-values calculated by *ANOVA* with Tukey's multiple comparison post-test across mutant strains: ns, not significant, $^{*}p < 0.05$, $^{**}p < 0.01$, $^{***}p < 0.001$.

whether overexpressing these ETC genes in the wild type background would affect axon regeneration. Interestingly, rescuing transgenes for the iron-sulfur proteins *nduf-2.2* and *isp-1* using either a ubiquitous or a pan-neuronal promoter, respectively, enhanced PLM axon regeneration in the wild type background (**Figures 6A,B**). Although, *nduf-2.2* and *gas-1* are over 90% identical in amino acid sequence and share similar functions (Kayser et al., 2001), transgenes of wild type *gas-1* using a pan-neuronal promoter did not enhance axon regeneration in the wild type background (**Figure 6C**). Similarly, neuronal overexpression of wild type *rad-8* also had no effect (**Figure 6D**). With the caveat that expression levels have not been directly measured in these strains, our data suggest that overexpression of *nduf-2.2* or *isp-1* can be sufficient to enhance axon regrowth above normal levels.

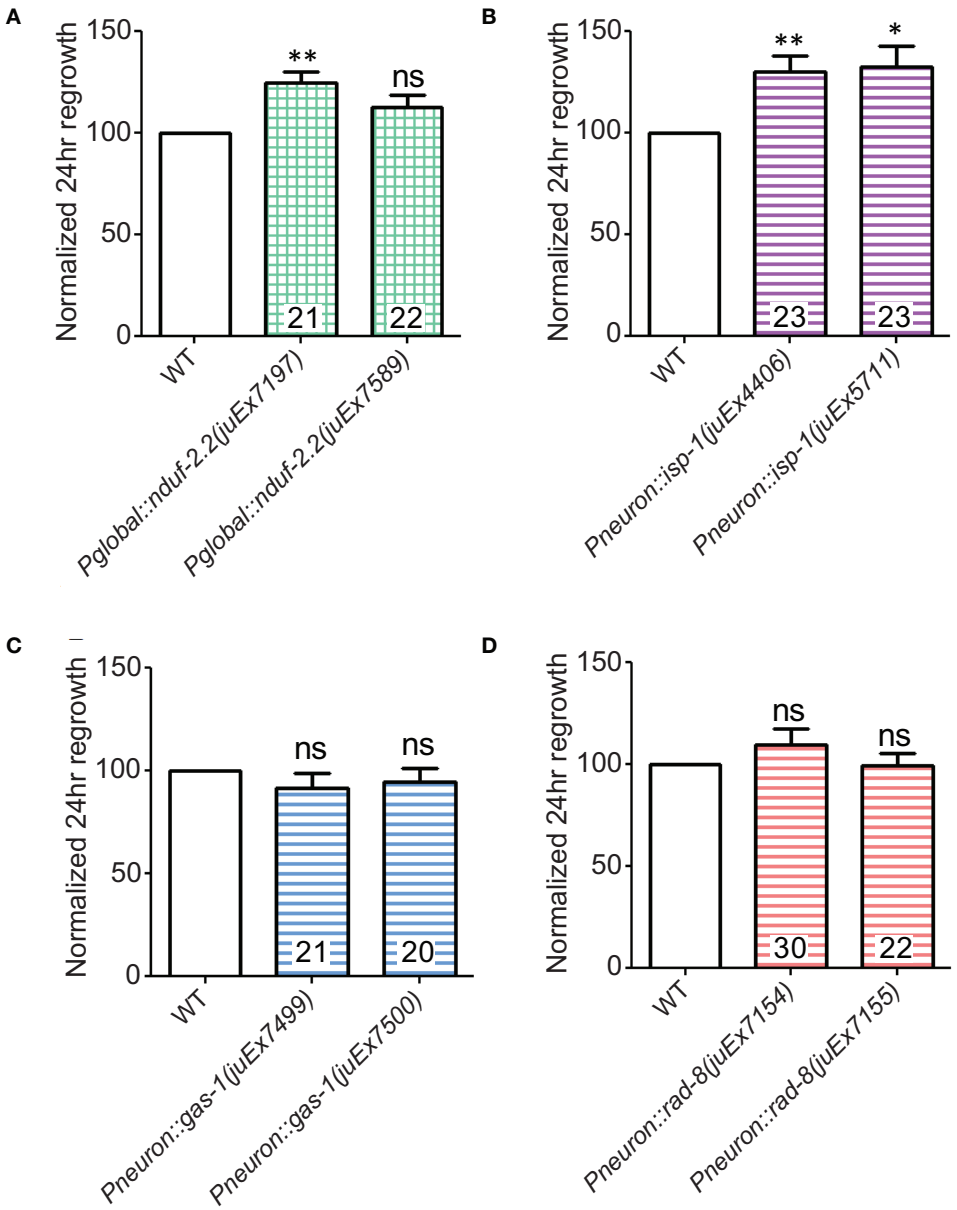

FIGURE 6 | Overexpression of either *nduf-2.2* or *isp-1* enhances regeneration in the wild type background. (A) One of the mutant-rescuing arrays of *nduf-2.2* under a global promoter enhanced axon regrowth in the wild type background. **(B)** Both transgenic arrays with pan-neuronal overexpression of *isp-1* were sufficient to increase regrowth in the wild type background. However, neuronal overexpression of neither **(C)** *gas-1* nor **(D)** *rad-8* had a significant effect in wild type animals. *p*-values were calculated using Student's *t*-test vs. same-day control: ns, not significant, $^{*}p < 0.05$ $^{**}p < 0.01$.

Interactions of *rad-8* with the Mitochondrial Electron Transport Chain

Our finding that *rad-8* is required for efficient axon regrowth prompted us to investigate this gene in more depth, since the cellular function of RAD-8 remains unclear. *rad-8* mutants were originally isolated by virtue of their hypersensitivity to radiation (Hartman and Herman, 1982) and later found to exhibit reduced electron transport between Complexes II and III (Fujii et al., 2011). *rad-8* encodes a putative mitochondrial dehydrogenase/reductase (Fujii et al., 2011) related to the mammalian Nogo-interacting protein RTN4IP/NIMP (Hu et al., 2002). To assess whether RAD-8 is required in mitochondria, we mis-targeted the protein to the cytoplasm by deleting the N-terminal mitochondrial localization sequence (MLS) as described by Hu et al. (2002). Wild type animals expressing RAD-8ΔMLS pan-neuronally displayed normal development and behavior, but in the *rad-8(mn163)* background the RAD-8ΔMLS transgene significantly decreased viability, precluding axon regeneration testing. These experiments suggest the N-terminal MLS is important for RAD-8 function, consistent with a role in mitochondria.

We next constructed compound mutants of *rad-8(mn163)* with other ETC mutants. Double mutants between *rad-8(mn163)* and *nduf-2.2(ok437)* or *isp-1(qm150)* were extremely slow growing yet displayed sub-additive interactions in axon regrowth, such that the double mutants resembled the strongest single mutant phenotype (**Figure 7A**). We were unsuccessful in our attempts to generate viable double mutants between *rad-8(mn163)* and *gas-1(fc21), mev-1(kn1),* and the C-terminal deletion mutant *ucr-2.3(ok3073)*. Double mutants of *rad-8(mn163)* with *ucr-2.3(pk732)*, a point mutant in the insulinase domain of a Complex III core subunit that is phenotypically similar to *mev-1(kn1)* (Butler et al., 2010) and had normal axon regrowth, showed axon regeneration levels similar to *rad-8(mn163)* mutants.

Additionally, we tested whether *rad-8(mn163)* interacts with *clk-1*. As noted above, the null allele *clk-1(qm30)* had no effect on axon regeneration alone, and double mutants resembled *rad-8(mn163)* in regrowth (**Figure 7B**). Unexpectedly, when *rad-8(mn163)* was combined with the *clk-1(e2519)* point mutation, the *rad-8(mn163)* axon regeneration defect was suppressed to wild type levels. Both *clk-1* alleles partially suppressed the slow growth and small body size of the *rad-8(mn163)* mutants when grown at 20°C, but only *e2519* suppressed *rad-8* axon regrowth defects, further supporting a conclusion that axon regrowth is separable from organismal growth rate.

Inhibiting the mitoUPR Suppresses *nduf-2.2* Regeneration Defects

One response to mitochondrial dysfunction is the mitochondrial unfolded protein response (mitoUPR), in which the transcription factor ATFS-1 is released from mitochonrdria and translocates to the cell nucleus to turn on the expression of adaptive genes (Nargund et al., 2012; Kornmann, 2014). We tested two deletion alleles of *atfs-1* that affect the N-terminal region of the gene, likely causing strong loss of function. We observed a mild improvement in axon regeneration in one allele, and another allele showed wild type levels of regrowth (**Figure 8**), suggesting that inhibiting the mitoUPR has no major effect on axon regeneration. However, double mutants of either *atfs-1* allele with the ETC gene *nduf-2.2* showed suppression of the regeneration defect seen in *nduf-2.2* single mutants. Our attempts to generate double mutant strains between *atfs-1* and the other affected ETC genes were unsuccessful because these mutants were either extremely slow-growing or lethal. Together with the interaction between *rad-8* and *clk-1* observed above, these data suggest that absence of *rad-8* or *nduf-2.2* likely trigger special cellular adaptations and stress signaling cascades, which are compensated upon impairment in mitoUPR function, resulting in normal regrowth of injured axons.

DISCUSSION

Increasing evidence from diverse model systems points to an important role for mitochondria in regenerative axon regrowth. Here, building on initial observations from our large-scale axon regeneration screen (Chen et al., 2011), we explored the role of mitochondria in depth. Using *C. elegans* mechanosensory neurons, we find that injured neurons maintain their axonal mitochondrial density as they regrow and do not send mitochondria to the tips of regrowing axons. Regeneration is generally resistant to loss-of-function mutations in most mitochondrial biogenesis or fission/fusion pathways, with the exception of *eat-3*/Opa1, which may affect assembly of the electron transport chain. We identify a subset of ETC components required for efficient regrowth, and show that these likely act cell autonomously during the axon extension phase of regrowth.

We find that in *C. elegans* PLM mechanosensory neurons, axon injury does not trigger dramatic alterations in mitochondrial distribution. By 24 h post injury, the total number of axonal mitochondria in the regrowing axon has increased so as to maintain mitochondrial density at ∼10 per 100 μm of axon length, with the most distal mitochondrion located ∼25 μm from the regrowing axon tip. These observations may be compared with recent studies of *C. elegans* motor neuron commissures, which display an increase in mitochondrial density within 12 h of injury due to increased axonal transport and translocation into growth cones (Han et al., 2016). Axon regeneration of mammalian neurons also appears to involve axonal mitochondrial transport, as loss of function in the mammalian-specific mitochondrial anchor protein syntaphilin results in enhanced axon regeneration (Zhou et al., 2016). Furthermore, the mammalian-specific transport protein Armcx1 is required for the enhanced regenerative capacity of some retinal ganglion axons in a regeneration-enhanced background (Cartoni et al., 2016). In contrast, Rawson and colleagues reported that in *C. elegans ric-7* mutant worms, which cannot transport mitochondria into PLM axons, severed axons retained their regenerative competence (Rawson et al., 2014).

In addition to mitochondrial transport, studies in mammalian peripheral axons or in *Drosophila* have found that injury triggers

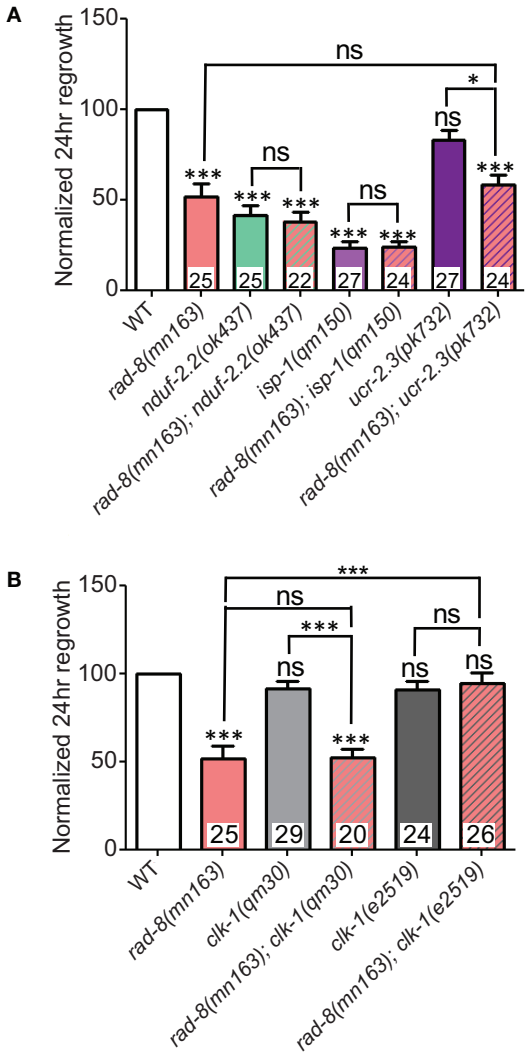

FIGURE 7 | *rad-8* epistasis places it in the same pathway as other ETC genes. (A) Axon regrowth in double mutants of *rad-8(mn163)* with either *nduf-2.2(ok437)* or *isp-1(qm150)* were identical to either *nduf-2.2(ok437)* or *isp-1(qm150)* single mutants, while double mutants of *rad-8(mn163)* with *ucr-2.3(pk732)* were identical to *rad-8(mn163)* single mutants. **(B)** *rad-8(mn163); clk-1(qm30)* double mutants were identical to *rad-8(mn163)* single mutants, while *rad-8(mn163); clk-1(e2519)* double mutants had wild type levels of axon regrowth. Lower tier *p*-values calculated by Student's *t*-test vs. same-day control and upper tier *p*-values calculated by *ANOVA* with Tukey's multiple comparison post-test across mutant strains: ns, not significant, $^{*}p < 0.05$, $^{***}p < 0.001$.

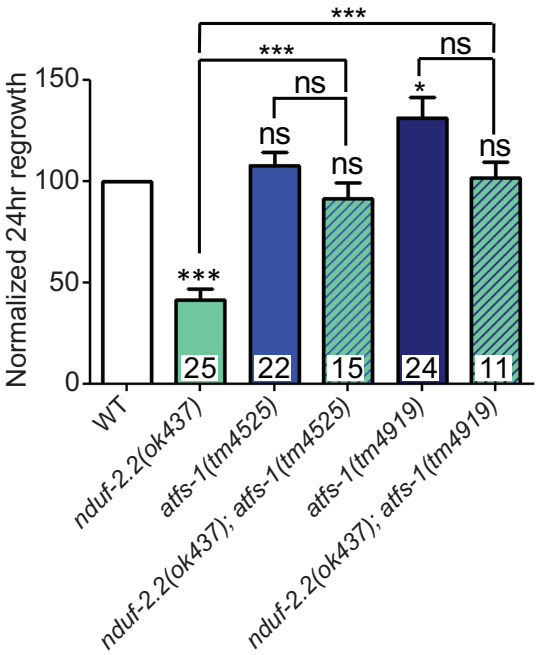

FIGURE 8 | Mutations in the mitoUPR response gene *atfs-1* suppress axon regeneration defects in *nduf-2.2*. Two deletion mutants of *atfs-1* have either no effect or a small increase in axon regeneration on their own, but double mutants of either *atfs-1* allele and *nduf-2.2* have wild type axon regrowth. Lower tier *p*-values calculated by Student's *t*-test vs. same-day control and upper tier *p*-values calculated by *ANOVA* with Tukey's multiple comparison post-test across mutant strains: ns, not significant, $^{*}p < 0.05$, $^{***}p < 0.001$.

mitochondrial fission (Chen et al., 2016; Kiryu-Seo et al., 2016). In contrast to our findings in PLM sensory neurons, the fission-defective mutant *drp-1* is defective in *C. elegans* motor commissure regrowth (Han et al., 2016), although it is unclear if this reflects a requirement for fission during the injury response or if it results from the chronic depletion of axonal mitochondria in these mutants. Taken together, these studies suggest the effects of injury on axonal mitochondrial distribution may vary depending on the species and neuronal subtype.

In PLM neurons, injury does not appear to trigger drastic remodeling of axonal mitochondria. Nonetheless, our data show that mitochondrial function is important in PLM axon regrowth. We tested over 20 genes with known or predicted roles in mitochondrial biogenesis or function, assessing mitochondrial transport, calcium uptake, mitophagy, the fission/fusion cycle, and the electron transport chain. We find no evidence that mitophagy on its own is essential for regrowth, as also reported for *C. elegans* motor neurons (Han et al., 2016). Adaptors for mitochondrial transport along microtubules also did not appear to play direct roles in PLM regrowth, although we have not excluded possible redundancy between the two *miro* genes. Axon regrowth was essentially normal in *drp-1* mutants (fission defective) or *fzo-1* mutants (fusion defective) implying that the fission/fusion cycle is not rate limiting to PLM axon regrowth. In contrast, *eat-3* (inner mitochondrial membrane fusion defective) mutants displayed significantly reduced regrowth, potentially reflecting an influence on the electron transport chain.

Our observations that loss of function in only five out of eleven ETC subunits resulted in significantly impaired axon regrowth support a more specific role for the electron transport chain in axon regrowth. Consistent with our findings, Han and colleagues also found that *isp-1* mutants are strongly defective in GABAergic motor neuron commissure regrowth (Han et al.,

2016). However, in contrast, Han and colleagues found that *nuo-6* mutants are mildly defective in motor neuron regrowth, whereas we find *nuo-6* mutants show normal PLM regrowth. This suggests that GABAergic motor neurons may be more sensitive to lowered ETC function than are PLM neurons, or that different neuron types depend on different ETC components for regrowth.

A key question is why axon regrowth is sensitive to loss of function in some but not other components of the ETC. It should be noted that in addition to their best-known roles in ATP synthesis, mitochondrial function affects diverse aspects of cellular metabolism. Chronic disruption of electron transport, as in the mutants studied here, triggers complex cellular responses, including remodeling of metabolism to preserve energy production. Electron transport dysfunction can trigger the mitochondrial retrograde signaling pathway (Liu and Butow, 2006), the mitochondrial unfolded protein response (Nargund et al., 2012), as well as a host of other metabolic responses (Morgan et al., 2015) including aberrant NADH:NAD^+ ratios (Falk et al., 2008) and altered one-carbon metabolism (Bao et al., 2016). A common result of ETC dysfunction is elevated production of mitochondrial ROS, which in some cases induces elevated levels of detoxifying enzymes. However, our data together with those of Han et al. (2016) argue against a role for mitochondrial calcium handling or ROS production in axon regeneration.

Focusing on the energetic phenotypes of the *C. elegans* mutants studied here, disruption of Complex I—as in *gas-1(fc21)* mutants—impairs Complex I activity, but animals compensate by elevating Complex II function and organismal ATP levels are normal (Kayser et al., 2004). Conversely, loss of Complex II function—as in *mev-1(kn1)* mutants—leads to a compensatory increase in Complex I function resulting in overall normal ATP levels (Braeckman et al., 2000; Senoo-Matsuda et al., 2001). Defects in ubiquinone synthesis, such as in *clk-1* mutants, strongly reduce Complex I-dependent respiration, but overall metabolism and ATP content are normal, presumably due to compensatory upregulation of glycolytic pathways for ATP production (Braeckman et al., 1999). Complex III-impaired *isp-1* mutants display the most dramatic axon regrowth defects in our assay and have been reported to have either normal (Yang and Hekimi, 2010a) or reduced (Yee et al., 2014) ATP levels. Conversely, *rad-8* mutants have normal ATP levels (Braeckman et al., 2000), yet display reduced regrowth. ATP levels have not been examined in *nduf-2.2* or *nduf-7* mutants. *nuo-6* mutants, which had normal PLM regrowth, have been reported to have either elevated (Yang and Hekimi, 2010a) or reduced (Yee et al., 2014) ATP levels. Thus, there is so far no clear correlation between respiratory chain outputs and regeneration, although it should be noted that whole organism measurements of ATP or other metabolites may not necessarily extend to individual neurons.

In seeking possible commonalities among the subset of mitochondria- and ETC-related genes required for axon regeneration, we note that several genes have human orthologs implicated in hereditary optic neuropathies, wherein retinal ganglion cells or their axons degenerate, leading to blindness. The *eat-3* ortholog *OPA1* is well known for its association with dominant optic atrophy, an inherited condition characterized by retinal ganglion cell degeneration (Lenaers et al., 2012). Mutations in *NDUFS2* and *NDUFS7,* orthologs of *nduf-2.2/gas-1* and *nduf-7,* respectively, are associated with mitochondrial Complex I deficiency, which can cause hereditary optic neuropathy (Triepels et al., 1999; Bugiani et al., 2004; Tuppen et al., 2010). Human mutations in *UQCRFS1*, the human ortholog of *isp-1*, the Complex III Rieske iron-sulfur protein, have not been directly associated with human disease, but Complex III deficiency in general is linked to optic neuropathy (Benit et al., 2009). A recent report found that mutations in *RTN4IP1,* the *rad-8* ortholog, lead to inherited optic neuropathy (Angebault et al., 2015). Although many of the other genes screened in this study have human orthologs associated with a variety of diseases, including degenerative diseases affecting the nervous system, none are currently associated with optic neuropathies. Speculatively, this suggests that *C. elegans* sensory neurons and human retinal ganglion cells share similarities in their dependence on specific components of the ETC, perhaps for metabolic or other homeostatic purposes. The finding that inhibition of the mitoUPR in the *nduf-2.2* mutant background could restore axon regeneration to wild type levels presents the possibility that specific cellular adaptations and signaling cascades remain active in this subset of ETC mutants.

An additional common feature among four of the six genes identified here as being required in axon regrowth is their biochemical function as iron-sulfur proteins, the key electron donors and acceptors in the ETC. Why these proteins are specifically required while other components of the same ETC complexes are not required is unclear. One possibility is that these proteins, due to their interface with electrons, experience a high rate of structural damage during respiration such that their degradation and replacement is rate-limiting. Another possibility is that under conditions of high respiratory demand—stresses such as axon injury—dysfunction of iron-sulfur proteins might lead to release of labile iron, leading to further cellular damage or the initiation of processes such as ferroptosis (Dixon and Stockwell, 2014; Yang and Stockwell, 2016). In support of both of these options, we found that overexpression of the iron-sulfur proteins NDUF-2.2 and ISP-1 can enhance regrowth, which may provide a ready pool of replacement proteins or might sequester labile iron, or both. It remains unclear why overexpression of the NDUF-2.2 paralog GAS-1 did not enhance regrowth; perhaps NDUF-2.2 plays a more dominant or specific role in neurons, while GAS-1 has a larger role in non-neuronal tissues. Together these data suggest that ETC iron-sulfur proteins play a specialized role in neurons and in axon regeneration.

Our finding that we could genetically suppress *rad-8* growth phenotypes with either of the *clk-1* mutant alleles was a serendipitous observation during double mutant construction. It is possible that loss of *clk-1* function leads to mild stress and upregulation of stress response pathways that might suppress the *rad-8* defects. However, other ETC mutants—which may also

activate stress response pathways—did not similarly suppress *rad-8(mn163)* phenotypes in the viable double-mutants, in some cases (*nduf-2.2, isp-1)* actually exacerbating the slow growth of *rad-8* mutants. Moreover, although both *clk-1* alleles suppressed *rad-8* growth rate defects, only the point mutant (*e2519*) and not the null allele suppressed the *rad-8(mn163)* regeneration defect, suggesting the *e2519* allele might possess altered function, as has been noted (Branicky et al., 2006). Similarly, RAD-8 may also has tissue-specific functions. It was notable that restoration of RAD-8 expression only in neurons also rescued organismal growth rates (this study and Fujii et al., 2011), while expression of the RAD-8ΔMLS construct in neurons strongly impaired overall growth rates. These findings support a link between neuronal mitochondria and overall animal growth rates (Ndegwa and Lemire, 2004; Berendzen et al., 2016), although overall growth rates and axon regeneration after injury are not themselves correlated. Future studies on the molecular mechanisms of these ETC-related genes may help shed further light on the role that mitochondria play in the axon regenerative program and may, through homology with human genes, provide insights into human optic atrophies.

AUTHOR CONTRIBUTIONS

WK: Designed and performed experiments, analyzed data, and wrote the paper. TH: Designed and performed experiments, analyzed data, and commented the paper. ZW: Performed experiments. AC and YJ: Designed experiments, analyzed data, and wrote the paper.

ACKNOWLEDGMENTS

We thank Laura Toy for help with strain construction and Suhong Xu, Sam Cherra, Kate McCulloch, and other members of the Jin and Chisholm labs for helpful comments and advice. Supported by NIH R01 NS057317 and NS093588 to AC and YJ, and NIH 5T32NS007220 (to N. C. Spitzer) and 1F32NS089187 to WK. ZW is an Associate, and YJ an Investigator, of the HHMI.

SUPPLEMENTARY MATERIAL

The Supplementary Material for this article can be found online at: http://journal.frontiersin.org/article/10.3389/fnins.2017.00263/full#supplementary-material

Figure S1 | Mitochondria in the worm nervous system. (A) Brightfield and fluorescence images of wild type worms expressing mitoGFP under the pan-neuronal *rgef-1* promoter. Zoomed in views of the **(A')** head and **(A")** tail ganglia are outlined. **(B)** Expression of mitoGFP in the PLM neuron using the *mec-4* promoter. **(C)** The density of axonal mitochondrial puncta in the first ∼100 μm from the cell body in the PLM neuron remains stable from the final larval stage (L4) through the seventh day of adulthood (A7). *p*-values calculated using Student's *t*-test vs. L4: ns, not significant.

Figure S2 | Mutants in cristae shape-related genes have normal axon regeneration. Single mutant analysis of genes linked to cristae formation or shape show no significant defects in axon regeneration. *p*-values calculated using Student's *t*-test vs. same day control: ns, not significant.

Table S1 | Mutant strains and genotyping primer sequences used.

Table S2 | Plasmids and cloning primer sequences used.

Table S3 | Transgenic array strain information.

Table S4 | Genotyping primer sequences used for strains with transgenic arrays.

REFERENCES

Angebault, C., Guichet, P. O., Talmat-Amar, Y., Charif, M., Gerber, S., Fares-Taie, L., et al. (2015). Recessive mutations in RTN4IP1 cause isolated and syndromic optic neuropathies. *Am. J. Hum. Genet.* 97, 754–760. doi: 10.1016/j.ajhg.2015.09.012

Bao, X. R., Ong, S. E., Goldberger, O., Peng, J., Sharma, R., Thompson, D. A., et al. (2016). Mitochondrial dysfunction remodels one-carbon metabolism in human cells. *Elife* 5:e10575. doi: 10.7554/eLife.10575

Benit, P., Lebon, S., and Rustin, P. (2009). Respiratory-chain diseases related to complex III deficiency. *Biochim. Biophys. Acta* 1793, 181–185. doi: 10.1016/j.bbamcr.2008.06.004

Berendzen, K. M., Durieux, J., Shao, L. W., Tian, Y., Kim, H. E., Wolff, S., et al. (2016). Neuroendocrine coordination of mitochondrial stress signaling and proteostasis. *Cell* 166, 1553, e10–1563.e10. doi: 10.1016/j.cell.2016.08.042

Braeckman, B. P., Houthoofd, K., De Vreese, A., and Vanfleteren, J. R. (1999). Apparent uncoupling of energy production and consumption in long-lived Clk mutants of *Caenorhabditis elegans*. *Curr. Biol.* 9, 493–496. doi: 10.1016/S0960-9822(99)80216-4

Braeckman, B. P., Houthoofd, K., and Vanfleteren, J. R. (2000). Patterns of metabolic activity during aging of the wild type and longevity mutants of *Caenorhabditis elegans*. *J. Am. Aging Assoc.* 23, 55–73. doi: 10.1007/s11357-000-0007-8

Branicky, R., Nguyen, P. A., and Hekimi, S. (2006). Uncoupling the pleiotropic phenotypes of clk-1 with tRNA missense suppressors in *Caenorhabditis elegans*. *Mol. Cell. Biol.* 26, 3976–3985. doi: 10.1128/MCB.26.10.3976-3985.2006

Breckenridge, D. G., Kang, B. H., Kokel, D., Mitani, S., Staehelin, L. A., and Xue, D. (2008). *Caenorhabditis elegans* drp-1 and fis-2 regulate distinct cell-death execution pathways downstream of ced-3 and independent of ced-9. *Mol. Cell* 31, 586–597. doi: 10.1016/j.molcel.2008.07.015

Bugiani, M., Invernizzi, F., Alberio, S., Briem, E., Lamantea, E., Carrara, F., et al. (2004). Clinical and molecular findings in children with complex I deficiency. *Biochim. Biophys. Acta* 1659, 136–147. doi: 10.1016/j.bbabio.2004.09.006

Butler, J. A., Ventura, N., Johnson, T. E., and Rea, S. L. (2010). Long-lived mitochondrial (Mit) mutants of *Caenorhabditis elegans* utilize a novel metabolism. *FASEB J.* 24, 4977–4988. doi: 10.1096/fj.10-162941

Cartoni, R., Norsworthy, M. W., Bei, F., Wang, C., Li, S., Zhang, Y., et al. (2016). The mammalian-specific protein armcx1 regulates mitochondrial transport during axon regeneration. *Neuron* 92, 1294–1307. doi: 10.1016/j.neuron.2016.10.060

Chen, L., Chuang, M., Koorman, T., Boxem, M., Jin, Y., and Chisholm, A. D. (2015). Axon injury triggers EFA-6 mediated destabilization of axonal microtubules via TACC and doublecortin like kinase. *Elife* 4:e08695. doi: 10.7554/eLife.08695

Chen, L., Nye, D. M., Stone, M. C., Weiner, A. T., Gheres, K. W., Xiong, X., et al. (2016). Mitochondria and caspases tune nmnat-mediated stabilization to promote axon regeneration. *PLoS Genet.* 12:e1006503. doi: 10.1371/journal.pgen.1006503

Chen, L., Wang, Z., Ghosh-Roy, A., Hubert, T., Yan, D., O'Rourke, S., et al. (2011). Axon regeneration pathways identified by systematic genetic screening in *C. elegans*. *Neuron* 71, 1043–1057. doi: 10.1016/j.neuron.2011.07.009

Chisholm, A. D., Hutter, H., Jin, Y., and Wadsworth, W. G. (2016). The genetics of axon guidance and axon regeneration in *Caenorhabditis elegans*. *Genetics* 204, 849–882. doi: 10.1534/genetics.115.186262

Cogliati, S., Frezza, C., Soriano, M. E., Varanita, T., Quintana-Cabrera, R., Corrado, M., et al. (2013). Mitochondrial cristae shape determines respiratory

chain supercomplexes assembly and respiratory efficiency. *Cell* 155, 160–171. doi: 10.1016/j.cell.2013.08.032

Dancy, B. M., Sedensky, M. M., and Morgan, P. G. (2015). Mitochondrial bioenergetics and disease in *Caenorhabditis elegans*. *Front. Biosci.* 20, 198–228. doi: 10.2741/4305

Dixon, S. J., and Stockwell, B. R. (2014). The role of iron and reactive oxygen species in cell death. *Nat. Chem. Biol.* 10, 9–17. doi: 10.1038/nchembio.1416

Ewbank, J. J., Barnes, T. M., Lakowski, B., Lussier, M., Bussey, H., and Hekimi, S. (1997). Structural and functional conservation of the *Caenorhabditis elegans* timing gene clk-1. *Science* 275, 980–983. doi: 10.1126/science.275.5302.980

Falk, M. J., Zhang, Z., Rosenjack, J. R., Nissim, I., Daikhin, E., Sedensky, M., et al. (2008). Metabolic pathway profiling of mitochondrial respiratory chain mutants in *C. elegans*. *Mol. Genet. Metab.* 93, 388–397. doi: 10.1016/j.ymgme.2007.11.007

Fatouros, C., Pir, G. J., Biernat, J., Koushika, S. P., Mandelkow, E., Mandelkow, M., et al. (2012). Inhibition of tau aggregation in a novel *Caenorhabditis elegans* model of tauopathy mitigates proteotoxicity. *Hum. Mol. Genet.* 21, 3587–3603. doi: 10.1093/hmg/dds190

Felkai, S., Ewbank, J. J., Lemieux, J., Labbe, J. C., Brown, G. G., and Hekimi, S. (1999). CLK-1 controls respiration, behavior and aging in the nematode *Caenorhabditis elegans*. *EMBO J.* 18, 1783–1792. doi: 10.1093/emboj/18.7.1783

Feng, J., Bussiere, F., and Hekimi, S. (2001). Mitochondrial electron transport is a key determinant of life span in *Caenorhabditis elegans*. *Dev. Cell* 1, 633–644. doi: 10.1016/S1534-5807(01)00071-5

Fujii, M., Yasuda, K., Hartman, P. S., Ayusawa, D., and Ishii, N. (2011). A mutation in a mitochondrial dehydrogenase/reductase gene causes an increased sensitivity to oxidative stress and mitochondrial defects in the nematode *Caenorhabditis elegans*. *Genes Cells* 16, 1022–1034. doi: 10.1111/j.1365-2443.2011.01547.x

Ghosh-Roy, A., Goncharov, A., Jin, Y., and Chisholm, A. D. (2012). Kinesin-13 and tubulin posttranslational modifications regulate microtubule growth in axon regeneration. *Dev. Cell* 23, 716–728. doi: 10.1016/j.devcel.2012.08.010

Ghosh-Roy, A., Wu, Z., Goncharov, A., Jin, Y., and Chisholm, A. D. (2010). Calcium and cyclic AMP promote axonal regeneration in *Caenorhabditis elegans* and require DLK-1 kinase. *J. Neurosci.* 30, 3175–3183. doi: 10.1523/JNEUROSCI.5464-09.2010

Hammarlund, M., Nix, P., Hauth, L., Jorgensen, E. M., and Bastiani, M. (2009). Axon regeneration requires a conserved MAP kinase pathway. *Science* 323, 802–806. doi: 10.1126/science.1165527

Han, S. M., Baig, H. S., and Hammarlund, M. (2016). Mitochondria localize to injured axons to support regeneration. *Neuron* 92, 1308–1323. doi: 10.1016/j.neuron.2016.11.025

Hartman, P. S., and Herman, R. K. (1982). Radiation-sensitive mutants of *Caenorhabditis elegans*. *Genetics* 102, 159–178.

He, Z., and Jin, Y. (2016). Intrinsic control of axon regeneration. *Neuron* 90, 437–451. doi: 10.1016/j.neuron.2016.04.022

Head, B. P., Zulaika, M., Ryazantsev, S., and van der Bliek, A. M. (2011). A novel mitochondrial outer membrane protein, MOMA-1, that affects cristae morphology in *Caenorhabditis elegans*. *Mol. Biol. Cell* 22, 831–841. doi: 10.1091/mbc.E10-07-0600

Hu, W. H., Hausmann, O. N., Yan, M. S., Walters, W. M., Wong, P. K., and Bethea, J. R. (2002). Identification and characterization of a novel Nogo-interacting mitochondrial protein (NIMP). *J. Neurochem.* 81, 36–45. doi: 10.1046/j.1471-4159.2002.00788.x

Ishii, N., Fujii, M., Hartman, P. S., Tsuda, M., Yasuda, K., Senoo-Matsuda, N., et al. (1998). A mutation in succinate dehydrogenase cytochrome b causes oxidative stress and ageing in nematodes. *Nature* 394, 694–697. doi: 10.1038/29331

Kanazawa, T., Zappaterra, M. D., Hasegawa, A., Wright, A. P., Newman-Smith, E. D., Buttle, K. F., et al. (2008). The *C. elegans* Opa1 homologue EAT-3 is essential for resistance to free radicals. *PLoS Genet.* 4:e1000022. doi: 10.1371/journal.pgen.1000022

Kayser, E. B., Morgan, P. G., Hoppel, C. L., and Sedensky, M. M. (2001). Mitochondrial expression and function of GAS-1 in *Caenorhabditis elegans*. *J. Biol. Chem.* 276, 20551–20558. doi: 10.1074/jbc.M011066200

Kayser, E. B., Morgan, P. G., and Sedensky, M. M. (1999). GAS-1: a mitochondrial protein controls sensitivity to volatile anesthetics in the nematode *Caenorhabditis elegans*. *Anesthesiology* 90, 545–554. doi: 10.1097/00000542-199902000-00031

Kayser, E. B., Morgan, P. G., and Sedensky, M. M. (2004). Mitochondrial complex I function affects halothane sensitivity in *Caenorhabditis elegans*. *Anesthesiology* 101, 365–372. doi: 10.1097/00000542-200408000-00017

Kiryu-Seo, S., Tamada, H., Kato, Y., Yasuda, K., Ishihara, N., Nomura, M., et al. (2016). Mitochondrial fission is an acute and adaptive response in injured motor neurons. *Sci. Rep.* 6:28331. doi: 10.1038/srep28331

Kornmann, B. (2014). Quality control in mitochondria: use it, break it, fix it, trash it. *F1000Prime Rep.* 6:15. doi: 10.12703/P6-15

Lenaers, G., Hamel, C., Delettre, C., Amati-Bonneau, P., Procaccio, V., Bonneau, D., et al. (2012). Dominant optic atrophy. *Orphanet J. Rare Dis.* 7:46. doi: 10.1186/1750-1172-7-46

Liu, Z., and Butow, R. A. (2006). Mitochondrial retrograde signaling. *Annu. Rev. Genet.* 40, 159–185. doi: 10.1146/annurev.genet.40.110405.090613

Mello, C. C., Kramer, J. M., Stinchcomb, D., and Ambros, V. (1991). Efficient gene transfer in *C. elegans*: extrachromosomal maintenance and integration of transforming sequences. *EMBO J.* 10, 3959–3970.

Mercer, K. B., Szlam, S. M., Manning, E., Gernert, K. M., Walthall, W. W., Benian, M., et al. (2009). A *C. elegans* homolog of huntingtin-associated protein 1 is expressed in chemosensory neurons and in a number of other somatic cell types. *J. Mol. Neurosci.* 37, 37–49. doi: 10.1007/s12031-008-9109-z

Mishra, P., and Chan, D. C. (2014). Mitochondrial dynamics and inheritance during cell division, development and disease. *Nat. Rev. Mol. Cell Biol.* 15, 634–646. doi: 10.1038/nrm3877

Miyadera, H., Amino, H., Hiraishi, A., Taka, H., Murayama, K., Miyoshi, H., et al. (2001). Altered quinone biosynthesis in the long-lived clk-1 mutants of *Caenorhabditis elegans*. *J. Biol. Chem.* 276, 7713–7716. doi: 10.1074/jbc.C000889200

Morgan, P. G., Higdon, R., Kolker, N., Bauman, A. T., Ilkayeva, O., Newgard, B., et al. (2015). Comparison of proteomic and metabolomic profiles of mutants of the mitochondrial respiratory chain in *Caenorhabditis elegans*. *Mitochondrion* 20, 95–102. doi: 10.1016/j.mito.2014.12.004

Morsci, N. S., Hall, D. H., Driscoll, M., and Sheng, Z. H. (2016). Age-related phasic patterns of mitochondrial maintenance in adult *Caenorhabditis elegans* neurons. *J. Neurosci.* 36, 1373–1385. doi: 10.1523/JNEUROSCI.2799-15.2016

Mun, J. Y., Lee, T. H., Kim, J. H., Yoo, B. H., Bahk, Y. Y., Koo, H. S., et al. (2010). *Caenorhabditis elegans* mitofilin homologs control the morphology of mitochondrial cristae and influence reproduction and physiology. *J. Cell. Physiol.* 224, 748–756. doi: 10.1002/jcp.22177

Munkacsy, E., and Rea, S. L. (2014). The paradox of mitochondrial dysfunction and extended longevity. *Exp. Gerontol.* 56, 221–233. doi: 10.1016/j.exger.2014.03.016

Nargund, A. M., Pellegrino, M. W., Fiorese, C. J., Baker, B. M., and Haynes, C. M. (2012). Mitochondrial import efficiency of ATFS-1 regulates mitochondrial UPR activation. *Science* 337, 587–590. doi: 10.1126/science.1223560

Ndegwa, S., and Lemire, B. D. (2004). *Caenorhabditis elegans* development requires mitochondrial function in the nervous system. *Biochem. Biophys. Res. Commun.* 319, 1307–1313. doi: 10.1016/j.bbrc.2004.05.108

Palikaras, K., Lionaki, E., and Tavernarakis, N. (2015). Coordination of mitophagy and mitochondrial biogenesis during ageing in *C. elegans*. *Nature* 521, 525–528. doi: 10.1038/nature14300

Pernas, L., and Scorrano, L. (2016). Mito-morphosis: mitochondrial fusion, fission, and cristae remodeling as key mediators of cellular function. *Annu. Rev. Physiol.* 78, 505–531. doi: 10.1146/annurev-physiol-021115-105011

Pickrell, A. M., and Youle, R. J. (2015). The roles of PINK1, parkin, and mitochondrial fidelity in Parkinson's disease. *Neuron* 85, 257–273. doi: 10.1016/j.neuron.2014.12.007

Rauthan, M., Ranji, P., Abukar, R., and Pilon, M. (2015). A mutation in *Caenorhabditis elegans* NDUF-7 activates the mitochondrial stress response and prolongs lifespan via ROS and CED-4. *G3 (Bethesda)* 5, 1639–1648. doi: 10.1534/g3.115.018598

Rawson, R. L., Yam, L., Weimer, R. M., Bend, E. G., Hartwieg, E., Horvitz, H. R., et al. (2014). Axons degenerate in the absence of mitochondria in *C. elegans*. *Curr. Biol.* 24, 760–765. doi: 10.1016/j.cub.2014.02.025

Rolland, S. G., Lu, Y., David, C. N., and Conradt, B. (2009). The BCL-2-like protein CED-9 of *C. elegans* promotes FZO-1/Mfn1,2- and EAT-3/Opa1-dependent mitochondrial fusion. *J. Cell Biol.* 186, 525–540. doi: 10.1083/jcb.200905070

Samann, J., Hegermann, J., von Gromoff, E., Eimer, S., Baumeister, R., and Schmidt, E. (2009). *Caenorhabditits elegans* LRK-1 and PINK-1 act

antagonistically in stress response and neurite outgrowth. *J. Biol. Chem.* 284, 16482–16491. doi: 10.1074/jbc.M808255200

Sancak, Y., Markhard, A. L., Kitami, T., Kovacs-Bogdan, E., Kamer, K. J., Udeshi, N. D., et al. (2013). EMRE is an essential component of the mitochondrial calcium uniporter complex. *Science* 342, 1379–1382. doi: 10.1126/science.1242993

Schwarz, T. L. (2013). Mitochondrial trafficking in neurons. *Cold Spring Harb. Perspect. Biol.* 5:a011304. doi: 10.1101/cshperspect.a011304

Senoo-Matsuda, N., Yasuda, K., Tsuda, M., Ohkubo, T., Yoshimura, S., Nakazawa, H., et al. (2001). A defect in the cytochrome b large subunit in complex II causes both superoxide anion overproduction and abnormal energy metabolism in *Caenorhabditis elegans*. *J. Biol. Chem.* 276, 41553–41558. doi: 10.1074/jbc.M104718200

Shen, Q., Yamano, K., Head, B. P., Kawajiri, S., Cheung, J. T., Wang, C., et al. (2014). Mutations in Fis1 disrupt orderly disposal of defective mitochondria. *Mol. Biol. Cell* 25, 145–159. doi: 10.1091/mbc.E13-09-0525

Shen, Y., Ng, L. F., Low, N. P., Hagen, T., Gruber, J., and Inoue, T. (2016). *C. elegans* miro-1 mutation reduces the amount of mitochondria and extends life span. *PLoS ONE* 11:e0153233. doi: 10.1371/journal.pone.0153233

Song, S., Jang, S., Park, J., Bang, S., Choi, S., Kwon, K. Y., et al. (2013). Characterization of PINK1 (PTEN-induced putative kinase 1) mutations associated with Parkinson disease in mammalian cells and Drosophila. *J. Biol. Chem.* 288, 5660–5672. doi: 10.1074/jbc.M112.430801

Springer, W., Hoppe, T., Schmidt, E., and Baumeister, R. (2005). A *Caenorhabditis elegans* Parkin mutant with altered solubility couples alpha-synuclein aggregation to proteotoxic stress. *Hum. Mol. Genet.* 14, 3407–3423. doi: 10.1093/hmg/ddi371

Tedeschi, A., and Bradke, F. (2016). Spatial and temporal arrangement of neuronal intrinsic and extrinsic mechanisms controlling axon regeneration. *Curr. Opin. Neurobiol.* 42, 118–127. doi: 10.1016/j.conb.2016.12.005

Triepels, R. H., van den Heuvel, L. P., Loeffen, J. L., Buskens, C. A., Smeets, R. J., Rubio Gozalbo, M. E., et al. (1999). Leigh syndrome associated with a mutation in the NDUFS7 (PSST) nuclear encoded subunit of complex I. *Ann. Neurol.* 45, 787–790. doi: 10.1002/1531-8249(199906)45:6<787::AID-ANA13>3.0.CO;2-6

Tsang, W. Y., and Lemire, B. D. (2003). The role of mitochondria in the life of the nematode, *Caenorhabditis elegans*. *Biochim. Biophys. Acta* 1638, 91–105. doi: 10.1016/S0925-4439(03)00079-6

Tuppen, H. A., Hogan, V. E., He, L., Blakely, E. L., Worgan, L., Al-Dosary, M., et al. (2010). The p.M292T NDUFS2 mutation causes complex I-deficient Leigh syndrome in multiple families. *Brain* 133, 2952–2963. doi: 10.1093/brain/awq232

Valenci, I., Yonai, L., Bar-Yaacov, D., Mishmar, D., and Ben-Zvi, A. (2015). Parkin modulates heteroplasmy of truncated mtDNA in *Caenorhabditis elegans*. *Mitochondrion* 20, 64–70. doi: 10.1016/j.mito.2014.11.001

Wu, Z., Ghosh-Roy, A., Yanik, M. F., Zhang, J. Z., Jin, Y., and Chisholm, A. D. (2007). *Caenorhabditis elegans* neuronal regeneration is influenced by life stage, ephrin signaling, and synaptic branching. *Proc. Natl. Acad. Sci. U.S.A.* 104, 15132–15137. doi: 10.1073/pnas.0707001104

Xu, S., and Chisholm, A. D. (2014). *C. elegans* epidermal wounding induces a mitochondrial ROS burst that promotes wound repair. *Dev. Cell* 31, 48–60. doi: 10.1016/j.devcel.2014.08.002

Xu, S., Wang, Z., Kim, K. W., Jin, Y., and Chisholm, A. D. (2016). Targeted mutagenesis of duplicated genes in *Caenorhabditis elegans* using CRISPR-Cas9. *J. Genet. Genomics* 43, 103–106. doi: 10.1016/j.jgg.2015.11.004

Yan, D., and Jin, Y. (2012). Regulation of DLK-1 kinase activity by calcium-mediated dissociation from an inhibitory isoform. *Neuron* 76, 534–548. doi: 10.1016/j.neuron.2012.08.043

Yan, D., Wu, Z., Chisholm, A. D., and Jin, Y. (2009). The DLK-1 kinase promotes mRNA stability and local translation in *C. elegans* synapses and axon regeneration. *Cell* 138, 1005–1018. doi: 10.1016/j.cell.2009.06.023

Yang, W., and Hekimi, S. (2010a). A mitochondrial superoxide signal triggers increased longevity in *Caenorhabditis elegans*. *PLoS Biol.* 8:e1000556. doi: 10.1371/journal.pbio.1000556

Yang, W., and Hekimi, S. (2010b). Two modes of mitochondrial dysfunction lead independently to lifespan extension in *Caenorhabditis elegans*. *Aging Cell* 9, 433–447. doi: 10.1111/j.1474-9726.2010.00571.x

Yang, W. S., and Stockwell, B. R. (2016). Ferroptosis: death by lipid peroxidation. *Trends Cell Biol.* 26, 165–176. doi: 10.1016/j.tcb.2015.10.014

Yanik, M. F., Cinar, H., Cinar, H. N., Chisholm, A. D., Jin, Y., and Ben-Yakar, A. (2004). Neurosurgery: functional regeneration after laser axotomy. *Nature* 432:822. doi: 10.1038/432822a

Yee, C., Yang, W., and Hekimi, S. (2014). The intrinsic apoptosis pathway mediates the pro-longevity response to mitochondrial ROS in *C. elegans*. *Cell* 157, 897–909. doi: 10.1016/j.cell.2014.02.055

Zhou, B., Yu, P., Lin, M. Y., Sun, T., Chen, Y., and Sheng, Z. H. (2016). Facilitation of axon regeneration by enhancing mitochondrial transport and rescuing energy deficits. *J. Cell Biol.* 214, 103–119. doi: 10.1083/jcb.201605101

Conflict of Interest Statement: The authors declare that the research was conducted in the absence of any commercial or financial relationships that could be construed as a potential conflict of interest.

frontiers in Neuroscience

REVIEW
published: 30 March 2017
doi: 10.3389/fnins.2017.00146

Metabolic Vulnerability in the Neurodegenerative Disease Glaucoma

*Denise M. Inman * and Mohammad Harun-Or-Rashid*

Department of Pharmaceutical Sciences, Northeast Ohio Medical University, Rootstown, OH, USA

Axons can be several orders of magnitude longer than neural somas, presenting logistical difficulties in cargo trafficking and structural maintenance. Keeping the axon compartment well supplied with energy also presents a considerable challenge; even seemingly subtle modifications of metabolism can result in functional deficits and degeneration. Axons require a great deal of energy, up to 70% of all energy used by a neuron, just to maintain the resting membrane potential. Axonal energy, in the form of ATP, is generated primarily through oxidative phosphorylation in the mitochondria. In addition, glial cells contribute metabolic intermediates to axons at moments of high activity or according to need. Recent evidence suggests energy disruption is an early contributor to pathology in a wide variety of neurodegenerative disorders characterized by axonopathy. However, the degree to which the energy disruption is intrinsic to the axon vs. associated glia is not clear. This paper will review the role of energy availability and utilization in axon degeneration in glaucoma, a chronic axonopathy of the retinal projection.

Keywords: mitochondria, lactate, axonopathy, Wallerian degeneration, optic neuropathy

OPEN ACCESS

Edited by:
Irving E. Vega,
Michigan State University, USA

Reviewed by:
Lee J. Martin,
Johns Hopkins School of Medicine, USA
Alberto Granzotto,
Centro Scienze dell'Invecchiamento e Medicina Traslazionale, Italy
James C. Vickers,
University of Tasmania, Australia

****Correspondence:***
Denise M. Inman
dinman@neomed.edu

Specialty section:
This article was submitted to Neurodegeneration, a section of the journal Frontiers in Neuroscience

Received: *20 January 2017*
Accepted: *08 March 2017*
Published: *30 March 2017*

Citation:
Inman DM and Harun-Or-Rashid M (2017) Metabolic Vulnerability in the Neurodegenerative Disease Glaucoma. Front. Neurosci. 11:146. doi: 10.3389/fnins.2017.00146

METABOLIC VULNERABILITY IN GLAUCOMA

Glaucoma is the leading cause of irreversible blindness worldwide (Tham et al., 2014). It blinds through the dysfunction and degeneration of retinal ganglion cell (RGC) axons that carry visual information from the eye to the brain (Calkins and Horner, 2012; Casson et al., 2012). There is emerging evidence for a critical role for energy management in the axon degeneration observed in this disease. In our work, we have been using the DBA/2J mouse model of glaucoma, an inbred strain that develops increased intraocular pressure (IOP) secondary to an iris pigment dispersion disease (John et al., 1998; Anderson et al., 2002). IOP is the main modifiable risk factor in primary open angle glaucoma, and lowering IOP is the mainstay of treatment. Increased IOP in the DBA/2J (D2) leads to optic neuropathy and eventual RGC death in a manner that emulates human patients with the most common forms of glaucoma, with pathology developing slowly over time (John et al., 1998), and occurring in contiguous retinal regions (Jakobs et al., 2005). IOP elevations in D2 mice are similar in scale to human patients, and the magnitude of these increases correlates with axon degeneration (Inman et al., 2006).

The potential role of energy availability and utilization in glaucoma became apparent through optic nerve physiology experiments. We measured compound action potential (CAP), the summation of all action potentials after stimulation, in freshly isolated D2 optic nerves. CAP amplitude decreased significantly by 6 months of age (Baltan et al., 2010), prior to measurable axon

structural pathology (Inman et al., 2006) or axon transport deficit (Dengler-Crish et al., 2014) in this model. The reduction in elicited neural activity was inversely correlated with IOP elevation in the D2; the higher the IOP exposure within an age group, the lower the CAP amplitude (Baltan et al., 2010). Notably, there was no difference in CAP latency or duration in the D2 at 6 or 10 months, and no impact of the K^+ channel blocker 4-aminopyridine. Both observations argue against significant changes in myelination as observed in multiple sclerosis-associated optic neuropathy in humans (Chan, 2002). However, when D2 optic nerves were subjected to oxygen-glucose deprivation and then allowed to recover, nerves from 6-month-old mice in the high IOP group demonstrated impaired recovery when compared to their low IOP companions. By 10 months of age, however, D2 optic nerves could not sustain recovery from oxygen-glucose deprivation in any mice, independent of IOP history. These results suggested that both IOP and age influence energy reserves in this pathology. To corroborate energy depletion, ATP measurements from D2 optic nerve showed significantly decreased ATP in the high IOP groups within each age, and significantly depleted ATP levels when comparing 6 to 10-month-olds within IOP group (see **Figure 1** for summary) (Baltan et al., 2010). The low ATP and clear lack of energy reserve in the D2 optic nerve with increased IOP suggested glaucoma-associated metabolic dysfunction. Strikingly, the metabolic dysfunction in the axon occurs quite early in the D2, prior to overt structural changes in the optic nerve. This suggests that resolution of the metabolic dysfunction could prevent axon degeneration and preserve visual function.

The observations of a potential metabolic dysfunction in glaucoma raise a number of interesting possibilities about the mechanism of pathophysiology. Several fundamental concepts have implications for how glaucoma could be managed and what might be fruitful therapeutic approaches to combat the disease: (1) how energy is produced and utilized in axons, (2) how energy is associated with axon degeneration, (3) the nature of axon degeneration in glaucoma, and (4) how axon degeneration might be prevented. As discussed below, the entry points for the final destruction of the axon vary between neurodegenerative disorders but have much in common beyond initiation. The focus here is energy depletion, which arises from a number of circumstances, including ischemia, mitochondrial dysfunction, age-related changes in the NAD+-sirtuin-PGC-1α axis, loss of axon support factors, and activation of axon degeneration factors. Below we review the current understanding of energy production in white matter and possible intervention points in glaucoma and, by extension, other chronic axonopathies.

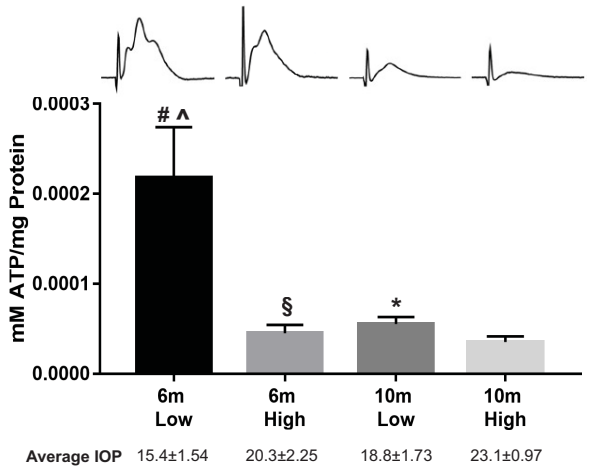

FIGURE 1 | Optic nerve ATP levels in the DBA/2J model of glaucoma at 6 and 10 months of age, separated into low and high intraocular pressure (IOP) groups. Optic nerves were rapidly isolated then flash frozen in liquid nitrogen until assay. Upon thaw, the optic nerve was cut into small pieces while in 10% $HClO_4$, then homogenized by sonication, and centrifuged at 4,500 rpm for 10 min at 4°C. The supernatant was collected, neutralized with 30 μl of 2.5 M KOH, then centrifuged at 14,000 rpm for 10 min at 4°C. The precipitate was removed, and supernatant kept on ice. Total ATP concentration was measured using the ATP bioluminescence assay kit (Roche), based on the ATP dependence of luciferase catalyzed oxidation of luciferin. Samples were diluted and mixed with the luciferase reagent and then absorbance was measured at 560 nm. Blank values were subtracted from the raw data, and ATP concentrations were calculated from a log–log plot of the standard curve data and normalized by the protein concentration. The values are expressed as millimoles of ATP per milligrams of protein. There was a significant difference in ATP levels in low vs. high IOP groups (*t*-test, #$p = 0.012$ for 6 m; *$p = 0.049$ for 10 m), and a significant difference in the ATP levels across 6 m vs. 10 m at low (*t*-test, ∧$p = 0.014$) and high (*t*-test, §$p = 0.028$) IOP. Above: representative compound action potential traces from each group; below: average IOP for each group. Adapted from Baltan et al. (2010).

ENERGY IN AXONS

Energy is produced both within axons and around them using substrates delivered by the circulation and glial cells. Axons obtain most of their energy from ATP through oxidative phosphorylation in mitochondria. Glial cells that contact axons (oligodendrocytes and astrocytes) are capable of providing energy substrates to axons as well. This energy is necessary for axon function.

Within Axons: Oxidative Phosphorylation and Glycolysis

The central nervous system prefers glucose as its substrate; glucose enters the brain (and retina and optic nerve) through glucose transporters. Neurons express GLUT3, a high-affinity glucose transporter (Maher et al., 1991), while astrocytes and endothelial cells express GLUT1 (Garcia-Caceres et al., 2016). Both GLUT3 and GLUT1 can be upregulated through insulin signaling (Simpson et al., 2008). Glucose is converted through glycolysis to pyruvate; the resultant pyruvate is fed into the Krebs cycle in mitochondria for the generation of ATP. Glucose in axons can also be used to produce reducing equivalents like NADPH via the pentose-phosphate pathway in order to maintain redox balance (Stincone et al., 2015). Neurons are highly oxidative and dependent on their mitochondria. ATP produced by mitochondria in the average ON axon can comfortably sustain the observed firing rate of action potentials, the maintenance of

the resting potential, and maintenance processes, according to a computational model that drew on published values for rat CNS (Harris and Attwell, 2012). The model indicated mitochondria could support all optic nerve axons using roughly 50% of the ATP generation capacity. There is only a calculated ATP shortfall for small axons, those below 0.8 μm in diameter (Harris and Attwell, 2012). In humans, normal optic nerve axon mean diameter ranges from 0.72 ± 0.07 μm (Mikelberg et al., 1989), to 0.96 ± 0.07 μm (Quigley et al., 1988), and 1.00 ± 0.06 μm (Jonas et al., 1990). Even within these ranges, a significant portion of the axons in the human optic nerve are likely to experience ATP shortfall if the model accurately predicts energy availability. The same is true for mouse, with a frequency distribution of optic nerve fiber diameter that peaks at 0.7–0.9 μm; 50.4% of axons are 0.9 um in diameter or less (Honjin et al., 1977), suggesting that there could also be a mitochondrial-derived ATP shortfall in a large subset of axons. The energy sufficiency calculations also depend upon the axon having enough access to glucose.

In general, there are adequate concentrations of GLUT3, the primary glucose transporter in neuronal membranes (Maher et al., 1991), to provide the necessary glucose levels to axons (Harris and Attwell, 2012). These estimates assume glucose diffusion to the middle of an internode quickly (see **Figure 2**); rat internodes average 240 μm (Ransom et al., 1991) while internode lengths in mouse ON average 110 μm (O'Meara et al., 2013). This internode length suggests glucose will readily diffuse; however, the predicted ATP shortfall in axons below 0.8 μm in diameter indicates a potential vulnerability of small axons. Small axons have light myelination, shorter internodes, slow conduction rates (Hursh, 1939), and more sparse mitochondria (Perge et al., 2009; Ohno et al., 2011). It has recently been demonstrated that glucose transporters are upregulated in response to activity in mouse myelinated axons (Saab et al., 2016), a potential solution to the possible lack of glucose in small axons. There are two caveats to this interpretation, however: The glucose transporters were upregulated in oligodendrocytes, not axons; and protein upregulation is not a dynamic response to momentary need. Axons likely rely on alternatives to glucose for maintenance of function.

Around Axons: Glial-Derived Energy

Axons may be supplied with metabolic intermediates from astrocytes and oligodendrocytes to address potential shortfalls from glucose transport and diffusion. Several early studies demonstrated metabolic coupling between neuronal and glial compartments (Hamberger and Hyden, 1963; Pevzner, 1971, 1972). Glia-to-neuron energy substrate transfer was also revealed in early work on metabolic coupling between glia and neurons in the honeybee retina, indicating that glial cells released alanine that was taken up and metabolized by photoreceptor neurons (Tsacopoulos and Magistretti, 1996). In the mammalian CNS, glia mainly transfer monocarboxylates—L-lactate, pyruvate, or ketone bodies—rather than alanine, to neurons (Brown et al., 2003). The initial support for energy transfer from glia to axons came from studies of optic nerve explants that could maintain CAPs for approximately 30 min in the absence of glucose (Stys et al., 1991; Wender et al., 2000). Further study of optic nerve showed that CAP maintenance was dependent on transport of lactate (Wender et al., 2000; Tekkök et al., 2005). The critical evidence supporting intracellular metabolic substrate transfer is based on a number of observations, including: (1) the ability of glial cells to release L-lactate from their glycogen stores (Dringen et al., 1993), (2) the ability of neurons to take up L-lactate (Bouzier-Sore et al., 2003), (3) the cellular distribution of lactate dehydrogenase enzyme that converts lactate to pyruvate (Bittar et al., 1996), and (4) the cellular localization of monocarboxylate transporters (MCTs) within the CNS (Koehler-Stec et al., 1998; Pierre et al., 2002).

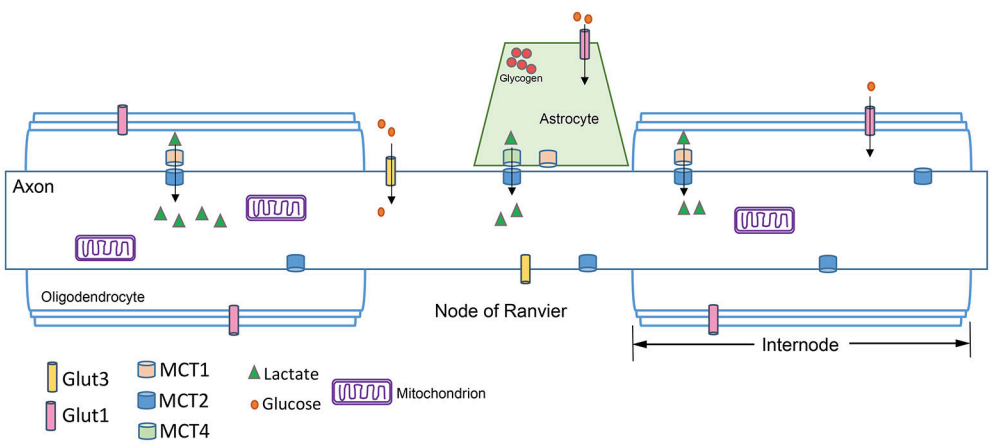

FIGURE 2 | Axon schematic showing the distribution of glucose transporters (GLUT), and monocarboxylate transporters (MCT) in the axon, astrocytes and oligodendrocytes. GLUTs move glucose into the cell, while MCTs transport monocarboxylates such as lactate, pyruvate, and β-hydroxybutyrate. Glia express MCT1 and MCT4, while axons express MCT2. The kinetics of the MCTs are such that MCT1 is best suited for lactate export and MCT2 for lactate uptake because of its higher affinity for lactate (see text). The node of Ranvier is concentrated with ion channels (not shown) necessary for saltatory conduction. Astrocytes can interface with the axon at the node of Ranvier. Oligodendrocytes myelinate the axon; the region between nodes of Ranvier is the internode.

Mounting evidence from different experimental studies indicates that oligodendrocytes and astrocytes significantly contribute to metabolic substrate transfer for axonal metabolic support.

Lactate, a glycolytic end product, can be converted to pyruvate for utilization in the Krebs cycle (**Figure 3**). Evidence from many different experiments indicates that lactate is an efficient oxidative energy substrate for neurons (Pellerin et al., 1998). The conversion of lactate to pyruvate is catalyzed by lactate dehydrogenase (LDH), and requires NAD+ as a cofactor. Cells that produce lactate glycolytically, like astrocytes, are abundant in one LDH isozyme, while cells that use lactate as a substrate, including neurons, are enriched in another (Tsacopoulos and Magistretti, 1996). Lactate is transported between glia and neurons through the monocarboxylate transporters (MCTs). MCTs are bidirectional extracellular membrane channels that transport lactate, pyruvate, and ketone bodies across the membrane depending on their concentration gradient (Pierre and Pellerin, 2005). The MCTs work by first binding a proton then one molecule of lactate; the transporter undergoes a conformational change that releases the proton and the lactate on the other side of the membrane (Dubinsky and Racker, 1978). MCT isoforms differ in their substrate-binding affinities and kinetics, making MCT1 best suited for lactate export and MCT2 for lactate uptake. Perhaps unsurprisingly, MCT1 is expressed preferentially in oligodendrocytes and astrocytes (Lee et al., 2012), while MCT2 is expressed in neurons and axons (Pierre et al., 2002; Simpson et al., 2007), and MCT4 is expressed in astrocytes (Rafiki et al., 2003). MCT2 has a much greater affinity than MCT1 or MCT4 for lactate and pyruvate (Simpson et al., 2007).

Glial Glycolysis Supports Axons

Glial cells and neurons form a metabolic unit in the CNS, with glial cells providing energy substrates that ensure neural function. In *Drosophila*, neurons die when glial cell glycolysis is impaired, indicating that glycolysis is essential to neuron survival (Volkenhoff et al., 2015). The metabolic unit is supported by communication among cells; axon firing can lead to upregulation of glucose transporter-1 in oligodendrocytes in mouse (Saab et al., 2016). Once fortified with additional glucose, oligodendrocytes release lactate, thereby maintaining energy supplies to myelinated axons in the optic nerve. Moreover, evidence from multiple sclerosis patient tissue suggests that oligodendrocytes in low glucose conditions decrease their lactate release (Rone et al., 2016), possibly imperiling myelin maintenance but allowing cell survival. This suggests that glia are responsive to axon activity through greater release of metabolic substrate, but they have limits.

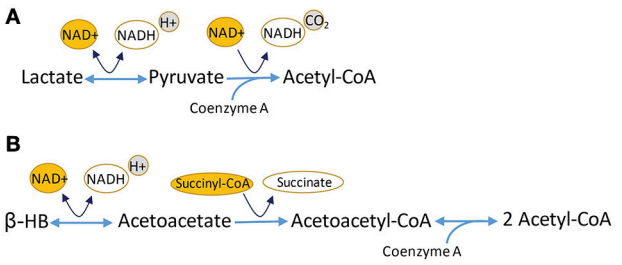

FIGURE 3 | Conversion of ketone bodies, including lactate and β-hydroxybutyrate (β-HB), intermediates that can be utilized in Krebs cycle. (A) Lactate conversion to pyruvate is catalyzed by lactate dehydrogenase and requires NAD+. The reaction is reversible. Pyruvate is oxidized to acetyl-CoA, using NAD+ and giving off NADH and CO_2. **(B)** β-HB can be utilized in Krebs cycle after a multi-step conversion reaction that results in the formation of two molecules of acetyl-CoA for every molecule of β-HB.

Glycogen

Astrocytes have glycogen stores that are capable of being mobilized to provide glucose or lactate to axons (Pellerin et al., 1998; Erlichman et al., 2008). Mobilized glycogen allows for continued optic nerve CAP generation when mouse optic nerves are deprived of glucose (Wender et al., 2000). *In vitro* evidence suggests that lactate derived from glycogen breakdown is preferentially exported (Sickmann et al., 2005). The glycogen stores get broken down into lactate, which gets transferred to and used by axons, as shown by CAP failure when lactate transporters are blocked in periods of aglycemia in mouse optic nerve (Wender et al., 2000; Tekkök et al., 2005). Blocking glycogen breakdown accelerated CAP failure in optic nerve subjected to high-frequency stimulation (Brown et al., 2005). Furthermore, neuronal function can be maintained and neuronal death averted during hypoglycemia by increasing astrocytic glycogen stores in rat brain (Suh et al., 2007). These data demonstrate that lactate from glial glycogen stores can and will be used by axons under stress. In brain parenchyma, astrocytes have unique morphological structures and phenotypical features, which ideally position them to sense neuronal activity (Lundgaard et al., 2014) and respond with the suitable metabolic substrate to their surrounding microenvironment (Rouach et al., 2008). Is something similar at work in white matter, between astrocytes and axons? Gap junctions known to connect astrocytes and oligodendrocytes (Orthmann-Murphy et al., 2007) could facilitate movement of glucose or lactate from astrocyte to oligodendrocyte, thereby providing lactate or other substrates directly through the axon-facing MCT-1 on oligodendrocytes. Alternatively, astrocytes are known to contact nodes of Ranvier (Serwanski et al., 2017) and may deliver metabolic substrates directly.

Energy and Axon Degeneration

Axon degeneration is a complex process that can initiate from different neuronal compartments, e.g., the soma, terminal boutons, or the axon itself. Regardless, the initial stages of neurodegeneration often manifest in the axon compartment. Axon degeneration mechanisms can share three common elements: intra-axonal Ca^{++} dysregulation, axon transport deficits, and mitochondrial dysfunction (Fagiolini et al., 1997; Stys, 2004). Both axon transport deficits and mitochondrial dysfunction are energy-related pathologies. For example, molecular motors require energy for axon transport. Earlier work on this subject posited that mitochondrial dysfunction would preclude axon transport until it was demonstrated that

molecular motors can use extra-mitochondrial sources of energy (Zala et al., 2013). This may dissociate axon transport deficit from mitochondria with regards to ATP demand; however, pathological change in mitochondrial dynamics can alter transport through other mechanisms (Crish and Calkins, 2011; Misko et al., 2012). Metabolic dysfunction could contribute to axon transport deficit, independent of mitochondria, through lack of substrate delivery to the axon. Anterograde axon transport deficit is known to be an important alteration in the pathology of glaucoma (Crish et al., 2010; Dengler-Crish et al., 2014). As will be discussed below, axon transport is required to maintain axon structure and function as well as traffic survival factors for the neuron (see Vrabec and Levin, 2007; Milde et al., 2013).

Mitochondria and Degeneration

Investigation into the mechanisms of axon degeneration underscores the central role of energy availability and mitochondria in keeping the axon compartment alive. For example, injured axons in zebrafish rapidly degenerate without mitochondria (Campbell et al., 2014). In *C. elegans*, mitochondrial targeting to axons can protect them from degeneration (Rawson et al., 2014). Similarly, releasing mitochondria from their syntaphilin tethers in axotomizedcultured cortical mouse axons can rescue energy deficits (Zhou et al., 2016), demonstrating the importance of ATP homeostasis to axon survival after injury. Some have determined mitochondria to be the site of axon protection (Avery et al., 2012), though preventing mitochondrial transport into axons prior to injury slowed, but did not stop, the course of axon degeneration in a *Drosophila* axotomy model (Kitay et al., 2013). Depolarizing mitochondria does not increase the rate of Wallerian degeneration in superior cervical ganglion axons *in vitro*, indicating that degeneration-associated Ca^{++} increases are extra-mitochondrial (Loreto et al., 2015). Axon regeneration, quite separate from degeneration, in mouse RGC axons (Cartoni et al., 2016) and *C. elegans* nerve cord axons (Han et al., 2016), does require mitochondria.

Glial Lactate Critical for Axon Survival

Recent experimental data demonstrates that MCTs are critical for maintaining axon health and integrity. Mice with 50% lower than normal MCT1 expression developed axonopathy in the optic nerve, suggesting that axons are quite sensitive to reduction in the provision of lactate from oligodendrocytes (Lee et al., 2012). Neurons in organotypic cultures could not survive without MCT1, and axons without it degenerated. MCT1 was also shown to be reduced in patients with amyotrophic lateral sclerosis (ALS) and in a mouse model of ALS (Lee et al., 2012). Deletion of MCT1 in oligodendrocytes substantially reduces the availability of local energy metabolites to the axon (Lee et al., 2012), potentially affecting the axonal energy-dependent processes such as axonal transport (Nave, 2010).

The crucial role of MCT1, a mover of energy substrate from the oligodendroglial compartment to axons, in axon function and survival spurred investigation into the regulation of energy exchange between oligodendrocyte and neuron (Saab et al., 2016). Stimulation of oligodendroglial NMDA receptors in response to axonal glutamate release upregulates glucose transporter GLUT1 in the oligodendrocyte. Increased uptake of glucose in the myelin as a result of GLUT1 expression ensures greater glucose delivery to the oligodendrocytes at a time when the axon is engaged in high spiking activity, thereby establishing a path to greater lactate release by the oligodendrocyte to the myelinated axon. Axons recovered from oxygen-glucose deprivation better with lactate than with glucose, indicating the oligodendrocytes were not merely passing along glucose to the axons (Saab et al., 2016).

A multi-pronged approach to supplying axons with energy, as outlined in the section on energy described above, is necessary because of the dire consequences of axonal energy depletion. Axons expend the bulk of their energy budget on the Na^{+}-K^{+} ATPase which moves these ions across the axolemma during and after action potential firing (Ritchie, 1967). Without sufficient energy for Na^{+}-K^{+} ATPase function, axons experience Na^{+} and Ca^{++} overload and then structural decline when Ca^{++}-dependent proteases such as calpain (and potentially others) lay waste to the cytoskeleton, disrupting axon transport, physiology, and other vital axon maintenance processes. Extracellular Ca^{++} influx is both necessary and sufficient for axon degeneration (Court and Coleman, 2012); it is part of a "final common pathway" for various mechanisms of axon degeneration such as developmental axon pruning and Wallerian degeneration (Yang et al., 2013); reviewed in (Stirling and Stys, 2010; Tsutsui and Stys, 2013; Conforti et al., 2014).

Energy and Mechanisms of Axon Degeneration: Wallerian

A role for energy in the mechanism of axon degeneration emerged from research into the mechanism of axon protection in the Wallerian degeneration-slow (Wld^{s}) mouse. Wld^{s} mice carry a naturally occurring mutation that greatly slows axon degeneration, allowing axons that are separated from the cell body to maintain structural and conduction integrity for 2 weeks after transection in mice (Lunn et al., 1989). In a series of follow-up studies, it was demonstrated that the slow degeneration phenotype was intrinsic to the axon (Perry et al., 1990a) and was controlled by a single autosomal dominant gene (Perry et al., 1990b; Lyon et al., 1993). It was ultimately determined that the Wld^{s} gene encodes a chimeric protein, a fusion of the N-terminal 70 amino acids of ubiquitination factor E4B (Ube4b) with nicotinamide mononucleotide adenylyltransferase-1 (NMNAT1) (Conforti et al., 2000; Mack et al., 2001). Subsequent research activity has indicated that the NMNAT1 portion of the fusion protein is primarily responsible for the Wld^{s} phenotype, as shown in in dorsal root ganglion culture (Araki et al., 2004). It is the ATP-dependent activity of NMNAT that converts nicotinamide mononucleotide (NMN) to NAD+ (**Figure 4**). NAD+ is an essential coenzyme in four steps of the Krebs cycle, an essential cofactor in the GAPDH step of glycolysis, and the conversion of lactate into pyruvate requires NAD+, reducing it to NADH. Determining that NMNAT activity contributes to axon survival after axotomy placed energy as a central issue to the mechanism of axon degeneration.

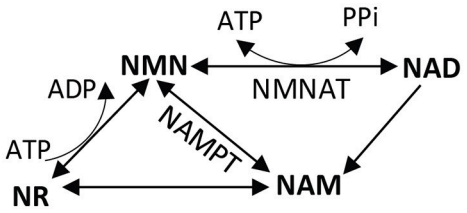

FIGURE 4 | Nicotinamide dinucleotide (NAD+) salvage pathway. NAD+ can be synthesized *de novo* using tryptophan (not shown), or through a salvage pathway using vitamin precursors niacin (vitamin B3), nicotinamide (NAM), or nicotinamide riboside (NR). In the salvage pathway, NMNAT catalyzes the formation of NAD+ from NMN and ATP. The reverse reaction converts NAD+ into NMN, giving off ATP. NMN, nicotinamide mononucleotide; NAD, nicotinamide dinucleotide; NMNAT, nicotinamide mononucleotide adenylyltransferase; NAMPT, nicotinamide phosphoribosyltransferase.

Given the critical role of NMNAT in axon survival after injury, logic would dictate that the product of NMNAT activity, NAD+, is the currency of axon protection. Mammals use a variant of vitamin B3, nicotinamide, as the precursor for NAD+ synthesis (Galli et al., 2013) (**Figure 4**). Roughly 50% of the pyridine nucleotide NAD+ pool is in mitochondria, and 50% is in the cytoplasm in cultured neurons (Alano et al., 2010). NADH and NAD+ cannot themselves be transported into or out of the mitochondria. Cytosolic NAD+ depletion has been shown to block glucose utilization, consistent with its requirement in glycolysis. NAD+ is regenerated in cells by the activity of lactate dehydrogenase, through the electron transport chain in mitochondria, or the movement of malate and/or aspartate transport across the inner mitochondrial membrane. The major consumers of NAD+ in a cell include poly (ADP-ribose) polymerases (PARPs), and sirtuins (class III histone deacetylases) (Blander and Guarente, 2004; Belenky et al., 2007). Strikingly, eliminating two major NAD+ consuming enzymes (PARP1 and CD38) does not prevent axon degeneration in mouse sciatic nerve transection (Sasaki et al., 2009). *In vivo*, NMNAT1 overexpression was not sufficient for axon protection, but NMNAT3 targeted to the mitochondrial matrix protected sciatic nerves after axotomy (Yahata et al., 2009). NMNAT3 likely regenerates NAD+ in the mitochondria for cellular energetics (Lau et al., 2009). Since the mitochondrial NAD+ pool is segregated from the cytoplasmic, NMNAT3-based protection from degeneration implicates mitochondrial dysfunction in the energy depletion that contributes to axon degeneration. The mitochondria isolated from these axons had normal respiratory chain components but were making more ATP (Yahata et al., 2009). The centrality of NAD+ in energy production and utilization suggest a mechanism linking loss of mitochondrial function to axon degeneration (Di Lisa and Ziegler, 2001).

Mitochondria isolated from Wld^s -expressing, protected mouse axons exhibit increased ATP production (Yahata et al., 2009) and enhanced Ca^{++} buffering (Avery et al., 2012). Importantly, Wld^s can ameliorate decreases in ATP after axon injury *in vitro* (Wang et al., 2005). There are multiple NMNATs, each one localized to a cellular compartment. NMNAT1 is nuclear, NMNAT2 is cytoplasmic and associated with Golgi-derived vesicles, and NMNAT3 is found in the mitochondria (Ali et al., 2013). Each of these NAD+-synthesizing enzymes has been investigated individually and found to impact axon survival. Mutations in NMNAT1 cause Leber's congenital amaurosis, a retinal degeneration disease (Falk et al., 2012). Targeting NMNAT1 expression to the cytoplasm then inducing ocular hypertension protects RGCs from death (Zhu et al., 2013). The protective effect of a cytoplasmic version of NMNAT1 depended upon mitochondrial axon transport (Fang et al., 2014a). NMNAT2, however, has turned out to be the essential axon protection factor; when not transported to the axon, a degenerative program ensues (Gilley and Coleman, 2010). Mutations that extend the half-life of NMNAT2 increase its ability to delay axon degeneration, beyond that observed with the Wld^s mutation (Milde et al., 2013). The Wld^s protein can protect a cut axon for up to 4 h *in vitro*, while NMNAT2 depletion within 5 h commits the axon to degeneration (Gilley and Coleman, 2010; Wang et al., 2015). The longer half-life of Wld^s over NMNAT2 may explain its ability to radically extend axon survival.

Identification of NMNAT2 as an axon protection factor has been accompanied by identification of two proteins that appear to be axon death factors (see **Figure 5**). PHR1, an E3 ubiquitin ligase, promotes axon degeneration after injury (Babetto et al., 2013) by influencing the turnover of NMNAT2. PHR1 deletion delays Wallerian degeneration. SARM1, a Toll-like receptor adaptor protein tethered to the mitochondria (Kim et al., 2007; Summers et al., 2014), contributes to axon degeneration such that its deletion significantly delays Wallerian degeneration after nerve transection (Osterloh et al., 2012). The mechanism of that delay includes increased NAD+ synthesis in the axon (Gerdts et al., 2015). SARM1 activation rapidly breaks down NAD+ after injury. SARM1 is required for activation of a post-injury MAPK cascade that disrupts energy homeostasis through ATP depletion in the axon (Yang et al., 2015). Cut neurites from SARM1−/− mice showed higher extracellular acidification rate (glycolysis) and higher maximal respiration than wildtype (Godzik and Coleman, 2015), suggesting a complex picture of the role of oxidative phosphorylation and glycolysis in maintaining ATP levels in injured axons. Isolated neurites show just a partial view of what is likely happening *in vivo*, where oligodendrocytes and astrocytes are capable of contributing to the overall energy scheme.

The prospect of axon survival has become quite complex with the further identification of elements capable of contributing to axon degeneration. Dual leucine zipper kinase (DLK), a MAP3K upstream of JNK, is necessary and sufficient for RGC death after optic nerve crush (Welsbie et al., 2013). Inhibiting the JNK cascade in DLK1−/− sensory neuron cultures delays Wallerian degeneration (Miller et al., 2009), suggesting that DLK1 acts through JNK to promote axon degeneration. There is some disagreement regarding the role of DLK1 in RGCs. Axon degeneration was not delayed after optic nerve crush in DLK1-deficient mice (Fernandes et al., 2014). While this suggests that kinases other than DLK1 may be capable of JNK activation for axon degeneration, a separate study showed that phosphorylation of c-Jun, a target of JNK, was dependent on

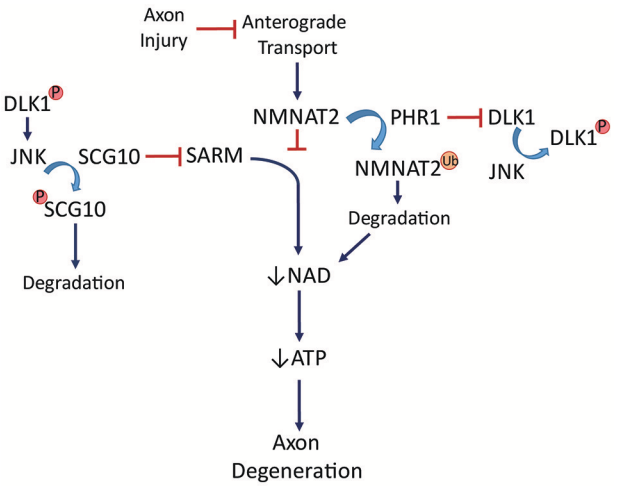

FIGURE 5 | NMNAT2 is transported into the axon to support/protect axon integrity. PHR1, an E3 ubiquitin ligase, can ubiquitinate NMNAT2, promoting its degradation. This leads to decreases in NAD+, low ATP levels, and eventual axon degeneration. SARM activation also leads to axon degeneration through loss of NAD+ and ATP. Ubiquitination-deubiquitination of PHR1 keeps DLK1 in balance until it is phosphorylated by JNK. DLK1 can then activate JNK, which phosphorylates SCG10, leading to its degradation. Axonal degeneration can be blocked by SCG10. Loss of SARM or PHR1 delays degeneration. See text for details.

DLK1 after optic nerve crush (Watkins et al., 2013). DLK1 was significantly upregulated in post-crush optic nerve and governed both the pro-apoptotic and pro-regenerative responses of RGCs (Watkins et al., 2013). JNK works in the commitment phase of the degeneration cascade since inhibiting it 3 h after axotomy of mouse or *Drosophila* axons was not sufficient to prevent axon loss (Miller et al., 2009). A protein phosphorylated early after axotomy in the distal segments of sensory nerve, SCG10, is a microtubule binding protein and JNK substrate whose phosphorylation targets it for degradation. SCG10 can delay degeneration of crushed mouse optic nerve if overexpressed (Shin et al., 2012). Loss of SCG10 alone, however, does not lead to axon degeneration. JNK regulates SCG10 turnover, linking it to DLK1. Interestingly, SCG10 is lost after axotomy even when NMNAT overexpression prevents axon degeneration (Shin et al., 2012).

After axotomy, PHR1 contributes to NMNAT2 degradation while SARM1 is similarly contributing to NAD+ depletion (**Figure 5**). DLK1 activates JNK, which ensures loss of SCG10. These events commit an axon to the degeneration cascade, and it is not yet known how the various elements interact or the precise timing. There are most certainly modifiers of the cascade as well as variations by mode of injury and type of neuron, as will be discussed below. Caveats to the general degeneration scheme include the fact that some of these mechanisms have been worked out *in vitro*, in isolated neurites. While this has established that Wld^s, SARM, and DLK-1 are cell-autonomous in their impact on axon degeneration, the various unexplained aspects of degeneration mechanisms are being assiduously investigated.

Glaucomatous Axonopathy: What Form Does It Take?

The success of axon protection strategies that have emerged from investigation into the Wld^s mutant applied to glaucoma may enable a determination about the mechanisms of axon degeneration in this disorder. In Wallerian degeneration, axons degenerate caudal to a lesion and in an asynchronous way over a population of axons within a nerve (Waller, 1850). The nature of the injury dictates its course since Wld^s axons degenerate anterogradely (from the injury toward the synapse) after transection but retrogradely (from the synapse back toward the injury) after crush injury in peripheral nerve (Beirowski et al., 2005). Wallerian degeneration can be triggered even without physical axonal injury (Ferri et al., 2003; Gilley and Coleman, 2010). In distal axonopathy, for which there is evidence in mouse models of glaucoma (Schlamp et al., 2006; Crish et al., 2010), an axon degenerates from the distal-most point and moves retrogradely. It may be the case that "dying back," or distal axonopathy is not separable from Wallerian degeneration in glaucoma, especially if glaucoma injury resembles a crush injury with retrograde degeneration. Support for shared mechanisms of distal axonopathy and Wallerian degeneration comes from models of Charcot-Marie-Tooth disease, a distal axonopathy that is significantly slowed by the expression of the Wld^s (Meyer zu Horste et al., 2011). Wld^s can also reduce the number of axon varicosities, enlarged portions of axons containing protein aggregates that are hallmarks of most neurodegenerative diseases. Despite this, Wld^s cannot delay all axon degeneration (Vande Velde et al., 2004), and there may be age-related limits to axon degeneration delay (Samsam et al., 2003). Wld^s has been shown to effectively delay the optic neuropathy of glaucoma in the mouse (Howell et al., 2007; Beirowski et al., 2008), though it did not prevent or delay RGC death. A comparison of pre-laminar and laminar axons (see **Figure 6**) in the optic nerve head of D2 mice with glaucoma show a significant decrease in axon number from pre-lamina to lamina, suggesting that axon damage initiates in the pre-lamina and distal axons degenerate (Howell et al., 2007). This would be consistent with an anterograde Wallerian degeneration as observed in transected axons (Beirowski et al., 2005). However, axon endbulbs can be observed throughout the optic nerve in the D2 mouse model of glaucoma (Buckingham et al., 2008; Crish et al., 2010; Dengler-Crish et al., 2014), suggesting a retrograde degeneration course that would be more in alignment with the response to crush injury (Beirowski et al., 2005). Consistent with this, one analysis of D2 optic nerve showed a distal to proximal pattern of degeneration that preceded loss of the corresponding RGCs (Schlamp et al., 2006). Without the ability to monitor the axons along their course, it cannot be ruled out that the end bulbs and axon fragmentation observed beyond the optic nerve head are distal portions of axons with an initiating injury at the optic nerve head.

Neurotrophin deprivation has been considered an important potential mechanism of RGC decline and death. Manipulating receptor tyrosine kinase (Trk) signaling concomitant with growth factor provision has proven to be supportive of RGC survival (Cheng et al., 2002; Lebrun-Julien et al., 2009; Weber and Harman, 2013). Developmental axon pruning is an example

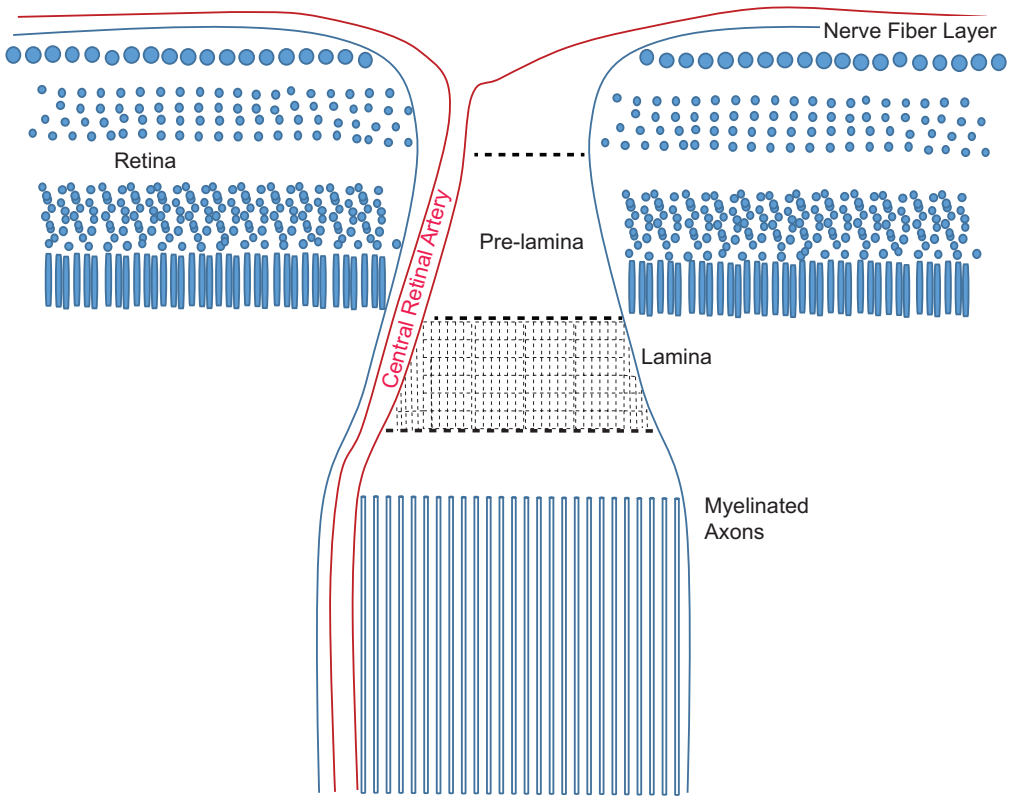

FIGURE 6 | Schematic of the optic nerve head in the mouse. Retinal ganglion cell axons converge at the optic disk and then make a ~90° turn to form the optic nerve. The pre-lamina region is formed from the fasciculated axons as they traverse the retina. Columns of astrocytes maintain the fasciculated bundles of unmyelinated axons through the lamina. Beyond the lamina, retinal ganglion axons are myelinated by oligodendrocytes.

of axon degeneration that can be triggered by loss of growth factor support from target areas. Axon pruning may share downstream mechanisms of degeneration with post-injury Wallerian degeneration, but the commitment phase differs. Wld^s cannot prevent pruning in mice or *Drosophila* (Hoopfer et al., 2006). Since Wld^s mice show normal CNS circuitry instead of a gross overabundance of unpruned connections, this is not unexpected. Evidence indicates there may be two mechanisms by which axons get pruned, one that is caspase-dependent and the other requiring loss of NAD+; the two may work together or run parallel to eliminate unneeded circuitry (Schoenmann et al., 2010). Growth factor deprivation initiates activation of caspases; Wld^s and cytoplasmic NMNAT1, even SARM1 deletion (Gerdts et al., 2013), can protect against nerve growth factor (NGF) withdrawal-induced axon degeneration. DLK-1, after trophic deprivation, is JNK dependent and contributes to both axon degeneration and cell body apoptosis (Ghosh et al., 2011). Interestingly, DLK1 knockout in a optic nerve crush model did not protect RGC axon structure or function as measured by CAP amplitude (Fernandes et al., 2014), suggesting that degeneration in these axons is governed differently than those in development (Hoopfer et al., 2006) and potentially other sensory systems (Miller et al., 2009). Others determined that deficiency in DLK1 protected RGC somas from apoptosis and proximal axons from degeneration after optic nerve crush (Watkins et al., 2013). The pro-apoptotic factor BAX, when deleted in mice of the D2 background, preserved RGC somas but axons degenerated (Libby et al., 2005). These data indicate that degeneration of the optic nerve in the D2 model of glaucoma may be caspase-independent. The preponderance of evidence suggests that glaucomatous degeneration occurs through Wallerian degeneration rather than trophic deprivation-related pathways, though the initial kinase signaling has yet to be determined.

ENERGY AND GLAUCOMA-SPECIFIC AXON DEGENERATION

RGCs Vulnerable to Energy Depletion

RGCs are not uniformly susceptible to cell death in glaucoma (Li et al., 2006; Della Santina et al., 2013), and whether specific axons are particularly vulnerable to degeneration is not known. In the cat optic nerve, 50% of the axons are in the category of small and lightly myelinated, and are therefore potentially susceptible to ATP shortfall. It is believed these axons correspond to γRGCs (Williams and Chalupa, 1983) which are the W cells by functional type. W cells include on- or off-tonic, on- or off-phasic, and on-off phasic cells (Fukuda et al., 1984; Watanabe et al., 1993). Axon caliber correlates relatively well with soma size (Huxlin and Goodchild, 1997; Coombs et al., 2006), suggesting that the

sizable group comprising the slowest conducting axons should include RGCs with small to medium cell somas. A number of studies have determined that OFF transient RGCs show early morphological and functional changes in the microbead injection and laser photocoagulation models of glaucoma (Della Santina et al., 2013; El-Danaf and Huberman, 2015; Ou et al., 2016). These OFF transients are believed to be αRGCs, those with large somas and extensive dendritic arbors; however, there are a number of RGC morphological types with arbor stratification at 50% of inner plexiform layer (IPL) depth typical of OFF transient cells (Della Santina and Ou, 2016) that could have small to medium cell somas and axons possibly in the smaller ranges. The D2 CAP data (**Figure 1**) and OFF transient data are not necessarily in opposition since the traces clearly show that CAPs are lost from all axon calibers (Baltan et al., 2010); large αRGCs can be preferentially lost among other cells that also succumb. Interestingly, after optic nerve transection in mouse, αRGCs preferentially survive, including OFF transients; when treated with osteopontin and IGF-1 or by downregulating PTEN, regeneration only occurs in αRGCs (Duan et al., 2015). Though αRGCs are a diverse group, it would seem unlikely that cells particularly susceptible to raised IOP would be resistant to axon transection.

Mitochondria in Glaucoma

To understand the mechanism of metabolic dysfunction in D2 optic nerve, the mitochondria would be a reasonable starting point for investigation since axons obtain most of their energy from ATP through oxidative phosphorylation. One very relevant study determined that mitochondria isolated from patients resistant to optic neuropathy—exposed to high IOP but absent pathology—showed greater levels of systemic "mitochondrial efficiency," including higher rates of ADP phosphorylation, hyperpolarized mitochondrial membrane potential, and enhanced Ca^{++} buffering capacity compared to control and glaucoma patient groups (Lascaratos et al., 2015). These observations single out the mitochondrial function as a potential biomarker for individuals susceptible to increased IOP. Our electron microscopic analysis of mitochondria in the D2 optic nerve is consistent with lower mitochondrial support in glaucoma patients. We observed a linear relationship between mitochondrial volume and axon volume in DBA/2J-Gpnmb^{+} (control strain that does not develop glaucoma) and pre-pathological D2 optic nerve. That relationship is abolished in the transport dysfunctional D2 optic nerve, for which we observed axon volumes that were not matched by appropriate mitochondrial volumes (Kleesattel et al., 2015). Interestingly, CAP amplitude measures suggest that the third peak of the CAP trace, corresponding to the slowest conducting axons, are lost earliest and in the greatest numbers, and in accordance to magnitude of IOP exposure, in the D2 mouse model of glaucoma (see **Figure 1**; Baltan et al., 2010).

What ties metabolism to susceptible RGCs? In short, very little is directly known about the specifics of OFF transient cell energy homeostasis, though mitochondrial distribution could be a factor. Whereas mitochondria take up greater axon volume in unmyelinated axons, lightly myelinated axons in mouse (Ohno et al., 2011) and guinea pig have slightly fewer mitochondria than predicted (Perge et al., 2009). Mitochondria in the D2 optic nerve are significantly smaller and possess reduced cristae with aging and increased IOP (Coughlin et al., 2015); this supports widespread fission of these organelles, as has been observed by others (Ju et al., 2008). Smaller mitochondria with reduced cristae have less machinery for oxidative phosphorylation, and therefore, lower energetic capacity. This would spell particular trouble if the optic nerve were ever to experience glucose shortage (for example, if glucose transporters were downregulated) because functional mitochondria are required for an axon to survive on lactate. Lactate conversion to pyruvate bypasses glycolysis. The resultant pyruvate is converted to acetyl-CoA for use in Krebs cycle (**Figure 3**). The intermediates produced there are used to establish the electron transport chain and the proton motive force for ATP Synthase (Complex V) and ATP production. Hence, survival on lactate requires functional mitochondria.

Unfortunately for axon survival, poorly functioning mitochondria are not being efficiently recycled in the D2 optic nerve (Coughlin et al., 2015). By not being replaced, these mitochondria can contribute to metabolic vulnerability by producing lower levels of ATP and comparatively more reactive oxygen species (ROS). Mitochondrial biosynthetic proteins such as PGC-1α decrease with age, including in the retina of D2 mice (Guo et al., 2014). Low PGC-1α levels likely limit mitochondrial biogenesis. With no prospect of generating new mitochondria, the lack of recycling of malfunctioning organelles is likely a survival mechanism.

Investigating the impact of upregulating mitophagy in glaucoma could resolve whether maintaining compromised mitochondria can ensure continued, albeit weakened, axon function. Some insight can be gleaned from a study in which autophagy was inhibited in glaucoma using 3-methyladenine (Seglen and Gordon, 1982). The authors observed significant axon degeneration after inhibiting autophagy, and axon protection when promoting autophagy through rapamycin treatment (Kitaoka et al., 2013). Conflicting results have accompanied those examining the role of autophagy in glaucoma, with autophagy induction detrimental to RGC soma survival in an ocular hypertension glaucoma model (Park et al., 2012), but rapamycin-induced autophagy protective of RGC somas after axotomy (Rodriguez-Muela and Boya, 2012).

Glial Cells

As outlined above, astrocytes and oligodendrocytes can exert significant control over the availability and utilization of energy in the optic nerve. Analyses of optic nerve head and axonal glia in glaucoma to date have focused on morphological change (Lampert et al., 1968; Dai et al., 2012; Sun and Jakobs, 2012; Lye-Barthel et al., 2013; Bosco et al., 2016; Cooper et al., 2016), or cell loss. In the D2 optic nerve, astrocyte hypertrophy occurred early in the disease process and was maintained; oligodendrocytes were lost only after axon loss (Son et al., 2010). Alternatively, a model of laser induced ocular hypertension led to significant oligodendrocyte loss within 1 week of IOP elevation (Nakazawa et al., 2006). Oligodendrocyte loss could be ameliorated with an antibody against TNFα, suggesting a

role for microglial-associated inflammation in the loss of myelin. Specific attributes of oligodendrocytes in glaucoma have not been investigated, though NG2+ cells proliferate and generate new oligodendrocytes after axon degeneration in the optic nerve (Son et al., 2010). In considering what is understood about the other macroglial cell in the optic nerve during glaucoma, the relationship between astrocyte hypertrophy and metabolic support of axons is unknown. These knowledge gaps provide many fertile areas of investigation for the metabolic role of optic nerve glia in glaucomatous neurodegeneration.

ADDRESSING ENERGY FAILURE IN GLAUCOMA

Glaucoma is an asynchronous degeneration of the optic nerve. Does axon degeneration occur from loss of protection factors or activation of death factors, or is it both? Where and when does energy dysregulation occur? How does one support axons before they fail? One approach to prevent axon degeneration is to develop ways to target cells that are likely to succumb. As noted above, specific RGCs and compartments seem particularly susceptible. As research refines the susceptible populations, targeting strategies can also become more sophisticated, though certain protection strategies may show positive consequences to targeting all RGCs. Aging remains an important risk factor, as suggested by the significant decreases in ATP with age (**Figure 1**) as well as degree of IOP exposure. Various energy-related approaches have been used to prevent axon degeneration in models of neurodegeneration, including providing creatine, manipulating members of the NAD+-sirtuin-PGC1α axis, and upregulating the NMNATs. Strategies used to protect against axon degeneration in glaucoma in particular consist of providing glucose, upregulating NMNAT1 and NMNAT3, providing ketone bodies, and inhibiting histone deacetylases (HDACs).

Glucose

Protection from glaucoma-induced optic neuropathy can occur by increasing energy substrates such as glucose. In a rat laser photocoagulation model of glaucoma, induction of hyperglycemia 4 days prior to ocular hypertension was shown to decrease axon loss in the optic nerve by more than 50% and increase ganglion cell survival also by roughly 50% (Ebneter et al., 2011). While glial activation was decreased in the optic nerve, retinal glial showed comparable levels of reactivity (microglia and astrocytes/Müller glia). A caveat to this study included the relatively brief study period (2 weeks) (Ebneter et al., 2011). Longer periods of hyperglycemia (6 weeks to 3 months) after ocular hypertension did not show neuroprotection in the retina (Kanamori et al., 2004a), though a distinction between neuronal and glial cell death was not made. A critical issue with increasing blood glucose levels is that hyperglycemia does not necessarily translate into greater glucose availability to the CNS without matching levels of high affinity glucose transporters such as GLUT3, or GLUT1. Whereas GLUT1 appears to be upregulated by NMDA-R activation (Saab et al., 2016), insulin can promote translocation of GLUT1 and GLUT3 to the cell surface (Uemura and Greenlee, 2006). In chronic glaucoma models, the likelihood of NMDA-R activation sufficient to upregulate GLUT1 seems unlikely because RGCs generally fire at low rates (more than 90% fire at 10 Hz or less) (Koch et al., 2004), and axons are being lost. The ectopic glutamate release observed in the optic nerve head in one glaucoma model (Fu and Sretavan, 2012) would not be directed at oligodendrocytes because axons in the nerve head are unmyelinated, but might its target be laminar astrocytes in an attempt to upregulate glucose transporters? Episcleral cauterization to initiate ocular hypertension in rats led to increased insulin and insulin-like growth factor receptor levels, concomitant with phosphorylated Akt, in retina in the acute post-injury period (Kanamori et al., 2004b). In the R28 rat retina neural cell line subjected to serum deprivation, insulin has been shown to be a retinal neuron survival factor by acting through the PI3K-Akt signaling pathway to decrease caspase-3 activation (Barber et al., 2001). It is unknown if glucose transporters were upregulated by these insulin increases. Traumatic brain injury, known to result in an 8-fold increase in extracellular lactate (Nilsson et al., 1990), led to an increase in neural (GLUT3), but not glial (GLUT1) glucose transporters (Hamlin et al., 2001). This would be consistent with increased need for energy in the neural compartment.

Glycogen

Astrocytes are the primary storage location for glycogen (Cataldo and Broadwell, 1986). Glycogen is broken down to glucose, but studies have shown that glycogen mobilization in astrocytes provides lactate, not glucose, to the extracellular milieu (Dringen et al., 1993). During periods of aglycemia, astrocytic glycogen is rapidly depleted, able to sustain function for no more than a few minutes (Brown, 2004). Increasing glycogen stores, though, can maintain axon firing longer during periods of hypoglycemia in rat brain (Suh et al., 2007). Astrocytes form the glia lamina of the optic nerve head in rodents (**Figure 6**), and these cells undergo profound morphological change with ocular hypertension (Sun et al., 2009; Dai et al., 2012; Bosco et al., 2016; Cooper et al., 2016). Of note, the optic nerve head glia impacted by glaucoma no longer contact the basal lamina of the nerve (Dai et al., 2012), the ultrastructural location of glycogen granules (Brown, 2004). This suggests astrocyte glycogen might be a source of metabolic vulnerability in the glaucomatous optic nerve due to possible depletion. Increasing glycogen stores, however, may not make a significant difference to energy homeostasis in a chronic disease like glaucoma because of its rapid depletion. Glycogen has other potential roles though, such as support of glutamatergic neurotransmission (Obel et al., 2012). Glycogen production through glycogen synthase is regulated by three kinases, including glycogen synthase kinase 3 (GSK-3). GSK-3 in particular has probable implications for glaucoma through its targets and its promiscuity; GSK-3 has more predicted substrates than any other kinase (Linding et al., 2007). GSK-3 phosphorylation regulates transcription factors such as NF-κB, STAT3, Fos/Jun AP-1, p53 (Beurel et al., 2015); histone deacetylases; and proteins like the microtubule binding tau (Mandelkow et al., 1992), critical to Alzheimer's disease and neurodegenerative disease pathology (Stamer et al., 2002;

Mandelkow et al., 2003). It is as yet unknown whether a connection exists between astrocyte glycogen production and neurodegenerative disease pathology through GSK-3.

Creatine

Ischemia is also postulated to occur as a result of poor blood flow at the optic nerve head, as observed in glaucoma patients (Schwartz, 1994; Grunwald et al., 1998); it also occurs in models of acute IOP increase (Sun et al., 2010). ATP turnover in cells is fast, but more so in tissues subjected to ischemia. ATP supply is maintained by a pool of phosphocreatine that exists at sites of high energy consumption because phosphocreatine can be converted by creatine kinase into ATP + creatine more quickly than ATP can be generated. Creatine is neuroprotective in many models of hypoxia, including for cerebral ischemia when delivered intercerebroventricularly (Lensman et al., 2006), and after experimental stroke when the creatine is in a formulation that extends half-life (Perasso et al., 2009). Pre-treating cortical axons with creatine prevented ischemia-induced damage as well as alleviating ATP depletion (Shen and Goldberg, 2012). This protection was independent of glial cells. Nevertheless, protection from ischemia corroborated previous studies demonstrating that creatine is not effective when delivered post-ischemia injury (Lensman et al., 2006; Shen and Goldberg, 2012). It may be the case that sufficient levels of creatine could not be delivered in a timely manner to counteract the depolarization and subsequent energy depletion in ischemia.

NMNATs

Similar to studies in sensory neurons, NMNATs have significant impact on RGCs and their axons. Embryonic mice (E18.5) nullizygous for NMNAT2 showed truncated RGC axons; the axons did not reach the optic chiasm, and there was no optic tract. RGC bodies appeared normal, with proximal axons that formed the optic nerve (Gilley et al., 2013). These results suggested a developmental role for NMNAT2 in axon extension. NMNAT3 upregulation in two different mouse models of glaucoma exerted significant protection of axons that could be reversed with treatment by 3-methyladenine, a PI3K inhibitor that reduces autophagy (Kitaoka et al., 2013). Cytoplasmic NMNAT1 upregulation protected RGC somas and axons in models of retinal ischemia and ocular hypertension (Zhu et al., 2013). The studies did not thoroughly examine the mechanism of NMNAT protection, though the apparent connection to autophagy in the Kitaoka study suggests that recycling of all but the most basic cellular components can help maintain energy homeostasis in RGCs subjected to pressure-induced insult.

NAD+-Sirtuin-PGC-1α Axis Manipulation

NAD+ levels decrease with aging (Guarente, 2014), and various studies of NAD+ replenishment (either direct or through precursors) demonstrated better metabolic health and mitochondrial function in diet-related diabetes (Yoshino et al., 2011), and in muscle stem cells in aged mice (Zhang et al., 2016). After axotomy *in vitro*, exogenous application of NAD+ was sufficient to slow the degeneration (Wang et al., 2005). Thus, a successful strategy for slowing or preventing axon degeneration has been to indirectly provide energy (Araki et al., 2004; Chung et al., 2013). Wallerian degeneration, the most likely mechanism by which glaucomatous RGC axons die, can be halted through increased NAD+ biosynthesis (Araki et al., 2004) and the action of a serine protease inhibitor that prevents ATP decrease (Ikegami et al., 2004). Despite NAD+ being an obvious candidate effector for axon protection, overexpression of Wld^s and NMNAT prevents axon degeneration but does not increase basal NAD+ levels (Mack et al., 2001; Araki et al., 2004), and NAD+ levels are not essential to axon preservation (Sasaki et al., 2009). If NAD+ levels are dispensable, then perhaps it is ATP levels that are crucial to axon protection. Reducing axon ATP causes irreversible axon damage (Shen et al., 2013).

NMNAT overexpression has had some success in models of glaucoma (Kitaoka et al., 2013), though if energy support is the goal, a very promising candidate is the NAD+ precursor nicotinamide riboside (**Figure 4**). Nicotinamide riboside (NR), when orally delivered to humans and mice, exhibits superior bioavailability and pharmacokinetics than either nicotinamide or nicotinic acid. NR significantly increases NMN, NAM, and NAD+ levels in humans by the fourth dose of a daily 1,000 mg intake, and maintains those increases up to 24 h after the seventh dose (Trammell et al., 2016).

Sirtuins

The sirtuins, class III histone deacetylases (HDACs), have had variable impact on degeneration in the CNS, their activation effective at delaying neurodegeneration in some situations, but not all (Conforti et al., 2007). Indirect maintenance of NAD+ pools through HDAC *inhibition* has been demonstrated in neurodegenerative diseases (Langley et al., 2005). In a transgenic mouse model of Alzheimer's disease, nicotinamide treatment inhibited SIRT1 activity, reduced phosphorylated tau, and restored cognitive ability (Green et al., 2008). As was discussed above, PARP1 and SIRT1 are enzymes that require NAD+ for activity. PARP1 inhibition or elimination did not improve axon regeneration after optic nerve transection in mice (Wang et al., 2016), though treatment started 3 days after injury and there is only a few hours between injury and commencement of Wallerian degeneration.

Resveratrol, a SIRT1 activator, has been utilized as a tool to probe the complexities of SIRT1 and degeneration. Resveratrol delayed Wallerian degeneration in sensory neuron cultures and after sciatic nerve crush (Calliari et al., 2013). The degeneration delay could be blocked by eliminating an endogenous SIRT1 inhibitor, DBC-1. DBC-1 knockout nerves degenerated just as quickly as wildtype if NAD+ was not present, indicating that NAD+ was necessary for full SIRT1 activity and subsequent axon protection (Calliari et al., 2013). Resveratrol also induced phosphorylation of AMPK, a master regulator of energy homeostasis (Dasgupta and Milbrandt, 2007), which when activated, stimulates glucose uptake in the brain (Hardie et al., 2012).

Resveratrol increased mitochondrial number and improved mitochondrial function primarily through SIRT1 deacetylation of PGC-1α and subsequent increased PGC-1α activity in mice (Lagouge et al., 2006). These effects were observed in skeletal

muscle and adipose tissue. In the CNS, resveratrol was found to increase brain lactate production and limit movement of radiolabeled pyruvate through Krebs cycle, thereby limiting oxidative phosphorylation (Rowlands et al., 2015). Is limiting oxidative phosphorylation a viable approach for preventing axon degeneration? The variable impact (positive and negative) of SIRT1 on Wallerian degeneration indicates the likelihood that the timing and overall energy state of the system dictate the response to SIRT1 activation. Blocking oxidative phosphorylation would limit ROS production, though blocking mitochondrial function, especially if axons are being supported by glial-derived lactate, would seem to be a risky approach.

SIRT1 manipulation has not been wholly favorable in glaucoma-related models. SIRT1 overexpression promoted RGC survival after optic nerve crush in mouse, an effect that was more pronounced than resveratrol treatment (Zuo et al., 2013). SIRT1 knockout did not increase RGC death over wildtype mice after optic nerve crush, suggesting complex interactions of cell death mechanisms. Moreover, functional testing of the RGCs showed no difference among the SIRT1 activation, overexpression, or knockout groups, suggesting that axon degeneration occurred regardless of SIRT1 status (Zuo et al., 2013). The SIRT1 downregulation that resulted from 60 min of retina ischemia in mice could be reversed with once daily mangiferin treatment, a xanthonoid antioxidant (Kim et al., 2015). Resolution of the potential impact of manipulating these key regulators of energy homeostasis in glaucoma will require closer investigation in order to determine if they might be reasonable therapeutic targets.

Mitochondria

Upregulating mitochondrial biogenesis would provide more energy-producing organelles to susceptible RGCs, but may place stressors on protein synthesis machinery, especially with aging. Greater numbers of mitochondria would still need to get trafficked along the axon, which may pose a significant problem depending on the stage of glaucoma. One regulatory complex important for mitochondrial biogenesis, mTOR, was no different in tissues between patients with ocular hypertension (OHT) and those with glaucoma (Lascaratos et al., 2015) even though the OHT patients demonstrated increased mitochondrial efficiency and no optic neuropathy. No change in mTOR suggests that the advantage conferred to OHT patients resistant to optic neuropathy did not include a drive toward making more mitochondria. Rather than make more mitochondria, a better strategy could be to improve mitochondrial function. Compensation for impaired oxidative phosphorylation in OPA1-linked autosomal dominant optic atrophy (ADOA) patients has been associated with preservation of vision (van Bergen et al., 2011). Complex II and III activity was higher in ADOA patients with better vision, and these patients had higher respiration rate. Improving mitochondrial function has been the asserted outcome for many of the abovementioned axon protection strategies such as insulin-associated PI3K/Akt activation, SIRT1 activation, and antioxidant treatment. The variable outcomes with these treatments suggest more specific changes as opposed to generalized improved mitochondrial function are necessary.

Mitochondrial Biogenesis

If unhealthy mitochondria contribute to glaucoma pathogenesis, ridding RGCs of the ROS-producing organelles would have to be coupled with mitochondrial biogenesis. A number of other neurodegenerative disease models have manipulated mitochondrial recycling or production to neuroprotective effect. Increased DNA damage response through hyperactivation of PARP-1 [poly (ADP-ribose) polymerase-1] can inhibit mitophagy by disrupting the NAD+-sirtuin-PGC-1α axis in cells developed from xeroderma pigmentosum group A patients (Fang et al., 2014b). Mitophagy in this context can be rescued by upregulating mitochondrial uncoupling protein 2 (UCP2) or providing the NAD+ precursors nicotinamide riboside (NR) or nicotinamide mononucleotide (NMN). Resumption of mitophagy reduced mitochondrial mass, but also reactive oxygen species in cultured hippocampal neurons subjected to H_2O_2 or oxygen glucose deprivation (Fang et al., 2014a). Upregulation of UCP2, a target of PGC-1α, increases ATP levels, reduces ROS and can protect neurons from mitochondrial Complex I disruption in a *Drosophila* model of Parkinson's disease (Islam et al., 2012). However, UCP2 overexpression in the G93A SOD1 mouse model of ALS led to lower levels of ROS but acceleration of the disease course (Peixoto et al., 2013). The proton conductance function of UCP2 requires the presence of specific activators that include fatty acids and ROS-derived alkenals (Brand and Esteves, 2005), the lack of which might explain why UCP2 overexpression is not always protective. Necdin, a protein that binds SIRT1, can stabilize PGC-1α and inhibit its ubiquitin-dependent degradation, thereby enhancing mitochondrial biogenesis (Hasegawa et al., 2016). The neuroprotection against mitochondrial-related injury afforded by necdin resembles that shown by PGC-1α upregulation (Mudò et al., 2012).

Ketone Bodies

Insight into the potential role of metabolism in the pathogenesis of glaucoma has emerged from several recent studies. In the EAAC1−/− model of normal tension glaucoma, every-other-day-fasting (EODF) led to significant protection of FluoroGold-positive retrogradely labeled RGCs, as well as the b wave of multi-focal ERG (Guo et al., 2016). EODF appeared to exert its effects through elevated β-hydroxybutyrate (β-HB), a ketone and endogenous histone deacetylase (HDAC) inhibitor. Increased β-HB levels led to increased histone acetylation that occurred concomitantly with increased mRNA expression of BDNF, bFGF, and catalase (Guo et al., 2016). β-HB can inhibit the class I HDACs (HDAC1, 2, 3, and 8) and at least one class II HDAC (HDAC4) (Shimazu et al., 2013). Ketogenic or medium chain fatty acid diets that lead to high levels of β-HB have long been effective at controlling seizure in children with epilepsy (Yellen, 2008), and have also demonstrated neuroprotection in models of Parkinson's disease (Yang and Cheng, 2010), Alzheimer's disease (Henderson et al., 2009), and ALS (Zhao et al., 2006). An important question is whether increasing ketone levels and subsequent manipulation of energy pathways is responsible for the observed neuroprotection, or if the results can be ascribed particularly

to the inhibition of histone acetylation. Inhibiting HDACs has been mostly effective at limiting damage in models of glaucoma. For example, inhibiting HDAC3 protected RGCs from death after optic nerve crush (Schmitt et al., 2014), and HDAC inhibition with valproic acid protected RGCs from death and preserved pERG amplitude in a rat model of ocular hypertension (Alsarraf et al., 2014). A broad HDAC inhibitor, trichostatin A, when delivered to D2 mice weekly for 4 months, did not protect the optic nerve from degeneration (Pelzel et al., 2012). What of the possibility that β-HB limits damage because it is a ketone body? Ketone bodies get converted into acetyl-CoA for utilization in the Krebs cycle (**Figure 3**), the biosynthetic hub whose intermediates provide the building blocks for fatty acids, nucleotides and the carbons for gluconeogenesis. In the near term, then, increased levels of monocarboxylates like ketone bodies would require the Krebs cycle and oxidative phosphorylation for energy generation. In mammals, more lactate could feed the production of glucose through gluconeogenesis, though this is an energy-expending process. L-lactate can protect cortical neurons from excitotoxic cell death *in vitro* (Llorente-Folch et al., 2016); this effect depends upon the aspartate-glutamate carrier in CNS mitochondria, ARALAR/AGC. This carrier is one half of the malate-aspartate shuttle that moves malate/aspartate and α-ketoglutarate/glutamate between the cytoplasm and the mitochondria in order to regenerate NAD+ from NADH in both compartments. Neuronal utilization of L-lactate depends on the this pathway (Llorente-Folch et al., 2016), underscoring the importance of NAD+ availability to managing the effects of too much NMDA receptor activation. This is one potential mechanism of ketone body neural protection that is separate from HDAC inhibition.

RESOLVING METABOLIC VULNERABILITY

Aging is a primary risk factor in glaucoma. There is recognition across neurodegenerative diseases that glucoregulatory control decreases with aging, spawning clinical trials designed to ameliorate the effects of aging through the use of compounds like metformin (ClinicalTrials.gov Identifier: NCT02432287) or acarbose (Brewer et al., 2016). These trials do not address glaucoma in particular, but may impact the disease through improved glucoregulatory control. Serum citrate as a potential biomarker for glaucoma was the subject of a recently completed clinical trial that showed significantly decreased citrate in the serum of Caucasian glaucoma patients (Fraenkl et al., 2011). Citrate is a byproduct of the Krebs cycle, so decreased values support the idea that mitochondrial function is impaired in glaucoma patients. Mitochondrial function can be monitored in patient retinas using the green fluorescence emitted by oxidized flavoproteins, a byproduct of oxidative stress (Field et al., 2011). This development may improve diagnosis as well as provide a means to monitor future metabolic therapy.

The complexity of optic nerve degeneration in glaucoma—its chronic timing, its asynchronicity, its non-cell autonomous nature—presents many challenges to medicine. Having reviewed the various ways energy plays a role in axon degeneration, we have also summarized several metabolic-related mechanisms of protection. The evidence indicates energy plays a critical role in the timing and organization of axon degeneration, including in glaucoma.

Note Added in Proof

Significant RGC soma and axon protection from glaucoma-related degeneration in the D2 mouse was achieved through dietary supplementation of nicotinamide (Williams et al., 2017). The finding is quite robust, with significant protection at both low (550 mg/kg/day) and high levels (2,000 mg/kg/day) of nicotinamide delivery. The study used RNA-sequencing to show a reversion of gene expression to that demonstrated by the control strain, DBA/2-Gpnmb^{+}, across clusters of genes that included those involved in oxidative phosphorylation; reactive oxygen species, glucose, and fatty acid metabolism; and DNA repair. These results support the existence of a metabolic vulnerability in glaucoma; the mechanism of protection is yet to be elucidated.

AUTHOR CONTRIBUTIONS

DI conceived of the topic and outlined the review; DI and MH wrote the review.

FUNDING

This work was supported by NIH EY026662 (DI).

ACKNOWLEDGMENTS

The authors thank Dr. Samuel Crish for helpful comments and discussion.

REFERENCES

Alano, C. C., Garnier, P., Ying, W., Higashi, Y., Kauppinen, T. M., and Swanson, R. A. (2010). NAD+ depletion is necessary and sufficient for poly (ADP-ribose) polymerase-1-mediated neuronal death. *J. Neurosci.* 30, 2967–2978. doi: 10.1523/JNEUROSCI.5552-09.2010

Ali, Y. O., Li-Kroeger, D., Bellen, H. J., Zhai, R. G., and Lu, H.C. (2013). NMNATs, evolutionarily conserved neuronal maintenance factors. *Trends Neurosci.* 36, 632–640. doi: 10.1016/j.tins.2013.07.002

Alsarraf, O., Fan, J., Dahrouj, M., Chou, C. J., Yates, P. W., and Crosson, C. E. (2014). Acetylation preserves retinal ganglion cell structure and function in a chronic model of ocular hypertension. *Invest. Ophthalmol. Vis. Sci.* 55, 7486–7493. doi: 10.1167/iovs.14-14792

Anderson, M. G., Smith, R. S., Hawes, N. L., Zabaleta, A., Chang, B., Wiggs, J. L., et al. (2002). Mutations in genes encoding melanosomal proteins cause pigmentary glaucoma in DBA/2J mice. *Nat. Genet.* 30, 81–85. doi: 10.1038/ng794

Araki, T., Sasaki, Y., and Milbrandt, J. (2004). Increased nuclear NAD biosynthesis and SIRT1 activation prevent axonal degeneration. *Science* 305, 1010–1013. doi: 10.1126/science.1098014

Avery, M. A., Rooney, T. M., Pandya, J. D., Wishart, T. M., Gillingwater, T. H., Geddes, J. W., et al. (2012). WldS prevents axon degeneration through increased mitochondrial flux and enhanced mitochondrial Ca2+ buffering. *Curr. Biol.* 22, 596–600. doi: 10.1016/j.cub.2012.02.043

Babetto, E., Beirowski, B., Russler, E. V., Milbrandt, J., and DiAntonio, A. (2013). The Phr1 ubiquitin ligase promotes injury-induced axon self-destruction. *Cell Rep.* 3, 1422–1429. doi: 10.1016/j.celrep.2013.04.013

Baltan, S., Inman, D. M., Danilov, C. A., Morrison, R. S., Calkins, D. J., and Horner, P. J. (2010). Metabolic vulnerability disposes retinal ganglion cell axons to dysfunction in a model of glaucomatous degeneration. *J. Neurosci.* 30, 5644–5652. doi: 10.1523/JNEUROSCI.5956-09.2010

Barber, A. J., Nakamura, M., Wolpert, E. B., Reiter, C. E., Seigel, G. M., Antonetti, D. A., et al. (2001). Insulin rescues retinal neurons from apoptosis by a phosphatidylinositol 3-kinase/Akt-mediated mechanism that reduces the activation of caspase-3. *J. Biol. Chem.* 276, 32814–32821. doi: 10.1074/jbc.M104738200

Beirowski, B., Adalbert, R., Wagner, D., Grumme, D. S., Addicks, K., Ribchester, R. R., et al. (2005). The progressive nature of Wallerian degeneration in wild-type and slow Wallerian degeneration (WldS) nerves. *BMC Neurosci.* 6:6. doi: 10.1186/1471-2202-6-6

Beirowski, B., Babetto, E., Coleman, M. P., and Martin, K. R. (2008). The WldS gene delays axonal but not somatic degeneration in a rat glaucoma model. *Eur. J. Neurosci.* 28, 1166–1179. doi: 10.1111/j.1460-9568.2008.06426.x

Belenky, P., Bogan, K. L., and Brenner, C. (2007). NAD+ metabolism in health and disease. *Trends Biochem. Sci.* 32, 12–19. doi: 10.1016/j.tibs.2006.11.006

Beurel, E., Grieco, S. F., and Jope, R. S. (2015). Glycogen synthase kinase-3 (GSK3): regulation, actions, and diseases. *Pharmacol. Ther.* 148, 114–131. doi: 10.1016/j.pharmthera.2014.11.016

Bittar, P. G., Charnay, Y., Pellerin, L., Bouras, C., and Magistretti, P. J. (1996). Selective distribution of lactate dehydrogenase isoenzymes in neurons and astrocytes of human brain. *J. Cereb. Blood Flow Metab.* 16, 1079–1089. doi: 10.1097/00004647-199611000-00001

Blander, G., and Guarente, L. (2004). The Sir2 family of protein deacetylases. *Annu. Rev. Biochem.* 73, 417–435. doi: 10.1146/annurev.biochem.73.011303.073651

Bosco, A., Breen, K. T., Anderson, S. R., Steele, M. R., Calkins, D. J., and Vetter, M. L. (2016). Glial coverage in the optic nerve expands in proportion to optic axon loss in chronic mouse glaucoma. *Exp. Eye Res.* 150, 34–43. doi: 10.1016/j.exer.2016.01.014

Bouzier-Sore, A. K., Voisin, P., Canioni, P., Magistretti, P. J., and Pellerin, L. (2003). Lactate is a preferential oxidative energy substrate over glucose for neurons in culture. *J. Cereb. Blood Flow Metab.* 23, 1298–1306. doi: 10.1097/01.WCB.0000091761.61714.25

Brand, M. D., and Esteves, T. C. (2005). Physiological functions of the mitochondrial uncoupling proteins UCP2 and UCP3. *Cell Metab.* 2, 85–93. doi: 10.1016/j.cmet.2005.06.002

Brewer, R. A., Gibbs, V. K., and Smith, D. L. (2016). Targeting glucose metabolism for healthy aging. *Nutr. Heal. Aging* 4, 31–46. doi: 10.3233/NHA-160007

Brown, A. M. (2004). Brain glycogen re-awakened. *J. Neurochem.* 89, 537–552. doi: 10.1111/j.1471-4159.2004.02421.x

Brown, A. M., Sickmann, H. M., Fosgerau, K., Lund, T. M., Schousboe, A., Waagepetersen, H. S., et al. (2005). Astrocyte glycogen metabolism is required for neural activity during aglycemia or intense stimulation in mouse white matter. *J. Neurosci. Res.* 79, 74–80. doi: 10.1002/jnr.20335

Brown, A. M., Tekkök, S. B., and Ransom, B. R. (2003). Glycogen regulation and functional role in mouse white matter. *J. Physiol.* 549, 501–512. doi: 10.1113/jphysiol.2003.042416

Buckingham, B. P., Inman, D. M., Lambert, W. S., Oglesby, E., Calkins, D. J., Steele, M. R., et al. (2008). Progressive ganglion cell degeneration precedes neuronal loss in a mouse model of glaucoma. *J. Neurosci.* 28, 2735–2744. doi: 10.1523/JNEUROSCI.4443-07.2008

Calkins, D. J., and Horner, P. J. (2012). The cell and molecular biology of glaucoma: axonopathy and the brain. *Invest. Ophthalmol. Vis. Sci.* 53, 2482–2484. doi: 10.1167/iovs.12-9483i

Calliari, A., Bobba, N., Escande, C., and Chini, E. N. (2013). Resveratrol delays Wallerian degeneration in a NAD(+) and DBC1 dependent manner. *Exp. Neurol.* 251C, 91–100. doi: 10.1016/j.expneurol.2013.11.013

Campbell, P. D., Shen, K., Sapio, M. R., Glenn, T. D., Talbot, W. S., and Marlow, F. L. (2014). Unique function of kinesin Kif5A in localization of mitochondria in axons. *J. Neurosci.* 34, 14717–14732. doi: 10.1523/JNEUROSCI.2770-14.2014

Cartoni, R., Norsworthy, M. W., Bei, F., Wang, C., Li, S., Zhang, Y., et al. (2016). The mammalian-specific protein Armcx1 regulates mitochondrial transport during axon regeneration. *Neuron* 92, 1294–1307. doi: 10.1016/j.neuron.2016.10.060

Casson, R. J., Chidlow, G., Wood, J. P., Crowston, J. G., and Goldberg, I. (2012). Definition of glaucoma: clinical and experimental concepts. *Clin. Exp. Ophthalmol.* 40, 341–349. doi: 10.1111/j.1442-9071.2012.02773.x

Cataldo, A. M., and Broadwell, R. D. (1986). Cytochemical identification of cerebral glycogen and glucose-6-phosphatase activity under normal and experimental conditions. II. Choroid plexus and ependymal epithelia, endothelia and pericytes. *J. Neurocytol.* 15, 511–524. doi: 10.1007/BF01611733

Chan, J. W. (2002). Optic neuritis in multiple sclerosis. *Ocul. Immunol. Inflamm.* 10, 161–186. doi: 10.1076/ocii.10.3.161.15603

Cheng, L., Sapieha, P., Kittlerova, P., Hauswirth, W. W., and Di Polo, A. (2002). TrkB gene transfer protects retinal ganglion cells from axotomy-induced death *in vivo*. *J. Neurosci.* 22, 3977–3986.

Chung, S. H., Shen, W., and Gillies, M. C. (2013). Laser capture microdissection-directed profiling of glycolytic and mTOR pathways in areas of selectively ablated Müller cells in the murine retina. *Invest. Ophthalmol. Vis. Sci.* 54, 6578–6585. doi: 10.1167/iovs.13-12311

Conforti, L., Fang, G., Beirowski, B., Wang, M. S., Sorci, L., Asress, S., et al. (2007). NAD(+) and axon degeneration revisited: Nmnat1 cannot substitute for Wld(S) to delay Wallerian degeneration. *Cell Death Differ.* 14, 116–127. doi: 10.1038/sj.cdd.4401944

Conforti, L., Gilley, J., and Coleman, M. P. (2014). Wallerian degeneration: an emerging axon death pathway linking injury and disease. *Nat. Rev. Neurosci.* 15, 394–409. doi: 10.1038/nrn3680

Conforti, L., Tarlton, A., Mack, T. G., Mi, W., Buckmaster, E. A., Wagner, D., et al. (2000). A Ufd2/D4Cole1e chimeric protein and overexpression of Rbp7 in the slow Wallerian degeneration (WldS) mouse. *Proc. Natl. Acad. Sci. U.S.A.* 97, 11377–11382. doi: 10.1073/pnas.97.21.11377

Coombs, J., van der List, D., Wang, G. Y., and Chalupa, L. M. (2006). Morphological properties of mouse retinal ganglion cells. *Neuroscience* 140, 123–136. doi: 10.1016/j.neuroscience.2006.02.079

Cooper, M. L., Crish, S. D., Inman, D. M., Horner, P. J., and Calkins, D. J. (2016). Early astrocyte redistribution in the optic nerve precedes axonopathy in the DBA/2J mouse model of glaucoma. *Exp. Eye Res.* 150, 22–33. doi: 10.1016/j.exer.2015.11.016

Coughlin, L., Morrison, R. S., Horner, P. J., and Inman, D. M. (2015). Mitochondrial morphology differences and mitophagy deficit in murine glaucomatous optic nerve. *Invest. Ophthalmol. Vis. Sci.* 56, 1437–1446. doi: 10.1167/iovs.14-16126

Court, F. A., and Coleman, M. P. (2012). Mitochondria as a central sensor for axonal degenerative stimuli. *Trends Neurosci.* 35, 364–372. doi: 10.1016/j.tins.2012.04.001

Crish, S. D., and Calkins, D. J. (2011). Neurodegeneration in glaucoma: progression and calcium- dependent intracellular mechanisms. *Neuroscience* 176, 1–11. doi: 10.1016/j.neuroscience.2010.12.036

Crish, S. D., Sappington, R. M., Inman, D. M., Horner, P. J., and Calkins, D. J. (2010). Distal axonopathy with structural persistence in glaucomatous neurodegeneration. *Proc. Natl. Acad. Sci. U.S.A.* 107, 5196–5201. doi: 10.1073/pnas.0913141107

Dai, C., Khaw, P. T., Yin, Z. Q., Li, D., Raisman, G., and Li, Y. (2012). Structural basis of glaucoma: the fortified astrocytes of the optic nerve head are the target of raised intraocular pressure. *Glia* 60, 13–28. doi: 10.1002/glia.21242

Dasgupta, B., and Milbrandt, J. (2007). Resveratrol stimulates AMP kinase activity in neurons. *Proc. Natl. Acad. Sci. U.S.A.* 104, 7217–7222. doi: 10.1073/pnas.0610068104

Della Santina, L., Inman, D. M., Lupien, C. B., Horner, P. J., and Wong, R. O. (2013). Differential progression of structural and functional alterations in distinct retinal ganglion cell types in a mouse model of glaucoma. *J. Neurosci.* 33, 17444–17457. doi: 10.1523/JNEUROSCI.5461-12.2013

Della Santina, L., and Ou, Y. (2016). Who's lost first? Susceptibility of retinal ganglion cell types in experimental glaucoma. *Exp. Eye Res.* doi: 10.1016/j.exer.2016.06.006. [Epub ahead of print].

Dengler-Crish, C. M., Smith, M. A., Inman, D. M., Wilson, G. N., Young, J. W., and Crish, S. D. (2014). Anterograde transport blockade precedes deficits in retrograde transport in the visual projection of the DBA / 2J mouse model of glaucoma. *Front. Neurosci.* 8:290. doi: 10.3389/fnins.2014.00290

Di Lisa, F., and Ziegler, M. (2001). Pathophysiological relevance of mitochondria in NAD(+) metabolism. *FEBS Lett.* 492, 4–8. doi: 10.1016/S0014-5793(01)02198-6

Dringen, R., Gebhardt, R., and Hamprecht, B. (1993). Glycogen in astrocytes: possible function as lactate supply for neighboring cells. *Brain Res.* 623, 208–214. doi: 10.1016/0006-8993(93)91429-V

Duan, X., Qiao, M., Bei, F., Kim, I. J., He, Z., and Sanes, J. R. (2015). Subtype-specific regeneration of retinal ganglion cells following axotomy: Effects of osteopontin and mtor signaling. *Neuron* 85, 1244–1256. doi: 10.1016/j.neuron.2015.02.017

Dubinsky, W. P., and Racker, E. (1978). The mechanism of lactate transport in human erythrocytes. *J. Membr. Biol.* 44, 25–36. doi: 10.1007/bf01940571

Ebneter, A., Chidlow, G., Wood, J. P., and Casson, R. J. (2011). Protection of retinal ganglion cells and the optic nerve during short-term hyperglycemia in experimental glaucoma. *Arch. Ophthalmol.* 129, 1337–1344. doi: 10.1001/archophthalmol.2011.269

El-Danaf, R. N., and Huberman, A. D. (2015). Characteristic patterns of dendritic remodeling in early-stage glaucoma: evidence from genetically identified retinal ganglion cell types. *J. Neurosci.* 35, 2329–2343. doi: 10.1523/JNEUROSCI.1419-14.2015

Erlichman, J. S., Hewitt, A., Damon, T. L., Hart, M., Kurascz, J., Li, A., et al. (2008). Inhibition of monocarboxylate transporter 2 in the retrotrapezoid nucleus in rats: a test of the astrocyte-neuron lactate-shuttle hypothesis. *J. Neurosci.* 28, 4888–4896. doi: 10.1523/JNEUROSCI.5430-07.2008

Fagiolini, M., Caleo, M., Strettoi, E., and Maffei, L. (1997). Axonal transport blockade in the neonatal rat optic nerve induces limited retinal ganglion cell death. *J. Neurosci.* 17, 7045–7052.

Falk, M., Zhang, Q., and Nakamaru-Ogiso, E. (2012). NMNAT1 mutations cause Leber congenital amaurosis. *Nat. Genet.* 44, 1040–1045. doi: 10.1038/ng.2361

Fang, C., Decker, H., and Banker, G. (2014a). Axonal transport plays a crucial role in mediating the axon-protective effects of NmNAT. *Neurobiol. Dis.* 68, 78–90. doi: 10.1016/j.nbd.2014.04.013

Fang, E. F., Scheibye-Knudsen, M., Brace, L. E., Kassahun, H., SenGupta, T., Nilsen, H., et al. (2014b). Defective mitophagy in XPA via PARP-1 hyperactivation and NAD(+)/SIRT1 reduction. *Cell* 157, 882–896. doi: 10.1016/j.cell.2014.03.026

Fernandes, K. A., Harder, J. M., John, S. W., Shrager, P., and Libby, R. T. (2014). DLK-dependent signaling is important for somal but not axonal degeneration of retinal ganglion cells following axonal injury. *Neurobiol. Dis.* 69, 108–116. doi: 10.1016/j.nbd.2014.05.015

Ferri, A., Sanes, J. R., Coleman, M. P., Cunningham, J. M., and Kato, A. C. (2003). Inhibiting axon degeneration and synapse loss attenuates apoptosis and disease progression in a mouse model of motoneuron disease. *Curr. Biol.* 13, 669–673. doi: 10.1016/S0960-9822(03)00206-9

Field, M. G., Yang, D., Bian, Z. M., Petty, H. R., and Elner, V. M. (2011). Retinal flavoprotein fluorescence correlates with mitochondrial stress, apoptosis, and chemokine expression. *Exp. Eye Res.* 93, 548–555. doi: 10.1016/j.exer.2011.06.023

Fraenkl, S. A., Muser, J., Groell, R., Reinhard, G., Orgul, S., Flammer, J., et al. (2011). Plasma citrate levels as a potential biomarker for glaucoma. *J. Ocul. Pharmacol. Ther.* 27, 577–580. doi: 10.1089/jop.2011.0062

Fu, C. T., and Sretavan, D. W. (2012). Ectopic vesicular glutamate release at the optic nerve head and axon loss in mouse experimental glaucoma. *J. Neurosci.* 32, 15859–15876. doi: 10.1523/JNEUROSCI.0038-12.2012

Fukuda, Y., Hsiao, C. F., Watanabe, M., and Ito, H. (1984). Morphological correlates of physiologically identified Y-, X-, and W-cells in cat retina. *J. Neurophysiol.* 52, 999–1013.

Galli, U., Travelli, C., Massarotti, A., Fakhfouri, G., Rahimian, R., Tron, G. C., et al. (2013). Medicinal chemistry of nicotinamide phosphoribosyltransferase (NAMPT) inhibitors. *J. Med. Chem.* 56, 6279–6296. doi: 10.1021/jm4001049

Garcia-Caceres, C., Quarta, C., Varela, L., Gao, Y., Gruber, T., Legutko, B., et al. (2016). Astrocytic insulin signaling couples brain glucose uptake with nutrient availability. *Cell* 166, 867–880. doi: 10.1016/j.cell.2016.07.028

Gerdts, J., Brace, E. J., Sasaki, Y., Diantonio, A., and Milbrandt, J. (2015). SARM1 activation triggers axon degeneration locally via NAD+ destruction. *Science* 348, 453–457. doi: 10.1126/science.1258366

Gerdts, J., Summers, D. W., Sasaki, Y., DiAntonio, A., and Milbrandt, J. (2013). Sarm1-mediated axon degeneration requires both SAM and TIR interactions. *J. Neurosci.* 33, 13569–13580. doi: 10.1523/JNEUROSCI.1197-13.2013

Ghosh, A. S., Wang, B., Pozniak, C. D., Chen, M., Watts, R. J., and Lewcock, J. W. (2011). DLK induces developmental neuronal degeneration via selective regulation of proapoptotic JNK activity. *J. Cell Biol.* 194, 751–764. doi: 10.1083/jcb.201103153

Gilley, J., Adalbert, R., Yu, G., and Coleman, M. P. (2013). Rescue of peripheral and CNS axon defects in mice lacking NMNAT2. *J. Neurosci.* 33, 13410–13424. doi: 10.1523/JNEUROSCI.1534-13.2013

Gilley, J., and Coleman, M. P. (2010). Endogenous Nmnat2 is an essential survival factor for maintenance of healthy axons. *PLoS Biol.* 8:e1000300. doi: 10.1371/journal.pbio.1000300

Godzik, K., and Coleman, M. P. (2015). The axon-protective WLDS protein partially rescues mitochondrial respiration and glycolysis after axonal injury. *J. Mol. Neurosci.* 55, 865–871. doi: 10.1007/s12031-014-0440-2

Green, K. N., Steffan, J. S., Martinez-Coria, H., Sun, X., Schreiber, S. S., Thompson, L. M., et al. (2008). Nicotinamide restores cognition in Alzheimer's disease transgenic mice via a mechanism involving sirtuin inhibition and selective reduction of Thr231-phosphotau. *J. Neurosci.* 28, 11500–11510. doi: 10.1523/JNEUROSCI.3203-08.2008

Grunwald, J. E., Piltz, J., Hariprasad, S. M., and DuPont, J. (1998). Optic nerve and choroidal circulation in glaucoma. *Investig. Ophthalmol. Vis. Sci.* 39, 2329–2336.

Guarente, L. (2014). Aging research - where do we stand and where are we going? *Cell* 159, 15–19. doi: 10.1016/j.cell.2014.08.041

Guo, X., Dason, E. S., Zanon-Moreno, V., Jiang, Q., Nahirny, A., Chan, D., et al. (2014). PGC-1α signaling coordinates susceptibility to metabolic and oxidative injury in the inner retina. *Am. J. Pathol.* 184, 1017–1029. doi: 10.1016/j.ajpath.2013.12.012

Guo, X., Kimura, A., Azuchi, Y., Akiyama, G., Noro, T., Harada, C., et al. (2016). Caloric restriction promotes cell survival in a mouse model of normal tension glaucoma. *Sci. Rep.* 6:33950. doi: 10.1038/srep33950

Hamberger, A., and Hyden, H. (1963). Inverse enzymatic changes in neurons and glia during increased function and hypoxia. *J. Cell Biol.* 16, 521–525. doi: 10.1083/jcb.16.3.521

Hamlin, G. P., Cernak, I., Wixey, J. A., and Vink, R. (2001). Increased expression of neuronal glucose transporter 3 but not glial glucose transporter 1 following severe diffuse traumatic brain injury in rats. *J. Neurotrauma* 18, 1011–1018. doi: 10.1089/08977150152693700

Han, S. M., Baig, H. S., and Hammarlund, M. (2016). Mitochondria localize to injured axons to support regeneration. *Neuron* 92, 1308–1323. doi: 10.1016/j.neuron.2016.11.025

Hardie, D. G., Ross, F. A., and Hawley, S. A. (2012). AMPK: a nutrient and energy sensor that maintains energy homeostasis. *Nat. Rev. Mol. Cell Biol.* 13, 251–262. doi: 10.1038/nrm3311

Harris, J. J., and Attwell, D. (2012). The energetics of CNS white matter. *J. Neurosci.* 32, 356–371. doi: 10.1523/JNEUROSCI.3430-11.2012

Hasegawa, K., Yasuda, T., Shiraishi, C., Fujiwara, K., Przedborski, S., Mochizuki, H., et al. (2016). Promotion of mitochondrial biogenesis by necdin protects neurons against mitochondrial insults. *Nat. Commun.* 7:10943. doi: 10.1038/ncomms10943

Henderson, S. T., Vogel, J. L., Barr, L. J., Garvin, F., Jones, J. J., and Costantini, L. C. (2009). Study of the ketogenic agent AC-1202 in mild to moderate Alzheimer's disease: a randomized, double-blind, placebo-controlled, multicenter trial. *Nutr. Metab. (Lond).* 6, 1–25. doi: 10.1186/1743-7075-6-31

Honjin, R., Sakato, S., and Yamashita, T. (1977). Electron microscopy of the mouse optic nerve: a quantitative study of the total optic nerve fibers. *Arch. Histol. Jpn.* 40, 321–332. doi: 10.1679/aohc1950.40.321

Hoopfer, E. D., McLaughlin, T., Watts, R. J., Schuldiner, O., O'Leary, D. D., and Luo, L. (2006). Wlds protection distinguishes axon degeneration following injury from naturally occurring developmental pruning. *Neuron* 50, 883–895. doi: 10.1016/j.neuron.2006.05.013

Howell, G. R., Libby, R. T., Jakobs, T. C., Smith, R. S., Phalan, F. C., Barter, J. W., et al. (2007). Axons of retinal ganglion cells are insulted in the optic nerve early in DBA/2J glaucoma. *J Cell Biol* 179, 1523–1537. doi: 10.1083/jcb.200706181

Hursh, J. (1939). Conduction velocity and diameter of nerve fibers. *Am. J. Physiol.* 127, 131–139.

Huxlin, K. R., and Goodchild, A. K. (1997). Retinal ganglion cells in the albino rat: revised morphological classification. *J. Comp. Neurol.* 385, 309–323.

Ikegami, K., Kato, S., and Koike, T. (2004). N-alpha-p-tosyl-L-lysine chloromethyl ketone (TLCK) suppresses neuritic degeneration caused by different experimental paradigms including *in vitro* Wallerian degeneration. *Brain Res.* 1030, 81–93. doi: 10.1016/j.brainres.2004.09.050

Inman, D. M., Sappington, R. M., Horner, P. J., and Calkins, D. J. (2006). Quantitative correlation of optic nerve pathology with ocular pressure and corneal thickness in the DBA/2 mouse model of glaucoma. *Invest. Ophthalmol. Vis. Sci.* 47, 986–996. doi: 10.1167/iovs.05-0925

Islam, R., Yang, L., Sah, M., Kannan, K., Anamani, D., Vijayan, C., et al. (2012). A neuroprotective role of the human uncoupling protein 2 (hUCP2) in a Drosophila Parkinson's Disease model. *Neurobiol. Dis.* 46, 137–146. doi: 10.1016/j.nbd.2011.12.055

Jakobs, T. C., Libby, R. T., Ben, Y., John, S. W., and Masland, R. H. (2005). Retinal ganglion cell degeneration is topological but not cell type specific in DBA/2J mice. *J Cell Biol* 171, 313–325. doi: 10.1083/jcb.200506099

John, S. W., Smith, R. S., Savinova, O. V., Hawes, N. L., Chang, B., Turnbull, D., et al. (1998). Essential iris atrophy, pigment dispersion, and glaucoma in DBA/2J mice. *Invest. Ophthalmol. Vis. Sci.* 39, 951–962.

Jonas, J. B., Muller-Bergh, J. A., Schlotzer-Schrehardt, U. M., and Naumann, G. O. (1990). Histomorphometry of the human optic nerve. *Investig. Ophthalmol. Vis. Sci.* 31, 736–744.

Ju, W. K., Kim, K. Y., Lindsey, J. D., Angert, M., Duong-Polk, K. X., Scott, R. T., et al. (2008). Intraocular pressure elevation induces mitochondrial fission and triggers OPA1 release in glaucomatous optic nerve. *Invest. Ophthalmol. Vis. Sci.* 49, 4903–4911. doi: 10.1167/iovs.07-1661

Kanamori, A., Nakamora, M., Mukuno, H., Maeda, H., and Negi, A. (2004a). Diabetes has an additive effect on neural apoptosis in rat retina with chronically elevated intraocular pressure. *Curr. Eye Res.* 28, 47–54. doi: 10.1076/ceyr.28.1.47.23487

Kanamori, A., Nakamura, M., Nakanishi, Y., Nagai, A., Mukuno, H., Yamada, Y., et al. (2004b). Akt is activated via insulin/IGF-1 receptor in rat retina with episcleral vein cauterization. *Brain Res.* 1022, 195–204. doi: 10.1016/j.brainres.2004.06.077

Kim, S.-J., Sung, M.-S., Heo, H., Lee, J.-H., and Park, S.-W. (2015). Mangiferin protects retinal ganglion cells in ischemic mouse retina via SIRT1. *Curr. Eye Res.* 0, 1–12. doi: 10.3109/02713683.2015.1050736

Kim, Y., Zhou, P., Qian, L., Chuang, J. Z., Lee, J., Li, C., et al. (2007). MyD88-5 links mitochondria, microtubules, and JNK3 in neurons and regulates neuronal survival. *J. Exp. Med.* 204, 2063–2074. doi: 10.1084/jem.20070868

Kitaoka, Y., Munemasa, Y., Kojima, K., Hirano, A., Ueno, S., and Takagi, H. (2013). Axonal protection by Nmnat3 overexpression with involvement of autophagy in optic nerve degeneration. *Cell Death Dis.* 4:e860. doi: 10.1038/cddis.2013.391

Kitay, B. M., McCormack, R., Wang, Y., Tsoulfas, P., and Zhai, R. G. (2013). Mislocalization of neuronal mitochondria reveals regulation of Wallerian degeneration and NMNAT/WLD(S)-mediated axon protection independent of axonal mitochondria. *Hum. Mol. Genet.* 22, 1601–1614. doi: 10.1093/hmg/ddt009

Kleesattel, D., Crish, S. D., and Inman, D. M. (2015). Decreased energy capacity and increased autophagic activity in optic nerve axons with defective anterograde transport. *Investig. Ophthalmol. Vis. Sci.* 56, 8215–8227. doi: 10.1167/iovs.15-17885

Koch, K., Mclean, J., Berry, M., Sterling, P., Balasubramanian, V., and Freed, M. A. (2004). Efficiency of information transmission by retinal ganglion cells. 14, 1523–1530. doi: 10.1016/j.cub.2004.08.060

Koehler-Stec, E. M., Simpson, I. A., Vannucci, S. J., Landschulz, K. T., and Landschulz, W. H. (1998). Monocarboxylate transporter expression in mouse brain Monocarboxylate transporter expression in mouse brain. *Am. J. Physiol. Endocrinol. Metab.* 275, E516–E524.

Lagouge, M., Argmann, C., Gerhart-Hines, Z., Meziane, H., Lerin, C., Daussin, F., et al. (2006). Resveratrol improves mitochondrial function and protects against metabolic disease by activating SIRT1 and PGC-1α. *Cell* 127, 1109–1122. doi: 10.1016/j.cell.2006.11.013

Lampert, P. W., Vogel, M. H., and Zimmerman, L. E. (1968). Pathology of the optic nerve in experimental acute glaucoma: electron microscopic studies. *Invest. Ophthalmol. Vis. Sci.* 7, 199–213.

Langley, B., Gensert, J. M., Beal, M. F., and Ratan, R. R. (2005). Remodeling chromatin and stress resistance in the central nervous system: histone deacetylase inhibitors as novel and broadly effective neuroprotective agents. *Curr Drug Targets CNS Neurol Disord.* 4, 41–50. doi: 10.2174/1568007053005091

Lascaratos, G., Chau, K. Y., Zhu, H., Gkotsi, D., King, R., Gout, I., et al. (2015). Resistance to the most common optic neuropathy is associated with systemic mitochondrial efficiency. *Neurobiol. Dis.* 82, 78–85. doi: 10.1016/j.nbd.2015.05.012

Lau, C., Niere, M., and Ziegler, M. (2009). The NMN/NaMN adenylyltransferase (NMNAT) protein family. *Front. Biosci.* 14, 410–431. doi: 10.2741/3252

Lebrun-Julien, F., Morquette, B., Douillette, A., Saragovi, H. U., and Di Polo, A. (2009). Inhibition of p75(NTR) in glia potentiates TrkA-mediated survival of injured retinal ganglion cells. *Mol. Cell. Neurosci.* 40, 410–420. doi: 10.1016/j.mcn.2008.12.005

Lee, Y., Morrison, B. M., Li, Y., Lengacher, S., Farah, M. H., Hoffman, P. N., et al. (2012). Oligodendroglia metabolically support axons and contribute to neurodegeneration. *Nature* 487, 443–448. doi: 10.1038/nature11314

Lensman, M., Korzhevskii, D. E., Mourovets, V. O., Kostkin, V. B., Izvarina, N., Perasso, L., et al. (2006). Intracerebroventricular administration of creatine protects against damage by global cerebral ischemia in rat. *Brain Res.* 1114, 187–194. doi: 10.1016/j.brainres.2006.06.103

Li, R. S., Chen, B. Y., Tay, D. K., Chan, H. H., Pu, M. L., and So, K. F. (2006). Melanopsin-expressing retinal ganglion cells are more injury-resistant in a chronic ocular hypertension model. *Investig. Ophthalmol. Vis. Sci.* 47, 2951–2958. doi: 10.1167/iovs.05-1295

Libby, R. T., Li, Y., Savinova, O. V., Barter, J., Smith, R. S., Nickells, R. W., et al. (2005). Susceptibility to neurodegeneration in a glaucoma is modified by Bax gene dosage. *PLoS Genet* 1, 17–26. doi: 10.1371/journal.pgen.0010004

Linding, R., Jensen, L. J., Ostheimer, G. J., van Vugt, M. A., Jørgensen, C., Miron, I. M., et al. (2007). Systematic discovery of *in vivo* phosphorylation networks. *Cell* 129, 1415–1426. doi: 10.1016/j.cell.2007.05.052

Llorente-Folch, I., Rueda, C. B., Pérez-Liébana, I., Satrústegui, J., and Pardo, B. (2016). l-Lactate-mediated neuroprotection against glutamate-induced excitotoxicity requires ARALAR/AGC1. *J. Neurosci.* 36, 4443–4456. doi: 10.1523/JNEUROSCI.3691-15.2016

Loreto, A., Di Stefano, M., Gering, M., and Conforti, L. (2015). Wallerian degeneration is executed by an NMN-SARM1-dependent Late Ca2+ influx but only modestly influenced by mitochondria. *Cell Rep.* 13, 2539–2552. doi: 10.1016/j.celrep.2015.11.032

Lundgaard, I., Osório, M. J., Kress, B. T., Sanggaard, S., and Nedergaard, M. (2014). White matter astrocytes in health and disease. *Neuroscience* 276, 161–173. doi: 10.1016/j.neuroscience.2013.10.050

Lunn, E. R., Perry, V. H., Brown, M. C., Rosen, H., and Gordon, S. (1989). Absence of wallerian degeneration does not hinder regeneration in peripheral nerve. *Eur. J. Neurosci.* 1, 27–33. doi: 10.1111/j.1460-9568.1989.tb00771.x

Lye-Barthel, M., Sun, D., and Jakobs, T. C. (2013). Morphology of astrocytes in a glaucomatous optic nerve. *Invest. Ophthalmol. Vis. Sci.* 54, 909–917. doi: 10.1167/iovs.12-10109

Lyon, M. F., Ogunkolade, B. W., Brown, M. C., Atherton, D. J., and Perry, V. H. (1993). A gene affecting Wallerian nerve degeneration maps distally on mouse chromosome 4. *Proc. Natl. Acad. Sci. U.S.A.* 90, 9717–9720. doi: 10.1073/pnas.90.20.9717

Mack, T. G., Reiner, M., Beirowski, B., Mi, W., Emanuelli, M., Wagner, D., et al. (2001). Wallerian degeneration of injured axons and synapses is delayed by a Ube4b/Nmnat chimeric gene. *Nat. Neurosci.* 4, 1199–1206. doi: 10.1038/nn770

Maher, F., Davies-Hill, T. M., Lysko, P. G., Henneberry, R. C., and Simpson, I. A., (1991). Expression of two glucose transporters, GLUT1 and GLUT3, in cultured cerebellar neurons: evidence for neuron-specific expression of GLUT3. *Mol. Cell. Neurosci.* 2, 351–360. doi: 10.1016/1044-7431(91)90066-W

Mandelkow, E. M., Drewes, G., Biernat, J., Gustke, N., Van Lint, J., Vandenheede, J. R., et al. (1992). Glycogen synthase kinase-3 and the Alzheimer-like

state of microtubule-associated protein tau. *FEBS Lett.* 314, 315–321. doi: 10.1016/0014-5793(92)81496-9

Mandelkow, E. M., Stamer, K., Vogel, R., Thies, E., and Mandelkow, E. (2003). Clogging of axons by tau, inhibition of axonal traffic and starvation of synapses. *Neurobiol. Aging* 24, 1079–1085. doi: 10.1016/j.neurobiolaging.2003.04.007

Meyer zu Horste, G., Miesbach, T. A., Muller, J. I., Fledrich, R., Stassart, R. M., Kieseier, B. C., et al. (2011). The Wlds transgene reduces axon loss in a Charcot-Marie-Tooth disease 1A rat model and nicotinamide delays post-traumatic axonal degeneration. *Neurobiol. Dis.* 42, 1–8. doi: 10.1016/j.nbd.2010.12.006

Mikelberg, F. S, Drance, S. M., Schulzer, M., Yidegiligne, H. M., and Weis, M. M. (1989). The normal human optic nerve. Axon count and axon diameter distribution. *Ophthalmology* 96, 1325–1328. doi: 10.1016/S0161-6420(89)32718-7

Milde, S., Gilley, J., and Coleman, M. P. (2013). Subcellular localization determines the stability and axon protective capacity of axon survival factor Nmnat2. *PLoS Biol.* 11:e1001539. doi: 10.1371/journal.pbio.1001539

Miller, B. R., Press, C., Daniels, R. W., Sasaki, Y., Milbrandt, J., and DiAntonio, A. (2009). A DLK-dependent axon self-destruction program promotes Wallerian degeneration. *Nat. Neurosci.* 12, 387–389. doi: 10.1038/nn.2290

Misko, A. L., Sasaki, Y., Tuck, E., Milbrandt, J., and Baloh, R. H. (2012). Mitofusin2 mutations disrupt axonal mitochondrial positioning and promote axon degeneration. *J. Neurosci.* 32, 4145–4155. doi: 10.1523/JNEUROSCI.6338-11.2012

Mudò, G., Mäkelä, J., Di Liberto, V., Tselykh, T. V, Olivieri, M., Piepponen, P., et al. (2012). Transgenic expression and activation of PGC-1α protect dopaminergic neurons in the MPTP mouse model of Parkinson's disease. *Cell. Mol. Life Sci.* 69, 1153–1165. doi: 10.1007/s00018-011-0850-z

Nakazawa, T., Nakazawa, C., Matsubara, A., Noda, K., Hisatomi, T., She, H., et al. (2006). Tumor necrosis factor-alpha mediates oligodendrocyte death and delayed retinal ganglion cell loss in a mouse model of glaucoma. *J. Neurosci.* 26, 12633–12641. doi: 10.1523/JNEUROSCI.2801-06.2006

Nave, K. A. (2010). Myelination and the trophic support of long axons. *Nat. Rev. Neurosci.* 11, 275–283. doi: 10.1038/nrn2797

Nilsson, P., Hillered, L., Pontén, U., and Ungerstedt, U. (1990). Changes in cortical extracellular levels of energy-related metabolites and amino acids following concussive brain injury in rats. *J. Cereb. Blood Flow Metab.* 10, 631–637. doi: 10.1038/jcbfm.1990.115

O'Meara, R. W., Michalski, J. P., Anderson, C., Bhanot, K., Rippstein, P., and Kothary, R. (2013). Integrin-linked kinase regulates process extension in oligodendrocytes via control of actin cytoskeletal dynamics. *J. Neurosci.* 33, 9781–9793. doi: 10.1523/JNEUROSCI.5582-12.2013

Obel, L. F., Müller, M. S., Walls, A. B., Sickmann, H. M., Bak, L. K., Waagepetersen, H. S., et al. (2012). Brain glycogen - new perspectives on its metabolic function and regulation at the subcellular level. *Front. Neuroenergetics* 4:3. doi: 10.3389/fnene.2012.00003

Ohno, N., Kidd, G. J., Mahad, D., Kiryu-Seo, S., Avishai, A., Komuro, H., et al. (2011). Myelination and axonal electrical activity modulate the distribution and motility of mitochondria at CNS nodes of Ranvier. *J. Neurosci.* 31, 7249–7258. doi: 10.1523/JNEUROSCI.0095-11.2011

Orthmann-Murphy, J. L., Freidin, M., Fischer, E., Scherer, S. S., and Abrams, C. K. (2007). Two distinct heterotypic channels mediate gap junction coupling between astrocyte and oligodendrocyte connexins. *J. Neurosci.* 27, 13949–13957. doi: 10.1523/JNEUROSCI.3395-07.2007

Osterloh, J. M., Yang, J., Rooney, T. M., Fox, A. N., Adalbert, R., Powell, E. H., et al. (2012). dSarm/Sarm1 is required for activation of an injury-induced axon death pathway. *Science* 337, 481–484. doi: 10.1126/science.1223899

Ou, Y., Jo, R. E., Ullian, E. M., Wong, R. O., and Della Santina, L., (2016). Selective vulnerability of specific retinal ganglion cell types and synapses after transient ocular hypertension. *J. Neurosci.* 36, 9240–9252. doi: 10.1523/JNEUROSCI.0940-16.2016

Park, H. Y. L., Kim, J. H., and Park, C. K. (2012). Activation of autophagy induces retinal ganglion cell death in a chronic hypertensive glaucoma model. *Cell Death Dis.* 3:e290. doi: 10.1038/cddis.2012.26

Peixoto, P. M., Kim, H.-J., Sider, B., Starkov, A., Horvath, T. L., and Manfredi, G. (2013). UCP2 overexpression worsens mitochondrial dysfunction and accelerates disease progression in a mouse model of amyotrophic lateral sclerosis. *Mol. Cell. Neurosci.* 57, 104–110. doi: 10.1016/j.mcn.2013.10.002

Pellerin, L., Pellegri, G., Bittar, P., Charnay, Y., Bouras, C., Martin, J., et al. (1998). Evidence supporting the existence of an activity-dependent astrocyte-neuron lactate shuttle. *Dev. Neurosci.* 20, 291–299. doi: 10.1159/000017324

Pelzel, H. R., Schlamp, C. L., Waclawski, M., Shaw, M. K., and Nickells, R. W. (2012). Silencing of Fem1cR3 gene expression in the DBA/2J mouse precedes retinal ganglion cell death and is associated with histone deacetylase activity. *Invest. Ophthalmol. Vis. Sci.* 53, 1428–1435. doi: 10.1167/iovs.11-8872

Perasso, L., Adriano, E., Ruggeri, P., Burov, S. V., Gandolfo, C., and Balestrino, M. (2009). *In vivo* neuroprotection by a creatine-derived compound: phosphocreatine-Mg-complex acetate. *Brain Res.* 1285, 158–163. doi: 10.1016/j.brainres.2009.06.009

Perge, J. A., Koch, K., Miller, R., Sterling, P., and Balasubramanian, V. (2009). How the optic nerve allocates space, energy capacity, and information. *J. Neurosci.* 29, 7917–7928. doi: 10.1523/JNEUROSCI.5200-08.2009

Perry, V., Brown, M., Lunn, E., Tree, P., and Gordon, S. (1990a). Evidence that very slow Wallerian degeneration in the C57Bl/Ola mice is an intrinsic property of the peripheral nerve. *Eur. J. Neurosci.* 2, 802–808. doi: 10.1111/j.1460-9568.1990.tb00472.x

Perry, V. H., Brown, M. C., Lunn, E. R., Tree, P., Gordon, S., and Cahusac, C. (1990b). Evidence that the rate of wallerian degeneration is controlled by a single autosomal dominant gene. *Eur. J. Neurosci.* 2, 408–413. doi: 10.1111/j.1460-9568.1990.tb00433.x

Pevzner, L. Z. (1971). Topochemical aspects of nucleic acid and protein metabolism within the neuron-neuroglia unit of the spinal cord anterior horn. *J. Neurochem.* 18, 895–907. doi: 10.1111/j.1471-4159.1971.tb12019.x

Pevzner, L. Z. (1972). Topochemical aspects of nucleic acid metabolism within the neuronal-neuroglia unit of cerebellum Purkinje cells. *Brain Res.* 46, 329–339. doi: 10.1016/0006-8993(72)90023-6

Pierre, K., Magistretti, P. J., and Pellerin, L. (2002). MCT2 is a major neuronal monocarboxylate transporter in the adult mouse brain. *J. Cereb. Blood Flow Metab.* 22, 586–595. doi: 10.1097/00004647-200205000-00010

Pierre, K., and Pellerin, L. (2005). Monocarboxylate transporters in the central nervous system: distribution, regulation and function. *J. Neurochem.* 94, 1–14. doi: 10.1111/j.1471-4159.2005.03168.x

Quigley, H. A., Dunkelberger, G. R., and Green, W. R. (1988). Chronic human glaucoma causing selectively greater loss of large optic nerve fibers. *Ophthalmology* 95, 357–363. doi: 10.1016/S0161-6420(88)33176-3

Rafiki, A., Boulland, J. L., Halestrap, A. P., Ottersen, O. P., and Bergersen, L. (2003). Highly differential expression of the monocarboxylate transporters MCT2 and MCT4 in the developing rat brain. *Neuroscience* 122, 677–688. doi: 10.1016/j.neuroscience.2003.08.040

Ransom, B. R., Butt, A. M., and Black, J. A. (1991). Ultrastructural identification of HRP-injected oligodendrocytes in the intact rat optic nerve. *Glia* 4, 37–45. doi: 10.1002/glia.440040105

Rawson, R. L., Yam, L., Weimer, R. M., Bend, E. G., Hartwieg, E., Horvitz, H. R., et al. (2014). Axons degenerate in the absence of mitochondria in *C. elegans*. *Curr. Biol.* 24, 760–765. doi: 10.1016/j.cub.2014.02.025

Ritchie, J. (1967). The oxygen consumption of mammalian non-myelinated nerve fibers at rest and during activity. *J. Physiol.* 188, 309–329. doi: 10.1113/jphysiol.1967.sp008141

Rodriguez-Muela, N., and Boya, P. (2012). Axonal damage, autophagy and neuronal survival. *Autophagy* 8, 286–288. doi: 10.4161/auto.8.2.18982

Rone, M. B., Cui, Q.-L., Fang, J., Wang, L.-C., Zhang, J., Khan, D., et al. (2016). Oligodendrogliopathy in multiple sclerosis: low glycolytic metabolic rate promotes oligodendrocyte survival. *J. Neurosci.* 36, 4698–4707. doi: 10.1523/JNEUROSCI.4077-15.2016

Rouach, N., Koulakoff, A., Abudara, V., Willecke, K., and Giaume, C. (2008). Astroglial metabolic networks sustain hippocampal synaptic transmission. *Science* 322, 1551–1555. doi: 10.1126/science.1164022

Rowlands, B. D., Lau, C. L., Ryall, J. G., Thomas, D. S., Klugmann, M., Beart, P. M., et al. (2015). Silent information regulator 1 modulator resveratrol increases brain lactate production and inhibits mitochondrial metabolism, whereas SRT1720 increases oxidative metabolism. *J. Neurosci. Res.* 93, 1147–1156. doi: 10.1002/jnr.23570

Saab, A. S., Tzvetavona, I. D., Trevisiol, A., Baltan, S., Dibaj, P., Kusch, K., et al. (2016). Oligodendroglial NMDA receptors regulate glucose import and axonal energy metabolism. *Neuron* 91, 119–132. doi: 10.1016/j.neuron.2016.05.016

Samsam, M., Mi, W., Wessig, C., Zielasek, J., Toyka, K. V., Coleman, M. P., et al. (2003). The *Wld*^{s} mutation delays robust loss of motor and sensory axons in a genetic model for myelin-related axonopathy. *J. Neurosci.* 23, 2833–2839.

Sasaki, Y., Vohra, B. P. S., Lund, F. E., and Milbrandt, J. (2009). Nicotinamide mononucleotide adenylyl transferase-mediated axonal protection requires enzymatic activity but not increased levels of neuronal nicotinamide adenine dinucleotide. *J. Neurosci.* 29, 5525–5535. doi: 10.1523/JNEUROSCI.5469-08.2009

Schlamp, C. L., Li, Y., Dietz, J. A., Janssen, K. T., and Nickells, R. W. (2006). Progressive ganglion cell loss and optic nerve degeneration in DBA/2J mice is variable and asymmetric. *BMC Neurosci.* 7:66. doi: 10.1186/1471-2202-7-66

Schmitt, H. M., Pelzel, H. R., Schlamp, C. L., and Nickells, R. W. (2014). Histone deacetylase 3 (HDAC3) plays an important role in retinal ganglion cell death after acute optic nerve injury. *Mol. Neurodegener.* 9, 39–54. doi: 10.1186/1750-1326-9-39

Schoenmann, Z., Assa-Kunik, E., Tiomny, S., Minis, A., Haklai-Topper, L., Arama, E., et al. (2010). Axonal degeneration is regulated by the apoptotic machinery or a NAD+-sensitive pathway in insects and mammals. *J. Neurosci.* 30, 6375–6386. doi: 10.1523/JNEUROSCI.0922-10.2010

Schwartz, B. (1994). Circulatory defects of the optic disk and retina in ocular hypertension and high pressure open-angle glaucoma. *Surv. Ophthalmol.* 38(Suppl):S23–S34. doi: 10.1016/0039-6257(94)90044-2

Seglen, P. O., and Gordon, P. B. (1982). 3-Methyladenine: specific inhibitor of autophagic/lysosomal protein degradation in isolated rat hepatocytes. *Proc. Natl. Acad. Sci. U.S.A.* 79, 1889–1892. doi: 10.1073/pnas.79.6.1889

Serwanski, D. R., Jukkola, P., and Nishiyama, A. (2017). Heterogeneity of astrocyte and NG2 cell insertion at the node of ranvier. *J. Comp. Neurol.* 525, 535–552. doi: 10.1002/cne.24083

Shen, H., and Goldberg, M. P. (2012). Creatine pretreatment protects cortical axons from energy depletion *in vitro*. *Neurobiol. Dis.* 47, 184–193. doi: 10.1016/j.nbd.2012.03.037

Shen, H., Hyrc, K. L., and Goldberg, M. P. (2013). Maintaining energy homeostasis is an essential component of Wld(S)-mediated axon protection. *Neurobiol. Dis.* 59, 69–79. doi: 10.1016/j.nbd.2013.07.007

Shimazu, T., Hirschey, M. D., Newman, J., He, W., Shirakawa, K., Le Moan, N., et al. (2013). Suppression of oxidative stress by β-hydroxybutyrate, an endogenous histone deacetylase inhibitor. *Science* 339, 211–214. doi: 10.1126/science.1227166

Shin, J. E., Miller, B. R., Babetto, E., Cho, Y., Sasaki, Y., Qayum, S., et al. (2012). SCG10 is a JNK target in the axonal degeneration pathway. *Proc. Natl. Acad. Sci. U.S.A.* 109, E3696–E3705. doi: 10.1073/pnas.1216204109

Sickmann, H. M., Schousboe, A., Fosgerau, K., and Waagepetersen, H. S. (2005). Compartmentation of lactate originating from glycogen and glucose in cultured astrocytes. *Neurochem. Res.* 30, 1295–1304. doi: 10.1007/s11064-005-8801-4

Simpson, I. A., Carruthers, A., and Vannucci, S. J. (2007). Supply and demand in cerebral energy metabolism: the role of nutrient transpoters. *J. Cereb. Blood Flow Metab.* 27, 1766–1791. doi: 10.1038/sj.jcbfm.9600521

Simpson, I., A., Dwyer, D., Malide, D., Moley, K. H., Travis, A., and Vannucci, S. J. (2008). The facilitative glucose transporter GLUT3: 20 years of distinction. *Am. J. Physiol. Endocrinol. Metab.* 295, E242–E253. doi: 10.1152/ajpendo.90388.2008

Son, J. L., Soto, I., Oglesby, E., Lopez-Roca, T., Pease, M. E., Quigley, H. A., et al. (2010). Glaucomatous optic nerve injury involves early astrocyte reactivity and late oligodendrocyte loss. *Glia* 58, 780–789. doi: 10.1002/glia.20962

Stamer, K., Vogel, R., Thies, E., Mandelkow, E., and Mandelkow, E. M. (2002). Tau blocks traffic of organelles, neurofilaments, and APP vesicles in neurons and enhances oxidative stress. *J. Cell Biol.* 156, 1051–1063. doi: 10.1083/jcb.200108057

Stincone, A., Prigione, A., Cramer, T., Wamelink, M. M. C., Campbell, K., Cheung, E., et al. (2015). The return of metabolism: biochemistry and physiology of the pentose phosphate pathway. *Biol. Rev.* 90, 927–963. doi: 10.1111/brv.12140

Stirling, D. P., and Stys, P. K. (2010). Mechanisms of axonal injury: internodal nanocomplexes and calcium deregulation. *Trends Mol. Med.* 16, 160–170. doi: 10.1016/j.molmed.2010.02.002

Stys, P. K. (2004). White matter injury mechanisms. *Curr. Mol. Med.* 4, 113–130. doi: 10.2174/1566524043479220

Stys, P. K., Waxman, S. G., and Ransom, B. R. (1991). Na(+)-Ca2+ exchanger mediates Ca2+ influx during anoxia in mammalian central nervous system white matter. *Ann. Neurol.* 30, 375–380. doi: 10.1002/ana.410300309

Suh, S. W., Bergher, J. P., Anderson, C. M., Treadway, J. L., Fosgerau, K., and Swanson, R. A. (2007). Astrocyte glycogen sustains neuronal activity during hypoglycemia : studies with the glycogen phosphorylase inhibitor CP-316,819. *J. Pharmacol. Exp. Ther.* 321, 45–50. doi: 10.1124/jpet.106.115550

Summers, D. W., DiAntonio, A., and Milbrandt, J. (2014). Mitochondrial dysfunction induces sarm1-dependent cell death in sensory neurons. *J. Neurosci.* 34, 9338–9350. doi: 10.1523/JNEUROSCI.0877-14.2014

Sun, D., and Jakobs, T. C. (2012). Structural remodeling of astrocytes in the injured CNS. *Neuroscientist* 18, 567–588. doi: 10.1177/1073858411423441

Sun, D., Lye-Barthel, M., Masland, R. H., and Jakobs, T. C. (2009). The morphology and spatial arrangement of astrocytes in the optic nerve head of the mouse. *J. Comp. Neurol.* 516, 1–19. doi: 10.1002/cne.22058

Sun, M.-H., Pang, J.-H. S., Chen, S.-L., Han, W.-H., Ho, T.-C., Chen, K.-J., et al. (2010). Retinal protection from acute glaucoma-induced ischemia-reperfusion injury through pharmacologic induction of heme oxygenase-1. *Invest. Ophthalmol. Vis. Sci.* 51, 4798–4808. doi: 10.1167/iovs.09-4086

Tekkök, S. B., Brown, A. M., Westenbroek, R., Pellerin, L., and Ransom, B. R. (2005). Transfer of glycogen-derived lactate from astrocytes to axons via specific monocarboxylate transporters supports mouse optic nerve activity. *J. Neurosci. Res.* 81, 644–652. doi: 10.1002/jnr.20573

Tham, Y. C., Li, X., Wong, T. Y., Quigley, H. A., Aung, T., and Cheng, C. Y. (2014). Global prevalence of glaucoma and projections of glaucoma burden through 2040: a systematic review and meta-analysis. *Ophthalmology* 121, 2081–2090. doi: 10.1016/j.ophtha.2014.05.013

Trammell, S. A. J., Schmidt, M. S., Weidemann, B. J., Redpath, P., Jaksch, F., Dellinger, R. W., et al. (2016). Nicotinamide riboside is uniquely and orally bioavailable in mice and humans. *Nat. Commun.* 7:12948. doi: 10.1038/ncomms12948

Tsacopoulos, M., and Magistretti, P. J. (1996). Metabolic coupling glia and neurons. *J. Neurosci.* 16, 877–885.

Tsutsui, S., and Stys, P. K. (2013). Metabolic injury to axons and myelin. *Exp. Neurol.* 246, 26–34. doi: 10.1016/j.expneurol.2012.04.016

Uemura, E., and Greenlee, H. W. (2006). Insulin regulates neuronal glucose uptake by promoting translocation of glucose transporter GLUT3. *Exp. Neurol.* 198, 48–53. doi: 10.1016/j.expneurol.2005.10.035

van Bergen, N. J., Crowston, J. G., Kearns, L. S., Staffieri, S. E., Hewitt, A. W., Cohn, A. C., et al. (2011). Mitochondrial oxidative phosphorylation compensation may preserve vision in patients with OPA1-linked autosomal dominant optic atrophy. *PLoS ONE* 6:e21347. doi: 10.1371/journal.pone.0021347

Vande Velde, C., Garcia, M. L., Yin, X., Trapp, B. D., and Cleveland, D. W. (2004). The neuroprotective factor Wlds does not attenuate mutant SOD1-mediated motor neuron disease. *Neuromol. Med.* 5, 193–203. doi: 10.1385/NMM:5:3:193

Volkenhoff, A., Weiler, A., Letzel, M., Stehling, M., Klämbt, C., and Schirmeier, S. (2015). Glial glycolysis is essential for neuronal survival in drosophila. *Cell Metab.* 22, 437–447. doi: 10.1016/j.cmet.2015.07.006

Vrabec, J. P., and Levin, L. A. (2007). The neurobiology of cell death in glaucoma. *Eye (Lond).* 21(Suppl. 1), S11–S14. doi: 10.1038/sj.eye.6702880

Waller, A. (1850). Experiments on the section of the glossopharyngeal and hypoglossal nerves of the frog, and observations of the alterations produced thereby in the structure of their primitive fibres. *Philos. Trans. R. Soc. London* 140, 423–429. doi: 10.1098/rstl.1850.0021

Wang, J. T., Medress, Z. A., Vargas, M. E., and Barres, B. A. (2015). Local axonal protection by WldS as revealed by conditional regulation of protein stability. *Proc. Natl. Acad. Sci. U.S.A.* 112, 10093–10100. doi: 10.1073/pnas.1508337112

Wang, J., Zhai, Q., Chen, Y., Lin, E., Gu, W., McBurney, M. W., et al. (2005). A local mechanism mediates NAD-dependent protection of axon degeneration. *J. Cell Biol.* 170, 349–355. doi: 10.1083/jcb.200504028

Wang, X., Sekine, Y., Byrne, A. B., and Cafferty, W. B. J. (2016). Inhibition of poly-ADP-ribosylation fails to increase axonal regeneration or improve functional recovery after adult mammalian CNS injury. *eNeuro* 3, 1–10. doi: 10.1523/ENEURO.0270-16.2016

Watanabe, M., Sawai, H., and Fukuda, Y. (1993). Number, distribution, and morphology of retinal ganglion cells with axons regenerated into peripheral nerve graft in adult cats. *J. Neurosci.* 13, 2105–2117.

Watkins, T. A., Wang, B., Huntwork-Rodriguez, S., Yang, J., Jiang, Z., Eastham-Anderson, J., et al. (2013). DLK initiates a transcriptional program that couples

apoptotic and regenerative responses to axonal injury. *Proc. Natl. Acad. Sci. U.S.A.* 110, 4039–4044. doi: 10.1073/pnas.1211074110

Weber, A. J., and Harman, C. D. (2013). BDNF treatment and extended recovery from optic nerve trauma in the cat. *Invest. Ophthalmol. Vis. Sci.* 54, 6594–6604. doi: 10.1167/iovs.13-12683

Welsbie, D. S., Yang, Z., Ge, Y., Mitchell, K. L., Zhou, X., Martin, S. E., et al. (2013). Functional genomic screening identifies dual leucine zipper kinase as a key mediator of retinal ganglion cell death. *Proc. Natl. Acad. Sci. U.S.A.* 110, 4045–4050. doi: 10.1073/pnas.1211284110

Wender, R., Brown, A. M., Fern, R., Swanson, R. A., Farrell, K., and Ransom, B. R. (2000). Astrocytic glycogen influences axon function and survival during glucose deprivation in central white matter. *J. Neurosci.* 20, 6804–6810.

Williams, P. A., Harder, J. M., Foxworth, N. E., Cochran, K. E., Philip, V. M., Porciatti, V., et al. (2017). Vitamin B3 modulates mitochondrial vulnerability and prevents glaucoma in aged mice. *Science* 760, 756–760. doi: 10.1126/science.aal0092

Williams, R. W., and Chalupa, L. M. (1983). An analysis of axon caliber within the optic nerve of the cat: evidence of size groupings and regional organization. *J. Neurosci.* 3, 1554–1564.

Yahata, N., Yuasa, S., and Araki, T. (2009). Nicotinamide mononucleotide adenylyltransferase expression in mitochondrial matrix delays Wallerian degeneration. *J. Neurosci.* 29, 6276–6284. doi: 10.1523/JNEUROSCI.4304-08.2009

Yang, J., Weimer, R. M., Kallop, D., Olsen, O., Wu, Z., Renier, N., et al. (2013). Regulation of axon degeneration after injury and in development by the endogenous calpain inhibitor calpastatin. *Neuron* 80, 1175–1189. doi: 10.1016/j.neuron.2013.08.034

Yang, J., Wu, Z., Renier, N., Simon, D. J., Uryu, K., Park, D. S., et al. (2015). Pathological axonal death through a Mapk cascade that triggers a local energy deficit. *Cell* 160, 161–176. doi: 10.1016/j.cell.2014.11.053

Yang, X., and Cheng, B. (2010). Neuroprotective and anti-inflammatory activities of ketogenic diet on MPTP-induced neurotoxicity. *J. Mol. Neurosci.* 42, 145–153. doi: 10.1007/s12031-010-9336-y

Yellen, G. (2008). Ketone bodies, glycolysis, and KATP channels in the mechanism of the ketogenic diet. *Epilepsia* 49, 80–82. doi: 10.1111/j.1528-1167.2008.01843.x

Yoshino, J., Mills, K. F., Yoon, M. J., and Imai, S. (2011). Nicotinamide mononucleotide, a key NAD+ intermediate, treats the pathophysiology of diet- and age-induced diabetes in mice. *Cell. Metab.* 14, 528–536. doi: 10.1016/j.cmet.2011.08.014

Zala, D., Hinckelmann, M.-V., Yu, H., Lyra da Cunha, M. M., Liot, G., Cordelières, F. P., et al. (2013). Vesicular glycolysis provides on-board energy for fast axonal transport. *Cell* 152, 479–491. doi: 10.1016/j.cell.2012.12.029

Zhang, H., Ryu, D., Wu, Y., Gariani, K., Wang, X., Luan, P., et al. (2016). NAD+ repletion improves mitochondrial and stem cell function and enhances life span in mice. *Science* 352, 1436–1443. doi: 10.1126/science.aaf2693

Zhao, Z., Lange, D. J., Voustianiouk, A., MacGrogan, D., Ho, L., Suh, J., et al. (2006). A ketogenic diet as a potential novel therapeutic intervention in amyotrophic lateral sclerosis. *BMC Neurosci.* 7:29. doi: 10.1186/1471-2202-7-29

Zhou, B., Yu, P., Lin, M.-Y., Sun, T., Chen, Y., and Sheng, Z.-H. (2016). Facilitation of axon regeneration by enhancing mitochondrial transport and rescuing energy deficits. *J. Cell Biol.* 214, 103–119. doi: 10.1083/jcb.201605101

Zhu, Y., Zhang, L., Sasaki, Y., Milbrandt, J., and Gidday, J. M. (2013). Protection of mouse retinal ganglion cell axons and soma from glaucomatous and ischemic injury by cytoplasmic overexpression of Nmnat1. *Invest. Ophthalmol. Vis. Sci.* 54, 25–36. doi: 10.1167/iovs.12-10861

Zuo, L., Khan, R. S., Lee, V., Dine, K., Wu, W., and Shindler, K. S. (2013). SIRT1 promotes RGC survival and delays loss of function following optic nerve crush. *Invest. Ophthalmol. Vis. Sci.* 54, 5097–5102. doi: 10.1167/iovs.13-12157

Conflict of Interest Statement: The authors declare that the research was conducted in the absence of any commercial or financial relationships that could be construed as a potential conflict of interest.

frontiers in Neuroscience

ORIGINAL RESEARCH
published: 25 August 2017
doi: 10.3389/fnins.2017.00473

Impaired Mitophagy Plays a Role in Denervation of Neuromuscular Junctions in ALS Mice

*Robert S. Rogers[1], Sudheer Tungtur[1], Tomohiro Tanaka[1], Lisa L. Nadeau[1], Yomna Badawi[1], Hua Wang[2], Hong-Min Ni[2], Wen-Xing Ding[2] and Hiroshi Nishimune[1]**

[1] Department of Anatomy and Cell Biology, University of Kansas School of Medicine, Kansas City, KS, United States,
[2] Department of Pharmacology, Toxicology and Therapeutics, University of Kansas School of Medicine, Kansas City, KS, United States

Motor neurons in amyotrophic lateral sclerosis (ALS) patients and animal models show degeneration from the nerve terminal, known as dying-back neuropathy. To investigate the mechanism underlying this neuropathy, we analyzed the neuromuscular junctions (NMJs) and motor neuron cell bodies in SOD1^{G93A} mice using electron microscopy. NMJs of SOD1^{G93A} mice exhibited significantly higher numbers of autophagosomes and degenerated mitochondria compared to wild-type controls. Mitophagosomes were identified in the NMJ presynaptic terminals of wild-type mice and SOD1^{G93A} mice. However, the number of mitophagosomes did not increase significantly in SOD1^{G93A} NMJs indicating a defect in mitophagy, the autophagic process to degrade mitochondria. Consistent with this, proteins essential for mitophagy, p62/SQSTM1, Bnip3, Pink1, and Parkin were down-regulated in motor neurons in SOD1^{G93A} mice. Importantly, SQSTM1 is one of the genes mutated in familial ALS patients. We evaluated the effect of impaired mitophagy on motor neurons by analyzing the double knockout mice of Pink1 and Parkin, two genes responsible for sensing depolarized mitochondria and delivering degenerated mitochondria to mitophagosomes. The double knockout mice exhibited NMJ degeneration, including axon swelling and NMJ fragmentation at 4 months of age. These phenotypes were rarely observed in wild-type control mice of the same age. The protein level of ATP synthase β subunit increased in the NMJ presynaptic terminals, suggesting the accumulation of mitochondria at NMJs of the double knockout mice. Importantly, NMJ denervation was observed in the double knockout mice. These data suggest that the reduced mitophagy function in motor neurons of SOD1^{G93A} mice is one of the mechanisms causing degeneration of ALS NMJs.

Keywords: ALS, autophagy, denervation, mitophagy, NMJ, p62/SQSTM1, SOD1^{G93A} mice

OPEN ACCESS

Edited by:
Robert W. Burgess, The Jackson Laboratory, United States

Reviewed by:
Kim A. Staats, University of Southern California, United States
Peter Gerrard Noakes, The University of Queensland, Australia
Gregorio Valdez, Virginia Tech, United States

****Correspondence:***
Hiroshi Nishimune
hnishimune@kumc.edu

Specialty section:
This article was submitted to Neurodegeneration, a section of the journal Frontiers in Neuroscience

Received: *01 April 2017*
Accepted: *10 August 2017*
Published: *25 August 2017*

Citation:
Rogers RS, Tungtur S, Tanaka T, Nadeau LL, Badawi Y, Wang H, Ni H-M, Ding W-X and Nishimune H (2017) Impaired Mitophagy Plays a Role in Denervation of Neuromuscular Junctions in ALS Mice. Front. Neurosci. 11:473. doi: 10.3389/fnins.2017.00473

INTRODUCTION

Amyotrophic lateral sclerosis (ALS) is a common and fatal motor neuron disease, but the etiology has not been elucidated fully (Bordet et al., 2001; Acsadi et al., 2002; Kaspar et al., 2003; Azzouz et al., 2004; Gould et al., 2006; Sorenson et al., 2008; Howe et al., 2009; Reyes et al., 2010; Jeong et al., 2011). In familial ALS patients, causal or risk-increasing roles in the pathogenesis of ALS have been reported for mutations in autophagy- and mitophagy-related genes, including ALS2/Alsin, charged

multivesicular protein 2B (CHMP2B), C9orf72, dynactin 1 (DCTN1), Optineurin, p62/SQSTM1 (sequestosome 1), Ubiquilin 2, and Valosin-containing protein (VCP) (Yang et al., 2001; Munch et al., 2004; Parkinson et al., 2006; Johnson et al., 2010; Maruyama et al., 2010; DeJesus-Hernandez et al., 2011; Deng et al., 2011; Fecto et al., 2011; Rubino et al., 2012; Williams et al., 2012; Farg et al., 2014). Autophagy is a selective process by which proteins and organelles are enveloped by a double membrane structure, the autophagosome, for delivery to lysosomes for degradation (Klionsky et al., 2016). The autophagy markers microtubule-associated protein 1 light chain 3 (LC3) and p62/SQSTM1 were detected in aggregated structures in spinal cord motor neurons of sporadic ALS patients suggesting a modulation of autophagy-related proteins in ALS (Sasaki, 2011). Interestingly, mice with nervous system-restricted knockout of the autophagy-essential genes *Atg5* or *Atg7* exhibited motor impairment, including impaired coordination and balance, reduced grip strength by 3–4 weeks of age, and axon degeneration (Hara et al., 2006; Komatsu et al., 2006, 2007). Nervous system-restricted knockout of the autophagy genes *Atg5* or *Atg9a* exhibited axon degeneration of central nervous system neurons (Nishiyama et al., 2007; Yamaguchi et al., 2017). Together, these observations suggest that autophagy dysfunction contributes to the etiology of ALS (Otomo et al., 2012; Ruffoli et al., 2015; Edens et al., 2016).

In SOD1^{G93A} mice, an ALS animal model, a defect of autophagosome fusion with lysosomes has been reported in the motor neuron cell body (Xie et al., 2015). Furthermore, electron microscopy analyses of motor neurons in SOD1^{G93A} mice and ALS patients have revealed autophagic vacuoles possibly arising from altered mitochondria (Hart et al., 1977; Wong et al., 1995). Increasing evidence suggests that defective mitochondrial function and impaired autophagy play roles in ALS etiology (Edens et al., 2016). Degenerated mitochondria are removed by a specific autophagic mechanism called mitophagy, which targets degenerated mitochondria (Youle and Narendra, 2011; Ding and Yin, 2012). Mitophagy is mediated by the following two major pathways. PTEN-induced putative kinase 1 (PINK1, *pink1*) is normally degraded rapidly, but it is stabilized at the surface of depolarized mitochondria, where it recruits and activates Parkin (a component of E3 ubiquitin ligase, *park2*; Matsuda et al., 2010; Narendra et al., 2010). Activated Parkin ubiquitinates outer mitochondrial membrane proteins including mitofusin 1/2 and voltage-dependent anion-selective channel protein 1 (VDAC1; Geisler et al., 2010). p62/SQSTM1 has a ubiquitin binding domain at the C-terminus that recognizes ubiquitinated mitochondrial proteins, accumulates to depolarized mitochondria, and recruits LC3 to mitochondria to induce mitophagy (Geisler et al., 2010; Okatsu et al., 2010). Phagophores are recruited by LC3 to form autophagosomes, and LC3 becomes lipidated to form LC3-II, which is a marker for autophagy levels (Kabeya et al., 2000; Klionsky et al., 2016). In a separate pathway, Nix and BCL2/adenovirus E18 19 kDa protein-interacting protein 3 (Bnip3) are also responsible for recruiting LC3 to the mitochondria to initiate mitophagy (Ding et al., 2010; Hanna et al., 2012). However, the functional level of mitophagy in ALS motor neurons is not well known.

Does mitophagy play a role in ALS etiology, and if so, where in motor neurons would mitophagy cause degeneration? Motor neuron degeneration is preceded by denervation of neuromuscular junctions (NMJs) in ALS patients and animal models, producing what is known as a dying-back neuropathy (Kennel et al., 1996; Siklos et al., 1996; Frey et al., 2000; Fischer et al., 2004; Dadon-Nachum et al., 2011). Furthermore, degenerated mitochondria have been detected at motor neuron presynaptic terminals of SOD1^{G93A} mice (Gould et al., 2006), suggesting that mitochondrial degeneration at the NMJs plays a role in this dying-back neuropathy. Interestingly, NMJ denervation cannot be prevented by blocking motor neuron apoptosis in ALS mice, suggesting that a mechanism other than apoptosis is responsible for the degeneration of axons and NMJs (Gould et al., 2006; Reyes et al., 2010). Therefore, degenerative changes in ALS motor neurons occur at the NMJ. However, the roles of autophagy and mitophagy at the NMJ have not been explored extensively. In this study, we performed ultrastructural analysis to investigate autophagosomes and mitophagosomes at NMJs. We also tested the role of mitophagy in the maintenance of NMJs by depleting both Pink1 and Parkin genes in mice and analyzing the NMJ innervation rate of the double knockout mice.

MATERIALS AND METHODS

Animals

Animal experiments were carried out in accordance with the animal care and use protocol approved by the Institutional Animal Care and Use Committee of University of Kansas Medical Center (KUMC) and in accordance with the Guidelines for the Care and Use of Laboratory Animals of KUMC. SOD1^{G93A} transgenic mice (JAX stock No. 004435, high copy number of transgene SOD1^{G93A}), *pink1* knockout mice (JAX stock No. 017946), and *park2* knockout mice (JAX stock No. 006582) were purchased from the Jackson Laboratory (Bar Harbor, Maine, USA) and maintained in the animal facility at KUMC until analysis. Three to five animals were analyzed per genotype per age, and the animal numbers of animals are reported in the appropriate figure legend or the Results Section.

SOD1^{G93A} mice on a C57BL/6J background survive longer than those on an SJL/J background (Heiman-Patterson et al., 2005; Wooley et al., 2005). With the C57Bl/6J background, disease onset, as determined by the limb tremor, occurs between P91-111 (Dobrowolny et al., 2005; Hayworth and Gonzalez-Lima, 2009). The survival rate starts to fall below 100% around P125-130 (Heiman-Patterson et al., 2005; Wooley et al., 2005), and the mean survival duration is between P142-161 (Dobrowolny et al., 2005; Heiman-Patterson et al., 2005; Wooley et al., 2005; Hayworth and Gonzalez-Lima, 2009). We analyzed the SOD1^{G93A} mice at three stages: presymptomatic stage (P57) (Wooley et al., 2005; Hayworth and Gonzalez-Lima, 2009), a stage with denervation (P85) (Dobrowolny et al., 2005), and a symptomatic stage (P140) (Dobrowolny et al., 2005; Hayworth and Gonzalez-Lima, 2009).

Transgene Copy Number Analysis

All male $SOD1^{G93A}$ mice produced at our institute by mating $SOD1^{G93A}$ mice with C57BL/6J female mice were analyzed for human SOD1 transgene copy number variation using the TaqMan qPCR genotype method as described in the Jackson Laboratory website (protocol name: Sod TgN Copy Number). Mice were excluded from analyses when they had low transgene copy numbers that showed more than a half cycle difference in qPCR (Leitner et al., 2009).

Electron Microscopy

The methods employed for electron microscopy have been described previously (Nishimune et al., 2004; Chen et al., 2011). In brief, diaphragm muscles and spinal cord at cervical level four were fixed in 5% glutaraldehyde, 4% paraformaldehyde in phosphate-buffered saline (PBS, pH 7.1, Delbucco's PBS), washed, refixed in 1% OsO_4, dehydrated, and embedded in resin. Ultrathin transverse sections were cut by skipping 30 μm minimum between sections for muscles and 100 μm minimum between sections for spinal cords to avoid analyzing the same NMJs or motor neurons. Sections were stained with lead citrate and uranyl acetate and systematically scanned using a transmission electron microscope. All profiles of NMJs and motor neuron cell bodies encountered in the micrographs were quantified. Motor neuron cell bodies were reconstructed by stitching multiple electron micrographs. The levels of electron micrographs in **Figures 3A–D** were adjusted to maximize the gray scale range of the images.

Autophagosomes were defined as double membrane structures that sequester a portion of the cytoplasm and/or organelles at various stages of degeneration from the cytoplasm, as described in the Guidelines for the Use and Interpretation of Assays for Monitoring Autophagy (3rd edition) (Klionsky et al., 2016). As described in these guidelines, autophagy can be both selective and nonselective for the autophagosome content. Mitophagosomes were defined as autophagosomes containing normal or degenerating mitochondria (Klionsky et al., 2016). Degenerated mitochondria were defined as double-membrane organelles with cristae, in which the cristae are not aligned regularly in more than 50% of the mitochondria profile. Mitochondria with large vacuole-like spaces within or between the cristae were recognized as degenerated mitochondria.

Immunohistochemistry and Image Analysis

The following antibodies were used: ATP synthase β subunit (A21351, Molecular Probes), choline acetyltransferase (AB144P, Millipore), Bnip3 (3769, Cell Signaling Tech.), LC3 (NB100-2220SS, Novus), neurofilament (2H3, DSHB, or N4142, Sigma), p62/SQSTM1 (2C11, Abnova), Pink1 (Abcam, ab75487), Parkin (sc-32282, Santa Cruz), SV2 (DSHB), Synaptophysin (18-0130, Zymed), Alexa Fluor 488 and 568 conjugated secondary antibodies, DAPI (4′,6-diamidino-2-phenylindole, dihydrochloride), and Alexa Fluor 594-conjugated α-bungarotoxin (Molecular Probes).

Immunohistochemical analyses have been described previously (Nishimune et al., 2004; Chen et al., 2011). Briefly, mice were fixed by transcardiac perfusion with 2% paraformaldehyde in PBS. Muscles and T12-L1 portions of the lumbar spinal cord were removed and post-fixed in 2% paraformaldehyde at room temperature, washed with PBS, and cryoprotected in 20% sucrose/PBS before being frozen in Optimal Cutting Temperature compound (Sakura, Torrance, CA), and sections were cut using a cryostat (transverse for lumbar spinal cords and both transverse and longitudinal for muscles). Muscles and lumbar spinal cords were sectioned at a thickness of 20 μm, blocked in PBS containing 2% bovine serum albumin (BSA), 2% normal goat serum, and 0.1–0.3% Triton X-100. For the goat anti-choline acetyltransferase antibody, BSA and normal goat serum were replaced with donkey serum for the blocking solution. Sections were then incubated with primary antibodies for 1 day at room temperature or 3 days at 4°C, washed with PBS, and incubated in appropriate secondary antibodies for 2 h at room temperature. Muscle sections were also incubated with Alexa Fluor 594-conjugated α-bungarotoxin. Lumbar spinal cord sections were also incubated with DAPI. Sections were then washed with PBS and mounted using VectaShield (Vector, Burlingame, CA).

Whole-mount immunohistochemical staining of diaphragm muscles was performed as follows. Muscles were fixed in 2% paraformaldehyde/PBS, washed in PBS, permeabilized in 0.5% Triton/0.1 M glycine/PBS overnight at 4°C, and blocked for 48 h at 4°C in 2% BSA/2% normal goat serum/0.5% Triton/PBS. Tissues were incubated with primary antibodies (anti-neurofilament and anti-SV2) for 48 h at 4°C, washed with PBS, and incubated with Alexa Fluor 488-conjugated anti-mouse IgG1 secondary antibody along with Alexa Fluor 594-conjungated α-bungarotoxin for 24 h at 4°C. After final washing, tissues were mounted in mounting medium (glycerol, PBS, *p*-phenylenediamine).

NMJs with LC3 Puncta

Immunohistochemical staining of LC3 showed puncta with strong signal intensity in presynaptic terminals of NMJ profiles. The NMJs were identified in transverse sections of diaphragm muscles by staining the nerve with anti-neurofilament and SV2 antibodies, and the acetylcholine receptors with Alexa Fluor 594-conjugated α-bungarotoxin. The number of NMJs with LC3 punctate signal overlapping with the nerve signal was quantified and described as the percentage of total NMJs counted.

Immunohistochemical Signal Intensity Quantification

The signal intensities of autophagy- and mitophagy-related proteins in motor neurons were measured using the method described in our previous publication (Chen et al., 2011). In brief, confocal images were obtained using Nikon A1R confocal microscope using PlanApo 20x, NA = 0.75 or PlanFluor 40x, NA = 1.30 lenses. The circumference of the motor neuron cell bodies in the lumbar spinal cord transverse sections was defined by the anti-choline acetyltransferase staining patterns. The average signal intensity within motor neurons was measured using the Show Region Statistics function in MetaMorph software ver. 7.0 (Molecular Devices).

The signal intensities of ATP synthase β subunit in the presynaptic terminals of NMJs were measured using the method

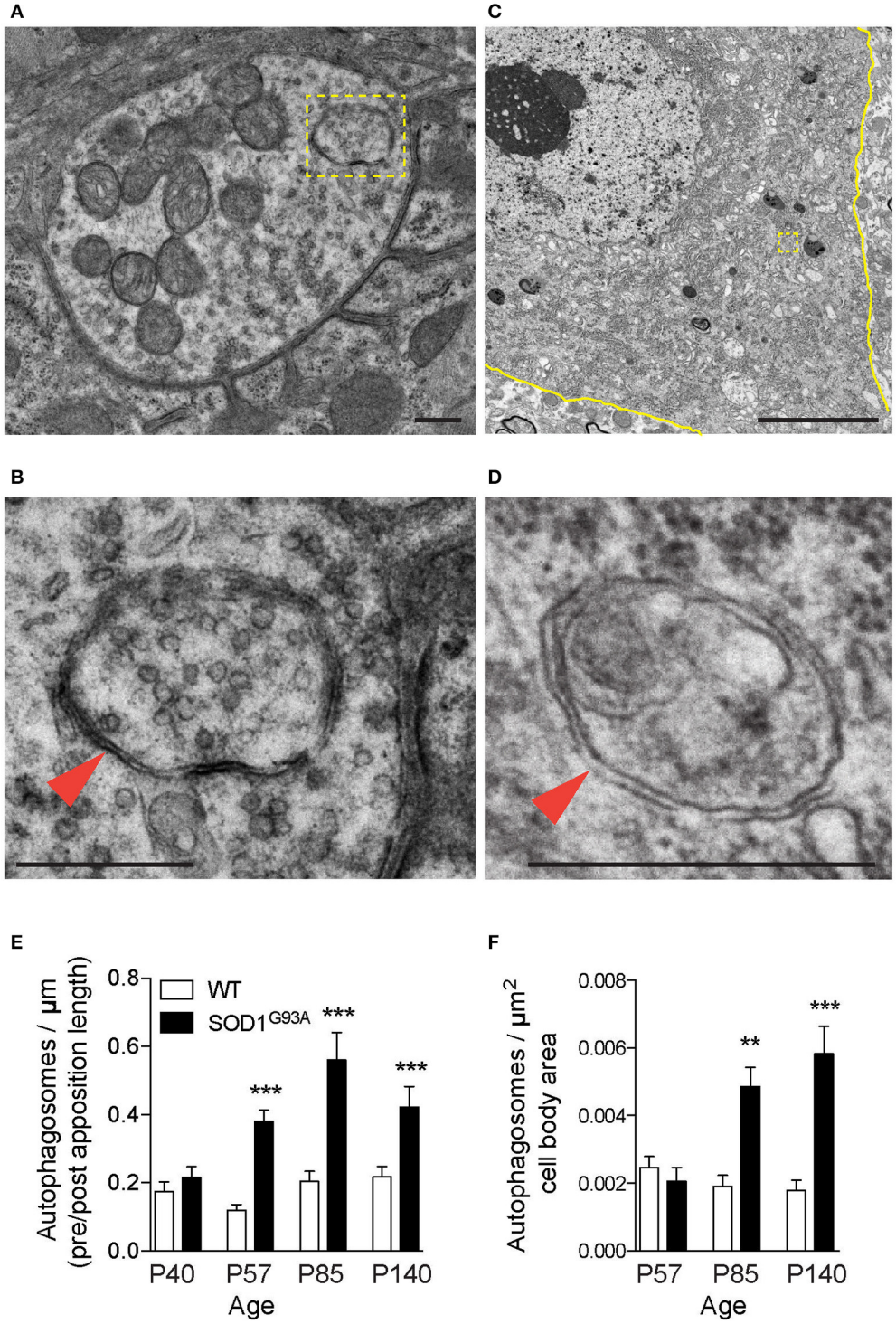

FIGURE 1 | Autophagosomes increase at NMJs in SOD1^{G93A} mice. Representative electron micrographs of autophagosomes in SOD1^{G93A} mice in **(A,B)** the presynaptic terminals of NMJs at P57 and **(C,D)** motor neuron cell bodies at P140. Higher-magnification images of **(A,C)** are shown in **(B,D)**. The colored marks on the micrographs are as follows: plasma membrane of motor neuron cell bodies (yellow) and autophagosomes (yellow boxes and orange arrowheads). Scale bars: **(A,B,D)** = 500 nm, **(C)** = 5 µm. Quantification revealed significantly increased numbers of autophagosomes in **(E)** the presynaptic terminals of NMJs and **(F)** motor neuron cell bodies of SOD1^{G93A} mice compared to wild-type mice (WT). The number of autophagosomes was normalized by pre- and postsynaptic apposition length for NMJs (synapse profile size) or the area of motor neuron cell bodies (µm^2). Graphs show mean ± SEM indicated by whiskers. Asterisks indicate significant differences by one-way ANOVA with Tukey's multiple comparison test (**$p < 0.01$, ***$p < 0.001$). NMJ quantifications are from n = five animals and 80–123 NMJs for each age and each genotype. Motor neuron cell body quantifications are from n = two animals for P57, three animals for P85, five animals for P140, and 40–73 cell bodies for each age and each genotype.

described above. The presynaptic terminals of NMJs in the muscle sections were defined by anti-neurofilament and anti-synaptophysin staining patterns. The average signal intensity within the presynaptic terminals of NMJs was measured using the Show Region Statistics function in MetaMorph software. The observer was blinded for the genotype.

P62 Aggregation

Motor neuron cell bodies were identified using ChAT staining to identify their location in the ventral horn of the lumbar spinal cord. The number of motor neurons that displayed large p62 positive structures was quantified and described as a percentage of total motor neurons counted.

NMJs with Axon Swelling

Adjacent to NMJs, axons have a constant diameter similar to the axon diameter that branches from the axon fascicle (Court et al., 2008; Samuel et al., 2012). Axons with abnormal enlargement near NMJs that is greater than the axon near the fascicle were qualitatively assessed, and the number of NMJs with abnormally enlarged axons were quantified as NMJs with axon swelling.

Fragmented NMJs

We used the analytical criteria described previously by Valdez et al. (Valdez et al., 2010; Taetzsch et al., 2017). Briefly, fragmented acetylcholine receptors were defined as acetylcholine receptor cluster with five or more islands and/or a segment of receptor cluster showing small and/or irregularly shaped receptor clusters. In young adult NMJs, acetylcholine receptor clusters show pretzel-like distribution patterns that are connected and not separated.

Denervation Analysis

The denervation analysis has been described previously (Chen et al., 2012). Briefly, muscle sections were stained using antibodies against nerves (anti-neurofilament and anti-SV2) and Alexa Fluor 594-conjugated α-bungarotoxin for acetylcholine receptors. Adult motor nerve terminals show perfect overlap with acetylcholine receptor clusters, which indicates fully innervated NMJs. NMJs were assessed for areas of the acetylcholine receptor clusters that were not occupied by nerves, whether in part or in full, as partially innervated NMJs or denervated NMJs. Quantifications are from four mice of each genotype and more than 98 NMJs per animal. The observer was blinded for the genotype.

Statistics

All statistics were performed using GraphPad Prism software version 6. Significance was assessed by un-paired *t*-test or one-way ANOVA with Tukey's multiple comparison test. The *p*- and *n*-values are reported in the text. All data in the graphs are shown as the mean ± S.E.M.

RESULTS

Increased Autophagosomes at ALS NMJs

Autophagy-related genes are mutated in ALS patients, which suggested altered autophagy function in motor neurons. Therefore, autophagosomes in motor neurons of $SOD1^{G93A}$ mice were analyzed using electron microscopy. The diaphragm was analyzed because ALS patients suffer from respiratory problems (Braun, 1987; Arnulf et al., 2000; Miller et al., 2009; Tateishi et al., 2010). NMJs in diaphragms of $SOD1^{G93A}$ mice revealed double-membraned autophagosomes containing synaptic vesicles and mitochondria at the nerve terminals (**Figures 1A,B**, **3A**, Supplementary Figure 1). The number of autophagosomes in NMJ profiles were significantly higher in the presynaptic terminals of $SOD1^{G93A}$ NMJs compared to those of age- and sex-matched wild-type mice beginning in the presymptomatic stage at postnatal day (P) 57, at stage with denervation (P85), and at symptomatic stage (P140) (**Figure 1E**; P40: $SOD1^{G93A}$, 0.22 ± 0.031 autophagosome/synapse profile size (μm), WT, 0.17 ± 0.029; P57: $SOD1^{G93A}$, 0.38 ± 0.033, WT, 0.12 ± 0.018; P85: $SOD1^{G93A}$, 0.56 ± 0.080, WT, 0.20 ± 0.030; P140: $SOD1^{G93A}$, 0.42 ± 0.061, WT, 0.22 ± 0.031; mean ± S.E.M.). Spinal cords of the same set of animals were dissected at cervical level four to analyze the motor neuron cell bodies of phrenic nerves innervating the diaphragms. Similar autophagosomes were detected in the cell bodies of motor neurons (**Figures 1C,D**). The number of autophagosomes in motor neuron cell bodies in $SOD1^{G93A}$ mice were similar at P57 but significantly higher at P85 and P140 compared to those of age- and sex-matched wild-type mice (**Figure 1F**; P57: $SOD1^{G93A}$, 0.0021 ± 0.00040 autophagosomes/μm^2, WT, 0.0025 ± 0.00034; P85: $SOD1^{G93A}$, 0.0049 ± 0.00057, WT, 0.0019 ± 0.00033; P140: $SOD1^{G93A}$, 0.0058 ± 0.00081, WT, 0.0018 ± 0.00031). These results indicate that autophagosomes accumulate in the presynaptic terminals of NMJs earlier than in motor neuron cell bodies in $SOD1^{G93A}$ mice.

Increased Levels of Autophagosome Marker at ALS NMJs

To validate the autophagosome accumulation in the presynaptic terminals of NMJs detected by electron microscopy, immunohistochemistry was used to detect an autophagosome marker, LC3 (microtubule-associated protein 1 light chain 3; Kabeya et al., 2000). LC3 proteins accumulated as large puncta in NMJ presynaptic terminals in diaphragms of $SOD1^{G93A}$ mice (**Figure 2A** lower panels). However, these LC3 puncta were rarely detected in the presynaptic terminals of wild-type NMJs (**Figure 2A** upper panels). The proportion of NMJs bearing LC3 puncta in the presynaptic terminal was significantly higher in $SOD1^{G93A}$ mice (23.9 ± 1.9%) than in wild-type mice (10.5 ± 2.2%, **Figure 2B**). These results suggest accumulation of autophagosomes in the NMJ presynaptic terminals of $SOD1^{G93A}$ mice and are consistent with the electron microscopic quantifications.

Mitochondria Degeneration and Mitophagy at ALS NMJs

The early increase in autophagosomes in the presynaptic terminals of NMJs suggested that the initiation of NMJ degeneration occurred during the presymptomatic stage in $SOD1^{G93A}$ mice. To further investigate the degeneration in

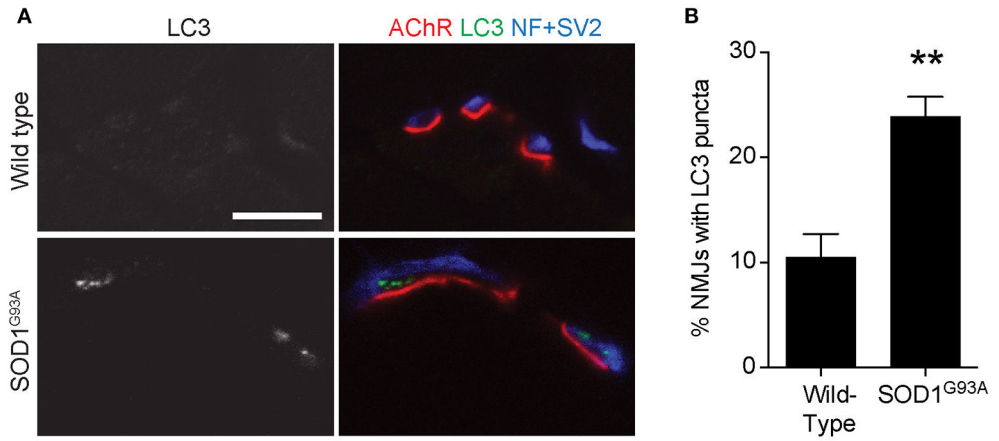

FIGURE 2 | Accumulation of an autophagosome marker in the presynaptic terminals of NMJs of SOD1^{G93A} mice **(A)** Representative confocal micrographs of immunohistochemistry showing accumulation of the autophagosome marker LC3 (grayscale in left panels, green in right panels) in presynaptic terminals of diaphragm NMJs in SOD1^{G93A} mice at P120, but not at NMJs of wild-type mice at P140. Nerves were stained using anti-neurofilament and anti-SV2 antibodies (blue), and postsynaptic acetylcholine receptors were labeled with Alexa 594-conjugated α-bungarotoxin (red). In these cross-section images of NMJs, presynaptic terminals are above the bungarotoxin signal, and postsynaptic myotubes are below the bungarotoxin signal. Scale bar: 10 μm. **(B)** The number of NMJs with LC3 puncta was significantly higher in SOD1^{G93A} mice than in wild-type mice. Quantifications are from n = three animals and 268–305 NMJs each genotype in confocal images. Asterisks indicate a significant difference by un-paired t-test (**$p < 0.01$).

ALS motor neurons, the electron micrographs of NMJs and motor neuron cell bodies used in **Figure 1** were analyzed for mitochondria. NMJs in diaphragms of SOD1^{G93A} mice contained significantly higher number of degenerated mitochondria in the presynaptic terminals that were still innervating endplates. The degenerated mitochondria had irregular cristae spacing, large vacuoles or degenerated cristae inside a double membrane structure, which were not detected in normal mitochondria in the NMJ presynaptic terminals of age-and sex-matched wild-type mice (**Figures 3A,B**). The representative example SOD1^{G93A} NMJ contained an autophagosome in the presynaptic terminal, but the autophagosome did not contain any degenerated mitochondria. The numbers of degenerated mitochondria at NMJs were 3–15 times higher in SOD1^{G93A} mice than in that of wild-type mice at the presymptomatic stage P57 and remained higher at P85 and P140 [**Figure 3E**; P40: SOD1^{G93A}, 0.13 ± 0.038 mitochondria/synapse profile size (μm), WT, 0.047 ± 0.013; P57: SOD1^{G93A}, 0.32 ± 0.034, WT, 0.021 ± 0.0069; P85: SOD1^{G93A}, 0.36 ± 0.045, WT, 0.042 ± 0.012; P140: SOD1^{G93A}, 0.45 ± 0.052, WT, 0.085 ± 0.022]. In the same sets of animals, the numbers of degenerated mitochondria in the cell bodies of motor neurons were three to four times greater in SOD1^{G93A} mice than in wild-type mice among from P57 to P140 (**Figure 3F**; P57: SOD1^{G93A}, 0.05814 ± 0.0041 degenerated mitochondria/μm^2, WT, 0.020 ± 0.0017; P85: SOD1^{G93A}, 0.11 ± 0.0087, WT, 0.029 ± 0.0028; P140: SOD1^{G93A}, 0.15 ± 0.0069, WT, 0.041 ± 0.0026).

As we have shown previously, the number of autophagosomes increased significantly in ALS motor neurons and NMJs; however, the degenerated mitochondria do not seem to be degraded efficiently by mitophagy in SOD1^{G93A} mice. Mitophagy mediated degradation of damaged mitochondria has been shown to occur locally in distal axons (Ashrafi et al., 2014). Therefore, we searched for mitophagosomes in the electron micrographs and identified clear examples of mitophagy in the NMJ presynaptic terminals of wild-type mice and SOD1^{G93A} mice (**Figures 3C,D**). A representative micrograph of a wild-type NMJ shows synaptic vesicles accumulating near the presynaptic membrane and an active zone, and dark synaptic cleft and postsynaptic junctional folds are visible (**Figure 3C**). A mitophagosome was identified near the presynaptic membrane and was surrounded by synaptic vesicles (an arrowhead in **Figure 3C**). A representative micrograph of a SOD1^{G93A} NMJ shows a phagophore surrounding a degenerated mitochondrion with irregular cristae (arrowheads in **Figure 3D**). Degenerated mitochondria and synaptic vesicles are visible nearby. Therefore, the number of mitophagosome was analyzed in the presynaptic terminals of NMJs and motor neuron cell bodies. However, mitophagosome number in NMJ was not different between SOD1^{G93A} mice and age- and sex-matched wild-type mice among all the stages analyzed, between P40–140 (**Figure 3G**; P40: SOD1^{G93A}, 0.0098 ± 0.0047 mitophagosome / synapse profile size (μm), WT, 0.012 ± 0.0062; P57: SOD1^{G93A}, 0.0044 ± 0.0044, WT, 0.0016 ± 0.0016; P85: SOD1^{G93A}, 0.010 ± 0.0049, WT, 0.0097 ± 0.0047; P140: SOD1^{G93A}, 0.015 ± 0.0066, WT, 0.0084 ± 0.0050). These results suggest insufficient function of mitophagy in the presynaptic terminals of ALS NMJs despite the accumulation of degenerated mitochondria. Meanwhile, in motor neuron cell bodies, the number of mitophagosomes was higher in SOD1^{G93A} mice than in wild-type mice at P85 (**Figure 3H**; P57: SOD1^{G93A}, 0.00037 ± 0.00016 mitophagosomes/μm^2, WT, 0.00022 ± 0.000097; P85: SOD1^{G93A}, 0.00090 ± 0.00022, WT, 0.00021 ± 0.000080; P140: SOD1^{G93A}, 0.00091 ± 0.00026, WT, 0.00028 ± 0.000095). However, there were significantly fewer mitophagosomes than

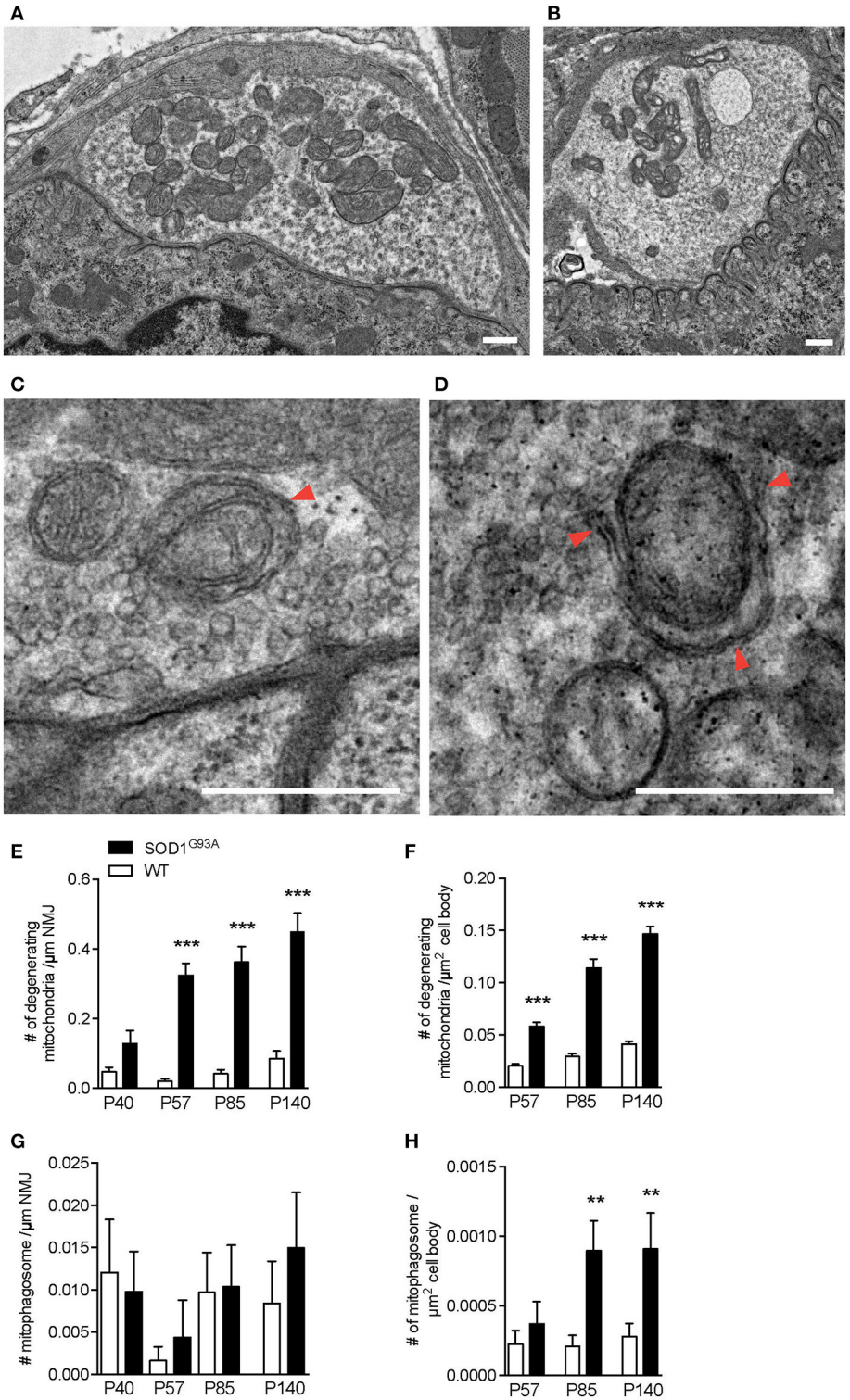

FIGURE 3 | Numbers of degenerating mitochondria in the presynaptic terminals of NMJs and in motor neurons. Representative electron micrographs of **(A)** a NMJ in wild-type mouse, **(B)** degenerated mitochondria in a NMJ of a $SOD1^{G93A}$ mouse, **(C)** mitophagosomes (arrowhead) near the presynaptic membrane in a NMJ of wild-type mouse, and **(D)** a phagophore (arrowheads) around degenerated mitochondria in a NMJ of a $SOD1^{G93A}$ mouse. Scale bar: 500 nm. Quantification of electron micrographs revealed significantly increased numbers of degenerated mitochondria in **(E)** NMJs and **(F)** motor neuron cell bodies and of mitophagosomes in **(G)** NMJs ($p = 0.6295$) and **(H)** motor neuron cell bodies of $SOD1^{G93A}$ mice (black bar) compared to age- and sex-matched wild-type mice (white bar). Graphs show mean ± SEM. Asterisks indicate significant differences ($^{**}p < 0.005$, $^{***}p < 0.0001$) between $SOD1^{G93A}$ mice and wild-type mice at each age by one-way ANOVA with Tukey's multiple comparison test. Numbers of animals, NMJs, and motor neuron cell bodies are the same as in **Figure 1**.

autophagosomes in motor neuron cell bodies of SOD1^{G93A} mice (compare **Figures 1F**, **3H**). In addition, the numbers of mitophagosomes increased more slowly than the increase in degenerated mitochondria in motor neuron cell bodies (compare **Figures 3F,H**). Together, these results suggest decreased function of mitophagy in SOD1^{G93A} mice, especially at NMJs, and this may lead to the accumulation of degenerated mitochondria in the presynaptic terminals of NMJs.

Reduction in Mitophagy-Related Proteins in ALS Motor Neurons

p62/Sequestosome 1 (SQSTM1) is mutated in ALS patients (Fecto et al., 2011; Hirano et al., 2013; Teyssou et al., 2013). p62/SQSTM1 has a ubiquitin binding domain at the C-terminus and accumulates to depolarized and ubiquitinated mitochondria (Geisler et al., 2010; Okatsu et al., 2010). p62/SQSTM1 recruits LC3 to mitochondria to induce mitophagy (Geisler et al., 2010). Pink1/Parkin-mediated mitophagy is dependent on p62/SQSTM1 and VDAC1 (Geisler et al., 2010). Interestingly, a large number of p62 aggregated structure was observed among motor neurons and non-motor neuron cells in the gray matter of lumbar spinal cord of SOD1^{G93A} mice at P85, which was hardly detected in wild-type age- and sex-matched control mice (**Figure 4A**). This feature was more prevalent in SOD1^{G93A} mice at P140 compared to that of P85 (compare lower panels in **Figures 4A,C**).

First, we examined the number of motor neuron cell bodies of the lumbar spinal cord that displayed large p62/SQSTM1 aggregated structures. At P85, 20.5 ± 4.6% of motor neuron cell bodies of SOD1^{G93A} mice contained p62/SQSTM1 aggregated structures compared to zero observed in wild-type control mice (**Figures 4A,B**). At P140, 10.4 ± 0.8% of motor neuron cell bodies in SOD1^{G93A} mice displayed large p62/SQSTM1 aggregated structures compared to 0.5 ± 0.5% of that in wild-type control mice (**Figures 4C,D**).

Next, we used immunohistochemistry to quantify the expression level of p62/SQSTM1 specifically in motor neuron cell bodies without the contamination from other cells in the gray matter. Importantly, the expression level of p62/SQSTM1 in motor neuron cell bodies estimated by average signal intensity was 10.3% lower at P85 and 19.7% lower at P140 in the lumbar spinal cord of SOD1^{G93A} mice compared to that of wild-type control mice (**Figures 4E–H,** P85: SOD1^{G93A}, 4,936 ± 130; WT, 5,501 ± 133; P140: SOD1^{G93A}, 4,415 ± 119; WT, 5,496 ± 185; arbitrary unit). The decreased protein level of p62/SQSTM1 suggested a reduction of autophagy and/or mitophagy function in SOD1^{G93A} motor neurons.

To investigate whether mitophagy function is altered in motor neurons of SOD1^{G93A} mice, expression levels of mitophagy-related proteins were analyzed using immunohistochemistry to specifically detect protein levels in motor neurons. Bnip3 (BCL2 and adenovirus E1B 19-kDa-interacting protein 3) forms a homodimer and is integrated into the mitochondrial outer membrane by C-terminal transmembrane domains. The LC3-interacting region in the N-terminal domain interacts with LC3-II at the phagophores to induce mitophagy (Springer and MacLeod, 2016). The expression level of Bnip3 in motor neuron cell bodies was 29% lower at P85 and 52% lower at P140 in lumbar spinal cords in SOD1^{G93A} mice compared to that of age- and sex-matched wild-type control mice at P85 and P140 (**Figure 5**; P85: SOD1^{G93A}, 4,343 ± 140; WT, 6,151 ± 124; P140: SOD1^{G93A}, 2,335 ± 144; WT, 4,864 ± 301; arbitrary unit).

Mitochondrial protein PTEN-induced putative kinase 1 (Pink1) is degraded rapidly in normal mitochondria, but is stabilized at the surface of depolarized mitochondria, where it recruits and activates Parkin (Matsuda et al., 2010; Narendra et al., 2010). Activated Parkin ubiquitinates mitochondrial outer membrane proteins, which recruit LC3 to initiate mitophagy (Geisler et al., 2010). Pink1 levels were significantly lower in motor neuron cell bodies of lumbar spinal cord of SOD1^{G93A} mice at P85 and P140 (18 and 19% lower, respectively) compared to that of age- and sex-matched wild-type control mice (**Figures 6A–D**; P85: SOD1^{G93A}, 10,013 ± 447; WT, 12,199 ± 407; P140: SOD1^{G93A}, 9,241 ± 390; WT, 11,385± 395; arbitrary unit). Furthermore, Parkin signal intensity in motor neuron cell bodies was significantly lower in motor neuron cell bodies of lumbar spinal cords of SOD1^{G93A} mice at P85 and P140 (14 and 7% lower, respectively) compared to wild-type control mice (**Figures 6E–H**; P85: SOD1^{G93A}, 6,851 ± 171; WT, 7,988 ± 239; P140: SOD1^{G93A}, 3,698 ± 76; WT, 4,004 ± 61; arbitrary unit). These protein-level analyses also suggested a reduction of mitophagy function in motor neurons of SOD1^{G93A} mice.

Pink1/Parkin Double Knockout Mice Exhibit Severe Degeneration of NMJs in Young Adults

The potential reduction of mitophagy function may lead to accumulation of degenerated mitochondria at NMJs and dying-back neuropathy of ALS motor neurons in SOD1^{G93A} mice. We have identified that the levels of p62/SQSTM1, Bnip3, Pink1, and Parkin are significantly reduced in motor neuron cell bodies of SOD1^{G93A} mice (**Figures 4–6**). p62/SQSTM1 is necessary for Pink1/Parkin-mediated mitophagy (Geisler et al., 2010). Therefore, double knockout mice (DKO) mice for Pink1 (*pink1*) and Parkin (*park2*) were analyzed to investigate the role of mitophagy in NMJ maintenance.

The loss of Pink1 and Parkin caused significant degeneration of NMJs in young adult mice. Diaphragm NMJs were analyzed at ages between P85 and P110 using whole-mount immunohistochemistry to minimize potential damage to NMJs due to sectioning. We have not detected premature death of DKO mice for Pink1 and Parkin to the age of 3.5 months. Both presynaptic nerve terminals and postsynaptic specialization showed abnormalities. Axons adjacent to NMJs showed swelling at a significantly higher rate in the DKO mice (22.5 ± 4.5%) than in age matched wild-type mice (4.9 ± 1.7%, **Figures 7A,B**). Postsynaptic acetylcholine receptors are clustered in a pretzel-like morphology that are mostly connected to each other in the muscles of wild-type mice. However, NMJs in the DKO mice showed fragmentation of acetylcholine receptor clusters at a significantly higher rate (16.7 ± 1.8%) than in wild-type NMJs (4.9 ± 1.7%, **Figures 7A,C**). Importantly, the DKO

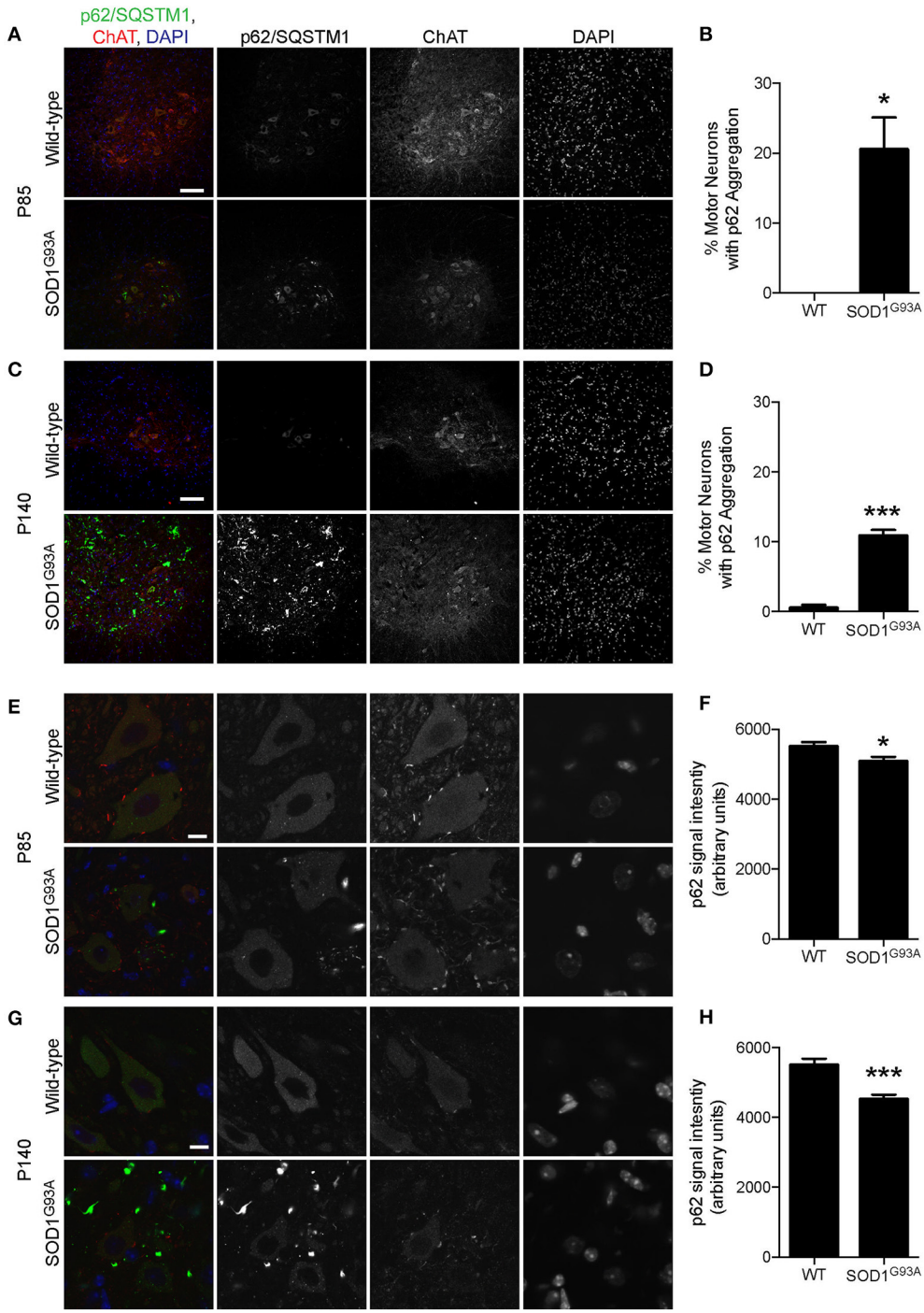

FIGURE 4 | Aggregation of p62/SQSTM1 in a subpopulation of motor neurons despite lower p62 levels in SOD1^{G93A} mice. **(A–D)** Aggregation of p62/SQSTM1 was observed in a greater percentage of motor neuron cell bodes of the lumbar spinal cord of SOD1^{G93A} mice compared with age- and sex-matched wild-type controls. Representative confocal micrographs of immunohistochemistry for p62/SQSTM1, choline acetyltransferase (ChAT), and DAPI are shown for **(A)** P85 and **(C)** P140 mice. Quantification of the percentage of motor neuron cell bodies with p62/SQSTM1 aggregates is shown for **(B)** P85 and **(C)** P140 mice and includes 46–86 motor neurons at P85 and 45–101 motor neurons at P140 from n = three animals for each genotype. **(E–H)** Decreased intensity of p62/SQSTM1 was observed in motor neuron cell bodes of the lumbar spinal cord of SOD1^{G93A} mice compared with age- and sex-matched wild-type controls. Representative confocal micrographs of immunohistochemistry for p62/SQSTM1, choline acetyltransferase (ChAT), and DAPI are shown for **(E)** P85 and **(G)** P140 mice. Quantification of average signal intensity shows decreased intensity of p62/SQSTM1 in motor neuron cell bodies for **(F)** P85 and for **(H)** P140 mice. Quantification for signal intensity are from n = three animals include 47–56 motor neurons for P85 **(F)** and 45–50 motor neurons for P140 **(H)** mice for each genotype. Graphs show mean ± SEM. Asterisks indicate significant differences as analyzed by un-paired t-test (*$p < 0.05$, ***$p < 0.001$) **(B,D,F,H)**. Different confocal scanning conditions were used between the two ages; therefore, the signal intensity arbitrary units should not be compared between ages. Scale bar: 100 μm **(A,C)** and 10 μm **(E,G)**.

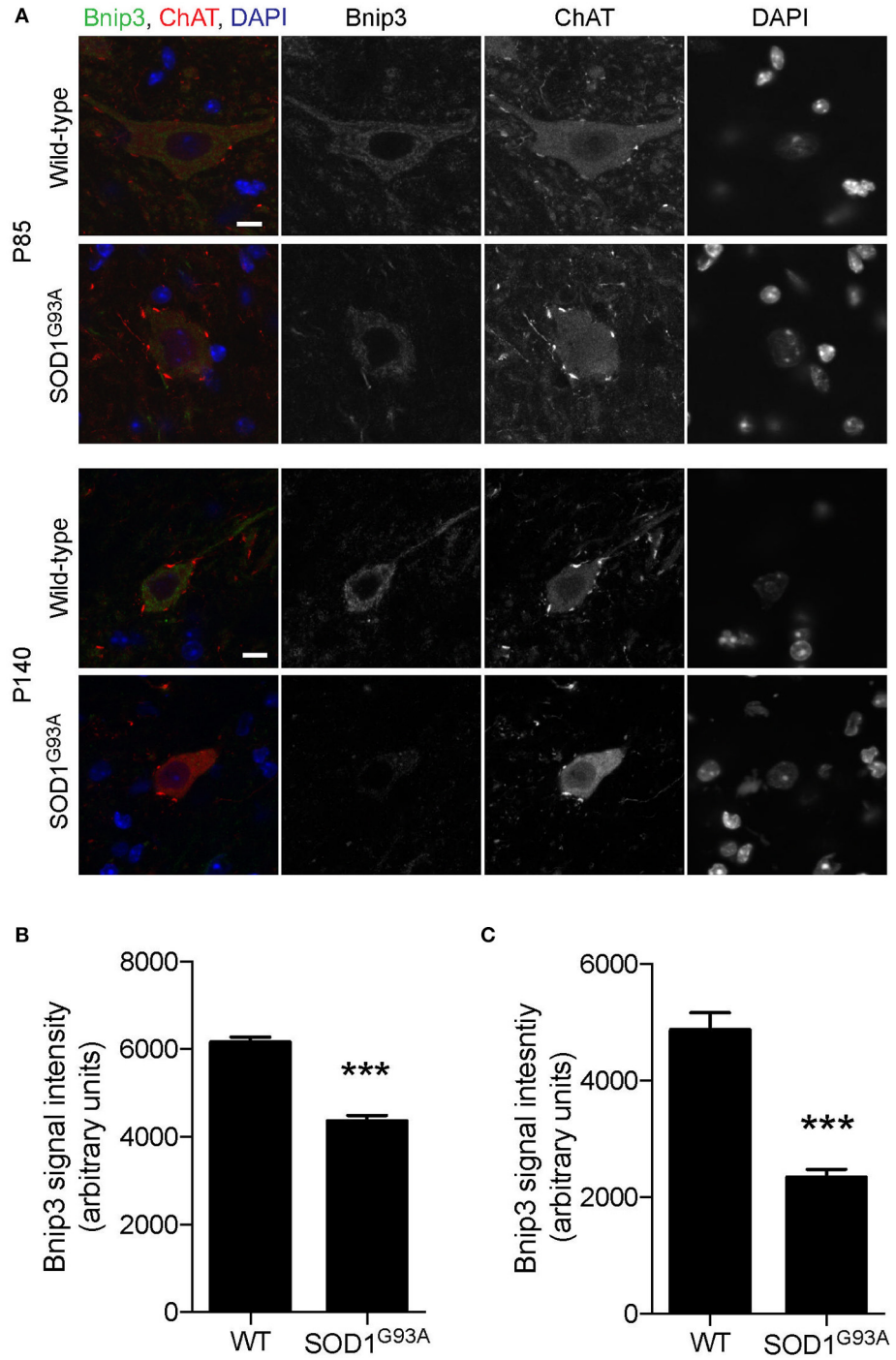

FIGURE 5 | Decreased expression of Bnip3 in motor neurons in SOD1^{G93A} mice. Bnip3 protein expression levels were significantly reduced in motor neurons in lumbar spinal cords of SOD1^{G93A} mice compared to age- and sex-matched wild-type controls. Representative confocal micrographs of immunohistochemistry for Bnip3, choline acetyltransferase (ChAT), and DAPI are shown for P85 and P140 mice **(A)**. Quantification for signal intensity is shown for **(B)** P85 and **(C)** P140 mice. Quantification for signal intensity are from n = three animals include 42–56 motor neurons for P85 and 31–34 motor neurons for P140 mice for each genotype. Graphs show mean ± SEM. Asterisks indicate significant differences as analyzed by un-paired t-test (***$p < 0.001$). Different confocal scanning conditions were used between the two ages; therefore, the signal intensity arbitrary units should not be compared between ages. Scale bar: 10 μm.

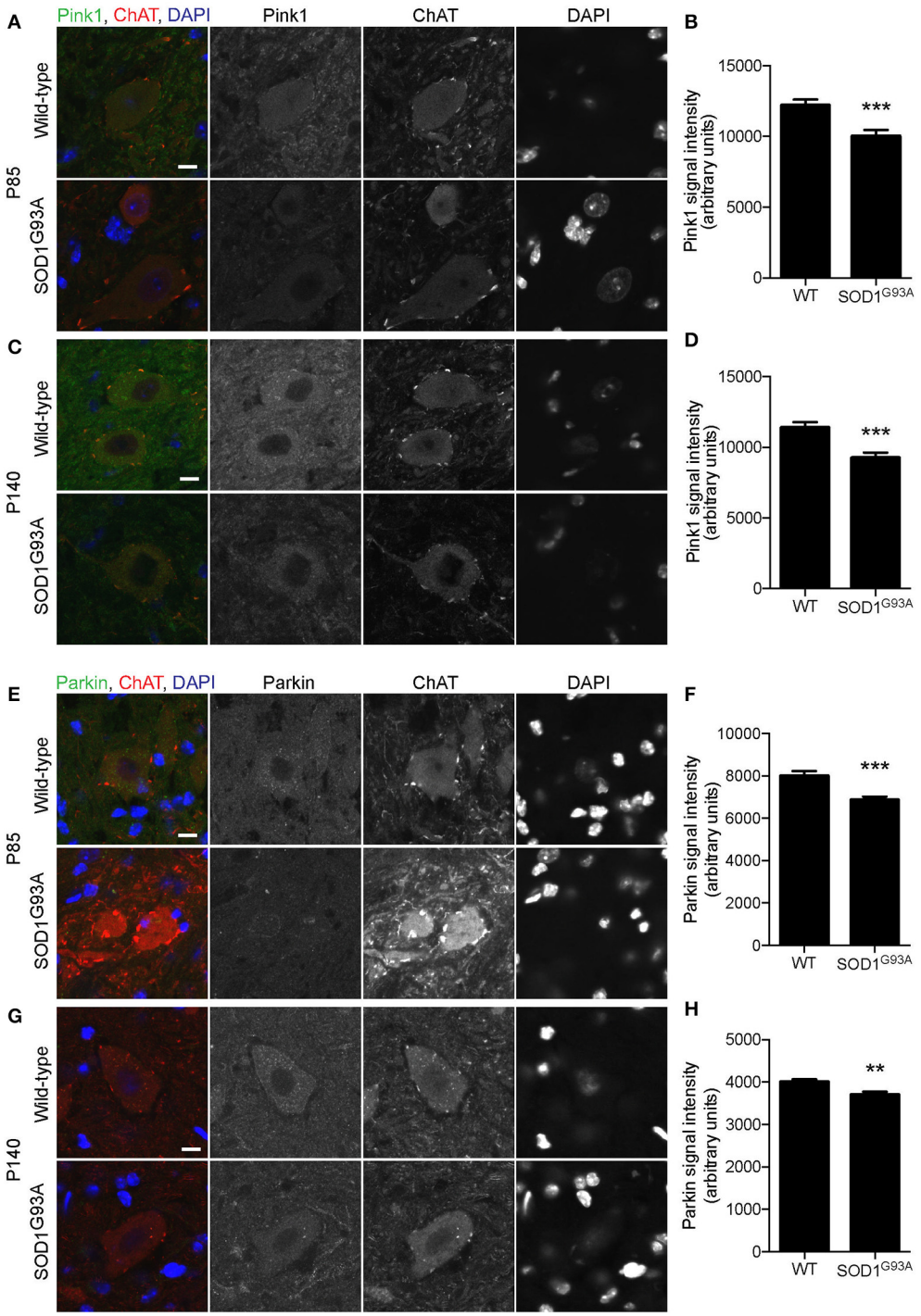

FIGURE 6 | Decreased expression of mitophagy-related proteins in motor neurons of SOD1^{G93A} mice. Pink1 and Parkin protein expression levels were significantly reduced in motor neurons in lumbar spinal cords of SOD1^{G93A} mice compared to age- and sex-matched wild-type controls. **(A–D)** Representative confocal micrographs of immunohistochemistry for Pink1, choline acetyltransferase (ChAT), and DAPI are shown for **(A)** P85 and **(C)** P140 mice. Quantification for signal intensity is shown for Pink1 at P85 **(B)** and P140 **(D)** mice. Quantification for signal intensity are from n = three animals include 37–43 motor neurons for P85 and 41–50 motor neurons for P140 mice for each genotype. **(E–H)** Representative confocal micrographs of immunohistochemistry for Parkin, choline acetyltransferase (ChAT), and DAPI are shown for **(E)** P85 and **(G)** P140 mice. Quantification for signal intensity is shown for Parkin at P85 **(F)** and P140 **(H)** mice. Quantification for signal intensity are from n = three animals include 32–38 motor neurons for P85 and 28–43 motor neurons for P140 for each genotype. Graphs show mean ± SEM. Asterisks indicate significant differences as analyzed by un-paired t-test (**$p < 0.01$, ***$p < 0.001$) **(B,D,F,H)**. Different confocal scanning conditions were used between the two ages; therefore, the signal intensity arbitrary units should not be compared between ages. Scale bar: 10 μm.

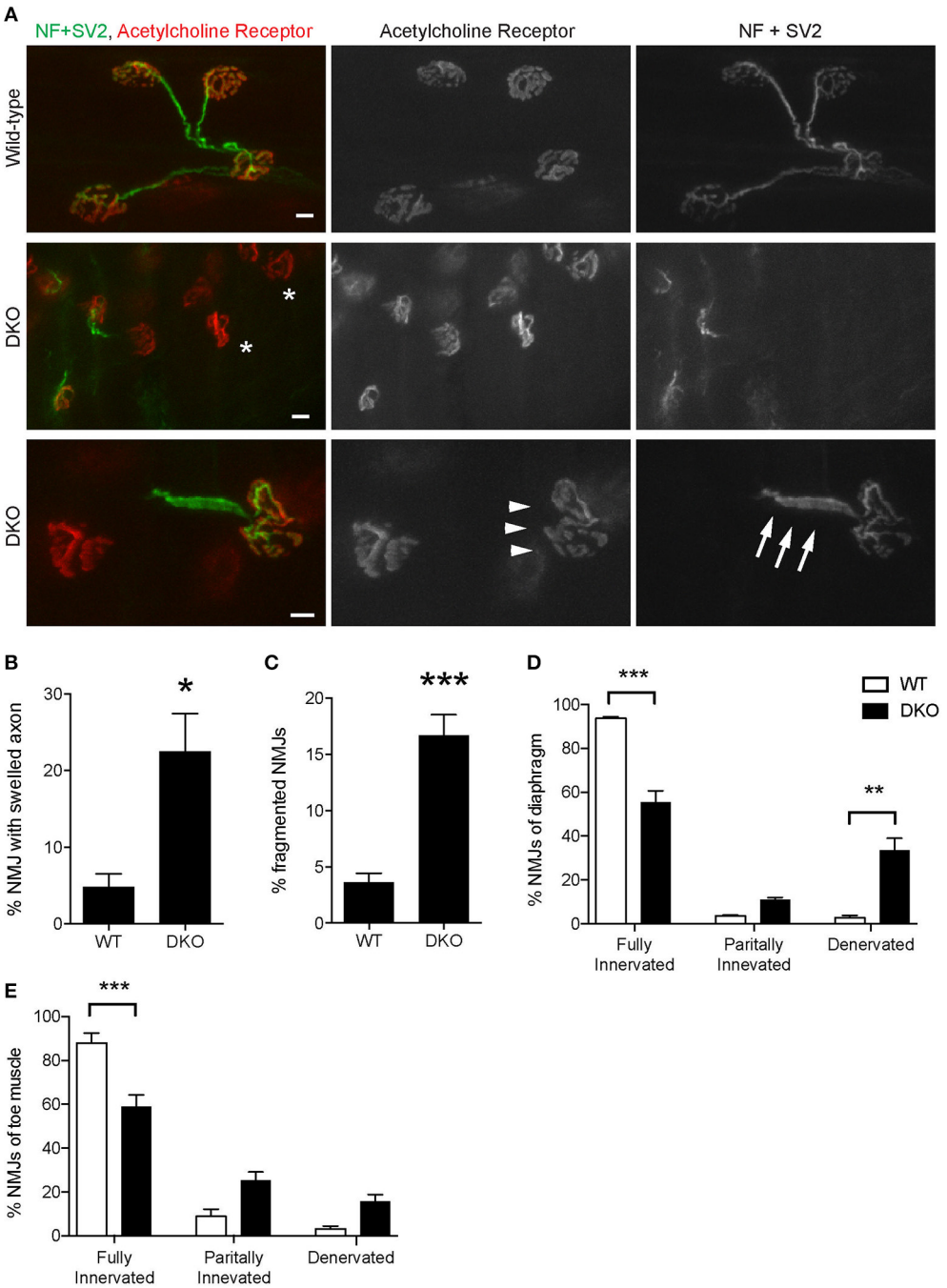

FIGURE 7 | Pink1/Parkin DKO mice have denervated NMJs. **(A)** Representative confocal images of individual NMJs in diaphragms of age-matched wild-type control mouse (top row) and Pink1/Parkin DKO mouse (middle and bottom rows). DKO diaphragm showed significantly increased NMJ denervation (white asterisks). NMJs of DKO mice showed axon swelling (white arrows) and fragmentation of acetylcholine receptor cluster (white arrowheads) at ages between P85 and P110. NMJs of wild-type mice of the same age did not show these phenotypes. Quantifications of **(B)** NMJ with axon swelling and **(C)** fragmented NMJs are from $n = $ four animals (3 male, 1 female) for each genotype, and **(B)** 45–161 NMJs and **(C)** 58–206 NMJs were counted for each animal. NMJ denervation rate of DKO mice was compared to wild-type mice in diaphragm **(D)** and toe **(E)** muscles. Quantification data are presented as a percent of NMJs that are either fully innervated, partially innervated, or denervated. Quantifications are from $n = $ four animals for each genotype and **(D)** 175–407 NMJs and **(E)** 98–212 NMJs were counted for each animal. Graphs show mean ± SEM. Asterisks indicate significant differences as analyzed by un-paired *t*-test **(C,D)** and one-way ANOVA with Tukey's multiple comparison test **(D,E)** (*$p < 0.05$, **$p < 0.01$, ***$p < 0.001$). Scale bar: 10 μm.

mice had significantly lower numbers of fully innervated NMJs in diaphragm (55.6 ± 5.1%) than wild-type mice (93.7 ± 0.8%, **Figure 7D**). Denervated NMJs were significantly more common in the DKO mice (33.5 ± 5.5%) but were rarely detected in wild-type mice (2.8 ± 1.0%). Furthermore, the toe muscle of DKO mice showed similar NMJ innervation rate and had significantly lower numbers of fully innervated NMJs (58.9 ± 5.5%) than wild-type mice (88.0 ± 4.5%, **Figure 7E**). The increased NMJ denervation is less likely to be caused by muscle fiber degeneration and regeneration because the muscle fiber cross-sectional area was not significantly different between the DKO mice and wild-type control mice (DKO, 7,146 ± 309 μm^2; WT 6,225 ± 369 μm^2), and central nuclei was not observed in muscle fibers. These data demonstrate that mitophagy is essential for the maintenance of NMJ innervation.

Finally, we asked whether reduced mitophagy cause accumulation of mitochondria at motor nerve terminals. Immunohistochemical signal intensity of the ATP synthase β subunit was measured at NMJ presynaptic terminals. The ATP synthase signal intensity was significantly higher in the DKO mice than in wild-type mice (DKO, 729.3 ± 10.86; WT, 499.8 ± 12.54; arbitrary unit, **Figure 8**). These results suggest that a lack of one of the mitophagy pathways, here, Pink1 and Parkin, results in the accumulation of mitochondria at nerve terminals. The reduced mitophagy function and the accumulation of degenerated mitochondria is likely to cause NMJ denervation in ALS model $SOD1^{G93A}$ mice.

DISCUSSION

Ultrastructural analysis revealed clear examples of mitophagy in the presynaptic terminals of NMJs of wild-type mice and $SOD1^{G93A}$ mice (**Figure 3**). To our knowledge, this report is the first to show electron micrographs of mitophagosomes at mammalian NMJs. We identified significant increases in the number of autophagosomes and degenerated mitochondria in the NMJ presynaptic terminals of $SOD1^{G93A}$ mice compared to wild-type controls. The accumulation of degenerated mitochondria at NMJs is consistent with that observed at ALS patient NMJs (Siklos et al., 1996). However, mitophagosome number did not increase significantly, and the expression levels of mitophagy-related proteins, p62/SQSTM1, Bnip3, Pink1, and Parkin were significantly lower in $SOD1^{G93A}$ mice than in aged- and sex-matched wild-type controls. These results suggest a reduced function of mitophagy in the NMJ presynaptic terminals of $SOD1^{G93A}$ mice, which may lead to accumulation of degenerated mitochondria, NMJ denervation, and dying back neuropathy. Consistent with this hypothesis, Pink1 and Parkin DKO mice exhibited NMJ denervation at young adult ages and increased immunohistochemical signal intensity of the ATP synthase β subunit, which suggested an accumulation of mitochondria in the NMJ presynaptic terminals. To our knowledge, this study is the first report to test the effect of deleting both Pink1 and Parkin in the maintenance of NMJs. Overexpression of human wild-type SOD1 in mice has been reported to cause mitochondrial vacuolization and axonopathy around 1 year of age (Jaarsma et al., 2000). We have not analyzed the phenotype of the transgenic mouse overexpressing wild-type SOD1 to compare against that of $SOD1^{G93A}$ mice, which is a limitation of the current study.

We have detected both autophagosomes and mitophagosomes in the presynaptic terminals of wild-type NMJs by using electron microscopy. This observation is consistent with a previous report that describes mitophagy in the distal axons of hippocampal neurons (Ashrafi et al., 2014). These functions of autophagy and mitophagy at the distal end of axons allow local mechanisms to preserve the function of nerve terminals without relying on the mechanisms in the cell body, which is a long distance away. However, the mitophagy function seems to show defects in presynaptic terminals of ALS NMJs and is not capable of depleting the accumulation of degenerated mitochondria. This reduced mitophagy function may be related to the lysosomal deficits that have been identified in $SOD1^{G93A}$ mice (Xie et al., 2015).

As a potential mechanism of the mitophagy defect, we revealed the down regulation of p62 in motor neurons of $SOD1^{G93A}$ mice. However, a previous publication reported progressive accumulation of p62 in lumbar spinal cord of $SOD1^{G93A}$ mice at P125 (Gal et al., 2007). We also observed increased level of p62 aggregates in the lumbar spinal cords of $SOD1^{G93A}$ mice at P85 and P140, but the increased signal derived mostly from cells other than motor neurons (**Figure 4**). The discrepancy between the two studies seems to stem from the difference in the antibodies used to detect p62/SQSTM1 protein. The specificity of the anti-p62/SQSTM1 antibody used in our study was verified using knockout mouse tissue in our previously published study (Yang et al., 2016). The antibody used by Gal et al. (Santa Cruz, SQSTM1 antibody, sc-10117) has not been verified using knockout animals and recognizes a second non-specific band in the western blot analysis, based on the information on the manufacturer's website. This antibody has been discontinued; therefore, the two antibodies could not be compared at this time.

As dysregulation autophagy has been shown in spinal cords of ALS patients, autophagy modulation has been explored as a potential treatment for ALS motor neuron dysfunction. Results of studies stimulating autophagy have been somewhat conflicting. Enhancing autophagy using rapamycin to inhibit mammalian target of rapamycin (mTOR) was shown to worsen ALS related symptomology, decrease life span, and result in a more severe mitochondrial dysfunction, possibly activating apoptosis, in $SOD1^{G93A}$ mice (Zhang et al., 2011). While another study showed that rapamycin treatment of $SOD1^{G93A}$ mice had no effect on survival, but did increase survival of $SOD1^{G93A}$ mice devoid of mature lymphocytes, indicating a delicate interplay with the immune system (Staats et al., 2013). Rapamycin also worsens ALS symptomology in valosin-containing protein mutant mice (Ching and Weihl, 2013), and had no effect on SOD1 H46R/H48Q mutant mice (Bhattacharya et al., 2012), both

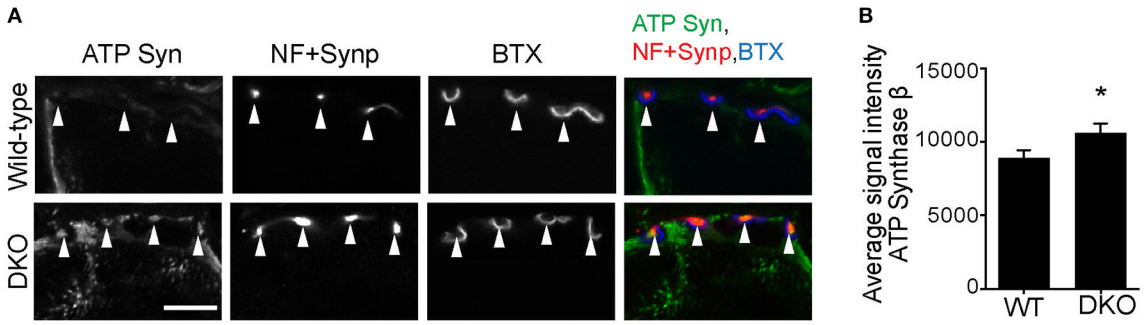

FIGURE 8 | Higher level of ATP synthase protein in presynaptic terminals of Pink1/Parkin DKO mice. **(A)** Representative confocal micrographs of immunohistochemistry for mitochondrial protein ATP synthase β subunit (ATP Syn) in presynaptic terminals (arrowheads) of tibialis anterior NMJs in the Pink1/Parkin DKO mice at ages between P85 and P110 compared to wild–type mice of the same age. Presynaptic terminals of NMJs were defined by anti-neurofilament and anti-synaptophysin staining pattern (NF + Synp). Postsynaptic acetylcholine receptors were labeled with Alexa 594-conjugated α-bungarotoxin (BTX). In these cross-section images of NMJs, presynaptic terminals are above the bungarotoxin signal, and postsynaptic myotubes are below the bungarotoxin signal. Scale bar: 10 μm. **(B)** Average signal intensity of ATP synthase β subunit is greater in presynaptic terminals of Pink1/Parkin DKO mice than in those of wild-type mice. Quantifications are from n = four animals and 97–101 NMJs for each genotype in confocal images. Graph shows mean ± SEM. Asterisks indicate significant differences as analyzed by un-paired t-test (*$p < 0.05$).

separate mouse models of ALS. However, enhancing autophagy using trehalose, independent of mTOR, delayed disease onset in SOD1^{G93A} mice, increased life span, reduced motor neuron loss in spinal cord, reduced NMJ denervation, and preserved mitochondrial function (Castillo et al., 2013; Zhang et al., 2014; Li et al., 2015). Furthermore, TAR DNA-binding protein 43 (TDP43) mutations have been identified in familial ALS patients, and animal and cell culture models have been studied. Enhancing autophagy increased cell survival *in vitro* of primary rat neurons transfected with TDP43(A315T)-GFP or human iPSC-derived motor neurons with TDP43 M337V mutation (Barmada et al., 2014). In addition, enhancing autophagy in mice overexpressing wild-type TDP43 alleviated the progression motor function loss (Wang et al., 2012). Taken together these results provide promise that modulating autophagy may be a treatment option for ALS.

This study has shown that the reduced mitophagy function and the accumulation of degenerated mitochondria are likely to contribute to the dying-back neuropathy of ALS NMJs. Further analyses are necessary to elucidate the mechanism by which mitophagy is down regulated in ALS motor neurons. Homeostatic feedback loop signals link the biogenesis of mitochondria and the level of mitophagy (Palikaras et al., 2015). Therefore, better understanding of the mitophagy defect can aid in the development of a novel intervention to ameliorate mitochondrial defects in ALS.

AUTHOR CONTRIBUTIONS

RR, WD, HN designed the work; RR, ST, TT, YB, LN, HW, HMN, WD, HN acquired, analyzed, and interpreted the data; RR, HN wrote the manuscript. All participated in the final approval of the manuscript.

FUNDING

This work was supported by grants from NIH, R01 NS078214 and R01 AG051470 (HN), R01 AA020518 (WD), from NIH K-INBRE postdoctoral award P20 GM103418 (RR), and core facility supports from the NIH-NCRR (P20RR016475 and P20RR024214) and NIGMS (P20GM104936 and P30GM122731).

ACKNOWLEDGMENTS

We thank B. Fegley for technical assistance on the electron microscope. The monoclonal antibodies SV2 and 2H3 developed by Drs. K.M. Buckley and Tom Jessell were obtained from the Developmental Studies Hybridoma Bank maintained by the NICHD and the University of Iowa, Department of Biological Sciences, Iowa City, IA 52242.

SUPPLEMENTARY MATERIAL

The Supplementary Material for this article can be found online at: http://journal.frontiersin.org/article/10.3389/fnins.2017.00473/full#supplementary-material

Supplementary Figure 1 | Examples of autophagosomes at NMJs in SOD1^{G93A} mice. Representative electron micrographs of autophagosomes in SOD1^{G93A} mice in the presynaptic terminals of NMJs at P57. Orange arrowheads point to the autophagosomes. **(D,E,F)** Higher-magnification images of autophagosomes in **(A,B,C)**. **(A,D)** Double membrane autophagosome structure surrounds synaptic vesicles between the presynaptic membrane and mitochondria, which contains cristae. **(B,E)** In the four membrane autophagosome structure, the outside double membrane has not closed yet. An autophagosome forms a double-membrane structure or a structure with multiple layers of double-membrane (Klionsky et al., 2016). Given the large evidence suggesting that autophagosomes are originated from endoplasmic reticulum membrane, these structures may reflect the early formation stage of autophagosomes. **(C,F)** Four membrane autophagosome structure surrounds synaptic vesicles between the presynaptic membrane and degenerating mitochondria. Scale bars: 500 nm.

REFERENCES

Acsadi, G., Anguelov, R. A., Yang, H., Toth, G., Thomas, R., Jani, A., et al. (2002). Increased survival and function of SOD1 mice after glial cell-derived neurotrophic factor gene therapy. *Hum. Gene Ther.* 13, 1047–1059. doi: 10.1089/104303402753812458

Arnulf, I., Similowski, T., Salachas, F., Garma, L., Mehiri, S., Attali, V., et al. (2000). Sleep disorders and diaphragmatic function in patients with amyotrophic lateral sclerosis. *Am. J. Respir. Crit. Care Med.* 161(3 Pt. 1), 849–856. doi: 10.1164/ajrccm.161.3.9805008

Ashrafi, G., Schlehe, J. S., LaVoie, M. J., and Schwarz, T. L. (2014). Mitophagy of damaged mitochondria occurs locally in distal neuronal axons and requires PINK1 and Parkin. *J. Cell Biol.* 206, 655–670. doi: 10.1083/jcb.201401070

Azzouz, M., Ralph, G. S., Storkebaum, E., Walmsley, L. E., Mitrophanous, K. A., Kingsman, S. M., et al. (2004). VEGF delivery with retrogradely transported lentivector prolongs survival in a mouse ALS model. *Nature* 429, 413–417. doi: 10.1038/nature02544

Barmada, S. J., Serio, A., Arjun, A., Bilican, B., Daub, A., Ando, D. M., et al. (2014). Autophagy induction enhances TDP43 turnover and survival in neuronal ALS models. *Nat. Chem. Biol.* 10, 677–685. doi: 10.1038/nchembio.1563

Bhattacharya, A., Bokov, A., Muller, F. L., Jernigan, A. L., Maslin, K., Diaz, V., et al. (2012). Dietary restriction but not rapamycin extends disease onset and survival of the H46R/H48Q mouse model of ALS. *Neurobiol. Aging* 33, 1829–1832. doi: 10.1016/j.neurobiolaging.2011.06.002

Bordet, T., Lesbordes, J. C., Rouhani, S., Castelnau-Ptakhine, L., Schmalbruch, H., Haase, G., et al. (2001). Protective effects of cardiotrophin-1 adenoviral gene transfer on neuromuscular degeneration in transgenic ALS mice. *Hum. Mol. Genet.* 10, 1925–1933. doi: 10.1093/hmg/10.18.1925

Braun, S. R. (1987). Respiratory system in amyotrophic lateral sclerosis. *Neurol. Clin.* 5, 9–31.

Castillo, K., Nassif, M., Valenzuela, V., Rojas, F., Matus, S., Mercado, G., et al. (2013). Trehalose delays the progression of amyotrophic lateral sclerosis by enhancing autophagy in motoneurons. *Autophagy* 9, 1308–1320. doi: 10.4161/auto.25188

Chen, J., Billings, S. E., and Nishimune, H. (2011). Calcium channels link the muscle-derived synapse organizer laminin beta2 to Bassoon and CAST/Erc2 to organize presynaptic active zones. *J. Neurosci.* 31, 512–525. doi: 10.1523/JNEUROSCI.3771-10.2011

Chen, J., Mizushige, T., and Nishimune, H. (2012). Active zone density is conserved during synaptic growth but impaired in aged mice. *J. Comp. Neurol.* 520, 434–452. doi: 10.1002/cne.22764

Ching, J., and Weihl, C. (2013). Rapamycin-induced autophagy aggravates pathology and weakness in a mouse model of VCP-associated myopathy. *Autophagy* 9, 799–800. doi: 10.4161/auto.23958

Court, F. A., Brophy, P. J., and Ribchester, R. R. (2008). Remodeling of motor nerve terminals in demyelinating axons of periaxin-null mice. *Glia* 56, 471–479. doi: 10.1002/glia.20620

Dadon-Nachum, M., Melamed, E., and Offen, D. (2011). The "dying-back" phenomenon of motor neurons in ALS. *J. Mol. Neurosci.* 43, 470–477. doi: 10.1007/s12031-010-9467-1

DeJesus-Hernandez, M., MacKenzie, I. R., Boeve, B. F., Boxer, A. L., Baker, M., Rutherford, N. J., et al. (2011). Expanded GGGGCC hexanucleotide repeat in noncoding region of C9ORF72 causes chromosome 9p-linked FTD and ALS. *Neuron* 72, 245–256. doi: 10.1016/j.neuron.2011.09.011

Deng, H. X., Chen, W., Hong, S. T., Boycott, K. M., Gorrie, G. H., Siddique, N., et al. (2011). Mutations in UBQLN2 cause dominant X-linked juvenile and adult-onset ALS and ALS/dementia. *Nature* 477, 211–215. doi: 10.1038/nature10353

Ding, W. X., Ni, H. M., Li, M., Liao, Y., Chen, X., Stolz, D. B., et al. (2010). Nix is critical to two distinct phases of mitophagy, reactive oxygen species-mediated autophagy induction and Parkin-ubiquitin-p62-mediated mitochondrial priming. *J. Biol. Chem.* 285, 27879–27890. doi: 10.1074/jbc.M110.119537

Ding, W. X., and Yin, X. M. (2012). Mitophagy: mechanisms, pathophysiological roles, and analysis. *Biol. Chem.* 393, 547–564. doi: 10.1515/hsz-2012-0119

Dobrowolny, G., Giacinti, C., Pelosi, L., Nicoletti, C., Winn, N., Barberi, L., et al. (2005). Muscle expression of a local Igf-1 isoform protects motor neurons in an ALS mouse model. *J. Cell Biol.* 168, 193–199. doi: 10.1083/jcb.200407021

Edens, B. M., Miller, N., and Ma, Y. C. (2016). Impaired autophagy and defective mitochondrial function: converging paths on the road to motor neuron degeneration. *Front. Cell. Neurosci.* 10:44. doi: 10.3389/fncel.2016.00044

Farg, M. A., Sundaramoorthy, V., Sultana, J. M., Yang, S., Atkinson, R. A., Levina, V., et al. (2014). C9ORF72, implicated in amytrophic lateral sclerosis and frontotemporal dementia, regulates endosomal trafficking. *Hum. Mol. Genet.* 23, 3579–3595. doi: 10.1093/hmg/ddu068

Fecto, F., Yan, J., Vemula, S. P., Liu, E., Yang, Y., Chen, W., et al. (2011). SQSTM1 mutations in familial and sporadic amyotrophic lateral sclerosis. *Arch. Neurol.* 68, 1440–1446. doi: 10.1001/archneurol.2011.250

Fischer, L. R., Culver, D. G., Tennant, P., Davis, A. A., Wang, M. S., Castellano-Sanchez, A., et al. (2004). Amyotrophic lateral sclerosis is a distal axonopathy: evidence in mice and man. *Exp. Neurol.* 185, 232–240. doi: 10.1016/j.expneurol.2003.10.004

Frey, D., Schneider, C., Xu, L., Borg, J., Spooren, W., and Caroni, P. (2000). Early and selective loss of neuromuscular synapse subtypes with low sprouting competence in motoneuron diseases. *J. Neurosci.* 20, 2534–2542. Available online at: http://www.jneurosci.org/content/20/7/2534/tab-article-info

Gal, J., Strom, A. L., Kilty, R., Zhang, F., and Zhu, H. (2007). p62 accumulates and enhances aggregate formation in model systems of familial amyotrophic lateral sclerosis. *J. Biol. Chem.* 282, 11068–11077. doi: 10.1074/jbc.M608787200

Geisler, S., Holmstrom, K. M., Skujat, D., Fiesel, F. C., Rothfuss, O. C., Kahle, P. J., et al. (2010). PINK1/Parkin-mediated mitophagy is dependent on VDAC1 and p62/SQSTM1. *Nat. Cell Biol.* 12, 119–131. doi: 10.1038/ncb2012

Gould, T. W., Buss, R. R., Vinsant, S., Prevette, D., Sun, W., Knudson, C. M., et al. (2006). Complete dissociation of motor neuron death from motor dysfunction by Bax deletion in a mouse model of ALS. *J. Neurosci.* 26, 8774–8786. doi: 10.1523/JNEUROSCI.2315-06.2006

Hanna, R. A., Quinsay, M. N., Orogo, A. M., Giang, K., Rikka, S., and Gustafsson, A. B. (2012). Microtubule-associated protein 1 light chain 3 (LC3) interacts with Bnip3 protein to selectively remove endoplasmic reticulum and mitochondria via autophagy. *J. Biol. Chem.* 287, 19094–19104. doi: 10.1074/jbc.M111.322933

Hara, T., Nakamura, K., Matsui, M., Yamamoto, A., Nakahara, Y., Suzuki-Migishima, R., et al. (2006). Suppression of basal autophagy in neural cells causes neurodegenerative disease in mice. *Nature* 441, 885–889. doi: 10.1038/nature04724

Hart, M. N., Cancilla, P. A., Frommes, S., and Hirano, A. (1977). Anterior horn cell degeneration and Bunina-type inclusions associated with dementia. *Acta Neuropathol.* 38, 225–228. doi: 10.1007/BF00688069

Hayworth, C. R., and Gonzalez-Lima, F. (2009). Pre-symptomatic detection of chronic motor deficits and genotype prediction in congenic B6.SOD1(G93A) ALS mouse model. *Neuroscience* 164, 975–985. doi: 10.1016/j.neuroscience.2009.08.031

Heiman-Patterson, T. D., Deitch, J. S., Blankenhorn, E. P., Erwin, K. L., Perreault, M. J., Alexander, B. K., et al. (2005). Background and gender effects on survival in the TgN(SOD1-G93A)1Gur mouse model of ALS. *J. Neurol. Sci.* 236, 1–7. doi: 10.1016/j.jns.2005.02.006

Hirano, M., Nakamura, Y., Saigoh, K., Sakamoto, H., Ueno, S., Isono, C., et al. (2013). Mutations in the gene encoding p62 in Japanese patients with amyotrophic lateral sclerosis. *Neurology* 80, 458–463. doi: 10.1212/WNL.0b013e31827f0fe5

Howe, C. L., Bergstrom, R. A., and Horazdovsky, B. F. (2009). Subcutaneous IGF-1 is not beneficial in 2-year ALS trial. *Neurology* 73, 1247; author reply: 1247–1248. doi: 10.1212/WNL.0b013e3181b26ae6

Jaarsma, D., Haasdijk, E. D., Grashorn, J. A., Hawkins, R., van Duijn, W., Verspaget, H. W., et al. (2000). Human Cu/Zn superoxide dismutase (SOD1) overexpression in mice causes mitochondrial vacuolization, axonal degeneration, and premature motoneuron death and accelerates motoneuron disease in mice expressing a familial amyotrophic lateral sclerosis mutant SOD1. *Neurobiol. Dis.* 7(6 Pt. B), 623–643. doi: 10.1006/nbdi.2000.0299

Jeong, G. B., Mojsilovic-Petrovic, J., Boccitto, M., and Kalb, R. (2011). Signaling events in axons and/or dendrites render motor neurons vulnerable to mutant superoxide dismutase toxicity. *J. Neurosci.* 31, 295–299. doi: 10.1523/JNEUROSCI.4824-10.2011

Johnson, J. O., Mandrioli, J., Benatar, M., Abramzon, Y., Van Deerlin, V. M., Trojanowski, J. Q., et al. (2010). Exome sequencing reveals VCP mutations as a cause of familial ALS. *Neuron* 68, 857–864. doi: 10.1016/j.neuron.2010.11.036

Kabeya, Y., Mizushima, N., Ueno, T., Yamamoto, A., Kirisako, T., Noda, T., et al. (2000). LC3, a mammalian homologue of yeast Apg8p, is localized in autophagosome membranes after processing. *EMBO J.* 19, 5720–5728. doi: 10.1093/emboj/19.21.5720

Kaspar, B. K., Llado, J., Sherkat, N., Rothstein, J. D., and Gage, F. H. (2003). Retrograde viral delivery of IGF-1 prolongs survival in a mouse ALS model. *Science* 301, 839–842. doi: 10.1126/science.1086137

Kennel, P. F., Finiels, F., Revah, F., and Mallet, J. (1996). Neuromuscular function impairment is not caused by motor neurone loss in FALS mice: an electromyographic study. *Neuroreport* 7, 1427–1431. doi: 10.1097/00001756-199605310-00021

Klionsky, D. J., Abdelmohsen, K., Abe, A., Abedin, M. J., Abeliovich, H., Acevedo Arozena, A., et al. (2016). Guidelines for the use and interpretation of assays for monitoring autophagy (3rd edition). *Autophagy* 12, 1–222. doi: 10.4161/auto.19496

Komatsu, M., Waguri, S., Chiba, T., Murata, S., Iwata, J., Tanida, I., et al. (2006). Loss of autophagy in the central nervous system causes neurodegeneration in mice. *Nature* 441, 880–884. doi: 10.1038/nature04723

Komatsu, M., Wang, Q. J., Holstein, G. R., Friedrich, V. L. Jr., Iwata, J., Kominami, E., et al. (2007). Essential role for autophagy protein Atg7 in the maintenance of axonal homeostasis and the prevention of axonal degeneration. *Proc. Natl. Acad. Sci. U.S.A.* 104, 14489–14494. doi: 10.1073/pnas.0701311104

Leitner, M., Menzies, S., and Lutz, C. (2009). *Working with ALS Mice, Guidelines for Preclinical Testing & Colony Management.* PRIZE4LIFE, The Jackson Laboratory, 1–28.

Li, Y., Guo, Y., Wang, X., Yu, X., Duan, W., Hong, K., et al. (2015). Trehalose decreases mutant SOD1 expression and alleviates motor deficiency in early but not end-stage amyotrophic lateral sclerosis in a SOD1-G93A mouse model. *Neuroscience* 298, 12–25. doi: 10.1016/j.neuroscience.2015.03.061

Maruyama, H., Morino, H., Ito, H., Izumi, Y., Kato, H., Watanabe, Y., et al. (2010). Mutations of optineurin in amyotrophic lateral sclerosis. *Nature* 465, 223–226. doi: 10.1038/nature08971

Matsuda, N., Sato, S., Shiba, K., Okatsu, K., Saisho, K., Gautier, C. A., et al. (2010). PINK1 stabilized by mitochondrial depolarization recruits Parkin to damaged mitochondria and activates latent Parkin for mitophagy. *J. Cell Biol.* 189, 211–221. doi: 10.1083/jcb.200910140

Miller, R. G., Jackson, C. E., Kasarskis, E. J., England, J. D., Forshew, D., Johnston, W., et al. (2009). Practice parameter update: the care of the patient with amyotrophic lateral sclerosis: drug, nutritional, and respiratory therapies (an evidence-based review): report of the Quality Standards Subcommittee of the American Academy of Neurology. *Neurology* 73, 1218–1226. doi: 10.1212/WNL.0b013e3181bc0141

Munch, C., Sedlmeier, R., Meyer, T., Homberg, V., Sperfeld, A. D., Kurt, A., et al. (2004). Point mutations of the p150 subunit of dynactin (DCTN1) gene in ALS. *Neurology* 63, 724–726. doi: 10.1212/01.WNL.0000134608.83927.B1

Narendra, D. P., Jin, S. M., Tanaka, A., Suen, D. F., Gautier, C. A., Shen, J., et al. (2010). PINK1 is selectively stabilized on impaired mitochondria to activate Parkin. *PLoS Biol.* 8:e1000298. doi: 10.1371/journal.pbio.1000298

Nishimune, H., Sanes, J. R., and Carlson, S. S. (2004). A synaptic laminin-calcium channel interaction organizes active zones in motor nerve terminals. *Nature* 432, 580–587. doi: 10.1038/nature03112

Nishiyama, J., Miura, E., Mizushima, N., Watanabe, M., and Yuzaki, M. (2007). Aberrant membranes and double-membrane structures accumulate in the axons of Atg5-null Purkinje cells before neuronal death. *Autophagy* 3, 591–596. doi: 10.4161/auto.4964

Okatsu, K., Saisho, K., Shimanuki, M., Nakada, K., Shitara, H., Sou, Y. S., et al. (2010). p62/SQSTM1 cooperates with Parkin for perinuclear clustering of depolarized mitochondria. *Genes Cells* 15, 887–900. doi: 10.1111/j.1365-2443.2010.01426.x

Otomo, A., Pan, L., and Hadano, S. (2012). Dysregulation of the autophagy-endolysosomal system in amyotrophic lateral sclerosis and related motor neuron diseases. *Neurol. Res. Int.* 2012:498428. doi: 10.1155/2012/498428

Palikaras, K., Lionaki, E., and Tavernarakis, N. (2015). Coordination of mitophagy and mitochondrial biogenesis during ageing in *C. elegans*. *Nature* 521, 525–528. doi: 10.1038/nature14300

Parkinson, N., Ince, P. G., Smith, M. O., Highley, R., Skibinski, G., Andersen, P. M., et al. (2006). ALS phenotypes with mutations in CHMP2B (charged multivesicular body protein 2B). *Neurology* 67, 1074–1077. doi: 10.1212/01.wnl.0000231510.89311.8b

Reyes, N. A., Fisher, J. K., Austgen, K., VandenBerg, S., Huang, E. J., and Oakes, S. A. (2010). Blocking the mitochondrial apoptotic pathway preserves motor neuron viability and function in a mouse model of amyotrophic lateral sclerosis. *J. Clin. Invest.* 120, 3673–3679. doi: 10.1172/JCI42986

Rubino, E., Rainero, I., Chio, A., Rogaeva, E., Galimberti, D., Fenoglio, P., et al. (2012). SQSTM1 mutations in frontotemporal lobar degeneration and amyotrophic lateral sclerosis. *Neurology* 79, 1556–1562. doi: 10.1212/WNL.0b013e31826e25df

Ruffoli, R., Bartalucci, A., Frati, A., and Fornai, F. (2015). Ultrastructural studies of ALS mitochondria connect altered function and permeability with defects of mitophagy and mitochondriogenesis. *Front. Cell. Neurosci.* 9:341. doi: 10.3389/fncel.2015.00341

Samuel, M. A., Valdez, G., Tapia, J. C., Lichtman, J. W., and Sanes, J. R. (2012). Agrin and synaptic laminin are required to maintain adult neuromuscular junctions. *PLoS ONE* 7:e46663. doi: 10.1371/journal.pone.0046663

Sasaki, S. (2011). Autophagy in spinal cord motor neurons in sporadic amyotrophic lateral sclerosis. *J. Neuropathol. Exp. Neurol.* 70, 349–359. doi: 10.1097/NEN.0b013e3182160690

Siklos, L., Engelhardt, J., Harati, Y., Smith, R. G., Joo, F., and Appel, S. H. (1996). Ultrastructural evidence for altered calcium in motor nerve terminals in amyotropic lateral sclerosis. *Ann. Neurol.* 39, 203–216. doi: 10.1002/ana.410390210

Sorenson, E. J., Windbank, A. J., Mandrekar, J. N., Bamlet, W. R., Appel, S. H., Armon, C., et al. (2008). Subcutaneous IGF-1 is not beneficial in 2-year ALS trial. *Neurology* 71, 1770–1775. doi: 10.1212/01.wnl.0000335970.78664.36

Springer, M. Z., and MacLeod, K. F. (2016). In brief: mitophagy: mechanisms and role in human disease. *J. Pathol.* 240, 253–255. doi: 10.1002/path.4774

Staats, K. A., Hernandez, S., Schonefeldt, S., Bento-Abreu, A., Dooley, J., Van Damme, P., et al. (2013). Rapamycin increases survival in ALS mice lacking mature lymphocytes. *Mol. Neurodegener.* 8:31. doi: 10.1186/1750-1326-8-31

Taetzsch, T., Tenga, M. J., and Valdez, G. (2017). Muscle fibers secrete FGFBP1 to slow degeneration of neuromuscular synapses during aging and progression of ALS. *J. Neurosci.* 37, 70–82. doi: 10.1523/JNEUROSCI.2992-16.2016

Tateishi, T., Hokonohara, T., Yamasaki, R., Miura, S., Kikuchi, H., Iwaki, A., et al. (2010). Multiple system degeneration with basophilic inclusions in Japanese ALS patients with FUS mutation. *Acta Neuropathol.* 119, 355–364. doi: 10.1007/s00401-009-0621-1

Teyssou, E., Takeda, T., Lebon, V., Boillee, S., Doukoure, B., Bataillon, G., et al. (2013). Mutations in SQSTM1 encoding p62 in amyotrophic lateral sclerosis: genetics and neuropathology. *Acta Neuropathol.* 125, 511–522. doi: 10.1007/s00401-013-1090-0

Valdez, G., Tapia, J. C., Kang, H., Clemenson, G. D. Jr., Gage, F. H., Lichtman, J. W., et al. (2010). Attenuation of age-related changes in mouse neuromuscular synapses by caloric restriction and exercise. *Proc. Natl. Acad. Sci. U.S.A.* 107, 14863–14868. doi: 10.1073/pnas.1002220107

Wang, I. F., Guo, B. S., Liu, Y. C., Wu, C. C., Yang, C. H., Tsai, K. J., et al. (2012). Autophagy activators rescue and alleviate pathogenesis of a mouse model with proteinopathies of the TAR DNA-binding protein 43. *Proc. Natl. Acad. Sci. U.S.A.* 109, 15024–15029. doi: 10.1073/pnas.1206362109

Williams, K. L., Warraich, S. T., Yang, S., Solski, J. A., Fernando, R., Rouleau, G. A., et al. (2012). UBQLN2/ubiquilin 2 mutation and pathology in familial amyotrophic lateral sclerosis. *Neurobiol. Aging* 33, 2527.e3–2527.e10. doi: 10.1016/j.neurobiolaging.2012.05.008

Wong, P. C., Pardo, C. A., Borchelt, D. R., Lee, M. K., Copeland, N. G., Jenkins, N. A., et al. (1995). An adverse property of a familial ALS-linked SOD1 mutation causes motor neuron disease characterized by vacuolar degeneration of mitochondria. *Neuron* 14, 1105–1116. doi: 10.1016/0896-6273(95)90259-7

Wooley, C. M., Sher, R. B., Kale, A., Frankel, W. N., Cox, G. A., and Seburn, K. L. (2005). Gait analysis detects early changes in transgenic SOD1(G93A) mice. *Muscle Nerve* 32, 43–50. doi: 10.1002/mus.20228

Xie, Y., Zhou, B., Lin, M. Y., Wang, S., Foust, K. D., and Sheng, Z. H. (2015). Endolysosomal deficits augment mitochondria pathology in spinal motor neurons of asymptomatic fALS mice. *Neuron* 87, 355–370. doi: 10.1016/j.neuron.2015.06.026

Yamaguchi, J., Suzuki, C., Nanao, T., Kakuta, S., Ozawa, K., Tanida, I., et al. (2017). Atg9a deficiency causes axon-specific lesions including neuronal circuit

dysgenesis. *Autophagy*. doi: 10.1080/15548627.2017.1314897. [Epub ahead of print].

Yang, H., Ni, H. M., Guo, F., Ding, Y., Shi, Y. H., Lahiri, P., et al. (2016). Sequestosome 1/p62 protein is associated with autophagic removal of excess hepatic endoplasmic reticulum in mice. *J. Biol. Chem.* 291, 18663–18674. doi: 10.1074/jbc.M116.739821

Yang, Y., Hentati, A., Deng, H. X., Dabbagh, O., Sasaki, T., Hirano, M., et al. (2001). The gene encoding alsin, a protein with three guanine-nucleotide exchange factor domains, is mutated in a form of recessive amyotrophic lateral sclerosis. *Nat. Genet.* 29, 160–165. doi: 10.1038/ng1001-160

Youle, R. J., and Narendra, D. P. (2011). Mechanisms of mitophagy. *Nat. Rev. Mol. Cell Biol.* 12, 9–14. doi: 10.1038/nrm3028

Zhang, X., Chen, S., Song, L., Tang, Y., Shen, Y., Jia, L., et al. (2014). MTOR-independent, autophagic enhancer trehalose prolongs motor neuron survival and ameliorates the autophagic flux defect in a mouse model of amyotrophic lateral sclerosis. *Autophagy* 10, 588–602. doi: 10.4161/auto.27710

Zhang, X., Li, L., Chen, S., Yang, D., Wang, Y., Zhang, X., et al. (2011). Rapamycin treatment augments motor neuron degeneration in SOD1(G93A) mouse model of amyotrophic lateral sclerosis. *Autophagy* 7, 412–425. doi: 10.4161/auto.7.4.14541

Conflict of Interest Statement: The authors declare that the research was conducted in the absence of any commercial or financial relationships that could be construed as a potential conflict of interest.

frontiers in Neuroscience

MINI REVIEW
published: 31 May 2017
doi: 10.3389/fnins.2017.00312

Accumulating Evidence for Axonal Translation in Neuronal Homeostasis

Emily L. Spaulding[1,2] *and Robert W. Burgess*[1,2]*

[1] The Jackson Laboratory, Bar Harbor, ME, United States, [2] Graduate School of Biomedical Sciences and Engineering, University of Maine, Orono, ME, United States

The specialized structure of the neuron requires that homeostasis is sustained over the meter or more that may separate a cell body from its axonal terminus. Given this impressive distance and an axonal volume that is many times that of the cell body, how is such a compartment grown during development, re-grown after injury, and maintained throughout adulthood? While early answers to these questions focused on the local environment or the cell soma as supplying the needs of the axon, it is now well-established that the axon has some unique needs that can only be met from within. Decades of research have revealed local translation as an indispensable mechanism of axonal homeostasis during development and regeneration in both invertebrates and vertebrates. In contrast, the extent to which the adult, mammalian axonal proteome is maintained through local translation remains unclear and controversial. This mini-review aims to highlight important experiments that have helped to shape the field of axonal translation, to discuss conceptual arguments and recent evidence that supports local translation as important to the maintenance of adult axons, and to suggest experimental approaches that have the potential to further illuminate the role of axonal translation in neuronal homeostasis.

Keywords: axon degeneration, local translation, peripheral neuropathy, axonal transport, hereditary sensory and motor neuropathy

OPEN ACCESS

Edited by:
Kurt De Vos,
University of Sheffield,
United Kingdom

Reviewed by:
Dianna E. Willis,
Burke-Cornell Medical Research Institute, United States
Kim A. Staats,
University of Southern California, United States

***Correspondence:**
Robert W. Burgess
robert.burgess@jax.org

Specialty section:
This article was submitted to Neurodegeneration, a section of the journal Frontiers in Neuroscience

Received: *03 April 2017*
Accepted: *17 May 2017*
Published: *31 May 2017*

Citation:
Spaulding EL and Burgess RW (2017) Accumulating Evidence for Axonal Translation in Neuronal Homeostasis. Front. Neurosci. 11:312. doi: 10.3389/fnins.2017.00312

SOMAL PROVISION OF THE AXONAL PROTEOME

In the early twentieth century popular opinion stated that the axon drew the majority of its nutrients from the local environment. Classic experiments by Weiss and Hiscoe challenged this idea by providing observable evidence for the directed movement of material from the neuronal soma to the axon terminal (Weiss and Hiscoe, 1948). Rat peripheral nerves were crushed, ligated, and allowed to regenerate. Within days, the axon segment just proximal to the ligation became swollen and enlarged. Upon removal of the ligation, the accumulated axoplasm moved from the soma to the axon, suggesting the presence of a dynamic communication system between the cell body and the axon and establishing the field of axonal transport.

Soon the idea that the neuronal soma supplied the axonal proteome prevailed. Radiolabeled amino acids systemically injected into rats were incorporated into new proteins in the soma and at the base of large dendrites within minutes of injection, but were observed in the axon hillock 1 day after injection, in the ventral root 2 days after injection, and 20 mm down the sciatic nerve 16 days after injection (Droz and Leblond, 1963). It was concluded that proteins are continuously synthesized in the cell body and at the base of large dendritic spines, and are subsequently

transported into distal dendrites and axons. Although background from supporting cells would have made it difficult to observe low signals in axons, this evidence supported the idea that would dominate the field for the next several decades; translation does not occur in axons.

DENDRITIC TRANSLATION REVEALS THE POTENTIAL FOR LOCAL CONTROL OF THE PROTEOME IN NEURONS

The earliest electron microscopy studies of neurons established the soma as the primary site of protein synthesis, based on the presence of well-defined endoplasmic reticulum (ER) and a large number of polyribosomes (Palay and Palade, 1955). Thus, the observation of newly synthesized proteins at the base of large dendrites led to the search and eventual identification of additional components of translation machinery in this compartment. The presence of polyribosomes and specific mRNA species, including microtubule associated protein 2 (MAP2) and the alpha subunit of calcium/calmodulin-dependent protein kinase II (CAMKIIα) were soon identified (Steward and Levy, 1982; Steward, 1983; Caceres et al., 1988).

Decades after the first behavioral studies in mammals showed that memory is dependent upon new protein synthesis, Kang and Schuman assigned physiological significance to dendritic translation by showing it is a requirement for synaptic plasticity in the mammalian hippocampus (Flexner et al., 1963; Kang and Schuman, 1996). Aakalu et al. provided visual evidence of dendritic translation in mammalian neurons using a reporter in which the coding sequence of green fluorescence protein (GFP) was flanked by the 5′ and 3′ untranslated ends of CAMKIIα, resulting in dendritic mRNA localization (Aakalu et al., 2001). Stimulation of cultured rat hippocampal neurons with Brain-derived neurotrophic factor (BDNF) resulted in dendritic synthesis of the GFP reporter, which was abolished by treatment with protein synthesis inhibitors. Possible diffusion from the cell body was eliminated by transection of dendrites from the soma and by including a membrane tether to the reporter protein. This study supplied the evidence needed to acknowledge dendritic translation as a mechanism of neuronal homeostasis.

AXONS POSSESS TRANSLATION MACHINERY

While the field of dendritic translation advanced, the search for evidence of axonal translation despite the apparent absence of polyribosomes and rRNA in the axon continued (Lasek et al., 1973). A series of *in vitro* metabolic labeling studies in goldfish, squid, and rabbit established that proteins can be synthesized in invertebrate and vertebrate axons (Koenig, 1967; Giuditta et al., 1968; Edstrom and Sjostrand, 1969). Eventually, more sensitive techniques enabled the identification of rRNA, mRNA, and actively translating polysomes in squid giant axons (Giuditta et al., 1980, 1986, 1991). In mammalian axons, ribosomes were identified at embryonic stages both in culture and *in vivo* (Tennyson, 1970; Bunge, 1973; Bassell et al., 1998). Polyribosomes were observed by electron microscopy in the axonal initial segment of mature mammalian central nervous system (CNS) neurons, although not in myelinated sections. Polyribosomes were tightly associated with synapses, suggesting that axonal translation may occur during times of extensive synaptic growth, such as development (Steward and Ribak, 1986).

Electron microscopy failed to detect rough ER or golgi apparatus in vertebrate axons, raising the question of whether or not axons have the ability to process or secrete locally synthesized proteins (Tennyson, 1970; Bunge, 1973). However, the Twiss lab addressed this question using cultured rat sensory neurons. Their extensive studies have shown that (1) ER and golgi components needed for classical protein synthesis and secretion are present in the axon, (2) ER chaperone proteins can be axonally translated, and (3) axons can target locally synthesized proteins to the membrane (Willis et al., 2005; Merianda et al., 2009). This evidence strongly suggests that neurons can post-translationally modify and secrete axonally synthesized proteins, although the associated machinery may exist in very small quantities or adopt unique morphologies in the axon, perhaps explaining how the axon is able to maintain the energetic burden of translation machinery.

AXONAL TRANSLATION OCCURS DURING NERVOUS SYSTEM DEVELOPMENT

Given that axonal ribosomes are present in embryonic axons and preferentially associated with synapses, many of the earliest studies in the field of axonal translation were related to its role in neuronal development. Axonal mRNA localization was revealed as a general mechanism of protein sorting and proteome management in the developing axon (Jung et al., 2012). In growing neurons, mRNA is sorted to neuronal processes in granules that also contain ribosomal subunits and translation factors (Knowles et al., 1996; Olink-Coux and Hollenbeck, 1996). β-actin was among the first such mRNA species to be identified as enriched within growth cones and axonal processes of developing neurons, and the axonal synthesis of actin protein in embryonic neurons was established soon after (Bassell et al., 1998; Eng et al., 1999).

It is now known that axonal translation is important for many aspects of neuronal development. Some neurotrophins can induce growth cones to turn toward their source in an actin-dependent manner (Zheng et al., 1996; Ming et al., 1997). The finding that β-actin mRNA is translated in the axon made this mechanism a good candidate for how axons can quickly and independently modulate the cytoskeleton for growth cone turning during development. Confirming this hypothesis, stimulation of either embryonic or adult neurons with neutrotrophins increases the transport of β-actin mRNA into the axon (Zhang et al., 1999, 2001; Willis et al., 2005). A directional gradient of netrin-1 induces translation of β-actin that directly precedes attractive growth cone turning (Leung et al., 2006). Repulsion is just as important as attraction for

axonal pathfinding during development, and axonal translation contributes to this phenomenon as well. The guidance cue Semaphorin 3A results in axonal translation of RhoA mRNA and subsequent collapse of the growth cone, preventing the axon from innervating incorrect targets (Wu et al., 2005). Overall neuronal growth and size-sensing is also dependent upon mRNA localization and axonal translation. In growing sensory neurons importin β1 mRNA is anterogradely transported to the axon, where it associates with ribosomes. Perturbation of this localization by 3′ UTR knockout or by sequestration of the importin β1-ribonucleoprotein complex to the cell body results in significantly longer axons (Perry et al., 2016). Finally, axonal protein synthesis is essential for localized BDNF-induced synaptic potentiation in developing neurons (Zhang and Poo, 2002). Thus, axonal translation is a mechanism by which growing neurons correctly pathfind, innervate target tissues, sense their own size, and modulate synaptic strength during development.

AXONAL TRANSLATION OCCURS DURING NERVOUS SYSTEM REGENERATION

Immunohistological studies eventually revealed that mature mammalian axons of the peripheral nervous system contain ribosomal proteins and rRNA, which are irregularly distributed and located close to the plasma membrane, possibly explaining the difficulty in identifying them (Koenig et al., 2000). The importance of axonal translation to neuronal growth during development and the identification of ribosomes in adult peripheral axons raised the possibility that axonal translation plays an additional role during peripheral nerve regeneration. Adult rat dorsal root ganglion (DRG) cells were shown to regenerate neuronal processes *in vitro* after *in vivo* axonal crush by regulating the translation of an existing pool of mRNAs (Twiss et al., 2000). Moreover, translation of these mRNAs within the axon itself is required for normal regeneration *in vitro*. *In vivo*, rat motor axons of the sciatic nerve isolated 7 days after a crush injury contain translation factors, ribosomal proteins, and rRNA (Zheng et al., 2001). Whether translation components originate from the neuron or from glial cells is still under question. Glia-to-axon transfer of proteins occurs in squid giant axons transected from their cell bodies (Lasek et al., 1977). In perfused squid axons cell-to-cell transfer of RNA occurs upon stimulation of glial receptors by axonal neurotransmitters, indicating that signaling from active or injured axons can induce glial cells to provide axonal translation components (Eyman et al., 2007). In mammals, the *in vivo* transfer of ribosomal components from Schwann cells to peripheral axons after injury suggests the presence of a dynamic collaboration between these cell types during regeneration (Court et al., 2008, 2011). Independent of the origin of translation machinery in uninjured axons, the glia-axon collaboration during injury conditions, along with increased aggregation of axonal ER components, suggests an increased capacity for axonal translation, processing, and secretion of newly synthesized proteins during regeneration (Merianda et al., 2009; Court et al., 2011).

CONCEPTUAL ARGUMENTS FOR AXONAL TRANSLATION IN NEURONAL HOMEOSTASIS

One of the most common conceptual arguments for the role of axonal translation in neuronal maintenance centers around efficiency. Mature mammalian neurons are the largest cells in the body and are highly compartmentalized. Transport of mRNA to distant locations within a neuron followed by local translation may be more efficient than transportation and storage of proteins. One mRNA molecule can be translated many times, allowing for communication with the use of fewer resources, fewer space restrictions, and less risk of aberrant protein accumulation. In addition, nascent proteins may provide opportunities for unique post-translational processing crucial to specific functions in the mature axonal compartment (**Figures 1A,C**; Jung et al., 2012; Perry and Fainzilber, 2014).

Axonal translation could also confer molecular flexibility at individual synapses. This could be especially useful during periods of high synaptic activity, providing synapse-specific, "on demand" adaptations to the proteome. Replenishment of proteins used for neurotransmission may be needed at some synapses after intense use such as during motor activity or learning. An example of this is found in growing axons, in which the membrane-bound receptor DCC physically associates with translation machinery and mediates local protein synthesis upon stimulation with netrin (Tcherkezian et al., 2010). In this example, the availability of extracellular signals coupled with the expression of presynaptic membrane receptors provides translational control at the level of individual synapses (**Figure 1B**).

Local translation may help axons maintain a healthy supply of functional mitochondria. Mutations that affect either the function or transport of axonal mitochondria result in neurodegeneration (Schwarz, 2013; Pease and Segal, 2014). Nigrostriatal dopamine neurons have extensive axonal arbors, estimated to form up to 245,000 synapses (Matsuda et al., 2009; Bolam and Pissadaki, 2012). Given that mitochondria are enriched at synapses, the cell body may be unable to synthesize the complete nuclear mitochondrial proteome at a rate sufficient for an uninterrupted supply of axonal mitochondria (Court and Coleman, 2012; Schwarz, 2013). Proteins of the inner and outer mitochondrial membranes possess different turnover rates, thus, axonally translated mitochondrial proteins may also allow for finer control of mitochondrial replenishment (Beattie, 1969). In support of axonal synthesis of nuclear-encoded mitochondrial proteins, rat superior cervical ganglia (SCG) axons contain mRNA for several of these proteins and inhibition of axonal protein synthesis decreases mitochondrial membrane potential (Hillefors et al., 2007). SCG axons also contain the micro RNA (miR), miR-338, which is known to post-transcriptionally modulate the expression of cytochrome c oxidase IV (COXIV), a nuclear protein important to oxidative phosphorylation. Overexpression of miR-338 in the axon reduces COXIV protein levels, mitochondrial oxygen consumption, and axonal ATP levels (**Figure 1D**; Aschrafi et al., 2008).

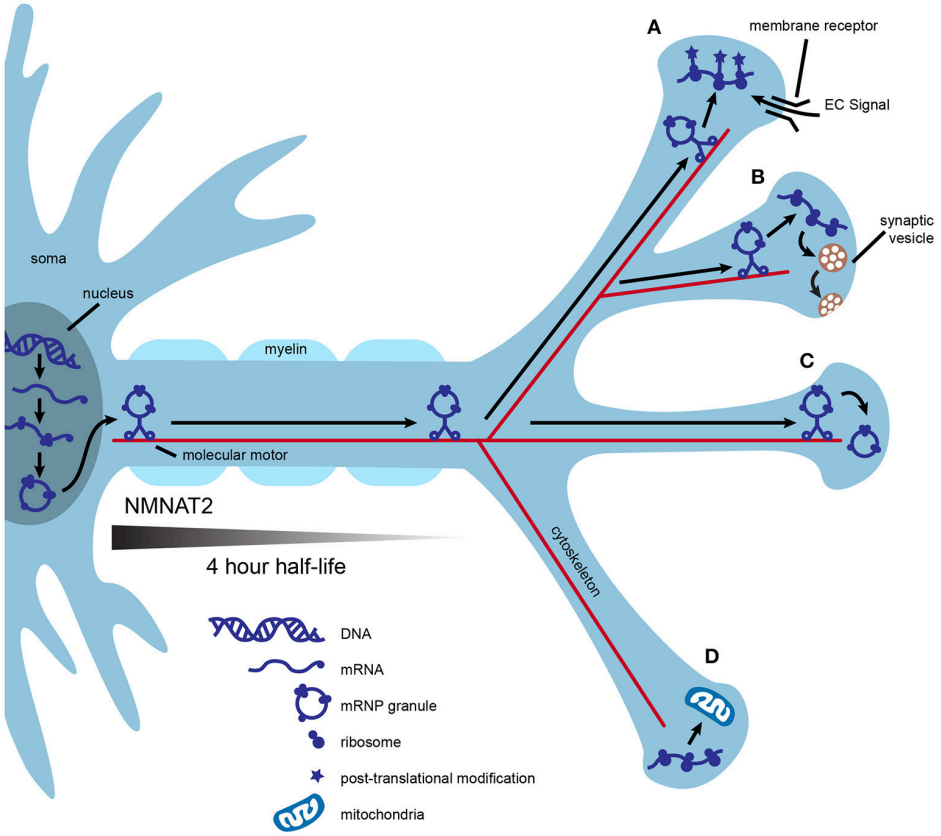

FIGURE 1 | Local translation may contribute to axonal efficiency and compartmentalization. mRNA is transcribed in the nucleus, packaged into mRNP granules, and transported by multiple molecular motors down the axon. Granules are transported into some synapses and mRNA is immediately translated into polypeptides **(A,B)**. Nascent polypeptides may present the opportunity for unique post-translational modification, as in synapse **(A)** or may be used to fulfill specific activity-based needs of individual synapses, as in **(B)**. Local translation of some mRNAs may be controlled at the synaptic level by the interaction of local extracellular signals, such as neurotrophins, with membrane receptors **(A)**. Alternatively, mRNP granules can be transported into synapses and stored for later use **(C)**, or excluded from other synapses **(D)**. Local translation of mitochondrial proteins could help to maintain a healthy supply of axonal mitochondria **(D)**. Axonal survival factors may also be translated locally. For example, NMNAT2 has a half-life of 4 h, and even if transported via fast axonal transport, would not make it to the most distance synapses before significant degradation.

Finally, axonal translation may provide a local supply of essential axon survival factors. Neurotrophins are important regulators of axonal survival that rely on both transported and locally translated proteins to exert their protective effects. For example, stimulation of axons by neurotrophins coordinates transcription of the antiapoptotic gene *bcl-w* with transport of bcl-w mRNA to the axon and subsequent local translation (Cosker et al., 2013). Because the inhibition of axonal protein synthesis with cycloheximide abolishes the protective effects of neurotrophins, local synthesis of other axonal survival proteins is likely (Pazyra-Murphy et al., 2009; Pease and Segal, 2014). A possible example is nicotinamide nucleotide adenylyltransferase 2 (NMNAT2), an essential axon survival factor with a half-life of only 4 h (Gilley and Coleman, 2010). Even if NMNAT2 were transported by fast axonal transport, estimated to move cargo at a speed of 400 mm/day, the protein would only travel ~67 mm before 50 percent degradation (Hirokawa et al., 2010). This would result in vanishingly low levels of NMNAT2 in the most distal axons in large mammals, including humans. Distinct neuronal types may require different balances of transported vs. locally translated NMNAT2 (**Figure 1**).

RECENT EVIDENCE FOR LOCAL TRANSLATION IN ADULT MAMMALIAN AXONS

Despite these arguments, the physiological significance of axonal translation in nervous system maintenance remains ambiguous. Asymmetrical mRNA localization is a commonly utilized communication strategy for many types of mature polarized cells. (Xing and Bassell, 2013). It is tempting to hypothesize that the longest axons *in vivo*, such as mature sensory and motor peripheral axons, may be the most reliant on mRNA transport and local translation for homeostasis. Mature sensory axons possess a complex repertoire of mRNA, and it is suspected that the microtubule stabilizing agent, Paclitaxel, causes sensory neuropathy at least in part by impairing axonal

transport (Scripture et al., 2006; Gumy et al., 2011). More direct evidence of neurodegeneration as a result of dysregulation of mRNA transport is found with mutations in the RNA binding protein, SMN1, which cause the severe motor neuron disease, spinal muscular atrophy (Wang et al., 2016). Mutations in at least five members of the ubiquitously expressed family of proteins, tRNA synthetases, cause the specific degeneration of sensory and motor axons, supporting the idea that local translation of transported mRNA is crucial for axonal maintenance (Antonellis and Green, 2008).

A challenge in establishing axonal translation in mature mammalian neurons is studying axons in isolation from their cell bodies and other supporting cell types *in vivo*. The genetic method, translating ribosome affinity purification (TRAP), now allows for axonally-derived populations of ribosomes and their associated RNA to be analyzed without fear of contamination from other cell types. Shigeoka, et al. used the RiboTag knockin mouse line, in which Cre-mediated recombination results in expression of a triple HA-tagged ribosomal protein, RPL22 (Sanz et al., 2009; Shigeoka et al., 2016). Ribosome-bound mRNAs in retinal ganglion cell (RGC) axons were isolated from their CNS targets in developing and adult mice. Comparison of cell somas in the retina to axons in the brain revealed distinct populations of ribosome-associated mRNAs in axons. Axons at all ages were enriched for the gene ontology (GO) terms "cellular metabolism" and "mitochondrial respiratory chain," suggesting that mitochondrial proteins are indeed locally translated in developing and adult axons. Analysis of developmental stages revealed that axonal translation is intimately associated with RGC circuit assembly. In contrast, adult axons are enriched for transcripts related to the maintenance of neurotransmission, including components of the trans-SNARE complex, glutamate receptors, and neurotrophin receptors. NMNAT2 transcript is associated with ribosomes in both developing and adult axons, but more highly enriched at the adult stage. Neurotrophin-induced survival signals, including components of the CREB and STAT3 pathways, are also enriched in the adult axon. This study provides key evidence that axonal translation in adult RGCs supports metabolic function, neurotransmission, axon survival, and many other aspects of axonal homeostasis.

APPROACHES TO ILLUMINATE THE ROLE OF AXONAL TRANSLATION IN NEURONAL HOMEOSTASIS

Additional studies are needed to provide a complete picture of the physiological relevance of translation in adult mammalian axons *in vivo,* and to definitively show when and where axonal translation is occurring. Visualization of nascent protein would provide the strongest evidence for axonal translation. Similar to the approach used by Aakalu et al. (2001) for the visualization of dendritic translation, Willis et al. used the 3′ UTR of rat β-actin mRNA to drive axonal localization of a GFP reporter protein containing a membrane tether. GFP protein was indeed locally synthesized in cultured axons of adult, rat DRGs and mRNA was transported to axons of adult central and peripheral neurons *in vivo* (Willis et al., 2007, 2011). Single molecule translation imaging (SMTI) was recently used to determine the temporal and spatial dynamics of β-actin translation in cultured *Xenopus* RGC axons (Strohl et al., 2017). The fast-folding, fast-bleaching fluorescent protein, Venus, was fused to the full-length β-actin sequence, and translation was visualized under baseline conditions and with Netrin-1 stimulation. Real-time visualization of axonally translated protein *in vivo* in a mammalian system is the next step. *In vivo* expression of a construct similar to that used by Strohl et al. could be driven in neurons and temporally and spatially analyzed using SMTI. TRAP studies could provide a list of axonally translated proteins in a given cell type with which to drive axonal localization of the reporter.

While the above experiment would unequivocally demonstrate axonal translation *in vivo*, it is limited in scope to demonstrating the synthesis of one protein at a time. New *in vivo* techniques for large-scale labeling of nascent proteins will be invaluable to the full characterization of the axonal proteome. Ultimately, a complete catalog of axonally translated proteins at developmental and adult stages of life in each neuronal cell type will be needed to understand the intricacies of axonal translation, its contribution to neuronal homeostasis, and how its disruption can lead to neurodegeneration.

AUTHOR CONTRIBUTIONS

RB assisted in the planning and editing of the paper, ES researched and wrote the manuscript.

FUNDING

This work was supported by Ruth L. Kirschstein National Research Service Award (NRSA) Individual Predoctoral Fellowship, Grant number: 1F31NS100328-01 to ES, and RO1 NS054154 and R13 NS098725 to RB.

REFERENCES

Aakalu, G., Smith, W. B., Nguyen, N., Jiang, C., and Schuman, E. M. (2001). Dynamic visualization of local protein synthesis in hippocampal neurons. *Neuron* 30, 489–502. doi: 10.1016/S0896-6273(01)00295-1

Antonellis, A., and Green, E. D. (2008). The role of aminoacyl-tRNA synthetases in genetic diseases. *Annu. Rev. Genomics Hum. Genet.* 9, 87–107. doi: 10.1146/annurev.genom.9.081307.164204

Aschrafi, A., Schwechter, A. D., Mameza, M. G., Natera-Naranjo, O., Gioio, A. E., and Kaplan, B. B. (2008). MicroRNA-338 regulates local cytochrome c oxidase IV mRNA levels and oxidative phosphorylation in the axons of sympathetic neurons. *J. Neurosci.* 28, 12581–12590. doi: 10.1523/JNEUROSCI.3338-08.2008

Bassell, G. J., Zhang, H., Byrd, A. L., Femino, A. M., Singer, R. H., Taneja, K. L., et al. (1998). Sorting of beta-actin mRNA and protein to neurites and growth cones in culture. *J. Neurosci.* 18, 251–265.

Beattie, D. S. (1969). The biosynthesis of the protein and lipid components of the inner and outer membranes of rat liver mitochondria. *Biochem. Biophys. Res. Commun.* 35, 67–74. doi: 10.1016/0006-291X(69)90483-5

Bolam, J. P., and Pissadaki, E. K. (2012). Living on the edge with too many mouths to feed: why dopamine neurons die. *Mov. Disord.* 27, 1478–1483. doi: 10.1002/mds.25135

Bunge, M. B. (1973). Fine structure of nerve fibers and growth cones of isolated sympathetic neurons in culture. *J. Cell Biol.* 56, 713–735. doi: 10.1083/jcb.56.3.713

Caceres, A., Busciglio, J., Ferreira, A., and Steward, O. (1988). An immunocytochemical and biochemical study of the microtubule-associated protein MAP-2 during post-lesion dendritic remodeling in the central nervous system of adult rats. *Brain Res.* 427, 233–246. doi: 10.1016/0169-328X(88)90046-0

Cosker, K. E., Pazyra-Murphy, M. F., Fenstermacher, S. J., and Segal, R. A. (2013). Target-derived neurotrophins coordinate transcription and transport of bclw to prevent axonal degeneration. *J. Neurosci.* 33, 5195–5207. doi: 10.1523/JNEUROSCI.3862-12.2013

Court, F. A., and Coleman, M. P. (2012). Mitochondria as a central sensor for axonal degenerative stimuli. *Trends Neurosci.* 35, 364–372. doi: 10.1016/j.tins.2012.04.001

Court, F. A., Hendriks, W. T., MacGillavry, H. D., Alvarez, J., and van Minnen, J. (2008). Schwann cell to axon transfer of ribosomes: toward a novel understanding of the role of glia in the nervous system. *J. Neurosci.* 28, 11024–11029. doi: 10.1523/JNEUROSCI.2429-08.2008

Court, F. A., Midha, R., Cisterna, B. A., Grochmal, J., Shakhbazau, A., Hendriks, W. T., et al. (2011). Morphological evidence for a transport of ribosomes from Schwann cells to regenerating axons. *Glia* 59, 1529–1539. doi: 10.1002/glia.21196

Droz, B., and Leblond, C. P. (1963). Axonal migration of proteins in the central nervous system and peripheral nerves as shown by radioautography. *J. Comp. Neurol.* 121, 325–346. doi: 10.1002/cne.901210304

Edstrom, A., and Sjostrand, J. (1969). Protein synthesis in the isolated Mauthner nerve fibre of goldfish. *J. Neurochem.* 16, 67–81. doi: 10.1111/j.1471-4159.1969.tb10344.x

Eng, H., Lund, K., and Campenot, R. B. (1999). Synthesis of beta-tubulin, actin, and other proteins in axons of sympathetic neurons in compartmented cultures. *J. Neurosci.* 19, 1–9.

Eyman, M., Cefaliello, C., Ferrara, E., De Stefano, R., Lavina, Z. S., Crispino, M., et al. (2007). Local synthesis of axonal and presynaptic RNA in squid model systems. *Eur. J. Neurosci.* 25, 341–350. doi: 10.1111/j.1460-9568.2007.05304.x

Flexner, J. B., Flexner, L. B., and Stellar, E. (1963). Memory in mice as affected by intracerebral puromycin. *Science* 141, 57–59. doi: 10.1126/science.141.3575.57

Gilley, J., and Coleman, M. P. (2010). Endogenous Nmnat2 is an essential survival factor for maintenance of healthy axons. *PLoS Biol.* 8:e1000300. doi: 10.1371/journal.pbio.1000300

Giuditta, A., Cupello, A., and Lazzarini, G. (1980). Ribosomal RNA in the axoplasm of the squid giant axon. *J. Neurochem.* 34, 1757–1760. doi: 10.1111/j.1471-4159.1980.tb11271.x

Giuditta, A., Dettbarn, W. D., and Brzin, M. (1968). Protein synthesis in the isolated giant axon of the squid. *Proc. Natl. Acad. Sci. U.S.A.* 59, 1284–1287. doi: 10.1073/pnas.59.4.1284

Giuditta, A., Hunt, T., and Santella, L. (1986). Rapid important paper Messenger RNA in squid axoplasm. *Neurochem. Int.* 8, 435–442. doi: 10.1016/0197-0186(86)90019-7

Giuditta, A., Menichini, E., Perrone Capano, C., Langella, M., Martin, R., Castigli, E., et al. (1991). Active polysomes in the axoplasm of the squid giant axon. *J. Neurosci. Res.* 28, 18–28. doi: 10.1002/jnr.490280103

Gumy, L. F., Yeo, G. S., Tung, Y. C., Zivraj, K. H., Willis, D., Coppola, G., et al. (2011). Transcriptome analysis of embryonic and adult sensory axons reveals changes in mRNA repertoire localization. *RNA* 17, 85–98. doi: 10.1261/rna.2386111

Hillefors, M., Gioio, A. E., Mameza, M. G., and Kaplan, B. B. (2007). Axon viability and mitochondrial function are dependent on local protein synthesis in sympathetic neurons. *Cell. Mol. Neurobiol.* 27, 701–716. doi: 10.1007/s10571-007-9148-y

Hirokawa, N., Niwa, S., and Tanaka, Y. (2010). Molecular motors in neurons: transport mechanisms and roles in brain function, development, and disease. *Neuron* 68, 610–638. doi: 10.1016/j.neuron.2010.09.039

Jung, H., Yoon, B. C., and Holt, C. E. (2012). Axonal mRNA localization and local protein synthesis in nervous system assembly, maintenance and repair. *Nat. Rev. Neurosci.* 13, 308–324. doi: 10.1038/nrn3274

Kang, H., and Schuman, E. M. (1996). A requirement for local protein synthesis in neurotrophin-induced hippocampal synaptic plasticity. *Science* 273, 1402–1406. doi: 10.1126/science.273.5280.1402

Knowles, R. B., Sabry, J. H., Martone, M. E., Deerinck, T. J., Ellisman, M. H., Bassell, G. J., et al. (1996). Translocation of RNA granules in living neurons. *J. Neurosci.* 16, 7812–7820.

Koenig, E. (1967). Synthetic mechanisms in the axon. IV. *In vitro* incorporation of [^{3}H]precursors into axonal protein and RNA. *J. Neurochem.* 14, 437–446. doi: 10.1111/j.1471-4159.1967.tb09542.x

Koenig, E., Martin, R., Titmus, M., and Sotelo-Silveira, J. R. (2000). Cryptic peripheral ribosomal domains distributed intermittently along mammalian myelinated axons. *J. Neurosci.* 20, 8390–8400.

Lasek, R. J., Dabrowski, C., and Nordlander, R. (1973). Analysis of axoplasmic RNA from invertebrate giant axons. *Nat. New Biol.* 244, 162–165. doi: 10.1038/newbio244162a0

Lasek, R. J., Gainer, H., and Barker, J. L. (1977). Cell-to-cell transfer of glial proteins to the squid giant axon. The glia-neuron protein trnasfer hypothesis. *J. Cell Biol.* 74, 501–523. doi: 10.1083/jcb.74.2.501

Leung, K. M., van Horck, F. P., Lin, A. C., Allison, R., Standart, N., and Holt, C. E. (2006). Asymmetrical beta-actin mRNA translation in growth cones mediates attractive turning to netrin-1. *Nat. Neurosci.* 9, 1247–1256. doi: 10.1038/nn1775

Matsuda, W., Furuta, T., Nakamura, K. C., Hioki, H., Fujiyama, F., Arai, R., et al. (2009). Single nigrostriatal dopaminergic neurons form widely spread and highly dense axonal arborizations in the neostriatum. *J. Neurosci.* 29, 444–453. doi: 10.1523/JNEUROSCI.4029-08.2009

Merianda, T. T., Lin, A. C., Lam, J. S., Vuppalanchi, D., Willis, D. E., Karin, N., et al. (2009). A functional equivalent of endoplasmic reticulum and Golgi in axons for secretion of locally synthesized proteins. *Mol. Cell. Neurosci.* 40, 128–142. doi: 10.1016/j.mcn.2008.09.008

Ming, G., Lohof, A. M., and Zheng, J. Q. (1997). Acute morphogenic and chemotropic effects of neurotrophins on cultured embryonic Xenopus spinal neurons. *J. Neurosci.* 17, 7860–7871.

Olink-Coux, M., and Hollenbeck, P. J. (1996). Localization and active transport of mRNA in axons of sympathetic neurons in culture. *J. Neurosci.* 16, 1346–1358.

Palay, S. L., and Palade, G. E. (1955). The fine structure of neurons. *J. Biophys. Biochem. Cytol.* 1, 69–88. doi: 10.1083/jcb.1.1.69

Pazyra-Murphy, M. F., Hans, A., Courchesne, S. L., Karch, C., Cosker, K. E., Heerssen, H. M., et al. (2009). A retrograde neuronal survival response: target-derived neurotrophins regulate MEF2D and bcl-w. *J. Neurosci.* 29, 6700–6709. doi: 10.1523/JNEUROSCI.0233-09.2009

Pease, S. E., and Segal, R. A. (2014). Preserve and protect: maintaining axons within functional circuits. *Trends Neurosci.* 37, 572–582. doi: 10.1016/j.tins.2014.07.007

Perry, R. B., and Fainzilber, M. (2014). Local translation in neuronal processes—*in vivo* tests of a "heretical hypothesis." *Dev. Neurobiol.* 74, 210–217. doi: 10.1002/dneu.22115

Perry, R. B., Rishal, I., Doron-Mandel, E., Kalinski, A. L., Medzihradszky, K. F., Terenzio, M., et al. (2016). Nucleolin-Mediated RNA localization regulates neuron growth and cycling cell size. *Cell Rep.* 16, 1664–1676. doi: 10.1016/j.celrep.2016.07.005

Sanz, E., Yang, L., Su, T., Morris, D. R., McKnight, G. S., and Amieux, P. S. (2009). Cell-type-specific isolation of ribosome-associated mRNA from complex tissues. *Proc. Natl. Acad. Sci. U.S.A.* 106, 13939–13944. doi: 10.1073/pnas.0907143106

Schwarz, T. L. (2013). Mitochondrial trafficking in neurons. *Cold Spring Harb. Perspect. Biol.* 5:a011304. doi: 10.1101/cshperspect.a011304

Scripture, C. D., Figg, W. D., and Sparreboom, A. (2006). Peripheral neuropathy induced by paclitaxel: recent insights and future perspectives. *Curr. Neuropharmacol.* 4, 165–172. doi: 10.2174/157015906776359568

Shigeoka, T., Jung, H., Jung, J., Turner-Bridger, B., Ohk, J., Lin, J. Q., et al. (2016). Dynamic axonal translation in developing and mature visual circuits. *Cell* 166, 181–192. doi: 10.1016/j.cell.2016.05.029

Steward, O. (1983). Polyribosomes at the base of dendritic spines of central nervous system neurons–their possible role in synapse construction and modification. *Cold Spring Harb. Symp. Quant Biol.* 48(Pt 2), 745–759. doi: 10.1101/SQB.1983.048.01.077

Steward, O., and Levy, W. B. (1982). Preferential localization of polyribosomes under the base of dendritic spines in granule cells of the dentate gyrus. *J. Neurosci.* 2, 284–291.

Steward, O., and Ribak, C. E. (1986). Polyribosomes associated with synaptic specializations on axon initial segments: localization of protein-synthetic machinery at inhibitory synapses. *J. Neurosci.* 6, 3079–3085.

Strohl, F., Lin, J. Q., Laine, R. F., Wong, H. H., Urbancic, V., Cagnetta, R., et al. (2017). Single molecule translation imaging visualizes the dynamics of local beta-actin synthesis in retinal axons. *Sci. Rep.* 7, 709. doi: 10.1038/s41598-017-00695-7

Tcherkezian, J., Brittis, P. A., Thomas, F., Roux, P. P., and Flanagan, J. G. (2010). Transmembrane receptor DCC associates with protein synthesis machinery and regulates translation. *Cell* 141, 632–644. doi: 10.1016/j.cell.2010.04.008

Tennyson, V. M. (1970). The fine structure of the axon and growth cone of the dorsal root neuroblast of the rabbit embryo. *J. Cell Biol.* 44, 62–79. doi: 10.1083/jcb.44.1.62

Twiss, J. L., Smith, D. S., Chang, B., and Shooter, E. M. (2000). Translational control of ribosomal protein L4 mRNA is required for rapid neurite regeneration. *Neurobiol. Dis.* 7, 416–428. doi: 10.1006/nbdi.2000.0293

Wang, E. T., Taliaferro, J. M., Lee, J. A., Sudhakaran, I. P., Rossoll, W., Gross, C., et al. (2016). Dysregulation of mRNA localization and translation in genetic disease. *J. Neurosci.* 36, 11418–11426. doi: 10.1523/JNEUROSCI.2352-16.2016

Weiss, P., and Hiscoe, H. B. (1948). Experiments on the mechanism of nerve growth. *J. Exp. Zool.* 107, 315–395. doi: 10.1002/jez.1401070302

Willis, D. E., van Niekerk, E. A., Sasaki, Y., Mesngon, M., Merianda, T. T., Williams, G. G., et al. (2007). Extracellular stimuli specifically regulate localized levels of individual neuronal mRNAs. *J. Cell Biol.* 178, 965–980. doi: 10.1083/jcb.200703209

Willis, D. E., Xu, M., Donnelly, C. J., Tep, C., Kendall, M., Erenstheyn, M., et al. (2011). Axonal localization of transgene mRNA in mature PNS and CNS neurons. *J. Neurosci.* 31, 14481–14487. doi: 10.1523/JNEUROSCI.2950-11.2011

Willis, D., Li, K. W., Zheng, J. Q., Chang, J. H., Smit, A. B., Kelly, T., et al. (2005). Differential transport and local translation of cytoskeletal, injury-response, and neurodegeneration protein mRNAs in axons. *J. Neurosci.* 25, 778–791. doi: 10.1523/JNEUROSCI.4235-04.2005

Wu, K. Y., Hengst, U., Cox, L. J., Macosko, E. Z., Jeromin, A., Urquhart, E. R., et al. (2005). Local translation of RhoA regulates growth cone collapse. *Nature* 436, 1020–1024. doi: 10.1038/nature03885

Xing, L., and Bassell, G. J. (2013). mRNA localization: an orchestration of assembly, traffic and synthesis. *Traffic* 14, 2–14. doi: 10.1111/tra.12004

Zhang, H. L., Eom, T., Oleynikov, Y., Shenoy, S. M., Liebelt, D. A., Dictenberg, J. B., et al. (2001). Neurotrophin-induced transport of a beta-actin mRNP complex increases beta-actin levels and stimulates growth cone motility. *Neuron* 31, 261–275. doi: 10.1016/S0896-6273(01)00357-9

Zhang, H. L., Singer, R. H., and Bassell, G. J. (1999). Neurotrophin regulation of beta-actin mRNA and protein localization within growth cones. *J. Cell Biol.* 147, 59–70. doi: 10.1083/jcb.147.1.59

Zhang, X., and Poo, M. M. (2002). Localized synaptic potentiation by BDNF requires local protein synthesis in the developing axon. *Neuron* 36, 675–688. doi: 10.1016/S0896-6273(02)01023-1

Zheng, J. Q., Kelly, T. K., Chang, B., Ryazantsev, S., Rajasekaran, A. K., Martin, K. C., et al. (2001). A functional role for intra-axonal protein synthesis during axonal regeneration from adult sensory neurons. *J. Neurosci.* 21, 9291–9303.

Zheng, J. Q., Wan, J. J., and Poo, M. M. (1996). Essential role of filopodia in chemotropic turning of nerve growth cone induced by a glutamate gradient. *J. Neurosci.* 16, 1140–1149.

Conflict of Interest Statement: The authors declare that the research was conducted in the absence of any commercial or financial relationships that could be construed as a potential conflict of interest.

frontiers in Neuroscience

ORIGINAL RESEARCH
published: 24 August 2017
doi: 10.3389/fnins.2017.00478

Investigations into Hypoxia and Oxidative Stress at the Optic Nerve Head in a Rat Model of Glaucoma

Glyn Chidlow, John P. M. Wood and Robert J. Casson*

Ophthalmic Research Laboratories, Discipline of Ophthalmology and Visual Sciences, University of Adelaide, Adelaide, SA, Australia

The vascular hypothesis of glaucoma proposes that retinal ganglion cell axons traversing the optic nerve head (ONH) undergo oxygen and nutrient insufficiency as a result of compromised local blood flow, ultimately leading to their degeneration. To date, evidence for the hypothesis is largely circumstantial. Herein, we made use of an induced rat model of glaucoma that features reproducible and widespread axonal transport disruption at the ONH following chronic elevation of intraocular pressure. If vascular insufficiency plays a role in the observed axonal transport failure, there should exist a physical signature at this time point. Using a range of immunohistochemical and molecular tools, we looked for cellular events indicative of vascular insufficiency, including the presence of hypoxia, upregulation of hypoxia-inducible, or antioxidant-response genes, alterations to antioxidant enzymes, increased formation of superoxide, and the presence of oxidative stress. Our data show that ocular hypertension caused selective hypoxia within the laminar ONH in 11/13 eyes graded as either medium or high for axonal transport disruption. Hypoxia was always present in areas featuring injured axons, and, the greater the abundance of axonal transport disruption, the greater the likelihood of a larger hypoxic region. Nevertheless, hypoxic regions were typically focal and were not necessarily evident in sections taken deeper within the same ONH, while disrupted axonal transport was frequently encountered without any discernible hypoxia. Ocular hypertension caused upregulation of heme oxygenase-1—an hypoxia-inducible and redox-sensitive enzyme—in ONH astrocytes. The distribution and abundance of heme oxygenase-1 closely matched that of axonal transport disruption, and encompassed hypoxic regions and their immediate penumbra. Ocular hypertension also caused upregulations in the iron-regulating protein ceruloplasmin, the anaerobic glycolytic enzyme lactate dehydrogenase, and the transcription factors cFos and p-cJun. Moreover, ocular hypertension increased the generation of superoxide radicals in the retina and ONH, as well as upregulating the active subunit of the superoxide-generating enzyme NADPH oxidase, and invoking modest alterations to antioxidant-response enzymes. The results of this study provide further indirect support for the hypothesis that reduced blood flow to the ONH contributes to axonal injury in glaucoma.

Keywords: glaucoma, optic nerve head, axonal transport, hypoxia, oxidative stress, astrocyte, retinal ganglion cell

OPEN ACCESS

Edited by:
Samuel David Crish,
Northeast Ohio Medical University,
United States

Reviewed by:
Denise M. Inman,
Northeast Ohio Medical University,
United States
Roland Brandt,
University of Osnabrück, Germany
Wendi Lambert,
Vanderbilt University Medical Center,
United States

****Correspondence:***
Glyn Chidlow
glyn.chidlow@sa.gov.au

Specialty section:
This article was submitted to Neurodegeneration, a section of the journal Frontiers in Neuroscience

Received: *07 May 2017*
Accepted: *11 August 2017*
Published: *24 August 2017*

Citation:
Chidlow G, Wood JPM and Casson RJ (2017) Investigations into Hypoxia and Oxidative Stress at the Optic Nerve Head in a Rat Model of Glaucoma. Front. Neurosci. 11:478. doi: 10.3389/fnins.2017.00478

INTRODUCTION

Glaucoma, the leading cause of irreversible blindness worldwide (Quigley and Broman, 2006), encompasses a family of neurodegenerative diseases, all of which feature a clinically characteristic optic neuropathy (Casson et al., 2012). Despite significant progress in recent decades, the pathogenesis of glaucoma remains poorly understood, while therapeutic options are restricted to reducing intraocular pressure (IOP), the foremost treatable risk factor for the disease. In rodent (Howell et al., 2007; Crish et al., 2010; Salinas-Navarro et al., 2010; Chidlow et al., 2011b; Dengler-Crish et al., 2014), as well as primate (Anderson and Hendrickson, 1974; Quigley and Anderson, 1976; Minckler et al., 1977), models of glaucoma, failure of orthograde axonal transport has emerged as the earliest detectable pathological event. While the primary site of axonal injury in glaucoma has not been unequivocally identified, data from clinical, as well as animal, studies have highlighted the crucial role played by the optic nerve head (ONH)—the location where retinal ganglion cell (RGC) axons converge to form the optic nerve and traverse the lamina—in this process. In simple terms, two theories have been proposed to account for axonal injury at the ONH in glaucoma: "the mechanical" and "the vascular" theories (Fechtner and Weinreb, 1994).

The vascular hypothesis proposes that RGC axons passing through the ONH undergo chronic or intermittent hypoxia, ischemia, and/or hypoglycemia as a result of compromised local blood flow (Flammer et al., 2002). The unmyelinated axons of the ONH are thought to be highly vulnerable to a decreased oxygen/nutrient supply owing to their prodigious energy requirements, which are served by a high local density of mitochondria (Barron et al., 2004). Deficits in nutrients or oxygen will not only result in RGC axons becoming bioenergetically compromised (Inman and Harun-Or-Rashid, 2017), but, importantly, will also dramatically increase production of reactive oxygen species (ROS), leading to oxidative stress (Chrysostomou et al., 2013). The relationship between ischemia-reperfusion and oxidative stress is well-known (Chen et al., 2011). It seems paradoxical that low oxygen availability *per se* would also result in an increase in ROS; however, numerous studies have reported that hypoxia increases generation of ROS within complex III of mitochondria (see Guzy and Schumacker, 2006). The rationale for this phenomenon is that during hypoxia, mitochondrial electron transport slows, augmenting the reduction state of electron carriers. This accumulation of reducing equivalents favors superoxide production at low oxygen concentrations. Thus, reperfusion is not essential for oxidative stress. Oxidative stress itself represents the failure of endogenous antioxidant defenses, which comprise both enzymatic and non-enzymatic components, to efficiently detoxify oxidative free radical species. Cumulative oxidative stress causes damage to DNA, proteins and lipids.

There is a wealth of physiological data supporting blood flow incompetence at the ONH in glaucoma individuals (Satilmis et al., 2003; Schmidl et al., 2011; Yanagi et al., 2011); however, direct evidence for the presence of ischemia/hypoxia within the ONH is predictably sparse. Nevertheless, there is an increasing body of indirect evidence for the vascular hypothesis, which includes reports of increases in oxidative stress markers in the serum, aqueous humor, and retina of glaucoma patients (Farkas et al., 2004; Aslan et al., 2013; Benoist d'Azy et al., 2016). These studies suggest a general compromise of antioxidant defenses in glaucoma. Interestingly, oxidative stress-related events have also been documented in ONH astrocyte and lamina cribrosa cell cultures from glaucoma patients (Malone and Hernandez, 2007; McElnea et al., 2011). In rodent models of glaucoma, convincing evidence exists for enhanced ROS levels and increased oxidative stress within the retina (see for example Moreno et al., 2004; Ko et al., 2005; Inman et al., 2013); somewhat surprisingly, however, the ONH itself has received scant attention.

In the current study, we made use of an induced rat model of glaucoma that features reproducible and widespread axonal transport disruption at the ONH by 24 h after chronic elevation of IOP (Salinas-Navarro et al., 2010; Chidlow et al., 2011b). It has been postulated that the model precipitates a crush-like injury to ON axons (Vidal-Sanz et al., 2011); however, if vascular insufficiency at the ONH—caused by ocular hypertension (OHT)—plays a role in the observed axonal transport failure, there should be a physical signature at this time point. Using a range of immunohistochemical and molecular tools, we looked for cellular events indicative of vascular insufficiency, including the presence of hypoxia, upregulation of hypoxia-inducible or antioxidant-response genes, alterations to antioxidant enzymes, increased formation of superoxide, upregulation in ROS-generating NADPH oxidase, and the presence of oxidative stress.

MATERIALS AND METHODS

Animals and Procedures

This study was approved by the South Australia Pathology/Central Health Network Animal Ethics committee and conforms with the Australian Code of Practice for the Care and Use of Animals for Scientific Purposes, 2013. All procedures were performed under anesthesia (100 mg/kg ketamine and 10 mg/kg xylazine), and all efforts were made to minimize suffering. All experiments also conformed to the ARVO Statement for the Use of Animals in Ophthalmic and Vision Research. Adult Sprague-Dawley rats (220–300 g) were housed in a temperature- and humidity-controlled environment with a 12-h light, 12-h dark cycle, and were provided with food and water *ad libitum*.

Ocular hypertension was induced in the right eye of each animal by laser photocoagulation of the trabecular meshwork, as previously described (Ebneter et al., 2010). IOPs were measured in both eyes using a rebound tonometer, factory calibrated for use in rats. All animals demonstrated an adequate IOP elevation (minimum increase in IOP of 10 mmHg). One animal was excluded as a result of death under anesthesia and 1 due to hyphema. The number of rats analyzed for immunohistochemistry was as follows: 1 d time point, $n = 28$; 3 d time point, $n = 16$. Of the total number of rats analyzed at 1 d, $n = 16$ received an injection of pimonidazole for localization of regions of hypoxia (see below), while $n = 4$ received an injection of dihydroethidium for localization of superoxide radicals (see below). Of the total number of rats analyzed at 3 d, $n = 4$ received

an injection of dihydroethidium for localization of superoxide. In addition to animals used for immunohistochemistry, a further 14 (1 d time point) and 12 (3 d time point) rats were analyzed by qPCR/Western blotting. In all cases throughout the manuscript, "*n*" number refers to the number of animals analyzed.

Tissue Processing and Immunohistochemistry

For tissue harvesting of ONH for protein and RNA extraction, all rats were humanely killed by transcardial perfusion with physiological saline under terminal anesthesia. Eyes were immediately enucleated and ONH samples were prepared using the following method: the anterior portion and vitreous body from each eye were removed. The remaining eye-cup was subsequently dissected into a flattened whole-mount in the shape of a "maltese-cross." A biopsy punch of 2 mm in diameter (Stiefel Laboratories, Brentford, United Kingdom, cat # BIOPSY-5918) was then utilized to separate the ONH area from the remainder of the ocular tissue. The initial 1 mm length of optic nerve was also included within each sample, as was the very central central portion of the retina. ONH samples were placed in 400 μl of TRI-reagent and then sonicated. Subsequently, both total protein and total RNA were extracted.

For tissue harvesting for paraffin embedding, all rats were killed by transcardial perfusion with physiological saline under terminal anesthesia. Eyes were immediately enucleated and immersion fixed in 10% (w/v) neutral buffered formalin or, in some cases, in Davidson's fixative [22% formalin (37–40%) solution, 33% ethanol (95%), 11.5% glacial acetic acid] for 24 h, followed by routine processing for paraffin embedding. Eyes were marked in a specific and recorded location to ensure correct orientation during embedding and 4 μm serial sections were cut using a rotary microtome.

Colorimetric immunohistochemistry was performed as previously described (Chidlow et al., 2011a). Briefly, tissue sections were deparaffinized and endogenous peroxidase activity was blocked with H_2O_2. Antigen retrieval was performed by microwaving sections in 10 mM citrate buffer (pH 6.0) and non-specific labeling blocked with PBS containing 3% normal horse serum. Sections were incubated overnight at room temperature in primary antibody (see **Table 1**), followed by consecutive incubations with biotinylated secondary antibody (Vector, Burlingame, CA) and streptavidin-peroxidase conjugate (Pierce,

TABLE 1 | Primary Antibodies used in the study.

Protein	Source	Clone/Cat. No.	Species	Immunogen	Dilution
8-Hydroxy-2′-deoxyguanosine	Abcam	Cat# ab48508	Mouse	8-Hydroxy-2′-deoxyguanosine conjugated Keyhole Limpet Hemocyanin	1:20,000
Actin	Sigma	Clone AC-15	Mouse	Slightly modified β-cytoplasmic actin N-terminal peptide	1:20,000[W]
APP	[*]C Masters	Clone 22C11	Mouse	Purified recombinant Alzheimer precursor A4 (pre A4695) fusion protein.	1:1,500
Ceruloplasmin	Dako	Cat# Q0121	Rabbit	*Ceruloplasmin* isolated from human plasma	1:10,000[W]
cFOS	Santa-Cruz	Cat# sc-253	Rabbit	Epitope mapping within an internal region of c-Fos of human origin	1:5,000
CRALBP	Abcam	Cat# ab15051	Mouse	Recombinant full length human CRALBP	1:2,000
gp91^{phox}	BD Biosciences	Clone 53/gp91[phox]	Mouse	Mouse gp91[phox] aa. 450–556	1:500
HO-1	Enzo Life Sciences	Cat# SPA-895	Rabbit	Recombinant rat HO-1 (Hsp32) lacking the membrane spanning region	1:2,500, 1:2,000[W]
Interleukin-6	R&D Systems	Cat# AF506	Goat	*E. coli*-derived recombinant rat IL-6 Phe25-Thr211	1:500
Iba1	Wako	Cat# 019-19741	Rabbit	Synthetic peptide corresponding to the Iba1carboxy-terminal sequence	1:4,000[f]
LDH-A	Santa-Cruz	Cat# sc-27230	Goat	Epitope mapping at the N-terminus of LDH-A of human origin	1:2,000
Myelin basic protein	Dako	Cat# A0623	Rabbit	*Myelin basic, protein* isolated from human brain	1:3,000
p67^{phox}	BD Biosciences	Clone 29/p67phox	Mouse	Human p67 [phox] aa. 317-469	1:1,000[W]
p-cJUN	CST	Cat# 3270	Rabbit	Synthetic phosphopeptide corresponding to residues around Ser73 of human c-Jun	1:5,000
Pimonidazole	Hypoxyprobe Inc	Clone 4.3.11.3	Mouse	Pimonidazole adducts	1:500
SOD-1	Calbiochem	Clone 6F5	Mouse	Purified recombinant fragment of human SOD1 expressed in *E. Coli*	1:2,500
SOD-2	Antibody Technology Australia Pty Ltd	Cat# SOD2R	Rabbit	Human/rat/mouse SOD2 aa. 25–43	1:2,500
Transferrin receptor	ThermoFisher	Clone H68.4	Mouse	Recombinant human transferrin receptor	1:500
Vimentin	Dako	Clone V9	Mouse	Purified vimentin from porcine eye lens	1:200[f]

[f] Dilution used for 2-step fluorescent immunostaining procedure; [W] Dilution used for Western blotting; [*] Gifted by C Masters, University of Melbourne.

Rockford, IL). Color development was achieved using NovaRed substrate kit (Vector, Burlingame, CA) for 3 min. Sections were counterstained with hematoxylin, dehydrated, cleared in histolene, and mounted. Confirmation of the specificity of antibody labeling was judged by the morphology and distribution of the labeled cells, by the absence of signal when the primary antibody was replaced by isotype/serum controls, by comparison with the expected staining pattern based on our own, and other, previously published results, and, in some instances, by the detection within retinal samples of a protein at the expected molecular weight by Western blotting.

For double labeling fluorescent immunohistochemistry, visualization of one antigen was achieved using a 3-step procedure (primary antibody, biotinylated secondary antibody, streptavidin-conjugated AlexaFluor 488 or 594), while the second antigen was labeled by a 2-step procedure (primary antibody, secondary antibody conjugated to AlexaFluor 488 or 594). Sections were prepared as above, then incubated overnight at room temperature in the appropriate combination of primary antibodies. On the following day, sections were incubated with the appropriate biotinylated secondary antibody for the 3-step procedure plus the correct secondary antibody conjugated to AlexaFluor 488 or 594 for the 2-step procedure, followed by streptavidin-conjugated AlexaFluor 488 or 594. Sections were then mounted using anti-fade mounting medium and examined under a confocal fluorescence microscope.

Evaluation of Immunohistochemistry

All assessments were performed in a randomized, blinded manner. The presence or absence of a hypoxic region within each pimonidazole-injected rat was compared to the IOP of that rat and also to the magnitude of axonal transport disruption at the ONH. Disrupted axonal transport was assessed semi-quantitatively by immunolabeling either for interleukin-6 (IL-6) or β-Amyloid precursor protein (APP) accumulation throughout the ONH using a 4-point grading system (undetectable, low, medium, high; see **Figure 1**) as previously described (Chidlow et al., 2011b, 2012). Our previous data have shown that IL-6 and APP can be used interchangeably; they provide identical patterns of immunolabeling within the ONH at 24 h after IOP elevation and identical responses to tissue injury.

For assessment of the amount of heme oxygenase-1 (HO-1), lactate dehydrogenase-A (LDH-A), p-cJun, cFos, transferrin receptor, and NADPH oxidase immunoreactivities in treated and control animals, photomicrographs (350 × 260 μm) of the ONH (centered at ∼0.4 mm from the scleral margin), and of the proximal myelinated ON (centered at ∼1.4 mm from the scleral margin) were captured from each animal. The area of axonal tissue available for analysis within each ONH typically did not encompass the entire area of the photomicrograph, hence the image was cropped. The corresponding image from the ON of that animal was cropped identically, which permits direct comparison of the % area stained in the ONH vs. the ON. For HO-1, LDH-A, transferrin receptor, and NADPH oxidase, images underwent color deconvolution to eliminate haematoxylin staining. After manual thresholding, the area of positive immunolabeling was measured. Evaluations were performed using the ImageJ 1.42q software package platform (http://rsb.info.nih.gov/ij/) and data are presented as % area of immunolabeling ± SEM. For p-cJun and cFos, the number of cells with unambiguous positive nuclear staining were counted in each photomicrograph. The threshold for identification of positive labeling was performed manually and took into account comparison with template photomicrographs and inter-animal variability in background labeling. Data are presented as number of positive cells ± SEM. In addition, for HO-1, two photomicrographs (350 × 260 μm) of the central retina, taken at ∼500 μm from the ONH, were also captured and analyzed for % area of immunolabeling, as outlined above. Statistical analysis (control group vs. OHT group) was carried out by Student's unpaired *t*-test where parametric assumptions were met or Mann–Whitney Rank Sum Test where they were not.

Localization of Hypoxia

To detect cellular hypoxia, 60 mg/kg bodyweight pimonidazole hydrochloride (Hypoxyprobe^{TM}-1 kit, Hypoxyprobe Inc, Burlington, Massachusetts) diluted in sterile PBS was administered by intraperitoneal injection 3 h prior to killing, as previously described (Gardiner et al., 2005; Mowat et al., 2010). Pimonidazole forms covalent adducts in cells that have an partial pressure of oxygen which is <10 mmHg (Arteel et al., 1995). The subsequent staining of tissue sections with an anti-pimonidazole antibody reveals the presence of hypoxic cells (Holcombe et al., 2008). Rats were killed by transcardial perfusion with physiological saline, following which they were immersion fixed in 10% neutral buffered formalin and processed for paraffin embedding and immunohistochemistry, as described above. In pimonidazole-injected animals, tissue sections from three levels of the ONH were typically evaluated for hypoxia.

Localization of Intracellular Superoxide

The spatial production of superoxide was investigated by *in situ* detection of the oxidation product of dihydroethidium (DHE, Molecular Probes, USA). DHE, which is cell permeant, is converted intracellularly to an ethidium derivative, in the presence of superoxide (but not by hydrogen peroxide, hydroxyl radical or peroxynitrite). This ethidium derivative exhibits peak fluorescence in the red spectrum and binds to DNA (Zanetti et al., 2005). Five microliters of DHE solution (stock solution of 5 mM in dimethyl sufoxide, diluted to 200 μM in PBS) was administrated by intravitreal injection to both eyes 3 h prior to humane killing. Assuming a volume of vitreous humor of 100 μl, this equated to a final DHE concentration of ∼10 μM. Rats were killed by transcardial perfusion with physiological saline followed by 10% (w/v) neutral buffered formalin. After post-fixation overnight, also in 10% (w/v) neutral buffered formalin, 10 μm sagital sections were prepared on a cryostat, rinsed with PBS and then mounted in fluorescence-preserving mounting medium. Slides were photographed using a confocal fluorescence microscope with an excitation of 510–550 nm and an emission of >580 nm.

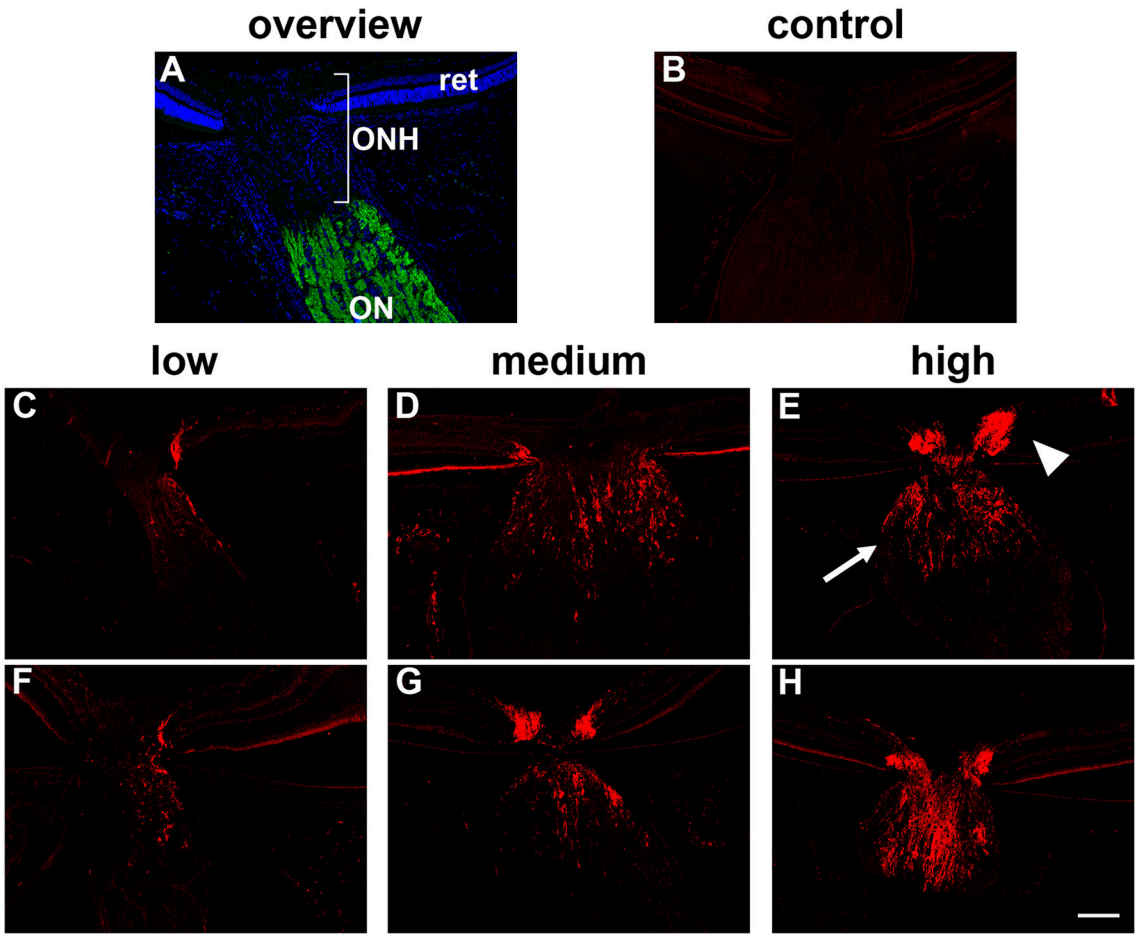

FIGURE 1 | Inter-animal variability in axonal transport disruption at the optic nerve head (ONH) 24 h after induction of ocular hypertension. **(A)** Overview of the anatomy of the rat ONH, as labeled with the nuclear dye DAPI. The location at which RGC axons become myelinated is demarcated by myelin basic protein (green). **(B)** In normal rats, minimal interleukin-6 is associated with RGC axons. **(C–H)** At 24 h after induction of chronic ocular hypertension, accumulation of interleukin-6 is evident within axons in the prelaminar (arrowhead) and laminar (arrow) ONH. The abundance of axonal transport disruption varies markedly between animals, ranging from a few to numerous immunopositive fibers, which can be classified, using a simple scoring system, as low, medium, or high; two examples are shown for each category. ON, optic nerve; ret, retina. Scale bar: 100 μm.

Real-Time RT-PCR

Real time PCR (qPCR) studies were carried out essentially as described previously (Chidlow et al., 2008). In brief, tissues were dissected, total RNA was isolated and first strand cDNA was synthesized from DNase-treated RNA samples. Real-time PCR reactions were carried out in 96-well optical reaction plates using the cDNA equivalent of 10 ng total RNA for each sample in a total volume of 20 μl containing 1 × SYBR Green or 1 × SSO Advanced PCR master mix (BioRad, Gladesville, Australia), forward and reverse primers. Thermal cycling conditions were 95°C for 3 min followed by 40 cycles of amplification comprising 95°C for 12 s, appropriate annealing temperature for 30 s and 72°C for 30 s. Primer pairs (**Table 2**) were designed from sequences contained in the Genbank database using the primer design software Primer 3 (http://bioinfo.ut.ee/primer3-0.4.0/primer3/) and were selected wherever possible to amplify sequences that spanned at least one intron. Primer sequences were analyzed for T_m (melting temperature), secondary structure and primer-dimer formation with NetPrimer analysis software (http://www.premierbiosoft.com/netprimer). PCR assays were performed using the CFX cycler (Bio-Rad) and all samples were run in duplicate. All mRNAs amplified with high efficiency and linearity during real-time PCR. Mean amplification efficiencies, as determined by plotting cycle threshold as a function of initial cDNA quantity, were in the range of 1.90–2.00. Results obtained from the qPCR experiments were, therefore, quantified using the comparative threshold cycle (C_T) method ($\Delta\Delta C_T$) for relative quantitation of gene expression, with a minor correction for amplification efficiency (Pfaffl, 2001). The ONH tissue extracts prepared via biopsy punch contain relatively low, but variable, amounts of central retina. Consequently, investigation into whether certain mRNAs, for example LDH-A, are upregulated in ONH astrocytes following induction of

ocular hypertension, is complicated by the fact that LDH-A, for example, is abundantly expressed in healthy photoreceptors and bipolar cells. To eliminate the influence of endogenous expression of mRNAs within the retina, all pPCR values were normalized to rhodopsin (which acts as a control for retinal content) and then expressed relative to controls. Statistical analysis was carried out by Student's unpaired *t*-test. The null hypothesis tested was that normalized C_T differences of target genes would be the same in control and treated ONH samples.

Western Immunoblotting

Electrophoresis/Western blotting was performed as previously described (Chidlow et al., 2010). In brief, ONH protein samples were prepared from TRI-reagent extracts as per the manufacturer's protocol. Extracted proteins were solubilized in homogenization buffer containing 1% SDS, diluted with an equal volume of sample buffer, and boiled for 3 min. Electrophoresis was performed using non-denaturing 10% polyacrylamide gels. After separation, proteins were transferred to polyvinylidine fluoride membranes for immunoprobing. Blocking of membranes was carried out in a solution of tris-buffered saline containing 0.1% (v/v) Tween-20 and 5% (w/v) non-fat dried skimmed milk. Membranes were then incubated consecutively with the appropriate primary antibody (**Table 1**), biotinylated secondary antibody and streptavidin-peroxidase conjugate; inter-step washes were carried out in tris-buffered saline (pH 7.4) containing 0.1% (v/v) Tween-20. Color development was achieved using 3-amino-9-ethylcarbazole. Images were captured and analyzed for densitometry using the program, Adobe PhotoShop CS2. Densitometry values were normalized for actin. Statistical analysis was carried out by Student's unpaired *t*-test (control group vs. OHT group). The null hypothesis tested was that densitometry measurements for target proteins (normalized for actin) would be the same in control and OHT samples.

RESULTS

Ocular Hypertension Causes a Variable Degree of Axonal Transport Disruption at the Optic Nerve Head

Previous studies, including our own, have shown that laser photocoagulation of the limbal tissues leads to a substantial and immediate elevation of IOP in the treated eye with the peak value occurring within the first 24 h (see Vidal-Sanz et al., 2011). Of the 16 rats injected with pimonidazole and detailed in **Table 3**, the mean baseline IOP was 12.1 ± 2.9 mm Hg (mean ± *SD*) and the mean IOP at time of death (24 h post-laser) was 36.7 ± 6.0

TABLE 3 | Characteristics of pimonidazole-injected rats.

Rat	IOP (baseline)	IOP (at 1 d)	Axonal transport disruption grade	Pimonidazole labeling (ONH)	HO-1 labeling (ONH)
1	12	40	Medium	No	Yes
2	10	36	Low	No	Yes
3	14	38	High	Yes	Yes
4	16	39	High	Yes	Yes
5	16	47	High	Yes	Yes
6	15	44	Medium	Yes	Yes
7	8	35	Medium	Yes	Yes
8	9	34	Low	No	Yes
9	11	25	Low	No	Yes
10	9	31	Medium	No	Yes
11	12	27	Medium	Yes	Yes
12	14	44	High	Yes	Yes
13	16	38	High	Yes	Yes
14	14	38	Medium	Yes	Yes
15	8	32	Medium	Yes	Yes
16	10	39	Medium	Yes	Yes

TABLE 2 | Primer sequences for mRNAs amplified by real-time RT-PCR.

mRNA	Primer sequences	Product size (bp)	Annealing temperature	Accession number
Rhodopsin	5′-CTCCATCTACAACCCAATCATC-3′ 5′-ACTCCTACAGTCAGCCACAGTC-3′	187	63°C	NM_033441
GCLM	5′-ATCTTGCCTCCTGCTGTGT-3′ 5′-CAGTTCTTTTGGGTCATTGTG-3′	95	60°C	NM_017305
LDH-A	5′-GCACTAAGCGGTCCCAAAAG-3′ 5′-ACAGCACCAACCCCAACAAC-3′	126	63°C	NM_017025
NQO1	5′-GGCTCTGAAGAAGAAAGGATGG-3′ 5′-GCTCCCCTGTGATGTCGTT-3′	95	62°C	NM_017000
NOX-2	5′-CACCCTTTCACCCTGACCTCT-3′ 5′-GCTCCCACTAACATCACCACCT-3′	215	63°C	NM_023965
Nrf2	5′-CGAAAAGGAGAGACAAGAGCAA-3′ 5′-GTGGGCAACCTGGGAGTAG-3′	160	62°C	NM_031789
Prdx6	5′-AAACTAAAACTGTCCATCCTCTACC-3′ 5′-ACCATCACACTCTCTCCCTTCT-3′	143	59°C	NM_053576
Transferrin receptor	5′-GTTTCCGCCATCTCAGTCATC-3′ 5′-CGGTCTGGTTCCTCATAGCC-3′	243	61°C	NM_022712

mm Hg. A similar magnitude of OHT was attained with all of the other rats analyzed in this study (data not shown).

Following 24 h of OHT, a proportion of RGC fibers passing through the ONH feature disrupted orthograde axonal transport. This can be visualized using the neural tracer cholera toxin B subunit, or by immunolabeling with antibodies directed against amyloid precursor protein (APP), or interleukin-6 (Chidlow et al., 2011b, 2012). In the current study, we used both APP and interleukin-6 to visualize compromised axons. There can be marked inter-animal variability in the extent of axonal transport disruption after induction of OHT. Using a semi-quantitative scoring system, ONH sections can be categorized as low, medium or high (see **Figure 1** for representative images). In general, rats with higher IOPs display greater axonal transport injury (Chidlow et al., 2011b). Categorization of the rats detailed in **Table 3** highlights this correlation: mean IOP for animals having their level of damage categorized as low = 31.7 ± 5.9 mm Hg; medium = 35.8 ± 5.5 mm Hg; high = 41.2 ± 4.1 mm Hg. Nevertheless, on an individual basis, IOP (as determined by rebound tonometry) is not a reliable predictor of pathology. Moreover, due to the sectorial nature of RGC injury in glaucoma, variability in the amount of axonal transport disruption is even evident when comparing different levels within the same ONH. It is important to consider these issues when assessing whether OHT is associated with hypoxia.

Ocular Hypertension Leads to Selective Hypoxia at the Optic Nerve Head

To detect any cellular hypoxia, pimonidazole was infused systemically 3 h prior to rats being humanely killed. As detailed in the Materials and Methods Section, pimonidazole forms stable covalent adducts with cells that have an oxygen partial pressure of <10 mmHg (Arteel et al., 1995), which can then be localized immunohistochemically in tissue sections. No pimonidazole labeling was evident in the optic nerve, ONH or retina of any of the untreated eyes (data not shown). Of the 16 OHT eyes, positive staining was detected within the ONH of 11 of them (**Table 3**). The 11 eyes positive for pimonidazole had a mean IOP of 38.3 ± 5.7 mm Hg, while the 5 negative eyes had a mean IOP of 33.2 ± 5.6 mm Hg, a difference that did not reach statistical significance ($P = 0.11$ by Student's unpaired *t*-test). Subdivision of the eyes by axonal transport disruption category revealed the following: 0/3 graded low for axonal transport disruption were positive for pimonidazole; 6/8 graded medium were positive; 5/5 graded high were positive (**Table 3**). A number of points are worth making regarding pimonidazole staining in OHT eyes: (1) no two animals were alike as regards the area or position of hypoxia; (2) pimonidazole always labeled in areas of the ONH featuring injured axons; (3) the greater the abundance of axonal transport disruption, the greater the likelihood of a large hypoxic region; (4) pimonidazole staining was observed in glial cells as well as axons; (5) hypoxic regions were sometimes very focal and not evident in sections taken deeper within the same ONH; (6) disrupted axonal transport was frequently encountered without any pimonidazole labeling; (7) no pimonidazole staining was observed in the prelaminar ONH, even in animals with prominent axonal transport disruption at this location; (8) no pimonidazole staining was observed in the portion of the optic nerve distal to the ONH. Representative images of pimonidazole staining in OHT eyes are provided in **Figures 2–4**. The images shown illustrate the points made above. Overall, the experiments with pimonidazole show that oxygen availability to regions within the ONH is reduced to hypoxic levels in some OHT eyes. It is highly likely that oxygen availability is reduced to some degree throughout the ONH, just not to the extent needed to produce covalent adducts of pimonidazole.

With regard to the retina, pimonidazole stained occassional RGCs in OHT eyes, typically in specimens categorized as high for axonal transport disruption. No unambiguous positive staining was observed in other classes of cells within the retina (**Figure 3**).

Ocular Hypertension Induces Heme Oxygenase-1 Expression in Optic Nerve Head Astrocytes

Low tissue oxygen availability can lead to a multitude of gene transcription changes mediated primarily via stabilization of two key transcription factors: hypoxia-inducible factor-1a (HIF-1) and nuclear factor erythroid 2-related factor 2 (Nrf2). HIF-1α and Nrf2, respectively, bind to and activate genes that possess the hypoxia response element and the antioxidant response element. HRE target genes are classically involved in oxygen homeostasis and anaerobic energy metabolism (Guillemin and Krasnow, 1997), while ARE target genes are characteristically antioxidant and detoxification enzymes (Wasserman and Fahl, 1997). Heme oxygenase-1 (HO-1) is a gene target of both Nrf2 and HIF-1. If low oxygen availability and increased production of ROS are involved in axonal transport disruption following induction of OHT, then HO-1 would be expected to be induced by neighboring glial cells, as occurs in the brain (Schipper et al., 2009).

Initially, we investigated HO-1 protein expression in dissected ONH samples (see Section Materials and Methods) from rats subjected to 1 and 3 d of OHT. The data showed a robust, statistically significant ($P < 0.001$) upregulation of HO-1 in treated ONH extracts at both time points (**Figure 4**). Next, we performed immunolabeling of HO-1 in tissue sections. No consistent patterns of HO-1 immunolabeling were evident in the optic nerve, ONH or retina of any of the contralateral, untreated eyes (data not shown). After 1 d of OHT, HO-1 immunolabeling was upregulated within ONH astrocytes (**Figure 5**, Supplementary Figure 1, **Table 3**). All rats analyzed, including the 16 pimonidazole-injected rats, displayed positive staining by ONH astrocytes (**Figure 5**). In the pimonidazole-injected rats, HO-1 was upregulated in the hypoxic region and immediate penumbra (**Figures 5A–C**). HO-1 expression was also observed in ONH sections of pimonidazole rats that did not feature an overt hypoxic region, including ONHs categorized as low for axonal transport disruption (**Figures 5D–G**). The extent of HO-1 expression closely matched the abundance of axonal transport disruption (**Figures 5H–K**). At 1 d after induction of OHT, HO-1 was largely restricted to the ONH. Quantification of the area of HO-1 labeling in images taken from the central retina,

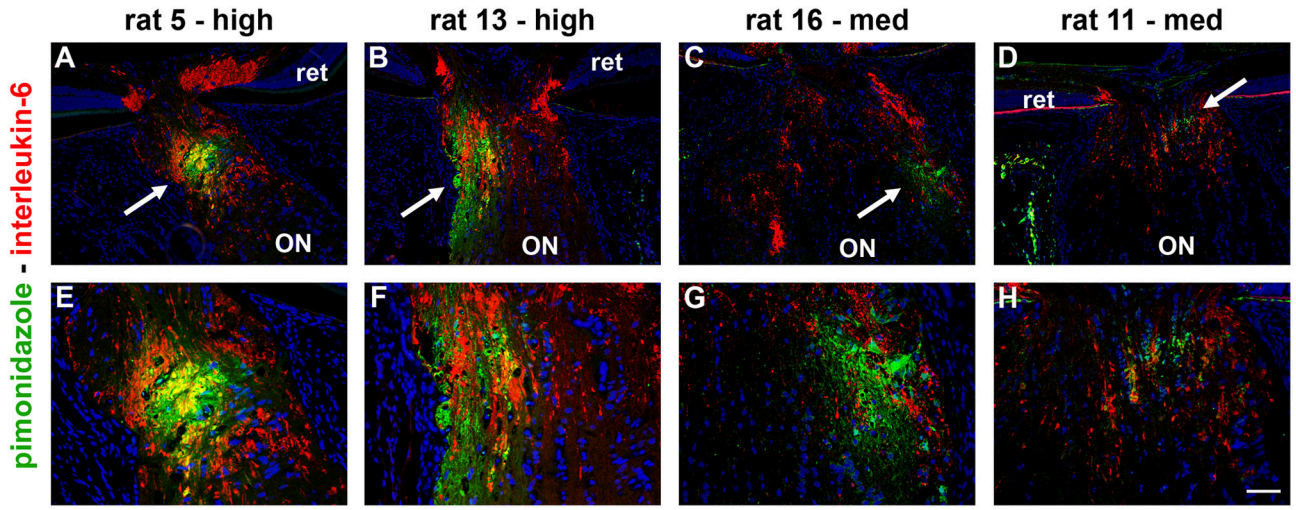

FIGURE 2 | Localization of hypoxia within the optic nerve head (ONH) at 24 h following induction of ocular hypertension. **(A–H)** Double labeling immunofluorescence of interleukin-6 (red), to demarcate those axons with disrupted axonal transport, with pimonidazole (green), to highlight hypoxic regions (arrows), in four representative animals. **(A–D)** are low magnification images, while **(E–H)** show the same sections at higher magnification. In the examples presented, the rats with high axonal transport disruption feature larger hypoxic regions than the rats with medium axonal transport disruption. The position of the hypoxic region can be seen to vary markedly between animals. ON, optic nerve; ret, retina. Scale bars: **(A–D)** = 100 μm; **(E–H)** = 50 μm.

ONH and myelinated optic nerve revealed a dramatic increase within the ONH, but only subtle changes in the retina and optic nerve (**Figure 5O**). In the retina, HO-1 was most commonly associated with astrocytes/Müller cell end feet in the prelaminar ONH. Occasional astrocytes, Müller cells, and microglia were HO-1-positive within the body of the retina (**Figures 5L–N**). After 3 d of OHT, the distribution of HO-1 immunolabeling was more widespread, encompassing retinal and ONH microglia, as well as astrocytes, patches of Müller cells and occassional RGCs (Supplementary Figure 1).

Ocular Hypertension Upregulates Lactate Dehydrogenase-A Expression in the Optic Nerve Head

Under conditions of reduced oxygen availability, metabolism of glucose to lactate via anaerobic glycolysis becomes the principal route by which cells generate ATP. Glycolytic genes have been repeatedly identified as inducible by hypoxia (Hu et al., 2003). To explore whether there is an alteration in glycolytic machinery within the ONH at 1 d after induction of OHT, we investigated expression of lactate dehydrogenase-A (LDH-A). qPCR analysis of dissected ONH samples revealed a statistically significant two-fold upregulation of LDH-A mRNA in the treated eye compared to the contralateral eye ($P < 0.05$; **Figure 6A**). Immunolabeling for LDH-A in control eyes revealed abundant expression within photoreceptors and bipolar cells in the retina, and weak labeling of axons and glial cells in the optic nerve (**Figures 6C–E**), in agreement with previous work (Casson et al., 2016). Following induction of elevated IOP, stronger expression of LDH-A was observed within the ONH, but never more distally in the optic nerve (**Figures 6F–H**). The upregulated expression within the ONH encompassed glial cells and possibly axons. Quantification of the area of LDH-A labeling in images taken from the ONH and myelinated optic nerve confirmed the observed increase within the ONH ($P < 0.01$), but not the optic nerve (**Figure 6B**).

Ocular Hypertension Selectively Affects Iron-Regulating Proteins in the Optic Nerve Head

Iron is crucial to the transport of molecular oxygen to tissues and its depletion has the capacity to invoke or worsen hypoxia (Chepelev and Willmore, 2011). A number of iron homeostasis genes, including transferrin, transferrin receptor, ceruloplasmin, and HO-1, are transcriptionally upregulated by hypoxia in a HIF-dependent manner (Chepelev and Willmore, 2011), while ceruloplasmin has additionally been credited with possessing antioxidant properties. To explore whether there is an alteration in iron-regulating proteins within the ONH during OHT, we investigated expression of transferrin receptor and ceruloplasmin. qPCR analysis of dissected ONH samples revealed no alteration in transferrin receptor mRNA in the treated eye compared to the contralateral eye ($P = 0.74$; **Figure 7C**). Immunolabeling for transferrin receptor in controls showed punctate labeling of glial cells in the ONH and optic nerve (**Figure 7A**). In agreement with earlier work (Moos, 1996), capillary endothelial cells and columns of oligodendrocytes were clearly positive for transferrin receptor (Supplementary Figure 2). Following induction of elevated IOP, no discernible alteration to the distribution of transferrin receptor was evident (**Figure 7B**). Quantification of the area of immunolabeling in images taken from the ONH confirmed this observation ($P = 0.22$; **Figure 7C**).

In contrast to transferrin receptor, ceruloplasmin protein levels in dissected ONH samples from rats subjected to both 1 or 3 d of OHT were found to be significantly higher than

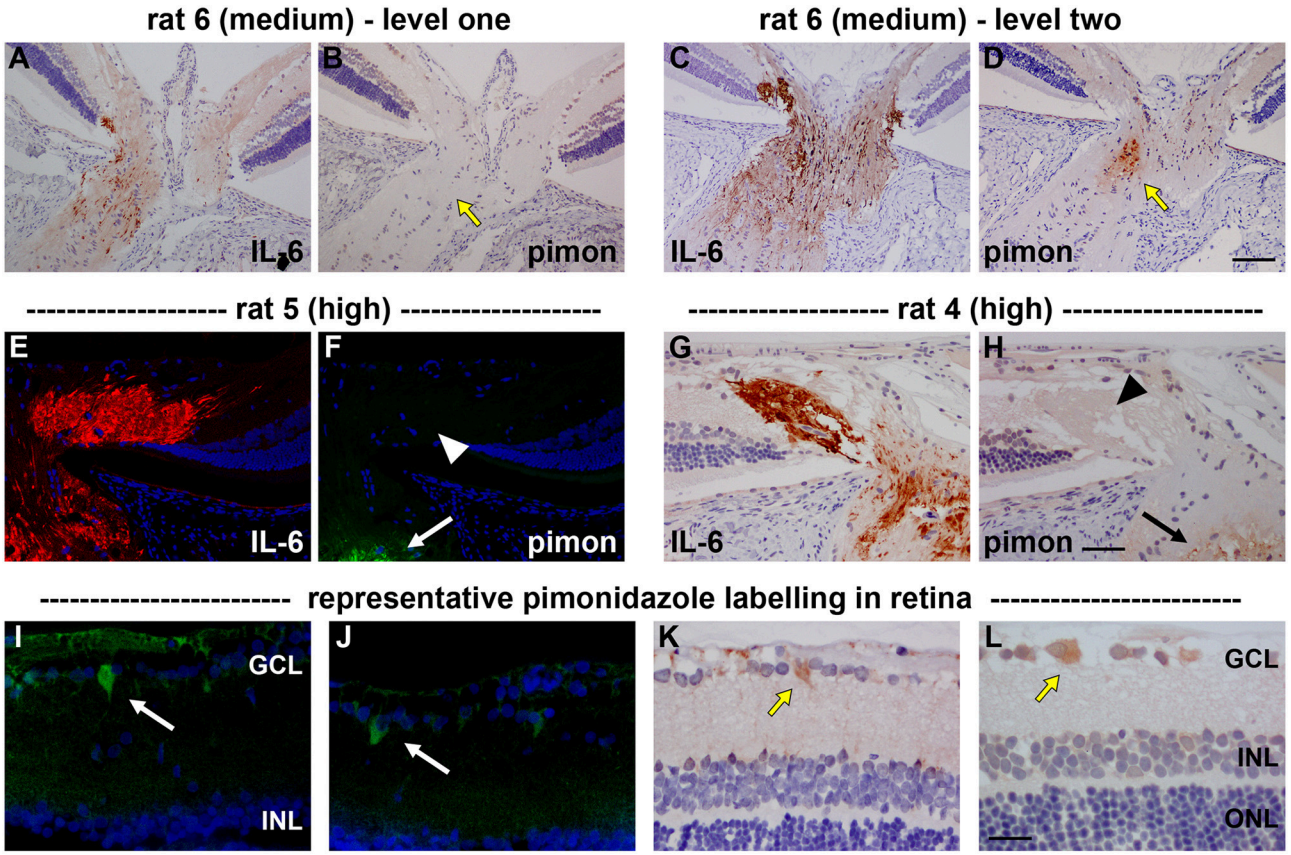

FIGURE 3 | Localization of hypoxia within the optic nerve head (ONH) and retina at 24 h following induction of ocular hypertension. **(A–D)** Hypoxic regions can be very focal, as shown by two images of pimonidazole (pimon) staining in the same rat ONH **(B,D)**, each with an accompanying image of interleukin-6 (IL-6) to demarcate the number of axons with disrupted axonal transport **(A,C)**: hypoxia is not detectable in (**B,** yellow arrow), but a small hypoxic region is apparent in (**D**; yellow arrow). It is notable that positive staining for pimonidazole is only observed in the portion of the ONH that displays greater axonal transport disruption (**C** vs. **A**). **(E–H)** Pimonidazole staining is not evident in the prelaminar ONH (**F**,**H**, white and black arrowheads), even in animals with prominent axonal transport disruption at this location **(E,G)** and featuring hypoxic regions within the laminar ONH (**F,H**, white and black arrows). **(I–L)** In the retina, very few cells stain positively for pimonidazole. In animals with high axonal transport disruption, occassional cells in the GCL are observed (white and yellow arrows). GCL, ganglion cell layer; INL, inner nuclear layer; ONL, outer nuclear layer. Scale bars: **(A–D)** = 100 μm; **(E–H)** = 50 μm; **(I–L)** = 25 μm.

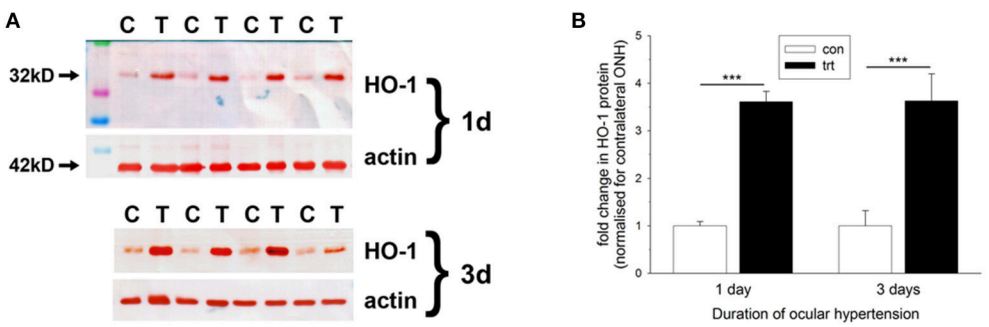

FIGURE 4 | Evaluation of heme oxygenase-1 (HO-1) expression in optic nerve head (ONH) extracts at 1 and 3 d after induction of ocular hypertension, as determined by Western immunoblotting. **(A)** Representative immunoblots from four animals at each time point are shown (C, control ONH; T, treated ONH). Single bands of the expected molecular weight are apparent. β-actin immunoblots for the same samples are also shown, as gel-loading controls. **(B)** Quantification of HO-1 protein data. Values (represented as mean ± SEM, where $n = 12–14$) are normalized for actin and expressed relative to controls. $^{***}P < 0.001$, by Student's unpaired *t*-test.

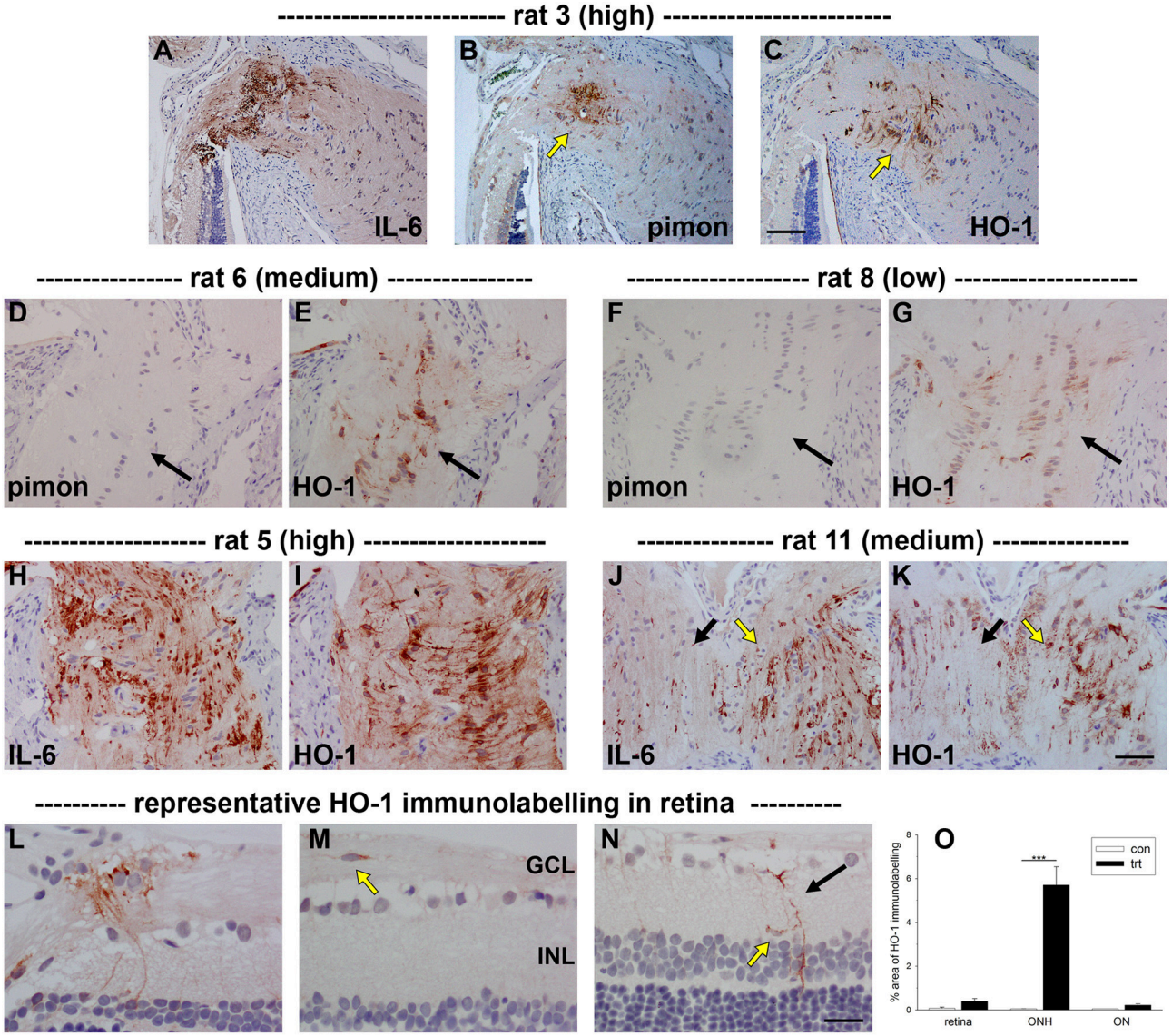

FIGURE 5 | Localization of heme oxygenase-1 (HO-1) immunolabeling within the optic nerve head (ONH) and retina at 24 h following induction of ocular hypertension. **(A–C)** Images of axonal transport disruption as delineated by interleukin-6 (IL-6), pimonidazole (pimon) staining to demarcate any hypoxia, and HO-1, all within the same plane of the ONH of rat 3. It can be seen that the distribution of HO-1 overlaps closely with those of axonal injury and hypoxia, but is somewhat more extensive than the latter (arrows). **(D–G)** Of note, HO-1 is upregulated by ONH glial cells in ocular hypertensive rats that do not feature an overt hypoxic region. **(H–K)** HO-1 is upregulated more robustly in rats that feature abundant axonal transport disruption. The distribution of HO-1 immunolabeling closely parallels that of IL-6 (see **J,K**: black arrows, low IL-6/HO-1 expression; yellow arrows, high IL-6/HO-1 expression). **(L–N)** In the retina, HO-1 immunolabeling is sparse at 24 h. Macroglial cells in the prelaminar ONH are often HO-1-positive **(L)**. HO-1-labeled microglia located within the nerve fiber layer can sometimes also be observed **(M)**. In the mid-central retina, Müller cell processes (black arrow) and microglia present within the inner plexiform layer (yellow arrow) occassionally express HO-1 **(N)**. GCL, ganglion cell layer; INL, inner nuclear layer. Scale bars: **(A–C)** = 100 μm; **(D–K)** = 50 μm; **(H–J)** = 25 μm. **(O)** Quantification of HO-1 immunolabeling in the retina, optic nerve head (ONH) and myelinated optic nerve (ON). Values represent mean ± SEM, where $n = 24$. ***$P < 0.001$, by Student's unpaired *t*-test.

in controls ($P < 0.01$ for both) when analyzed by Western blotting (**Figures 7D,E**). Ceruloplasmin displays a pattern of immunolabeling within the control (Supplementary Figure 2) and treated (data not shown) ONH that is characteristic of astrocytes, suggesting that the increase in protein expression following ocular hypertension derives from upregulation by this cell type.

Ocular Hypertension Induces AP-1 Expression in the Optic Nerve Head

Activating protein-1 (AP-1), a pleiotropic transcription factor and member of the leucine zipper family, is a dimer composed of JUN/FOS or JUN/JUN subunits. AP-1 activation by transient and prolonged hypoxia is a well-described phenomenon (Cummins and Taylor, 2005). To explore whether AP-1 activation at the

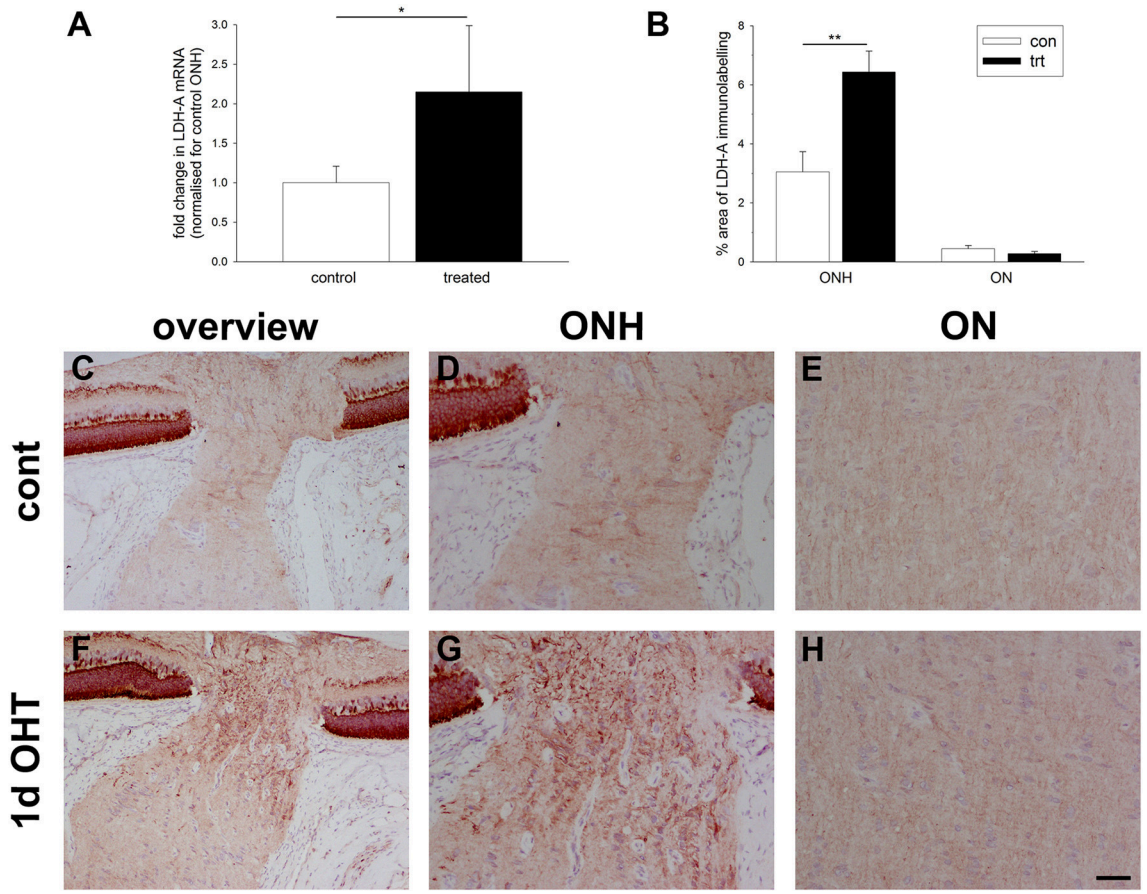

FIGURE 6 | Evaluation of lactate dehydrogenase-A (LDH-A) expression in the optic nerve head (ONH) at 1 d after induction of ocular hypertension. **(A)** Level of LDH-A mRNA in ONH samples from OHT eyes, as measured by qPCR. Data are normalized for rhodopsin and expressed relative to controls. Values represent mean ± SEM, where $n = 14$. $^{*}P < 0.05$, by Student's unpaired *t*-test. **(B)** Quantification of LDH-A immunolabeling in the ONH and myelinated optic nerve (ON). Values represent mean ± SEM, where $n = 14$. $^{**}P < 0.01$, by Student's unpaired *t*-test. **(C–H)** Representative images of LDH-A immunolabeling within the ONH and proximal portion of the myelinated optic nerve (ON) of a control eye and an eye analyzed at 24 h after induction of ocular hypertension. **(C**,**F)** are low magnification images, while **(D**,**E**,**G**,**H)** show the same sections at higher magnification. In control rats, LDH-A is weakly expressed throughout retinal ganglion cell axons and by glial cells of the ONH. In treated animals, LDH-A expression is markedly upregulated within the ONH, but not ON. Scale bar: **(C,F)** = 100 μm; **(D,E,G,H)** = 50 μm.

ONH corresponds temporally with axonal transport disruption, we quantified the number of nuclei expressing cFos and the active, phosphorylated form of cJun (p-cJun) at 1 d after induction of OHT in images taken from the ONH and myelinated optic nerve. In control eyes, very few cells in either the ONH or proximal optic nerve displayed nuclear expression of cFos or p-cJun (**Figures 8B,C,J,K**). In treated eyes, however, there was a striking increase in expression of both cFos ($P < 0.001$) and p-cJun ($P < 0.001$) at the ONH (**Figures 8E,F,J,K**). The inductions of cFos ($P = 0.11$) and p-cJun ($P = 0.10$) did not extend spatially into the optic nerve (**Figures 8H–K**). The spatial extent of cFos and p-cJun upregulations were comparable to that of HO-1 (**Figures 8A,D,G**). Moreover, double labeling with the glial marker S100 revealed that expression of both cFos and p-cJun was restricted to astrocytes (Supplementary Figure 3).

Ocular Hypertension Induces Only Modest Alterations to Nrf2 and Nrf2-Driven Antioxidant Enzymes in the Optic Nerve Head

Oxidative stress, brought about by excessive production of ROS, is implicated in the pathogenesis of RGC loss during glaucoma (Tezel, 2006). Upon redox perturbation, the transcription factor Nrf2 controls the inducible expression of a multitude of genes involved in protection against oxidative stress (Tebay et al., 2015). We investigated expression of Nrf2 itself and some Nrf2-responsive genes at the ONH during OHT. qPCR data of dissected ONH samples revealed an increase in Nrf2 mRNA in the treated vs. the contralateral eye of approximately two-fold ($P < 0.01$) after 1 d of OHT (**Figure 9A**); however, by 3 d Nrf2 mRNA was no longer significantly elevated ($P = 0.28$).

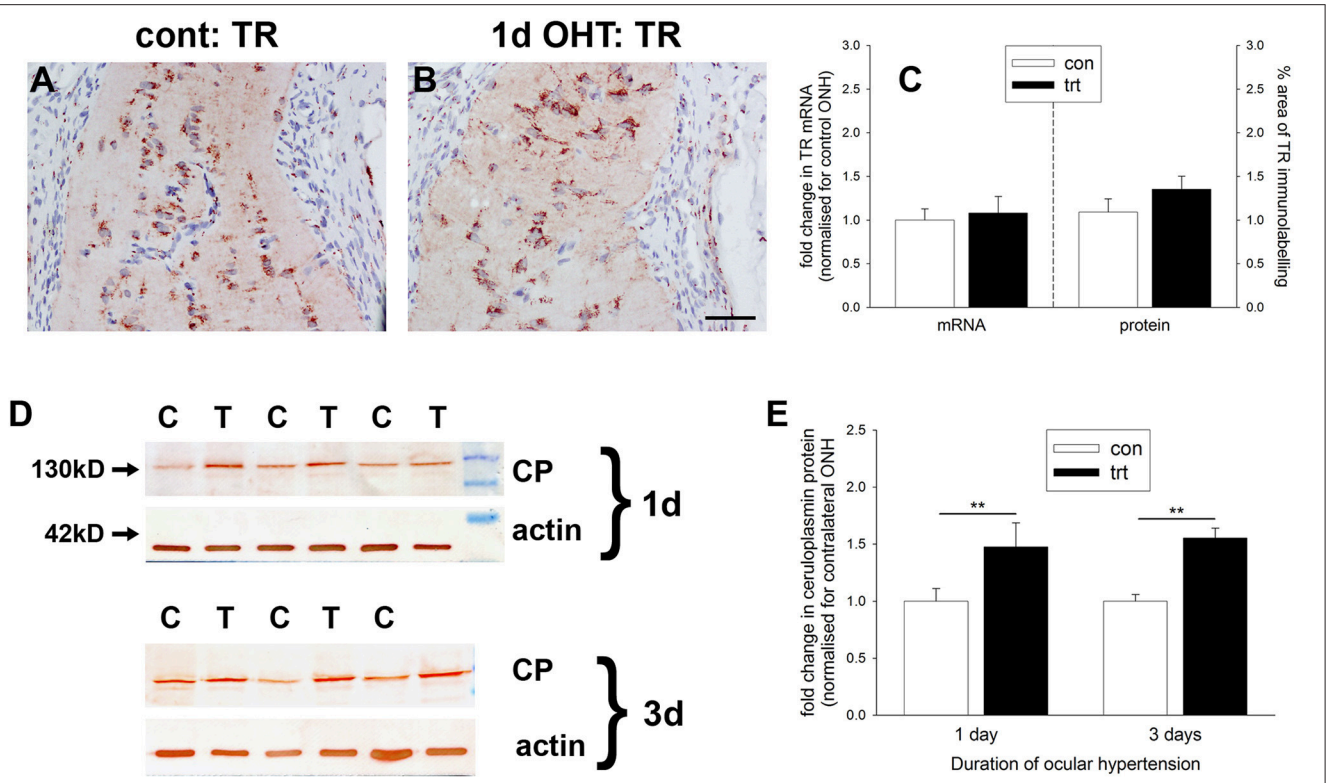

FIGURE 7 | Evaluation of iron-regulating proteins transferrin receptor and ceruloplasmin in the optic nerve head (ONH) at 1 and 3 d after induction of ocular hypertension **(A,B)** Representative images of transferrin receptor (TR) immunolabeling within the ONH of a control eye and an eye analyzed at 24 h after induction of ocular hypertension. Scale bar: 50 μm. **(C)** Quantification of transferrin receptor mRNA expression in ONH extracts, as measured by qPCR, and transferrin receptor protein expression in tissue sections of the ONH. All values represent mean ± SEM, where $n = 14$. pPCR data are normalized for rhodopsin and expressed relative to controls. **(D)** Representative immunoblots from three animals at each time point are shown (C, control ONH; T, treated ONH). Single bands of the expected molecular weight are apparent. β-actin immunoblots for the same samples are also shown, as gel-loading controls. **(E)** Quantification of ceruloplasmin protein data. Values (represented as mean ± SEM, where $n = 12$–14) are normalized for actin and expressed relative to controls. $^{**}P < 0.01$, by Student's unpaired *t*-test.

Examination of the levels of two key Nrf2 target genes, NQO1 and GCLM, failed to show any robust increases in expression at either time point (**Figures 9B,C**), although the former transcript almost reached significance at the 1 d time point ($P = 0.06$).

Western blotting data (**Figures 9D–G**) of dissected ONH samples probed with antibodies directed against the cytoplasmic (SOD-1) and mitochondrial (SOD-2) isoforms of superoxide dismutase and the peroxide scavenging enzyme peroxiredoxin-6 (Prdx6) revealed no alterations in any of the three enzymes after 1 d of OHT ($P = 0.50$, $P = 0.51$, $P = 0.80$, respectively). By 3 d of OHT, SOD-1, and Prdx6 remained unchanged relative to normotensive eyes ($P = 0.24$, $P = 0.30$, respectively). Interestingly, SOD-2 was consistently elevated at this later time point ($P < 0.001$). We augmented these Western blotting results by performing qPCR on ONH extracts and immunolabeling for Prdx6 and SOD-2 in ONH tissue sections. The rationale for these experiments was simply that Prdx6 is the peroxiredoxin isoform expressed exclusively by astrocytes within the ONH (Chidlow et al., 2016) and hence is of obvious interest, whilst SOD-2 displayed an upregulated profile at the 3 d time point and the cellular origin of this increase is of relevance. As regards Prdx6, neither qPCR nor immunohistochemistry suggested an upregulation of this enzyme during the early stages of OHT (**Figures 9H–J**). In contrast, SOD-2 is present in all cells, but within the ONH is predominantly visible, as expected, within the unmyelinated axons (**Figure 9K**). After 3 d of OHT, more intense, punctate SOD-2 labeling of axons was evident in zones of axonal injury (**Figures 9L,M**); thus, it appears plausible that axons rather than astrocytes represent the source of the additional SOD-2 that was detected by Western blotting.

Ocular Hypertension Increases Generation of Superoxide in the Retina and Optic Nerve Head

Superoxide represents the primary ROS generated during oxidative stress. Analysis of superoxide formation, accordingly, represents a useful tool for identifying the likely sites of any oxidative stress. Notwithstanding the mitochondrial respiratory chain, the major cellular source of superoxide in disease scenario is thought to be the dedicated superoxide-generating enzyme NADPH oxidase (NOX), in particular the NOX-2 isoform (Bedard and Krause, 2007). To shed light on superoxide production during OHT, we performed *in situ* detection of

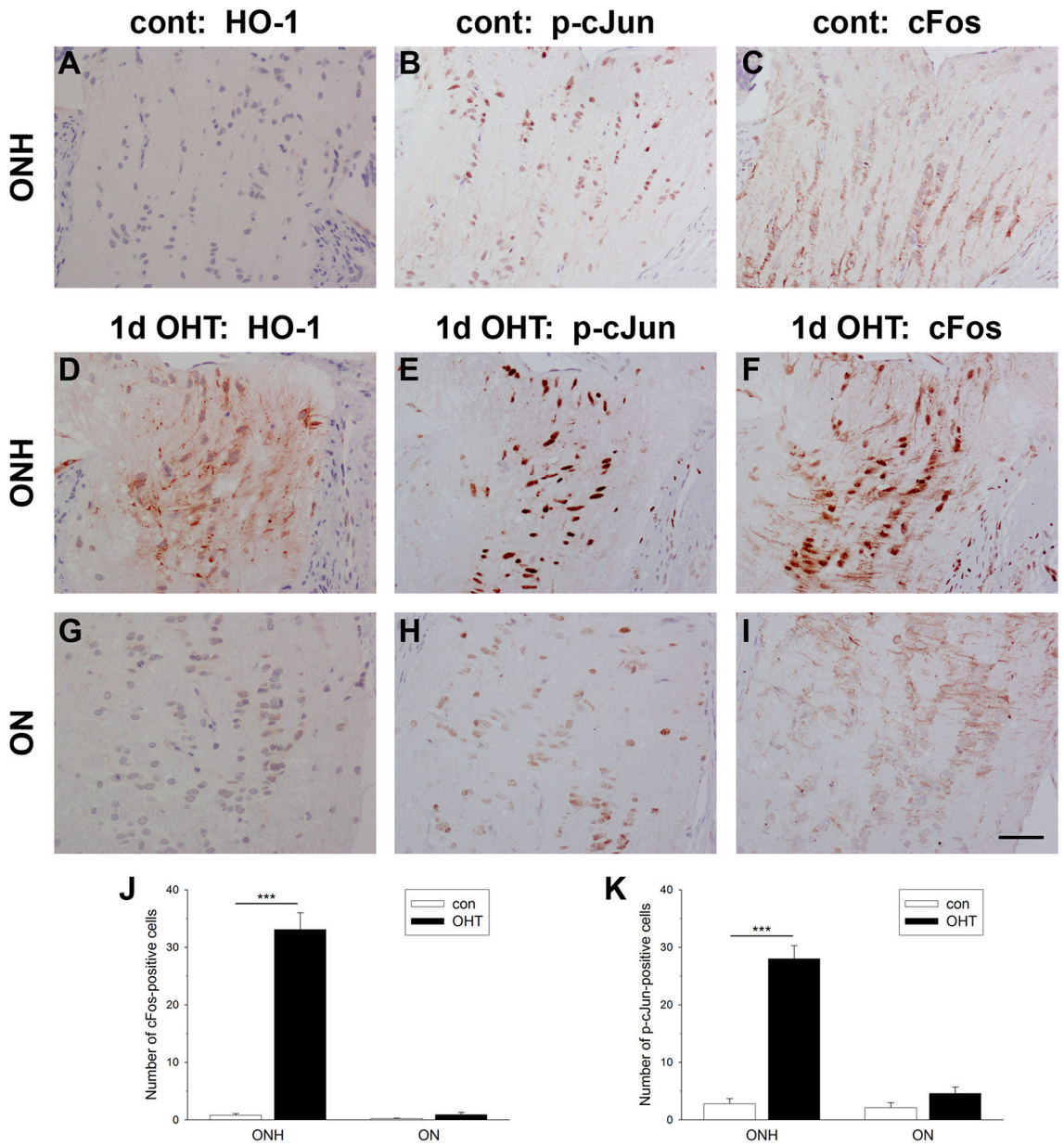

FIGURE 8 | Evaluation of cFos and p-cJun expression in the optic nerve head (ONH) at 1 d after induction of ocular hypertension (OHT). **(A–C)** Representative images of heme oxygenase-1 (HO-1), cFos, and p-cJun immunolabeling within a control ONH. **(D–I)** Representative images of HO-1, cFos, and p-cJun immunolabeling within the ONH and proximal portion of the optic nerve (ON) of a rat analyzed at 24 h after induction of ocular hypertension. In the control ONH, few cell nuclei label positively for cFos or p-cJun. In contrast, at 24 h after induction of OHT, numerous nuclei within the ONH, but not the ON, are cFos- and p-cJun-positive. Heme oxygenase-1 (HO-1) immunolabeling from the same rat is shown for comparative purposes. Scale bar: 50 μm. **(J,K)** Quantification of cFos and p-cJun immunolabeling in the ONH and ON. Values represent mean ± SEM, where $n = 24$. ***$P < 0.001$, by Student's unpaired *t*-test.

the oxidation product of dihydroethidium, and investigated the levels and activity of NOX-2 by qPCR, Western blotting, and immunohistochemistry.

In control eyes, superoxide formation, as determined by oxidation of dihydroethidium, was barely detectable (**Figures 10A,D**). After 1 d of OHT, RGCs throughout the retina and glial cells at the prelaminar ONH were prominently stained, whilst some Müller cells and axonal bundles in the central nerve fiber layer displayed fainter staining (**Figures 10B,E**). After 3 d of OHT, a similar pattern of staining was observed, although by this later time point both Müller cell and axonal staining were stronger (**Figures 10C,F**). Confirmation that superoxide staining within the retinal inner nuclear layer principally reflected Müller cells was achieved by double labeling with

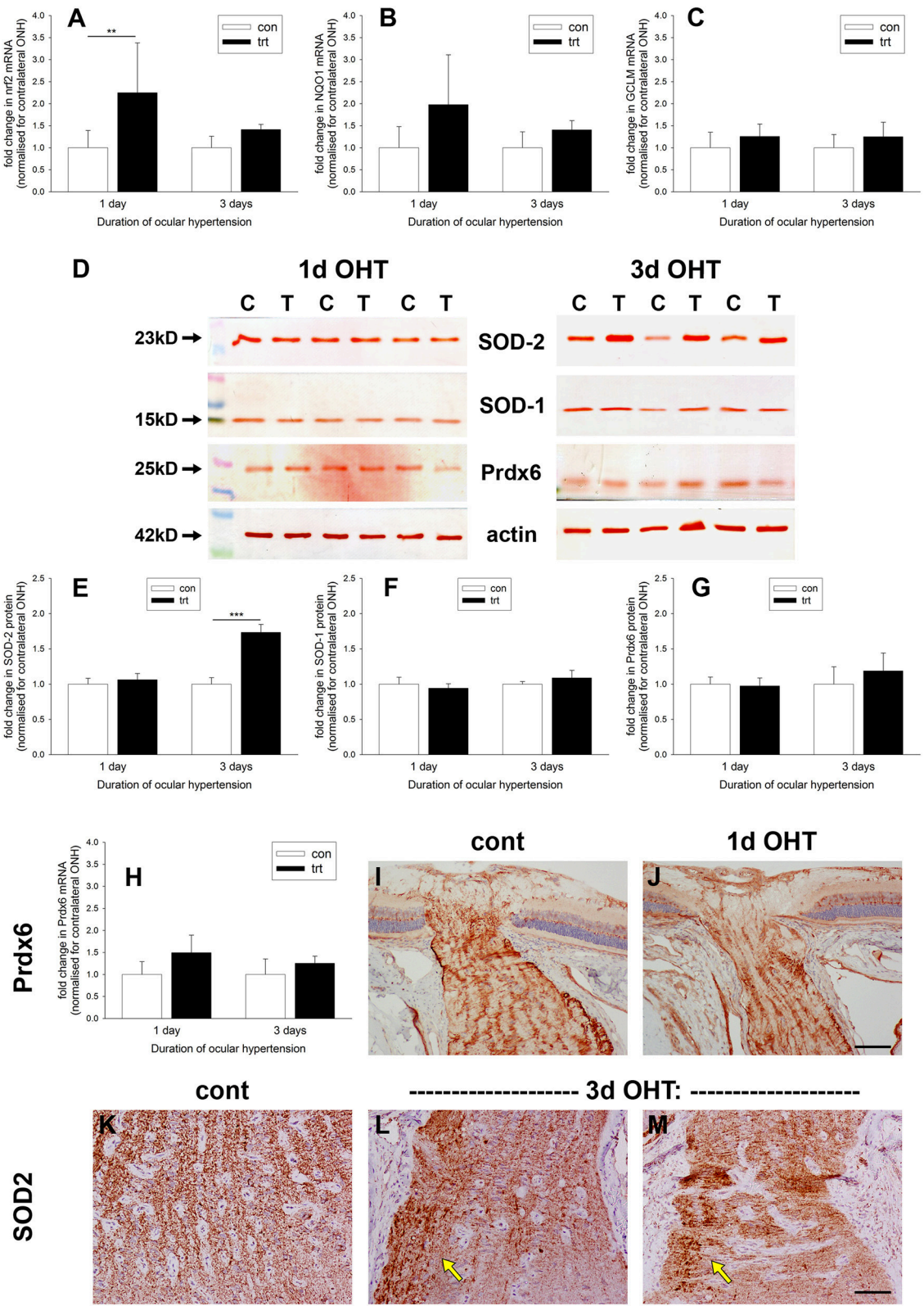

FIGURE 9 | Evaluation of antioxidant defenses in the optic nerve head (ONH) after induction of ocular hypertension (OHT). **(A–C)** Quantification of mRNAs encoding the antioxidant response element genes Nrf2, GCLM, and NQO1 in ONH extracts, as measured by qPCR. Data are normalized for rhodopsin and expressed relative to controls. Values represent mean ± SEM, where $n = 12–14$. $^{**}P < 0.01$, by Student's unpaired *t*-test. **(D–G)** Expression of the antioxidant enzymes SOD-1, SOD-2, *(Continued)*

FIGURE 9 | Continued
and Prdx6 in optic nerve head (ONH) extracts at 1 and 3 d after induction of ocular hypertension, as determined by Western immunoblotting. Representative immunoblots from three animals at each time point are shown (C, control ONH; T, treated ONH). Single bands of the expected molecular weight are apparent. β-actin immunoblots for the same samples are also shown, as gel-loading controls. Values (represented as mean ± SEM, where $n = 12$–14) are normalized for actin and expressed relative to controls. ***$P < 0.001$, by Student's unpaired t-test. **(H)** Quantification of Prdx6 mRNA expression in ONH extracts, as measured by qPCR. All values represent mean ± SEM, where $n = 14$. Data are normalized for rhodopsin and expressed relative to controls. **(I,J)** Representative images of Prdx6 immunolabeling in ONH tissue sections from control and OHT eyes. Prdx6 is associated with astrocytes, but appears unchanged following OHT. **(K–M)** Representative images of SOD-2 immunolabeling in ONH tissue sections from control and eyes subjected to 3 d of OHT. In controls optic nerves, SOD-2 expression is conspicuous within axon bundles. Following 3 d of OHT, injured axon bundles display robust, punctate SOD-2 immunolabeling (arrows). Scale bar: **(I,J)** = 100 μm; **(K–M)** = 50 μm.

CRALBP (**Figures 10G–I**). All four animals at each time point displayed analogous patterns of fluorescence. The protocol used for determination of superoxide detection entailed intravitreal injection of dihydroethidium. As such, penetration of the compound to the optic nerve was likely highly inadequate and the laminar region of the ONH stained only faintly. For this reason, and also owing to the low "*n*" numbers, quantification was not carried out.

qPCR data of dissected ONH samples revealed increases in NOX-2 mRNA in the treated vs. the untreated, contralateral eye of ∼1.5-fold at 1 d, and three-fold at 3 d, after induction of OHT (**Figure 11A**). This difference only reached statistical significance ($P = 0.13$ at 1 d; $P < 0.05$ at 3 d) at the latter time point. Western blotting analysis of the regulatory subunit of NOX-2, $p67^{phox}$, revealed a similar trend: the protein was barely detectable in control ONH extracts, was unchanged at 1 d after induction of OHT, but was significantly elevated after 3 d of OHT ($P < 0.01$; **Figures 11B,C**). To provide a more informative spatial perspective, as well as insight into activity, we immunolabeled tissue sections with an antibody directed against the catalytic subunit of NOX-2, $gp91^{phox}$. In control eyes, occasional $gp91^{phox}$-positive cells were detected (data not shown). After 1 d of OHT, some ONH sections displayed numerous $gp91^{phox}$-positive cells, others featured occasional faintly-labeled cells, while other ONHs had no discernible $gp91^{phox}$ immunolabeling (**Figures 11E,G**). Surprisingly, the expression of $gp91^{phox}$ did not reflect the abundance of axonal transport disruption (**Figures 11D,F**). Double labeling with the macrophage/microglial-specific marker iba1 indicated that expression of $gp91^{phox}$ was restricted to this cell type (data not shown). By 3 d of OHT, $gp91^{phox}$-positive microglia were observed in all ONH sections and also within the inner retina (**Figures 11H–K**, Supplementary Figure 4), whilst $gp91^{phox}$-positive macrophages were prominent at the site of laser trabeculoplasty, signifying inflammation at this location (Supplementary Figure 4). Quantification of the area of $gp91^{phox}$ immunolabeling in images taken from the ONH (**Figure 11L**) revealed a significant increase within this region at 3 d ($P < 0.01$), but not 1 d ($P = 0.08$).

Ocular Hypertension Does Not Appear to be Associated with Oxidative DNA Damage in the Optic Nerve Head

Oxidative stress leads to DNA, protein and lipid damage. The guanine base in DNA or RNA is oxidized by ROS and changes to 8-hydroxy-2′-deoxyguanosine, which can be monitored immunohistochemically. 8-Hydroxy-2′-deoxyguanosine, thus, serves as a useful measure of oxidative stress. We analyzed ONH tissue sections from 1 and 3 d OHT eyes, but at neither of the time points did we detect any positive labeling for -hydroxy-2′-deoxyguanosine, even in ONH sections with numerous $gp91^{phox}$-positive cells and axonal injury (**Figure 11N**). The validity of the assay was proven by positive staining in eyes injected with the excitotoxic glutamatergic agonist, N-methyl-D-aspartate (**Figure 11M**).

DISCUSSION

Failure of orthograde axonal transport at the ONH has been hitherto identified as the earliest pathological event following chronic elevation of IOP. Analogous results have been found in primates (Anderson and Hendrickson, 1974; Quigley and Anderson, 1976, 1977; Minckler et al., 1977) and pigs (Balaratnasingam et al., 2007), which possess a collagenous lamina cribrosa, as well as rodents (Howell et al., 2007; Salinas-Navarro et al., 2010; Chidlow et al., 2011b), which feature an astrocyte-rich glial lamina (Sun et al., 2009). The underlying cause of axonal injury at the ONH in response to OHT is unknown, but conceivably involves bioenergetic deficiency resulting from a decreased oxygen/nutrient supply (Inman and Harun-Or-Rashid, 2017). In the current study, we have employed a rat model of OHT that features reproducible and widespread axonal transport disruption at the ONH by 24 h after chronic elevation of IOP (Salinas-Navarro et al., 2010; Chidlow et al., 2011b). Using a range of immunohistochemical and molecular tools, we looked for cellular events that may be indicative of vascular insufficiency.

Initially, we examined whether OHT-induced axonal transport disruption is spatially and temporally associated with oxygen deprivation. The hypoxia marker pimonidazole binds cells with an oxygen tension of <10 mmHg (Arteel et al., 1995), and has been successfully employed to reveal hypoxia within the optic nerve in a rat model of anterior ischemic optic neuropathy (Danylkova et al., 2006), and, within the retina in a murine model of oxygen-induced retinopathy (Gardiner et al., 2005; Mowat et al., 2010) and in rats subjected to acute elevation of IOP (Holcombe et al., 2008). Our results revealed some hypoxic staining within the laminar ONH in 11/13 eyes graded as either medium or high for axonal transport disruption. Pimonidazole always labeled in areas of the ONH featuring injured axons, and, the greater the abundance of axonal transport disruption, the greater the likelihood of a larger hypoxic region. Nevertheless,

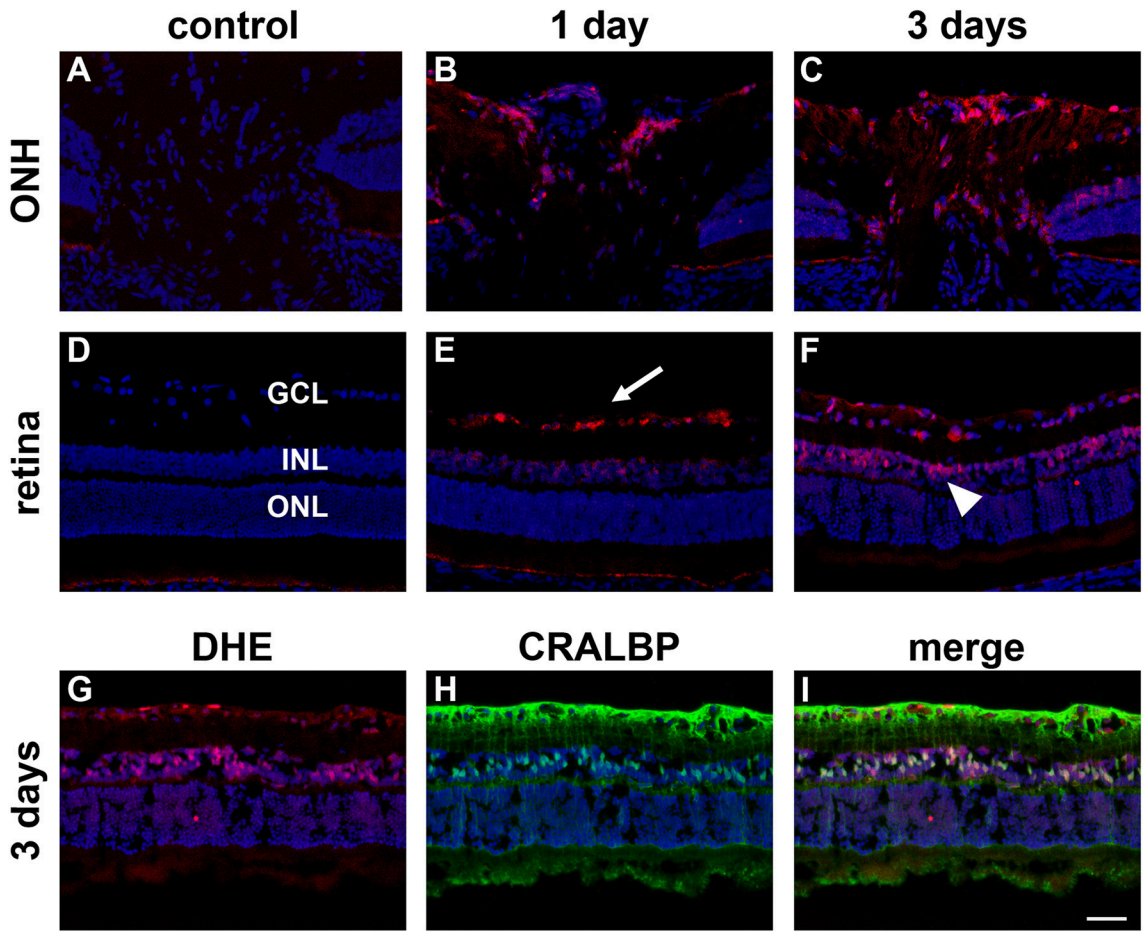

FIGURE 10 | Increased superoxide production in the retina and prelaminar optic nerve head (ONH) after induction of ocular hypertension (OHT). **(A–F)** Representative images of sections of the prelaminar ONH and retina incubated with dihydroethidium (DHE, red) from a control eye, and from eyes subjected to ocular hypertension for 1 and 3 days. Sections are counterstained with the nuclear dye DAPI. Negligible fluorescence is evident in sections from the control. In contrast, after 1 day of OHT, cells residing within the retinal ganglion cell layer (GCL, arrow), some cells within the inner nuclear layer (INL), and glial cells at the ONH display DHE fluorescence. After 3d of OHT, DHE staining is more prominent, notably by cells in the INL (arrowhead) and at the ONH. ONL, outer nuclear layer. **(G–I)** Double labeling immunofluorescence of DHE (red) with the Müller cell marker CRALBP (green) at 3 days after induction of OHT. Scale bar: 50 μm.

hypoxic regions were typically focal and were not necessarily evident in sections taken deeper within the same ONH, while disrupted axonal transport was frequently encountered without any pimonidazole labeling, and, hypoxia was not evident in animals graded as low for axonal transport disruption. Overall, it can be concluded that there is a negative effect of moderate, chronic OHT upon ONH tissue oxygenation, coinciding with axonal transport failure, but that the deficit in oxygen is not uniform throughout the ONH. It is reasonable to postulate the existence of areas of non-, or low, perfusion in watershed zones in the ONH. In future, it may be worth analyzing serial sections through the entire ONH for hypoxia and constructing 3-dimensional models. It is a weakness of the current study that only three levels of each ONH were analyzed for the presence of hypoxia.

In the cat, oxygen tension within the prelaminar ONH has been reported to exist within the range of 10–32 mm Hg (Shonat et al., 1992; Ahmed et al., 1994). Acute elevation of IOP to ∼40 mm Hg—a level very similar to that measured in our "high injury" cohort—yielded negligible impact upon oxygen tension within the prelaminar ONH or retina (Shonat et al., 1992; Ahmed et al., 1994), indicating a system with effective autoregulation. As such, we might not have expected to detect hypoxia at the ONH in the current study. A number of factors might account for the apparent dissimilarity: firstly, we only observed pimonidazole staining within the laminar, not the prelaminar, ONH. To knowledge, oxygen tension within the laminar ONH in response to elevation of IOP has not been reported and may differ from the prelaminar region; secondly, autoregulation may not function as efficiently during prolonged OHT as compared to acute OHT; thirdly, the ONH vasculature of the cat differs considerably from that of the rat. Despite the low oxygen tension present in the inner retina of the healthy rat eye (Yu and Cringle, 2001), chronic OHT

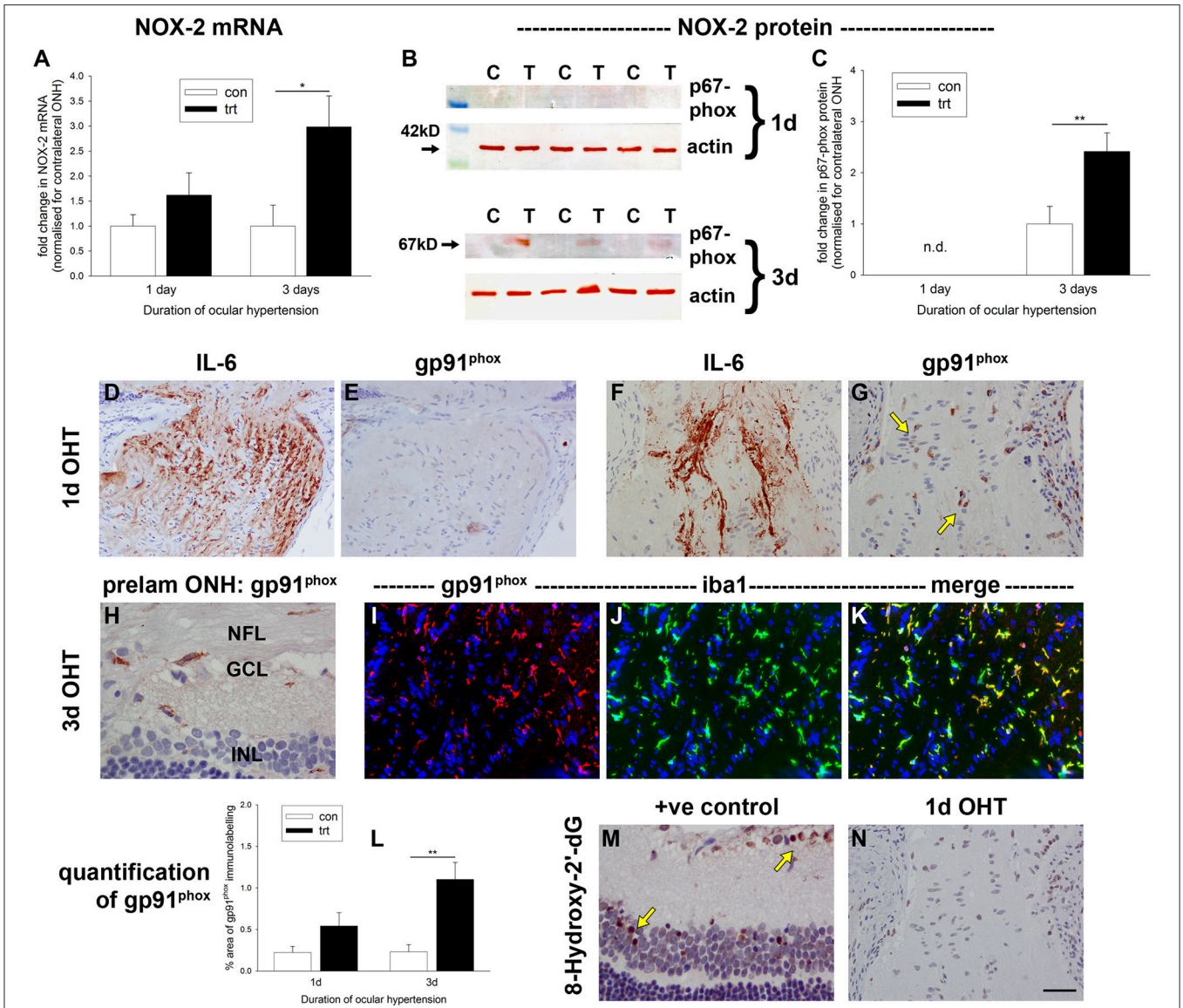

FIGURE 11 | Evaluation of NADPH oxidase-2 (NOX-2) and 8-hydroxy-2′-deoxyguanosine in the optic nerve head (ONH) after induction of ocular hypertension (OHT). **(A)** Quantification of NOX-2 mRNA in ONH extracts, as measured by qPCR. Data are normalized for rhodopsin and expressed relative to controls. Values represent mean ± SEM, where $n = 12–14$. $^{*}P < 0.05$, by Student's unpaired *t*-test. **(B,C)** Expression of the regulatory subunit for NOX-2, p67^{phox}, in optic nerve head (ONH) extracts at 1 and 3 d after induction of ocular hypertension, as determined by Western immunoblotting. Representative immunoblots from three animals at each time point are shown (C, control ONH; T, treated ONH). Single bands of the expected molecular weight are apparent. β-actin immunoblots for the same samples are also shown, as gel-loading controls. Values (represented as mean ± SEM, where $n = 12–14$) are normalized for actin and expressed relative to controls. $^{**}P < 0.01$, by Student's unpaired *t*-test. **(D–K)** Representative images of gp91^{phox} (the catalytic subunit of NOX-2) immunolabeling in tissue sections from control and OHT eyes. **(D–G)** After 24 h of OHT, gp91^{phox}-positive cells (**G**, arrows) are evident in ONHs from some OHT rats, but not in others **(F)**. The presence of gp91^{phox} expression appears not to be related to the exent of axonal transport disruption, shown alongside for comparative purposes **(D,F)**. **(H–K)** After 3 d of OHT, all OHT eyes feature gp91^{phox}-positive cells, throughout the prelaminar **(H)** and laminar ONH **(I–K)**. Double labeling immunofluorescence of gp91^{phox} (red) with iba1 (green) reveals an almost complete co-localization in microglia **(I–K)**. **(L)** Quantification of gp91^{phox} immunolabeling in the ONH. Values represent mean ± SEM, where $n = 12–16$. $^{**}P <$ 0.01, by Student's unpaired *t*-test. **(M,N)** Representative images of 8-hydroxy-2′-deoxyguanosine (8-hydroxy-2′-dG) immunolabeling in the retina following injection of the excitotoxic glutamatergic agonist, N-methyl-D-aspartate, and in the ONH (also shown in **G**) after 24 h of OHT. 8-Hydroxy-2′-dG-positive cells are numerous in the positive control specimen, but not within the ONH of OHT rats. Scale bar: **(D–G,N)** = 50 μm; **(H–K,M)** = 25 μm.

did not give rise to noteworthy hypoxia in the retina, with staining limited to occasional pimonidazole-positive cells in the ganglion cell layer. These results essentially reflect those previously reported following acute elevation of IOP, where RGC hypoxia was not observed below an IOP of 70 mm Hg (Holcombe et al., 2008). Our results show that autoregulation maintains perfusion to the rat retina reasonably effectively even during OHT.

We did not assess vascular damage in the current study, as we considered it unlikely as such early time points prior to axon loss. In humans and monkeys with glaucoma, capillary drop out within the optic disc has been shown to occur in proportion to axon loss: as fibers atrophy, so do capillaries. Thus, capillaries are not disproportionately lost early in glaucoma (Quigley et al., 1984). Such results match those of Valiente-Soriano et al. (2015), who found no abnormalities in the inner retinal vasculature after 2 weeks of raised IOP that could account for the sectorial loss of RGCs. As regards microvascular function, it has been argued that raised IOP compresses capillaries, reducing blood supply to axons, without causing actual capillary loss. There is no strong evidence from fluorescein angiography that defects at the ONH substantially precede neuron loss, but the great difficulty, as noted by Quigley et al. (1984), is that the capillaries of greatest interest in glaucoma pathogenesis are hidden from clinical and angiographic view. In our study, hypoxia was not detected at the superficial ONH, only within the laminar region. As such, localized sub-optimal microvascular perfusion remains a likely explanation for the observed hypoxia. As a final point, rats in our study with a lower magnitude pressure rise tended not to have detectable ONH hypoxia; thus, it might be predicted that elevation of IOP for long periods of time may likewise not produce hypoxia; however, longer term moderate ocular hypertension may slowly damage ONH capillaries, eventually resulting in hypoxia. Moreover, rats in this study were young and ostensibly healthy; elevation of IOP in older humans may conceivably elicit hypoxia at lower pressures owing to a diminished abililty of capillaries to withstand any mechanical stress.

We next investigated expression of HO-1, the inducible, rate-limiting enzyme in heme catabolism. HO-1, a gene target of both HIF-1 and Nrf2, is one of the most studied genes in conditions of hypoxia and oxidative stress and is believed to play an important role in the endogenous response of tissues to oxidative injuries (Ryter et al., 2006; Jazwa and Cuadrado, 2010). Our results showed a robust and consistent induction of HO-1 by astrocytes within the ONH after 1 d of OHT. The distribution and abundance of HO-1 closely matched that of axonal transport disruption. HO-1 expression encompassed hypoxic regions and their immediate penumbra, but was also observed in ONH sections of pimonidazole rats that did not feature an overt hypoxic region, indicating that HO-1 is a sensitive and early glial-expressed marker of axonal injury during OHT. At present, it is unclear whether HO-1 within the ONH is upregulated in response to lower-than-normal oxygen tension or a higher-than-normal concentration of ROS. In cultured brain astrocytes, both hypoxia (Kuwabara et al., 1996; Imuta et al., 2007) and exogenously-applied oxidative stress (Lee et al., 2003) have been shown to induce HO-1 expression. Of particular relevance to glaucoma, oxidative stress also upregulates HO-1 expression in cultured ONH astrocytes (Yu et al., 2009; Noh et al., 2013) and cultured retinal astrocytes (Nahirnyj et al., 2013). Contrary to the unambiguous results of this study, HO-1 mRNA was not found to be upregulated in ONH extracts taken from rats with early or advanced optic nerve injury profiles in the hypertonic saline model of OHT (Johnson et al., 2011). An explanation for the differing results likely relates to the chronology of IOP elevation, axonal injury and HO-1 mRNA induction in the OHT model used. While neuronal injury can lead to a prolonged upregulation in HO-1 protein, the mRNA itself is typically upregulated for only a short time window.

In contrast to the ONH, HO-1 was not widely expressed by retinal glial cells until 3 d after induction of OHT, a time point coincident with a demonstrably increased signal for the superoxide-sensitive marker DHE. Interestingly, RGCs displayed strong labeling for DHE after just 1 d of OHT, but no HO-1 immunolabeling was evident in the GCL until 3 d after induction of OHT, and even then only in occasional cells. The results are consistent with those of brain studies, for example Dwyer et al. (1995), who compared HO-1 induction in cultured cortical neurons and forebrain astrocytes following an oxidative stress challenge and showed that in spite of increased generation of free radicals in neurons, the HO-1 protein level was relatively unchanged, whilst it was upregulated seven-fold within a few hours in the astrocyte cultures. The efficacy of astrocytes may be a factor in their own survival, and that of neighboring neurons, in the face of oxidative challenge. Indeed, the consensus reached from a wealth of studies is that acute induction of HO-1 by oxidative stress is an adaptive mechanism that controls the severity of neuronal damage. Over-expression or pharmacological induction of HO-1 is neuroprotective in numerous models of CNS injury (Schipper et al., 2009; Jazwa and Cuadrado, 2010), including retinal ischemia-reperfusion (Peng et al., 2008; Sun et al., 2010), optic nerve crush (Himori et al., 2014), and diabetic retinopathy (Fan et al., 2012). The products of HO-1 activity have potent antioxidant and anti-inflammatory properties that are thought to mediate the observed neuroprotection. Future studies should investigate whether overexpression of HO-1 is neuroprotective in experimental glaucoma.

HO-1 is one of many oxygen-regulated genes involved in the adaptative response of cells to hypoxia. Other iron metabolism genes, such as ceruloplasmin, transferrin receptor and transferrin, have also been implicated (Chepelev and Willmore, 2011), alongside genes encoding glucose transport and glycolytic enzymes (Wenger, 2002). We found increased levels of LDH-A and ceruloplasmin in the hypertensive ONH concurrent with axonal transport disruption, HO-1 expression and pimonidazole staining. The results are in agreement with previous work showing that brain astrocytes upregulate glycolytic genes, including LDH-A, in response to hypoxia (Marrif and Juurlink, 1999; Mense et al., 2006). As a note of caution, it should be acknowledged that analyzing LDH-A expression is less informative than studying enzyme activity or lactate levels in terms of demonstrating anaerobic glycolysis. Our finding of upregulated ceruloplasmin likewise corresponds with previous reports demonstrating increased expression of ceruloplasmin in murine, primate and human glaucomatous retinas (Farkas et al., 2004; Stasi et al., 2007).

Hypoxia-induced modification of gene expression is not solely mediated via HIF-1. Other transcription factors, notably AP-1—a dimer composed of JUN/FOS or JUN/JUN subunits—can also be activated by hypoxia (Cummins and Taylor, 2005). Dimerization between JUN/FOS subunits as well as phosphorylation of either JUN or FOS is required for DNA-binding and transcriptional

activity of AP-1. In the current study, we observed a striking induction of both cFos and the phosphorylated form of cJun by astrocytes within the ONH after 1 d of OHT. An identical response was previously reported in monkeys with longer-term experimental glaucoma (Hashimoto et al., 2005). AP-1 is a redox-sensitive transcription factor, thus, increased ROS rather than hypoxia may be the stimulus for its activation; nevertheless, this finding underscores the rapid response of ONH astrocytes to perturbations in homeostasis.

Any hypoxia or nutrient deficiency in the ONH (resulting from vascular insufficiency) during OHT will likely result in impaired mitochondrial functioning, an increased production of ROS, and eventually, in oxidative stress-induced cell damage (Chrysostomou et al., 2013). In an attempt to safeguard homeostasis from oxidative stress, cells have evolved the means to upregulate antioxidant genes under the control of the redox-sensitive transcription factor Nrf2 (Tebay et al., 2015). Astrocytes in the ONH occupy up to one half of the tissue volume—a much greater percentage than in the myelinated optic nerve (Skoff et al., 1986)—and they likely have a significant influence upon the progression of glaucoma, whether supporting axonal survival or contributing to neuroinflammation (Soto and Howell, 2014; Williams et al., 2017). Recent studies using cultured ONH astrocytes have demonstrated that exogenously-administered oxidative stress fortifies their antioxidant defenses, resulting in elevated levels of Nrf2, SOD-2, HO-1, and Hsp27 (Malone and Hernandez, 2007; Yu et al., 2008, 2009; Noh et al., 2013). In the current study, we undertook preliminary analysis of ROS formation and antioxidant defenses at 1 d after induction of OHT when axonal transport disruption at the ONH is maximal, and, following 3 d of OHT when axonal degeneration has commenced. We found a significant upregulation of Nrf2—the master regulator of antioxidant defenses (Tebay et al., 2015)—in ONH extracts, but not of other well-described antioxidant enzymes, such as NQO1, GCLM, Prdx6, or SOD-1. Prdx6, which is expressed exclusively by astrocytes in the ONH (Chidlow et al., 2016), was of particular interest given the finding of increased expression in reactive astrocytes following ischemia-reperfusion in the hippocampus (Zhang et al., 2013). Moreover, we failed to detect any oxidative DNA damage to astrocytes at either time point. While these results are suggestive of a lack of detrimental oxidative stress within ONH astrocytes concurrent with axonal transport injury, it should be noted that only modest inductions of antioxidant genes were reported in primary cortical astrocyte cultures subjected to oxidative stress (Lee et al., 2003). Moreover, we did observe an increased level of superoxide in ONH astrocytes, as well as a consistent elevation of the mitochondrial isoform of superoxide dismutase (SOD-2) in ONH extracts. Since SOD-2 is present in all cells with mitochondria, and is abundant in non-myelinated axons in the ONH, it was not feasible to delineate whether the increased signal reflected any upregulation by astrocytes. Interestingly, RGC somas also displayed increased superoxide after 1 d of OHT. This finding matches the earlier work of Kanamori et al. (2010), who identified superoxide labeling of RGC somas at 1 d after optic nerve transection, and suggested that this represented an upstream signal for RGC apoptosis following axonal injury.

While the mitochondrial respiratory chain is the major contributor to excessive ROS, the dedicated superoxide-generating enzyme NADPH oxidase (NOX), in particular the phagocytic NOX-2 isoform, is increasingly being implicated as a source of detrimental ROS in acute and chronic neurodegenerative conditions (Ma et al., 2017). We postulated that ONH glia, chiefly microglia, triggered by elevation of IOP, upregulate NOX-2, and release a burst of superoxide, which contributes to axonal transport failure. In fact, our data show that there was no consistent pattern of NOX-2 expression after 1 d of OHT, concomitant with axonal transport disruption. It must be concluded that NOX-2 does not contribute significantly to initial axonal injury. Expression of NOX-2 by ONH microglia was, however, widespread after 3 d of OHT. Presumably, this response contributes to phagocytosis of injured axons. Future work should determine whether inhibition of NOX-2 augments axonal survival in glaucoma, as has been shown to be the case in numerous other neurodegenerative conditions.

The overall results of this study provide tentative support for the hypothesis that reduced blood flow to the ONH contributes to RGC axonal injury; however, the data cannot be viewed as providing direct evidence for a causative relationship between hypoxia—or cellular events downstream of hypoxia—and axonal transport failure. Future work needs to identify if reducing the existence, or even the extent, of hypoxia, or if augmenting energy availability and/or antioxidant defenses prevents the axonal transport failure that occurs during OHT.

AUTHOR CONTRIBUTIONS

All authors had full access to all the data in the study and take responsibility for the integrity of the data and the accuracy of the data analysis. Study concept and design: GC, JW, and RC. Acquisition of data: GC and JW. Analysis and interpretation of data: GC and JW. Drafting of the manuscript: GC. Critical revision of the manuscript for important intellectual content: JW and RC. Statistical analysis: GC and RC. Obtained funding: GC. Administrative, technical, and material support: RC.

FUNDING

Research supported by the Ophthalmic Research Institute of Australia (ORIA/Quinlivan & Glaucoma Australia Grant) and the National Health and Medical Research Council of Australia (APP1050982).

ACKNOWLEDGMENTS

The authors are also indebted to Mark Daymon and Teresa Mammone for expert technical assistance.

SUPPLEMENTARY MATERIAL

The Supplementary Material for this article can be found online at: http://journal.frontiersin.org/article/10.3389/fnins.2017.00478/full#supplementary-material

REFERENCES

Ahmed, J., Linsenmeier, R. A., and Dunn, R. Jr. (1994). The oxygen distribution in the prelaminar optic nerve head of the cat. *Exp. Eye Res.* 59, 457–465. doi: 10.1006/exer.1994.1131

Anderson, D. R., and Hendrickson, A. (1974). Effect of intraocular pressure on rapid axoplasmic transport in monkey optic nerve. *Invest. Ophthalmol.* 13, 771–783.

Arteel, G. E., Thurman, R. G., Yates, J. M., and Raleigh, J. A. (1995). Evidence that hypoxia markers detect oxygen gradients in liver: pimonidazole and retrograde perfusion of rat liver. *Br. J. Cancer* 72, 889–895. doi: 10.1038/bjc.1995.429

Aslan, M., Dogan, S., and Kucuksayan, E. (2013). Oxidative stress and potential applications of free radical scavengers in glaucoma. *Redox Rep.* 18, 76–87. doi: 10.1179/1351000212Y.0000000033

Balaratnasingam, C., Morgan, W. H., Bass, L., Matich, G., Cringle, S. J., and Yu, D. Y. (2007). Axonal transport and cytoskeletal changes in the laminar regions after elevated intraocular pressure. *Invest. Ophthalmol. Vis. Sci.* 48, 3632–3644. doi: 10.1167/iovs.06-1002

Barron, M. J., Griffiths, P., Turnbull, D. M., Bates, D., and Nichols, P. (2004). The distributions of mitochondria and sodium channels reflect the specific energy requirements and conduction properties of the human optic nerve head. *Br. J. Ophthalmol.* 88, 286–290. doi: 10.1136/bjo.2003.027664

Bedard, K., and Krause, K. H. (2007). The NOX family of ROS-generating NADPH oxidases: physiology and pathophysiology. *Physiol. Rev.* 87, 245–313. doi: 10.1152/physrev.00044.2005

Benoist d'Azy, C., Pereira, B., Chiambaretta, F., and Dutheil, F. (2016). Oxidative and anti-oxidative stress markers in chronic glaucoma: a systematic review and meta-analysis. *PLoS ONE* 11:e0166915. doi: 10.1371/journal.pone.0166915

Casson, R. J., Chidlow, G., Wood, J. P., Crowston, J. G., and Goldberg, I. (2012). Definition of glaucoma: clinical and experimental concepts. *Clin. Exp. Ophthalmol.* 40, 341–349. doi: 10.1111/j.1442-9071.2012.02773.x

Casson, R. J., Wood, J. P., Han, G., Kittipassorn, T., Peet, D. J., and Chidlow, G. (2016). M-type pyruvate kinase isoforms and lactate Dehydrogenase A in the mammalian retina: metabolic implications. *Invest. Ophthalmol. Vis. Sci.* 57, 66–80. doi: 10.1167/iovs.15-17962

Chen, H., Yoshioka, H., Kim, G. S., Jung, J. E., Okami, N., Sakata, H., et al. (2011). Oxidative stress in ischemic brain damage: mechanisms of cell death and potential molecular targets for neuroprotection. *Antioxid. Redox Signal.* 14, 1505–1517. doi: 10.1089/ars.2010.3576

Chepelev, N. L., and Willmore, W. G. (2011). Regulation of iron pathways in response to hypoxia. *Free Radic. Biol. Med.* 50, 645–666. doi: 10.1016/j.freeradbiomed.2010.12.023

Chidlow, G., Daymon, M., Wood, J. P., and Casson, R. J. (2011a). Localization of a wide-ranging panel of antigens in the rat retina by immunohistochemistry: comparison of Davidson's solution and formalin as fixatives. *J. Histochem. Cytochem.* 59, 884–898. doi: 10.1369/0022155411418115

Chidlow, G., Ebneter, A., Wood, J. P., and Casson, R. J. (2011b). The optic nerve head is the site of axonal transport disruption, axonal cytoskeleton damage and putative axonal regeneration failure in a rat model of glaucoma. *Acta Neuropathol.* 121, 737–751. doi: 10.1007/s00401-011-0807-1

Chidlow, G., Holman, M. C., Wood, J. P., and Casson, R. J. (2010). Spatiotemporal characterization of optic nerve degeneration after chronic hypoperfusion in the rat. *Invest. Ophthalmol. Vis. Sci.* 51, 1483–1497. doi: 10.1167/iovs.09-4603

Chidlow, G., Wood, J. P., Ebneter, A., and Casson, R. J. (2012). Interleukin-6 is an efficacious marker of axonal transport disruption during experimental glaucoma and stimulates neuritogenesis in cultured retinal ganglion cells. *Neurobiol. Dis.* 48, 568–581. doi: 10.1016/j.nbd.2012.07.026

Chidlow, G., Wood, J. P., Knoops, B., and Casson, R. J. (2016). Expression and distribution of peroxiredoxins in the retina and optic nerve. *Brain Struct. Funct.* 221, 3903–3925. doi: 10.1007/s00429-015-1135-3

Chidlow, G., Wood, J. P., Manavis, J., Osborne, N. N., and Casson, R. J. (2008). Expression of osteopontin in the rat retina: effects of excitotoxic and ischemic injuries. *Invest. Ophthalmol. Vis. Sci.* 49, 762–771. doi: 10.1167/iovs.07-0726

Chrysostomou, V., Rezania, F., Trounce, I. A., and Crowston, J. G. (2013). Oxidative stress and mitochondrial dysfunction in glaucoma. *Curr. Opin. Pharmacol.* 13, 12–15. doi: 10.1016/j.coph.2012.09.008

Crish, S. D., Sappington, R. M., Inman, D. M., Horner, P. J., and Calkins, D. J. (2010). Distal axonopathy with structural persistence in glaucomatous neurodegeneration. *Proc. Natl. Acad. Sci. U.S.A.* 107, 5196–5201. doi: 10.1073/pnas.0913141107

Cummins, E. P., and Taylor, C. T. (2005). Hypoxia-responsive transcription factors. *Pflugers Arch.* 450, 363–371. doi: 10.1007/s00424-005-1413-7

Danylkova, N. O., Pomeranz, H. D., Alcala, S. R., and McLoon, L. K. (2006). Histological and morphometric evaluation of transient retinal and optic nerve ischemia in rat. *Brain Res.* 1096, 20–29. doi: 10.1016/j.brainres.2006.04.061

Dengler-Crish, C. M., Smith, M. A., Inman, D. M., Wilson, G. N., Young, J. W., and Crish, S. D. (2014). Anterograde transport blockade precedes deficits in retrograde transport in the visual projection of the DBA/2J mouse model of glaucoma. *Front. Neurosci.* 8:290. doi: 10.3389/fnins.2014.00290

Dwyer, B. E., Nishimura, R. N., and Lu, S. Y. (1995). Differential expression of heme oxygenase-1 in cultured cortical neurons and astrocytes determined by the aid of a new heme oxygenase antibody. Response to oxidative stress. *Brain Res. Mol. Brain Res.* 30, 37–47. doi: 10.1016/0169-328X(94)00273-H

Ebneter, A., Casson, R. J., Wood, J. P., and Chidlow, G. (2010). Microglial activation in the visual pathway in experimental glaucoma: spatiotemporal characterization and correlation with axonal injury. *Invest. Ophthalmol. Vis. Sci.* 51, 6448–6460. doi: 10.1167/iovs.10-5284

Fan, J., Xu, G., Jiang, T., and Qin, Y. (2012). Pharmacologic induction of heme oxygenase-1 plays a protective role in diabetic retinopathy in rats. *Invest. Ophthalmol. Vis. Sci.* 53, 6541–6556. doi: 10.1167/iovs.11-9241

Farkas, R. H., Chowers, I., Hackam, A. S., Kageyama, M., Nickells, R. W., Otteson, D. C., et al. (2004). Increased expression of iron-regulating genes in monkey and human glaucoma. *Invest. Ophthalmol. Vis. Sci.* 45, 1410–1417. doi: 10.1167/iovs.03-0872

Fechtner, R. D., and Weinreb, R. N. (1994). Mechanisms of optic nerve damage in primary open angle glaucoma. *Surv. Ophthalmol.* 39, 23–42. doi: 10.1016/S0039-6257(05)80042-6

Flammer, J., Orgül, S., Costa, V. P., Orzalesi, N., Krieglstein, G. K., Serra, L. M., et al. (2002). The impact of ocular blood flow in glaucoma. *Prog. Retin. Eye Res.* 21, 359–393. doi: 10.1016/S1350-9462(02)00008-3

Gardiner, T. A., Gibson, D. S., de Gooyer, T. E., de la Cruz, V. F., McDonald, D. M., and Stitt, A. W. (2005). Inhibition of tumor necrosis factor-alpha improves physiological angiogenesis and reduces pathological neovascularization in ischemic retinopathy. *Am. J. Pathol.* 166, 637–644. doi: 10.1016/S0002-9440(10)62284-5

Guillemin, K., and Krasnow, M. A. (1997). The hypoxic response: huffing and HIFing. *Cell* 89, 9–12. doi: 10.1016/S0092-8674(00)80176-2

Guzy, R. D., and Schumacker, P. T. (2006). Oxygen sensing by mitochondria at complex III: the paradox of increased reactive oxygen species during hypoxia. *Exp. Physiol.* 91, 807–819. doi: 10.1113/expphysiol.2006.033506

Hashimoto, K., Parker, A., Malone, P., Gabelt, B. T., Rasmussen, C., Kaufman, P. S., et al. (2005). Long-term activation of c-Fos and c-Jun in optic nerve head astrocytes in experimental ocular hypertension in monkeys and after exposure to elevated pressure *in vitro*. *Brain Res.* 1054, 103–115. doi: 10.1016/j.brainres.2005.06.050

Himori, N., Maruyama, K., Yamamoto, K., Yasuda, M., Ryu, M., Omodaka, K., et al. (2014). Critical neuroprotective roles of heme oxygenase-1 induction against axonal injury-induced retinal ganglion cell death. *J. Neurosci. Res.* 92, 1134–1142. doi: 10.1002/jnr.23398

Holcombe, D. J., Lengefeld, N., Gole, G. A., and Barnett, N. L. (2008). The effects of acute intraocular pressure elevation on rat retinal glutamate transport. *Acta Ophthalmol.* 86, 408–414. doi: 10.1111/j.1600-0420.2007.01052.x

Howell, G. R., Libby, R. T., Jakobs, T. C., Smith, R. S., Phalan, F. C., Barter, J. W., et al. (2007). Axons of retinal ganglion cells are insulted in the optic nerve early in DBA/2J glaucoma. *J. Cell Biol.* 179, 1523–1537. doi: 10.1083/jcb.200706181

Hu, C. J., Wang, L. Y., Chodosh, L. A., Keith, B., and Simon, M. C. (2003). Differential roles of hypoxia-inducible factor 1alpha (HIF-1alpha) and HIF-2alpha in hypoxic gene regulation. *Mol. Cell. Biol.* 23, 9361–9374. doi: 10.1128/MCB.23.24.9361-9374.2003

Imuta, N., Hori, O., Kitao, Y., Tabata, Y., Yoshimoto, T., Matsuyama, T., et al. (2007). Hypoxia-mediated induction of heme oxygenase type I and carbon monoxide release from astrocytes protects nearby cerebral neurons from hypoxia-mediated apoptosis. *Antioxid. Redox Signal.* 9, 543–552. doi: 10.1089/ars.2006.1519

Inman, D. M., and Harun-Or-Rashid, M. (2017). Metabolic vulnerability in the neurodegenerative disease glaucoma. *Front. Neurosci.* 11:146. doi: 10.3389/fnins.2017.00146

Inman, D. M., Lambert, W. S., Calkins, D. J., and Horner, P. J. (2013). alpha-Lipoic acid antioxidant treatment limits glaucoma-related retinal ganglion cell death and dysfunction. *PLoS ONE* 8:e65389. doi: 10.1371/journal.pone.0065389

Jazwa, A., and Cuadrado, A. (2010). Targeting heme oxygenase-1 for neuroprotection and neuroinflammation in neurodegenerative diseases. *Curr. Drug Targets* 11, 1517–1531. doi: 10.2174/1389450111009011517

Johnson, E. C., Doser, T. A., Cepurna, W. O., Dyck, J. A., Jia, L., Guo, Y., et al. (2011). Cell proliferation and interleukin-6-type cytokine signaling are implicated by gene expression responses in early optic nerve head injury in rat glaucoma. *Invest. Ophthalmol. Vis. Sci.* 52, 504–518. doi: 10.1167/iovs.10-5317

Kanamori, A., Catrinescu, M. M., Kanamori, N., Mears, K. A., Beaubien, R., and Levin, L. A. (2010). Superoxide is an associated signal for apoptosis in axonal injury. *Brain* 133, 2612–2625. doi: 10.1093/brain/awq105

Ko, M. L., Peng, P. H., Ma, M. C., Ritch, R., and Chen, C. F. (2005). Dynamic changes in reactive oxygen species and antioxidant levels in retinas in experimental glaucoma. *Free Radic. Biol. Med.* 39, 365–373. doi: 10.1016/j.freeradbiomed.2005.03.025

Kuwabara, K., Matsumoto, M., Ikeda, J., Hori, O., Ogawa, S., Maeda, Y., et al. (1996). Purification and characterization of a novel stress protein, the 150-kDa oxygen-regulated protein (ORP150), from cultured rat astrocytes and its expression in ischemic mouse brain. *J. Biol. Chem.* 271, 5025–5032. doi: 10.1074/jbc.271.9.5025

Lee, J. M., Calkins, M. J., Chan, K., Kan, Y. W., and Johnson, J. A. (2003). Identification of the NF-E2-related factor-2-dependent genes conferring protection against oxidative stress in primary cortical astrocytes using oligonucleotide microarray analysis. *J. Biol. Chem.* 278, 12029–12038. doi: 10.1074/jbc.M211558200

Ma, M. W., Wang, J., Zhang, Q., Wang, R., Dhandapani, K. M., Vadlamudi, R. K., et al. (2017). NADPH oxidase in brain injury and neurodegenerative disorders. *Mol. Neurodegener.* 12:7. doi: 10.1186/s13024-017-0150-7

Malone, P. E., and Hernandez, M. R. (2007). 4-Hydroxynonenal, a product of oxidative stress, leads to an antioxidant response in optic nerve head astrocytes. *Exp. Eye Res.* 84, 444–454. doi: 10.1016/j.exer.2006.10.020

Marrif, H., and Juurlink, B. H. (1999). Astrocytes respond to hypoxia by increasing glycolytic capacity. *J. Neurosci. Res.* 57, 255–260. doi: 10.1002/(SICI)1097-4547(19990715)57:2<255::AID-JNR11>3.0.CO;2-6

McElnea, E. M., Quill, B., Docherty, N. G., Irnaten, M., Siah, W. F., Clark, A. F., et al. (2011). Oxidative stress, mitochondrial dysfunction and calcium overload in human lamina cribrosa cells from glaucoma donors. *Mol. Vis.* 17, 1182–1191.

Mense, S. M., Sengupta, A., Zhou, M., Lan, C., Bentsman, G., Volsky, D. J., et al. (2006). Gene expression profiling reveals the profound upregulation of hypoxia-responsive genes in primary human astrocytes. *Physiol. Genomics* 25, 435–449. doi: 10.1152/physiolgenomics.00315.2005

Minckler, D. S., Bunt, A. H., and Johanson, G. W. (1977). Orthograde and retrograde axoplasmic transport during acute ocular hypertension in the monkey. *Invest. Ophthalmol. Vis. Sci.* 16, 426–441.

Moos, T. (1996). Immunohistochemical localization of intraneuronal transferrin receptor immunoreactivity in the adult mouse central nervous system. *J. Comp. Neurol.* 375, 675–692. doi: 10.1002/(SICI)1096-9861(19961125)375:4<675::AID-CNE8>3.0.CO;2-Z

Moreno, M. C., Campanelli, J., Sande, P., Sánez, D. A., Keller Sarmiento, M. I., and Rosenstein, R. E. (2004). Retinal oxidative stress induced by high intraocular pressure. *Free Radic. Biol. Med.* 37, 803–812. doi: 10.1016/j.freeradbiomed.2004.06.001

Mowat, F. M., Luhmann, U. F., Smith, A. J., Lange, C., Duran, Y., Harten, S., et al. (2010). HIF-1alpha and HIF-2alpha are differentially activated in distinct cell populations in retinal ischaemia. *PLoS ONE* 5:e11103. doi: 10.1371/journal.pone.0011103

Nahirnyj, A., Livne-Bar, I., Guo, X., and Sivak, J. M. (2013). ROS detoxification and proinflammatory cytokines are linked by p38 MAPK signaling in a model of mature astrocyte activation. *PLoS ONE* 8:e83049. doi: 10.1371/journal.pone.0083049

Noh, Y. H., Kim, K. Y., Shim, M. S., Choi, S. H., Choi, S., Ellisman, M. H., et al. (2013). Inhibition of oxidative stress by coenzyme Q10 increases mitochondrial mass and improves bioenergetic function in optic nerve head astrocytes. *Cell Death Dis.* 4, e820. doi: 10.1038/cddis.2013.341

Peng, P. H., Ko, M. L., Chen, C. F., and Juan, S. H. (2008). Haem oxygenase-1 gene transfer protects retinal ganglion cells from ischaemia/reperfusion injury. *Clin. Sci.* 115, 335–342. doi: 10.1042/CS20070384

Pfaffl, M. W. (2001). A new mathematical model for relative quantification in real-time RT-PCR. *Nucleic Acids Res.* 29:e45. doi: 10.1093/nar/29.9.e45

Quigley, H., and Anderson, D. R. (1976). The dynamics and location of axonal transport blockade by acute intraocular pressure elevation in primate optic nerve. *Invest. Ophthalmol.* 15, 606–616.

Quigley, H. A., and Anderson, D. R. (1977). Distribution of axonal transport blockade by acute intraocular pressure elevation in the primate optic nerve head. *Invest. Ophthalmol. Vis. Sci.* 16, 640–644.

Quigley, H. A., and Broman, A. T. (2006). The number of people with glaucoma worldwide in 2010 and 2020. *Br. J. Ophthalmol.* 90, 262–267. doi: 10.1136/bjo.2005.081224

Quigley, H. A., Hohman, R. M., Addicks, E. M., and Green, W. R. (1984). Blood vessels of the glaucomatous optic disc in experimental primate and human eyes. *Invest. Ophthalmol. Vis. Sci.* 25, 918–931.

Ryter, S. W., Alam, J., and Choi, A. M. (2006). Heme oxygenase-1/carbon monoxide: from basic science to therapeutic applications. *Physiol. Rev.* 86, 583–650. doi: 10.1152/physrev.00011.2005

Salinas-Navarro, M., Alarcón-Martínez, L., Valiente-Soriano, F. J., Jiménez-López, M., Mayor-Torroglosa, S., Avilés-Trigueros, M., et al. (2010). Ocular hypertension impairs optic nerve axonal transport leading to progressive retinal ganglion cell degeneration. *Exp. Eye Res.* 90, 168–183. doi: 10.1016/j.exer.2009.10.003

Satilmis, M., Orgül, S., Doubler, B., and Flammer, J. (2003). Rate of progression of glaucoma correlates with retrobulbar circulation and intraocular pressure. *Am. J. Ophthalmol.* 135, 664–669. doi: 10.1016/S0002-9394(02)02156-6

Schipper, H. M., Song, W., Zukor, H., Hascalovici, J. R., and Zeligman, D. (2009). Heme oxygenase-1 and neurodegeneration: expanding frontiers of engagement. *J. Neurochem.* 110, 469–485. doi: 10.1111/j.1471-4159.2009.06160.x

Schmidl, D., Garhofer, G., and Schmetterer, L. (2011). The complex interaction between ocular perfusion pressure and ocular blood flow - relevance for glaucoma. *Exp. Eye Res.* 93, 141–155. doi: 10.1016/j.exer.2010.09.002

Shonat, R. D., Wilson, D. F., Riva, C. E., and Cranstoun, S. D. (1992). Effect of acute increases in intraocular pressure on intravascular optic nerve head oxygen tension in cats. *Invest. Ophthalmol. Vis. Sci.* 33, 3174–3180.

Skoff, R., Knapp, P. E., and Bartlett, W. P. (1986). "Astrocyte diversity in the optic nerve: a cytoarchitectural study," in *Astrocytes*, eds S. Fedoroff and A. Vernadakis (New York, NY: Academic Press), 269–291.

Soto, I., and Howell, G. R. (2014). The complex role of neuroinflammation in glaucoma. *Cold Spring Harb. Perspect. Med.* 4:a017269. doi: 10.1101/cshperspect.a017269

Stasi, K., Nagel, D., Yang, X., Ren, L., Mittag, T., and Danias, J. (2007). Ceruloplasmin upregulation in retina of murine and human glaucomatous eyes. *Invest. Ophthalmol. Vis. Sci.* 48, 727–732. doi: 10.1167/iovs.06-0497

Sun, D., Lye-Barthel, M., Masland, R. H., and Jakobs, T. C. (2009). The morphology and spatial arrangement of astrocytes in the optic nerve head of the mouse. *J. Comp. Neurol.* 516, 1–19. doi: 10.1002/cne.22058

Sun, M. H., Pang, J. H., Chen, S. L., Han, W. H., Ho, T. C., Chen, K. J., et al. (2010). Retinal protection from acute glaucoma-induced ischemia-reperfusion injury through pharmacologic induction of heme oxygenase-1. *Invest. Ophthalmol. Vis. Sci.* 51, 4798–4808. doi: 10.1167/iovs.09-4086

Tebay, L. E., Robertson, H., Durant, S. T., Vitale, S. R., Penning, T. M., Dinkova-Kostova, A. T., et al. (2015). Mechanisms of activation of the transcription factor Nrf2 by redox stressors, nutrient cues, and energy status and the pathways through which it attenuates degenerative disease. *Free Radic. Biol. Med.* 88, 108–146. doi: 10.1016/j.freeradbiomed.2015.06.021

Tezel, G. (2006). Oxidative stress in glaucomatous neurodegeneration: mechanisms and consequences. *Prog. Retin. Eye Res.* 25, 490–513. doi: 10.1016/j.preteyeres.2006.07.003

Valiente-Soriano, F. J., Nadal-Nicolas, F. M., Salinas-Navarro, M., Jimenez-Lopez, M., Bernal-Garro, J. M., Villegas-Perez, M. P., et al. (2015). BDNF rescues RGCs but not intrinsically photosensitive RGCs in ocular hypertensive albino rat retinas. *Invest. Ophthalmol. Vis. Sci.* 56, 1924–1936. doi: 10.1167/iovs.15-16454

Vidal-Sanz, M., Salinas-Navarro, M., Nadal-Nicolás, F. M., Alarcon-Martinez, L., Valiente-Soriano, F. J., Miralles de Imperial, J., et al. (2011). Understanding glaucomatous damage: Anatomical and functional data from ocular hypertensive rodent retinas. *Prog. Retin. Eye Res.* 31, 1–27. doi: 10.1016/j.preteyeres.2011.08.001

Wasserman, W. W., and Fahl, W. E. (1997). Functional antioxidant responsive elements. *Proc. Natl. Acad. Sci. U.S.A.* 94, 5361–5366. doi: 10.1073/pnas.94.10.5361

Wenger, R. H. (2002). Cellular adaptation to hypoxia: O2-sensing protein hydroxylases, hypoxia-inducible transcription factors, and O2-regulated gene expression. *FASEB J.* 16, 1151–1162. doi: 10.1096/fj.01-0944rev

Williams, P. A., Marsh-Armstrong, N., and Howell, G. R. (2017). Neuroinflammation in glaucoma: a new opportunity. *Exp. Eye Res.* 157, 20–27. doi: 10.1016/j.exer.2017.02.014

Yanagi, M., Kawasaki, R., Wang, J. J., Wong, T. Y., Crowston, J., and Kiuchi, Y. (2011). Vascular risk factors in glaucoma: a review. *Clin. Exp. Ophthalmol.* 39, 252–258. doi: 10.1111/j.1442-9071.2010.02455.x

Yu, A. L., Fuchshofer, R., Birke, M., Kampik, A., Bloemendal, H., and Welge-Lüssen, U. (2008). Oxidative stress and TGF-beta2 increase heat shock protein 27 expression in human optic nerve head astrocytes. *Invest. Ophthalmol. Vis. Sci.* 49, 5403–5411. doi: 10.1167/iovs.07-1478

Yu, A. L., Moriniere, J., Birke, M., Neumann, C., Fuchshofer, R., Kampik, A., et al. (2009). Reactivation of optic nerve head astrocytes by TGF-beta2 and H_2O_2 is accompanied by increased Hsp32 and Hsp47 expression. *Invest. Ophthalmol. Vis. Sci.* 50, 1707–1717. doi: 10.1167/iovs.08-1961

Yu, D. Y., and Cringle, S. J. (2001). Oxygen distribution and consumption within the retina in vascularised and avascular retinas and in animal models of retinal disease. *Prog. Retin. Eye Res.* 20, 175–208. doi: 10.1016/S1350-9462(00)00027-6

Zanetti, M., d'Uscio, L. V., Peterson, T. E., Katusic, Z. S., and O'Brien, T. (2005). Analysis of superoxide anion production in tissue. *Methods Mol. Med.* 108, 65–72. doi: 10.1385/1-59259-850-1:065

Zhang, X., Yeung, P. K., McAlonan, G. M., Chung, S. S., and Chung, S. K. (2013). Transgenic mice over-expressing endothelial endothelin-1 show cognitive deficit with blood-brain barrier breakdown after transient ischemia with long-term reperfusion. *Neurobiol. Learn. Mem.* 101, 46–54. doi: 10.1016/j.nlm.2013.01.002

Conflict of Interest Statement: The authors declare that the research was conducted in the absence of any commercial or financial relationships that could be construed as a potential conflict of interest.

The reviewer DI and handling Editor declared their shared affiliation.

frontiers in Neuroscience

ORIGINAL RESEARCH
published: 31 May 2017
doi: 10.3389/fnins.2017.00318

Interleukin-6 Deficiency Attenuates Retinal Ganglion Cell Axonopathy and Glaucoma-Related Vision Loss

Franklin D. Echevarria[1], *Cathryn R. Formichella*[2,3] *and Rebecca M. Sappington*[2,3,4]*

[1] Neuroscience Graduate Program, Vanderbilt University, Nashville, TN, United States, [2] Department of Ophthalmology and Visual Sciences, Vanderbilt University School of Medicine, Nashville, TN, United States, [3] Vanderbilt Eye Institute, Vanderbilt University Medical Center, Nashville, TN, United States, [4] Department of Pharmacology, Vanderbilt University School of Medicine, Nashville, TN, United States

The pleotropic cytokine interleukin-6 (IL-6) is implicated in retinal ganglion cell (RGC) survival and degeneration, including that associated with glaucoma. IL-6 protects RGCs from pressure-induced apoptosis *in vitro*. However, it is unknown how IL-6 impacts glaucomatous degeneration *in vivo*. To study how IL-6 influences glaucomatous RGC axonopathy, accompanying glial reactivity, and resultant deficits in visual function, we performed neural tracing, histological, and neurobehavioral assessments in wildtype (B6;129SF2/J; WT) and IL-6 knock-out mice (B6;129S2-*IL6*^{tm1kopf}/J; *IL-6-/-*) after 8 weeks of unilateral or bilateral microbead-induced glaucoma (microbead occlusion model). IOP increased by 20% following microbead injection in both genotypes ($p < 0.05$). However, deficits in wound healing at the site of corneal injection were noted. In WT mice, elevated IOP produced degenerating axon profiles and decreased axon density in the optic nerve by 15% ($p < 0.01$). In *IL-6-/-* mice, axon density in the optic nerve did not differ between microbead- and saline-injected mice ($p > 0.05$) and degenerating axon profiles were minimal. Preservation of RGC axons was reflected in visual function, where visual acuity decreased significantly in a time-dependent manner with microbead-induced IOP elevation in WT ($p < 0.001$), but not *IL-6-/-* mice ($p > 0.05$). Despite this preservation of RGC axons and visual acuity, both microbead-injected WT and *IL-6-/-* mice exhibited a 50% decrease in anterograde CTB transport to the superior colliculus, as compared to saline-injected controls ($p < 0.01$). Assessment of glial reactivity revealed no genotype- or IOP-dependent changes in retinal astrocytes. IOP elevation decreased microglia density and percent retinal area covered in WT mice ($p < 0.05$), while *IL-6-/-* mice exhibited only a decrease in density ($p < 0.05$). Together, our findings indicate that two defining features of RGC axonopathy—axon transport deficits and structural degeneration of axons—likely occur via independent mechanisms. Our data suggest that IL-6 is part of a mechanism that specifically leads to structural degeneration of axons. Furthermore, its absence is sufficient to prevent both structural degeneration of the optic nerve and vision loss. Overall, our work supports the proposition that functional deficits in axon transport represent a therapeutic window for RGC axonopathy and identify IL-6 signaling as a strong target for such a therapeutic.

Keywords: interleukin-6, cytokine, retinal ganglion cell, glaucoma, axonopathy, microbead, cornea, wound healing

OPEN ACCESS

Edited by:
Jason R. Richardson, Northeast Ohio Medical University, United States

Reviewed by:
Varun Kesherwani, University of Nebraska Medical Center, United States
Gregory W. J. Hawryluk, University of Utah, United States
Jena J. Steinle, Wayne State University School of Medicine, United States

***Correspondence:**
Rebecca M. Sappington
rebecca.m.sappington@vanderbilt.edu

Specialty section:
This article was submitted to Neurodegeneration, a section of the journal Frontiers in Neuroscience

Received: *27 March 2017*
Accepted: *19 May 2017*
Published: *31 May 2017*

Citation:
Echevarria FD, Formichella CR and Sappington RM (2017) Interleukin-6 Deficiency Attenuates Retinal Ganglion Cell Axonopathy and Glaucoma-Related Vision Loss. Front. Neurosci. 11:318. doi: 10.3389/fnins.2017.00318

INTRODUCTION

The pleotropic cytokine interleukin-6 (IL-6) is involved in a variety of central nervous system (CNS) pathologies including injury, infection, and neurodegeneration (Erta et al., 2012). Its classification as either protective or destructive within the CNS continues to be highly contested. Pre-treatment with IL-6 prevents apoptosis in neural cells exposed to a number of physiological stressors *in vitro*, supporting the idea that IL-6 is neuro-protective (Yamada and Hatanaka, 1994; Sappington et al., 2006; Spittau et al., 2012; Fang et al., 2013; Chucair-Elliott et al., 2014). In animal models of CNS disease, loss of IL-6 leads to an overall reduction in the neuroinflammatory response, including reduced expression of other inflammatory cytokines and diminished glial reactivity (Penkowa et al., 1999, 2000, 2001; Clark et al., 2000; Cardenas and Bolin, 2003). Interestingly, the effect on neuronal health is variable, as studies suggest that IL-6 signaling promotes both viability (Yamada and Hatanaka, 1994; Loddick et al., 1998; Zhong et al., 1999; Clark et al., 2000; Cardenas and Bolin, 2003; Inomata et al., 2003; Penkowa et al., 2003; Sappington et al., 2006; Spittau et al., 2012; Fang et al., 2013; Leibinger et al., 2013; Chucair-Elliott et al., 2014) and dysfunction (Campbell et al., 1993; Bluthe et al., 2000; Sparkman et al., 2006; Mukaino et al., 2010; Burton et al., 2011, 2013; Burton and Johnson, 2012) depending on the model of CNS injury. IL-6 mRNA and protein are upregulated near retinal ganglion cells (RGCs) and their axons in rodent models of glaucoma (Sappington and Calkins, 2008; Chidlow et al., 2012; Sims et al., 2012; Wilson et al., 2015). Glaucoma is a neurodegenerative disease characterized by RGC axonopathy and associated with both advanced age and elevated intraocular pressure (IOP) (Calkins, 2012). Like elsewhere in the CNS, the role of IL-6 in RGC axonopathy is unclear. Application of recombinant IL-6 to RGCs *in vitro* prevents pressure-induced apoptosis (Sappington et al., 2006). Similarly, IL-6 appears to protect RGCs and enhance axon regeneration following optic nerve crush (Leibinger et al., 2013, 2016). In contrast, other studies indicate that IL-6 deficiency protects RGCs in models of glutamate excitotoxicity and optic nerve crush (Fisher et al., 2001).

To better elucidate the impact of IL-6 signaling on RGC axonopathy in glaucoma, we comprehensively examined and compared optic nerve morphology, visual acuity, active axonal transport, and retinal glial reactivity in IL-6 deficient (*IL-6-/-*) and wildtype (WT) mice with 8 weeks of unilateral or bilateral microbead-induced glaucoma (microbead occlusion model). Together, our data indicate that IL-6 deficiency mitigates glaucoma-induced deficits in visual function and optic nerve structure without improvement in axon transport or reduction in microglia reactivity. This suggests that IL-6 may play specific role in the progression of RGC axonopathy from functional deficits to structural degeneration.

Abbreviations: IL-6, interleukin-6; IOP, intraocular pressure; CNS, central nervous system; RGC, retinal ganglion cell; GCL, ganglion cell layer; NFL, nerve fiber layer; SC, superior colliculus; GFAP, glial fibrillary acidic protein; Iba-1, ionized calcium-binding adapter molecule-1; CTB, cholera toxin beta-subunit; SD-OCT, spectral domain optical coherence tomography.

MATERIALS AND METHODS

Animals

Seven to nine month old male and female *IL-6-/-* mice (B6;129S2-*IL6*^{tm1kopf}/J) and respective genomic controls (B6;129SF2/J) were used for all experiments. *IL-6-/-* mice contain a neomycin selection cassette in exon 2 of the IL-6 gene preventing transcription of the mRNA product (Kopf et al., 1994). Founder mice were obtained from Jackson Laboratories (Bar Harbor, ME) and experimental mice were bred and genotyped in-house using the following primers provided by Jackson Labs: 5′-TTC-CAT-CCA-GTT-GCC-TTC-TTG-G-3′, 5′-TTC-TCA-TTT-CCA-CGA-TTT-CCC-AG-3′ and 5′-CCG-GAG-AAC-CTG-CGT-GCA-ATC-C-3′. Mice were housed in accordance with NIH guidelines and maintained on a 12 h light/dark cycle with *ad libitum* access to standard mouse chow and water. This study was carried out in accordance with the ARVO statement for the use of animals in ophthalmic and vision research and was approved by the IACUC of Vanderbilt University Medical Center.

Induction of Ocular Hypertension Using the Microbead Occlusion Model

Acute IOP elevation was induced in WT and *IL-6-/-* mice using the microbead occlusion model, as previously described (Sappington et al., 2010). For anterograde axonal transport, axon density measurements, and retinal gliosis, mice from both genotypes received a unilateral injection of 1.5 µl (1×10^6 microbeads/mL) of 15 µm polystyrene beads conjugated to an Alexa Fluor 488 chromophore. The contralateral eye served as a surgical control and was injected with an equal volume of saline. For experiments looking at visual acuity and corneal integrity, 7–11 mice from both genotypes received bilateral injections of 1.5 µl microbeads and a separate cohort of mice served as controls and received bilateral injections of an equivalent volume of saline. All mice received two microbead/saline injections 4 weeks apart to raise IOP for a total of 8 weeks. Following IOP elevation, mice were sacrificed by transcardial perfusion of 50 ml of 1X PBS followed by 100 ml of 4% paraformaldehyde. Eye and brain tissue were stored in 4% PFA at 4°C until use.

IOP Measurements

IOP was measured in awake, behaving mice, using a Tonolab rebound tonometer (TonoLab; Reichert, Depew, NY), as previously described (Echevarria et al., 2013; Formichella et al., 2014; Echevarria et al., 2016). Prior to initial injection, mean baseline IOP for each mouse was calculated from approximately 60 individual readings taken over a period of 6 days (10 measurements/day) within a 2 week timeline. Following microbead or saline injections, weekly IOP was determined as the mean of 20–30 measurements, taken over 2–3 days (10 measurements/day) each week for a total of 8 weeks. IOP measurements were taken at the same time of day to remove any effect of circadian rhythm on IOP measurements. To avoid

corneal irritation and discomfort, 0.5% proparacaine anesthetic drops (Akorn Inc, Lake Forest, IL), and lubricating eye drops were applied to each eye before and after IOP measurements were taken respectively.

Immunohistochemistry

Immunohistochemistry of whole mount retinas was done as previously described (Sims et al., 2012; Echevarria et al., 2013, 2016). Primary antibodies against glial fibrillary acidic protein (GFAP, 1:500; Cat# Z033429-2; DAKO) to label astrocytes, ionized calcium-binding adapter molecule-1 (Iba-1, 1:250; Cat# 019-19741; WAKO) to label microglia, and β-Tubulin III (TUJ1, 1:500; Cat#845501; BioLegend) to label RGCs were used. Secondary antibodies were used at a concentration of 1:200 and consisted of donkey α-rabbit attached to either a Rhodamine Red-X (Cat# 711-295-152; Jackson Immuno Labs) or Alexa-647 (Cat# 711-605-152; Jackson Immuno Labs) fluorophore.

Fluorescent *In-situ* Hybridization

Generation of IL-6 probes and FISH in naïve WT and *IL-6-/-* whole mount retina were done as previously described (Crish et al., 2013). Probes were made against a nucleotide sequence encompassing exons 2–5 of *IL-6* [nucleotides 107–651 of (NCBI Ref Seq: NM_031168.2)]. The transcript inserted into the pGEM-T Easy Vector (Promega, Madison WI) was generated by PCR using primers to IL-6 (forward 5′-ATCCAGTTGCCTTCTTGGGACTGA-3′ and reverse 5′TGGCTAAGGACCAAGACCATCCAA-3′). Following FISH, retinas underwent immunohistochemistry as described above to label RGCs.

Microscopy and Image Analysis

Imaging of whole mount retinas was done on an inverted confocal microscope (Olympus FV-1000; Center Valley, PA) through the Vanderbilt University Medical Center Cell Imaging Shared Resource Core. *IL-6* and β-Tubulin III labeling was imaged at 100X, while GFAP and Iba-1 was imaged at 60X. For both groups, 7–9 pseudo-random z-stack images in the mid central/mid-peripheral areas through the ganglion cell (GCL) and nerve fiber layers (NFL) of the retina were acquired using a digital camera and image analysis software (FV-100 ASW; Olympus). GFAP and Iba-1 percent area was calculated using NIS elements AR software (Nikon Instruments, Melville, NY), as previously described (Formichella et al., 2014). The area (mm^2) of the image containing above background signal intensity of Iba-1 or GFAP (See **Figures 6A,B**; red labeling) was calculated and reported as a percentage of the total area of the image. Total area of each image and background signal threshold was equal among all images. Microglia cell density was calculated by counting the number of Iba-1 positive cell somas and dividing the counts by the area of the image.

Anterograde Axon Transport Measurements

Anterograde axonal transport capabilities of RGCs were assessed with cholera toxin beta-subunit (CTB) conjugated to a 488 fluorophore, as previously described (Crish et al., 2010; Formichella et al., 2014; Ward et al., 2014; Bond et al., 2016). Briefly, mice were given a 1.5–2 μl intravitreal injection of CTB (10 μg/μl in sterile ddH_2O; Cat# C-34775, Life Technologies) using a 33 gauge needle attached to a Hamilton syringe under 2.5% isoflurane anesthesia. Five days after CTB injection, mice were sacrificed by transcardial perfusion as described above. To quantify axon transport, whole brains were cryopreserved in 30% sucrose for 24–48 h at 4°C. Using a sliding microtome, 50 μm sections were obtained through the superior colliculus (SC). CTB signal in these sections was imaged *en montage* at 10X, using a Nikon Eclipse T*i* inverted microscope (Nikon Instruments, Melville, NY). Anterograde axonal transport was quantified as previously described (Crish et al., 2010). Briefly, the SC from each image was outlined and CTB signal above background was divided by total pixel area to determine the volume of SC with CTB labeling. This value was used to create a colorimetric 2D retinotopic map of CTB transport ranging from 0% (blue) and 100% (red). Intact transport was defined as percent area with CTB signal $\geq$70% density (red/yellow).

Axon Density and Nerve Area

Axon density was measured in semi-thin sections of optic nerve as previously described (Sappington et al., 2010; Ward et al., 2014). Briefly, optic nerves were post fixed at least 48 h in 2.5% glutaraldehyde and embedded in epon. Semi-thin (700 nm) cross-sections of optic nerve near the chiasm were stained with 1% p-Phenylenediamine (PPD) and 1% toluidine blue to highlight myelin and glia, respectively. Optic nerve cross-sections were imaged *en montage* at 100X magnification on an upright Olympus Provis AX (Olympus, Melville, NY) microscope. To calculate axon density, a 50 × 50 μm grid mask was placed on the montaged image using NIS elements AR software. The number of axons was manually counted by a blind-observer in 8–10 squares of the grid. Each square counted was equal in area (0.0025 mm^2). To measure nerve area, the circumference of the nerve was traced in montaged images of optic nerve cross-sections. Nerve area was calculated as the area (mm^2) within this outline using NIS elements software.

Neurobehavioral Visual Testing Using Optomotry

The optokinetic response is a naturally occurring reflex that serves as a functional tool for quantitative analyses of visual system function in mice (Douglas et al., 2005). Briefly, each mouse was placed on a platform surrounded by four LCD computer monitors. A sinusoidal grating of alternating white and black bars rotating in either a clock-wise or counter clock-wise fashion was projected on the monitors. Mice able to perceive the moving stimulus produced a reflexive movement of the head in the direction of the stimulus. The visual acuity of each mouse was measured by changing the spatial frequency of the black and white bars. The visual acuity threshold was determined as the highest spatial frequency for which reflexive tracking was noted. The presence of the reflexive head movement was recorded by an observer using a camera mounted above the mouse. Mice were tested for baseline visual acuity threshold 1–2 weeks before microbead/saline injection and 4 and 8 weeks post-initial microbead/saline injection.

Corneal Imaging Using Spectral Domain Optical Coherence Tomography (SD-OCT)

Mice were anesthetized with a ketamine/xylazine cocktail (80/5 μg/gram of mouse), pupils were dilated with 0.5% Tropicamide, and eyes kept moist with lubricating eye drops. Live volumetric scans of the cornea were obtained using SD-OCT running the Bioptogen ultra-high resolution spectral domain OCT system with cornea bore (Bioptogen, Morrisville, NC). Quantification of injury area was performed using Image J software (National Institute of Health).

Statistical Analysis

Statistical analysis was conducted with SigmaPlot Version 11.1 (Systat Software Inc, San Jose, CA). For baseline and delta baseline IOP comparisons between WT and *IL-6-/-*, a Mann-Whitney Rank Sum test and a One-Way ANOVA with Holm-Sidak *post-hoc* correction was done respectively. For post injection IOP comparisons, a One-Way ANOVA on RANKS with Dunn's *post-hoc* correction was done. For corneal wound area measurements, a two-tailed *t*-test was done between WT and *IL-6-/-* mice at each time point. Differences in visual acuity throughout the 8 week experimental time course were assessed with a One-Way Repeated Measures ANOVA between baseline visual acuity, acuity at 4 weeks post initial injection, and 8 weeks post initial injection within each experimental group. Differences between all experimental groups at each time point were assessed with a One-Way ANOVA with Holm-Sidak *post-hoc* correction. Differences in percent baseline visual acuity at 8 weeks between all experimental groups were assessed with a One-Way ANOVA on RANKS with Dunn's *post-hoc* correction. All other comparisons were made with a One-Way ANOVA on RANKS with Dunn's *post-hoc* correction (percent glia coverage, microglia cell density) or a One-Way ANOVA with Holm-Sidak *post-hoc* correction (SC transport, axon density/nerve area). For all, $p < 0.05$ were considered statistically significant.

RESULTS

IL-6 Deficiency Does Not Affect Microbead-Induced Elevations in IOP

To confirm genetic ablation of IL-6, we conducted PCR to confirm the presence of the neomycin selection cassette in exon 2 of the *IL-6* gene. In all *IL-6-/-* mice used in this study, PCR amplification of exon 2 revealed a 380 bp product in the *IL-6-/-* mouse compared to the 174 bp PCR product in the WT mouse (**Figure 1A**). Loss of *IL-6* mRNA was corroborated using *in situ* hybridization. In a subset of WT and *IL-6-/-* whole mount retina co-immunolabeled with the RGC-specific marker β-Tubulin (TUJ1), labeling for *IL-6* mRNA using an antisense fluorescent *in situ* hybridization (FISH) probe showed robust signal that co-localized to TUJ1+ positive RGCs in WT mice (**Figure 1B**; left). Conversely, anti-sense labeling for *IL-6* mRNA was not detected in *IL-6-/-* mice (**Figure 1C**; left). Similarly, significant *IL-6* mRNA labeling was not detected following incubation with the sense probe in either genotype (**Figures 1B,C**; right). To examine the impact of IL-6 deficiency on the progression of IOP-induced

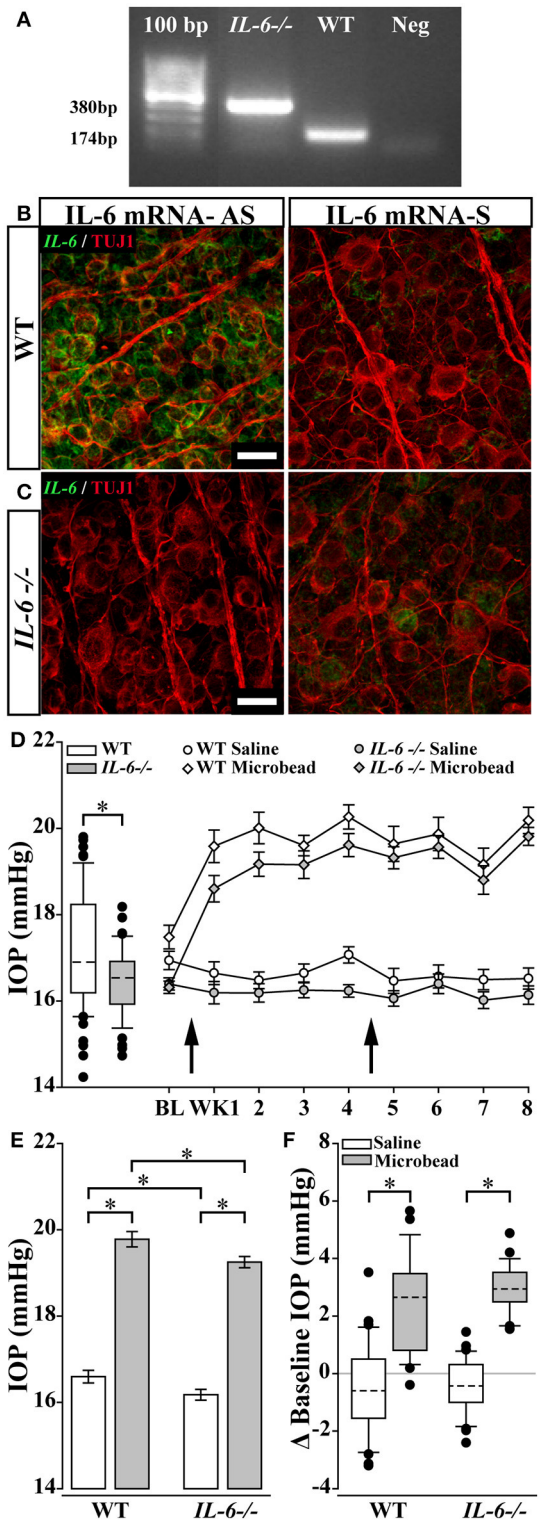

FIGURE 1 | IL-6 deficiency does not affect magnitude and duration of microbead induced ocular hypertension. **(A)** Representative gel from a PCR confirming the *IL-6-/-* genotype. PCR amplification of exon 2 leads to a PCR product of 380 bp in *IL-6-/-* mice and a 174 bp PCR product in WT mice. No band present in negative control lane. Products were run along a 100 bp

(Continued)

FIGURE 1 | Continued
ladder. **(B,C)**. Representative 100X confocal image of retinal whole mount from WT **(B)** and *IL-6-/-* mice **(C)** incubated with an anti-sense (AS; left) or sense probe (S; right) against *IL-6* mRNA (right). Signal from AS probe (**B**, green) is found within β-Tubulin (TUJ1) positive RGCs (red) in WT mice **(B)**. No significant signal was present in retinas from *IL-6-/-* mice (**C**; left) or during incubation with sense probe (**B,C**; right). Scale bars = 20 μm. **(D;** left) Boxplot of baseline IOP of WT (white) and *IL-6-/-* (gray) mice from all experimental cohorts prior to microbead/saline injection. Baseline IOP of *IL-6-/-* mice is decreased by 4% compared to baseline IOP of WT mice. (**D**; right) Line plot (mean ± SEM) showing baseline and weekly post saline (circle) or microbead (diamond) IOP in WT (white) or *IL-6-/-* (gray) eyes. Arrows indicate time of saline/microbead injections. Throughout the 8 week experiment, microbead injected eyes from both WT and *IL-6-/-* show a 15–20% increase in IOP compared to baseline measurements and saline injected eyes. **(E)** Bar graph of average IOPs (mean ± SEM) taken post initial microbead (gray) or saline (white) injection in both WT and *IL-6-/-* mice. A significant IOP increase in microbead- injected eyes vs. saline- injected eyes is seen in both genotypes. A genotype specific IOP reduction is seen in both saline- and microbead-injected *IL-6-/-* mice. **(F)** Boxplot showing magnitude of IOP difference in saline (white) and microbead (gray) injected WT and *IL-6-/-* mice compared to baseline measurements. A significant elevation in IOP is present in microbead-injected eyes compared to saline- injected eyes in both genotypes. However, no genotype specific differences in IOP seen. *$p < 0.05$. $n = 26$–34 eyes/genotype/condition. Dashed lines in box plot indicate median value.

RGC neurodegeneration, we utilized the microbead occlusion model (Sappington et al., 2010) of glaucoma to elevate IOP for a total of 8 weeks in WT and *IL-6-/-* mice. Baseline IOP was 4% lower in *IL-6-/-* mice (16.4 +/− 0.79 mmHg), compared to WT mice (17.1 +/− 1.32 mmHg; $p < 0.01$; **Figure 1D**; left). Microbead injection increased IOP by ∼ 20%, as compared to saline-injected controls for both genotypes (WT; $p < 0.001$, *IL-6-/-*; $p < 0.001$, **Figure 1D**; right and **Figure 1E**). In accordance with baseline IOP measurements, the mean IOP (mmHg) for both saline- ($p < 0.05$) and microbead-injected ($p < 0.05$) was lower in *IL-6-/-* mice than their WT counterparts (**Figure 1E**). However, with respect to baseline IOP, the magnitude of IOP elevation was similar (∼2.5 mmHg) in microbead-injected WT and *IL-6-/-* mice ($p > 0.05$, **Figure 1F**).

IL-6 Deficiency Preserves Optic Nerve Structure Following IOP Elevation

In glaucoma, degeneration of the optic nerve starts at the distal end of the optic nerve and progresses in a distal to proximal fashion (Crish et al., 2010). Unlike the distal optic nerve of saline-injected WT mice (**Figure 2A**; top), the distal optic nerve of microbead-injected WT mice presented with signs of structural pathology, including increased glial infiltration and degenerating axon profiles (**Figure 2A**; bottom). This was accompanied by a slight enlargement in nerve area (**Figure 2C**; left) and a 15% decrease in axon density, as compared to saline-injected mice ($p < 0.05$, **Figure 2D**; left). In contrast, while distal optic nerves from microbead-injected *IL-6-/-* mice presented with some gliosis, no change in degenerating axon profiles were noted (**Figure 2B**). Similarly, there were no measurable changes either in nerve area (**Figure 2C**; right) or myelinated axon density (*p*

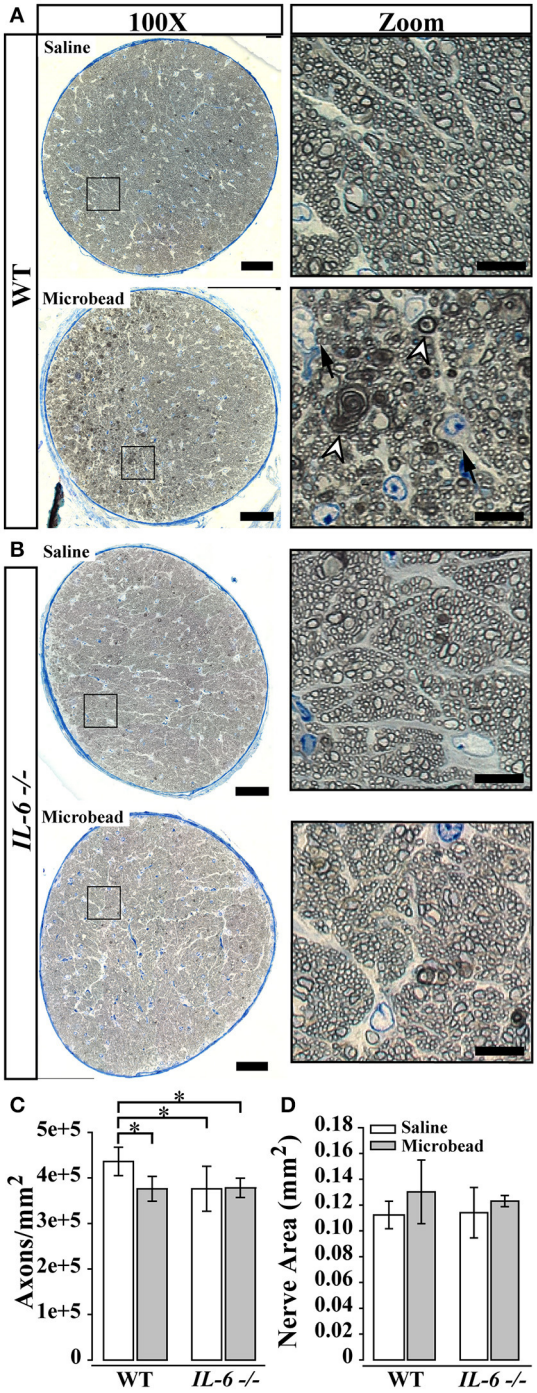

FIGURE 2 | IL-6 deficiency mitigates axon degeneration caused by IOP elevation. **(A,B)** Representative 100X montaged optic nerve cross sections from WT **(A)** and *IL-6-/-* **(B)** optic nerves following saline (top) or microbead (bottom) injection. Black box in montaged image (left) corresponds to location of zoomed images highlighting axon and glia (right). IOP elevation results in increased glial infiltration (black arrows) and degenerative axon profiles (white arrow heads) in optic nerves from microbead injected WT, but not *IL-6-/-* mice. **(C)** Bar graph of average (mean ± STDEV) myelinated axon density measurements in WT and *IL-6-/-* mice following saline (white) or microbead (gray) injection. Saline- injected *IL-6-/-* mice show a genotype

(Continued)

FIGURE 2 | Continued
specific decrease in myelinated axon density compared to saline- injected WT mice. However, microbead- injected WT eyes show a significant 15% decrease in myelinated axon density compared to saline- injected WT eyes, while no difference is seen between microbead- and saline- injected *IL-6-/-* eyes. **(D)** Bar graph of average nerve area (mean ± STDEV) among groups shows no significant difference. *$p < 0.05$. $n = 40$–50 density measurements/genotype/group. Scale bars= 50 μm for 100X montaged optic nerves and 10 μm for zoomed images.

> 0.05, **Figure 2D**; right), as compared to saline-injected *IL-6-/-* mice. However, independent of IOP, optic nerves from *IL-6-/-* mice contained approximately ∼15% fewer myelinated RGC axons than those from WT mice ($p < 0.05$, **Figure 2D**).

IL-6 Deficiency Does Not Prevent IOP-Induced Deficits in Anterograde Axon Transport

Previous reports indicate that functional deficits in anterograde axon transport along the optic projection precede structural degeneration of RGC axons in glaucoma (Crish et al., 2010, 2013). To measure active anterograde transport in RGC axons, we injected the active uptake, active transport tracer cholera toxin beta subunit (CTB) into the vitreous of *IL-6-/-* and WT mice 8 weeks after the initial microbead or saline injection. We measured anterograde transport of CTB from RGC soma in the retina to RGC terminals in the superior colliculus (SC) by quantifying CTB labeling in serial sections of SC and generating 2D reconstructions of CTB labeling in the SC (**Figure 3A**). In WT mice, 8 weeks of elevated IOP led to a ∼50% decrease in CTB transport to the SC, as compared to saline-injected mice ($p < 0.001$, **Figure 3A**; top, **Figure 3B**; left). Interestingly, in *IL-6-/-* mice, IOP elevation also resulted in a ∼50% decrease in CTB transport ($p < 0.001$, **Figure 3A**; bottom, **Figure 3B**; right). Similar to previously published studies (Crish et al., 2010; Lambert et al., 2011; Ward et al., 2014), these deficits occurred in a sectoral manner, extending from the periphery toward the optic disc in WT and *IL-6-/-* mice (**Figure 3A**). No differences in axon transport were noted between genotype in saline-injected animals ($p > 0.05$, **Figure 3B**).

IL-6 Deficiency Preserves Visual Acuity Following IOP Elevation

Loss of vision in glaucoma is irreversible and caused by degeneration of RGCs and their axons (Calkins, 2012). To ensure detection of any vision loss associated with microbead-induced glaucoma, we performed bilateral injections of microbeads in one cohort of WT and *IL-6-/-* mice. A second cohort received bilateral injections of saline. We measured visual acuity by optomotry every 4 weeks for the duration of the experiment. Over the course of 8 weeks, microbead-injected WT mice exhibited significant depreciation of visual acuity at each time point compared to baseline, resulting in an overall 22% decrease in visual acuity ($p < 0.001$ for all, **Figure 4A**; gray). However, in saline-injected WT mice, visual acuity did not significantly differ from baseline at either time point ($p > 0.05$, **Figure 4A**; white). Comparison of

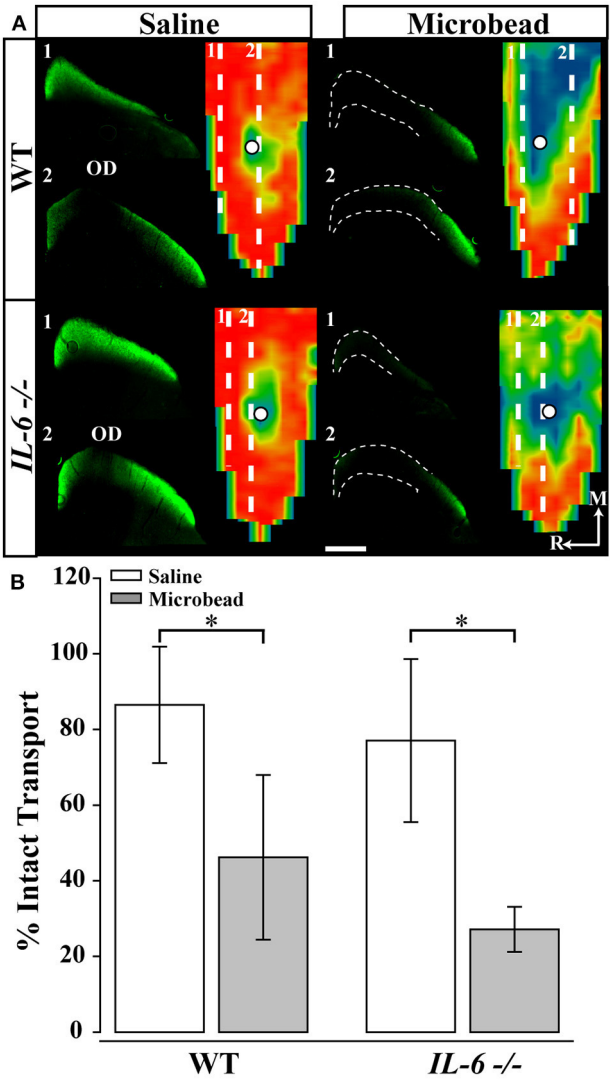

FIGURE 3 | IL-6 deficiency does not alter IOP-dependent deficits in anterograde axon transport. **(A)** Representative coronal sections through the superior colliculus (SC) and respective retinotopic heat maps after 5 days of CTB transport in WT (top) and (bottom) *IL-6-/-* mice. Outlines in coronal sections indicate areas of transport deficits. Dashed lines in map indicate position of coronal section. Density of the CTB signal for heat maps range from 0% (blue) to 50% (green) to 70% (yellow) to 100% (red). Numbered, dashed lines in retinotopic maps indicate the location of respective coronal section and white circles indicate position of the optic disk (OD). Medial (M) and rostral (R) orientations are indicated. **(B)** Bar graph showing average percent intact transport (mean ± STDEV, ≥70% density of CTB signal; red/yellow areas) from SC following saline (white) or microbead (gray) injection in WT (left) and *IL-6-/-* (right) mice. SC from both microbead- injected WT and *IL-6-/-* mice show a ∼50% deficit in intact axon transport compared to saline- injected mice. *$p < 0.05$. $n = 5$–6 SC/genotype/condition. Scale bars = 500 μm for all images.

visual acuity between saline- and microbead-injected WT mice revealed a significant ∼15% decrease in both raw visual acuity ($p < 0.05$, **Figure 4C**) and percent baseline visual acuity ($p < 0.05$, **Figure 4D**). In *IL-6-/-* mice, visual acuity dropped 8% with either saline ($p < 0.01$) or microbeads ($p < 0.05$), as compared

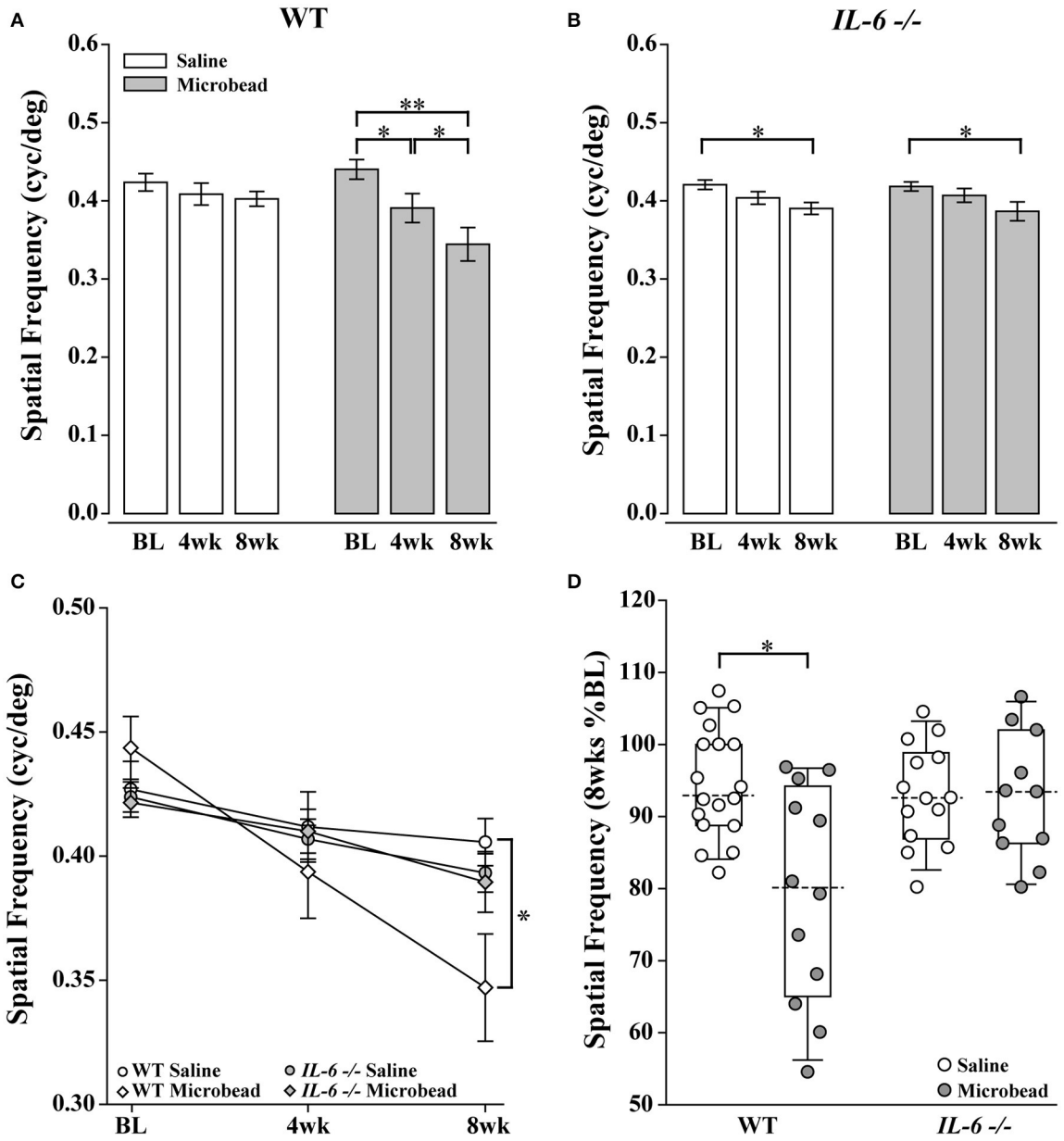

FIGURE 4 | *IL-6-/-* mice are resistant to IOP-induced deficits in visual acuity. **(A)** Bar graph showing average visual acuity threshold (mean ± SEM) of WT mice at baseline and 4 and 8 weeks post initial saline (white) or microbead (gray) injection. WT mice injected with microbeads show a significant decrease in visual acuity at both 4 weeks and 8 weeks post-injection compared to baseline. **(B)** Bar graph showing average visual acuity threshold (mean ± SEM) of *IL-6-/-* mice at baseline and 4 and 8 weeks post initial saline (white) or microbead (gray) injection. *IL-6-/-* mice injected with either saline or microbeads show a significant decrease in visual acuity at 8 weeks compared to baseline. **(C)** Line graph comparing visual acuity of WT saline (white circle), WT microbead (white diamond), *IL-6-/-* saline (gray circle) and *IL-6-/-* microbead (gray diamond) at each time point. Visual acuity decreases significantly in microbead-injected WT mice compared to saline-injected WT mice. Visual acuity does not differ between saline- and microbead- injected *IL-6-/-* or between genotypes. **(D)** Boxplot of the percent visual acuity remaining at 8 weeks compared to baseline measurements for WT and *IL-6-/-*. WT mice injected with microbeads show a significant decrease in the remaining visual acuity when compared to the saline- injected WT mice. *IL-6-/-* mice injected with microbeads show no difference in the remaining visual acuity when compared to the saline injected *IL-6-/-* cohort. $^{*}p < 0.05$, $^{**}p < 0.001$. $n = 13$–17/group. Dashed lines in boxplot indicate median value of data set.

to baseline acuity (**Figure 4B**). However, this initial reduction in visual acuity did not differ between saline- and microbead-injected *IL-6-/-* mice ($p > 0.05$, **Figures 4C,D**) and remained unchanged between 4 and 8 weeks for both groups (saline: $p > 0.05$; microbead: $p > 0.05$; **Figure 4B**). That this slight decrease in visual acuity was noted in both saline- and microbead-injected *IL-6-/-* mice and remained stable for the 8 week experiments suggest that it arises from an IOP-independent influence. No difference in visual acuity was noted between WT and *IL-6-/-* mice at any time point ($p > 0.05$, **Figure 4C**).

IL-6-/- Mice Exhibit Deficits in Corneal Wound Healing

Previous studies indicate *IL-6-/-* mice exhibit deficits in wound healing (Lin et al., 2003; McFarland-Mancini et al., 2010). As the microbead/saline injections require puncturing of the cornea, we used spectral-domain optical coherence tomography (SD-OCT) imaging to examine whether perturbed healing of the cornea could underlie the reduction in visual acuity noted in both saline and microbead-injected *IL-6-/-* mice. Two weeks following intracameral injection of saline or microbeads in WT eyes, SD-OCT imaging revealed complete closure of the epithelial layer and approximately 2/3 closure of the stroma and endothelial layers at the injection site (**Figure 5A**). Quantification of the remaining corneal wound revealed no significant change over the remaining 6 weeks ($p > 0.05$; **Figure 5C**). In *IL-6-/-* mice, SD-OCT imaging revealed complete closure of the epithelial layer by 2 weeks. However, limited closure of the stroma and endothelial layers was noted (**Figure 5B**). This reduction in stroma and endothelial wound healing was noted throughout the 8 week experiment (**Figure 5B**). Quantification of corneal injury revealed that the area of corneal wound was 2-fold larger in *IL-6-/-* mice than in WT mice at all three time points ($p < 0.05$; **Figure 5C**). Like WT mice, the area of the corneal wound did not change over the 8 week experiment in *IL-6-/-* ($p > 0.05$; **Figure 5C**).

IL-6 Deficiency Enlarges the Microglia Population in Retina

Recent studies suggest that changes in glial reactivity in the retina occur in response to IOP elevation, and impact RGC degeneration in both genomic and inducible models of glaucoma (Martin et al., 2003; Sappington and Calkins, 2006; Inman and Horner, 2007; Bosco et al., 2008; Johnson and Morrison, 2009; Johnson et al., 2011; Echevarria et al., 2013; Lye-Barthel et al., 2013; Formichella et al., 2014; Hines-Beard et al., 2016). To determine whether IL-6 deficiency alters glial reactivity associated with RGC axonopathy, we performed a morphological analysis of astrocyte and microglia reactivity in retina. We visualized astrocytes and microglia in whole-mount retina from saline- and microbead- injected WT and *IL-6-/-* mice with immunolabeling against the astrocyte- specific label glial fibrillary acidic protein (GFAP) and the microglia- specific marker ionized calcium binding adaptor molecule (Iba-1). While Iba-1 labels various types of myeloid cells, we selected this marker because (1) 100% of retinal microglia are Iba-1 positive (Bosco et al., 2011), (2) Iba-1 expression remains rather stable across activation states compared to other microglia/macrophage markers (Bosco et al., 2011) and (3) with the exception of amoeboid microglia, other myeloid cells and microglia can be readily distinguished by morphology. To account for changes in both glia density and hypertrophy/ramification, we quantified the percent of retinal area covered by GFAP+ astrocytes (**Figure 6A**) and Iba-1+ microglia (**Figure 6B**). Our previous work indicates that percent area coverage is a highly reliable measure of reactivity (Formichella et al., 2014). GFAP immunolabeling revealed no gross genotype- or IOP-dependent changes in astrocytic morphology (**Figure 6C**). Quantification of astrocyte coverage confirmed no significant change in astrocyte morphology with respect to either IOP or genotype ($p > 0.05$ for all; **Figure 6E**). In contrast, Iba-1 immunolabeling revealed qualitative changes in microglia that appeared to relate to both genotype and IOP (**Figure 6D**). Quantification revealed 32% more microglia coverage in saline-injected *IL-6-/-* mice vs. WT mice ($p < 0.05$; **Figure 6F**). IOP elevation decreased microglia coverage by 45% in WT retina ($p < 0.05$; **Figure 6F**), as compared to saline-injected controls (**Figure 6F**). While it appeared as if there was decreased microglial coverage in *IL-6-/-* retina following IOP elevation compared to saline-injected controls, it did not reach statistical significance ($p > 0.05$; **Figure 6F**). Additionally, microglia coverage remained higher in *IL-6-/-* mice than in WT mice following IOP elevation ($p < 0.05$, **Figure 6F**). Based on qualitative assessment, IOP-induced changes in percent area coverage appeared to arise from changes in microglia density (**Figure 6D**). To quantitatively test this observation, we measured the density of Iba-1+ microglia across all experimental groups. We found that microbead-induced IOP elevation decreased the density of microglia by 37% in WT retina ($p < 0.05$) and by 36% in *IL-6-/-* mice ($p < 0.05$), as compared to saline-injected controls (**Figure 6G**). There was no significant difference in the density of microglia between WT and *IL-6-/-* mice regardless of treatment ($p > 0.05$; **Figure 6G**).

DISCUSSION

The present work investigated the relevance of IL-6 signaling to RGC axonopathy following microbead-induced IOP elevation. By comparing functional and structural outcomes of RGC degeneration in *IL-6-/-* and WT mice, we were able to link IL-6 signaling with specific events in RGC axonopathy. These studies delineate a role for IL-6 in the progression from functional deficits to structural degeneration within the axonopathy continuum. Secondarily, our data also indicated a role for IL-6 in corneal wound healing and potentially, IOP regulation.

Glaucoma is associated with elevated IOP. Current therapies, directed toward lowering IOP, delay pathology (Calkins, 2012). Not surprisingly, animal models of glaucoma are generally characterized by elevated IOP and subsequent degeneration of RGCs. Despite modest differences in baseline IOP, the magnitude of IOP elevation achieved with microbead occlusion was identical in WT and *IL-6-/-* mice (**Figure 1**). This indicates that IL-6 deficiency does not impact efficacy of IOP elevation in this model. Intracameral injection of saline and microbeads requires a small diameter (approx. 100 μm) puncture in the cornea. OCT imaging revealed that IL-6 deficiency resulted in a larger corneal wound and impeded stitching and filling of the stromal and endothelial layers of the cornea, which was visible in WT mice within 2 weeks of puncture (**Figure 5**). Interestingly, the epithelial layer of the cornea in *IL-6-/-* mice was indistinguishable from WT mice (**Figure 5**). This suggests that IL-6 signaling plays a prominent role in healing of stromal and endothelial, but not epithelial, layers of cornea. That a deficit in corneal wound healing was noted in our studies is not surprising, as IL-6 is

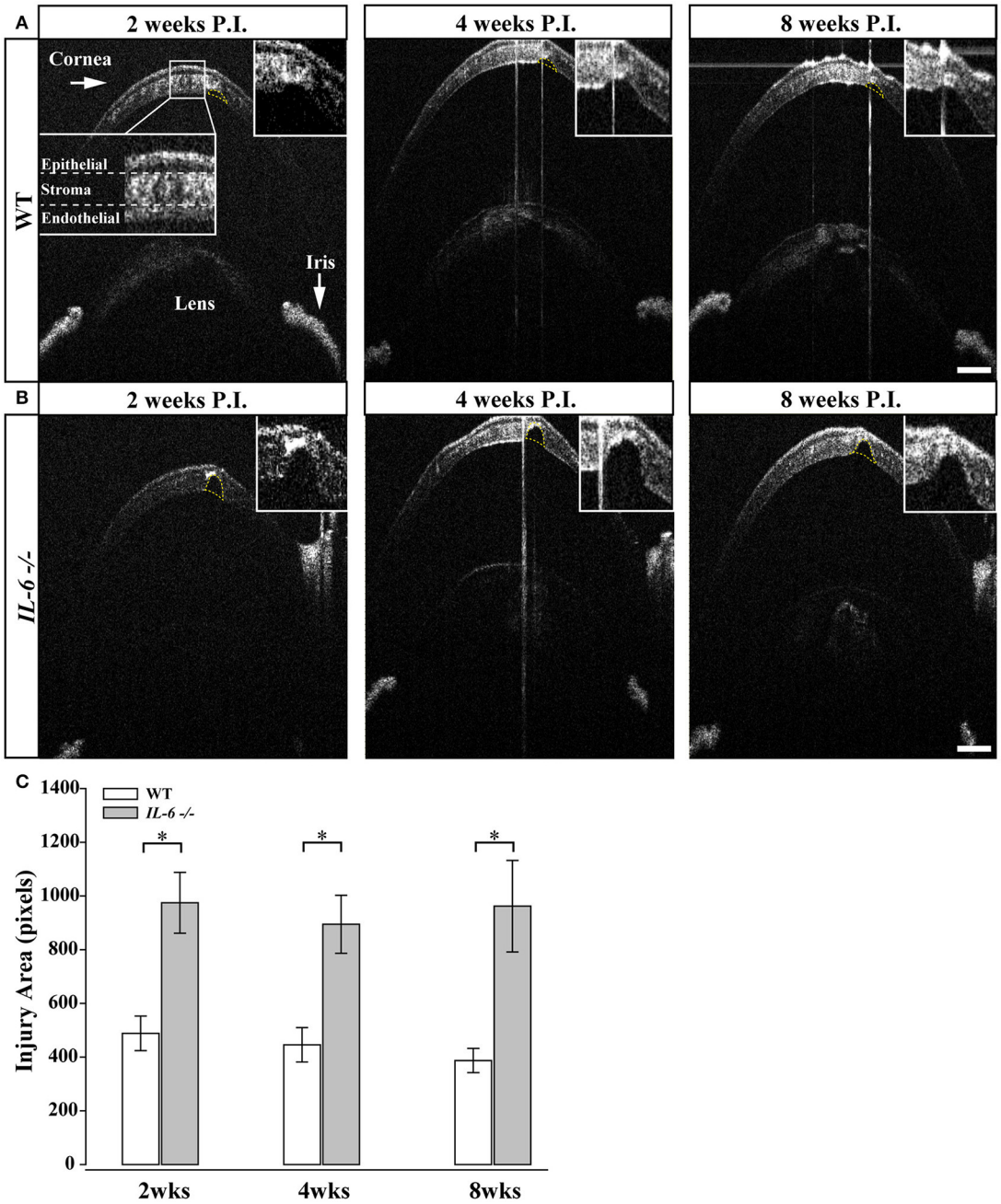

FIGURE 5 | *IL-6-/-* mice present with defects in corneal wound healing following microbead/saline injection.**(A)** Representative images of corneal wounds at 2, 4 and 8 weeks post initial injection in WT mice. Insert (**A;** far left) outlines layers of the cornea. 2 weeks after corneal puncture due to saline or microbead delivery, WT mice left display small gaps in the corneal stroma and endothelium (yellow dotted lines). The size of the injury persists after 4 (middle) and 8 (right) weeks after injury. **(B)** Representative images of corneal wounds at 2, 4, and 8 weeks post injection in *IL-6-/-* mice. *IL-6-/-* mice however, present with significantly larger gaps 2 weeks (left) in the corneal stroma after puncture that also persists at 4 (middle) and 8 (right) weeks after injury. **(C)** Bar graph showing quantification of corneal injury area (mean ± SEM). *IL-6-/-* mice have significantly larger corneal injuries at all time points. Size of the wound area did not change significantly over time in either WT or *IL-6-/-*. $^*p < 0.05$. $n = 9$ eyes/genotype/group. Scale bars= 100 μm for all images.

strongly associated with wound healing and tissue regeneration in other systems (Blindenbacher et al., 2003; Lin et al., 2003; Tiberio et al., 2008; McFarland-Mancini et al., 2010).

Structural degeneration of the optic nerve and vision loss are the two hallmarks of glaucoma. In our study, IL-6 deficiency preserved both the structure of RGC axons and visual acuity following 8 weeks of elevated IOP. Consistent with previous findings (Sappington et al., 2010; Lambert et al., 2011; Ward et al., 2014; Bond et al., 2016), microbead-induced IOP elevation decreased axon density, while increasing degenerative axon

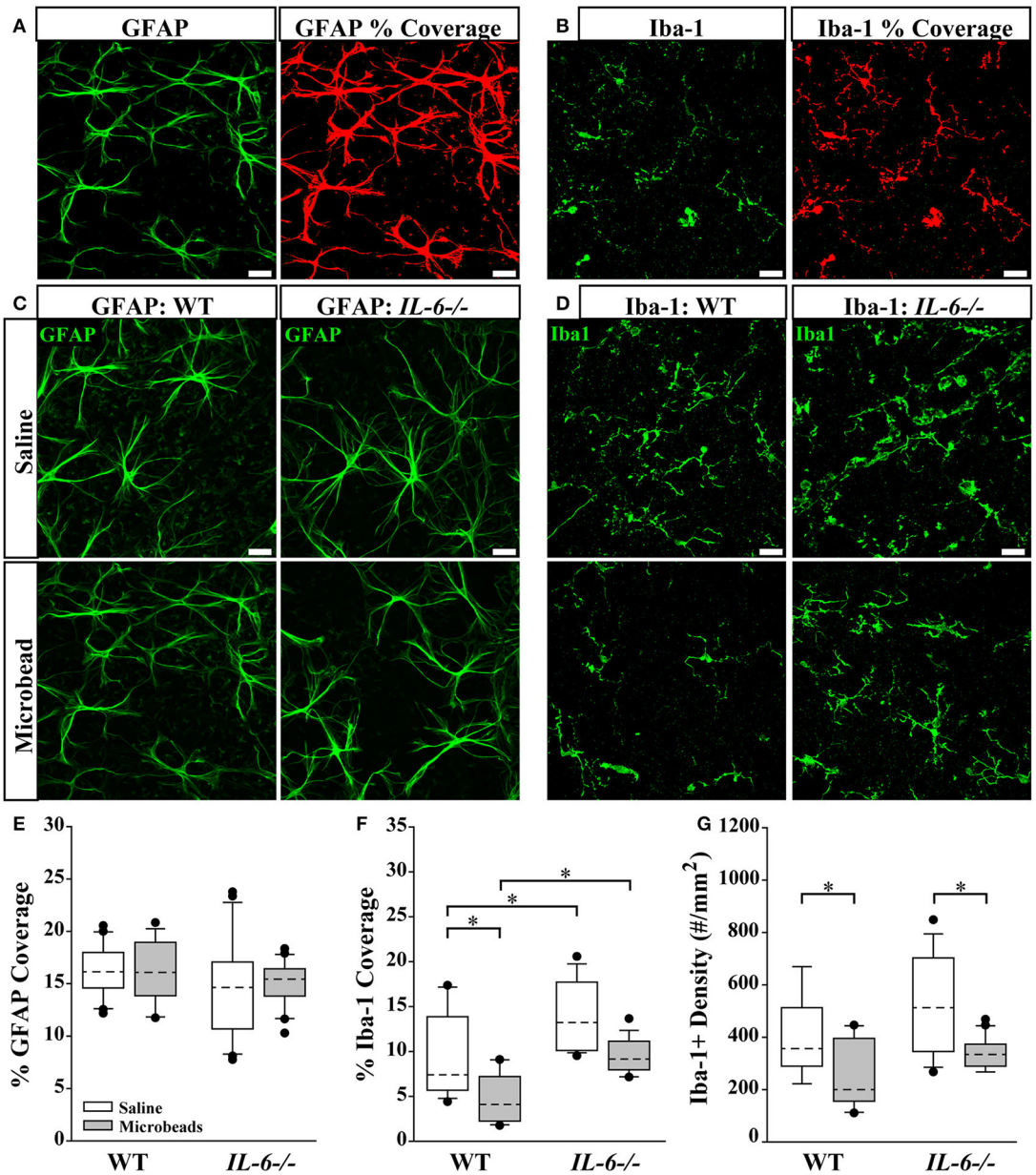

FIGURE 6 | IL-6 deficiency affects microglial coverage regardless of IOP. **(A,B)** Representative 60X confocal images depicting quantification of percent coverage of GFAP+ astrocytes (green; **A,** left) and Iba-1+ microglia (green; **B,** left). The area containing above background signal for GFAP and Iba-1 was highlighted in red (**A,B;** right) and divided against the total area of the image to obtain the percent coverage measurements. **(C,D)** Representative 60X confocal images depicting GFAP+ astrocyte (green; **C**) and Iba-1+ microglia (green; **D**) labeling in whole mount retina of microbead- and saline- injected WT and *IL-6-/-* eyes. **(E)** Boxplot of percent coverage of GFAP+ astrocytes in saline (white) and microbead (gray) injected WT (left) and *IL-6-/-* (right) eyes. No genotype or IOP dependent changes were calculated. **(F)** Boxplot of percent coverage of Iba-1+ microglia in saline- (white) and microbead- (gray) injected WT (left) and *IL-6-/-* (right) eyes. While an IL-6 dependent increase in percent coverage of microglia is seen in both saline and microbead- injected eyes, only an IOP dependent decrease is seen in microbead-injected WT eyes. **(G)** Boxplot of Iba-1+ microglia cell density (counts/mm^2) in saline- (white) and microbead- (gray) injected WT (left) and *IL-6-/-* (right) eyes. IOP dependent decreases in microglia counts are evident in microbead- injected eyes are evident in both WT and *IL-6-/-* eyes. $^*p < 0.05$. $n = 6$–8 images/eye/condition/genotype. Scale bars= 30 μm for all images. Dashed lines in boxplot indicate median value of data set.

profiles and macrogliosis in WT optic nerves (**Figure 2**). This was accompanied by a significant and IOP-dependent decrease in visual acuity (**Figure 4**). In contrast, *IL-6-/-* mice exhibited no *IOP-dependent* changes in visual acuity (**Figure 4**) or optic nerve outcomes, including axon density, degenerative axon profiles or macrogliosis (**Figure 2**). However, visual acuity decreased modestly, but significantly (8%), in an *IOP-independent* manner following both saline and microbead injection in *IL-6-/-* mice

(**Figure 4**). That this decrease was noted following both types of injection and did not change over time, it is highly likely that visual acuity was negatively impacted by the observed deficits in corneal wound healing (**Figure 5**). Together, these data indicate that IL-6 signaling impacts RGC axonopathy prior to the onset of both structural degeneration and decreased visual function.

Previous studies indicate that RGC axonopathy in glaucoma progresses in a distal to proximal fashion and that deficits in active, anterograde transport precede structural degeneration of the optic nerve (Crish et al., 2010, 2013). Consistent with previously published studies (Sappington et al., 2010; Lambert et al., 2011; Ward et al., 2014; Bond et al., 2016), microbead-induced IOP elevation in WT mice resulted in a 50% decrease in anterograde transport of CTB to the SC (**Figure 3**). Interestingly, *IL-6-/-* mice exhibited a similar decrease in anterograde transport (**Figure 3**). This suggests that IL-6 signaling does not play a significant role in the development of axon pathology that leads to deficits in axon transport. Together with the optic nerve and visual function analyses, these data delineate a temporal window in which IL-6 signaling contributes to RGC axonopathy. Specifically, this temporal window begins after the onset of axon transport deficits and prior to the onset of structural degeneration and decreased visual function. More generally, our data suggest that axon transport deficits and structural degeneration of axons occurs via, at least partially, independent mechanisms.

Given that IL-6 is typically associated with inflammatory functions, we assessed microglia and astrocyte reactivity in the GCL and NFL. Not surprisingly, our analysis revealed a strong association between IOP, IL-6, and microglia, the "resident" immune cell of the CNS. Elevated IOP decreased microglia coverage in the GCL/NFL of WT mice (**Figure 6**). This was attributable to a decrease in the density of microglia (**Figure 6**). Interestingly, elevated IOP also decreased the density of microglia in *IL-6-/-* mice, but did not sufficiently reduce microglia coverage to a statistically significant level (**Figure 6**). Microglia coverage was greater in *IL-6-/-* than in WT mice, regardless of IOP (**Figure 6**). This IL-6-dependent increase in microglia coverage was not attributable to changes in microglia density, suggesting that it likely arises from changes in size and extent of ramification. Based on previous literature, changes in microglia density likely arise from migration of microglia to other retinal layers, particularly the outer retina (Rojas et al., 2014). These findings suggest that IL-6 may be more relevant for microglia ramification/activation state than microglia migration or temporal onset of microglia reactivity in this model. Unlike microglia, astrocyte reactivity did not appear to associate with IOP elevation or IL-6 deficiency (**Figure 6**). The former is contrary to studies of astrocyte reactivity in other glaucoma models, where both retinal astrocyte hypertrophy and hypotrophy are associated with elevated IOP. Notably, most of these studies were conducted in either chronic models (Inman and Horner, 2007; Formichella et al., 2014) or inducible models with much higher IOP elevation (Wang et al., 2000; Gallego et al., 2012). Differences in the duration and magnitude of IOP elevation, as well as severity of RGC pathology, could account for our contradictory findings. Together, these data suggest that IL-6 signaling generally associates with microglia rather than astrocytes. This is supported by our previous work indicating that retinal microglia, but not retinal astrocytes, induce IL-6 expression in response to elevated pressure (Sappington and Calkins, 2006, 2008; Sappington et al., 2006).

While our findings support a role for IL-6 in the progression RGC degeneration in glaucoma, we utilized *IL-6-/-* mice that are generated from homozygous pairing. As such, these mice are deficient in IL-6 throughout development as well as in adulthood. In this case, we are unable to differentiate IL-6-dependent outcomes arising from IL-6 signaling during disease and those arising from developmental IL-6 signaling. Our findings indicate that there are at least two developmental ramifications pertinent to our investigation:

First, IL-6 deficiency modestly, but significantly, decreased baseline IOP by ∼4% compared to WT (**Figure 1**). There is some indication that modulation of IL-6 signaling accompanies IOP elevations in human patients, including both primary open angle and angle closure glaucoma (Takai et al., 2012; Engel et al., 2014; Huang et al., 2014; Du et al., 2016). However, in a recent study of porcine anterior segment, IL-6 did not appear to alter outflow facility that determines IOP (Birke et al., 2011). Our data suggest that, at least in mice, IL-6 signaling may impact the IOP "set-point" either through modulation of aqueous dynamics or during development of the anterior chamber. That the relative increase in IOP achieved with microbeads was equivalent in WT and *IL-6-/-* mice indicates the latter may be more relevant. Most importantly, the magnitude of change in IOP, rather than absolute IOP, appears to be of greater import for disease etiology in both animal models and human patients. In humans, IOP fluctuations, defined as the difference between the highest and lowest IOP, is greater in glaucoma patients than non-glaucoma patients (Nouri-Mahdavi et al., 2004; Sihota et al., 2005; De Moraes et al., 2011; Tan et al., 2017; Tojo et al., 2017) and is predictive of glaucoma progression (Nouri-Mahdavi et al., 2004; Sihota et al., 2005). Likewise, the magnitude of peak IOP measurement predicts progression in glaucoma patients, even for those with IOP successfully lowered by conventional treatments (Nouri-Mahdavi et al., 2004). In animal models, IOP elevations are often presented as a change in cumulative IOP, which documents the change in IOP from control eyes or baseline over time. This measure is well-documented as a strong predictor of RGC pathology (Gao and Jakobs, 2016). Additional studies of strain differences indicate that absolute IOP does not necessarily correlate with RGC pathology (Cone et al., 2010, 2012). In these studies, some strains present with less severity despite higher IOP elevations on the order of several mmHg (Cone et al., 2010, 2012). In our studies, the strain background is controlled and thus, also is the potential for susceptibility defined by this background. As such, it is unlikely that differences in disease outcomes noted in our *IL-6-/-* mice are attributable to the 0.7 mmHg difference in absolute IOP and likely arise from other IL-6-dependent outcomes.

Second, baseline axon density in the optic nerve of *IL-6-/-* mice was approximately 15% lower than that of WT mice. Our assessment of axon density in PPD-stained semi-thin sections allows counting of only myelinated axons. Previous literature

documents that IL-6 influences oligodendrocyte differentiation and gene expression associated with myelination *in vitro* (Valerio et al., 2002; Zhang et al., 2006, 2007). As such, it is probable that myelination of RGC axons is altered in our *IL-6-/-* mice. This may or may not have consequences beyond confounding axon density measurements. Further studies with conditional perturbation of IL-6 signaling will be needed to elucidate the source and impact of confounds arising from developmental deficiency of IL-6 signaling.

In conclusion, our findings indicate that IL-6 is part of a mechanism that specifically leads to structural degeneration of axons. Furthermore, its absence is sufficient to prevent both structural degeneration of the optic nerve and vision loss. That the functional and structural components of RGC axonopathy could be mechanistically separated has tremendous implications for therapeutic targeting, and our findings identify IL-6 as a potential candidate for such.

AUTHOR CONTRIBUTIONS

FE designed the study, performed experiments, analyzed data and wrote the manuscript. CF performed experiments and reviewed the manuscript. RS designed the study, analyzed data and revised the manuscript. All authors have read and approved the final manuscript.

FUNDING

These studies were supported by the National Eye Institute awards RO1EY020496 (RS) and P30EY08126 (Vanderbilt Vision Research Center) and Career Development (RS) and Unrestricted (Vanderbilt Eye Institute) awards from Research to Prevent Blindness, Inc.

ACKNOWLEDGMENTS

The authors would like to thank the Vanderbilt University Medical Center Cell Imaging Shared Resource Core for assistance in confocal imaging. We would also like to thank Mr. Brian Carlson and Wendi Lambert, PhD from the laboratory of David Calkins, PhD for assistance with microbead injections, Mrs. Abigayle Waterson for assistance with IOP measurements and genotyping and Ms. Rachel Fischer for assistance with IOP measurements.

REFERENCES

Birke, M. T., Birke, K., Lutjen-Drecoll, E., Schlotzer-Schrehardt, U., and Hammer, C. M. (2011). Cytokine-dependent ELAM-1 induction and concomitant intraocular pressure regulation in porcine anterior eye perfusion culture. *Invest. Ophthalmol. Vis. Sci.* 52, 468–475. doi: 10.1167/iovs.10-5990

Blindenbacher, A., Wang, X., Langer, I., Savino, R., Terracciano, L., and Heim, M. H. (2003). Interleukin 6 is important for survival after partial hepatectomy in mice. *Hepatology* 38, 674–682. doi: 10.1053/jhep.2003.50378

Bluthe, R. M., Michaud, B., Poli, V., and Dantzer, R. (2000). Role of IL-6 in cytokine-induced sickness behavior: a study with IL-6 deficient mice. *Physiol. Behav.* 70, 367–373. doi: 10.1016/S0031-9384(00)00269-9

Bond, W. S., Hines-Beard, J., GoldenMerry, Y. P., Davis, M., Farooque, A., Sappington, R. M., et al. (2016). Virus-mediated EpoR76E therapy slows optic nerve axonopathy in experimental glaucoma. *Mol. Ther.* 24, 230–239. doi: 10.1038/mt.2015.198

Bosco, A., Inman, D. M., Steele, M. R., Wu, G., Soto, I., Marsh-Armstrong, N., et al. (2008). Reduced retina microglial activation and improved optic nerve integrity with minocycline treatment in the DBA/2J mouse model of glaucoma. *Invest. Ophthalmol. Vis. Sci.* 49, 1437–1446. doi: 10.1167/iovs.07-1337

Bosco, A., Steele, M. R., and Vetter, M. L. (2011). Early microglia activation in a mouse model of chronic glaucoma. *J. Comp. Neurol.* 519, 599–620. doi: 10.1002/cne.22516

Burton, M. D., and Johnson, R. W. (2012). Interleukin-6 trans-signaling in the senescent mouse brain is involved in infection-related deficits in contextual fear conditioning. *Brain Behav. Immun.* 26, 732–738. doi: 10.1016/j.bbi.2011.10.008

Burton, M. D., Rytych, J. L., Freund, G. G., and Johnson, R. W. (2013). Central inhibition of interleukin-6 trans-signaling during peripheral infection reduced neuroinflammation and sickness in aged mice. *Brain Behav. Immun.* 30, 66–72. doi: 10.1016/j.bbi.2013.01.002

Burton, M. D., Sparkman, N. L., and Johnson, R. W. (2011). Inhibition of interleukin-6 trans-signaling in the brain facilitates recovery from lipopolysaccharide-induced sickness behavior. *J. Neuroinflammation* 8:54. doi: 10.1186/1742-2094-8-54

Calkins, D. J. (2012). Critical pathogenic events underlying progression of neurodegeneration in glaucoma. *Prog. Retin. Eye Res.* 31, 702–719. doi: 10.1016/j.preteyeres.2012.07.001

Campbell, I. L., Abraham, C. R., Masliah, E., Kemper, P., Inglis, J. D., Oldstone, M. B., et al. (1993). Neurologic disease induced in transgenic mice by cerebral overexpression of interleukin 6. *Proc. Natl. Acad. Sci. U.S.A.* 90, 10061–10065. doi: 10.1073/pnas.90.21.10061

Cardenas, H., and Bolin, L. M. (2003). Compromised reactive microgliosis in MPTP-lesioned IL-6 KO mice. *Brain Res.* 985, 89–97. doi: 10.1016/S0006-8993(03)03172-X

Chidlow, G., Wood, J. P., Ebneter, A., and Casson, R. J. (2012). Interleukin-6 is an efficacious marker of axonal transport disruption during experimental glaucoma and stimulates neuritogenesis in cultured retinal ganglion cells. *Neurobiol. Dis.* 48, 568–581. doi: 10.1016/j.nbd.2012.07.026

Chucair-Elliott, A. J., Conrady, C., Zheng, M., Kroll, C. M., Lane, T. E., and Carr, D. J. (2014). Microglia-induced IL-6 protects against neuronal loss following HSV-1 infection of neural progenitor cells. *Glia* 62, 1418–1434. doi: 10.1002/glia.22689

Clark, W. M., Rinker, L. G., Lessov, N. S., Hazel, K., Hill, J. K., Stenzel-Poore, M., et al. (2000). Lack of interleukin-6 expression is not protective against focal central nervous system ischemia. *Stroke* 31, 1715–1720. doi: 10.1161/01.STR.31.7.1715

Cone, F. E., Gelman, S. E., Son, J. L., Pease, M. E., and Quigley, H. A. (2010). Differential susceptibility to experimental glaucoma among 3 mouse strains using bead and viscoelastic injection. *Exp. Eye Res.* 91, 415–424. doi: 10.1016/j.exer.2010.06.018

Cone, F. E., Steinhart, M. R., Oglesby, E. N., Kalesnykas, G., Pease, M. E., and Quigley, H. A. (2012). The effects of anesthesia, mouse strain and age on intraocular pressure and an improved murine model of experimental glaucoma. *Exp. Eye Res.* 99, 27–35. doi: 10.1016/j.exer.2012.04.006

Crish, S. D., Dapper, J. D., MacNamee, S. E., Balaram, P., Sidorova, T. N., Lambert, W. S., et al. (2013). Failure of axonal transport induces a spatially coincident increase in astrocyte BDNF prior to synapse loss in a central target. *Neuroscience* 229, 55–70. doi: 10.1016/j.neuroscience.2012.10.069

Crish, S. D., Sappington, R. M., Inman, D. M., Horner, P. J., and Calkins, D. J. (2010). Distal axonopathy with structural persistence in glaucomatous neurodegeneration. *Proc. Natl. Acad. Sci. U.S.A.* 107, 5196–5201. doi: 10.1073/pnas.0913141107

De Moraes, C. G., Juthani, V. J., Liebmann, J. M., Teng, C. C., Tello, C., Susanna, R. Jr., et al. (2011). Risk factors for visual field progression in treated glaucoma. *Arch. Ophthalmol.* 129, 562–568. doi: 10.1001/archophthalmol.2011.72

Douglas, R. M., Alam, N. M., Silver, B. D., McGill, T. J., Tschetter, W. W., and Prusky, G. T. (2005). Independent visual threshold measurements in the two eyes of freely moving rats and mice using a virtual-reality optokinetic system. *Vis. Neurosci.* 22, 677–684. doi: 10.1017/S0952523805225166

Du, S., Huang, W., Zhang, X., Wang, J., Wang, W., and Lam, D. S. (2016). Multiplex cytokine levels of aqueous humor in acute primary angle-closure patients: fellow eye comparison. *BMC Ophthalmol.* 16:6. doi: 10.1186/s12886-016-0182-8

Echevarria, F. D., Rickman, A. E., and Sappington, R. M. (2016). Interleukin-6: a constitutive modulator of glycoprotein 130, neuroinflammatory and cell survival signaling in retina. *J. Clin. Cell. Iummunol.* 7:439. doi: 10.4172/2155-9899.1000439

Echevarria, F., Walker, C., Abella, S., Won, M., and Sappington, R. (2013). Stressor-dependent alterations in glycoprotein 130: implications for glial cell reactivity, cytokine signaling and ganglion cell health in glaucoma. *J. Clin. Exp. Ophthalmol.* 4:1000286. doi: 10.4172/2155-9570.1000286

Engel, L. A., Muether, P. S., Fauser, S., and Hueber, A. (2014). The effect of previous surgery and topical eye drops for primary open-angle glaucoma on cytokine expression in aqueous humor. *Graefes Arch. Clin. Exp. Ophthalmol.* 252, 791–799. doi: 10.1007/s00417-014-2607-5

Erta, M., Quintana, A., and Hidalgo, J. (2012). Interleukin-6, a major cytokine in the central nervous system. *Int. J. Biol. Sci.* 8, 1254–1266. doi: 10.7150/ijbs.4679

Fang, X. X., Jiang, X. L., Han, X. H., Peng, Y. P., and Qiu, Y. H. (2013). Neuroprotection of interleukin-6 against NMDA-induced neurotoxicity is mediated by JAK/STAT3, MAPK/ERK, and PI3K/AKT signaling pathways. *Cell. Mol. Neurobiol.* 33, 241–251. doi: 10.1007/s10571-012-9891-6

Fisher, J., Mizrahi, T., Schori, H., Yoles, E., Levkovitch-Verbin, H., Haggiag, S., et al. (2001). Increased post-traumatic survival of neurons in IL-6-knockout mice on a background of EAE susceptibility. *J. Neuroimmunol.* 119, 1–9. doi: 10.1016/S0165-5728(01)00342-3

Formichella, C., Abella, S. K., Sims, S. M., Cathcart, H. M., and Sappington, R. M. (2014). Astrocyte reactivity: a biomarker for ganglion cell health in retinal neurodegeneration. *J. Clin. Cell. Immunol.* 5:15. doi: 10.4172/2155-9899.1000188

Gallego, B. I., Salazar, J. J., de Hoz, R., Rojas, B., Ramirez, A. I., Salinas-Navarro, M., et al. (2012). IOP induces upregulation of GFAP and MHC-II and microglia reactivity in mice retina contralateral to experimental glaucoma. *J. Neuroinflammation* 9:92. doi: 10.1186/1742-2094-9-92

Gao, S., and Jakobs, T. C. (2016). Mice homozygous for a deletion in the glaucoma susceptibility locus INK4 show increased vulnerability of retinal ganglion cells to elevated intraocular pressure. *Am. J. Pathol.* 186, 985–1005. doi: 10.1016/j.ajpath.2015.11.026

Hines-Beard, J., Bond, W. S., Backstrom, J. R., and Rex, T. S. (2016). Virus-mediated EpoR76E gene therapy preserves vision in a glaucoma model by modulating neuroinflammation and decreasing oxidative stress. *J. Neuroinflammation* 13:39. doi: 10.1186/s12974-016-0499-5

Huang, W., Chen, S., Gao, X., Yang, M., Zhang, J., Li, X., et al. (2014). Inflammation-related cytokines of aqueous humor in acute primary angle-closure eyes. *Invest. Ophthalmol. Vis. Sci.* 55, 1088–1094. doi: 10.1167/iovs.13-13591

Inman, D. M., and Horner, P. J. (2007). Reactive nonproliferative gliosis predominates in a chronic mouse model of glaucoma. *Glia* 55, 942–953. doi: 10.1002/glia.20516

Inomata, Y., Hirata, A., Yonemura, N., Koga, T., Kido, N., and Tanihara, H. (2003). Neuroprotective effects of interleukin-6 on NMDA-induced rat retinal damage. *Biochem. Biophys. Res. Commun.* 302, 226–232. doi: 10.1016/S0006-291X(03)00127-X

Johnson, E. C., Doser, T. A., Cepurna, W. O., Dyck, J. A., Jia, L., Guo, Y., et al. (2011). Cell proliferation and interleukin-6-type cytokine signaling are implicated by gene expression responses in early optic nerve head injury in rat glaucoma. *Invest. Ophthalmol. Vis. Sci.* 52, 504–518. doi: 10.1167/iovs.10-5317

Johnson, E. C., and Morrison, J. C. (2009). Friend or foe? Resolving the impact of glial responses in glaucoma. *J. Glaucoma* 18, 341–353. doi: 10.1097/IJG.0b013e31818c6ef6

Kopf, M., Baumann, H., Freer, G., Freudenberg, M., Lamers, M., Kishimoto, T., et al. (1994). Impaired immune and acute-phase responses in interleukin-6-deficient mice. *Nature* 368, 339–342. doi: 10.1038/368339a0

Lambert, W. S., Ruiz, L., Crish, S. D., Wheeler, L. A., and Calkins, D. J. (2011). Brimonidine prevents axonal and somatic degeneration of retinal ganglion cell neurons. *Mol. Neurodegener.* 6:4. doi: 10.1186/1750-1326-6-4

Leibinger, M., Andreadaki, A., Gobrecht, P., Levin, E., and Fischer, D. (2016). Boosting CNS axon regeneration by circumventing limitations of natural cytokine signaling. *Mol. Ther.* 4, 1712–1725. doi: 10.1038/mt.2016.102

Leibinger, M., Muller, A., Gobrecht, P., Diekmann, H., Andreadaki, A., and Fischer, D. (2013). Interleukin-6 contributes to CNS axon regeneration upon inflammatory stimulation. *Cell Death Dis.* 4:e609. doi: 10.1038/cddis.2013.126

Lin, Z. Q., Kondo, T., Ishida, Y., Takayasu, T., and Mukaida, N. (2003). Essential involvement of IL-6 in the skin wound-healing process as evidenced by delayed wound healing in IL-6-deficient mice. *J. Leukoc. Biol.* 73, 713–721. doi: 10.1189/jlb.0802397

Loddick, S. A., Turnbull, A. V., and Rothwell, N. J. (1998). Cerebral interleukin-6 is neuroprotective during permanent focal cerebral ischemia in the rat. *J. Cereb. Blood Flow Metab.* 18, 176–179. doi: 10.1097/00004647-199802000-00008

Lye-Barthel, M., Sun, D., and Jakobs, T. C. (2013). Morphology of astrocytes in a glaucomatous optic nerve. *Invest. Ophthalmol. Vis. Sci.* 54, 909–917. doi: 10.1167/iovs.12-10109

Martin, A., Hofmann, H. D., and Kirsch, M. (2003). Glial reactivity in ciliary neurotrophic factor-deficient mice after optic nerve lesion. *J. Neurosci.* 23, 5416–5424.

McFarland-Mancini, M. M., Funk, H. M., Paluch, A. M., Zhou, M., Giridhar, P. V., Mercer, C. A., et al. (2010). Differences in wound healing in mice with deficiency of IL-6 versus IL-6 receptor. *J. Immunol.* 184, 7219–7228. doi: 10.4049/jimmunol.0901929

Mukaino, M., Nakamura, M., Yamada, O., Okada, S., Morikawa, S., Renault-Mihara, F., et al. (2010). Anti-IL-6-receptor antibody promotes repair of spinal cord injury by inducing microglia-dominant inflammation. *Exp. Neurol.* 224, 403–414. doi: 10.1016/j.expneurol.2010.04.020

Nouri-Mahdavi, K., Hoffman, D., Coleman, A. L., Liu, G., Li, G., Gaasterland, D., et al. (2004). Predictive factors for glaucomatous visual field progression in the Advanced Glaucoma Intervention Study. *Ophthalmology* 111, 1627–1635. doi: 10.1016/j.ophtha.2004.02.017

Penkowa, M., Giralt, M., Carrasco, J., Hadberg, H., and Hidalgo, J. (2000). Impaired inflammatory response and increased oxidative stress and neurodegeneration after brain injury in interleukin-6-deficient mice. *Glia* 32, 271–285. doi: 10.1002/1098-1136(200012)32:3<271::AID-GLIA70>3.0.CO;2-5

Penkowa, M., Giralt, M., Lago, N., Camats, J., Carrasco, J., Hernandez, J., et al. (2003). Astrocyte-targeted expression of IL-6 protects the CNS against a focal brain injury. *Exp. Neurol.* 181, 130–148. doi: 10.1016/S0014-4886(02)00051-1

Penkowa, M., Molinero, A., Carrasco, J., and Hidalgo, J. (2001). Interleukin-6 deficiency reduces the brain inflammatory response and increases oxidative stress and neurodegeneration after kainic acid-induced seizures. *Neuroscience* 102, 805–818. doi: 10.1016/S0306-4522(00)00515-7

Penkowa, M., Moos, T., Carrasco, J., Hadberg, H., Molinero, A., Bluethmann, H., et al. (1999). Strongly compromised inflammatory response to brain injury in interleukin-6-deficient mice. *Glia* 25, 343–357. doi: 10.1002/(SICI)1098-1136(19990215)25:4<343::AID-GLIA4>3.0.CO;2-V

Rojas, B., Gallego, B. I., Ramirez, A. I., Salazar, J. J., de Hoz, R., Valiente-Soriano, F. J., et al. (2014). Microglia in mouse retina contralateral to experimental glaucoma exhibit multiple signs of activation in all retinal layers. *J. Neuroinflammation* 11:133. doi: 10.1186/1742-2094-11-133

Sappington, R. M., and Calkins, D. J. (2006). Pressure-induced regulation of IL-6 in retinal glial cells: involvement of the ubiquitin/proteasome pathway and NFkappaB. *Invest. Ophthalmol. Vis. Sci.* 47, 3860–3869. doi: 10.1167/iovs.05-1408

Sappington, R. M., and Calkins, D. J. (2008). Contribution of TRPV1 to microglia-derived IL-6 and NFkappaB translocation with elevated hydrostatic pressure. *Invest. Ophthalmol. Vis. Sci.* 49, 3004–3017. doi: 10.1167/iovs.07-1355

Sappington, R. M., Carlson, B. J., Crish, S. D., and Calkins, D. J. (2010). The microbead occlusion model: a paradigm for induced ocular hypertension in rats and mice. *Invest. Ophthalmol. Vis. Sci.* 51, 207–216. doi: 10.1167/iovs.09-3947

Sappington, R. M., Chan, M., and Calkins, D. J. (2006). Interleukin-6 protects retinal ganglion cells from pressure-induced death. *Invest. Ophthalmol. Vis. Sci.* 47, 2932–2942. doi: 10.1167/iovs.05-1407

Sihota, R., Saxena, R., Gogoi, M., Sood, A., Gulati, V., and Pandey, R. M. (2005). A comparison of the circadian rhythm of intraocular pressure in primary phronic angle closure glaucoma, primary open angle glaucoma and normal eyes. *Indian J. Ophthalmol.* 53, 243–247. doi: 10.4103/0301-4738.18905

Sims, S. M., Holmgren, L., Cathcart, H. M., and Sappington, R. M. (2012). Spatial regulation of interleukin-6 signaling in response to neurodegenerative stressors in the retina. *Am. J. Neurodegener. Dis.* 1, 168–179.

Sparkman, N. L., Buchanan, J. B., Heyen, J. R., Chen, J., Beverly, J. L., and Johnson, R. W. (2006). Interleukin-6 facilitates lipopolysaccharide-induced disruption in working memory and expression of other proinflammatory cytokines in hippocampal neuronal cell layers. *J. Neurosci.* 26, 10709–10716. doi: 10.1523/JNEUROSCI.3376-06.2006

Spittau, B., Zhou, X., Ming, M., and Krieglstein, K. (2012). IL6 protects MN9D cells and midbrain dopaminergic neurons from MPP+-induced neurodegeneration. *Neuromolecular Med.* 14, 317–327. doi: 10.1007/s12017-012-8189-7

Takai, Y., Tanito, M., and Ohira, A. (2012). Multiplex cytokine analysis of aqueous humor in eyes with primary open-angle glaucoma, exfoliation glaucoma, and cataract. *Invest. Ophthalmol. Vis. Sci.* 53, 241–247. doi: 10.1167/iovs.11-8434

Tan, S., Baig, N., Hansapinyo, L., Jhanji, V., Wei, S., and Tham, C. C. (2017). Comparison of self-measured diurnal intraocular pressure profiles using rebound tonometry between primary angle closure glaucoma and primary open angle glaucoma patients. *PLoS ONE* 12:e0173905. doi: 10.1371/journal.pone.0173905

Tiberio, G. A., Tiberio, L., Benetti, A., Cervi, E., Montani, N., Dreano, M., et al. (2008). IL-6 Promotes compensatory liver regeneration in cirrhotic rat after partial hepatectomy. *Cytokine* 42, 372–378. doi: 10.1016/j.cyto.2008.03.012

Tojo, N., Abe, S., Ishida, M., Yagou, T., and Hayashi, A. (2017). The fluctuation of intraocular pressure measured by a contact lens sensor in normal-tension glaucoma patients and nonglaucoma subjects. *J. Glaucoma* 26, 195–200. doi: 10.1097/IJG.0000000000000517

Valerio, A., Ferrario, M., Dreano, M., Garotta, G., Spano, P., and Pizzi, M. (2002). Soluble interleukin-6 (IL-6) receptor/IL-6 fusion protein enhances *in vitro* differentiation of purified rat oligodendroglial lineage cells. *Mol. Cell. Neurosci.* 21, 602–615. doi: 10.1006/mcne.2002.1208

Wang, X., Tay, S. S. W., and Ng, Y. K. (2000). An immunohistochemical study of neuronal and glial cell reactions in retinae of rats with experimental glaucoma. *Exp. Brain Res.* 132, 476–484. doi: 10.1007/s002210000360

Ward, N. J., Ho, K. W., Lambert, W. S., Weitlauf, C., and Calkins, D. J. (2014). Absence of transient receptor potential vanilloid-1 accelerates stress-induced axonopathy in the optic projection. *J. Neurosci.* 34, 3161–3170. doi: 10.1523/JNEUROSCI.4089-13.2014

Wilson, G. N., Inman, D. M., Dengler Crish, C. M., Smith, M. A., and Crish, S. D. (2015). Early pro-inflammatory cytokine elevations in the DBA/2J mouse model of glaucoma. *J. Neuroinflammation* 12:176. doi: 10.1186/s12974-015-0399-0

Yamada, M., and Hatanaka, H. (1994). Interleukin-6 protects cultured rat hippocampal neurons against glutamate-induced cell death. *Brain Res.* 643, 173–180. doi: 10.1016/0006-8993(94)90023-X

Zhang, P. L., Izrael, M., Ainbinder, E., Ben-Simchon, L., Chebath, J., and Revel, M. (2006). Increased myelinating capacity of embryonic stem cell derived oligodendrocyte precursors after treatment by interleukin-6/soluble interleukin-6 receptor fusion protein. *Mol. Cell. Neurosci.* 31, 387–398. doi: 10.1016/j.mcn.2005.10.014

Zhang, P. L., Levy, A. M., Ben-Simchon, L., Haggiag, S., Chebath, J., and Revel, M. (2007). Induction of neuronal and myelin-related gene expression by IL-6-receptor/IL-6: a study on embryonic dorsal root ganglia cells and isolated Schwann cells. *Exp. Neurol.* 208, 285–296. doi: 10.1016/j.expneurol.2007.08.022

Zhong, J., Dietzel, I. D., Wahle, P., Kopf, M., and Heumann, R. (1999). Sensory impairments and delayed regeneration of sensory axons in interleukin-6-deficient mice. *J. Neurosci.* 19, 4305–4313.

Conflict of Interest Statement: The authors declare that the research was conducted in the absence of any commercial or financial relationships that could be construed as a potential conflict of interest.

frontiers in Neuroscience

ORIGINAL RESEARCH
published: 07 February 2017
doi: 10.3389/fnins.2017.00045

Oral Delivery of a Synthetic Sterol Reduces Axonopathy and Inflammation in a Rodent Model of Glaucoma

*Wendi S. Lambert[1], Brian J. Carlson[1], Cathryn R. Formichella[1], Rebecca M. Sappington[1], Clarence Ahlem[2] and David J. Calkins[1]**

[1] Vanderbilt University Medical Center, The Vanderbilt Eye Institute, Nashville, TN, USA, [2] NeurMedix, Inc., San Diego, CA, USA

Glaucoma is a group of optic neuropathies associated with aging and sensitivity to intraocular pressure (IOP). The disease is the leading cause of irreversible blindness worldwide. Early progression in glaucoma involves dysfunction of retinal ganglion cell (RGC) axons, which comprise the optic nerve. Deficits in anterograde transport along RGC axons to central visual structures precede outright degeneration, and preventing these deficits is efficacious at abating subsequent progression. HE3286 is a synthetic sterol derivative that has shown therapeutic promise in models of inflammatory disease and neurodegenerative disease. We examined the efficacy of HE3286 oral delivery in preventing loss of anterograde transport in an inducible model of glaucoma (microbead occlusion). Adult rats received HE3286 (20 or 100 mg/kg) or vehicle daily via oral gavage for 4 weeks. Microbead occlusion elevated IOP ∼30% in all treatment groups, and elevation was not affected by HE3286 treatment. In the vehicle group, elevated IOP reduced anterograde axonal transport to the superior colliculus, the most distal site in the optic projection, by 43% ($p = 0.003$); HE3286 (100 mg/kg) prevented this reduction ($p = 0.025$). HE3286 increased brain-derived neurotrophic factor (BDNF) in the optic nerve head and retina, while decreasing inflammatory and pathogenic proteins associated with elevated IOP compared to vehicle treatment. Treatment with HE3286 also increased nuclear localization of the transcription factor NFκB in collicular and retinal neurons, but decreased NFκB in glial nuclei in the optic nerve head. Thus, HE3286 may have a neuroprotective influence in glaucoma, as well as other chronic neurodegenerations.

Keywords: glaucoma, neuroinflammation, neuroprotection, axonopathy, HE3286, NF kappa B, axonal transport, brain derived neurotrophic factor

OPEN ACCESS

Edited by:
Jason R. Richardson, Northeast Ohio Medical University, USA

Reviewed by:
Adriana Di Polo, University of Montreal, Canada
Mohammad Harun-Or-Rashid, Northeast Ohio Medical University, USA

****Correspondence:***
David J. Calkins
david.j.calkins@vanderbilt.edu

Specialty section:
This article was submitted to Neurodegeneration, a section of the journal Frontiers in Neuroscience

Received: *28 September 2016*
Accepted: *20 January 2017*
Published: *07 February 2017*

Citation:
Lambert WS, Carlson BJ, Formichella CR, Sappington RM, Ahlem C and Calkins DJ (2017) Oral Delivery of a Synthetic Sterol Reduces Axonopathy and Inflammation in a Rodent Model of Glaucoma. Front. Neurosci. 11:45. doi: 10.3389/fnins.2017.00045

INTRODUCTION

Glaucoma is the leading cause of irreversible blindness worldwide (Quigley and Broman, 2006). The disease selectively targets retinal ganglion cells (RGCs) and their axons through stress conveyed at the optic nerve head (Calkins, 2012; Nickells et al., 2012). Age is a major risk factor for developing glaucoma, but sensitivity to intraocular pressure (IOP) is the only modifiable risk factor and sole target for clinical intervention (Heijl et al., 2002). Decreasing IOP with drugs or surgery can slow

disease progression, but for many patients does not prevent RGC degeneration and vision loss (Heijl et al., 2002). Given that by 2020 nearly 80 million people will have glaucoma, with an estimated 11.2 million with permanent vision loss (Quigley and Broman, 2006; Cheung et al., 2008; Schober et al., 2008), the identification of therapeutic agents that can protect RGCs independently of IOP is of paramount importance.

HE3286 (17α-Ethynyl-androst-5ene-3β, 7β, 17β-triol) is a synthetic derivative of androst-5-ene-3β,7β,17β-triol (AET), a non-glucocorticoid anti-inflammatory metabolite of the adrenal steroid, dehydroepiandrosterone (DHEA; Ahlem et al., 2011). DHEA and AET have shown therapeutic promise in rodent models of immune-mediated inflammatory disorders with varying results in clinical trials (Offner et al., 2002; Dillon, 2005; Ahlem et al., 2009). HE3286 shows better oral bioavailability in humans, has low potential for toxicity, does not bind to glucocorticoid receptor or any known nuclear hormone receptor, and is not immunosuppressive (Wang et al., 2010; Ahlem et al., 2011). Treatment with HE3286 improves outcome measures in models of autoimmune disease, lung inflammation, experimental optic neuritis and Parkinson's disease, and is currently being tested in clinical trials (Auci et al., 2007, 2010; Ahlem et al., 2009; Offner et al., 2009; Conrad et al., 2010; Lu et al., 2010; Kosiewicz et al., 2011; Nicoletti et al., 2012; Reading et al., 2013a,b; Khan et al., 2014). It is believed HE3286 may act via binding, regulation and/or activation of MAPK or ERK, or through modulation of NFκB (Lu et al., 2010; Ahlem et al., 2011; Nicoletti et al., 2012; Reading et al., 2012).

Neurodegeneration in glaucoma shows many similarities with other age-related neurodegenerative disorders, including early deficits in axon function that precede loss of neurons themselves (Crish and Calkins, 2011; Mckinnon, 2012; Ghiso et al., 2013; Jindal, 2013; Danesh-Meyer and Levin, 2015; Jain and Aref, 2015). In animal models of glaucoma, degradation of RGC anterograde transport to central brain targets occurs early and prior to outright loss of axons in the optic projection (Crish et al., 2010, 2013; Dengler-Crish et al., 2014). Experimental interventions that prevent transport deficits are efficacious at stopping subsequent degeneration of axons and cell bodies (Lambert et al., 2011; Dapper et al., 2013). Here, we tested whether HE3286 could rescue RGC axon transport and modulate markers for neuroinflammation in the optic projection using our inducible microbead occlusion model of glaucoma in rats (Crish et al., 2010; Sappington et al., 2010; Dapper et al., 2013). We found that while HE3286 had no effect on IOP, daily oral delivery for 4 weeks prevented deficits in anterograde transport to the superior colliculus (SC), the primary central projection for RGCs in rodents (Linden and Perry, 1983; Hofbauer and Drager, 1985). HE3286 also influenced the level of many proteins implicated in the pathogenesis of glaucoma and other neurodegenerative disorders throughout the optic projection. Finally, HE3286 increased activation of the transcription factor NFκB in colliculus and retina, while decreasing glial NFκB activation in the optic nerve head, which is a major pathogenic site of neuroinflammation in glaucoma (Soto and Howell, 2014; Russo et al., 2016). These data suggest HE3286 has therapeutic potential with regards to neurodegeneration in glaucoma by modulating common neuroinflammatory pathways.

MATERIALS AND METHODS

Animals

All experimental procedures were conducted in accordance with the guidelines of and approved by The Vanderbilt University Institutional Animal Care and Use Committee. Brown Norway rats (7–9 months old, male) were obtained from Charles River Laboratories (Wilmington, MA) and maintained in a 12-h light-dark cycle with standard rodent chow available *ad libitum*. Three cohorts of rats ($n = 6$ per cohort; 18 rats total) were randomly assigned to one of three treatment groups: vehicle, 20 mg/kg HE3286 or 100 mg/kg HE3286. We measured IOP bilaterally in awake rats using a TonoPen XL rebound tonometer (Medtronic Solan, Jacksonville, FL) as previously described (Sappington et al., 2010; Crish et al., 2013; Dapper et al., 2013). To avoid corneal irritation, hydrating eye drops were administered to each eye at the completion of IOP measurements. Prior to microbead occlusion (Sappington et al., 2010; Crish et al., 2013; Dapper et al., 2013), we monitored IOP for 2–3 days; these measurements were averaged to obtain a baseline value. We elevated IOP unilaterally (OS) by a single 5.0 μl injection of 15 μm polystyrene microbeads (Molecular Probes, Eugene, OR) into the anterior chamber. The fellow eye (OD) received an equivalent volume of saline to serve as an internal control. Beginning 24 h post-injection (day 1), we monitored IOP using tonometry at least three times weekly for the duration of the experiment (Sappington et al., 2010; Crish et al., 2013; Dapper et al., 2013). Beginning with the microbead injection (day 0), rats received 20 mg/kg or 100 mg/kg HE3286 (10 mg/mL HE3286 in an aqueous medium containing 1 mg/mL sodium carboxymethyl cellulose, 9 mg/mL sodium chloride, 20 mg/mL polysorbate-80, and 0.5 mg/mL phenol as abroad spectrum preservative, Harbor Therapeutics, San Diego, CA 92122) via oral gavage. For the vehicle group, half received 20 mg/kg vehicle and the other half 100 mg/kg vehicle (1 mg/mL sodium carboxymethyl cellulose, 9 mg/mL sodium chloride, 20 mg/mL polysorbate-80, and 0.5 mg/mL phenol in an aqueous medium, Harbor Therapeutics, San Diego, CA 92122). Rats received vehicle or HE3286 once daily via oral gavage for 28 days.

Anterograde Axonal Transport

Forty-eight hours prior to perfusion, rats were anesthetized with 2.5% isoflurane and injected intravitreally with 2 μl of 0.5 mg cholera toxin subunit B (CTB) conjugated to Alexa Fluor-488 (Molecular Probes, CA) as previously described (Crish et al., 2010; Dapper et al., 2013; Ward et al., 2014). Animals were transcardially perfused with phosphate buffered saline (PBS) followed with 4% paraformaldehyde in PBS. Brains were cryoprotected overnight in 30% sucrose/PBS and coronal midbrain sections (50 μm) cut on a freezing sliding microtome. Alternating sections of superior colliculus (SC) were imaged using a Nikon Ti Eclipse microscope (Nikon Instruments Inc., Melville, NY) and the intensity of CTB signal was quantified using a custom ImagePro macro (Media Cybernetics, Bethesda, MD) as previously described (Crish et al., 2010; Dapper et al.,

2013; Ward et al., 2014). After normalizing to background, CTB signal intensity was calculated to reconstruct a retinotopic map of intact anterograde transport across the SC. Percent of intact transport for each map was defined as the region of the SC with intensity ≥70% of the maximum CTB signal for that tissue. CTB uptake by RGCs in the retina was verified using a Zeiss FV-1000 inverted confocal microscope through the Vanderbilt University Medical Center Cell Imaging Shared Resource.

Immunohistochemistry

Whole eyes were dissected from perfused animals, paraffin-embedded and vertically sectioned (6 μm). Immunohistochemistry of whole eyes and brain was performed as previously described and at identical conditions between cohorts (Sappington et al., 2009; Crish et al., 2010; Weitlauf et al., 2014). Primary antibodies used to immunolabel proteins of interest in the brain, optic nerve head, and retina are listed in **Table 1**. Sections were incubated with appropriate secondary antibodies (1:200; Jackson ImmunoResearch Laboratories, Inc., West Grove, PA) and then cover-slipped with DAPI Fluoromount G (Southern Biotech, Birmingham, AL). Sections were imaged using a Zeiss FV-1000 inverted confocal microscope through the Vanderbilt University Medical Center Cell Imaging Shared Resource. For retina, all images were collected within the mid-peripheral region for comparison across eyes and cohorts. Identical microscope settings were used to acquire images for signal quantification, which was performed by a naïve observer using a custom macro in ImagePro (Media Cybernetics; Bethesda, MD) that determines the percent area of the positive label (Crish et al., 2013). The microbead to saline ratio (microbead:saline) of label in a specific tissue was calculated for each animal; ratios were averaged and reported as label (microbead:saline). Nuclear localization of NFkB was analyzed using a custom macro in ImageJ (Carmona et al., 2007; Schneider et al., 2012) followed by signal quantification in ImagePro. For quantifying label, a tissue section serving each saline and microbead eye from at least five animals per cohort was used. Retinal and nuclear layer thickness were measured at five different retinal locations per image using the Measurement tool in ImagePro. For RGC counts, the number of CTB-positive and DAPI-positive cells within the ganglion cell layer were counted using the Count tool in Photoshop. At least eight images per animal were quantified to determine an average retinal thickness.

TABLE 1 | Primary antibodies used for brain and whole eye immunohistochemistry.

Protein	Dilution used	Catalog number	Vendor
Alzheimer precursor protein (APP)	1:50	MAB348	1
β-amyloid (Aβ)	1:200	#2454	2
Brain derived neurotrophic factor (BDNF)	1:100	NBP2-42215	3
CD44	1:150	NB600-1317	3
C1q	1:1000	A301	4
Ceruloplasmin (Cp)	1:500	#611488	5
Choline acetyltransferase (ChAT)	1:100	AB144P	1
Glial fibrillary acidic protein (GFAP)	1:500	MAB360	1
Interleukin 1β (IL1β)	1:50	AF-501-NA	6
Interleukin 6 (IL6)	1:400	ab6672	7
IL6Rα membrane bound (IL6Rαm)	1:50	sc-600	8
Ionized Ca^{2+}-binding adapter molecule 1 (Iba1)	1:400	ab107159	7
NeuN	1:500	NBP1-92693	3
NF-κB	1:100	sc-372	8
p75 neurotrophin receptor (p75)	1:500	G323A	9
Phosphorylated neurofilament-H (pNF-H)	1:1000	801601	10
Tumor necrosis factor α (TNFα)	1:300	AF-510-NA	6

1, EMD Millipore, Billerica, MA; 2, Cell Signaling Technology, Danvers, MA; 3, Novus Biologicals, Littleton CO; 4, Quidel Corp., San Diego, CA; 5, BD Transductions Labs, San Jose, CA; 6, R and D Systems, Minneapolis, MN; 7, AbCam, Cambridge, MA; 8, Santa Cruz Biotechnologies, Dallas, TX; 9, Promega Corp., Madison, WI; 10, BioLegend, San Diego, CA.

Statistical Analysis

All data are expressed as mean ± standard error unless indicated otherwise. The number of samples used in each experiment is provided in the appropriate methods description or figure legend. Statistical comparisons between two independent measurements were made using two-sided *t*-tests, following confirmation of normality for each using the Shapiro-Wilk normality test; samples for which normality failed were compared using the Mann-Whitney Rank Sum Test (SigmaPlot 12.5, Systat Software, Inc., Chicago, IL). Comparisons between multiple groups were made using one way analysis of variance (ANOVA) followed by the Holm-Sidak Pairwise Multiple Comparison test (SigmaPlot 11.1, Systat Software, Inc., Chicago, IL). Comparisons of a sample mean to a hypothesized or predicted value were made using a one-sided *t*-test. Actual *p*-values of significance are indicated where appropriate in the results section or figure legends. All comparisons for which significance is reported achieved or exceeded a *post-hoc* calculation of power of 0.80.

RESULTS

Two rats, one from each HE3286 group, were euthanized before completion of the study due to complications from oral gavage. Treatment with HE3286 for 28 days had few directly observable adverse effects, as rats were active, responsive and showed no overt signs of distress. HE3286 did result in weight loss in both the 20 and 100 mg/kg groups (**Table 2**). Weights on day 0 (first day of treatment) ranged from 283 to 430 g, and mean

TABLE 2 | Weight loss with HE3286 treatment following microbead injection.

Treatment group	Weight day 0 (g)	Weight day 28 (g)	% Change (%)
Vehicle	357.2 ± 19.7	371.5 ± 21.0	+4.03
20 mg/kg HE3286	347.5 ± 6.5	326.3 ± 9.8	−6.16*
100 mg/kg HE3286	371.7 ± 15.0	333.7 ± 14.7	−10.26*†

$^{*}p < 0.001$ compared to vehicle; $^{\dagger}p = 0.042$ compared to 20 mg/kg dose ($n = 6$ rats per group).

weights for the three treatment groups were not significantly different ($p = 0.523$). Weights on day 28 (last day of treatment) ranged from 290 to 440 g, with no significant difference in mean weight between the three treatment groups ($p = 0.130$). However, rats that received vehicle gained 14.3 g during the experimental period, while rats that received 20 mg/kg HE3286 lost 21.2 g and rats that received 100 mg/kg HE3286 lost 38.0 g. Comparing percent change in weight over the course of treatment for each animal showed that HE3286 decreased weight in both the 20 mg/kg group ($p < 0.001$, compared to vehicle) and 100 mg/kg group ($p < 0.001$, compared to vehicle; $p = 0.042$ compared to 20 mg/kg).

Oral Delivery of HE3286 Has no Effect on Ocular Pressure

Baseline IOP measurements ranged from 19.15 ± 0.50 to 20.29 ± 0.55 mm Hg and were similar for all treatment groups ($p = 0.638$). Microbead injection elevated IOP in all eyes for the full 28 day period regardless of treatment (**Figure 1A**). In vehicle-treated rats, elevation was 32.7% compared to saline-injected eyes: 26.69 ± 2.73 vs. 20.12 ± 2.69 mm Hg; $p = 0.002$ (**Figure 1B**). Similar increases of 29.6% and 30.0% were observed for the 20 mg/kg HE3286-treated group (26.39 ± 2.51 vs. 20.37 ± 2.68 mm Hg, $p = 0.002$) and for the 100 mg/kg HE3286-treated group (26.49 ± 2.52 vs. 20.39 ± 2.53 mm Hg, $p = 0.002$), respectively. Mean IOP of saline eyes did not significantly differ for any treatment group ($p = 0.997$); the same was true for microbead eyes ($p = 0.997$).

HE3286 Rescues Anterograde Axonal Transport to the Superior Colliculus

Deficits in anterograde axonal transport from retina to SC are an early sign of pathogenesis in rodent models of glaucoma, including microbead occlusion (Crish et al., 2010; Lambert et al., 2011; Dapper et al., 2013; Ward et al., 2014). **Figure 2** compares the level of intact transport of fluorescently labeled CTB to the SC of vehicle-, 20 mg/kg HE3286-, and 100 mg/kg HE3286-treated rats. Deficits in transport are readily apparent in the SC from microbead-injected eyes of vehicle rats (dotted lines, **Figure 2A** top row). These deficits tend to fill in complete retinotopic sectors when reconstructed from serial sections through the SC (**Figure 2A** bottom row), consistent with our previous studies (Lambert et al., 2011; Dapper et al., 2013). Variability in transport was low in SC from saline-injected eyes (**Figure 2B**), which had similarly intact transport for all groups: 89.2 ± 2.7% for vehicle, 85.8 ± 3.9% for 20 mg/kg HE3286, and 90.9 ± 3.7% for 100 mg/kg HE3286 (**Figure 2C**; $p = 0.593$). Elevated IOP due to microbead injection decreased intact transport to the SC in vehicle-treated rats to 57.4 ± 6.0% intact transport (**Figure 2C**; $p = 0.003$ compared to saline). Treatment with HE3286 attenuated transport deficits dramatically, as intact transport to the SC from microbead-injected eyes was 71.9 ± 9.8 and 83.0 ± 7.1% for the 20 and 100 mg/kg HE3286 treatment groups, respectively (**Figure 2C**); neither differed from intact transport from the saline eye ($p \geq 0.270$). Compared to SC from microbead-injected eyes in the vehicle group, the improvement was significant for the 100 mg/kg HE3286 cohort ($p = 0.025$). No difference in SC volume was detected for any groups or any treatments ($p = 0.082$).

HE3286 Counters the Influence of Elevated IOP Throughout the Optic Projection

Brain-Derived Neurotrophic Factor (BDNF)

Deficits in anterograde transport to the SC of glaucomatous mice is accompanied by significant changes in local neurochemistry, including increased localization of BDNF (Crish et al., 2013). Within the SC of vehicle rats, BDNF also appeared to increase with microbead-induced elevated IOP (**Figure 3A**, left); treatment with HE3286 (20 mg/kg) appeared to blunt this increase (**Figure 3A**, right). In the optic nerve head (ONH; **Figure 3B**), which is a major site of stress in glaucoma (Hernandez, 2000), levels of BDNF appeared similar in saline- and microbead-injected eyes from vehicle treated rats. Treatment with HE3286 (20 mg/kg) appeared to increase BDNF in the ONH of microbead-injected eyes compared to saline. Finally, levels of BDNF in the retina decreased following microbead injection in vehicle-treated rats, with HE3286 again blunting this effect (**Figure 3C**).

When quantified (**Figure 3D**), the ratio of BDNF in microbead to saline SC for vehicle rats was significantly greater than an expected ratio of unity: 2.34 ± 0.12 ($p < 0.001$). This ratio was diminished by 70% compared to vehicle in the 20 mg/kg HE3286 group (0.71 ± 0.09; $p < 0.001$) and by 43% in the 100 mg/kg group (1.34 ± 0.08; $p < 0.001$). In the ONH (**Figure 3D**, middle), the ratio of microbead to saline BDNF increased with 20 mg/kg HE3286 by 69%: 1.43 ± 0.20 vs. 0.84 ± 0.16 for vehicle ($p = 0.042$). The 34% increase in this ratio for the 100 mg/kg dose was not significant compared to vehicle (0.93 ± 0.12; $p = 0.66$). Finally, in the retina, treatment with HE3286 increased the microbead:saline ratio of BDNF by 282% in the 20 mg/kg group (0.64 ± 0.05) and by 501% in the 100 mg/kg group (1.00 ± 0.05) when compared to vehicle (0.17 ± 0.04; $p < 0.002$); the 100 mg/kg HE3286 ratio was significantly below an expected ratio of unity ($p = 0.02$). Thus, as microbead-induced elevations in IOP degrade anterograde transport in the optic projection, HE3286 treatment generally has the effect of opposing the change in BDNF levels induced by elevated IOP.

Note that for BDNF and all other immunolabeled proteins we quantified, the total SC area for saline (7.013 ± 0.006 mm^2) and microbead (7.017 ± 0.003 mm^2) eyes or vehicle (7.019 ± 0.002 mm^2) and HE3286 groups (7.012 ± 0.005 mm^2) did not vary ($p \geq 0.088$). Similarly, total area quantified in the nerve head did not vary between saline (7.019 ± 0.002 mm^2) and microbead (7.022 ± 0.002 mm^2) eyes or between vehicle (7.018 ± 0.003 mm^2) and HE3286 groups (7.022 ± 0.002 mm^2; $p > 0.279$). Finally, total area quantified in the retina was similar between saline (2.756 ± 0.203 mm^2) and microbead (2.712 ± 0.198 mm^2) eyes or between vehicle (2.996 ± 0.204 mm^2) and HE3286 (2.603 ± 0.199 mm^2; $p > 0.076$) groups.

Microglia Activation

Given HE3286's proposed anti-inflammatory action and the contribution of microglia as neuroinflammatory mediators in

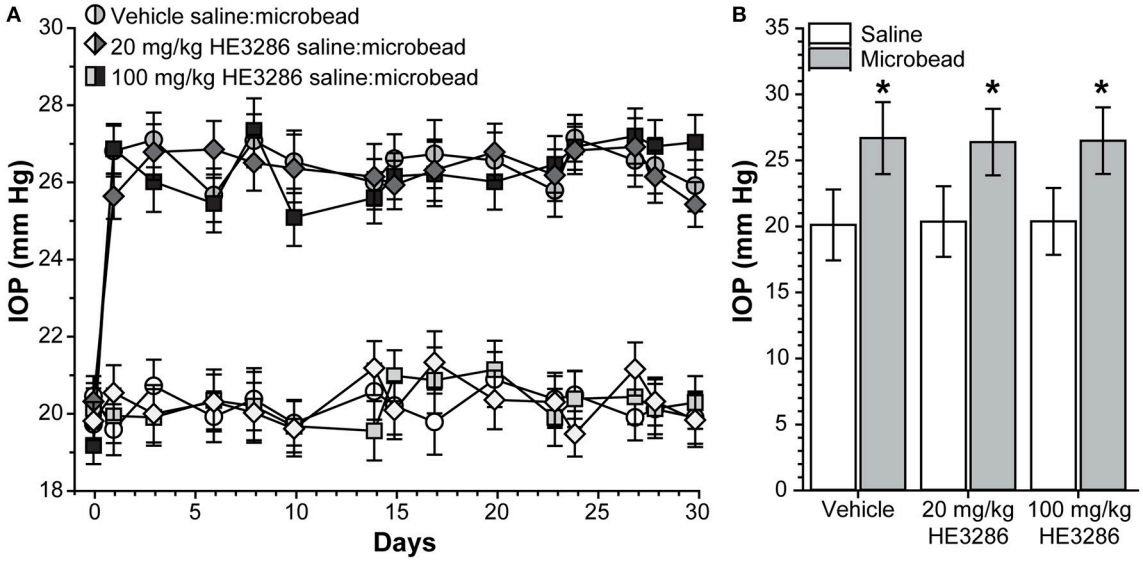

FIGURE 1 | HE3286 treatment does not lower ocular pressure following microbead occlusion. (A) Mean intraocular pressure (IOP) in rats before (day 0) and following (days ≥1) a single unilateral injection of polystyrene microbeads (5.0 μl) into the anterior chamber. The fellow eye was injected with an equivalent volume saline. **(B)** Microbead-injected eyes exhibited an increase in IOP following injection (mean ± SEM shown) compared to saline eyes, regardless of treatment. *$p \leq 0.002$, $n = 6$ per treatment group.

glaucoma, we examined how treatment influences levels of ionized calcium-binding adapter molecule 1 (Iba1), a microglia-specific marker (Ito et al., 1998; Soto and Howell, 2014; Mac Nair and Nickells, 2015). In the SC, microbead-induced elevated IOP elicited a modest increase in Iba1 levels in vehicle animals, which was mitigated by HE3286 (**Figure 4A**). In the ONH, elevated IOP sharply increased Iba1, which again was prevented in the HE3286 group (**Figure 4B**). Iba1 appeared elevated in microbead retina from vehicle-treated rats, while treatment with HE3286 had the opposite effect (**Figure 4C**). The influence of HE3286 was significant in all three tissues (**Figure 4D**). Treatment with the 20 mg/kg dose of HE3286 reduced the ratio of Iba1 in microbead to saline SC by 63%: 0.84 ± 0.11 compared to 1.29 ± 0.19 for vehicle ($p = 0.037$). The 100 mg/kg dose had a similar influence (0.86 ± 0.17, $p = 0.061$). The microbead:saline ratio of Iba1 in ONH for vehicle rats was significantly greater than an expected ratio of unity: 1.56 ± 0.12 ($p = 0.045$). This ratio was diminished by 83% in the 20 mg/kg HE3286 group (0.27 ± 0.03; $p = 0.005$); 100 mg/kg HE3286 had far less effect (1.09 ± 0.27; $p = 0.193$). For vehicle retina, the Iba1 microbead to saline ratio was significantly more than 1 (1.42 ± 0.04; $p = 0.007$). Treatment with both 20 mg/kg and 100 mg/kg HE3286 decreased this ratio compared to vehicle: 1.09 ± 0.08 for the 20 mg/kg group ($p = 0.018$) and 0.99 ± 0.07 ($p = 0.009$) for the 100 mg/kg group.

Markers of Neuroinflammation or Neurodegeneration

Other significant markers implicated in neuroinflammation or neurodegeneration were also modulated in the optic projection by HE3286. Interleukin 6 (IL6) is a pro-inflammatory cytokine that can promote RGC survival (Matousek et al., 2012; Song et al., 2013). In the SC of vehicle rats, IL6 localization appeared to diminish with elevated IOP; this was reversed with HE3286 (**Figure 5A**). The p75 neurotrophin receptor is a member of the tumor necrosis factor receptor family and has diverse roles in neuronal activity, plasticity, and injury response (Meeker and Williams, 2015). We found that p75 levels increased within the ONH of microbead eyes from vehicle rats; treatment with 20 mg/kg HE3286 prevented this increase (**Figure 5B**). Finally, amyloid precursor protein (APP) is cleaved to form β-amyloid, a major component of amyloid plaques. Recent evidence suggests this protein and its cleaved products may be involved in the pathogenesis of glaucoma (Jain and Aref, 2015). HE3286 appeared to increase APP levels in saline-injected eyes (**Figure 5D**). We found that microbead-induced elevations in IOP increased APP in the optic nerve head (**Figure 5C**) and retina (**Figure 5D**) of vehicle rats. In both tissues, HE3286 prevented this increase.

When quantified (**Figure 5E**), the ratio of IL6 in microbead to saline SC was significantly less than an expected value of unity: 0.55 ± 0.08 ($p = 0.005$). This trend was reversed by 100 mg/kg HE3286, which increased the IL6 ratio by 219% compared to vehicle: 1.75 ± 0.51 ($p = 0.047$). In the ONH (**Figure 5F**), the microbead to saline ratio for p75 was also significantly higher than unity: 2.41 ± 0.15 ($p = 0.011$). Treatment with both 20 mg/kg and 100 mg/kg HE3286 prevented the increase with elevated IOP, reducing the ratio by 58% (1.02 ± 0.14; $p = 0.002$) and 66% (0.82 ± 0.14; $p = 0.001$), respectively, compared to vehicle. For APP in ONH (**Figure 5G**), treatment with 20 mg/kg HE3286 decreased the microbead to saline ratio by 53% compared to vehicle: 5.71 ± 1.15 vs. 12.13 ± 1.49 ($p = 0.027$). Similarly, 100 mg/kg HE3286 elicited a 54% decrease to 5.63 ± 0.84 ($p = 0.019$). In the retina (**Figure 5H**), elevated IOP

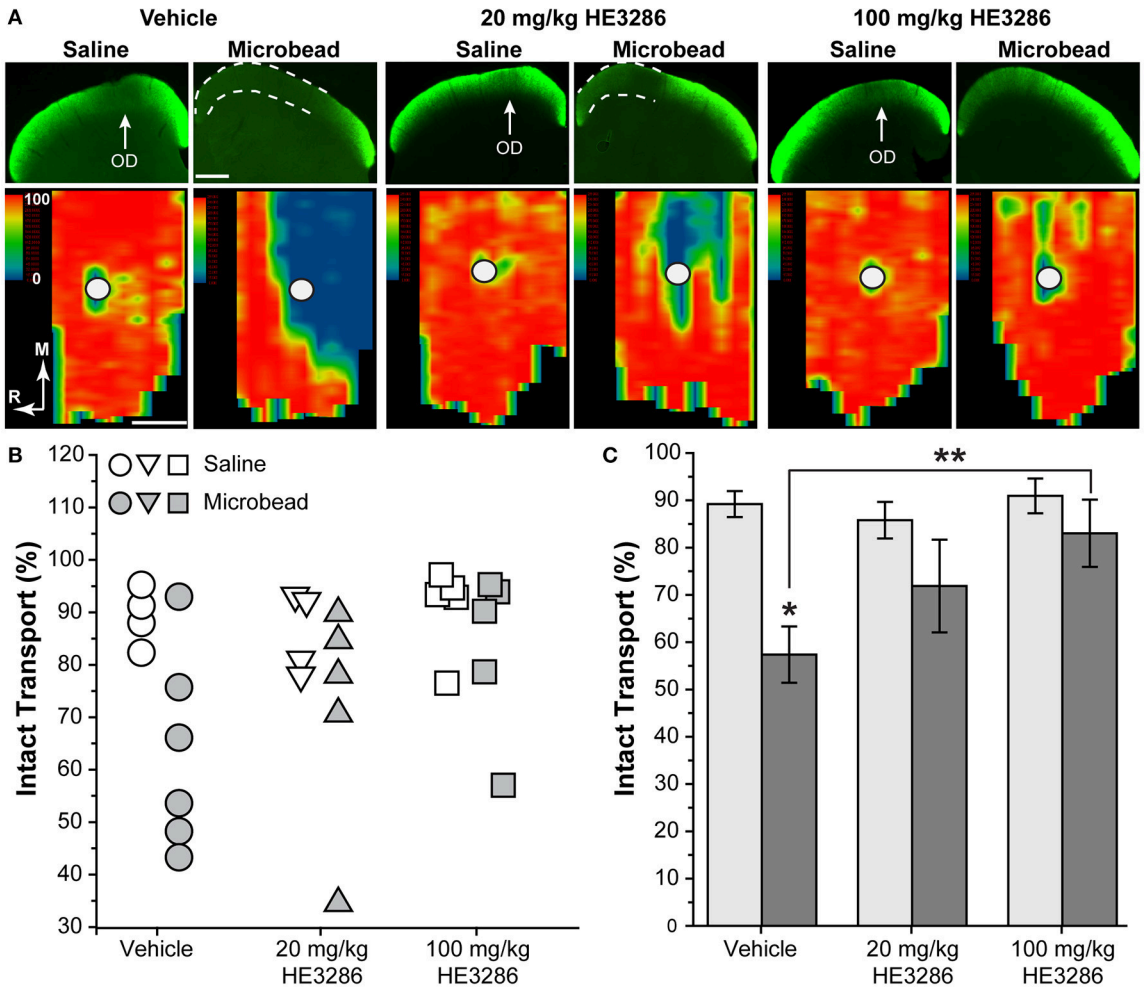

FIGURE 2 | HE3286 treatment rescues axonal transport following microbead occlusion. (A) Coronal sections (top row) through the superior colliculus following intravitreal injection of CTB (green) into saline- and microbead-injected eyes of vehicle- and HE3286-treated rats. Deficits in anterograde transport of CTB (dotted lines) due to microbead-induced elevations in IOP are most apparent in vehicle rats. Representation of the optic disc in the retina (OD) lacks transport due to absence of RGCs. Retinotopic maps (bottom row) reconstructed from serial sections of SC with optic disc indicated (circles). Density of the transported CTB signal ranges from 0% (blue) to 50% (green) to 100% (red). Medial (M) and rostral (R) orientations are indicated. Scale: 500 μm. **(B)** Intact transport for individual saline- and microbead-injected eyes per treatment group given as fraction of SC retinotopic map with CTB signal ≥70% of the maximum. Two SCs from saline-injected eyes of vehicle-treated rats and one SC from a saline-injected 20 mg/kg HE3286-treated rat were excluded from analysis due to lack of CTB uptake by RGC. **(C)** Mean level of intact transport in SC was reduced by elevated IOP in vehicle group compared to saline eye (*$p = 0.003$). Higher dose of HE3286 prevented this reduction (**$p = 0.025$). $n = 4$–6 animals per treatment group.

significantly increased the microbead to saline ratio for APP well above an expected ratio of unity: 8.05 ± 0.81 ($p = 0.013$). Treatment with HE3286 significantly decreased the ratio by 97 and 94% for the 20 mg/kg and 100 mg/kg doses, respectively, compared to vehicle ($p < 0.001$). Both the ratio for 20 mg/kg HE3286 (0.25 ± 0.05) and 100 mg/kg HE3286 (0.48 ± 0.14) were significantly lower than unity ($p \leq 0.035$).

As with BDNF (**Figure 3**) and Iba1 (**Figure 4**), in each of the cases illustrated in **Figure 5**, treatment with one or both doses of HE3286 tended to oppose the action of elevated IOP in the vehicle cohort, as indicated by the directionality of the change in the microbead:saline ratio for each. If the ratio >1 in vehicle tissue, HE3286 treatment pushed the ratio below unity; if the vehicle ratio <1, HE3286 increased the ratio above unity. This tendency held for other proteins we tested in SC, ONH, and retina and for which HE3286 elicited a significant change in expression level. These results are summarized in **Table 3**.

HE3286 Modulates Common Pathogenic Markers for Glaucoma in the Retina

Next we examined how HE3286 treatment influences localization of common markers for neurodegeneration in glaucomatous retina. Ceruloplasmin (Cp) is a positive acute phase protein upregulated during inflammation (Denko, 1979; Goldstein et al., 1979). In vehicle retina, Cp increased dramatically

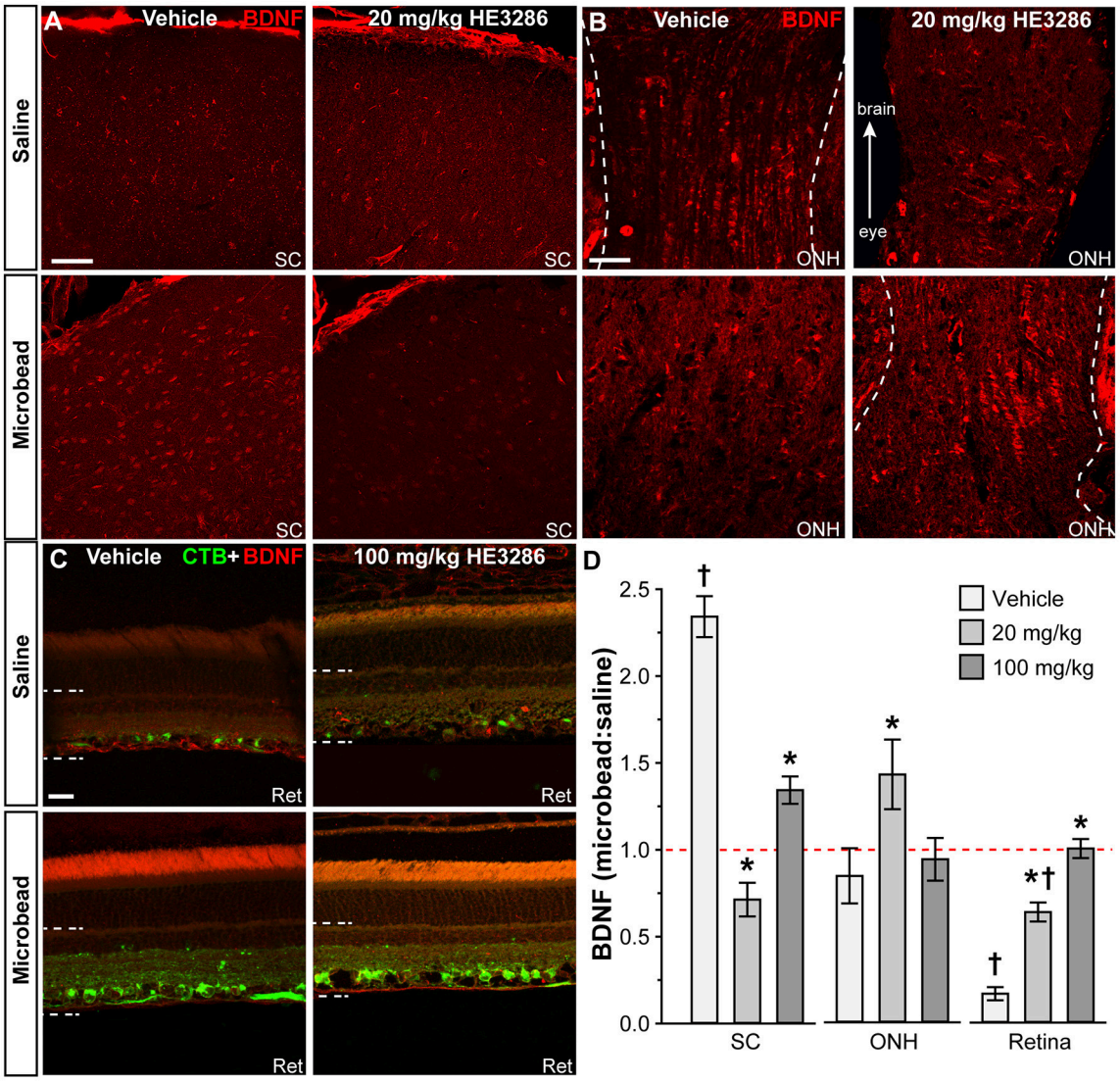

FIGURE 3 | HE3286 treatment influences BDNF levels in optic projection. Confocal micrographs of saline- and microbead-eye tissue from vehicle and HE3286 rats show immunolabeling for BDNF in superior colliculus (SC, **A**), optic nerve head (ONH, **B**), and retina (Ret, **C**), which also shows RGCs labeled by CTB uptake. Dotted lines indicate region of retina where immunolabel was quantified. Scale: 50 μm **(A,B)** and 20 μm **(C). (D)** Bar graphs indicate quantification of levels of BDNF in superior colliculus (SC), optic nerve head (ONH), and retina expressed as the microbead:saline ratio for vehicle and HE3286 treatment groups. †Indicates significant departure from expected ratio of unity ($p \leq 0.02$), which is indicated (dotted line). *indicates $p \leq 0.042$ compared to ratio for vehicle group. $n = 6$ animals per vehicle treatment group, 5 animals per 20 mg/kg and 100 mg/kg HE3286 groups for SC; $n = 3$ animals per treatment group for ONH and retina analysis.

with microbead-induced elevated IOP; HE3286 prevented this increase (**Figure 6A**). Interleukin 1β (IL1β) is a pro-inflammatory cytokine that can promote neurodegeneration or protection depending on whether the injury is acute or chronic (Matousek et al., 2012; Song et al., 2013). In vehicle retina, IL1β decreased with elevated IOP (**Figure 6B**, left). While treatment with 20 mg/kg HE3286 further reduced expression (images not shown), 100 mg/kg HE3286 reversed this trend (**Figure 6B**, right). In vehicle retina, elevated IOP appeared to increase expression of C1q, an early component of the classical complement pathway, especially in CTB-labeled RGCs (**Figure 6C**, left). This too was prevented by 100 mg/kg HE3286 (**Figure 6C**, right). Finally, we also tested localization of choline acetyltransferase (ChAT), a marker for cholinergic amacrine cell neurons, to determine if HE3286 affects levels of common proteins not typically associated with glaucoma progression. Neither elevated IOP nor treatment appeared to influence localization levels (**Figure 6D**), which were consistent with other studies (Kang et al., 2004; Feng et al., 2006; Samuel et al., 2011).

When quantified, the ratio of Cp in microbead to saline retina in the vehicle group was well above an expected value of unity: 4.61 ± 0.49 ($p = 0.018$; **Figure 6E**). Treatment with HE3286 abated this increase by 80% compared to vehicle in the 20 mg/kg group (0.92 ± 0.29; $p = 0.003$) and by 96% in the 100 mg/kg

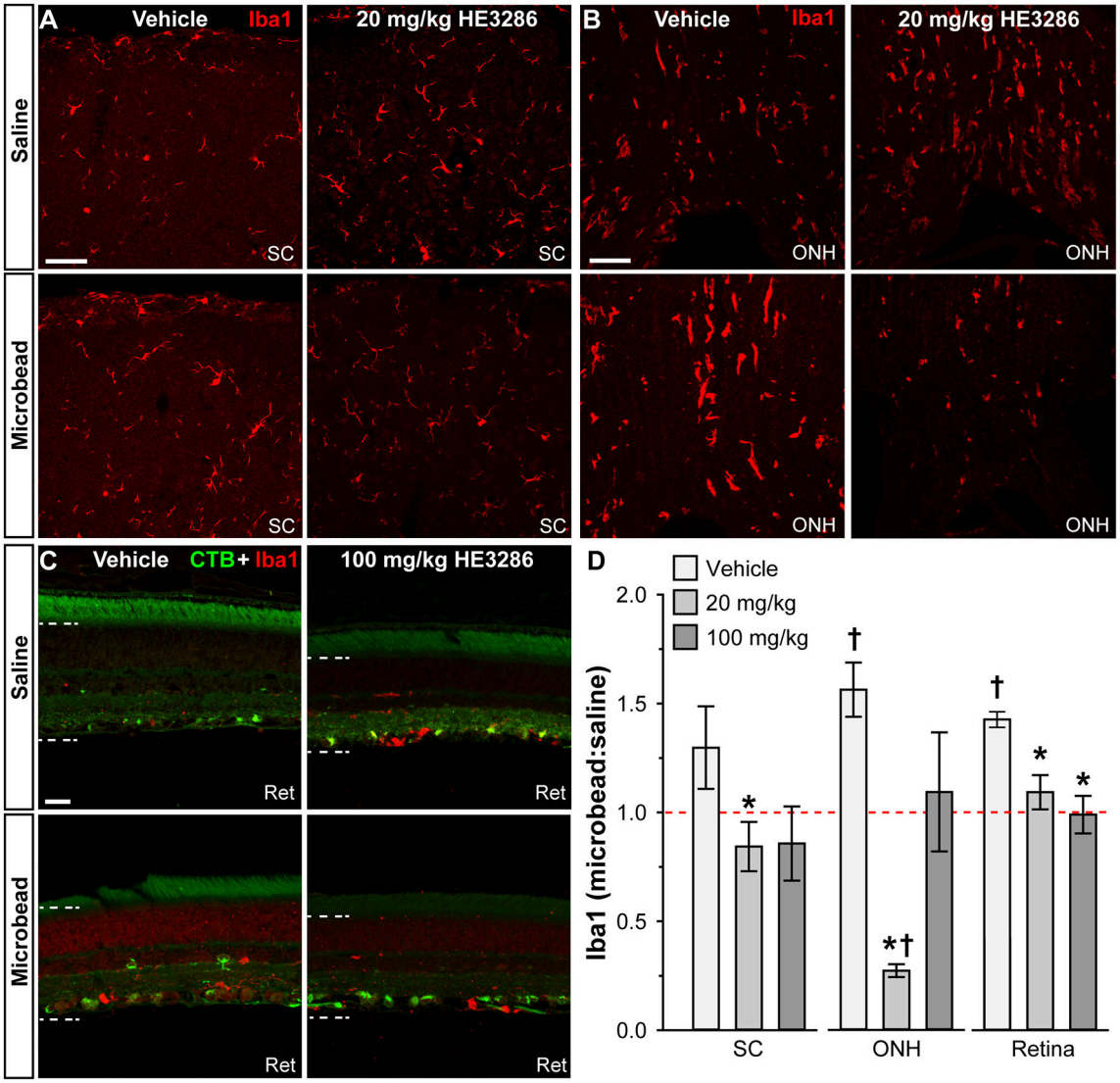

FIGURE 4 | HE3286 treatment influences Iba1-labeled microglia in optic projection. Confocal micrographs of saline- and microbead-injected tissue from vehicle and HE3286 rats show immunolabeling for the microglia marker Iba1 in superior colliculus (SC, **A**), optic nerve head (ONH, **B**), and retina (Ret, **C**), which also shows RGCs labeled by CTB uptake. Dotted lines indicate region of retina where immunolabel was quantified. Scale: 50 μm **(A,B)** and 20 μm **(C)**. **(D)** Bar graphs indicate quantification of Iba1 in superior colliculus (SC), optic nerve head (ONH), and retina expressed as the microbead:saline ratio for vehicle and HE3286 treatment groups. † indicates significant departure from expected ratio of unity ($p \leq 0.045$), which is indicated (dotted line). *Indicates $p \leq 0.037$ compared to ratio for vehicle group. $n = 6$ animals per vehicle treatment group, 5 animals per 20 mg/kg and 100 mg/kg HE3286 groups for SC; $n = 3$ animals per treatment group for ONH and retina analysis.

group (0.18 ± 0.03; $p < 0.001$). For IL1β (**Figure 6F**), elevated IOP significantly reduced levels compared to saline retina in the vehicle group, yielding a ratio of 0.28 ± 0.02 ($p = 0.001$). Treatment with 20 mg/kg HE3286 further reduced IL1β by 76% (0.07 ± 0.04; $p = 0.009$). However, 100 mg/kg HE3286 had the opposite effect, increasing levels by 440% compared to vehicle (1.49 ± 0.14; $p = 0.001$). Elevated IOP in vehicle rats significantly increased levels of C1q compared to saline retina: 1.225 ± 0.061 ($p = 0.033$, **Figure 6G**). While 20 mg/kg HE3286 had little effect (1.430 ± 0.096), 100 mg/kg HE3286 significantly reduced the C1q microbead to saline ratio compared to vehicle: 0.037 ± 0.007 ($p < 0.001$). As expected, levels of ChAT were the same in saline and microbead retinas in all treatment groups (**Figure 6H**, $p \geq 0.461$).

HE3286 Changes NFκB Localization in the Optic Projection

One proposed mechanism of action for HE3286 is to modulate the transcription factor NFκB, which translocates to the nucleus when activated (Offner et al., 2009). Using an antibody with proven efficacy in brain (Herkenham et al., 2011; **Figure 7A**), we examined and quantified the degree of

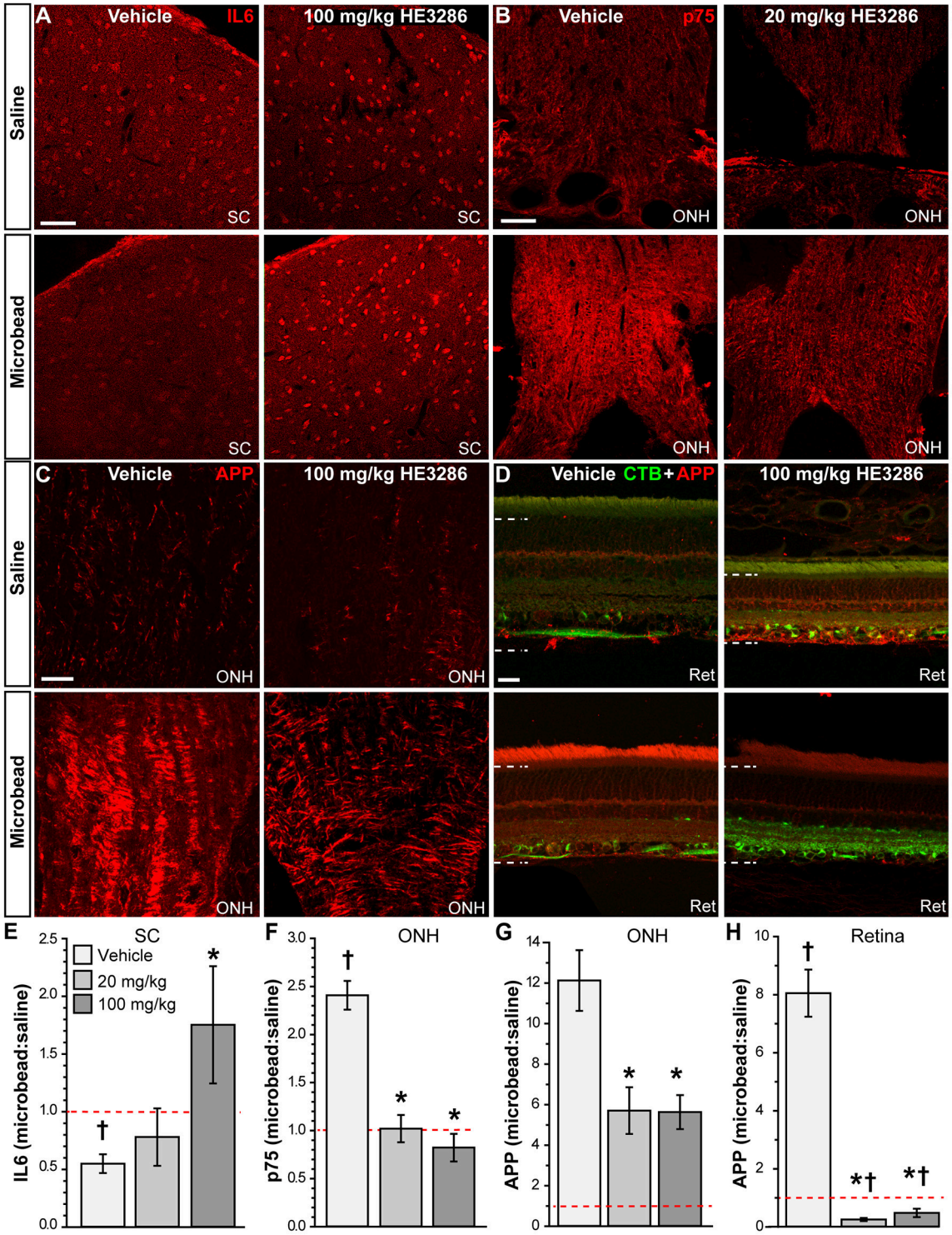

FIGURE 5 | HE3286 treatment influences other degenerative markers in optic projection. Confocal micrographs of saline- and microbead-injected tissue from vehicle and HE3286 rats show immunolabeling for IL6 in superior colliculus (SC, **A**), p75 in optic nerve head (ONH, **B**), and APP in optic nerve head (ONH, **C**) and retina (Ret, **D**), which also shows RGCs labeled by CTB uptake. Dotted lines indicate region of retina where immunolabel was quantified. Scale: 50 μm **(A–C)** and 20 μm **(D)**. Bar graphs **(E–H)** indicate quantification of each of these markers in the specified tissue expressed as the microbead:saline ratio for vehicle and HE3286 treatment groups. SC: superior colliculus; ONH: optic nerve head. †Indicates significant departure from expected ratio of unity ($p \leq 0.047$), which is indicated (dotted line). *indicates $p \leq 0.027$ compared to ratio for vehicle group. $n = 6$ animals per vehicle treatment group, 5 animals per 20 mg/kg and 100 mg/kg HE3286 groups for SC; $n = 3$ animals per treatment group for ONH and retina analysis.

TABLE 3 | Significant HE3286-induced changes in expression compared to vehicle.

Target	Tissue	Vehicle (*p*-value)	20 mg/kg	100 mg/kg	*p*-values
TNFα	ONH	1.68 ± 0.20 (0.038)	0.28 ± 0.10: 83%↓	No change	0.003
IL6Rαm	ONH	1.93 ± 0.09 (<0.001)	0.72 ± 0.03: 62%↓	0.74 ± 0.11: 63%↓	<0.001
IL6	Retina	5.43 ± 0.84 (0.006)	2.10 ± 0.37: 61%↓	2.55 ± 0.65: 53%↓	≤0.045
p75	Retina	2.41 ± 0.22 (0.022)	1.53 ± 0.20: 37%↓	1.26 ± 0.21: 48%↓	≤0.041
CD44	Retina	1.32 ± 0.10	No change	0.48 ± 0.11: 63%↓	0.005
Aβ	Retina	8.89 ± 0.58 (<0.001)	13.19 ± 1.33: 48%↑	5.02 ± 0.88: 44%↓	≤0.042

Tissue expression given as microbead:saline, mean ± SEM (n = 3 animals per groups). Vehicle p-value indicates significance for ratio compared expected value of unity. ONH, optic nerve head; IL6, interleukin-6; p75, low-affinity neurotrophin receptor; CD44, homing cell adhesion glycoprotein; TNFα, tumor necrosis factor α; IL6Rαm, membrane bound IL6 receptor α; Aβ, beta-amyloid. ↑, increase compared to vehicle; ↓, decrease compared to vehicle.

nuclear localization of NFκB in SC, optic nerve head, and retina. In vehicle-treated rats, NFκB localized both within and external to nuclei in SC; microbead SC appeared to have less nuclear localization (**Figure 7B**). Treatment with HE3286 increased NFκB particularly in microbead SC. Within the ONH (**Figure 7C**), microbead-induced elevations in IOP increased NFκB in nuclei for the vehicle group; this was prevented with HE3286 treatment. In retinal sections (**Figure 7D**), elevated IOP had little effect on NFκB localization. However, HE3286 appeared to increase NFκB translocation, particularly in RGCs of microbead retina.

Using an established algorithm (Carmona et al., 2007; Schneider et al., 2012), we quantified the degree of nuclear localization of NFκB as the ratio of levels in tissue from microbead to saline eyes (**Figures 7E–G**). For SC (**Figure 7E**), this ratio was significantly lower than an expected value of 1 for vehicle rats ($p = 0.006$), consistent with our qualitative observation (**Figure 7B**). Treatment with HE3286 reversed this trend as we found that the ratio of microbead to saline nuclear NFκB increased 77% (1.25 ± 0.09) in rats treated with 20 mg/kg HE3286 and by 39% (0.99 ± 0.09) in rats treated with 100 mg/kg HE3286; both changes were significant compared to vehicle (0.71 ± 0.5; $p \leq 0.031$). In the ONH (**Figure 7F**), NFκB in nuclei increased significantly with microbead elevations in IOP for the vehicle group (1.50 ± 0.18; $p = 0.047$). Treatment with 100 mg/kg HE3286 decreased the ratio of microbead to saline levels by 35% (0.97 ± 0.12), which was significant compared to vehicle ($p = 0.038$). Treatment with 20 mg/kg HE3286 had little effect compared to vehicle (1.41 ± 0.22; $p = 0.753$). Similar to the SC, nuclear NFκB in the retina increased with IOP elevation for the HE3286 treatment groups (**Figure 7G**). Treatment with 100 mg/kg HE3286 caused a 62% increase (1.47 ± 0.14) compared to the microbead:saline ratio in vehicle (0.90 ± 0.25; $p = 0.044$); this was also significantly different from an expected ratio of 1 ($p = 0.031$). The 20 mg/kg HE3286 dose also increased NFκB nuclear labeling in microbead retina (1.368 ± 0.185), but the 51% increase was not significant both compared to vehicle ($p = 0.087$) and to an expected ratio of unity ($p = 0.117$).

NFκB activation can promote degeneration or survival depending on the cell type (e.g., glia vs. neurons; Mattson and Camandola, 2001). In SC from each treatment group, NFκB localized to nuclei of GFAP-labeled astrocytes (**Figure 8A**), Iba1-labeled microglia (**Figure 4B**), and neurons labeled by NeuN or pNFH (**Figures 8C,D**). Whether nuclear localization was glial or neuronal did not appear to be influenced by elevated IOP in the vehicle cohort, since SC from saline and microbead eyes showed both. NFκB localization in neuronal nuclei did appear to increase with elevated IOP in HE3286-treated rats, consistent with the overall increase in NFκB we observed earlier (**Figures 7B,E**).

Within the ONH, the majority of NFκB appeared to localize in the cytoplasm surrounding DAPI-labeled nuclei, though nuclei of some astrocytes (**Figure 9A**) and microglia (**Figure 9B**) contained NFκB. Consistent with the overall increase within the ONH (**Figures 7C,F**), microbead-induced elevated IOP appeared to increase glial NFκB nuclear localization in vehicle rats, which was attenuated by HE3286. In retina, nuclei of RGCs identified by CTB uptake and GFAP-labeled astrocytes also demonstrated NFκB localization (**Figures 9C,D**). Elevated IOP appeared to decrease nuclear NFκB in vehicle rats, with HE3286 treatment reversing this trend. Again, this finding is consistent with the overall trend of NFκB localization we quantified in retina (**Figures 7D,G**).

HE3286 Decreased Retinal Thickness in Rats with Induced Ocular Hypertension

While examining vertical retinal sections following immunohistochemistry, we noted what appeared to be a decrease in retinal thickness within the mid-peripheral region of the retina in rats treated with HE3286 compared to vehicle (**Figure 10A**). To examine this further, we measured retinal thickness across groups and retinal locations. Comparing mean retinal thickness (**Figure 10C**) showed that for vehicle-treated and 20 mg/kg HE3286-treated rats, retinal thickness was decreased in microbead-injected eyes compared to saline-injected eyes, but this difference was not significant (vehicle: 132.51 ± 1.47 vs. 130.93 ± 1.99 μm, $p = 0.557$; 20 mg/kg dose: 116.35 ± 2.50 vs. 111.47 ± 2.11 μm, $p = 0.21$). In contrast, rats treated with 100 mg/kg HE3286 had significantly thinner retinas in saline-injected eyes (87.70 ± 0.59 μm) compared to microbead-injected eyes (96.91 ± 0.98 μm; $p = 0.001$). Comparing saline-injected eyes across the groups showed that treatment with HE3286 decreased retinal thickness 12–34% compared to treatment with vehicle ($p < 0.005$). Similarly, retinal thickness decreased 15–26% in microbead eyes treated with HE3286 compared to vehicle ($p < 0.002$). Retinal thinning was dependent on dosage, as a 13–25% decrease was observed in eyes that received 100 mg/kg HE3286 compared to 20 mg/kg

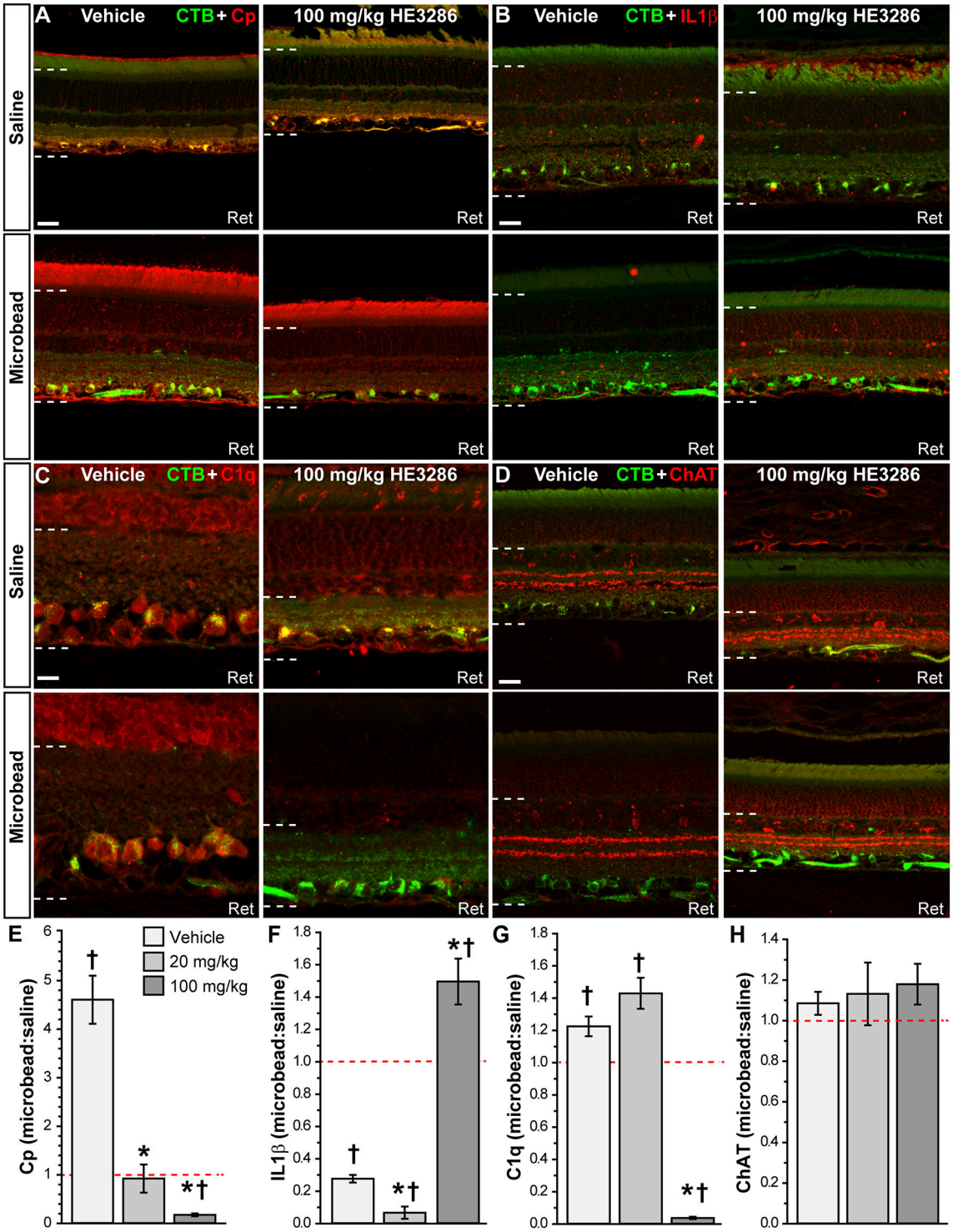

FIGURE 6 | HE3286 treatment influences retinal expression of common pathogenic markers. Confocal micrographs of saline- and microbead-injected from vehicle and HE3286 rats show immunolabeling in retina (Ret) for ceruloplasmin (Cp, **A**), interleukin 1β (IL1β, **B**), and C1q, the first component of the classical complement pathway **(C)**. Localization of amacrine cell neurons specific for ChAT (choline acetyltransferase) is shown for comparison **(D)**. CTB-labeled RGCs are shown in each panel. Dotted lines indicate region of retina where immunolabel was quantified. Scale: 20 μm **(A,B,D)** or 10 μm **(C)**. Bar graphs **(E–H)** indicate quantification of each of these markers expressed as the microbead:saline ratio for vehicle and HE3286 treatment groups. †Indicates significant departure from expected ratio of unity ($p \leq 0.037$), which is indicated (dotted line). *indicates $p \leq 0.033$ compared to ratio for vehicle group. $n = 3$ animals per treatment group.

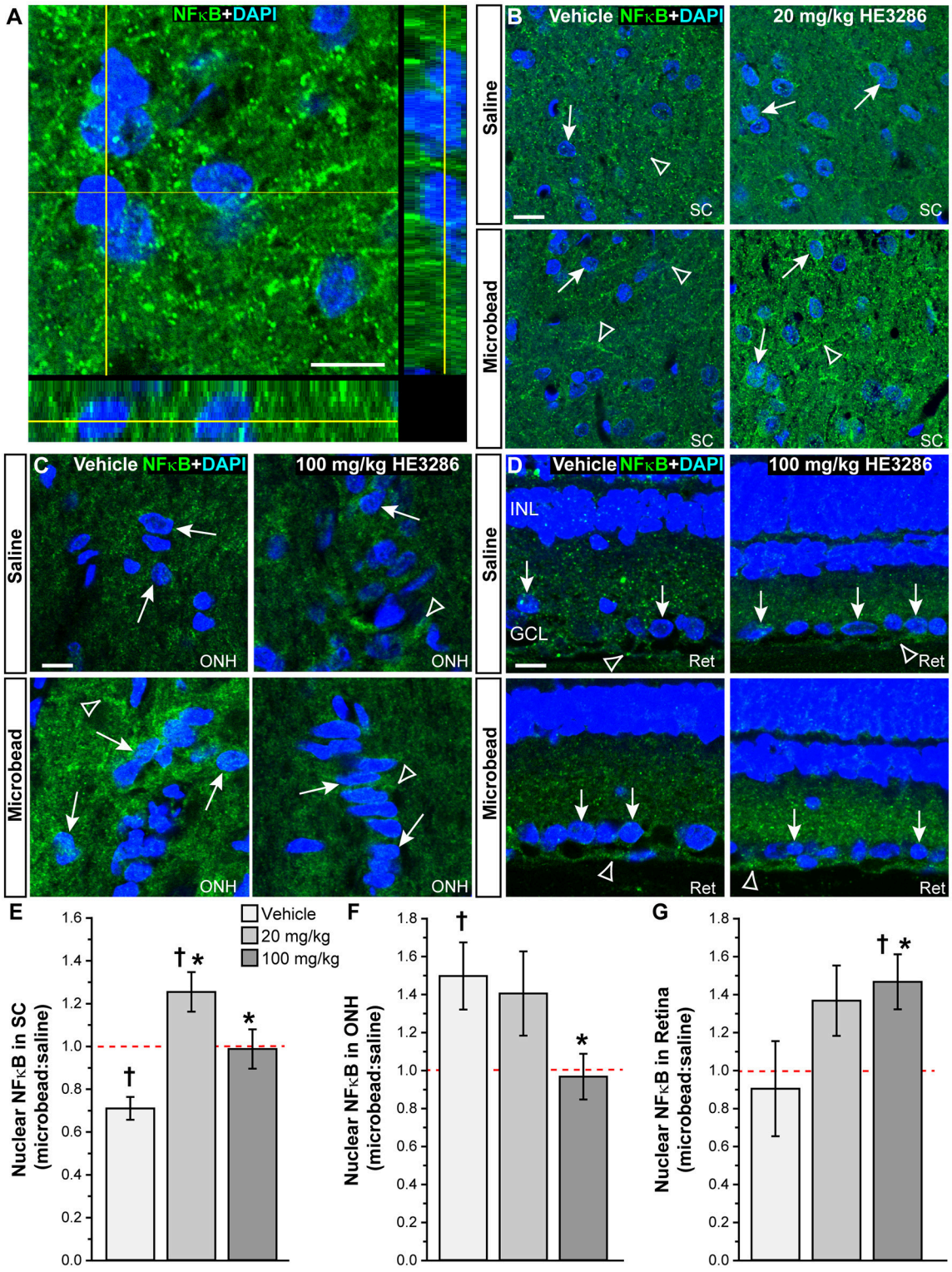

FIGURE 7 | HE3286 modulates NFκB nuclear localization in the optic projection. (A) Confocal micrograph of a coronal section through naïve rat SC shows localization of NFκB (green) both outside and within DAPI-labeled nuclei (blue). Lines indicate location of orthogonal rotations through nuclei. Scale: 10 μm. Representative images (single optical plane) of superior colliculus (SC, **B**), optic nerve head (ONH, **C**) and retina (Ret, **D**) from vehicle and HE3286 rats shows localization of NFκB (green) both within (arrows) and external to (arrowhead) DAPI-stained nuclei. INL: inner nuclear layer of retina; GCL: ganglion cell layer. Scale: 10 μm. Bar graphs show nuclear localization of NFκB in SC **(E)**, optic nerve head (ONH, **F**), and retina **(G)** expressed as the ratio of microbead:saline in vehicle and HE3286 treated tissue; ratio of 1, or unity, indicated by dotted line. †Indicates significant departure from expected ratio of unity ($p \leq 0.026$). *Indicates $p \leq 0.044$ compared to ratio for vehicle group. $n = 5$ animals per treatment group.

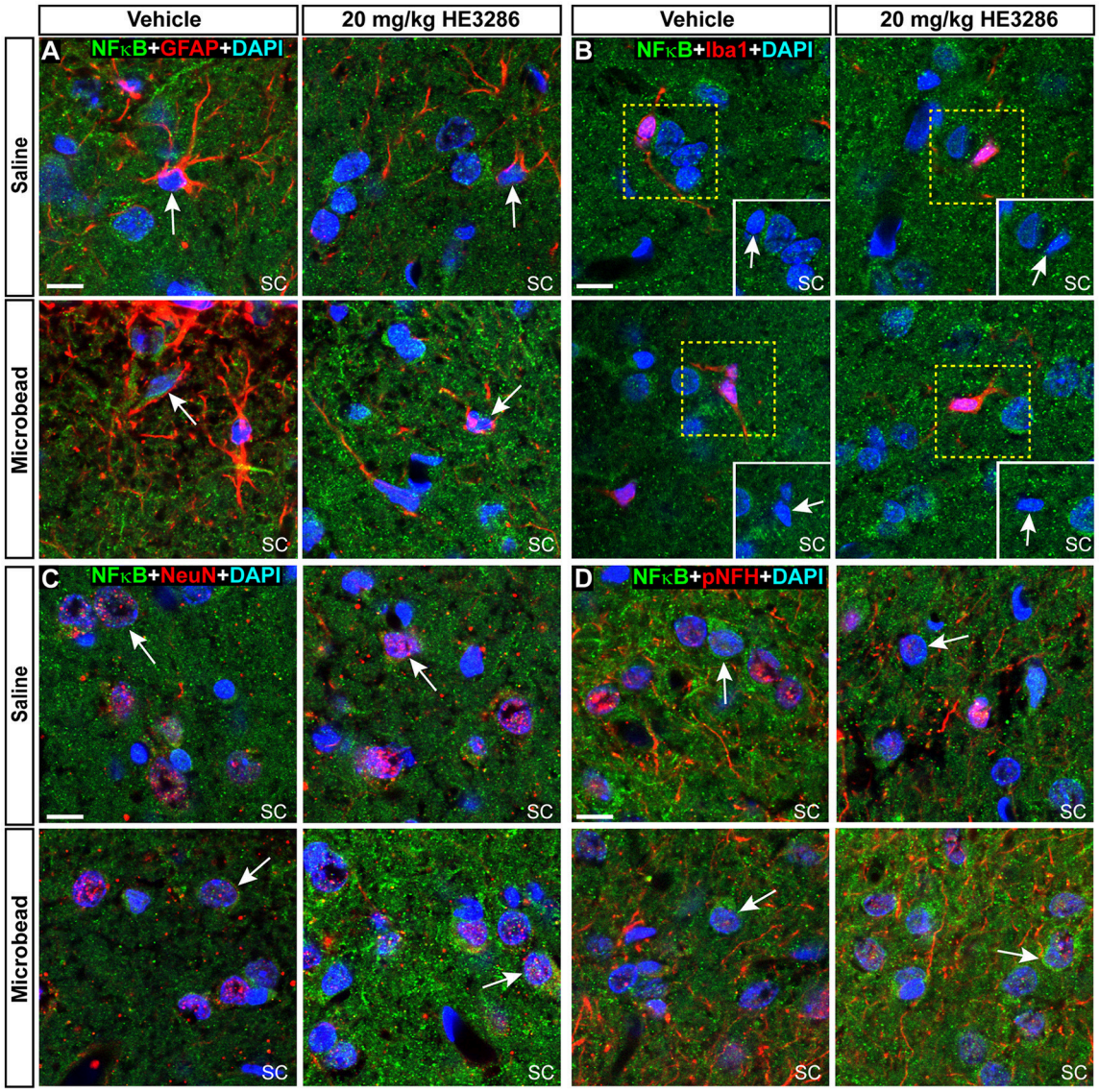

FIGURE 8 | NFκB localizes to both neuronal and glial nuclei in superior colliculus. Representative confocal images of NFκB in the superior colliculus (SC) of vehicle- and HE3286-treated rats with all nuclei indicated (DAPI). Sections were also labeled for astrocytes (**A**, GFAP), microglia (**B**, Iba1), or neurons using antibodies against either NeuN **(C)** or phosphorylated neurofilament heavy (pNFH; **D**). Representative nuclei from each cell class demonstrated NFκB localization (arrows). Insets (solid white, **B**) show region contained within dashed box with red channel removed to better visualize nuclear localization of NFκB. Scale: 10 μm.

($p < 0.003$). To determine if retinal thinning involved neuronal loss, we counted RGCs that were positive for CTB uptake and DAPI nuclear labeling and measured the thickness of the inner nuclear and outer nuclear layers of the retinas (**Figure 10D**). Treatment with HE3286 did not reduce the number of RGCs in 20 mg/kg ($3.14 \times 10^{-4} \pm 7.77 \times 10^{-6}$ RGCs/μm^2) or 100 mg/kg ($3.16 \times 10^{-4} \pm 7.48 \times 10^{-6}$ RGCs/μm^2) HE3296-treated retinas compared to vehicle-treated retinas ($3.14 \times 10^{-4} \pm 6.91 \times 10^{-6}$ RGCs/μm^2; $p > 0.963$). In contrast, HE3286 treatment reduced INL thickness 16% for the 20 mg/kg dose (14.1 ± 0.2 μm) and 21% for the 100 mg/kg dose (13.2 ± 0.1 μm) compared to vehicle (16.8 ± 0.3 mm; $p < 0.001$). This response was dose-dependent, as 100 mg/kg HE3286 reduced INL thickness a further 6% compared to 20 mg/kg ($p = 0.029$). A similar reduction in ONL thickness was observed at the higher dose of HE3286 (27.1 ± 0.2 μm) compared to vehicle (33.6 ± 0.4 μm) or the 20 mg/kg dose (33.4 ± 0.6 μm; $p > 0.001$)

DISCUSSION

In this study, we examined the therapeutic potential of a sterol derivative, HE3286, in an inducible model of glaucoma. Daily oral gavage with either 20 mg/kg or 100 mg/kg HE3286 did not affect IOP following microbead or saline injection. Even

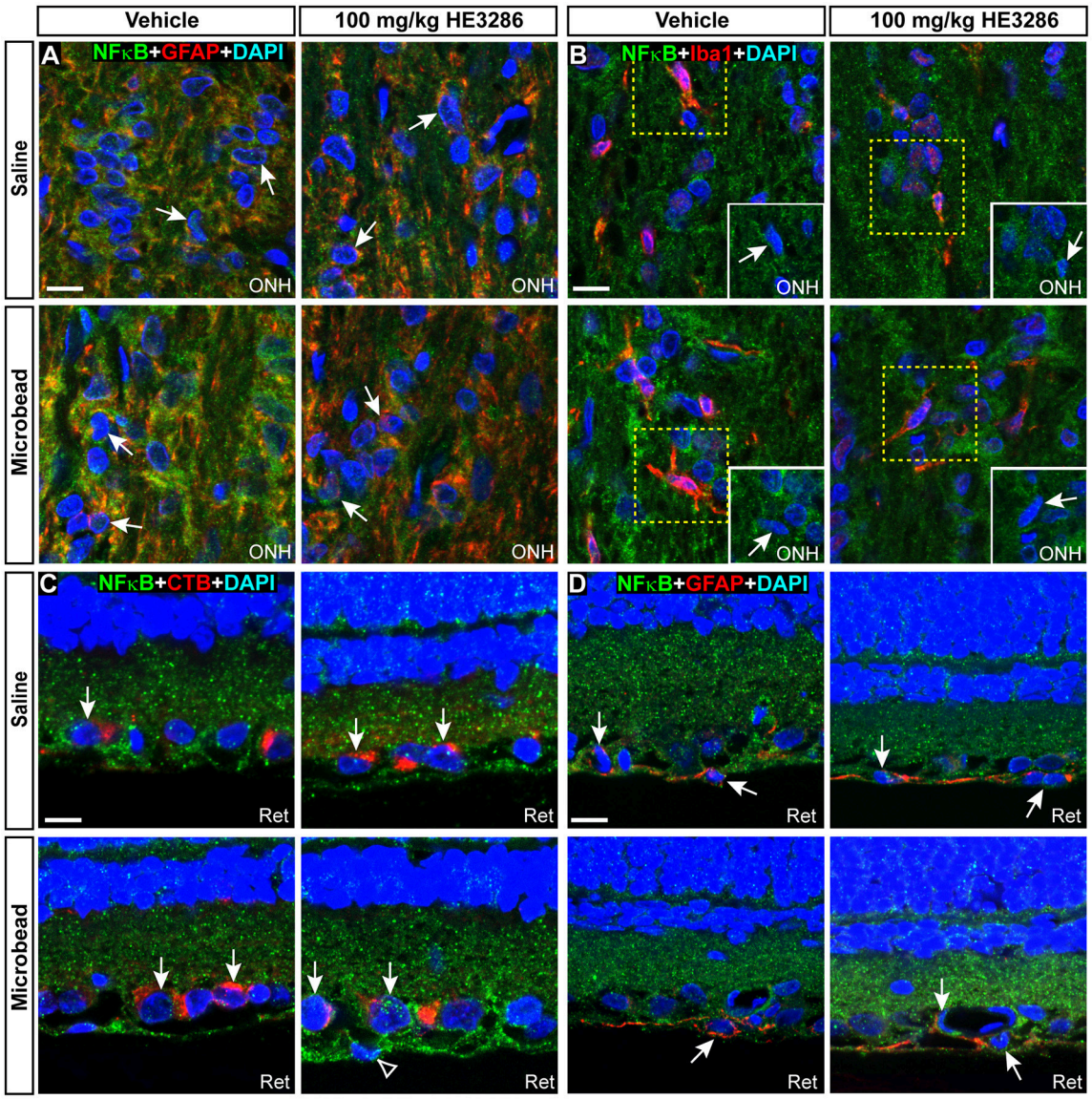

FIGURE 9 | NFκB localizes to glial nuclei in optic nerve head and to glial and neuronal nuclei in retina. Representative confocal images of NFκB (green) localization in DAPI-stained nuclei of astrocytes (**A**, GFAP) and microglia (**B**, Iba1) in optic nerve head (ONH) of vehicle- and HE3286-treated rats. Inset in **(B)** is region contained within dashed box with red channel removed to better visualize nuclear localization of NFκB. In retina **(C,D)**, NFκB localizes to nuclei of RGCs with CTB uptake and GFAP-labeled astrocytes within the retina (Ret). Arrows indicate cells positively-identified by specific label. Scale: 10 μm.

so, treatment with HE3286 did have tremendous influence on outcomes typically associated with IOP-related axonopathy. We found that HE3286 (1) preserved anterograde axonal transport of CTB from the retina to the superior colliculus in microbead-injected eyes, (2) countered the influence of elevated IOP throughout the optic projection with respect to levels of BDNF, Iba1 and other proteins associated with neuroinflammation and neurodegeneration, (3) modulated pathogenic markers of glaucoma within the retina, (4) increased NFκB localization to neuronal nuclei in the superior colliculus and retina, and (5) decreased NFκB localization to glial nuclei in the optic nerve head.

HE3286 treatment also resulted in weight loss and retinal thinning. In a safety and pharmacokinetic study, Ahlem et al. found that HE3286 had no adverse effects in chronic toxicity studies and was not immunosuppressive (Ahlem et al., 2011). Male rats that received daily oral gavage of 100 to 400 mg/kg HE3268 consumed less food and gained less weight than rats treated with vehicle, but showed no corresponding pathology or other effects on general health (Ahlem et al., 2011). We observed a similar weight loss (**Table 2**), with rats that received HE3286 losing ~6–10% of their body weight over the course of the study. We observed no adverse effects to general health (e.g., piloerection, hunched posture, decreased

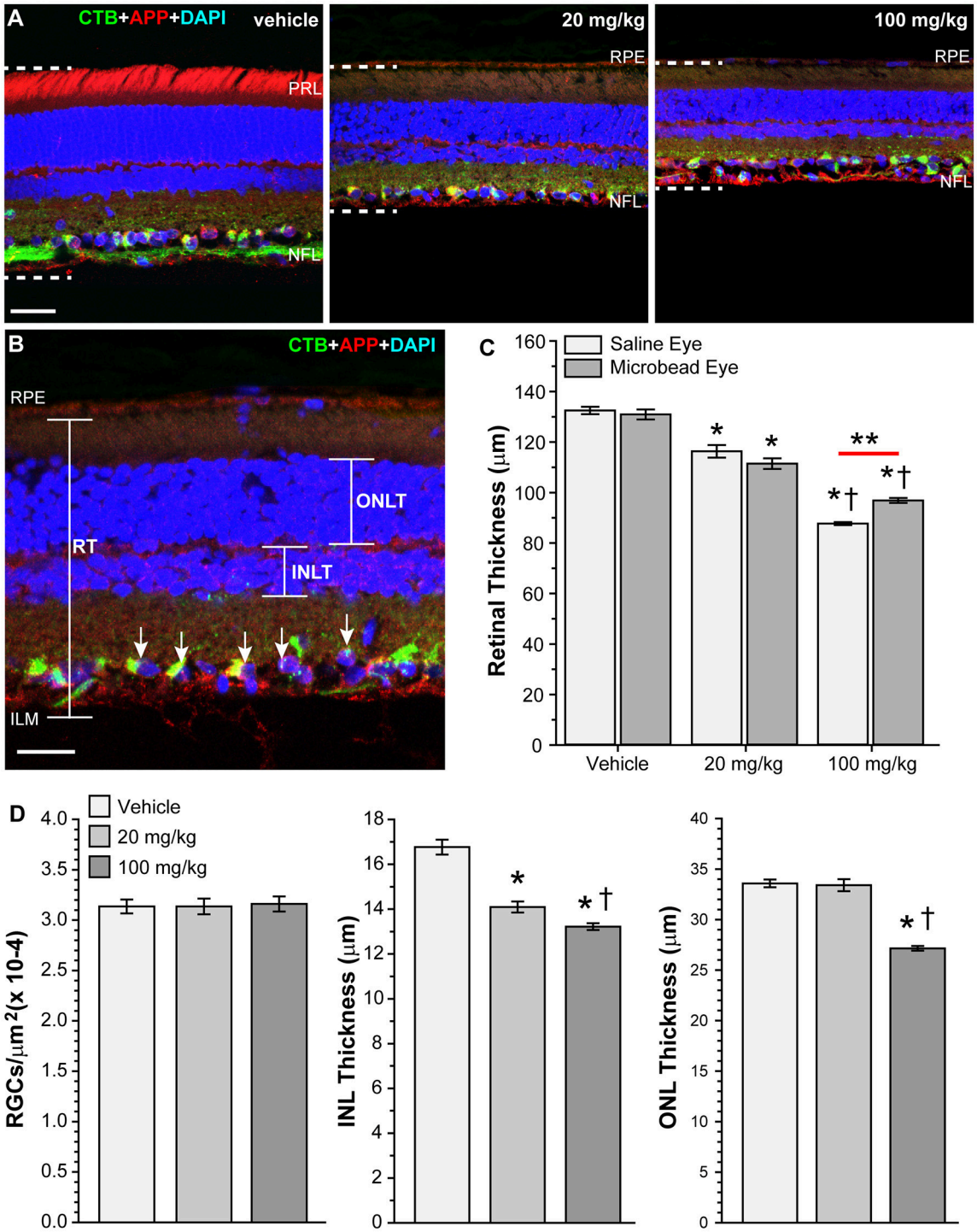

FIGURE 10 | HE3286 treatment decreases retinal thickness. (A) Confocal images of vertical retinal sections from vehicle- and HE3286-treated rats showing CTB uptake (green), immunolabeling for APP (red), and DAPI-labeled nuclei (blue). All images were captured in the mid-peripheral region of the retina. Dotted lines show retinal thickness from nerve fiber layer (NFL) to the retinal pigmented epithelial layer (RPE). Scale bar: 30 μm. PRL: photoreceptor layer. **(B)** Higher magnification of retinal section with same markers demonstrating how total retinal thickness (RT), inner nuclear layer thickness (INLT) and outer nuclear layer thickness (ONLT) were measured. RGCs positive for CTB and DAPI (arrows) were counted. Scale bar: 20 μm. ILM: inner limiting membrane. **(C)** Bar graph showing HE3286 treatment decreased retinal thickness. $^{*}p < 0.005$ compared to vehicle; $^{\dagger}p < 0.003$ compared to 20 mg/kg HE3286; $^{**}p = 0.0013$; $n = 8$ images per animal, three animals per treatment group. **(D)** Bar graphs showing HE3286 did not reduce RGC number, but did result in thinning of INL and ONL. $^{*}p < 0.001$ compared to vehicle; $^{\dagger}p < 0.029$ compared to 20 mg/kg HE3286 for INL thickness. $^{*}p < 0.001$ compared to vehicle; $^{\dagger}p < 0.001$ compared to 20 mg/kg HE3286 for ONL thickness. $n = 8$ images per animal, three animals per treatment group.

responsiveness, labored breathing, sudden lethargy, changes in muscle tone) other than weight loss. We did, however, note thinning of the retina and nuclear layers in rats that received HE3286 (**Figure 10**). Retinal thickness in vehicle treated rats (∼130 μm) was similar to what has been previously reported (Cavallotti et al., 2001; Jiao et al., 2013). Regardless of microbead treatment, retinas from rats treated with HE3286 were 12–34% thinner than rats that received vehicle. This could be a side effect of sterol treatment, as Razali et. al. reported reduced retinal thickness in a model of steroid induced ocular hypertension in rats (Razali et al., 2015). However, HE3286 is not a glucocorticoid or glucocorticoid mimetic, nor does it bind the glucocorticoid nuclear hormone receptor (Ahlem et al., 2011), so this explanation is unlikely. Also, HE3286 treatment did not elevate IOP (**Figure 1**), which other steroids can do (Razeghinejad and Katz, 2012).

Loss of retinal neurons can lead to thinning of the retina and has been observed in many neurodegenerative disorders or their models, including glaucoma, Alzheimer's disease, multiple sclerosis, and Parkinson's disease (Lee et al., 2014; Vidal-Sanz et al., 2015; Gupta et al., 2016; Knier et al., 2016a). The retinal thinning seen following HE3286 treatment is unlikely to be due to RGC loss, as counts of CTB+/DAPI+ cells (RGCs) in the ganglion cell layer showed no significant differences between vehicle- and HE3286-treated retinas. This was not surprising as RGC soma loss occurs late in the progression of glaucoma (Buckingham et al., 2008; Calkins, 2012). We did see significant thinning of the INL and ONL with HE3286 treatment. This could be a sign of effective treatment. Interestingly, thickening of the INL has been noted in multiple sclerosis patients and correlates with inflammatory disease severity and disease progression (Saidha et al., 2015; Knier et al., 2016a). This increase in INL volume is thought to be due to retinal inflammation; reducing inflammation via immunomodulatory therapy results in thinning of the INL (Saidha et al., 2015; Knier et al., 2016a,b). HE3286 treatment decreased levels of inflammatory markers in this study (**Figures 4–6**, **Table 3**). Thinning of the INL and ONL by HE3286 (**Figure 10**) may reflect a lower inflammatory response in these tissues.

In addition to preserving anterograde axonal transport (**Figure 2**), HE3286 also mitigated other indicators of dysfunction. For example, treatment with HE3286 resulted in a lack of BDNF elevation in the SC (**Figures 3A,D**). In a previous study, we observed focal increases in BDNF in regions of the SC where anterograde transport was depleted due to elevated IOP (Crish et al., 2013). Upregulation of BDNF in glaucoma is likely to result from retinorecipient targets responding to glaucoma-relevant stress to improve RGC survival (Chen and Weber, 2004; Lebrun-Julien and Di Polo, 2008; Weber et al., 2010). HE3286's preservation of anterograde transport prevented the need to increase BDNF in the SC, implying that restoration of RGC function (i.e., axonal transport) arrests the complex downstream cascades of gliosis and neuroinflammation normally observed in this condition. Conversely, HE3286 treatment also increased BDNF in the ONH and retina (**Figures 3B–D**). Neurotrophic factor deprivation due to impaired neurotrophin transport from the brain to the retina is a longstanding hypothesis in the pathogenesis of RGC degeneration in glaucoma (Johnson et al., 2011). Increased BDNF in the optic nerve and retina with IOP elevations suggests that HE3286 acts on the neurotrophin system, either directly, or indirectly by increasing transport, to preserve RGCs (Crish et al., 2013). Whether HE3296 increases BDNF by affecting the trafficking of BDNF or by stimulating local production of BDNF in the retina and optic nerve remains to be determined (Johnson et al., 2011; Crish and Calkins, 2015).

Treatment with HE3286 modulated other proteins implicated in neuroinflammation or neurodegeneration within the optic projection (**Figures 5**, **6**, **Table 3**). For certain proteins, one dose of HE3286 appeared more effective than the other; this has been observed previously for HE3286 (Ahlem et al., 2009). HE3286 may be more effective at regulating signaling pathways or maintaining homeostasis in a specific tissue at one dose versa another. Microglia become activated in response to injury and upregulate a variety of proteins, including Iba1 (Kreutzberg, 1996; Ito et al., 1998; Soto and Howell, 2014; Mac Nair and Nickells, 2015). Levels of Iba1 were elevated in the SC, ONH, and retina of vehicle-treated rats; this is not surprising since microglial activation has been observed in the optic projection in glaucoma (Wang et al., 2000; Yuan and Neufeld, 2001; Imamura et al., 2009; Ebneter et al., 2010; Shimazawa et al., 2012). HE3286 reduced Iba1 expression in all tissues examined, suggesting it abated microglia activation; a similar effect on microglia was observed in a model of optic neuritis (Khan et al., 2014). Treatment with HE3286 also reduced IL6 levels in the retina and levels of IL6Rαm and TNFα in ONH. Activated microglia produce these pro-inflammatory proteins during glaucoma pathogenesis (Tezel et al., 2001; Sappington and Calkins, 2008; Roh et al., 2012; Sims et al., 2012; Cueva Vargas et al., 2015; Wilson et al., 2015), so it's not unexpected that HE3286 would curb their expression in our model. Interestingly, HE3286 increased levels of IL6 within the SC and IL1β in the retina. While associated with neuroinflammation and implicated in neurodegeneration, both IL6 and IL1β have been shown to be neuroprotective under certain conditions (Sappington et al., 2006; Biber et al., 2008; Chidlow et al., 2012; Matousek et al., 2012; Noguchi et al., 2013; Song et al., 2013; Madeira et al., 2015; Wilson et al., 2015). HE3286 also increased APP levels in saline-injected eyes (**Figure 5D**). HE3286 is a synthetic derivative of a DHEA metabolite (Ahlem et al., 2011). DHEA levels have been linked to Alzheimer's disease, but the exact role of this neurosteroid in disease progression is currently under debate (Kim et al., 2003; Naylor et al., 2008; Aldred and Mecocci, 2010; Hampl and Bicikova, 2010; Rasmuson et al., 2011). DHEA treatment was neuroprotective in a rat model of AD, and *in vitro* DHEA increases the expression of APP and its cleavage to non-amyloidogenic fragments (Danenberg et al., 1996; Aly et al., 2011). It is possible the increase in APP levels observed in HE3286-treated saline-injected eyes is the result of DHEA-like APP processing. APP can be neuroprotective in some cases (Yankner et al., 1989; Schubert and Behl, 1993; Mucke et al., 1994; Allinquant et al., 1995; Zheng and Koo, 2011). Future studies could include elucidating the effects of HE3286 on APP and its processing in glaucoma and other

neurodegenerative diseases. Finally, HE3286 decreased APP and p75 in the ONH and retina, and dramatically reduced ceruloplasmin and C1q expression in the retina of microbead-injected eyes. Each of these factors has been implicated in RGC death, or has been shown to be elevated in the retina and optic nerve in human glaucomatous tissue and/or in models of glaucoma (Stasi et al., 2006, 2007; Goldblum et al., 2007; Stevens et al., 2007; Wei et al., 2007; Lebrun-Julien et al., 2009; Kipfer-Kauer et al., 2010; Howell et al., 2011, 2014; Ding et al., 2012; Meeker and Williams, 2015). Taken as a whole, it appears HE3286 mitigates the neuroinflammatory response by dampening microglial activation.

The expression of TNFα, IL6, APP in neurons and glia, as well as the production of β-amyloid, and the activation of microglia can all be regulated by NFκB activation (Mattson and Camandola, 2001; Camandola and Mattson, 2007). A suggested mechanism of action for HE3286 is the regulation of NFκB activity (Auci et al., 2007; Ahlem et al., 2009, 2011; Offner et al., 2009). NFκB is a transcription factor activated by a wide range of stimuli that in turn regulates the expression of genes involved inflammation, immune response, cell survival and cell death (Gilmore, 2008; Hayden and Ghosh, 2008; Lawrence, 2009). Activated NFκB translocates to the nucleus, and we observed nuclear localization of NFκB in neurons and glia within the optic projection of vehicle- and HE3286-treated rats following IOP elevation (**Figures 7–9**). Similar activation of NFκB in the visual pathway has been observed following injury and in models of glaucoma (Choi et al., 1998; Agapova et al., 2006; Haenold et al., 2014). Treatment with HE3286 increased NFκB localization in neuronal nuclei within the SC and retina and decreased NFκB localization in ONH glial nuclei in microbead-injected eyes. This cell-specific NFκB activation may explain the beneficial outcomes observed in HE3286-treated rats; NFκB activation in glial cells promotes neuronal degeneration, while activation in neurons promotes survival (Mattson and Camandola, 2001; Camandola and Mattson, 2007). Activated NFκB can enhance mitochondrial bioenergetics and prevent peripheral neuropathy in rodent models of diabetes (Saleh et al., 2013). Increased NFκB localization to RGC nuclei in HE3286-treated microbead-injected eyes may protect these neurons metabolically (Kong et al., 2009; Baltan et al., 2010; Lee et al., 2011; Coughlin et al., 2015; Kleesattel et al., 2015; Fahy et al., 2016), such that axonal transport is preserved compared to vehicle-treated eyes (**Figure 2**). Whether or not HE3286 maintains RGC functionality could be assessed using outcomes such as visual evoked potentials, electroretinogram, or two-alternative forced-choice visual behavioral testing in this or other models of glaucoma.

HE3286 has produced therapeutic benefits in various models of inflammatory disease, in a model of Parkinson's and in clinical trials for diabetic complications (Auci et al., 2007, 2010; Ahlem et al., 2009; Offner et al., 2009; Conrad et al., 2010; Lu et al., 2010; Kosiewicz et al., 2011; Nicoletti et al., 2012; Reading et al., 2013a,b; Khan et al., 2014). HE3286 has been well tolerated and has presented no adverse effects in human trials (Reading et al., 2013a,b). We observed positive therapeutic outcomes in terms of anterograde axonal transport, the expression of proteins associated with neuroinflammation, neurodegeneration, and glaucoma pathogenesis, and NFκB activation. The results of this study suggest HE3286 provides neuroprotection to RGCs and their axons, which helps preserve function in these neurons following exposure to elevated ocular pressure. This neuroprotection could be due to caloric restriction (**Table 2**), as has been observed in a mouse model of glaucoma (Guo et al., 2016). However, HE3286's anti-inflammatory activity has been observed *in vitro* and in mice without weight loss compared to vehicle controls, and in humans without caloric restriction or weight loss (Wang et al., 2010; Reading et al., 2013b). A matched feeding experimental design would be needed to understand the potential contribution of reduced caloric intake in our glaucoma model, but prior evidence in other models suggest the current results are not predominately a result of caloric restriction. Glaucoma shares many common features with other neurodegenerative diseases (Crish and Calkins, 2011; Mckinnon, 2012; Ghiso et al., 2013; Jindal, 2013; Danesh-Meyer and Levin, 2015; Jain and Aref, 2015). Given the number of people currently with or likely to develop glaucoma in the near future, the commonalities between glaucoma and other age-related neurodegenerative diseases, and that HE3286 is already being tested in clinical trials, further studies on HE3286 and the mechanism of its action in the central nervous system is warranted.

AUTHOR CONTRIBUTIONS

WL contributed substantially to the experimental design, the acquisition, analysis and interpretation of data, and the writing and revising the manuscript. BC, CF contributed substantially to the acquisition and analysis of data and assisted in manuscript revisions. RS contributed substantially to the experimental design with regards to neuroinflammation, and assisted in the critical revision of the manuscript. CA contributed substantially to the conception and experimental design, and assisted in the critical revision of the manuscript. DC contributed substantially to the conception and experimental design, interpretation of data, and assisted in the critical revision of the manuscript.

FUNDING

The authors declare that this research was supported by a grant from Harbor Therapeutics, Inc. (San Diego, CA). We also acknowledge support from the Vanderbilt Vision Research Center (5P30EY008126, DC).

ACKNOWLEDGMENTS

Confocal imaging was performed through the use of the VUMC Cell Imaging Shared Resource (supported by NIH grants CA68485, DK20593, DK58404, DK59637, and EY08126).

REFERENCES

Agapova, O. A., Kaufman, P. L., and Hernandez, M. R. (2006). Androgen receptor and NFkB expression in human normal and glaucomatous optic nerve head astrocytes *in vitro* and in experimental glaucoma. *Exp. Eye Res.* 82, 1053–1059. doi: 10.1016/j.exer.2005.10.021

Ahlem, C., Auci, D., Mangano, K., Reading, C., Frincke, J., Stickney, D., et al. (2009). HE3286: a novel synthetic steroid as an oral treatment for autoimmune disease. *Ann. N. Y. Acad. Sci.* 1173, 781–790. doi: 10.1111/j.1749-6632.2009.04798.x

Ahlem, C. N., Kennedy, M. R., Page, T. M., Reading, C. L., White, S. K., Mckenzie, J. J., et al. (2011). Studies of the pharmacology of 17α-ethynyl-androst-5-ene-3β,7β,17β-triol, a synthetic anti-inflammatory androstene. *Int. J. Clin. Exp. Med.* 4, 119–135.

Aldred, S., and Mecocci, P. (2010). Decreased dehydroepiandrosterone (DHEA) and dehydroepiandrosterone sulfate (DHEAS) concentrations in plasma of Alzheimer's disease (AD) patients. *Arch. Gerontol. Geriatr.* 51, e16–e18. doi: 10.1016/j.archger.2009.07.001

Allinquant, B., Hantraye, P., Mailleux, P., Moya, K., Bouillot, C., and Prochiantz, A. (1995). Downregulation of amyloid precursor protein inhibits neurite outgrowth *in vitro*. *J. Cell Biol.* 128, 919–927. doi: 10.1083/jcb.128.5.919

Aly, H. F., Metwally, F. M., and Ahmed, H. H. (2011). Neuroprotective effects of dehydroepiandrosterone (DHEA) in rat model of Alzheimer's disease. *Acta Biochim. Pol.* 58, 513–520.

Auci, D., Kaler, L., Subramanian, S., Huang, Y., Frincke, J., Reading, C., et al. (2007). A new orally bioavailable synthetic androstene inhibits collagen-induced arthritis in the mouse: androstene hormones as regulators of regulatory T cells. *Ann. N. Y. Acad. Sci.* 1110, 630–640. doi: 10.1196/annals.1423.066

Auci, D. L., Mangano, K., Destiche, D., White, S. K., Huang, Y., Boyle, D., et al. (2010). Oral treatment with HE3286 ameliorates disease in rodent models of rheumatoid arthritis. *Int. J. Mol. Med.* 25, 625–633. doi: 10.3892/ijmm_00000385

Baltan, S., Inman, D. M., Danilov, C. A., Morrison, R. S., Calkins, D. J., and Horner, P. J. (2010). Metabolic vulnerability disposes retinal ganglion cell axons to dysfunction in a model of glaucomatous degeneration. *J. Neurosci.* 30, 5644–5652. doi: 10.1523/JNEUROSCI.5956-09.2010

Biber, K., Pinto-Duarte, A., Wittendorp, M. C., Dolga, A. M., Fernandes, C. C., Von Frijtag Drabbe Kunzel, J., et al. (2008). Interleukin-6 upregulates neuronal adenosine A1 receptors: implications for neuromodulation and neuroprotection. *Neuropsychopharmacology* 33, 2237–2250. doi: 10.1038/sj.npp.1301612

Buckingham, B. P., Inman, D. M., Lambert, W., Oglesby, E., Calkins, D. J., Steele, M. R., et al. (2008). Progressive ganglion cell degeneration precedes neuronal loss in a mouse model of glaucoma. *J. Neurosci.* 28, 2735–2744. doi: 10.1523/JNEUROSCI.4443-07.2008

Calkins, D. J. (2012). Critical pathogenic events underlying progression of neurodegeneration in glaucoma. *Prog. Retin. Eye Res.* 31, 702–719. doi: 10.1016/j.preteyeres.2012.07.001

Camandola, S., and Mattson, M. P. (2007). NF-κB as a therapeutic target in neurodegenerative diseases. *Expert Opin. Ther. Targets* 11, 123–132. doi: 10.1517/14728222.11.2.123

Carmona, R., Macias, D., Guadix, J. A., Portillo, V., Perez-Pomares, J. M., and Munoz-Chapuli, R. (2007). A simple technique of image analysis for specific nuclear immunolocalization of proteins. *J. Microsc.* 225, 96–99. doi: 10.1111/j.1365-2818.2007.01719.x

Cavallotti, C., Artico, M., Pescosolido, N., and Feher, J. (2001). Age-related changes in rat retina. *Jpn. J. Ophthalmol.* 45, 68–75. doi: 10.1016/S0021-5155(00)00294-X

Chen, H., and Weber, A. J. (2004). Brain-derived neurotrophic factor reduces TrkB protein and mRNA in the normal retina and following optic nerve crush in adult rats. *Brain Res.* 1011, 99–106. doi: 10.1016/j.brainres.2004.03.024

Cheung, W., Guo, L., and Cordeiro, M. F. (2008). Neuroprotection in glaucoma: drug-based approaches. *Optom. Vis. Sci.* 85, 406–416. doi: 10.1097/OPX.0b013e31817841e5

Chidlow, G., Wood, J. P., Ebneter, A., and Casson, R. J. (2012). Interleukin-6 is an efficacious marker of axonal transport disruption during experimental glaucoma and stimulates neuritogenesis in cultured retinal ganglion cells. *Neurobiol. Dis.* 48, 568–581. doi: 10.1016/j.nbd.2012.07.026

Choi, J. S., Sungjoo, K. Y., and Joo, C. K. (1998). NF-κB activation following optic nerve transection. *Korean J. Ophthalmol.* 12, 19–24. doi: 10.3341/kjo.1998.12.1.19

Conrad, D., Wang, A., Pieters, R., Nicoletti, F., Mangano, K., Van Heeckeren, A. M., et al. (2010). HE3286, an oral synthetic steroid, treats lung inflammation in mice without immune suppression. *J. Inflamm.* 7:52. doi: 10.1186/1476-9255-7-52

Coughlin, L., Morrison, R. S., Horner, P. J., and Inman, D. M. (2015). Mitochondrial morphology differences and mitophagy deficit in murine glaucomatous optic nerve. *Invest. Ophthalmol. Vis. Sci.* 56, 1437–1446. doi: 10.1167/iovs.14-16126

Crish, S. D., and Calkins, D. J. (2011). Neurodegeneration in glaucoma: progression and calcium-dependent intracellular mechanisms. *Neuroscience* 176, 1–11. doi: 10.1016/j.neuroscience.2010.12.036

Crish, S. D., and Calkins, D. J. (2015). Central visual pathways in glaucoma: evidence for distal mechanisms of neuronal self-repair. *J. Neuroophthalmol.* 35(Suppl. 1), S29–S37. doi: 10.1097/wno.0000000000000291

Crish, S. D., Dapper, J. D., Macnamee, S. E., Balaram, P., Sidorova, T. N., Lambert, W. S., et al. (2013). Failure of axonal transport induces a spatially coincident increase in astrocyte BDNF prior to synapse loss in a central target. *Neuroscience* 229, 55–70. doi: 10.1016/j.neuroscience.2012.10.069

Crish, S. D., Sappington, R. M., Inman, D. M., Horner, P. J., and Calkins, D. J. (2010). Distal axonopathy with structural persistence in glaucomatous neurodegeneration. *Proc. Natl. Acad. Sci. U.S.A.* 107, 5196–5201. doi: 10.1073/pnas.0913141107

Cueva Vargas, J. L., Osswald, I. K., Unsain, N., Aurousseau, M. R., Barker, P. A., Bowie, D., et al. (2015). Soluble tumor necrosis factor alpha promotes retinal ganglion cell death in glaucoma via calcium-permeable ampa receptor activation. *J. Neurosci.* 35, 12088–12102. doi: 10.1523/JNEUROSCI.1273-15.2015

Danenberg, H. D., Haring, R., Fisher, A., Pittel, Z., Gurwitz, D., and Heldman, E. (1996). Dehydroepiandrosterone (DHEA) increases production and release of Alzheimer's amyloid precursor protein. *Life Sci.* 59, 1651–1657. doi: 10.1016/0024-3205(96)00496-1

Danesh-Meyer, H. V., and Levin, L. A. (2015). Glaucoma as a neurodegenerative disease. *J Neuroophthalmol* 35(Suppl. 1), S22–S28. doi: 10.1097/wno.0000000000000293

Dapper, J. D., Crish, S. D., Pang, I. H., and Calkins, D. J. (2013). Proximal inhibition of p38 MAPK stress signaling prevents distal axonopathy. *Neurobiol. Dis.* 59, 26–37. doi: 10.1016/j.nbd.2013.07.001

Dengler-Crish, C. M., Smith, M. A., Inman, D. M., Wilson, G. N., Young, J. W., and Crish, S. D. (2014). Anterograde transport blockade precedes deficits in retrograde transport in the visual projection of the DBA/2J mouse model of glaucoma. *Front. Neurosci.* 8:290. doi: 10.3389/fnins.2014.00290

Denko, C. W. (1979). Protective role of ceruloplasmin in inflammation. *Agents Actions* 9, 333–336. doi: 10.1007/BF01970657

Dillon, J. S. (2005). Dehydroepiandrosterone, dehydroepiandrosterone sulfate and related steroids: their role in inflammatory, allergic and immunological disorders. *Curr. Drug Targets Inflamm. Allergy* 4, 377–385. doi: 10.2174/1568010054022079

Ding, Q. J., Cook, A. C., Dumitrescu, A. V., and Kuehn, M. H. (2012). Lack of immunoglobulins does not prevent C1q binding to RGC and does not alter the progression of experimental glaucoma. *Invest. Ophthalmol. Vis. Sci.* 53, 6370–6377. doi: 10.1167/iovs.12-10442

Ebneter, A., Casson, R. J., Wood, J. P., and Chidlow, G. (2010). Microglial activation in the visual pathway in experimental glaucoma: spatiotemporal characterization and correlation with axonal injury. *Invest. Ophthalmol. Vis. Sci.* 51, 6448–6460. doi: 10.1167/iovs.10-5284

Fahy, E. T., Chrysostomou, V., and Crowston, J. G. (2016). Mini-Review: impaired axonal transport and glaucoma. *Curr. Eye Res.* 41, 273–283. doi: 10.3109/02713683.2015.1037924

Feng, L., Xie, X., Joshi, P. S., Yang, Z., Shibasaki, K., Chow, R. L., et al. (2006). Requirement for Bhlhb5 in the specification of amacrine and cone bipolar subtypes in mouse retina. *Development* 133, 4815–4825. doi: 10.1242/dev.02664

Ghiso, J. A., Doudevski, I., Ritch, R., and Rostagno, A. A. (2013). Alzheimer's disease and glaucoma: mechanistic similarities and differences. *J. Glaucoma* 22(Suppl. 5), S36–S38. doi: 10.1097/ijg.0b013e3182934af6

Gilmore, T. D. (2008). *NF-kB Transcription Factors.* Available online at: www.NF-kB.org (Accessed).

Goldblum, D., Kipfer-Kauer, A., Sarra, G. M., Wolf, S., and Frueh, B. E. (2007). Distribution of amyloid precursor protein and amyloid-beta immunoreactivity in DBA/2J glaucomatous mouse retinas. *Invest. Ophthalmol. Vis. Sci.* 48, 5085–5090. doi: 10.1167/iovs.06-1249

Goldstein, I. M., Kaplan, H. B., Edelson, H. S., and Weissmann, G. (1979). A new function for ceruloplasmin as an acute-phase reactant in inflammation: a scavenger of superoxide anion radicals. *Trans. Assoc. Am. Physicians* 92, 360–369.

Guo, X., Kimura, A., Azuchi, Y., Akiyama, G., Noro, T., Harada, C., et al. (2016). Caloric restriction promotes cell survival in a mouse model of normal tension glaucoma. *Sci. Rep.* 6:33950. doi: 10.1038/srep33950

Gupta, V. K., Chitranshi, N., Gupta, V. B., Golzan, M., Dheer, Y., Wall, R. V., et al. (2016). Amyloid beta accumulation and inner retinal degenerative changes in Alzheimer's disease transgenic mouse. *Neurosci. Lett.* 623, 52–56. doi: 10.1016/j.neulet.2016.04.059

Haenold, R., Weih, F., Herrmann, K. H., Schmidt, K. F., Krempler, K., Engelmann, C., et al. (2014). NF-κB controls axonal regeneration and degeneration through cell-specific balance of RelA and p50 in the adult CNS. *J. Cell Sci.* 127, 3052–3065. doi: 10.1242/jcs.140731

Hampl, R., and Bicikova, M. (2010). Neuroimmunomodulatory steroids in Alzheimer dementia. *J. Steroid Biochem. Mol. Biol.* 119, 97–104. doi: 10.1016/j.jsbmb.2010.02.007

Hayden, M. S., and Ghosh, S. (2008). Shared principles in NF-κB signaling. *Cell* 132, 344–362. doi: 10.1016/j.cell.2008.01.020

Heijl, A., Leske, M. C., Bengtsson, B., Hyman, L., and Hussein, M. (2002). Reduction of intraocular pressure and glaucoma progression: results from the early manifest glaucoma trial. *Arch. Ophthalmol.* 120, 1268–1279. doi: 10.1001/archopht.120.10.1268

Herkenham, M., Rathore, P., Brown, P., and Listwak, S. J. (2011). Cautionary notes on the use of NF-κB p65 and p50 antibodies for CNS studies. *J. Neuroinflammation* 8:141. doi: 10.1186/1742-2094-8-141

Hernandez, M. R. (2000). The optic nerve head in glaucoma: role of astrocytes in tissue remodeling. *Prog. Retin. Eye Res.* 19, 297–321. doi: 10.1016/S1350-9462(99)00017-8

Hofbauer, A., and Drager, U. C. (1985). Depth segregation of retinal ganglion cells projecting to mouse superior colliculus. *J. Comp. Neurol.* 234, 465–474. doi: 10.1002/cne.902340405

Howell, G. R., Macalinao, D. G., Sousa, G. L., Walden, M., Soto, I., Kneeland, S. C., et al. (2011). Molecular clustering identifies complement and endothelin induction as early events in a mouse model of glaucoma. *J. Clin. Invest.* 121, 1429–1444. doi: 10.1172/JCI44646

Howell, G. R., Macnicoll, K. H., Braine, C. E., Soto, I., Macalinao, D. G., Sousa, G. L., et al. (2014). Combinatorial targeting of early pathways profoundly inhibits neurodegeneration in a mouse model of glaucoma. *Neurobiol. Dis.* 71, 44–52. doi: 10.1016/j.nbd.2014.07.016

Imamura, K., Onoe, H., Shimazawa, M., Nozaki, S., Wada, Y., Kato, K., et al. (2009). Molecular imaging reveals unique degenerative changes in experimental glaucoma. *Neuroreport* 20, 139–144. doi: 10.1097/WNR.0b013e32831d7f82

Ito, D., Imai, Y., Ohsawa, K., Nakajima, K., Fukuuchi, Y., and Kohsaka, S. (1998). Microglia-specific localisation of a novel calcium binding protein, Iba1. *Brain Res. Mol. Brain Res.* 57, 1–9. doi: 10.1016/S0169-328X(98)00040-0

Jain, S., and Aref, A. A. (2015). Senile dementia and glaucoma: evidence for a common link. *J. Ophthalmic Vis. Res.* 10, 178–183. doi: 10.4103/2008-322X.163766

Jiao, J., Mo, B., Wei, H., and Jiang, Y. R. (2013). Comparative study of laser-induced choroidal neovascularization in rats by paraffin sections, frozen sections and high-resolution optical coherence tomography. *Graefes Arch. Clin. Exp. Ophthalmol.* 251, 301–307. doi: 10.1007/s00417-012-2204-4

Jindal, V. (2013). Glaucoma: an extension of various chronic neurodegenerative disorders. *Mol. Neurobiol.* 48, 186–189. doi: 10.1007/s12035-013-8416-8

Johnson, T. V., Bull, N. D., and Martin, K. R. (2011). Neurotrophic factor delivery as a protective treatment for glaucoma. *Exp. Eye Res.* 93, 196–203. doi: 10.1016/j.exer.2010.05.016

Kang, T. H., Ryu, Y. H., Kim, I. B., Oh, G. T., and Chun, M. H. (2004). Comparative study of cholinergic cells in retinas of various mouse strains. *Cell Tissue Res.* 317, 109–115. doi: 10.1007/s00441-004-0907-5

Khan, R. S., Dine, K., Luna, E., Ahlem, C., and Shindler, K. S. (2014). HE3286 reduces axonal loss and preserves retinal ganglion cell function in experimental optic neuritis. *Invest. Ophthalmol. Vis. Sci.* 55, 5744–5751. doi: 10.1167/iovs.14-14672

Kim, S. B., Hill, M., Kwak, Y. T., Hampl, R., Jo, D. H., and Morfin, R. (2003). Neurosteroids: cerebrospinal fluid levels for Alzheimer's disease and vascular dementia diagnostics. *J. Clin. Endocrinol. Metab.* 88, 5199–5206. doi: 10.1210/jc.2003-030646

Kipfer-Kauer, A., Mckinnon, S. J., Frueh, B. E., and Goldblum, D. (2010). Distribution of amyloid precursor protein and amyloid-beta in ocular hypertensive C57BL/6 mouse eyes. *Curr. Eye Res.* 35, 828–834. doi: 10.3109/02713683.2010.494240

Kleesattel, D., Crish, S. D., and Inman, D. M. (2015). Decreased energy capacity and increased autophagic activity in optic nerve axons with defective anterograde transport. *Invest. Ophthalmol. Vis. Sci.* 56, 8215–8227. doi: 10.1167/iovs.15-17885

Knier, B., Berthele, A., Buck, D., Schmidt, P., Zimmer, C., Muhlau, M., et al. (2016a). Optical coherence tomography indicates disease activity prior to clinical onset of central nervous system demyelination. *Mult. Scler.* 22, 893–900. doi: 10.1177/1352458515604496

Knier, B., Schmidt, P., Aly, L., Buck, D., Berthele, A., Muhlau, M., et al. (2016b). Retinal inner nuclear layer volume reflects response to immunotherapy in multiple sclerosis. *Brain* 139, 2855–2863. doi: 10.1093/brain/aww219

Kong, G. Y., Van Bergen, N. J., Trounce, I. A., and Crowston, J. G. (2009). Mitochondrial dysfunction and glaucoma. *J. Glaucoma* 18, 93–100. doi: 10.1097/IJG.0b013e318181284f

Kosiewicz, M. M., Auci, D. L., Fagone, P., Mangano, K., Caponnetto, S., Tucker, C. F., et al. (2011). HE3286, an orally bioavailable synthetic analogue of an active DHEA metabolite suppresses spontaneous autoimmune diabetes in the non-obese diabetic (NOD) mouse. *Eur. J. Pharmacol.* 658, 257–262. doi: 10.1016/j.ejphar.2011.02.016

Kreutzberg, G. W. (1996). Microglia: a sensor for pathological events in the CNS. *Trends Neurosci.* 19, 312–318. doi: 10.1016/0166-2236(96)10049-7

Lambert, W. S., Ruiz, L., Crish, S. D., Wheeler, L. A., and Calkins, D. J. (2011). Brimonidine prevents axonal and somatic degeneration of retinal ganglion cell neurons. *Mol. Neurodegener.* 6:4. doi: 10.1186/1750-1326-6-4

Lawrence, T. (2009). The nuclear factor NF-κB pathway in inflammation. *Cold Spring Harb. Perspect. Biol.* 1:a001651. doi: 10.1101/cshperspect.a001651

Lebrun-Julien, F., and Di Polo, A. (2008). Molecular and cell-based approaches for neuroprotection in glaucoma. *Optom. Vis. Sci.* 85, 417–424. doi: 10.1097/OPX.0b013e31817841f7

Lebrun-Julien, F., Morquette, B., Douillette, A., Saragovi, H. U., and Di Polo, A. (2009). Inhibition of p75(NTR) in glia potentiates TrkA-mediated survival of injured retinal ganglion cells. *Mol. Cell. Neurosci.* 40, 410–420. doi: 10.1016/j.mcn.2008.12.005

Lee, J. Y., Kim, J. M., Ahn, J., Kim, H. J., Jeon, B. S., and Kim, T. W. (2014). Retinal nerve fiber layer thickness and visual hallucinations in Parkinson's Disease. *Mov. Disord.* 29, 61–67. doi: 10.1002/mds.25543

Lee, S., Van Bergen, N. J., Kong, G. Y., Chrysostomou, V., Waugh, H. S., O'neill, E. C., et al. (2011). Mitochondrial dysfunction in glaucoma and emerging bioenergetic therapies. *Exp. Eye Res.* 93, 204–212. doi: 10.1016/j.exer.2010.07.015

Linden, R., and Perry, V. H. (1983). Massive retinotectal projection in rats. *Brain Res.* 272, 145–149. doi: 10.1016/0006-8993(83)90371-2

Lu, M., Patsouris, D., Li, P., Flores-Riveros, J., Frincke, J. M., Watkins, S., et al. (2010). A new antidiabetic compound attenuates inflammation and insulin resistance in Zucker diabetic fatty rats. *Am. J. Physiol. Endocrinol. Metab.* 298, E1036–E1048. doi: 10.1152/ajpendo.00668.2009

Mac Nair, C. E., and Nickells, R. W. (2015). Neuroinflammation in glaucoma and optic nerve damage. *Prog. Mol. Biol. Transl. Sci.* 134, 343–363. doi: 10.1016/bs.pmbts.2015.06.010

Madeira, M. H., Boia, R., Santos, P. F., Ambrosio, A. F., and Santiago, A. R. (2015). Contribution of microglia-mediated neuroinflammation to retinal degenerative diseases. *Mediators Inflamm.* 2015:673090. doi: 10.1155/2015/673090

Matousek, S. B., Ghosh, S., Shaftel, S. S., Kyrkanides, S., Olschowka, J. A., and O'banion, M. K. (2012). Chronic IL-1beta-mediated neuroinflammation mitigates amyloid pathology in a mouse model of Alzheimer's disease without inducing overt neurodegeneration. *J. Neuroimmune Pharmacol.* 7, 156–164. doi: 10.1007/s11481-011-9331-2

Mattson, M. P., and Camandola, S. (2001). NF-κB in neuronal plasticity and neurodegenerative disorders. *J. Clin. Invest.* 107, 247–254. doi: 10.1172/JCI11916

Mckinnon, S. J. (2012). The cell and molecular biology of glaucoma: common neurodegenerative pathways and relevance to glaucoma. *Invest. Ophthalmol. Vis. Sci.* 53, 2485–2487. doi: 10.1167/iovs.12-9483j

Meeker, R. B., and Williams, K. S. (2015). The p75 neurotrophin receptor: at the crossroad of neural repair and death. *Neural Regen. Res.* 10, 721–725. doi: 10.4103/1673-5374.156967

Mucke, L., Masliah, E., Johnson, W. B., Ruppe, M. D., Alford, M., Rockenstein, E. M., et al. (1994). Synaptotrophic effects of human amyloid beta protein precursors in the cortex of transgenic mice. *Brain Res.* 666, 151–167. doi: 10.1016/0006-8993(94)90767-6

Naylor, J. C., Hulette, C. M., Steffens, D. C., Shampine, L. J., Ervin, J. F., Payne, V. M., et al. (2008). Cerebrospinal fluid dehydroepiandrosterone levels are correlated with brain dehydroepiandrosterone levels, elevated in Alzheimer's disease, and related to neuropathological disease stage. *J. Clin. Endocrinol. Metab.* 93, 3173–3178. doi: 10.1210/jc.2007-1229

Nickells, R. W., Howell, G. R., Soto, I., and John, S. W. (2012). Under pressure: cellular and molecular responses during glaucoma, a common neurodegeneration with axonopathy. *Annu. Rev. Neurosci.* 35, 153–179. doi: 10.1146/annurev.neuro.051508.135728

Nicoletti, F., Philippens, I., Fagone, P., Ahlem, C. N., Reading, C. L., Frincke, J. M., et al. (2012). 17α-Ethynyl-androst-5-ene-3β,7β,17β-triol (HE3286) Is neuroprotective and reduces motor impairment and neuroinflammation in a murine MPTP Model of Parkinson's Disease. *Parkinsons Dis.* 2012:969418. doi: 10.1155/2012/969418

Noguchi, Y., Shinozaki, Y., Fujishita, K., Shibata, K., Imura, Y., Morizawa, Y., et al. (2013). Astrocytes protect neurons against methylmercury via ATP/P2Y(1) receptor-mediated pathways in astrocytes. *PLoS ONE* 8:e57898. doi: 10.1371/journal.pone.0057898

Offner, H., Firestein, G. S., Boyle, D. L., Pieters, R., Frincke, J. M., Garsd, A., et al. (2009). An orally bioavailable synthetic analog of an active dehydroepiandrosterone metabolite reduces established disease in rodent models of rheumatoid arthritis. *J. Pharmacol. Exp. Ther.* 329, 1100–1109. doi: 10.1124/jpet.108.145086

Offner, H., Zamora, A., Drought, H., Matejuk, A., Auci, D. L., Morgan, E. E., et al. (2002). A synthetic androstene derivative and a natural androstene metabolite inhibit relapsing-remitting EAE. *J. Neuroimmunol.* 130, 128–139. doi: 10.1016/S0165-5728(02)00214-X

Quigley, H. A., and Broman, A. T. (2006). The number of people with glaucoma worldwide in 2010 and 2020. *Br. J. Ophthalmol.* 90, 262–267. doi: 10.1136/bjo.2005.081224

Rasmuson, S., Nasman, B., and Olsson, T. (2011). Increased serum levels of dehydroepiandrosterone (DHEA) and interleukin-6 (IL-6) in women with mild to moderate Alzheimer's disease. *Int. Psychogeriatr.* 23, 1386–1392. doi: 10.1017/S1041610211000810

Razali, N., Agarwal, R., Agarwal, P., Kapitonova, M. Y., Kannan Kutty, M., Smirnov, A., et al. (2015). Anterior and posterior segment changes in rat eyes with chronic steroid administration and their responsiveness to antiglaucoma drugs. *Eur. J. Pharmacol.* 749, 73–80. doi: 10.1016/j.ejphar.2014.11.029

Razeghinejad, M. R., and Katz, L. J. (2012). Steroid-induced iatrogenic glaucoma. *Ophthalmic Res.* 47, 66–80. doi: 10.1159/000328630

Reading, C. L., Flores-Riveros, J., Stickney, D. R., and Frincke, J. M. (2013a). An anti-inflammatory sterol decreases obesity-related inflammation-induced insulin resistance and metabolic dysregulation. *Mediators Inflamm.* 2013:814989. doi: 10.1155/2013/814989

Reading, C. L., Frincke, J. M., and White, S. K. (2012). Molecular targets for 17α-ethynyl-5-androstene-3β,7β,17β-triol, an anti-inflammatory agent derived from the human metabolome. *PLoS ONE* 7:e32147. doi: 10.1371/journal.pone.0032147

Reading, C. L., Stickney, D. R., Flores-Riveros, J., Destiche, D. A., Ahlem, C. N., Cefalu, W. T., et al. (2013b). A synthetic anti-inflammatory sterol improves insulin sensitivity in insulin-resistant obese impaired glucose tolerance subjects. *Obesity* 21, E343–E349. doi: 10.1002/oby.20207

Roh, M., Zhang, Y., Murakami, Y., Thanos, A., Lee, S. C., Vavvas, D. G., et al. (2012). Etanercept, a widely used inhibitor of tumor necrosis factor-α (TNF-α), prevents retinal ganglion cell loss in a rat model of glaucoma. *PLoS ONE* 7:e40065. doi: 10.1371/journal.pone.0040065

Russo, R., Varano, G. P., Adornetto, A., Nucci, C., Corasaniti, M. T., Bagetta, G., et al. (2016). Retinal ganglion cell death in glaucoma: exploring the role of neuroinflammation. *Eur. J. Pharmacol.* 787, 134–142. doi: 10.1016/j.ejphar.2016.03.064

Saidha, S., Al-Louzi, O., Ratchford, J. N., Bhargava, P., Oh, J., Newsome, S. D., et al. (2015). Optical coherence tomography reflects brain atrophy in multiple sclerosis: a four-year study. *Ann. Neurol.* 78, 801–813. doi: 10.1002/ana.24487

Saleh, A., Roy Chowdhury, S. K., Smith, D. R., Balakrishnan, S., Tessler, L., Martens, C., et al. (2013). Ciliary neurotrophic factor activates NF-κB to enhance mitochondrial bioenergetics and prevent neuropathy in sensory neurons of streptozotocin-induced diabetic rodents. *Neuropharmacology* 65, 65–73. doi: 10.1016/j.neuropharm.2012.09.015

Samuel, M. A., Zhang, Y., Meister, M., and Sanes, J. R. (2011). Age-related alterations in neurons of the mouse retina. *J. Neurosci.* 31, 16033–16044. doi: 10.1523/JNEUROSCI.3580-11.2011

Sappington, R. M., and Calkins, D. J. (2008). Contribution of TRPV1 to microglia-derived IL-6 and NFκB translocation with elevated hydrostatic pressure. *Invest. Ophthalmol. Vis. Sci.* 49, 3004–3017. doi: 10.1167/iovs.07-1355

Sappington, R. M., Carlson, B. J., Crish, S. D., and Calkins, D. J. (2010). The microbead occlusion model: a paradigm for induced ocular hypertension in rats and mice. *Invest. Ophthalmol. Vis. Sci.* 51, 207–216. doi: 10.1167/iovs.09-3947

Sappington, R. M., Chan, M., and Calkins, D. J. (2006). Interleukin-6 protects retinal ganglion cells from pressure-induced death. *Invest. Ophthalmol. Vis. Sci.* 47, 2932–2942. doi: 10.1167/iovs.05-1407

Sappington, R. M., Sidorova, T., Long, D. J., and Calkins, D. J. (2009). TRPV1: contribution to retinal ganglion cell apoptosis and increased intracellular Ca^{2+} with exposure to hydrostatic pressure. *Invest. Ophthalmol. Vis. Sci.* 50, 717–728. doi: 10.1167/iovs.08-2321

Schneider, C. A., Rasband, W. S., and Eliceiri, K. W. (2012). NIH Image to ImageJ: 25 years of image analysis. *Nat. Methods* 9, 671–675. doi: 10.1038/nmeth.2089

Schober, M. S., Chidlow, G., Wood, J. P., and Casson, R. J. (2008). Bioenergetic-based neuroprotection and glaucoma. *Clin. Exp. Ophthalmol.* 36, 377–385. doi: 10.1111/j.1442-9071.2008.01740.x

Schubert, D., and Behl, C. (1993). The expression of amyloid beta protein precursor protects nerve cells from beta-amyloid and glutamate toxicity and alters their interaction with the extracellular matrix. *Brain Res.* 629, 275–282. doi: 10.1016/0006-8993(93)91331-L

Shimazawa, M., Ito, Y., Inokuchi, Y., Yamanaka, H., Nakanishi, T., Hayashi, T., et al. (2012). An alteration in the lateral geniculate nucleus of experimental glaucoma monkeys: *in vivo* positron emission tomography imaging of glial activation. *PLoS ONE* 7:e30526. doi: 10.1371/journal.pone.0030526

Sims, S. M., Holmgren, L., Cathcart, H. M., and Sappington, R. M. (2012). Spatial regulation of interleukin-6 signaling in response to neurodegenerative stressors in the retina. *Am. J. Neurodegener. Dis.* 1, 168–179.

Song, C., Zhang, Y., and Dong, Y. (2013). Acute and subacute IL-1β administrations differentially modulate neuroimmune and neurotrophic systems: possible implications for neuroprotection and neurodegeneration. *J. Neuroinflammation* 10:59. doi: 10.1186/1742-2094-10-59

Soto, I., and Howell, G. R. (2014). The complex role of neuroinflammation in glaucoma. *Cold Spring Harb. Perspect. Med.* 4:a017269. doi: 10.1101/cshperspect.a017269

Stasi, K., Nagel, D., Yang, X., Ren, L., Mittag, T., and Danias, J. (2007). Ceruloplasmin upregulation in retina of murine and human glaucomatous eyes. *Invest. Ophthalmol. Vis. Sci.* 48, 727–732. doi: 10.1167/iovs.06-0497

Stasi, K., Nagel, D., Yang, X., Wang, R. F., Ren, L., Podos, S. M., et al. (2006). Complement component 1Q (C1Q) upregulation in retina of murine, primate, and human glaucomatous eyes. *Invest. Ophthalmol. Vis. Sci.* 47, 1024–1029. doi: 10.1167/iovs.05-0830

Stevens, B., Allen, N. J., Vazquez, L. E., Howell, G. R., Christopherson, K. S., Nouri, N., et al. (2007). The classical complement cascade mediates CNS synapse elimination. *Cell* 131, 1164–1178. doi: 10.1016/j.cell.2007.10.036

Tezel, G., Li, L. Y., Patil, R. V., and Wax, M. B. (2001). TNF-alpha and TNF-alpha receptor-1 in the retina of normal and glaucomatous eyes. *Invest. Ophthalmol. Vis. Sci.* 42, 1787–1794.

Vidal-Sanz, M., Valiente-Soriano, F. J., Ortin-Martinez, A., Nadal-Nicolas, F. M., Jimenez-Lopez, M., Salinas-Navarro, M., et al. (2015). Retinal

neurodegeneration in experimental glaucoma. *Prog. Brain Res.* 220, 1–35. doi: 10.1016/bs.pbr.2015.04.008

Wang, T., Villegas, S., Huang, Y., White, S. K., Ahlem, C., Lu, M., et al. (2010). Amelioration of glucose intolerance by the synthetic androstene HE3286: link to inflammatory pathways. *J. Pharmacol. Exp. Ther.* 333, 70–80. doi: 10.1124/jpet.109.161182

Wang, X., Sam-Wah Tay, S., and Ng, Y. K. (2000). Nitric oxide, microglial activities and neuronal cell death in the lateral geniculate nucleus of glaucomatous rats. *Brain Res.* 878, 136–147. doi: 10.1016/S0006-8993(00)02727-X

Ward, N. J., Ho, K. W., Lambert, W. S., Weitlauf, C., and Calkins, D. J. (2014). Absence of transient receptor potential vanilloid-1 accelerates stress-induced axonopathy in the optic projection. *J. Neurosci.* 34, 3161–3170. doi: 10.1523/JNEUROSCI.4089-13.2014

Weber, A. J., Viswanathan, S., Ramanathan, C., and Harman, C. D. (2010). Combined application of BDNF to the eye and brain enhances ganglion cell survival and function in the cat after optic nerve injury. *Invest. Ophthalmol. Vis. Sci.* 51, 327–334. doi: 10.1167/iovs.09-3740

Wei, Y., Wang, N., Lu, Q., Zhang, N., Zheng, D., and Li, J. (2007). Enhanced protein expressions of sortilin and p75NTR in retina of rat following elevated intraocular pressure-induced retinal ischemia. *Neurosci. Lett.* 429, 169–174. doi: 10.1016/j.neulet.2007.10.012

Weitlauf, C., Ward, N. J., Lambert, W. S., Sidorova, T. N., Ho, K. W., Sappington, R. M., et al. (2014). Short-term increases in transient receptor potential vanilloid-1 mediate stress-induced enhancement of neuronal excitation. *J. Neurosci.* 34, 15369–15381. doi: 10.1523/JNEUROSCI.3424-14.2014

Wilson, G. N., Inman, D. M., Dengler Crish, C. M., Smith, M. A., and Crish, S. D. (2015). Early pro-inflammatory cytokine elevations in the DBA/2J mouse model of glaucoma. *J. Neuroinflammation* 12, 176. doi: 10.1186/s12974-015-0399-0

Yankner, B. A., Dawes, L. R., Fisher, S., Villa-Komaroff, L., Oster-Granite, M. L., and Neve, R. L. (1989). Neurotoxicity of a fragment of the amyloid precursor associated with Alzheimer's disease. *Science* 245, 417–420. doi: 10.1126/science.2474201

Yuan, L., and Neufeld, A. H. (2001). Activated microglia in the human glaucomatous optic nerve head. *J. Neurosci. Res.* 64, 523–532. doi: 10.1002/jnr.1104

Zheng, H., and Koo, E. H. (2011). Biology and pathophysiology of the amyloid precursor protein. *Mol. Neurodegener.* 6:27. doi: 10.1186/1750-1326-6-27

Conflict of Interest Statement: The authors declare that this research was supported by a grant from Harbor Therapeutics, Inc (San Diego, CA).

The reviewer MH and handling Editor declared their shared affiliation, and the handling Editor states that the process nevertheless met the standards of a fair and objective review.

frontiers in Neuroscience

ORIGINAL RESEARCH
published: 24 November 2016
doi: 10.3389/fnins.2016.00526

Loss of Fractalkine Signaling Exacerbates Axon Transport Dysfunction in a Chronic Model of Glaucoma

Kevin T. Breen[1], Sarah R. Anderson[1], Michael R. Steele[1], David J. Calkins[2], Alejandra Bosco[1†] and Monica L. Vetter[1†]*

[1] Departments of Neurobiology and Anatomy, University of Utah, Salt Lake City, UT, USA, [2] Department of Ophthalmology and Visual Sciences, Vanderbilt University, Nashville, TN, USA

Neurodegeneration in glaucoma results in decline and loss of retinal ganglion cells (RGCs), and is associated with activation of myeloid cells such as microglia and macrophages. The chemokine fractalkine (FKN or Cx3cl1) mediates communication from neurons to myeloid cells. Signaling through its receptor Cx3cr1 has been implicated in multiple neurodegenerative diseases, but the effects on neuronal pathology are variable. Since it is unknown how FKN-mediated crosstalk influences RGC degeneration in glaucoma, we assessed this in a chronic mouse model, DBA/2J. We analyzed a DBA/2J substrain deficient in Cx3cr1, and compared compartmentalized RGC degeneration and myeloid cell responses to those in standard DBA/2J mice. We found that loss of FKN signaling exacerbates axon transport dysfunction, an early event in neurodegeneration, with a significant increase in RGCs with somal accumulation of the axonal protein phosphorylated neurofilament, and reduced retinal expression of genes involved in axon transport, Kif1b, and Atp8a2. There was no change in the loss of Brn3-positive RGCs, and no difference in the extent of damage to the proximal optic nerve, suggesting that the loss of fractalkine signaling primarily affects axon transport. Since Cx3cr1 is specifically expressed in myeloid cells, we assessed changes in retinal microglial number and activation, changes in gene expression, and the extent of macrophage infiltration. We found that loss of fractalkine signaling led to innate immune changes within the retina, including increased infiltration of peripheral macrophages and upregulated nitric oxide synthase-2 (Nos-2) expression in myeloid cells, which contributes to the production of NO and can promote axon transport deficits. In contrast, resident retinal microglia appeared unchanged either in number, morphology, or expression of the myeloid activation marker ionized calcium binding adaptor molecule 1 (Iba1). There was also no significant increase in the proinflammatory gene interleukin 1 beta (Il1β). We conclude that loss of fractalkine signaling causes a selective worsening of axon transport dysfunction in RGCs, which is linked to enhanced Nos-2 expression in myeloid cells. Our findings suggest that distinct mechanisms may contribute to different aspects of RGC decline in glaucoma, with axonal transport selectively altered after loss of Cx3cr1 in microglia and/or macrophages.

Keywords: retina, glaucoma, microglia, macrophage, retinal ganglion cell, neurodegeneration, Cx3cr1, DBA/2J

OPEN ACCESS

Edited by:
Jason R. Richardson, Northeast Ohio Medical University, USA

Reviewed by:
Roland Brandt, University of Osnabrück, Germany
Tatjana C. Jakobs, Massachusetts Eye and Ear Infirmary, USA

****Correspondence:***
Monica L. Vetter
monica@neuro.utah.edu

† These authors have contributed equally to this work.

Specialty section:
This article was submitted to Neurodegeneration, a section of the journal Frontiers in Neuroscience

Received: *10 September 2016*
Accepted: *31 October 2016*
Published: *24 November 2016*

Citation:
Breen KT, Anderson SR, Steele MR, Calkins DJ, Bosco A and Vetter ML (2016) Loss of Fractalkine Signaling Exacerbates Axon Transport Dysfunction in a Chronic Model of Glaucoma. Front. Neurosci. 10:526. doi: 10.3389/fnins.2016.00526

INTRODUCTION

The myeloid innate immune system has long been of interest in the field of neurodegeneration, not only as a responder to neuronal stress and damage but also as a driver of neurodegeneration (Ilieva et al., 2009; Czeh et al., 2011). This is also the case for diverse neurodegenerative ocular diseases, including glaucoma (Karlstetter et al., 2015). In glaucoma, retinal ganglion cells (RGCs) progressively degenerate, with the different neuronal compartments (soma, axon, dendrites, and synapses) declining at different times and potentially by different mechanisms (Libby et al., 2005a; Whitmore et al., 2005; Conforti et al., 2007; Howell et al., 2007; Calkins, 2012; Fernandes et al., 2014). In addition, multiple studies in human and experimental glaucoma suggest a link between the progressive deterioration of RGCs and alterations of glial cell types (Yuan and Neufeld, 2001; Naskar et al., 2002; Neufeld and Liu, 2003; Nakazawa et al., 2006; Inman and Horner, 2007; Bosco et al., 2011, 2015b; Lye-Barthel et al., 2013; Chong and Martin, 2015). Microglia are the resident innate immune cells of the central nervous system, and in both glaucoma patients and in animal models of glaucoma, they display increased reactivity and cluster at the optic nerve head, which is a site of early damage (Bosco et al., 2011; Yuan and Neufeld, 2001; Roh et al., 2012; Soto and Howell, 2014). It has also been demonstrated that peripheral macrophages infiltrate the retina in animal models of glaucoma (Howell et al., 2012) suggesting that different myeloid cell types may participate in glaucoma progression. However, it remains unclear how microglia and macrophages affect RGC compartmentalized degeneration in glaucoma.

In order to address the role of myeloid cells in neurodegeneration, many studies have manipulated the fractalkine (FKN) signaling system, which serves as a major neuron-to-myeloid cell communication system (Hoarau et al., 2011; Limatola and Ransohoff, 2014). The FKN receptor, Cx3cr1, is specifically expressed by cells of the myeloid lineage, including microglia, while the FKN ligand, Cx3cl1, is highly expressed by neurons (Jung et al., 2000; Cook et al., 2001). Multiple studies have suggested that Cx3cl1/Cx3cr1 signaling functions to constrain microglial activation, and thus limit potentially neurotoxic effects (Cardona et al., 2006; Limatola and Ransohoff, 2014). However, it is now appreciated that diverse myeloid functions are regulated by FKN signaling, including cytokine secretion, microglial activation, phagocytosis, process dynamics, migration, survival of subsets of circulating monocytes, and infiltration of macrophages positive for chemokine C-C motif receptor 2 (Ccr2) (Cardona et al., 2006; Lee et al., 2008; Landsman et al., 2009; Liang et al., 2009; Sennlaub et al., 2013). Given these complex roles, it is not surprising that loss of FKN signaling has diverse and sometimes contradictory effects on neurodegeneration (Wolf et al., 2013). For example, loss of FKN signaling simultaneously reduces amyloid-β burden and increases tau pathology in the same mouse model of Alzheimer's disease (Lee et al., 2014). These findings suggest that myeloid cells may differentially influence distinct aspects of neurodegeneration. However, the role of these cells is still incompletely understood, particularly for progressive age-related neurodegeneration including glaucoma.

The DBA/2J mouse models key aspects of neurodegeneration in human glaucoma because the decline of RGCs occurs in an age-related and asynchronous manner with variable onset (John et al., 1998; Anderson et al., 2002; Jakobs et al., 2005; Libby et al., 2005a). Multiple quantitative readouts have been established demonstrating progressive compartmental degeneration of RGCs in the DBA/2J retina and optic nerve. These include early downregulation of RGC genes such as the transcription factor Brn3b, accumulation of axonal proteins such as phosphorylated neurofilament (pNF) within RGC somata as transport declines, and loss of axons with subsequent gliosis in the optic nerve (Libby et al., 2005a,b; Schlamp et al., 2006; Buckingham et al., 2008; Soto et al., 2008; Dengler-Crish et al., 2014; Bosco et al., 2015b; Cooper et al., 2016). Furthermore, alterations of both resident microglia and infiltrating macrophages have been documented in this model, although the impact of these cells on RGC degeneration remains poorly understood (Mo et al., 2003; Anderson et al., 2008; Bosco et al., 2011, 2015b; Howell et al., 2012).

To address this, we sought to manipulate microglia/macrophage function and assess the effects on RGC neurodegeneration. We therefore analyzed the retinas of 10–11 month-old DBA/2J mice lacking the FKN receptor, Cx3cr1, for neuroprotective, or deleterious effects in the retina and optic nerve. Thus, we measured the density of Brn3-positive nuclei and somal pNF-positive cells across whole retinas, and analyzed the respective optic nerves for the extent of glial coverage as a proxy for axon dropout. In these same samples, we assessed changes in myeloid cells in the retina by quantifying cell densities of myeloid cell populations and assessing microglial activation by Iba1 immunostaining. We then performed flow cytometry to assess infiltration of CCR2+ macrophages and measured gene expression changes by qRT-PCR. We show that loss of fractalkine signaling in myeloid cells increases infiltration of Ccr2+ macrophages into the DBA/2J retina, selectively worsens axon transport dysfunction in RGCs, and is associated with selective changes in the expression of genes related to axon transport deficits.

Abbreviations: RGC, retinal ganglion cell; pNF, phosphorylated neurofilament; RT-PCR, reverse transcriptase polymerase chain reaction; Gapdh, glyceraldehyde 3-phosphate dehydrogenase; FACS, fluorescence-activated cell sorting; PBS, phosphate buffered saline; PPD, paraphenylenediamine; Iba1, ionized calcium binding adaptor molecule 1; Nos-2, nitric oxide synthase 2; NO, nitric oxide; Il1β, interleukin 1 beta; Mfge8, milk fat globule-EGF factor 8 protein; Dlk, dual leucine kinase; Ccl2, chemokine C-C motif ligand 2; Ccr2, chemokine C-C motif receptor 2; Cx3cl1, fractalkine; Cx3cr1, fractalkine receptor; GFP, green fluorescent protein; $Cx3cr1^{gfp/gfp}$, Cx3cr1 -gfp knockin.

MATERIALS AND METHODS

Mice

$Cx3cr1^{gfp/gfp}$ DBA/2J mice were generated by breeding existing $Cx3cr1^{gfp/+}$ DBA/2J mice to homozygosity (Bosco et al., 2015b). DBA/2J mice were obtained from Jackson Labs, bred in-house, and were refreshed with new breeders every 3–4 generations. Both male and female mice were used for analysis ($n = 36$ $Cx3cr1^{gfp/gfp}$ DBA/2J mice, 21 male, 15 female; $n = 31$ DBA/2J

mice, 15 male, 16 female). Mice from both strains were aged to 10–11 months, when a majority of DBA/2J eyes typically show clear glaucoma pathology (Libby et al., 2005a). Although animals of mixed gender were used, we have excluded gender as a contributing factor, since our findings were confirmed by analysis of data from male animals alone (data not shown). Experiments and mouse care were performed in compliance with the ARVO Statement for the Use of Animals in Ophthalmic and Vision Research, and with the guidelines of the University of Utah Institutional Animal Care and Use Committee.

Tissue Collection

Perfusion and dissection of retinal tissue and optic nerves for both immunohistochemistry and RNA collection were performed as previously described (Bosco et al., 2011). Briefly, retinas were dissected fresh under RNAase-free conditions for RNA isolation, or dissected from transcardially perfused mice as whole mounts, which were stored in chilled 0.1 M phosphate-buffered saline (PBS) overnight at 4°C and utilized the next day for immunohistochemistry. Also, retinal eyecups were cryoprotected, cast in gelatin blocks that were stored at −80°C, and cryosectioned radially at 16 μm thickness for immunohistochemistry. Optic nerves were postfixed, embedded in resin and prepared as 1–2 μm-thick cross-sections for toluidine blue and paraphenylenediamine (PPD) staining (Bosco et al., 2015b).

Immunohistochemistry

Triple immunofluorescence staining was performed using established protocols and antibodies, as previously described in detail (Bosco et al., 2011). Retinal whole mount and cryosections were incubated with primary antibodies for 3 days at 4°C and incubated with secondary antibodies for 2 h. Primary antibodies used in this study included: goat anti-Brn3 (Santa Cruz sc-6026 at 1:50), mouse anti-phosphorylated neurofilament (pNF; including NFM and NFH; Dako M0762 at 1:100), rabbit anti-Iba1 (Wako at 1:1000), rat anti-CCR2 APC conjugated (R&D Systems FAB5538A at 1:10), and rabbit anti-cleaved caspase 3 (BD Biosciences BDB559565 at 1:500). pNF staining co-labeled with rabbit polyclonal neurofilament heavy antibody (Biolegend 801703) and in separate experiments was absent when primary antibody was omitted. All Alexa Fluor-conjugated (488, 568, or 647 nm) donkey secondary antibodies were used at 1:400 (Invitrogen); Alexa-Fluor 594-conjugated donkey anti rat secondary was used at 1:200 (Jackson ImmunoResearch Lab).

In situ Hybridization

Antisense and sense 3′UTR Dig labeled probes were generated from pCMV-SPORT6 Cx3cl1 (MGC 5859) obtained from ATCC. Probes were synthesized and hybridized using standard procedures as in Soto et al. (2008) without the use of proteinase K. Briefly, mice were perfused, eyes cast in gelatin, and 16 um radial cryosections were generated as described in their respective sections. Bound probes were detected using 1:300 Anti-Dig AP antibody (Sigma 11093274910) overnight at 4°C with 30 min color development using NBT/BCIP tablets (Sigma 11697471001).

Microscopy

All retinal samples were imaged on an inverted confocal microscope (Nikon A1 with NIS-Elements software 4.2) using a 20x objective and resonance scanning (Bosco et al., 2012). Entire retinas were imaged using a multipoint acquisition macro of the software, collecting 25 × 25 fields at 60x magnification (0.41 μm/pixel), each spanning 30–40 μm of the retinal inner surface through a step size of 0.8 μm. Maximum intensity projections of stitched, high-resolution images were then generated for each retina, and all images were identically and minimally adjusted for brightness and contrast for analysis. Optic nerves were imaged on a compound BX51 Olympus light microscope using a 60X objective and analyzed using cellSens software as 36 high-resolution multipoint images (Bosco et al., 2015b).

Quantification of Brn3+ Nuclei

Brn3+ nuclei, corresponding to RGCs expressing Brn3a and Brn3b (Bosco et al., 2011), were sampled within the central 1.77 μm^2 of the retina by dividing a circle centered on the optic disk into eight parts (2 dorsal, 2 ventral, 2 nasal, and 2 temporal). A 250 × 250 μm box was placed in each of these areas with blood vessels used as landmarks. RGC degeneration in the DBA/2J model is sectorial (Jakobs et al., 2005; Howell et al., 2007), so to avoid bias, when two sectors were visible within an eighth of the retina being analyzed, two boxes were placed one in each sector. The total number of Brn3+ nuclei were tallied and normalized to the area sampled (∼0.06 mm^2 per box). To be counted, nuclei had to be spherical/elliptical in shape and >1.5x the intensity of the background. Debris was uniformly more intense than Brn3+ nuclei and was excluded from the quantification. Retinas were then sorted from highest to lowest Brn3+ nuclei density. The distribution of densities of Brn3+ nuclei was not normally distributed therefore a Wilcoxon rank sum test was used to assess significance.

Quantification of Somal pNF+ RGCs

Cell somas with accumulated phosphorylated neurofilament (pNF) were quantified in the central 1.77 μm^2 of the retina, as described for Brn3. RGC somata were identified based on shape (reflecting either somatic or somato-dendritic accumulation), size being >10 μm in diameter and fluorescence intensity being >1.5x the background. Somal pNF positive RGCs were verified to be negative for Iba1. RGCs positive for both Brn3 and somal pNF or just somal pNF were quantified. Retinas were then sorted from lowest to highest somal pNF+ RGC density. The distribution of densities of pNF+ cells was not normally distributed therefore a Wilcoxon rank sum test was used to assess significance.

Quantification of Iba1+ Cells

Three categories of Iba1+ cell were determined based on morphology: branched Iba1+ cells with a small cell soma and more than two branches, perivascular Iba1+ cells having two main branches at polar opposite sides of the cell, and amoeboid Iba1+ cells having no branches. Branched Iba1+ and perivascular Iba1+ cells were quantified in the central 1.77 um^2 of the retina, as described for Brn3, excluding the optic disk. Amoeboid Iba1+ cells, being fewer in number, were quantified in

the entire retina, excluding the optic disk and the lumen of blood vessels. Retinas were then sorted from lowest to highest density of the respective Iba1+cell morphological class. The distribution of densities of perivascular and amoeboid Iba1+ cells was not normally distributed and was analyzed by Wilcoxon rank sum test. The distribution of branched Iba1+ cells was normally distributed and was analyzed by Student's *t*-test.

Optic Nerve Histopathology

Optic nerve cross-sections from the myelinated portion of the nerve, 1–1.5 mm proximal to the lamina, were embedded and 1 μm sections were cut on an ultramicrotome with a glass knife then transferred to slides. Sections were stained with PPD (Libby et al., 2005a) for 28 min using a modified protocol as previously described (Bosco et al., 2015a,b), and mounted under coverslips with Permount (Fisher).

Quantification of Non-axonal Area in the Proximal Optic Nerve

The relative area devoid of axons or dystrophic axons in individual optic nerve cross-sections was measured by segmentation of glial cells and/or glial scar and extracellular matrix from 8-bit stitched RGB images of PPD stained nerves, as previously described (Bosco et al., 2015a,b, 2016). The green channel of the RGB image provided the greatest contrast to segment glial area from non-glial elements including axons and blood vessels. Briefly, the green channel of RGB images minimally adjusted for contrast (0–10 on a scale to 0–100) and sharpness (Gauss Laplace between 1.0 and 1.1 on a scale of 0–2), were thresholded to generate a binary mask encompassing the total cross-sectional area of the optic nerve, excluding meninges and blood vessels. The axon-free nerve relative area was then calculated by determining the percent of the total optic nerve that is covered by non-axonal cells or matrix. Optic nerves were then sorted from lowest to highest percent non-axonal area. The distribution of percent optic nerve covered by non-axonal elements was not normally distributed and was analyzed by Wilcoxon rank sum test. To verify this analysis, a subset of 24 DBA/2J and 24 Cx3cr1$^{gfp/gfp}$ DBA/2J PPD-stained optic nerves were blindly scored using a three-category system as mild, moderate, or severe, as in Libby et al. (2005a). Mild degeneration consisted of nerves with no or very little loss of axons and no gliosis. Moderate degeneration consisted of little to no gliosis but a clear presence of dystrophic axons, while a majority remained healthy. Severe degeneration consisted of nerves with clear and frequently extensive gliosis and a majority of dystrophic axons with clear and significant loss of axons overall. No significant difference was found between the genotypes with a chi-squared value of 0.93.

Fluorescence-Activated Cell Sorting (FACS) and Flow Cytometry

Four female DBA/2J or three Cx3cr1$^{gfp/gfp}$ DBA/2J female mice at 12 months of age were perfused with saline. Retinas were dissociated in PBS, 50 mM HEPES, 0.05 mg/ml DNaseI (Sigma D4513), 0.025 mg/ml Liberase (Sigma 5401119001) for 35 min with intermediate trituration. Cells were passed through a 70 μm nylon cell strainer, washed with staining buffer (1X PBS, 2% BSA, 0.1% sodium azide, 0.05% EDTA), and red blood cells were lysed (eBioscience 00-4333-57). Cell counts were determined using a hemocytometer and Fc block (BD Biosciences 553142) was added 2 μl per 10^6 cells. Antibodies were applied for 30 min on ice (BV421-CD45 563890, PE-CD11b 553311, APC-Ccr2 FAB5538A100). Cells were washed, pelleted, and resuspended in 500 μl staining buffer. FACS was performed using a BD FACSAria cell sorter. CD11b$^+$, CD45$^+$, CCR2 ± were sorted directly into RLT buffer (Qiagen 79216) and stored at −20°C. RNA from sorted cells was purified using an RNeasy Plus Micro kit (Qiagen 74034) and reverse transcribed using SuperScript IV Reverse transcriptase (Invitrogen 18090019). 832,000–937,000 events were collected for flow analysis using BD FACSDiva software. CCR2$^+$ populations were analyzed gating on live CD11b$^+$ CD45$^+$ cells. Unstained retinas and spleens stained for CD11b, CD45 and CCR2 from the same animals were used as negative and positive controls, respectively.

Quantitative RT-PCR

Sample preparation, cDNA synthesis, and quantitative reverse transcriptase polymerase chain reaction (qRT-PCR) were performed as previously described (Bosco et al., 2011). Briefly, whole retinas were aspirated through a 22-gage needle and RNA was isolated using a Qiagen RNeasy micro kit according to manufacturer's instructions. The mRNA quality was determined on an Agilent Bioanalyzer and samples with RNA integrity numbers <8 were discarded. First strand cDNA was synthesized using an Invitrogen Superscript III First Strand cDNA synthesis kit according to manufacturer's recommendations, and quantities determined on a Nano-drop spectrophotometer. qRT-PCR was performed on an Applied Biosystems 7900 HT instrument with QuantStudio 12 K Flex software using an Invitrogen Platinum Sybr Green qPCR supermix-UDG kit according to manufacturer's instructions. For analysis of whole retina samples (all genes except Nos-2 and interleukin 1β (Il1β)), a standard curve was generated based on five serial one-half dilutions of pooled cDNAs from a large number of 1–12-month DBA/2J retinas, and genes were analyzed in the linear range based on these curves. For Nos-2 and Il1β, we used the ΔΔCt method to calculate the relative fold change in gene expression (Livak and Schmittgen, 2001), and statistical analysis was performed using Student's *t*-test on all genes. Analyzed genes were normalized to glyceraldehyde 3-phosphate dehydrogenase (Gapdh). For statistical analysis, genes that did not amplify were set to 40 cycles, which is the limit of detection.

Primers used 5′–3′:

GapdhF:	TGCACCACCAACTGCTTAGC
GapdhR:	GGCATGGACTGTGGTCATGAG
Iba1F:	CCTGATTGGAGGTGGATGTCA
Iba1R:	GGCTCACGACTGTTTCTTTTTTCC
Kif1bF:	TTATTGATACATCCATGGGGTC
Kif1bR:	TCTCCTGAATACTGGTCACA
Atp8a2F:	CTTTGTGTTTTGTTTTCCCCGC
Atp8a2R:	CGCTGTACTTGGCCGTACTGA
Mfge8F:	GGATAATCAGGGCAAGATCA

Mfge8R:	TAGGACGCCACATACTGGAT
Ccr2F:	AAGGAGCCATACCTGTAAATGC
Ccr2R:	ATGCCGTGGATGAACTGAGG
Ccl2F:	CACTCACCTGCTGCTACTCA
Ccl2R:	GCTTGGTGACAAAAACTACAGC
Nos-2F:	TCTTGGAGCGAGTTGTGGATT
Nos-2R:	CAGCCTCTTGTCTTTGACCCA
Il1βF:	ACATCAGCACCTCACAAGCAGAG
Il1βR:	TGGGGAAGGCATTAGAAACAGTC

Intraocular Pressure (IOP)

IOP was determined as previously described (Bosco et al., 2011) with the exception of Isoflurane being used as anesthesia instead of Avertin. Briefly, mice were anesthetized using Isoflurane (2% delivered in 2 L/min oxygen) and IOP was measured using a Tonolab (Colonial Medical Supply) positioned to strike the center of the eye. Twelve measurements were collected per eye before noon, the top and bottom measurement discarded, and the remainder averaged with a SEM <0.7. By assessing mice at 3, 6, and 9 mo of age ($n = 24$, 14, and 28 eyes respectively), we confirmed that in Cx3cr1$^{gfp/gfp}$ DBA/2J mice there was no enhancement of the existent elevation in IOP documented in DBA/2J mice (Libby et al., 2005a) and iris atrophy was present (data not shown).

Statistics

Statistical analyses for each method are described in their respective sections. Normality of the data was examined both by histogram distribution and by percentage of data falling 1 and 2 standard deviations away from the mean. When data were not normally distributed, we created a macro in Excel to run a Wilcoxon rank sum test to determine whether the rank of the population means were significantly different. Kolmogorov-Smirnov test was performed by utilizing an online tool developed at St. John's University (retrieved from http://www.physics.csbsju.edu/stats/KS-test.html).

RESULTS

Loss of Cx3cr1 Exacerbates RGC Axon Dysfunction in the DBA/2J Retina

Since the FKN ligand is enriched in the ganglion cell layer of the retina in both humans and mice (Silverman et al., 2003; Zieger et al., 2014) including RGCs in the DBA/2J (Supplemental Figure 1), we reasoned that loss of FKN signaling may influence key aspects of RGC decline in glaucoma. Deficits in axonal transport progressively affect RGC axon and somal integrity in glaucoma (Soto et al., 2008; Crish et al., 2010; Dengler-Crish et al., 2014). One marker of disrupted axonal transport is the build-up of phosphorylated neurofilament (pNF; medium and heavy) proteins within the proximal axon segment, cell body, and dendrites of RGCs (Soto et al., 2008). Within the central retina of DBA/2J and Cx3cr1$^{gfp/gfp}$ DBA/2J mice at 10–11 months of age we found regions with both low and high numbers of somal pNF+ RGCs (**Figures 1A–C**), consistent with the variable levels of pathology in the DBA/2J model. We observed an overall increase in the density of somal pNF+ RGCs in Cx3cr1$^{gfp/gfp}$ DBA/2J vs. DBA/2J retinas (**Figure 1D**), with a significant shift in the distribution toward higher mean densities of somal pNF+ RGCs for Cx3cr1$^{gfp/gfp}$ DBA/2J mice than in standard DBA/2J retinas ($p < 0.05$ by Kolmogorov-Smirnov test). This resulted in a significantly increased population mean density of somal pNF+ RGCs in Cx3cr1$^{gfp/gfp}$ DBA/2J compared to the DBA/2J retinas (10.51 vs. 6.46 cells/mm^2 respectively, **Figure 1D**; $p < 0.05$ by Wilcoxon rank sum test).

Since somal accumulation of pNF suggests deficits in axonal transport, we isolated whole retina mRNA and performed quantitative RT-PCR to determine whether there is altered expression of genes involved in axon transport. Previous work has shown reduced expression of the anterograde transport motor Kif1b within sectors of DBA/2J retinas depleted of Fluorogold positive RGCs (Panagis et al., 2010). Compared to DBA/2J, we found that expression of Kif1b was significantly reduced in Cx3cr1$^{gfp/gfp}$ DBA/2J retinas (25% reduction; $n = 9$ retinas Cx3cr1$^{gfp/gfp}$ DBA/2J, $n = 8$ DBA/2J; $p < 0.05$, Student's t-test, **Figure 1E**). Loss of the phosphatidyl-serine flippase, Atp8a2, also disrupts axonal transport with an increase in RGCs with somal pNF (Zhu et al., 2012). Expression of Atp8a2 by qRT-PCR was also significantly reduced in Cx3cr1$^{gfp/gfp}$ DBA/2J vs. DBA/2J retinas (15% reduction; $n = 9$ retinas Cx3cr1$^{gfp/gfp}$ DBA/2J, $n = 8$ DBA/2J; $p < 0.05$ Student's t-test, **Figure 1E**). Thus, we find multiple lines of evidence for increased axon transport dysfunction in the DBA/2J retina with loss of fractalkine signaling.

Loss of Cx3cr1 in DBA/2J Mice Increases the Number of Early Declining RGCs

Since loss of fractalkine signaling resulted in increased numbers of somal pNF+ RGCs, we reasoned that this could be due to increased numbers of affected RGCs, impaired clearance of degenerating RGCs, or both. To determine whether the increase in pNF RGCs was due to impaired clearance we identified RGCs in earlier and later stages of degeneration. Early declining RGCs downregulate the expression of characteristic genes such as members of the Brn3 transcription factor family in response to damage (Schlamp et al., 2001; Huang et al., 2006; Buckingham et al., 2008; Soto et al., 2008). In the DBA/2J retina Brn3 downregulation precedes the clearance of the RGC soma by several weeks (Soto et al., 2008). We quantified subsets of RGCs with somal buildup of pNF with or without nuclear Brn3 expression in DBA/2J and Cx3cr1$^{gfp/gfp}$ DBA/2J retinas. In both genotypes we identified three populations of RGCs at 10–11 months: healthy RGCs that express Brn3 and lack somal pNF (Brn3+/pNF-; **Figure 2A**); early declining RGCs that express Brn3 but accumulate somal/somatodendritic pNF (Brn3+/pNF+; **Figure 2B**); and RGCs in later stages of degeneration that lose Brn3 expression and retain somal/somatodendritic pNF (Brn3-/pNF+; **Figure 2C**) before ultimately being eliminated.

Quantification of the relative cell density for these three subsets of RGCs revealed a higher proportion of Cx3cr1$^{gfp/gfp}$ DBA/2J retinas that had Brn3+/pNF+ RGCs compared to age-matched DBA/2J mice and a significant increase in the

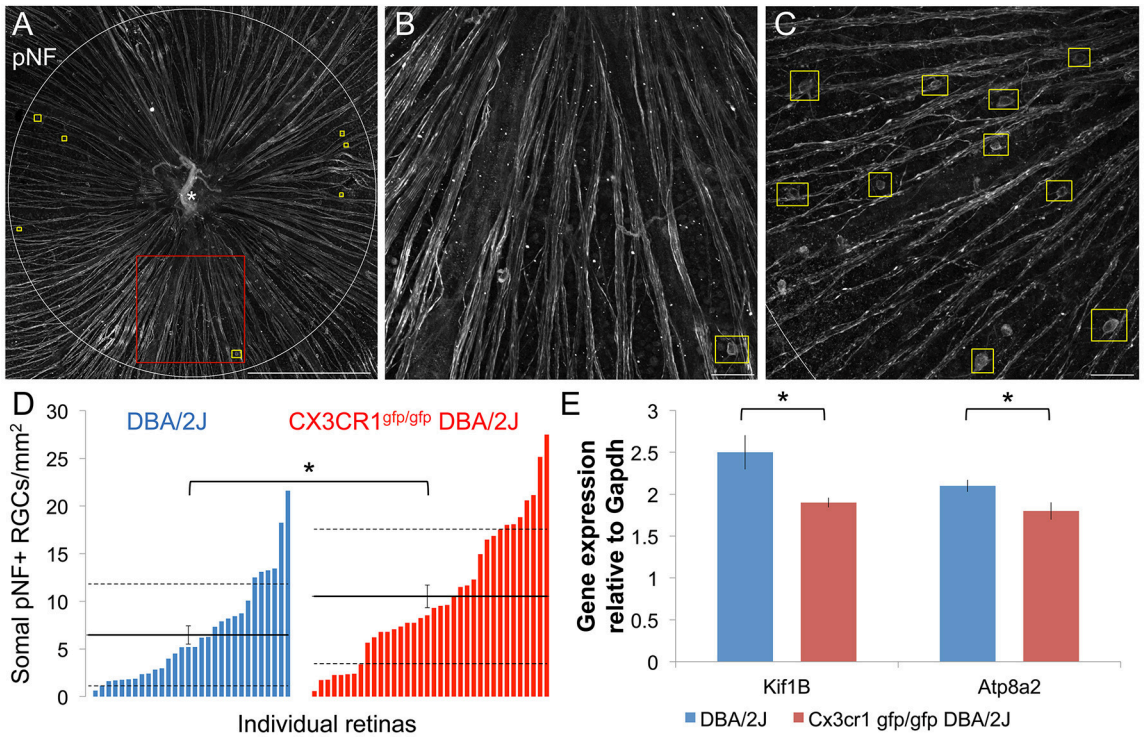

FIGURE 1 | More RGCs have somal accumulation of pNF and axonal transport genes are downregulated with loss of fractalkine signaling. (A) Confocal image of a Cx3cr1$^{gfp/gfp}$ DBA/2J retinal flat mount immunostained for phosphorylated-neurofilament (pNF), depicting the sampled central retinal area (1.77 mm^2). This retina has few somal pNF+ RGCs and smooth, fasciculated axons. Yellow boxes indicate cells that show pNF accumulated within the cell soma. **(B)** Higher magnification view of an area in A (red box), depicting a cell with accumulated somal pNF. **(C)** Higher magnification of the central retinal area from a different Cx3cr1$^{gfp/gfp}$ DBA/2J retina (same dimensions as in **B**) with abundant somal pNF+ RGCs as well as beaded and defasciculated axons. **(D)** Distribution of the number of cells with somal pNF within the central retina in DBA/2J (blue; $n = 31$ retinas) and Cx3cr1$^{gfp/gfp}$ DBA/2J (red; $n = 36$ retinas) sorted in ascending order. There are significantly more somal pNF+ cells in Cx3cr1$^{gfp/gfp}$ retinas ($^*p < 0.05$; Wilcoxon ranked sum test). Solid horizontal line indicates the population mean, dashed lines indicate 1 standard deviation above and below the mean. Error bars represent the SEM. **(E)** There is significantly less expression of axonal transport genes Kif1b and Atp8a2 in Cx3cr1$^{gfp/gfp}$ DBA/2J whole retina cDNA (25% and 15% less expression respectively, $^*p < 0.05$; Student's *t*-test; error bars represent the SEM, $n = 8$ DBA/2J retinas and 9 Cx3cr1$^{gfp/gfp}$ DBA/2J retinas). Scale bars: 500 μm **(A)**; 50 μm **(B,C)**.

mean density of Brn3+/pNF+ RGCs (1.47 vs. 1.03 cells/mm^2 respectively, **Figure 2D**; $p < 0.05$ by Wilcoxon rank sum test), demonstrating an increase in early declining RGCs in the absence of fractalkine signaling. We also measured a significant increase in the mean number of Brn3-/pNF+ RGCs in late stages of degeneration, consistent with the overall increase in pNF+ RGCs (9.02 vs. 5.43 cells/mm^2 respectively, **Figure 2E**; $p < 0.05$ by Wilcoxon rank sum test). Since there was not a selective increase in Brn3-/pNF+ RGCs, we conclude that the increased density of RGCs with somal pNF buildup is not simply a failure to clear RGCs in late stages of decline in Cx3cr1$^{gfp/gfp}$ DBA/2J retinas.

To further assess possible changes in clearance and cell death, we performed immunostaining for cleaved caspase 3, and found that none of the pNF+ cells were positive (0 out of 40 somal pNF+ RGCs, $n = 2$ retinas; Supplemental Figure 2). In addition, we observed that the nuclei of RGCs with somal pNF accumulation were not pyknotic (Supplemental Figure 3) suggesting they are not yet undergoing apoptosis. Since fractalkine has been shown to induce expression of the opsonin milk fat globule-EGF factor 8 (Mfge8), which stimulates myeloid cells to clear apoptotic neurons (Fuller and Van Eldik, 2008) we assessed levels of Mfge8 mRNA. However, we found no significant difference in Cx3cr1$^{gfp/gfp}$ DBA/2J ($n = 3$) vs. DBA/2J ($n = 3$) retinas ($p > 0.05$, Student's *t*-test; data not shown). Together, these findings suggest that loss of fractalkine signaling is amplifying the generation of dystrophic RGCs rather than impairing their clearance.

Loss of Cx3cr1 in the DBA/2J Mouse Does Not Alter Brn3-Positive RGC Numbers

To determine if loss of Cx3cr1 affected other retinal readouts of RGC compartmentalized degeneration we assessed whether loss of fractalkine signaling altered the density of cells expressing Brn3 within the ganglion cell layer (**Figure 3A**). We quantified the density of Brn3+ nuclei in eight sectors for each retina (**Figure 3A**), and found that regardless of genotype, there were regions with high and low numbers of Brn3+ nuclei (**Figures 3B–E**), consistent with sectorial downregulation of Brn3 expression in both DBA/2J and Cx3cr1$^{gfp/gfp}$ DBA/2J retinas. We then calculated average densities of Brn3+ nuclei for each retina (**Figure 3F**). There were similar maximum densities of Brn3+

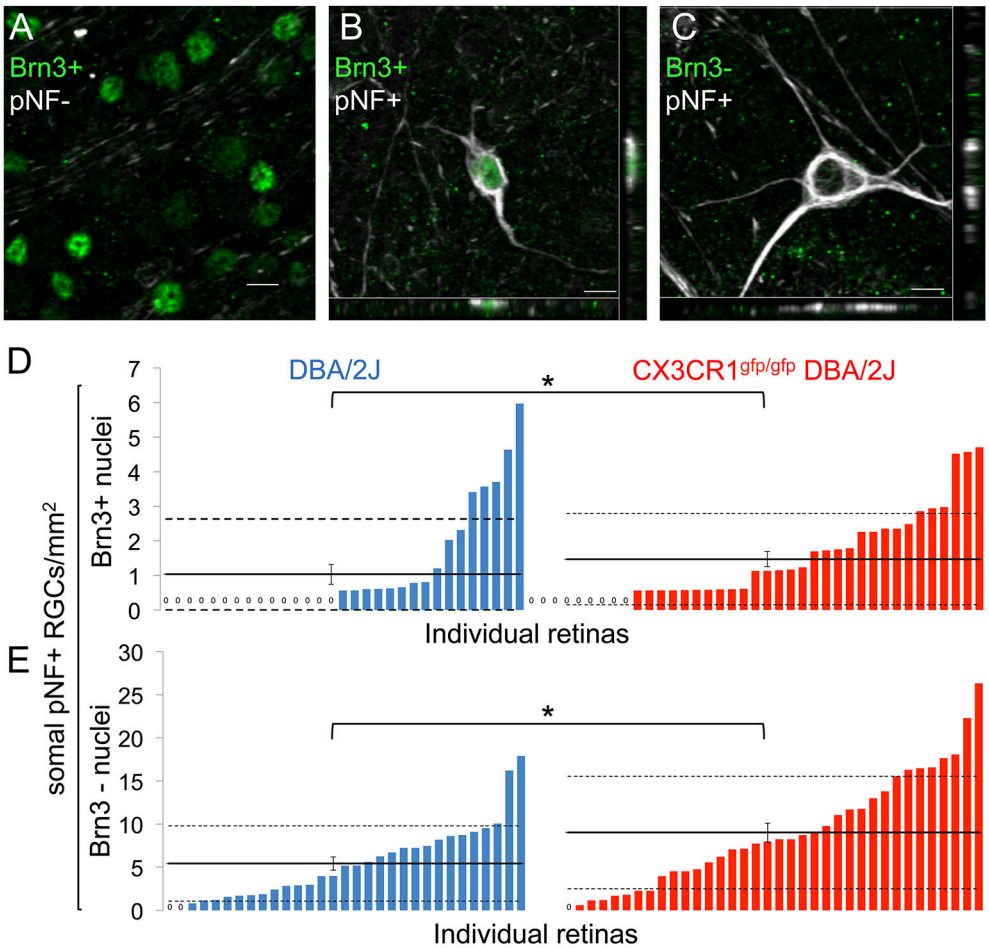

FIGURE 2 | Loss of fractalkine signaling results in increased numbers of RGCs in both early and late stages of decline. (A) Confocal image of retinal flat mount showing Brn3+ nuclei that lack accumulation of somal pNF. **(B,C)** Confocal image of cells with somal accumulation of pNF, and either expression **(B)** or absence **(C)** of Brn3. Orthogonal views in the x-y (bottom) and y-z (side) planes are shown. **(D,E)** Distribution of the density of cells that are Brn3+/somal pNF+ **(D)** or Brn3-/somal pNF+ **(E)** within the central retina in DBA/2J (blue $n = 31$ retinas) and Cx3cr1$^{gfp/gfp}$ DBA/2J (red $n = 36$ retinas) mice, sorted in ascending order. Cx3cr1$^{gfp/gfp}$ DBA/2J retinas contain significantly more Brn3+/somal pNF+ cells (**D**, $^*p < 0.05$; Wilcoxon ranked sum test) and Brn3-/somal pNF+ cells (**E**, $^*p < 0.05$; Wilcoxon ranked sum test) than DBA/2J retinas. Solid horizontal line indicates the population mean, dashed lines indicate 1 standard deviation above and below the mean. Error bars represent the SEM. Scale bars: 10 μm.

nuclei in each genotype (2400/mm^2 in DBA/2J and 2300/mm^2 in Cx3cr1$^{gfp/gfp}$ DBA/2J **Figure 3F**), and similar distribution of retinas with varying levels of Brn3 depletion (**Figure 3F**), consistent with the range of disease severity typically observed in the DBA/2J model (Buckingham et al., 2008). Likewise, the population mean densities of Brn3+ nuclei for each genotype were not significantly different (867 and 846 cells per mm^2 respectively, **Figure 3F**; $p > 0.05$ Wilcoxon rank sum test). To rule out sampling artifacts, we counted all Brn3+ nuclei within the central retina (1.77 mm^2) for a subset of retinas ($n = 6$ DBA/2J and 7 Cx3cr1$^{gfp/gfp}$ DBA/2J with similar ranges of pathology), and obtained similar results (data not shown). Therefore, we conclude that at this timepoint, loss of fractalkine signaling did not affect the characteristic downregulation of Brn3 expression in RGCs that occurs in the DBA/2J retina with age.

Loss Of Cx3cr1 in DBA/2J Mice Does Not Exacerbate Optic Nerve Degeneration

RGC degeneration in the DBA/2J model is well characterized within the optic nerve to include a progressive loss of RGC axons and a subsequent replacement by glia and extracellular matrix (John et al., 1998; Libby et al., 2005a; Schlamp et al., 2006; Lye-Barthel et al., 2013; Bosco et al., 2015a,b, 2016; Cooper et al., 2016). To determine if the potential impact on axonal transport by loss of Cx3cr1 affected optic nerve degeneration, we estimated the relative coverage of non-axonal area using segmentation of glia and extracellular matrix in nerve cross-sections (Bosco et al., 2015a,b, 2016). For both the DBA/2J and Cx3cr1$^{gfp/gfp}$ DBA/2J genotypes at 10–11 months, we observed a similar distribution of nerves with non-axonal area ranging from 10 to above 95% in individual nerves (**Figures 4A–E**). We did not observe a statistically significant difference in the mean non-axonal area

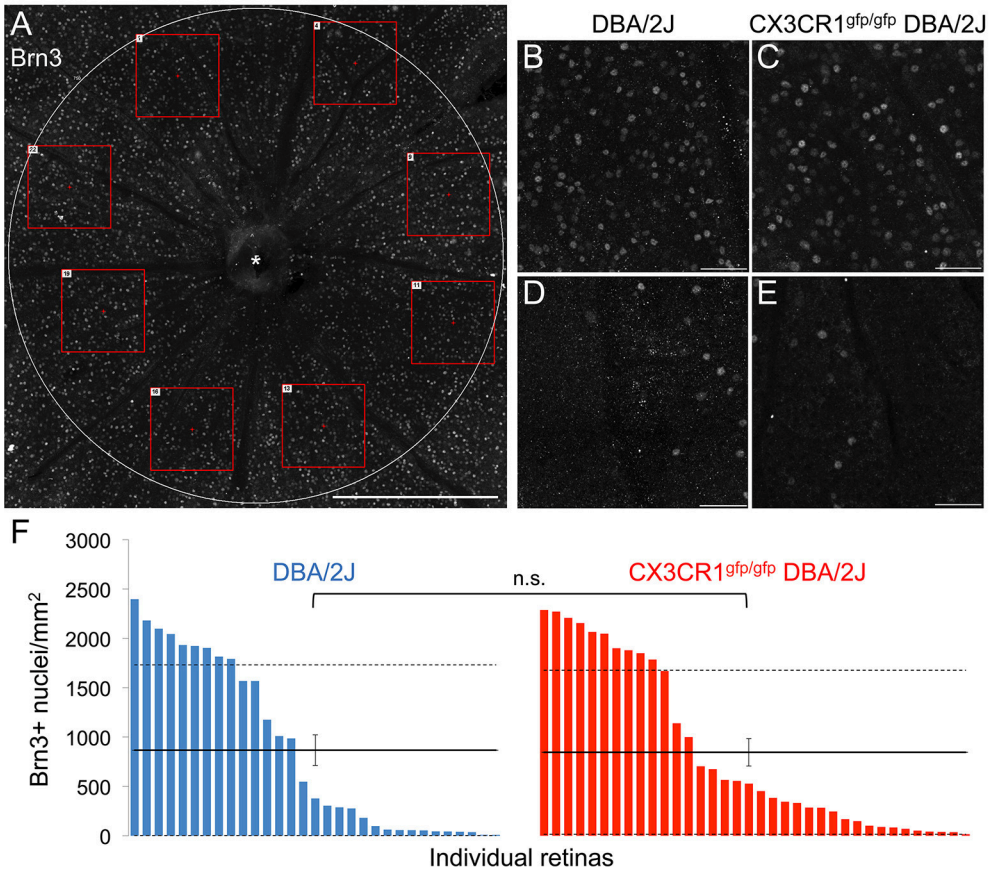

FIGURE 3 | The density of Brn3+ nuclei does not change with loss of fractalkine signaling. (A) Confocal image of a representative Cx3cr1$^{gfp/gfp}$ DBA/2J retinal flat mount showing the Brn3 immunofluorescence in the central retinal area (1.77 mm^2). Red boxes depict examples of 0.06 mm^2 fields sampled across 8 sectors. **(B–E)** Higher magnification images of 0.06 mm^2 fields (250 × 250 μm) in retinas from DBA/2J **(B,D)** or Cx3cr1$^{gfp/gfp}$ DBA/2J **(C,E)**, representative of high **(B,C)**, and low **(D,E)** Brn3+ nucleus density. **(F)** Distribution of Brn3+ nuclei densities per retina in DBA/2J (blue; $n = 31$ retinas) and Cx3cr1$^{gfp/gfp}$ DBA/2J (red; $n = 36$ retinas), sorted from high to low density. Solid horizontal lines indicate population means, dashed lines indicate 1 standard deviation above and below the mean. Error bars represent the SEM (n.s.: $p > 0.05$; Wilcoxon ranked sum test). Asterisk indicates optic nerve head. Scale bars: 500 μm **(A)**; 50 μm **(B–E)**.

for Cx3cr1$^{gfp/gfp}$ DBA/2J optic nerves as compared to DBA/2J (42 and 39% respectively; **Figure 4E**; $p > 0.05$ by Wilcoxon rank sum test). To confirm these findings, we used a qualitative scoring method (Libby et al., 2005a) on a subset of 24 nerves of each genotype, and did not find a significant difference in optic nerve degeneration between the genotypes (Chi-squared value of 0.93; data not shown). Therefore, we conclude that loss of fractalkine signaling did not alter proximal optic nerve degeneration on the DBA/2J background at this age.

Macrophage Infiltration Is Increased in Cx3cr1$^{gfp/Gfp}$ DBA/2J Retinas

Given that fractalkine signaling regulates many myeloid cell responses, including microglial activation, as well as peripheral monocyte recruitment and distribution (Cardona et al., 2006; Sennlaub et al., 2013; Wolf et al., 2013; Limatola and Ransohoff, 2014), we examined how loss of the fractalkine receptor affected myeloid cells in terms of morphology, number, distribution, and levels of the activation-associated gene, Iba1 in 10–11 month-old Cx3cr1$^{gfp/gfp}$ DBA/2J vs. DBA/2J retinas. We observed three distinct morphological subtypes of Iba1+ cells within the retina: cells with a small soma and many processes ("branched"), cells with two main processes on polar opposite sides typically outlining blood vessels ("perivascular"), and spherical cells with no processes ("amoeboid") (**Figures 5A–C**). We presume these Iba1+ cell subtypes to respectively represent resident parenchymal microglia, perivascular macrophages, and either infiltrating macrophages or highly activated resident microglia. We found no change in the density of branched Iba1+ cells (**Figure 5E**; $p > 0.05$ by Student's t-test) between Cx3cr1$^{gfp/gfp}$ DBA/2J retinas compared to DBA/2J retinas, suggesting no change in the resident microglia population. There was a trend toward an increase in the mean density of perivascular cells in Cx3cr1$^{gfp/gfp}$ DBA/2J retinas (**Figure 5F**, $p < 0.1$ by Wilcoxon rank sum test), and a significant 1.7-fold increase in the mean density of amoeboid Iba1+ cells (**Figure 5G**, $p < 0.05$ by Wilcoxon rank sum test).

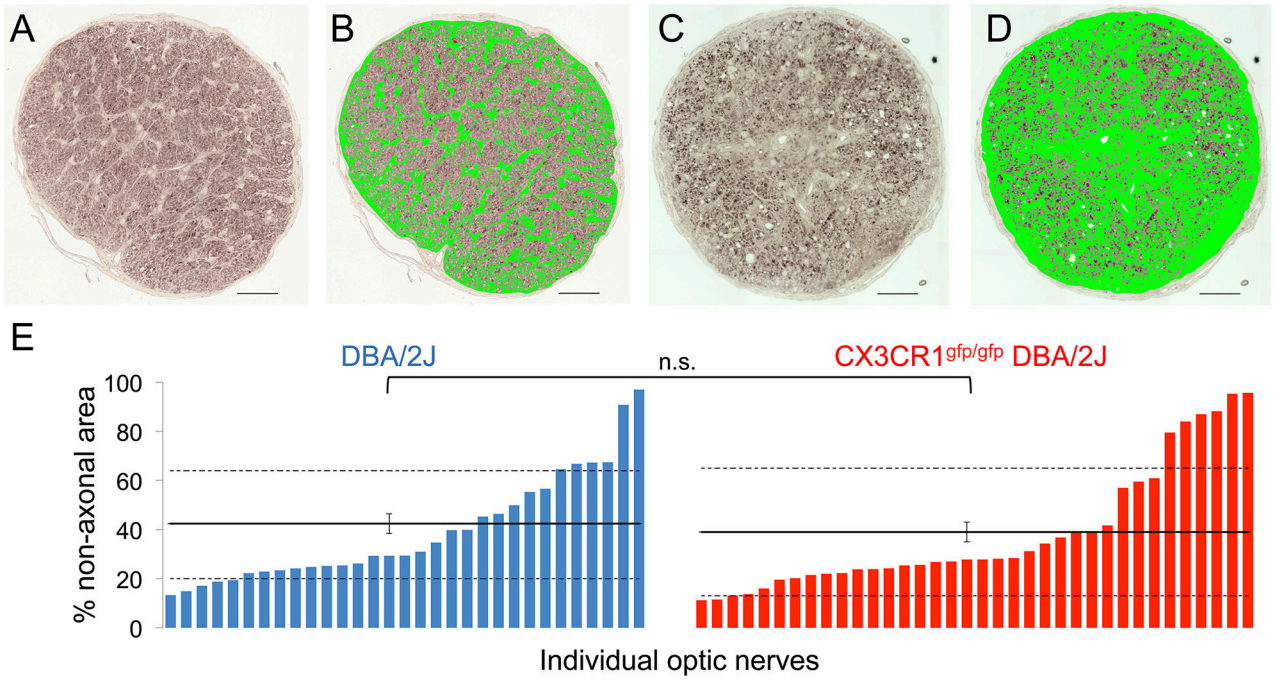

FIGURE 4 | There is no difference in the amount of gliosis and scarring in the optic nerve with loss of fractalkine signaling. (A) Low magnification micrograph of a healthy optic nerve cross section with low gliosis and few dystrophic axonal profiles used for subsequent image analysis. **(B)** The same nerve in **(A)** after threshold-based segmentation of non-axonal area, including glia, and extracellular matrix but excluding blood vessels (binary mask in green). **(C)** Low magnification micrograph of a diseased optic nerve cross section with high gliosis and many dystrophic axonal profiles used for subsequent image analysis. **(D)** The same nerve in **(C)** after segmentation of the non-axonal areas, including gliotic and scar areas (binary mask in green). **(E)** Distribution of the non-axonal area percentages per optic nerve in DBA/2J (blue, $n = 31$) and Cx3cr1$^{gfp/gfp}$ null DBA/2J (red $n = 36$) sorted in ascending order. There is no significant difference between the genotypes (n.s. $p > 0.05$; Wilcoxon ranked sum test). Horizontal lines indicate the population mean, dashed lines indicate 1 standard deviation above and below the mean. Error bars represent the SEM. Scale bars: 50 μm.

To determine whether the amoeboid Iba1+ cells were infiltrating macrophages, we first confirmed their exclusive localization to the nerve fiber layer by volumetric view of confocal image stacks (**Figure 6A**), a distribution previously reported for infiltrating macrophages in retinal injury paradigms (Garcia-Valenzuela and Sharma, 1999) and for macrophages that patrol the vitreous body (Vagaja et al., 2012). Furthermore, to positively identify these amoeboid Iba1+ cells as peripheral monocytes and not as microglia, we immunostained retinas for the peripheral macrophage marker CCR2 (Saederup et al., 2010). We determined that the amoeboid shaped Iba1+ cells stained positive for CCR2 in five whole mount DBA/2J retinas (**Figure 6B**) and in two whole mount Cx3cr1$^{gfp/gfp}$ DBA/2J retinas (**Figure 6C**), confirming their identity as peripherally derived macrophages. Consistent with this, qRT-PCR analysis showed a 3-fold increase in levels of Ccr2 expression in Cx3cr1$^{gfp/gfp}$ DBA/2J retinas ($n = 5$) vs. DBA/2J retinas ($n = 5$; $p < 0.05$; Student's t-test, **Figure 6D**). There was a concurrent 2-fold increase in levels of the ligand Ccl2 which can promote macrophage infiltration ($n = 5$ each; $p < 0.05$; Student's t-test, **Figure 6D**).

To selectively sort for myeloid cell types present in the DBA/2J retina, and further confirm an increase in peripherally-derived macrophages in the absence of fractalkine signaling, we performed flow cytometry analysis on Cx3cr1$^{gfp/gfp}$ DBA/2J ($n = 6$) and DBA/2J ($n = 8$) retinas, evaluating CD11b^{+}, CD45^{+}, CCR2 ± cells (**Figures 6E–G**). CCR2+ cells account for approximately 15% of the CD11b^{+} CD45^{+} double positive myeloid population in 12 month-old DBA/2J retinas, while they represent about 33% in age-matched Cx3cr1$^{gfp/gfp}$ DBA/2J retinas (**Figure 6H**). Thus, the CCR2+ cells, which represent peripherally-derived macrophages, are more than doubled in Cx3cr1$^{gfp/gfp}$ DBA/2J retinas, which is consistent with the observed increase in amoeboid Iba1+ cells in the retinas lacking Cx3cr1 (**Figure 5G**).

Loss of FKN Signaling Results in Selective Changes in Myeloid Cell Gene Expression

To determine how loss of fractalkine signaling in myeloid cells might impact pathways involved in RGC degeneration, we assessed changes in expression of genes associated with myeloid cell activation between Cx3cr1$^{gfp/gfp}$ DBA/2J and DBA/2J retinas. qRT-PCR analysis of whole retina RNA detected equal levels of Iba1 mRNA between the genotypes ($n = 5$ each, **Figure 5D**), suggesting no significant changes in the overall levels of myeloid

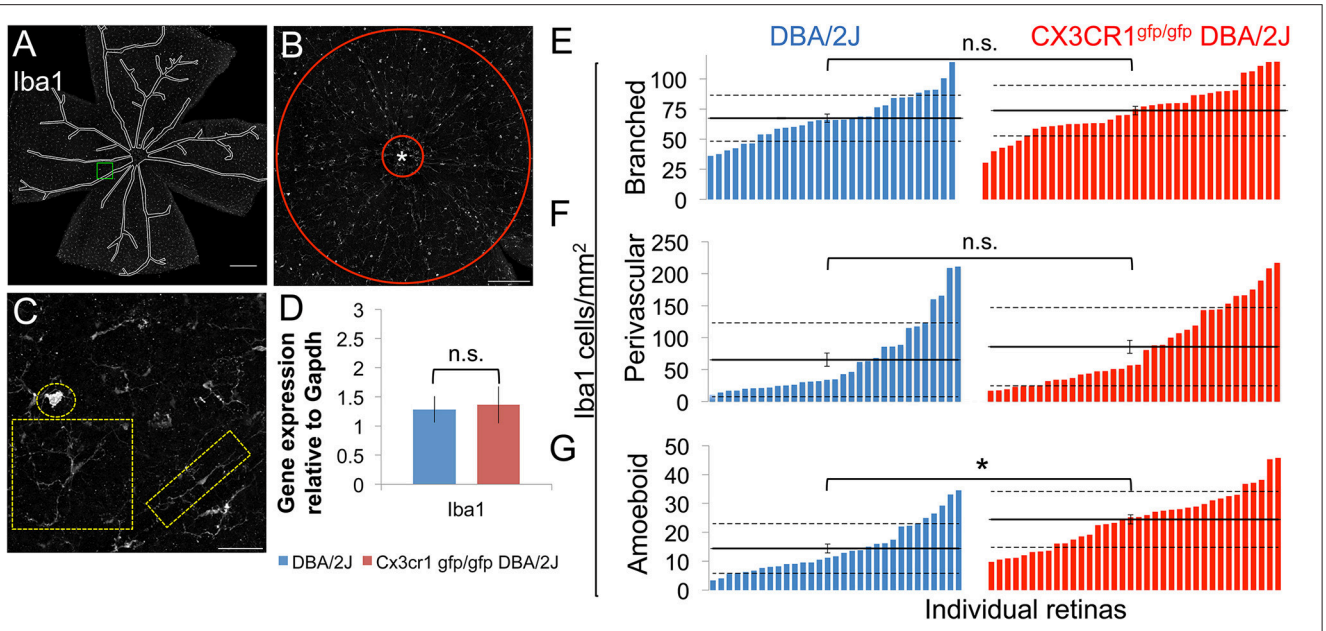

FIGURE 5 | Loss of fractalkine signaling results in greater numbers of amoeboid shaped Iba1+ cells. (A) Low magnification view of an entire retinal flat mount that was sampled for Iba1+ cells. Blood vessels (traced) were excluded from analysis. **(B)** Low magnification image of the central retina (1.77 mm^2) depicting the area sampled for branched and perivascular shaped Iba1+ cells excluding the optic nerve head (marked by an asterisk and traced by the red circle). **(C)** Higher magnification view of the area indicated in A demonstrating the 3 categories of shapes for Iba1+ cells, showing an amoeboid morphology (circle), complex branching (square), or perivascular distribution (rectangle). **(D)** There is no difference in the expression of Iba1 in Cx3CR1$^{gfp/gfp}$ DBA/2J retinas (n.s., *: $p > 0.05$; Student's *t*-test; error bars represent the SEM, 5 retinas per condition). **(E–G)**: Distribution of the number of branched **(E)**, perivascular **(F)**, and amoeboid shaped Iba1+ cells **(G)** within the central retina in DBA/2J (blue, $n = 31$) and Cx3cr1$^{gfp/gfp}$ DBA/2J (red $n = 36$) sorted in ascending order. There are significantly more amoeboid Iba1+ cells (1.7-fold *$p < 0.05$; Wilcoxon ranked sum test) in Cx3cr1$^{gfp/gfp}$ retinas. There are no statistically significant changes in the numbers of branched or perivascular Iba1+ cells (n.s. $p > 0.05$; Student's *t*-test and Wilcoxon ranked sum test respectively). Horizontal lines indicate the population mean, dashed lines indicate 1 standard deviation above and below the mean. Error bars represent the SEM. Scale bars: 500 μm **(A)**, 250 μm **(B)**, 50 μm **(C)**.

cell activation. We also assessed changes in expression of the proinflammatory gene Il1β in Cx3cr1$^{gfp/gfp}$ DBA/2J and DBA/2J retinas by qRT-PCR and found a 2.34-fold increase, but this was not significant ($n = 6$ each genotype; $p = 0.1$ by Student's *t*-test, data not shown). Since loss of Cx3cr1 has been shown to increase expression of Il1β [26, 57] we performed qRT-PCR on FACS-sorted CD11b+ CD45+ cells (**Figures 6E–G**). In contrast to whole retina mRNA levels, Il1β was reduced by 33% in myeloid cells from Cx3cr1$^{gfp/gfp}$ DBA/2J ($n = 6$) retinas vs. DBA/2J ($n = 8$) retinas, suggesting that this population is not contributing to increased expression of this gene in the DBA/2J retina.

Since reactive nitric oxide (NO) from activated microglia can induce axon transport deficits (Stagi et al., 2005), we performed qRT-PCR analysis to assess changes in the expression of Nos-2, which contributes to the production of NO. We found a 1.89-fold increase in Nos-2 expression in Cx3cr1$^{gfp/gfp}$ DBA/2J and DBA/2J whole retinas, which was not significant ($n = 6$ each genotype; $p = 0.1$ by Student's *t*-test, data not shown), but when we enriched for myeloid cells by FACS-sorting CD11b+ CD45+ cells (**Figures 6D–F**) we observed a 3-fold increase in Nos-2 in myeloid cells from Cx3cr1$^{gfp/gfp}$ DBA/2J ($n = 6$) retinas vs. DBA/2J ($n = 8$) retinas (**Figure 6I**). Thus, we find selective changes in the expression of genes in myeloid cells consistent with a role in disrupting axon transport.

DISCUSSION

Loss of Cx3cr1 Affects Compartmentalized RGC Degeneration

We found that loss of Cx3cr1 in the DBA/2J model of chronic glaucoma had a selective effect on somal accumulation of pNF in RGCs in 10–11 month-old mice, suggesting deficits in axonal transport. These effects were uncoupled from other RGC degenerative changes, including loss of Brn3 gene transcription or optic nerve histopathology. We also observed increased infiltration of CCR2+ peripheral macrophages, but no change in myeloid cell activation overall, since resident microglia were not altered in density, or morphology, and overall levels of Iba1 mRNA were unaffected. Our findings suggest that distinct mechanisms may contribute to different aspects of RGC decline in glaucoma, with axonal transport selectively altered after loss of Cx3cr1 in myeloid cells such as microglia and macrophages.

Loss of Cx3cr1 Enhances Axon Transport Deficits in RGC Neurodegeneration

We observed that loss of Cx3cr1 resulted in enhanced somal accumulation of pNF, as well as reduced expression of the anterograde transport motor Kif1b, consistent with exacerbation of axonal transport deficits. There is a correlate in humans

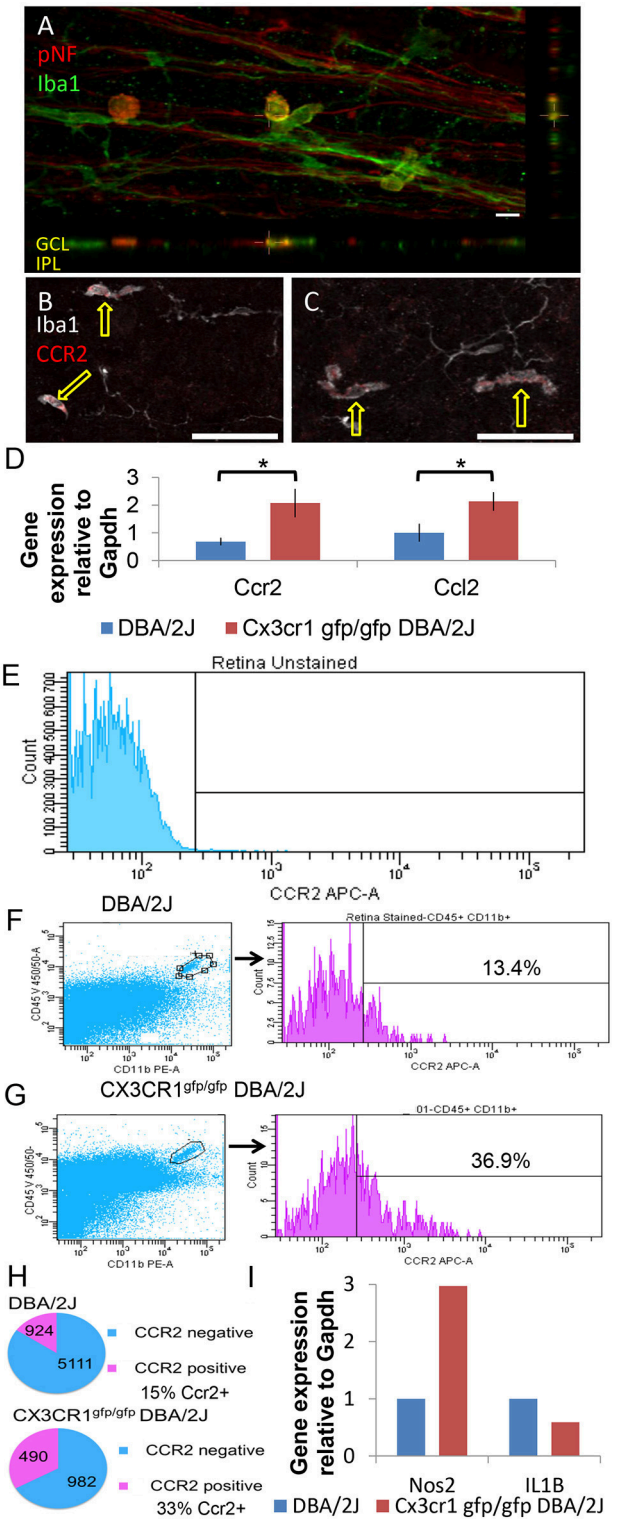

FIGURE 6 | Amoeboid Iba1+ cells are peripherally derived macrophages. (A) Amoeboid Iba1+ cells localize to the neurofibrillary layer. Volume view of a DBA/2J retinal whole mount stained for the axonal marker pNF (red) and the microglia/macrophage marker Iba1 (green). Orthogonal views shown below and to the right. Amoeboid Iba1+ cells showed

(Continued)

FIGURE 6 | Continued

non-specific reactivity with the donkey anti-mouse secondary antibody used to detect pNF (not shown). **(B)** Single z-plane (0.8 μm) from a control DBA/2J retinal whole mount immunostained for the peripheral macrophage marker Ccr2 (red) and Iba1 (white). The amoeboid shaped Iba1+ cells are positive for Ccr2 (arrows) while branched Iba1+ cells are negative. **(C)** Single z-plane (0.8 μm) from a $Cx3cr1^{gfp/gfp}$ DBA/2J retina immunostained for the peripheral macrophage marker Ccr2 (red) and Iba1 (white). As in **(B)** the amoeboid shaped Iba1+ cells are positive for Ccr2 (arrows) while branched Iba1+ cells are negative. **(D)** There is significantly more expression of Ccr2 and Ccl2 in $Cx3cr1^{gfp/gfp}$ DBA/2J whole retina cDNA (3 and 2-fold more expression respectively, $^*p < 0.05$; Student's *t*-test; error bars represent the SEM, 5 retinas per condition). **(E)** Gating parameters were set by dissociated retinal cells not exposed to antibodies. 56,935 viable cells collected. **(F)** Left, representative plot of DBA/2J assessing $CD45^+$ $CD11b^+$ (gate shown) from 129,000 to 200,000 viable cells. Right, histograms and percent $CCR2^+$ of gated $CD45^+CD11b^+$ population. **(G)** Left, representative plots of $Cx3cr1^{gfp/gfp}$ DBA/2J assessing $CD45^+$ $CD11b^+$ (gate shown) from 129,000 to 200,000 viable cells as in F. Right, histograms and percent $CCR2^+$ of gated $CD45^+CD11b^+$ population. **(H)** Top, total number and percent of $CCR2^+$ and $CCR2^-$ of all $CD45^+CD11b^+$ cells analyzed by flow cytometry in DBA/2J $n = 8$ pooled retinas (293,780 cells collected). Bottom, total number and percent of $CCR2^+$ and $CCR2^-$ of all $CD45^+CD11b^+$ cells analyzed by flow cytometry in $Cx3cr1^{gfp/gfp}$ DBA/2J $n = 6$ pooled retinas (453,727 cells collected). **(I)**: There is ~3-fold more expression of Nos2 but 33% less expression of IL1β in FACS sorted myeloid cells ($n = 8$ DBA/2J pooled retinas and $n = 6$ $CX3CR1^{gfp/gfp}$ DBA/2J pooled retinas). Scale bars: 50 μm **(B,C)** 10 μm **(A)**.

where mutations in KIF1A affect axonal transport and can lead to progressive neurodegeneration, including optic atrophy (Okamoto et al., 2014). Decline in axonal transport is an early and prevalent feature of many forms of neurodegeneration, including glaucoma, generally preceding signs of structural axon degeneration (Pease et al., 2000; Quigley et al., 2000; De Vos et al., 2008; Soto et al., 2008; Crish et al., 2010, 2013; Chidlow et al., 2011; Millecamps and Julien, 2013; Dengler-Crish et al., 2014). Our findings are consistent with previous studies showing that neuroinflammation, including microglia activation and oxidative stress, is a contributing factor to early axon transport dysfunction (Takeuchi et al., 2005). In an animal model of multiple sclerosis, which is characterized by significant neuroinflammation, axon transport deficits were found to be an early state of axonal dysfunction. These deficits preceded structural changes to axons and could be reversed by anti-inflammatory as well as anti-oxidant treatment (Sorbara et al., 2014).

We observed increased expression of Nos-2 in retinal DBA/2J myeloid cells lacking Cx3cr1. Reactive nitric oxide (NO) from microglia can focally induce axon transport deficits *in vitro* (Stagi et al., 2005), and promote axonal damage *in vivo* (Nikic et al., 2011). Nos-2 is not required for RGC death and axon degeneration in DBA/2J mice (Libby et al., 2007), but effects on axon transport have not been assessed. Therefore, it is possible that there is a selective role for this pathway in this aspect of neuronal decline, consistent with our findings. Notably, alleviating oxidative stress in the DBA/2J model with alpha-lipoic acid treatment results in improved axonal transport (Inman et al., 2013).

Optic Nerve Degeneration and Brn3 Downregulation Are Not Affected by Loss of Cx3cr1

While we observed an increase in somal accumulation of pNF, there was no change in structural degeneration of the optic nerve in Cx3cr1$^{gfp/gfp}$ DBA/2J mice relative to DBA/2J mice. This may be due to the fact that structural decline of axons can lag changes in transport, as shown in a model of multiple sclerosis (Sorbara et al., 2014). Consistent with this, there is structural persistence in the optic pathway well after axon transport failure in an ocular hypertension model of glaucoma (Crish et al., 2010; Crish and Calkins, 2011). Notably, in glaucoma patients, functional decline of RGCs as measured by pattern electroretinography (PERG) significantly precedes structural changes, such as loss of nerve fiber layer thickness (Banitt et al., 2013), and in animal models reduced PERG amplitude can result from blockade of axon transport (Chou et al., 2013). Alternatively, structural degeneration of axons may be independently regulated, for example by calpain-dependent cleavage of cytoskeletal components (Crish and Calkins, 2011; Wang et al., 2012).

Interestingly, there are other instances of somal accumulation of pNF in RGCs being uncoupled from optic nerve degeneration. The wabbler-lethal mutant mouse has a loss of function mutation in the phosphatidyl-serine flippase, Atp8a2 that is involved in apoptosis and vesicle trafficking (Zhu et al., 2012; van der Mark et al., 2013). This mutant mouse shows disrupted axonal transport with an increase in RGCs with somal pNF, without observed increased damage to the optic nerve (Zhu et al., 2012). Since we found a significant reduction in expression of Atp8a2 in Cx3cr1$^{gfp/gfp}$ DBA/2J vs. DBA/2J retinas, it is possible that loss of this pathway may be in part responsible for mediating the reduced RGC axonal transport phenotype. These results raise the question of whether exoplasmic-facing phosphatidyl-serine signaling to receptors on microglia or macrophages affects RGC degeneration, or if a cell autonomous role in membrane fluidity affects axonal transport.

In our study, Brn3 downregulation was also similar in both Cx3cr1$^{gfp/gfp}$ DBA/2J and DBA/2J retinas. This suggests the density of RGCs was not significantly different with loss of Cx3cr1, and that Cx3cr1 signaling does not influence this early aspect of RGC degeneration. Thus, different aspects of RGC decline may occur at different rates or be regulated by distinct mechanisms. Consistent with this, deficiency in the dual leucine kinase (Dlk) signaling pathway alters somal but not axonal RGC degeneration (Fernandes et al., 2014). In contrast to our findings, significant reductions in beta tubulin III labeled RGCs were observed in a transient ocular hypertension model of glaucoma in Cx3cr1$^{gfp/gfp}$ C57Bl6/J mice (Wang et al., 2014). Thus, it is possible that Cx3cr1 signaling has different effects in an acute injury vs. chronic model of RGC degeneration. Overall, our findings suggest that loss of fractalkine signaling selectively affects axon transport, providing evidence that distinct pathways mediate specific aspects of compartmentalized neurodegeneration.

Loss of Cx3cr1 Does Not Alter Microglial Activation

FKN signaling has been found to be a brake on microglial activation in many models of neurodegeneration (Cardona et al., 2006; Wolf et al., 2013; Limatola and Ransohoff, 2014). However, we found that the activation of the presumed resident microglia (branched, parenchymal Iba1+ cells) remained unchanged in terms of morphology and Iba1 mRNA levels with loss of Cx3cr1. A similar lack of change in microglia activation in Cx3cr1 knockouts was also observed in other disease models, such as prion-infected mice (Striebel et al., 2016). Activated microglia can secrete pro-inflammatory cytokines like Il1β (Patterson, 2015), and loss of Cx3cr1 has been shown to elevate levels of the pro-inflammatory cytokine Il1β (Cardona et al., 2006) In diabetic retinopathy, only a few genes associated with inflammation are significantly upregulated in Cx3cr1 knockout retina, including Il1β (Cardona et al., 2015). However, while we found that Nos2 was upregulated, as discussed above, we did not observe a significant increase in Il1β with loss of Cx3cr1 in the DBA/2J retina or in sorted myeloid cells including microglia. Thus, we conclude that overall levels of myeloid cell activation were not altered by loss of Cx3cr1 in this model, but that specific genes and pathways may be affected.

Other aspects of microglia function may also be affected by loss of Cx3cr1. For example, Cx3cr1 null microglia have been noted to more slowly remodel their processes (Liang et al., 2009), suggesting functional impairment. Whether this occurs in our model remains unclear. We also observed a perivascular population of Iba1+ cells that frequently lined up along axons (**Figure 6A**) in a manner reminiscent of that seen by CD11c+ dendritic cells in the optic nerve crush model of axonal injury (Lehmann et al., 2010; Heuss et al., 2014). Whether these cells represent a second niche of dendritic cells in the retina (Heuss et al., 2014) or a subpopulation of microglia (Dando et al., 2016) is unclear, but the proximity to RGC axons and retinal vessels suggest these cells would be a fruitful target in glaucoma research.

Loss of Cx3cr1 Promotes Enhanced Macrophage Infiltration

While we did not observe obvious changes in microglia activation, loss of Cx3cr1 clearly resulted in enhanced Ccr2+ monocyte/macrophage infiltration. Consistent with this, we also found increased levels of expression of the ligand for Ccr2, Ccl2, which can promote infiltration (Sennlaub et al., 2013). Ccl2 was also found to be increased in brains from prion-infected Cx3cr1 knockout vs. wild type C57Bl6/J mice (Striebel et al., 2016). Increased CCR2+ macrophage infiltration on a Cx3cr1 null background is consistent with what has been observed in age and light damage models of subretinal inflammation that clearly showed a pathogenic role for these infiltrating macrophages (Sennlaub et al., 2013). However, since macrophages have been implicated in RGC regeneration (Cui et al., 2009; Yin et al., 2009), it is unclear whether their role in RGC compartmentalized degeneration is beneficial or detrimental. However, the increase

in Ccr2+ macrophages in Cx3cr1$^{gfp/gfp}$ DBA/2J retinas makes them a candidate for impacting axonal transport in RGCs since the numbers of resident microglia and perivascular macrophages were unchanged between the genotypes. Since differences do exist between the DBA/2J and acute models of IOP elevation, such as microbead injection (Sappington et al., 2010) or injection of hypertonic saline into episcleral veins (Morrison et al., 2011; Johnson et al., 2014) it may prove fruitful to evaluate the role of microglia and macrophages in these models.

Overall, our findings indicate that loss of Cx3cr1 increased the infiltration of CCR2+ macrophages into the DBA/2J retina, and selectively increased axonal transport dysfunction in this mouse model of chronic glaucoma, potentially driven by increased Nos2 expression in Cx3cr1-null myeloid cells. Thus, alterations in myeloid function may contribute to the impaired axonal transport seen early in many neurodegenerative diseases (Millecamps and Julien, 2013).

AUTHOR CONTRIBUTIONS

MV, AB, and KB conceived the study and participated in its design and coordination. KB, MS, SA, and DC performed experiments and acquired data. KB and SA performed the analysis, and KB, SA, AB, and MV interpreted the data. KB and MV wrote the manuscript. All authors read and approved the final manuscript.

FUNDING

This work was supported by National Institutes of Health grants 1R01EY023621 and 1R01EY020878 to MV, and grants from the Glaucoma Research Foundation, and Melza M. and Frank Theodore Barr Foundation to MV and DC.

ACKNOWLEDGMENTS

We thank Dr. Samuel Crish for his ImageJ macro used to quantify cholera toxin B signal in the superior colliculus. We thank Cesar Romero for technical assistance, Kathryn Moore for comments on the manuscript, and thank Drs. Scott Rogers and Lorise Gahring for assistance with flow cytometry. Some of the data herein appear in an online archived thesis (Breen, 2015) published by ProQuest.

SUPPLEMENTARY MATERIAL

The Supplementary Material for this article can be found online at: http://journal.frontiersin.org/article/10.3389/fnins.2016.00526/full#supplementary-material

REFERENCES

Anderson, M. G., Nair, K. S., Amonoo, L. A., Mehalow, A., Trantow, C. M., Masli, S., et al. (2008). GpnmbR150X allele must be present in bone marrow derived cells to mediate DBA/2J glaucoma. *BMC Genet.* 9:30. doi: 10.1186/1471-2156-9-30

Anderson, M. G., Smith, R. S., Hawes, N. L., Zabaleta, A., Chang, B., Wiggs, J. L., et al. (2002). Mutations in genes encoding melanosomal proteins cause pigmentary glaucoma in DBA/2J mice. *Nat. Genet.* 30, 81–85. doi: 10.1038/ng794

Banitt, M. R., Ventura, L. M., Feuer, W. J., Savatovsky, E., Luna, G., Shif, O., et al. (2013). Progressive loss of retinal ganglion cell function precedes structural loss by several years in glaucoma suspects. *Invest. Ophthalmol. Vis. Sci.* 54, 2346–2352. doi: 10.1167/iovs.12-11026

Bosco, A., Breen, K. T., Anderson, S. R., Steele, M. R., Calkins, D. J., and Vetter, M. L. (2016). Glial coverage in the optic nerve expands in proportion to optic axon loss in chronic mouse glaucoma. *Exp. Eye Res.* 150, 34–43. doi: 10.1016/j.exer.2016.01.014

Bosco, A., Crish, S. D., Steele, M. R., Romero, C. O., Inman, D. M., Horner, P. J., et al. (2012). Early reduction of microglia activation by irradiation in a model of chronic glaucoma. *PLoS ONE* 7:e43602. doi: 10.1371/journal.pone.0043602

Bosco, A., Romero, C. O., Ambati, B. K., and Vetter, M. L. (2015a). *In vivo* dynamics of retinal microglial activation during neurodegeneration: confocal ophthalmoscopic imaging and cell morphometry in mouse glaucoma. *J. Vis. Exp.* 11:e52731. doi: 10.3791/52731

Bosco, A., Romero, C. O., Breen, K. T., Chagovetz, A. A., Steele, M. R., Ambati, B. K., et al. (2015b). Neurodegeneration severity can be predicted from early microglia alterations monitored *in vivo* in a mouse model of chronic glaucoma. *Dis. Model. Mech.* 8, 443–455. doi: 10.1242/dmm.018788

Bosco, A., Steele, M. R., and Vetter, M. L. (2011). Early microglia activation in a mouse model of chronic glaucoma. *J. Comp. Neurol.* 519, 599–620. doi: 10.1002/cne.22516

Breen, K. (2015). *Describing the Roles of Myeloid Cells in the Compartmental Degeneration of Retinal Ganglion Cells in the Neurodegenerative Disease Glaucoma*. Dissertation thesis. Salt Lake City (UT): University of Utah.

Buckingham, B. P., Inman, D. M., Lambert, W., Oglesby, E., Calkins, D. J., Steele, M. R., et al. (2008). Progressive ganglion cell degeneration precedes neuronal loss in a mouse model of glaucoma. *J. Neurosci.* 28, 2735–2744. doi: 10.1523/JNEUROSCI.4443-07.2008

Calkins, D. J. (2012). Critical pathogenic events underlying progression of neurodegeneration in glaucoma. *Prog. Retin. Eye Res.* 31, 702–719. doi: 10.1016/j.preteyeres.2012.07.001

Cardona, A. E., Pioro, E. P., Sasse, M. E., Kostenko, V., Cardona, S. M., Dijkstra, I. M., et al. (2006). Control of microglial neurotoxicity by the fractalkine receptor. *Nat. Neurosci.* 9, 917–924. doi: 10.1038/nn1715

Cardona, S. M., Mendiola, A. S., Yang, Y.-C., Adkins, S. L., Torres, V., and Cardona, A. E. (2015). Disruption of fractalkine signaling leads to microglial activation and neuronal damage in the diabetic retina. *ASN Neuro* 7:1759091415608204. doi: 10.1177/1759091415608204

Chidlow, G., Ebneter, A., Wood, J. P., and Casson, R. J. (2011). The optic nerve head is the site of axonal transport disruption, axonal cytoskeleton damage and putative axonal regeneration failure in a rat model of glaucoma. *Acta Neuropathol.* 121, 737–751. doi: 10.1007/s00401-011-0807-1

Chong, R. S., and Martin, K. R. (2015). Glial cell interactions and glaucoma. *Curr. Opin. Ophthalmol.* 26, 73–77. doi: 10.1097/ICU.0000000000000125

Chou, T. H., Park, K. K., Luo, X., and Porciatti, V. (2013). Retrograde signaling in the optic nerve is necessary for electrical responsiveness of retinal ganglion cells. *Invest. Ophthalmol. Vis. Sci.* 54, 1236–1243. doi: 10.1167/iovs.12-11188

Conforti, L., Adalbert, R., and Coleman, M. P. (2007). Neuronal death: where does the end begin? *Trends Neurosci.* 30, 159–166. doi: 10.1016/j.tins.2007.02.004

Cook, D. N., Chen, S. C., Sullivan, L. M., Manfra, D. J., Wiekowski, M. T., Prosser, D. M., et al. (2001). Generation and analysis of mice lacking the chemokine fractalkine. *Mol. Cell. Biol.* 21, 3159–3165. doi: 10.1128/MCB.21.9.3159-3165.2001

Cooper, M. L., Crish, S. D., Inman, D. M., Horner, P. J., and Calkins, D. J. (2016). Early astrocyte redistribution in the optic nerve precedes axonopathy in the DBA/2J mouse model of glaucoma. *Exp. Eye Res.* 150, 22–33. doi: 10.1016/j.exer.2015.11.016

Crish, S. D., and Calkins, D. J. (2011). Neurodegeneration in glaucoma: progression and calcium-dependent intracellular mechanisms. *Neuroscience* 176, 1–11. doi: 10.1016/j.neuroscience.2010.12.036

Crish, S. D., Dapper, J. D., MacNamee, S. E., Balaram, P., Sidorova, T. N., Lambert, W. S., et al. (2013). Failure of axonal transport induces a spatially coincident increase in astrocyte BDNF prior to synapse loss in a central target. *Neuroscience* 229, 55–70. doi: 10.1016/j.neuroscience.2012.10.069

Crish, S. D., Sappington, R. M., Inman, D. M., Horner, P. J., and Calkins, D. J. (2010). Distal axonopathy with structural persistence in glaucomatous neurodegeneration. *Proc. Natl. Acad. Sci. U.S.A.* 107, 5196–5201. doi: 10.1073/pnas.0913141107

Cui, Q., Yin, Y., and Benowitz, L. I. (2009). The role of macrophages in optic nerve regeneration. *Neuroscience* 158, 1039–1048. doi: 10.1016/j.neuroscience.2008.07.036

Czeh, M., Gressens, P., and Kaindl, A. M. (2011). The yin and yang of microglia. *Dev. Neurosci.* 33, 199–209. doi: 10.1159/000328989

Dando, S. J., Naranjo Golborne, C., Chinnery, H. R., Ruitenberg, M. J., and McMenamin, P. G. (2016). A case of mistaken identity: CD11c-eYFP(+) cells in the normal mouse brain parenchyma and neural retina display the phenotype of microglia, not dendritic cells. *Glia* 64, 1331–1349. doi: 10.1002/glia.23005

Dengler-Crish, C. M., Smith, M. A., Inman, D. M., Wilson, G. N., Young, J. W., and Crish, S. D. (2014). Anterograde transport blockade precedes deficits in retrograde transport in the visual projection of the DBA/2J mouse model of glaucoma. *Front. Neurosci.* 8:290. doi: 10.3389/fnins.2014.00290

De Vos, K. J., Grierson, A. J., Ackerley, S., and Miller, C. C. (2008). Role of axonal transport in neurodegenerative diseases. *Annu. Rev. Neurosci.* 31, 151–173. doi: 10.1146/annurev.neuro.31.061307.090711

Fernandes, K. A., Harder, J. M., John, S. W., Shrager, P., and Libby, R. T. (2014). DLK-dependent signaling is important for somal but not axonal degeneration of retinal ganglion cells following axonal injury. *Neurobiol. Dis.* 69, 108–116. doi: 10.1016/j.nbd.2014.05.015

Fuller, A. D., and Van Eldik, L. J. (2008). MFG-E8 regulates microglial phagocytosis of apoptotic neurons. *J. Neuroimmune Pharmacol.* 3, 246–256. doi: 10.1007/s11481-008-9118-2

Garcia-Valenzuela, E., and Sharma, S. C. (1999). Laminar restriction of retinal macrophagic response to optic nerve axotomy in the rat. *J. Neurobiol.* 40, 55–66.

Heuss, N. D., Pierson, M. J., Montaniel, K. R., McPherson, S. W., Lehmann, U., Hussong, S. A., et al. (2014). Retinal dendritic cell recruitment, but not function, was inhibited in MyD88 and TRIF deficient mice. *J. Neuroinflammation* 11:143. doi: 10.1186/s12974-014-0143-1

Hoarau, J. J., Krejbich-Trotot, P., Jaffar-Bandjee, M. C., Das, T., Thon-Hon, G. V., Kumar, S., et al. (2011). Activation and control of CNS innate immune responses in health and diseases: a balancing act finely tuned by neuroimmune regulators (NIReg). *CNS Neurol. Disord. Drug Targets* 10, 25–43. doi: 10.2174/187152711794488601

Howell, G. R., Libby, R. T., Jakobs, T. C., Smith, R. S., Phalan, F. C., Barter, J. W., et al. (2007). Axons of retinal ganglion cells are insulted in the optic nerve early in DBA/2J glaucoma. *J. Cell Biol.* 179, 1523–1537. doi: 10.1083/jcb.200706181

Howell, G. R., Soto, I., Zhu, X., Ryan, M., Macalinao, D. G., Sousa, G. L., et al. (2012). Radiation treatment inhibits monocyte entry into the optic nerve head and prevents neuronal damage in a mouse model of glaucoma. *J. Clin. Invest.* 122, 1246–1261. doi: 10.1172/JCI61135

Huang, W., Fileta, J., Guo, Y., and Grosskreutz, C. L. (2006). Downregulation of Thy1 in retinal ganglion cells in experimental glaucoma. *Curr. Eye Res.* 31, 265–271. doi: 10.1080/02713680500545671

Ilieva, H., Polymenidou, M., and Cleveland, D. W. (2009). Non-cell autonomous toxicity in neurodegenerative disorders: ALS and beyond. *J. Cell Biol.* 187, 761–772. doi: 10.1083/jcb.200908164

Inman, D. M., and Horner, P. J. (2007). Reactive nonproliferative gliosis predominates in a chronic mouse model of glaucoma. *Glia* 55, 942–953. doi: 10.1002/glia.20516

Inman, D. M., Lambert, W. S., Calkins, D. J., and Horner, P. J. (2013). alpha-Lipoic acid antioxidant treatment limits glaucoma-related retinal ganglion cell death and dysfunction. *PLoS ONE* 8:e65389. doi: 10.1371/journal.pone.0065389

Jakobs, T. C., Libby, R. T., Ben, Y., John, S. W., and Masland, R. H. (2005). Retinal ganglion cell degeneration is topological but not cell type specific in DBA/2J mice. *J. Cell Biol.* 171, 313–325. doi: 10.1083/jcb.200506099

John, S. W., Smith, R. S., Savinova, O. V., Hawes, N. L., Chang, B., Turnbull, D., et al. (1998). Essential iris atrophy, pigment dispersion, and glaucoma in DBA/2J mice. *Invest. Ophthalmol. Vis. Sci.* 39, 951–962.

Johnson, E. C., Cepuma, W. O., Choi, D., and Morrison, J. C. (2014). Radiation pretreatment does not protect the rat optic nerve from elevated intraocular pressure-induced injury. *Invest. Ophthalmol. Vis. Sci.* 56, 412–419. doi: 10.1167/iovs.14-15094

Jung, S., Aliberti, J., Graemmel, P., Sunshine, M. J., Kreutzberg, G. W., Sher, A., et al. (2000). Analysis of fractalkine receptor CX(3)CR1 function by targeted deletion and green fluorescent protein reporter gene insertion. *Mol. Cell. Biol.* 20, 4106–4114. doi: 10.1128/MCB.20.11.4106-4114.2000

Karlstetter, M., Scholz, R., Rutar, M., Wong, W. T., Provis, J. M., and Langmann, T. (2015). Retinal microglia: just bystander or target for therapy? *Prog. Retin. Eye Res.* 45, 30–57. doi: 10.1016/j.preteyeres.2014.11.004

Landsman, L., Bar-On, L., Zernecke, A., Kim, K. W., Krauthgamer, R., Shagdarsuren, E., et al. (2009). CX3CR1 is required for monocyte homeostasis and atherogenesis by promoting cell survival. *Blood* 113, 963–972. doi: 10.1182/blood-2008-07-170787

Lee, J. E., Liang, K. J., Fariss, R. N., and Wong, W. T. (2008). *Ex vivo* dynamic imaging of retinal microglia using time-lapse confocal microscopy. *Invest. Ophthalmol. Vis. Sci.* 49, 4169–4176. doi: 10.1167/iovs.08-2076

Lee, S., Xu, G., Jay, T. R., Bhatta, S., Kim, K. W., Jung, S., et al. (2014). Opposing effects of membrane-anchored CX3CL1 on amyloid and tau pathologies via the p38 MAPK pathway. *J. Neurosci.* 34, 12538–12546. doi: 10.1523/JNEUROSCI.0853-14.2014

Lehmann, U., Heuss, N. D., McPherson, S. W., Roehrich, H., and Gregerson, D. S. (2010). Dendritic cells are early responders to retinal injury. *Neurobiol. Dis.* 40, 177–184. doi: 10.1016/j.nbd.2010.05.022

Liang, K. J., Lee, J. E., Wang, Y. D., Ma, W., Fontainhas, A. M., Fariss, R. N., et al. (2009). Regulation of dynamic behavior of retinal microglia by CX3CR1 signaling. *Invest. Ophthalmol. Vis. Sci.* 50, 4444–4451. doi: 10.1167/iovs.08-3357

Libby, R. T., Anderson, M. G., Pang, I. H., Robinson, Z. H., Savinova, O. V., Cosma, I. M., et al. (2005a). Inherited glaucoma in DBA/2J mice: pertinent disease features for studying the neurodegeneration. *Vis. Neurosci.* 22, 637–648. doi: 10.1017/S0952523805225130

Libby, R. T., Howell, G. R., Pang, I. H., Savinova, O. V., Mehalow, A. K., Barter, J. W., et al. (2007). Inducible nitric oxide synthase, Nos2, does not mediate optic neuropathy and retinopathy in the DBA/2J glaucoma model. *BMC Neurosci.* 8:108. doi: 10.1186/1471-2202-8-108

Libby, R. T., Li, Y., Savinova, O. V., Barter, J., Smith, R. S., Nickells, R. W., et al. (2005b). Susceptibility to neurodegeneration in a glaucoma is modified by Bax gene dosage. *PLoS Genet.* 1, 17–26. doi: 10.1371/journal.pgen.0010004

Limatola, C., and Ransohoff, R. M. (2014). Modulating neurotoxicity through CX3CL1/CX3CR1 signaling. *Front. Cell. Neurosci.* 8:229. doi: 10.3389/fncel.2014.00229

Livak, K. J., and Schmittgen, T. D. (2001). Analysis of relative gene expression data using real-time quantitative PCR and the 2(-Delta Delta C(T)) Method. *Methods* 25, 402–408. doi: 10.1006/meth.2001.1262

Lye-Barthel, M., Sun, D., and Jakobs, T. C. (2013). Morphology of astrocytes in a glaucomatous optic nerve. *Invest. Ophthalmol. Vis. Sci.* 54, 909–917. doi: 10.1167/iovs.12-10109

Millecamps, S., and Julien, J. P. (2013). Axonal transport deficits and neurodegenerative diseases. *Nat. Rev. Neurosci.* 14, 161–176. doi: 10.1038/nrn3380

Mo, J. S., Anderson, M. G., Gregory, M., Smith, R. S., Savinova, O. V., Serreze, D. V., et al. (2003). By altering ocular immune privilege, bone marrow-derived cells pathogenically contribute to DBA/2J pigmentary glaucoma. *J. Exp. Med.* 197, 1335–1344. doi: 10.1084/jem.20022041

Morrison, J. C., Cepurna Ying Guo, W. O., and Johnson, E. C. (2011). Pathophysiology of human glaucomatous optic nerve damage: insights from rodent models of glaucoma. *Exp. Eye Res.* 93, 156–164. doi: 10.1016/j.exer.2010.08.005

Nakazawa, T., Nakazawa, C., Matsubara, A., Noda, K., Hisatomi, T., She, H., et al. (2006). Tumor necrosis factor-alpha mediates oligodendrocyte death and delayed retinal ganglion cell loss in a mouse model of glaucoma. *J. Neurosci.* 26, 12633–12641. doi: 10.1523/JNEUROSCI.2801-06.2006

Naskar, R., Wissing, M., and Thanos, S. (2002). Detection of early neuron degeneration and accompanying microglial responses in the retina of a rat model of glaucoma. *Invest. Ophthalmol. Vis. Sci.* 43, 2962–2968.

Neufeld, A. H., and Liu, B. (2003). Glaucomatous optic neuropathy: when glia misbehave. *Neuroscientist* 9, 485–495. doi: 10.1177/1073858403253460

Nikic, I., Merkler, D., Sorbara, C., Brinkoetter, M., Kreutzfeldt, M., Bareyre, F. M., et al. (2011). A reversible form of axon damage in experimental autoimmune encephalomyelitis and multiple sclerosis. *Nat. Med.* 17, 495–499. doi: 10.1038/nm.2324

Okamoto, N., Miya, F., Tsunoda, T., Yanagihara, K., Kato, M., Saitoh, S., et al. (2014). KIF1A mutation in a patient with progressive neurodegeneration. *J. Hum. Genet.* 59, 639–641. doi: 10.1038/jhg.2014.80

Panagis, L., Zhao, X., Ge, Y., Ren, L., Mittag, T. W., and Danias, J. (2010). Gene expression changes in areas of focal loss of retinal ganglion cells in the retina of DBA/2J mice. *Invest. Ophthalmol. Vis. Sci.* 51, 2024–2034. doi: 10.1167/iovs.09-3560

Patterson, S. L. (2015). Immune dysregulation and cognitive vulnerability in the aging brain: interactions of microglia, IL-1β, BDNF and synaptic plasticity. *Neuropharmacology* 96(Pt A), 11–18. doi: 10.1016/j.neuropharm.2014.12.020

Pease, M. E., McKinnon, S. J., Quigley, H. A., Kerrigan-Baumrind, L. A., and Zack, D. J. (2000). Obstructed axonal transport of BDNF and its receptor TrkB in experimental glaucoma. *Invest. Ophthalmol. Vis. Sci.* 41, 764–774.

Quigley, H. A., McKinnon, S. J., Zack, D. J., Pease, M. E., Kerrigan-Baumrind, L. A., Kerrigan, D. F., et al. (2000). Retrograde axonal transport of BDNF in retinal ganglion cells is blocked by acute IOP elevation in rats. *Invest. Ophthalmol. Vis. Sci.* 41, 3460–3466.

Roh, M., Zhang, Y., Murakami, Y., Thanos, A., Lee, S. C., Vavvas, D. G., et al. (2012). Etanercept, a widely used inhibitor of tumor necrosis factor-α (TNF-α), prevents retinal ganglion cell loss in a rat model of glaucoma. *PLoS ONE* 7:e40065. doi: 10.1371/journal.pone.0040065

Saederup, N., Cardona, A. E., Croft, K., Mizutani, M., Cotleur, A. C., Tsou, C. L., et al. (2010). Selective chemokine receptor usage by central nervous system myeloid cells in CCR2-red fluorescent protein knock-in mice. *PLoS ONE* 5:e13693. doi: 10.1371/journal.pone.0013693

Sappington, R. M., Carlson, B. J., Crish, S. D., and Calkins, D. J. (2010). The microbead occlusion model: a paradigm for induced ocular hypertension in rats and mice. *Invest. Ophthalmol. Vis. Sci.* 51, 207–216. doi: 10.1167/iovs.09-3947

Schlamp, C. L., Johnson, E. C., Li, Y., Morrison, J. C., and Nickells, R. W. (2001). Changes in Thy1 gene expression associated with damaged retinal ganglion cells. *Mol. Vis.* 7, 192–201.

Schlamp, C. L., Li, Y., Dietz, J. A., Janssen, K. T., and Nickells, R. W. (2006). Progressive ganglion cell loss and optic nerve degeneration in DBA/2J mice is variable and asymmetric. *BMC Neurosci.* 7:66. doi: 10.1186/1471-2202-7-66

Sennlaub, F., Auvynet, C., Calippe, B., Lavalette, S., Poupel, L., Hu, S. J., et al. (2013). CCR2(+) monocytes infiltrate atrophic lesions in age-related macular disease and mediate photoreceptor degeneration in experimental subretinal inflammation in Cx3cr1 deficient mice. *EMBO Mol. Med.* 5, 1775–1793. doi: 10.1002/emmm.201302692

Silverman, M. D., Zamora, D. O., Pan, Y., Texeira, P. V., Baek, S. H., Planck, S. R., et al. (2003). Constitutive and inflammatory mediator-regulated fractalkine expression in human ocular tissues and cultured cells. *Invest. Ophthalmol. Vis. Sci.* 44, 1608–1615. doi: 10.1167/iovs.02-0233

Sorbara, C. D., Wagner, N. E., Ladwig, A., Nikic, I., Merkler, D., Kleele, T., et al. (2014). Pervasive axonal transport deficits in multiple sclerosis models. *Neuron* 84, 1183–1190. doi: 10.1016/j.neuron.2014.11.006

Soto, I., and Howell, G. R. (2014). The complex role of neuroinflammation in glaucoma. *Cold Spring Harb. Perspect. Med.* 4:a017269. doi: 10.1101/cshperspect.a017269

Soto, I., Oglesby, E., Buckingham, B. P., Son, J. L., Roberson, E. D., Steele, M. R., et al. (2008). Retinal ganglion cells downregulate gene expression and lose their axons within the optic nerve head in a mouse glaucoma model. *J. Neurosci.* 28, 548–561. doi: 10.1523/JNEUROSCI.3714-07.2008

Stagi, M., Dittrich, P. S., Frank, N., Iliev, A. I., Schwille, P., and Neumann, H. (2005). Breakdown of axonal synaptic vesicle precursor transport by microglial nitric oxide. *J. Neurosci.* 25, 352–362. doi: 10.1523/JNEUROSCI.3887-04.2005

Striebel, J. F., Race, B., Carroll, J. A., Phillips, K., and Chesebro, B. (2016). Knockout of fractalkine receptor, *Cx3cr1,* does not alter disease or microglial activation in prion-infected mice. *J. Gen. Virol.* 97, 1481–1487. doi: 10.1099/jgv.0.000442

Takeuchi, H., Mizuno, T., Zhang, G., Wang, J., Kawanokuchi, J., Kuno, R., et al. (2005). Neuritic beading induced by activated microglia is an early feature of neuronal dysfunction toward neuronal death by inhibition of mitochondrial respiration and axonal transport. *J. Biol. Chem.* 280, 10444–10454. doi: 10.1074/jbc.M413863200

Vagaja, N. N., Chinnery, H. R., Binz, N., Kezic, J. M., Rakoczy, E. P., and McMenamin, P. G. (2012). Changes in murine hyalocytes are valuable early indicators of ocular disease. *Invest. Ophthalmol. Vis. Sci.* 53, 1445–1451. doi: 10.1167/iovs.11-8601

van der Mark, V. A., Elferink, R. P., and Paulusma, C. C. (2013). P4 ATPases: flippases in health and disease. *Int. J. Mol. Sci.* 14, 7897–7922. doi: 10.3390/ijms14047897

Wang, J. T., Medress, Z. A., and Barres, B. A. (2012). Axon degeneration: molecular mechanisms of a self-destruction pathway. *J. Cell Biol.* 196, 7–18. doi: 10.1083/jcb.201108111

Wang, K., Peng, B., and Lin, B. (2014). Fractalkine receptor regulates microglial neurotoxicity in an experimental mouse glaucoma model. *Glia* 62, 1943–1954. doi: 10.1002/glia.22715

Whitmore, A. V., Libby, R. T., and John, S. W. (2005). Glaucoma: thinking in new ways-a role for autonomous axonal self-destruction and other compartmentalised processes? *Prog. Retin. Eye Res.* 24, 639–662. doi: 10.1016/j.preteyeres.2005.04.004

Wolf, Y., Yona, S., Kim, K. W., and Jung, S. (2013). Microglia, seen from the CX3CR1 angle. *Front. Cell. Neurosci.* 7:26. doi: 10.3389/fncel.2013.00026

Yin, Y., Cui, Q., Gilbert, H. Y., Yang, Y., Yang, Z., Berlinicke, C., et al. (2009). Oncomodulin links inflammation to optic nerve regeneration. *Proc. Natl. Acad. Sci. U.S.A.* 106, 19587–19592. doi: 10.1073/pnas.0907085106

Yuan, L., and Neufeld, A. H. (2001). Activated microglia in the human glaucomatous optic nerve head. *J. Neurosci. Res.* 64, 523–532. doi: 10.1002/jnr.1104

Zhu, X., Libby, R. T., de Vries, W. N., Smith, R. S., Wright, D. L., Bronson, R. T., et al. (2012). Mutations in a P-type ATPase gene cause axonal degeneration. *PLoS Genet.* 8:e1002853. doi: 10.1371/journal.pgen.1002853

Zieger, M., Ahnelt, P. K., and Uhrin, P. (2014). CX3CL1 (fractalkine) protein expression in normal and degenerating mouse retina: *in vivo* studies. *PLoS ONE* 9:e106562. doi: 10.1371/journal.pone.0106562

Conflict of Interest Statement: The authors declare that the research was conducted in the absence of any commercial or financial relationships that could be construed as a potential conflict of interest.

frontiers in Neuroscience

ORIGINAL RESEARCH
published: 03 November 2016
doi: 10.3389/fnins.2016.00494

Early Cytoskeletal Protein Modifications Precede Overt Structural Degeneration in the DBA/2J Mouse Model of Glaucoma

*Gina N. Wilson[1,2], Matthew A. Smith[1,3], Denise M. Inman[1], Christine M. Dengler-Crish[1] and Samuel D. Crish[1]**

[1] Department of Pharmaceutical Sciences, Northeast Ohio Medical University, Rootstown, OH, USA, [2] School of Biomedical Sciences, Kent State University, Kent, OH, USA, [3] Integrated Pharmaceutical Medicine Program, Northeast Ohio Medical University, Rootstown, OH, USA

Axonal transport deficits precede structural loss in glaucoma and other neurodegenerations. Impairments in structural support, including modified cytoskeletal proteins, and microtubule-destabilizing elements, could be initiating factors in glaucoma pathogenesis. We investigated the time course of changes in protein levels and post-translational modifications in the DBA/2J mouse model of glaucoma. Using anterograde tract tracing of the retinal projection, we assessed major cytoskeletal and transported elements as a function of transport integrity in different stages of pathological progression. Using capillary-based electrophoresis, single- and multiplex immunosorbent assays, and immunofluorescence, we quantified hyperphosphorylated neurofilament-heavy chain, phosphorylated tau (ptau), calpain-mediated spectrin breakdown product (145/150 kDa), β–tubulin, and amyloid-β_{42} proteins based on age and transport outcome to the superior colliculus (SC; the main retinal target in mice). Phosphorylated neurofilament-heavy chain (pNF-H) was elevated within the optic nerve (ON) and SC of 8–10 month-old DBA/2J mice, but was not evident in the retina until 12–15 months, suggesting that cytoskeletal modifications first appear in the distal retinal projection. As expected, higher pNF-H levels in the SC and retina were correlated with axonal transport deficits. Elevations in hyperphosphorylated tau (ptau) occurred in ON and SC between 3 and 8 month of age while retinal ptau accumulations occurred at 12–15 months in DBA/2J mice. *In vitro* co-immunoprecipitation experiments suggested increased affinity of ptau for the retrograde motor complex protein dynactin. We observed a transport-related decrease of β-tubulin in ON of 10–12 month-old DBA/2J mice, suggesting destabilized microtubule array. Elevations in calpain-mediated spectrin breakdown product were seen in ON and SC at the earliest age examined, well before axonal transport loss is evident. Finally, transport-independent elevations of amyloid-β_{42}, unlike pNF-H or ptau, occurred first in the retina of DBA/2J mice, and then progressed to SC. These data demonstrate distal-to-proximal progression of cytoskeletal modifications in the progression of glaucoma, with many of these changes occurring prior to complete loss of functional transport and axon degeneration. The

OPEN ACCESS

Edited by:
Marco Antonio Maximo Prado, University of Western Ontario, Canada

Reviewed by:
Rafael Linden, Federal University of Rio de Janeiro, Brazil
Christian Gonzalez-Billault, University of Chile, Chile

***Correspondence:**
Samuel D. Crish
scrish@neomed.edu

Specialty section:
This article was submitted to Neurodegeneration, a section of the journal Frontiers in Neuroscience

Received: *22 August 2016*
Accepted: *14 October 2016*
Published: *03 November 2016*

Citation:
Wilson GN, Smith MA, Inman DM, Dengler-Crish CM and Crish SD (2016) Early Cytoskeletal Protein Modifications Precede Overt Structural Degeneration in the DBA/2J Mouse Model of Glaucoma. Front. Neurosci. 10:494. doi: 10.3389/fnins.2016.00494

earliest changes, such as elevated spectrin breakdown and amyloid-β levels, may make retinal ganglion cells susceptible to future stressors. As such, targeting modification of the axonal cytoskeleton in glaucoma may provide unique opportunities to slow disease progression.

Keywords: glaucoma, cytoskeleton, neurofilament, spectrin, tau, phosphorylation, axonal transport, amyloid-beta

INTRODUCTION

Glaucoma is a major cause of irreversible blindness, predicted to afflict nearly 112 million people worldwide by the year 2020 (Tham et al., 2014). While age and sensitivity to elevated intraocular pressure (IOP) are two major risk factors, ultimately it is the dysfunction and degeneration of retinal ganglion cells and their axons that lead to permanent vision loss in glaucoma (Quigley, 1999; Almasieh et al., 2012). As in many other chronic neurodegenerations, axonopathy is a component of early glaucoma pathogenesis (Libby et al., 2005; McKinnon et al., 2009; Crish et al., 2010; Dengler-Crish et al., 2014; Cooper et al., 2016). Furthermore, axonopathy is compartmentalized, with axonal transport deficits, morphological changes, and eventual axon loss initially manifested in the distal segments of retinal ganglion cell (RGC) axons (Libby et al., 2005; Schlamp et al., 2006; Crish et al., 2010, 2013; Dengler-Crish et al., 2014; Cooper et al., 2016). Functional axonal transport deficits are observed before structural loss—wherein lies a therapeutic window separating the earliest elements of dysfunction in this disease from stages of irrevocable neural loss (Crish et al., 2010; Sunico et al., 2011; Dengler-Crish et al., 2014).

Axonal transport blockade has been linked to aberrant cytoskeletal organization or breakdown (Coleman, 2005; Shea and Chan, 2008), and cytoskeletal proteins have been historically used as pathological markers in glaucoma (Soto et al., 2011). Recent work has redirected attention to these elements as potential mechanisms for disease progression (Balaratnasingam et al., 2008; Kang et al., 2014; Cooper et al., 2016). In the DBA/2J mouse, a well-characterized model that develops progressive glaucomatous pathology as a function of age (John et al., 1998), optic nerves (ON) from pathologically-advanced mice show striking evidence of large swellings (spheroids) exhibiting accumulated cargo and disorganized, highly phosphorylated neurofilaments (Crish et al., 2010). However, the nature and time course of cytoskeletal abnormalities within the axon have not been clearly defined; these changes may explain the underlying mechanics of early axonal transport deficits characteristic of glaucoma.

The axonal cytoskeleton is dynamic, and arrangement of its components is tightly regulated to produce the proper organization essential for normal structure and function of the axon (Köpke et al., 1993; Nicolas et al., 2002; Ackerley et al., 2003; Jung et al., 2005; Song et al., 2013; Xu et al., 2013; Wortman et al., 2014). Axonopathy often begins with post-translational modifications of proteins involved in axon structure and function (Petzold et al., 2008). Aberrations in several cytoskeletal proteins, such as neurofilaments, spectrin, microtubules, and tau, have been implicated in the pathogenesis of neurodegenerative diseases, including glaucoma (Braak et al., 1994; Schultz et al., 1997; Ahlijanian et al., 2000; Fischer et al., 2004; Tahzib et al., 2004; Cuchillo-Ibanez et al., 2008; Petzold et al., 2008; Chidlow et al., 2011; Haines et al., 2011; Ito et al., 2012; Yan and Jeromin, 2012). Amyloid-β (Aβ) has been a biomarker of neurodegeneration most commonly associated with Alzheimer's disease (AD), but is present in other pathological conditions, including glaucoma (McKinnon, 2003). Although it is not directly involved in the structural maintenance of the cytoskeleton, Aβ may play an active role in axonal transport deficits. Elevations in Aβ protein fibrils and oligomers coincide with elevated intracellular calcium concentrations (Kawahara and Kuroda, 2000), and oligomeric Aβ has been associated with inhibition of fast axonal transport (Morfini et al., 2009). Evidence of Aβ in animal models of glaucoma as well as in human glaucomatous eyes (McKinnon, 2003; Ito et al., 2012) further asserts the necessity of considering the role of such AD pathophysiological elements in the context of glaucoma.

In the current study, we assessed the relationship between cytoskeletal changes, axonal transport deficits, and primary risk factors (i.e., age) in glaucoma. Using a combination of neuronal tract tracing, immunofluorescence, and advanced protein quantitation techniques, we examined levels of extremely hyperphosphorylated (i.e., superphosphorylated) neurofilament (pNF-H), phosphorylated tau (ptau-231), spectrin breakdown product (SBDP 145/150; cleaved αII-spectrin), β-tubulin, and $A\beta_{42}$ throughout the retinal projection of DBA/2J mice as a function of age and extent of axonal transport deficits. Overall, our data support that initial cytoskeletal changes in the distal retinal projection occur before large-scale anterograde transport loss and subsequent axon degeneration, emphasizing the importance of these elements as potential targets for early intervention in the disease.

METHODS

DBA/2J Mouse Model of Glaucoma

Eighty-three mixed-sex (30 male, 53 female) DBA/2J and DBA/2J-*Gpnmb*$^+$ mice of different ages were used for protein quantification and immunofluorescence studies. The DBA/2J mouse has two loss of function mutations that produce iris atrophy, resulting in age-related elevation of IOP and progressive degeneration of visual structures that mimic human glaucoma (John et al., 1998; Burroughs et al., 2011). DBA/2J-*Gpnmb*$^+$ mice (D2G) have the same genetic background as DBA/2J mice;

Abbreviations: pNF-H, hyperphosphorylated heavy-chain neurofilament; SBDP, spectrin breakdown product; ON, optic nerve; SC, superior colliculus; GSK, glycogen synthase kinase; RGC, retinal ganglion cell.

however, they express a functioning wild-type *Gpnmb*$^{+}$ allele that prevents development of elevated IOP or glaucomatous pathology (Howell et al., 2007). For our experimental staging in the DBA/2J strain, we used 3–5 month old mice (D3-5) representing pre-glaucomatous ages, 8–10 month old mice (D8-10) representing early glaucomatous pathology where anterograde transport deficits and mild axonopathy are evident, and 12–15 month old mice (D12-15) representing increasing transport deficits, axonopathy, and RGC soma loss characteristic of late glaucomatous pathology. Staging of DBA/2J glaucomatous mice was consistent with previous work published by our lab as well as others and was based on anterograde and retrograde transport loss as well as eventual RGC loss in this model (John et al., 1998; Howell et al., 2007; Buckingham et al., 2008; Crish et al., 2010; Dengler-Crish et al., 2014; Wilson et al., 2015). For control comparisons, we used 3–5 and 12–15 month old D2G mice to represent ages targeted for pre-glaucomatous and late glaucomatous time points in the DBA/2J strain (G3-5 and G12-15 respectively). **Table 1** describes experimental and control group nomenclature and provides specific sample sizes. All mice were originally obtained from The Jackson Laboratory (Bar Harbor, ME, USA) and were housed and aged under the same conditions in the Comparative Medicine Unit at Northeast Ohio Medical University. Mice were maintained on a 12-h light/dark cycle with standard rodent chow available *ad libitum*. All experimental procedures were conducted in accordance with the guidelines of the Northeast Ohio Medical University Institutional Animal Care and Use Committee (IACUC). All protocols for animal use were approved by this IACUC prior to initiation of the study.

Anterograde Tracing

Anterograde tract tracing methods were used to assay anterograde transport integrity between each retina to the corresponding contralateral superior colliculus (Crish et al., 2010). Mice were anesthetized with 2.5% isoflurane and placed prone in a stereotaxic device (Stoelting, Wood Dale, IL). Cholera toxin B-subunit conjugated to Alexa Fluor 488 (CTB) was injected into the vitreous chamber of both eyes (1.5 µl of 0.1% CTB in sterile physiological saline per eye; Life Technologies: Grand Island, NY) using a 33-gage needle attached to a 25 µl Hamilton syringe. Mice were then allowed to recover and were returned to their home cages. Forty-eight hours later, mice were sacrificed by either transcardial perfusion with 4% paraformaldehyde for immunofluorescence assays or by decapitation under 5% isoflurane anesthesia to collect fresh tissue for protein quantitation procedures.

Tissue Collection

Eyes, brain, and ONs were harvested from mice perfused for immunofluorescence assays; brains were post-fixed overnight while eyes and ONs were post-fixed for 2 h. Tissue was transferred to 20% sucrose in phosphate buffered saline (PBS) prior to sectioning. Brains were sectioned coronally through the rostral-caudal extent of the SC at 50 µm on a freezing-sliding microtome; ONs were sliced longitudinally at 20 µm. Retinas were dissected from eyes.

In mice sacrificed for protein quantitation, retina, ONs, SC, and cerebellum (as a control structure) were collected and immediately frozen on dry ice, following the microdissection procedure previously described in Wilson et al. (2015). Whole-mount SC imaging was done with a Zeiss AxioZoom V16 epifluorescent microscope equipped with a digital high-resolution camera (AxioCam MRm Rev.3; Zeiss: Jena, Germany). Under 16.2x magnification, microdissection of the SC was performed to collect transport-intact (CTB-positive) and transport-absent (CTB-negative) regions which were analyzed separately in order to parse out the relationship between transport outcome and protein levels. Retinas were flattened and examined to determine success of the tracer injection as described in Dengler-Crish et al. (2014). Tissue was stored frozen at −80°C until use.

Sandwich ELISAs for pNF-H and Aβ_{42}

Enzyme-linked immunosorbent assays (ELISA) were used to quantify pNF-H (ELISA-pNFH-V1: EnCor Biotechnology Inc.; Oxfordshire, UK) and Aβ_{42} (#KMB3441: Life Technologies, Carlsbad, CA). Frozen tissue samples were homogenized via sonication (Branson Digital Sonifier; 10% amplitude for two 2-s pulses) in buffer (for pNF-H: 4 M Urea, 1 mM EDTA, 1 mM EGTA, 0.2 mM PMSF, with 1X Halt protease and phosphatase inhibitors; for Aβ_{42}: 5 M Guanidine-HCl in Dubellco's PBS, 0.2 mM PMSF, and 1X Halt protease inhibitor cocktail). Homogenate volume was approximately 100 µl buffer per mg of tissue. Homogenates were centrifuged at 15,200 × *g* and 4°C for 5 or 20 min, for pNF-H and Aβ_{42} samples, respectively. Supernatants were decanted into fresh Eppendorf tubes. Samples were diluted 1:50 with the EnCor protein block for pNF-H assays or 1:20 in PBS for Aβ_{42} assays and the assays were carried out according to the manufacturers' protocols. Protein standards were provided in each ELISA kit. Briefly, antibody-coated microplates were incubated with 100 µl of sample, standard, or background (assay buffer/diluent buffer) at room temperature (RT) for 2 h. Plates were washed three times with wash buffers provided in kits, then 100 µl of detection antibody was added to all wells and incubated for 1 h at RT. Plates were washed 3 times and 100 µl of HRP-conjugated secondary antibody was added to all wells and incubated for 1 h. After three washes, 100 µl of 3,3′,5,5′-tetramethylbenzidine (TMB) substrate was added to every well and incubated at RT for 25–30 min. Stop solution (2N H_2SO_4) was added and plates were read at 450 nm on a SpectraMax 340 PC plate reader (Molecular Devices, Sunnyvale, CA) using SoftMax Pro 5.2 analytical software. Mean absorbance values were recorded and calculated concentrations were based on the standard curve.

Tau Multiplex

Phosphorylated tau (ptau-231; phosphorylated at the threonine 231 site) and total tau proteins were measured using magnetic bead-based neurodegeneration multiplex plates for the Luminex platform (HND1Mag-39K; EMD Millipore, Billerica MA). Fresh tissue samples were homogenized via sonication in T-Per buffer supplemented with Halt protease and phosphatase inhibitors and centrifuged at 1000 × *g* for 10 min. Supernatants were

TABLE 1 | Group nomenclature.

Strain	Age	Group nomenclature	Projections analyzed					
			pNF-H	Aβ42	ptau-231	Total tau	SBDP	β-tubulin
D2G	3–5	D2G*	8	12	4	4	–	–
D2G	12–15		8	6	4	4	4	4
DBA/2J	3–5	D3–5	10	14	9	9	4	4
DBA/2J	8–10	D8–10	18	14	6	6	7**	7**
DBA/2J	12–15	D12–15	16	18	6	6		

Single asterisks denotes that both young and old controls were collapsed into a single group, when possible, to simplify analyses.

***Double asterisks denotes that a new combination of ages was used for the SBDP and β-tubulin analyses. An overarching "pathological" group consisting of animals aged 10–12 months was used here.*

collected for further analyses; pellets were re-suspended with 50–100 µl of additional T-Per buffer and were centrifuged a final time (1000 × *g*, 10 min, 4°C) with supernatants added to final sample volume. Multiplex analyses were conducted according to manufacturer's instructions. In brief, a solution containing antibody-coupled beads for total tau and ptau-231 were pipetted into a 96-well microplate (25 µl/well). Twenty-five microliters of assay diluent was then added, followed by 25 µl of sample or appropriate standard. Plates were light-protected and incubated for 16–18 h on an orbital shaker (500–600 rpm) at 4°C. Following incubation, plates were washed three times with manufacturer-provided detergent solution using a handheld magnet to keep beads in place. Twenty-five microliters of HRP-conjugated detection antibody was added to all wells and incubated at RT for 1 h (shaking at 500–600 rpm). Plates were washed three times as described and 25 µl of Streptavidin-RPE was added to wells. After a final wash, 100 µl of Magpix drive fluid was added to wells, plates were vigorously shaken for 3 min, and then plates were read on a Magpix Luminex 200. Xponent software was used to generate a standard curve for each analyte from which concentrations of unknown samples were calculated.

Automated Capillary-Based Western Blotting for SBDP and β-Tubulin

Analyses for SBDP and β-tubulin were performed using Wes, an automated capillary-based Western blotting platform (ProteinSimple, Santa Clara, CA). Brain samples used for Wes were selected from DBA/2J mice demonstrating either intact CTB transport (no visible deficit in the SC) or 0% transport (no detectable CTB label in the SC). T-Per buffer containing Halt protease and phosphatase inhibitors was added to samples (approximately 10 µl per 1 µg of tissue), tissue was then homogenized via sonication (20% amplitude for two, 2-s pulses), and brain homogenates were centrifuged at 14,000 rpm for 10 min at 4°C. Wes procedures were performed according to manufacturer protocol. Briefly, brain or ON homogenate was diluted to 0.1 µg/µl in 0.1X sample buffer and a fluorescent master mix (1 µl per 5 µl total volume) was added; the sample solutions and ladder were then placed in a thermocycler and heated to 95°C for 5 min and subsequently cooled to 25°C. The samples, blocking reagent, wash buffer, primary antibodies, HRP-conjugated secondary antibodies, chemiluminescent substrate, and separation/stacking matrices were dispensed into a pre-filled microplate (ProteinSimple, PS-PP03). After plate loading, immunodetection was fully automated using default instrument settings for size-based assays. Primary antibodies used were SBDP (mouse, 1:20; Santa Cruz, Dallas, TX) and β-tubulin (rabbit, 1:200: Covance/BioLegend, San Diego, CA). GAPDH (1:100: Sigma-Aldrich, St. Louis, MO) was used as a loading control. All antibodies were diluted with antibody diluent (ProteinSimple, 042-195). Resulting chemiluminescent signals were quantitated and analyzed with Compass software (ProteinSimple v2.5). Protein densitometry was calculated by dividing the area under the curve of each protein of interest by area under the curve of the loading control (GAPDH).

Bicinchoninic Acid Assay for Total Protein

Total protein content was assessed in tissue samples using the Pierce Bicinchoninic Acid (BCA) assay kit (Thermo Fisher; #23227) and individual protein levels were normalized to total protein content within tissue samples. Samples for pNF-H were diluted to a urea concentration compatible with the assay (<3 mM).

Calculating Percent Intact Transport

Whole-mount SC were imaged with the Zeiss AxioZoom microscope to capture the full extent of the dorsal surface of the SC. Captured images were imported into ImagePro Premier (Media Cybernetics; Rockville, MD) software where areas containing CTB signal were defined within the total SC area. To quantify percent intact transport of each SC, the area of intact CTB transport was divided by the total collicular area (Wilson et al., 2015).

Immunofluorescence

Sections from fixed retina, brain, and longitudinal ON were blocked with 5% normal donkey serum and 0.1% Triton-X 100 in PBS for 2 h and then incubated for 48 h at 4°C with the primary antibody cocktail (diluted in 3% serum, 0.1% Triton in PBS). Primary antibodies used consisted of the following: mouse anti-SMI-310 (superphosphorylated NF-H 1:1000; AbCam, Cambridge, MA), rabbit anti-tau p231 (1:400; Life Technologies), or rabbit anti-tubulin β-III (1:1000; BioLegend), and goat anti-Brn3a (1:400; Santa Cruz) for identification of retinal ganglion cell bodies. Staining for "superphosphorylated" NF

is distinguished from the more typical "hyperphosphorylated" phosphoisoforms seen with other pNF antibodies (e.g., SMI-31, SMI-34, RT97) in that the former represents the highest level of phosphorylation of all the antibody-detected NF phosphoisoforms, and is typically only found in a subset of axons in normal tissue. Assessment of superphosphorylated NF allows us to identify pathological changes in the axon that might be masked by the relatively high expression of other NF phosphoisoforms in normal tissue. Following primary antibody incubation, tissue was washed in PBS and Alexa Fluor secondary antibodies (Jackson Immunoresearch Laboratories, West Grove, PA) against mouse, rabbit, and/or goat (diluted 1:250 in PBS containing 0.1% Triton X-100 and 1% normal donkey serum) were then added and sections were incubated for 2 h at room temperature. Tissue was then washed with PBS, mounted onto slides and cover-slipped with Fluoromount-G (Southern Biotech, Birmingham, AL) prior to visualization.

Semi-Thin Optic Nerve Embedding, Sectioning, and Immunofluorescence

Perfusion-fixed ONs were immediately placed in 1% glutaraldehyde for 3 h and were then washed in buffer (3.5% sucrose/50 mM glycine in 0.01 M PBS) for 10 min. Tissue was dehydrated using cold 70% ethanol followed by 95% ethanol, and 100% ethanol each for 5 min. Tissue was then placed in a (1:1) mixture of LR white resin (#62662; Sigma-Aldrich) and 100% ethanol for 5 min. After removal from mixture on day 2, tissue was placed in fresh LR white twice, for 5 min each, prior to overnight incubation in LR white, at 4°C. On day 3, tissue was added to gelatin capsules (#7114, Electron Microscopy Sciences, Hatfield, PA) filled with LR white, covered, and placed in an oven at 50°C for overnight infiltration.

Using a Leica UC6 ultramicrotome (Buffalo Grove, IL) equipped with a Diatome diamond knife (Ultra 45, 3.0 mm), 1 μm cross-sections were collected and mounted onto subbed glass slides. Tissue was blocked with 5% normal donkey serum and 0.1% Triton-X 100 in PBS for 2 h. Tissue incubated for 48 h at room temperature in primary antibody solution (3% serum, 0.1% Triton in PBS) consisting of anti-β-tubulin III (1:50; BioLegend) and anti-SMI310 (1:400; AbCam). Following primary antibody incubation, tissue was washed in PBS (10 min, x3) before secondary antibody incubation using Alexa Fluor secondary antibodies (Jackson Immunoresearch Laboratories) against mouse, rabbit, and/or goat (diluted 1:200 in PBS containing 0.1% Triton X-100 and 1% normal donkey serum) overnight at room temperature. Tissue was then washed with PBS before slides were cover slipped using Fluoromount-G mounting media.

Immunofluorescence Imagining

Immunofluorescence imaging of retina, SC, and cross-section ON was completed using a Zeiss Axio Imager M2 epifluorescent microscope outfitted with an Apotome.2 for obtaining optically sectioned images, digital high resolution camera (AxioCam MRm Rev.3), and motorized Z and X-Y stage (Zeiss, Jena, Germany). Longitudinal ON were imaged using the Zeiss AxioZoom V16 epifluorescent microscope.

Tau-Dynactin Co-immunoprecipitation

To test the effect of tau hyperphosphorylation on its affinity for the retrograde motor component, dynactin, we performed co-immunoprecipitation comparing native tau (that exhibits a low level of phosphorylation) and tau hyperphosphorylated by pretreatment with glycogen synthase kinase 3β (GSK-3β; a kinase that has tau as one of its major substrates). In a 1.5 ml Eppendorf tube, 30 μl of Dynabeads-G (ThermoFisher, #10003D) was bound with 10 μl of antibody against dynactin-2 (AbCam, #EPR5095), which was then allowed to bind 5 μg recombinant dynactin-2 (0.5 μg/μl; OriGene Technologies Inc., Rockville, MD; #TP314771). The tubes were rotated for 20 min at RT to ensure thorough mixing. Five micrograms of human tau-412 isoform (1 μg/μl; rPeptide, LLC, Bogart GA), was treated with either GSK-3β, lambda phosphatase, or PBS and incubated at RT for 30 min. The tau solutions were then mixed with dynactin-bound Dynabeads and allowed to rotate for 20 min. Fifty microliters of Laemmli buffer was added to each reaction and tubes were heated at 70°C for 10 min. Forty microliters of each solution was used to perform Western blots which were run on 4–15% Mini-Protean TGX precast gels (Bio-Rad, Hercules, CA; #4561083SEDU) and Immun-Blot PVDF membranes (Bio-Rad; #1620177). Membranes were probed with an antibody against pan-tau (anti-Tau-5; AbCam #ab80579) to determine relative amounts of total tau pulled out in each reaction context. Blots were stripped (Restore™ Western Blot Stripping Buffer; ThermoFisher; #21059) and probed with a phospho-specific antibody (phospho-(Ser/Thr) Phe Antibody; Cell Signaling, Anvers, MA; #9631) to confirm differences in phosphorylation state. Control blots were run using either Dynabeads-only (30 μl), pure dynactin, or native tau protein (1 μg).

Statistical Analyses

IBM SPSS Statistics 22 (IBM Corp: Armonk, NY, USA) was used for all statistical analyses. To justify pooling D2G results into a unitary control group, two-tailed, independent samples student *t*-tests were performed to confirm similarity of results between young (3–5 months.) and old (12–15 months.) D2G control animals. Assessments regarding whether pooling was applicable were made separately for each protein (pNF-H, ptau, total tau, and $A\beta_{42}$) and tissue type (retina, ON, SC, and cerebellum). Independent samples *t*-tests were performed to determine any initial sex differences in protein quantification measurements within each strain/age group of mice prior to assessment of our overall hypotheses. To test our overall hypotheses, we conducted one-way analyses of variance (ANOVA) using protein concentration (pNF-H, ptau, total tau, and $A\beta_{42}$) per anatomical region (retina, ON, SC and cerebellum control) as the dependent variable and strain/age group as the independent variable. Bonferroni-corrected *post hoc* comparisons were performed to elucidate specific group differences. For other analyses, we used transport outcome as our independent variable to determine whether proteins levels in each region differed in transport-intact (CTB-positive) vs. transport-deficient (CTB-negative) projections. Since the distribution of projections with intact transport was variable in the D8-10 DBA/2J group (53% intact) and skewed substantially toward loss in the D12-15 group

(15% intact), we pooled data across these two age groups to have sufficient cases to support each level of our dichotomous transport-intact/deficient variable for analysis. In addition to this dichotomous transport variable, we also used a continuous variable of "percent intact transport" for our correlational analyses.

RESULTS

D2G Mice Show No Differences in Protein Concentrations Based on Age

To assess whether age-related differences in cytoskeletal components occur independent of strain, we compared pNF-H protein levels in retina, ON, SC, and cerebellum (control structure) between young (3–5 months.) and old (12–15 months.) D2G using independent samples *t*-tests. No significant differences in pNF-H levels were shown between young and old D2G for any structure (refer to **Table 2**). These results were recapitulated in analyses of Aβ and tau proteins as well. Therefore, young and old D2G were pooled into a single control group for all subsequent analyses. No significant sex differences were observed within either D2G age group.

pNF-H Levels in DBA/2J Mice are Elevated in an Age and Transport Dependent Manner

DBA/2J Mice Show Early pNF-H Elevations in SC and Late Increases in the Retina, with Transitional Changes Occurring in ON

Figure 1 depicts results for pNF-H analyses. As shown in **Figure 1A**, pNF-H protein concentration differed between strains in the retina [$F_{(3, 55)} = 3.116$, $p = 0.034$], ON [$F_{(3, 52)} = 17.206$, $p < 0.001$], and SC [$F_{(3, 50)} = 3.653$, $p = 0.019$] with no differences in cerebellar control tissue (**Table 2**).

TABLE 2 | Young and aged D2G comparisons.

Protein	Structure	*t*	Mean Difference	*p*-value
pNF-H	*Retina*	0.316	0.001547	0.757
	ON	2.28	0.063000	0.063
	SC	0.558	0.011460	0.578
	Cerebellum	−0.073	0.001700	0.949
Aβ42	*Retina*	0.688	0.749250	0.501
	ON	2.016	2.590410	0.075
	SC	0.424	0.753093	0.681
	Cerebellum	0.237	1.493809	0.834
Ptau-231	*Retina*	−0.64	0.002750	0.568
	ON	0.873	0.024179	0.447
	SC	−0.826	0.001414	0.561
Total tau	*Retina*	−0.534	0.000016	0.631
	ON	1.083	0.000459	0.358
	SC	−0.983	0.000000	0.506

An approximate 5-fold increase in collicular pNF-H was seen in the 8–10 month DBA/2J group ($p = 0.020$) compared to controls. Retinal pNF-H levels did not significantly differ between groups until DBA/2J mice were 12–15 months of age, whereby pNF-H levels were increased by nearly 5-fold in 12–15 month DBA/2Js compared to controls ($p = 0.033$). pNF-H results in the ON showed a transitional pattern of results, with D8-10 mice displaying significantly higher pNF-H levels—more than double—in comparison to D2G controls and D3-5 ($p = 0.003$) and D12-15 ($p < 0.01$) mice. Further, we saw elevations of pNF-H in the most superficial SC between groups (**Figure 1A**). Following the pattern of ON NF levels, we see an increase of pNF in D8-10 followed with a reduction in the oldest age group. **Figure 1B** shows immunofluorescent labeling of superphosphorylated NF-H (SMI-310) in retina and ON. Retinas show low levels of pNF and ptau in the control retina with the D8 retina showing greatly increased levels of pNF and ptau, with both proteins being aberrantly localized in the RGC somata (labeled with Brn3a), a sign of pathology. Immunofluorescence staining in our semithin cross-sections of ON is also consistent with results from the protein quantification. We found low levels of pNF-H in aged control mice with very robust staining evident in a D9 ON. This staining is greatly reduced in the D13 ON, likely due to axon loss, as evidenced by the massive reduction in β-tubulin seen in the same section. No sex differences were observed within retina, ON, or SC of any DBA/2J age group.

pNF-H Levels in Retina and SC Vary Based on Transport Outcome in DBA/2J Mice

Collicular tissue was microdissected to separate CTB+ from CTB- areas, each area was run separately. For retina, total CTB+ area of corresponding collicular lobe was used for classification. We contrasted pNF-H levels in retinal projections taken from mice with deficient (0–20%) anterograde transport (CTB-) in the SC with projections taken from SC displaying full tracer coverage (CTB+) and these data are presented in **Figure 2**. Only DBA/2J mice in the D8-10 and D12-15 groups displayed transport deficits (as anticipated based on the established trajectory of transport loss in this model) with only 15% of D12-15 colliculi exhibiting any detectable CTB label whatsoever. To maximize detection of differences in pNF-H levels as a function of transport outcome, we pooled data across the two pathologically-aged DBA/2J groups (D8-10 and D12-15). Significant elevations of pNF-H were indicated in both SC [$F_{(1, 53)} = 8.288$, $p = 0.006$] and retina [$F_{(1, 59)} = 5.816$, $p = 0.019$] of transport deficient (CTB-) projections compared to intact (CTB+) projections (**Figure 1A**). There were no differences in ON or cerebellum levels (not shown) of pNF-H as a function of transport outcome. For both SC and retina, the percent of intact transport was negatively correlated with pNF-H levels indicating that pNF-H levels increased as a function of transport deficit magnitude in these structures (SC: Pearson $r^2 = -0.358$; retina: Pearson $r^2 = -0.317$, $p < 0.05$ in both cases). pNF-H levels in the ON did not show this same relationship to transport deficit magnitude. There were no observed differences in transport outcome to the SC based on mouse sex.

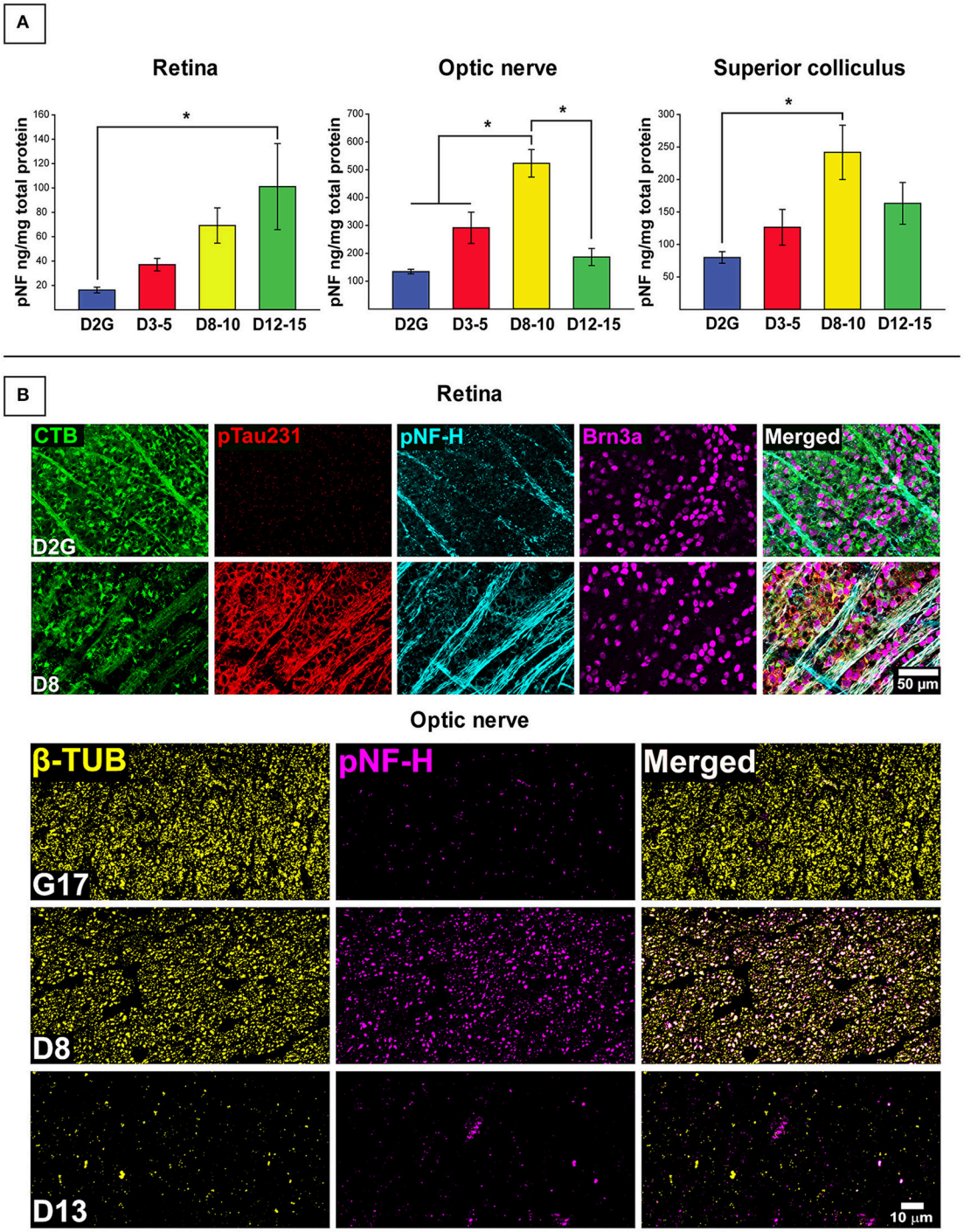

FIGURE 1 | Early elevations in pNF-H observed in distal RGC projection with effects of age and transport outcome. (A) Quantification of pNF-H by ELISA in retina, optic nerve (ON), and superior colliculus (SC). DBA/2J retinal pNF-H levels show trending increase with age peaking at 12–15 months at which point, is significantly elevated compared to the D2G controls. In the ON, pNF-H levels were highest at 8–10 months. in the DBA/2J mice but returned to levels similar to the D2G controls at 12–15 months. In the SC, pNF-H levels remained significantly elevated in the D8-10 group compared to controls. **(B)** (Top) Immunofluorescence of cytoskeletal markers, SMI-310 (specific for superphosphorylated, pNF-H) and the RGC marker Brn3a in the retina of an 8-mo. DBA/2J (D8) and D2G control. Micrographs show visibly increased pNF-H and somatic/axonal ptau-231 staining in the D8 retina. The D2G pNF-H labeling is typical of mature, non-pathological axons within the retina. (Bottom) Semithin (1 μm) cross-sections taken from 8-months. DBA/2J (D8), 13-months. DBA/2J (D13), and 17-months. D2G (G17) control ON immuno-stained for β-tubulin (β-TUB) and pNF-H. A significant increase in pNF-H is observed in the D8 ON compared to G17 control. In the D13, pNF-H in the ON is nearly absent corresponding to the prominent loss of axonal structure indicative by the reduction in β-TUB. Error bars depict SEM. Asterisk indicates significant statistical difference ($p < 0.05$).

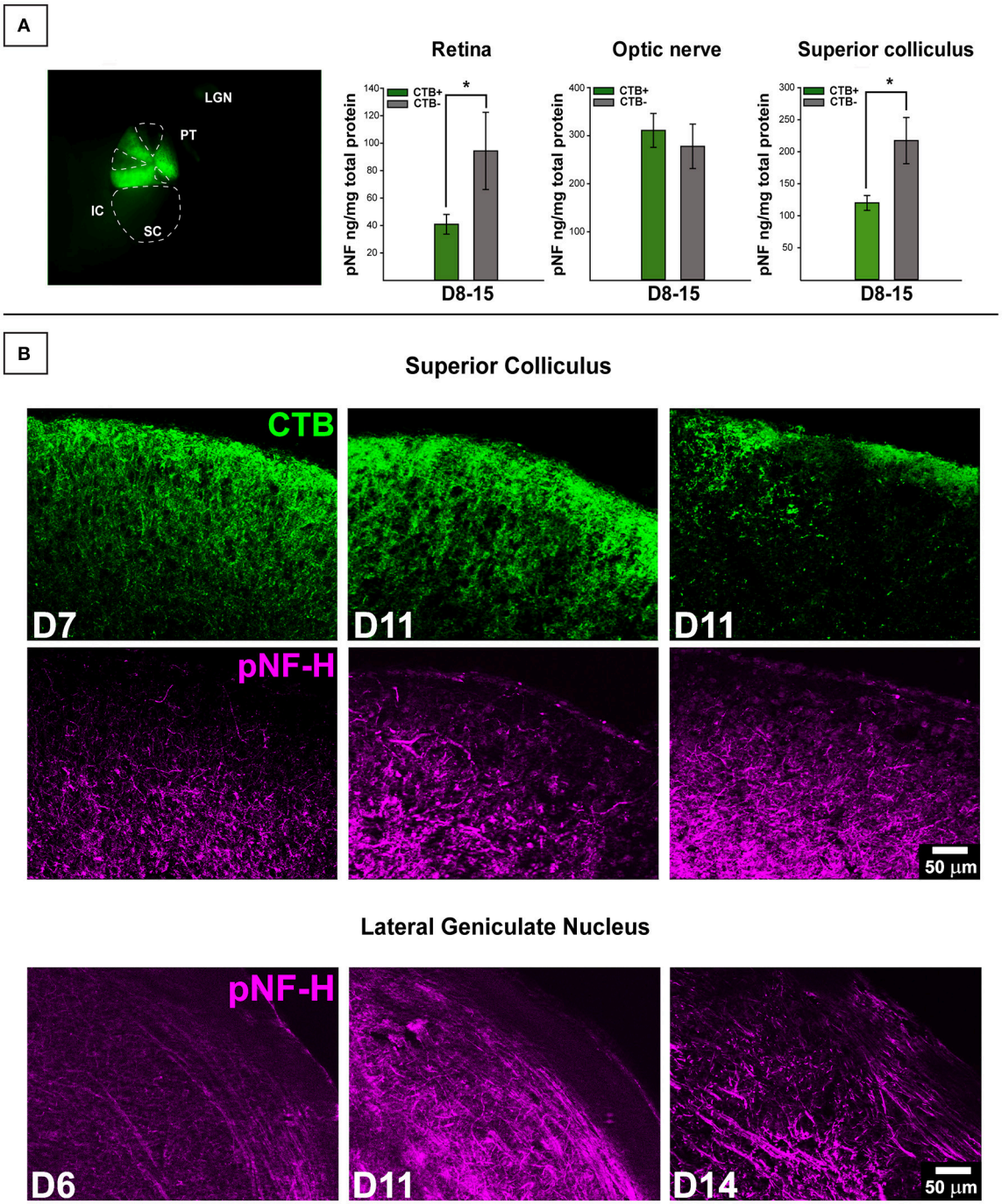

FIGURE 2 | Transport-dependent elevations in pNF-H observed in retina and SC of DBA/2J mice. (A) (Left) Photomicrograph from the dorsal surface of a whole-mount pathological SC in which the cortex has been removed and cholera toxin-B (CTB) labeling shows sectorial loss in the left (top) collicular lobe and complete loss in the right (bottom) lobe. Abbreviations: IC, inferior colliculus; PT, pre-tectum; LGN, lateral geniculate nucleus; SC, superior colliculus. The dotted lines demarcate areas absent of CTB indicating axonal transport deficit (CTB-). (Right) ELISA quantification of pNF-H in retina, optic nerve (ON), and SC. The transport status of retina and ON were determined by whether or not the SC was CTB+ (>90% CTB-label for partially transporting projections) or CTB- (<10% CTB-label for partially transporting projections). Levels of pNF-H were significantly elevated nearly 2-fold in both retina and SC of CTB- projections compared to CTB+ projections. Asterisks indicate significant statistical differences ($p < 0.05$). Error bars depict SEM. **(B)** Top panel shows immunofluorescence of the SC, comparing 7-months. (D7), and 11-months. (D11) DBA/2J with and without CTB transport. Visibly increased pNF-H is shown in CTB- D11 SC. Bottom panel illustrates an age-dependent increase in pNF-H staining in the LGN (the visual thalamus) of 6, 11, and 14-month DBA/2J mice.

Phosphorylated Tau Shows Age-Dependent Changes in Retina and ON

Age-Dependent Elevations in Ptau in DBA/2J Mouse SC and Retina

Concentrations of ptau-231 differed as a function of DBA/2J age group in retina [$F_{(3, 22)} = 3.850$, $p = 0.026$] and SC [$F_{(3, 16)} = 7.209$, $p = 0.004$] but not in ON or control cerebellar tissue. Specifically, collicular ptau-231 was elevated by more than 4-fold in the youngest DBA/2J group (D3-5) compared to D2G controls ($p = 0.007$) and D12-15 mice ($p = 0.011$) (**Figure 3**). In contrast, retinal levels of ptau-231 were significantly increased about 3-fold in the D12-15 group compared to D2G controls (ptau-231; $p = .022$) and displayed a stepwise pattern of age-related increase among DBA/2J mice (**Figure 3A**). As shown in **Figure 2B**, there was a notable elevation in ptau-231 immunofluorescent labeling in the somata and axons of an 8-month old DBA/2J retina compared to retina from an 11-month old D2G control, despite no differences in the distribution of the RGC marker Brn3a between retina of these mice. Although differences in ptau-231 protein levels between groups were not detected in of ON homogenates, immunofluorescent ptau labeling in fixed longitudinal ON sections of 14-month old DBA/2J showed an intriguing distal-to-proximal distribution. Ptau-231 label was obvious in myelinated proximal ON but was sparse in the distal portion of the nerve (**Figure 3C**), and this pattern was observed in three cases of D14 ON and not in any other age groups. Relationships between transport deficits and ptau-231 protein levels could not be determined due to high variability in tau protein concentrations and small sample sizes of transport-intact mice in the oldest DBA/2J age groups. No sex differences were observed within retina or SC of any DBA/2J age group.

Tau-Dynactin Co-Immunoprecipitation

To further explore the age-related distal-to-proximal distribution of ptau in the DBA/2J retinal projection, we conducted a co-immunoprecipitation assay for differences in binding affinity of different tau phosphoisoforms with dynactin-2, the link between the retrograde molecular motor dynein and cytoskeletal elements. Results indicated that more tau protein was pulled down by the dynactin protein after GSK-3β-mediated phosphorylation compared to native conditions or phosphatase pre-treatment, as observed by Western blot (**Figure 3C**). Dynabead-only, tau, or dynactin alone conditions showed little if any non-specific binding. Blots were stripped and probed with a phospho-specific antibody to confirm differences in phosphorylation state (not shown).

Elevations in SBDP Observed Early in ON and SC of DBA/2J Mice

Comparisons of spectrin breakdown product (SBDP) protein levels were only performed between groups of D2G, D3-5, and D10-12 DBA/2J mice with this oldest group exhibiting a bimodal distribution in terms of transport outcome (CTB+/CTB-). SBDP levels varied significantly between these groups in the ON [$F_{(3, 13)} = 32.36$, $p < 0.01$] and SC [$F_{(3, 13)} = 4.718$, $p = 0.027$]. Interestingly, D3-5 DBA/2J mice demonstrated significantly elevated SBDP in ON compared to all other groups ($p < 0.01$ for all comparisons; **Figure 4A**), a difference of more than 10-fold. These young DBA/2J mice also expressed collicular levels of SBDP that were more than double the levels detected in D2G controls ($p < 0.05$; **Figure 4B**). As expected based on this result, SBDP protein levels did not differ as a function of transport outcome in the D10-12 group exhibiting either fully intact or completely absent transport to individual SC. No sex differences were observed within ON or SC of any DBA/2J age group.

Decreased β-Tubulin in Pathologically-Aged DBA/2J Mice with Disrupted Transport

To determine whether lower levels of SBDP observed in ON and SC of 10–12 month old DBA/2J mice were potentially due to an overall loss or disorganization of structure in aged projections, we quantified β-tubulin (a major structural component of microtubules) in these structures. In 10–12 months old DBA/2J mice, β-tubulin was significantly decreased within the ON of transport deficient (CTB-) projections relative to transport intact (CTB+) projections [$F_{(1, 11)} = 9.11$, $p = 0.01$], and transport-deficient D10-12 projections also had lower levels of β-tubulin levels compared to D2G projections [$F_{(3, 11)} = 5.053$, $p = 0.030$] (**Figure 4A**). Immunofluorescent staining in the ON also reflected decreased β-tubulin and CTB label in 11-month old DBA/2J tissue compared to 6-month old DBA/2J ON (**Figure 1B**). No significant differences in collicular β-tubulin levels were detected between any groups (**Figure 4B**); however, β-tubulin levels in this region showed trends similar to those observed in the ON. No sex differences were observed within ON or SC of any DBA/2J age group.

Elevations in $A\beta_{42}$ Levels in DBA/2J

Retinal $A\beta_{42}$ Levels Are Elevated in all DBA/2J Mice Regardless of Age, but Show Age-Dependent Increases at the Level of the SC

Retinal and collicular $A\beta_{42}$ levels varied as a function of strain, age, and location [retina: $F_{(3, 61)} = 5.886$, $p < 0.01$; SC: $F_{(3, 38)} = 7.760$, $p < 0.01$]. Retinal $A\beta_{42}$ was elevated in all age groups of DBA/2J mice, by three to four times, relative to D2G controls ($p \leq 0.010$ in all analyses; **Figure 5A**, top). Collicular $A\beta_{42}$ was significantly elevated in D8–10 and D12–15 mice by more than double control levels, but not in the young D3–5 group ($p < 0.05$ in both cases; **Figure 5B**, top). In DBA/2J SC, $A\beta_{42}$ was highest in the D8–10 group, although statistically these $A\beta_{42}$ values only differed from the D3–5 group ($p = 0.03$). $A\beta_{42}$ levels in cerebellar tissue did not differ by age or strain. No sex differences were observed within retina or SC of any DBA/2J age group.

$A\beta_{42}$ Levels Are Elevated in DBA/2J SC as a Function of Transport Loss

As illustrated in **Figure 5B** (bottom), $A\beta_{42}$levels were increased in SC of transport-deficient (CTB-) projections relative to transport-intact (CTB+) projections of DBA/2J mice (collapsed across D8–10 and D12–15 groups) [$F_{(1,41)} = 8.044$, $p = 0.007$]. No transport-related differences were found in retina (**Figure 5A**, bottom) or ON samples (not shown).

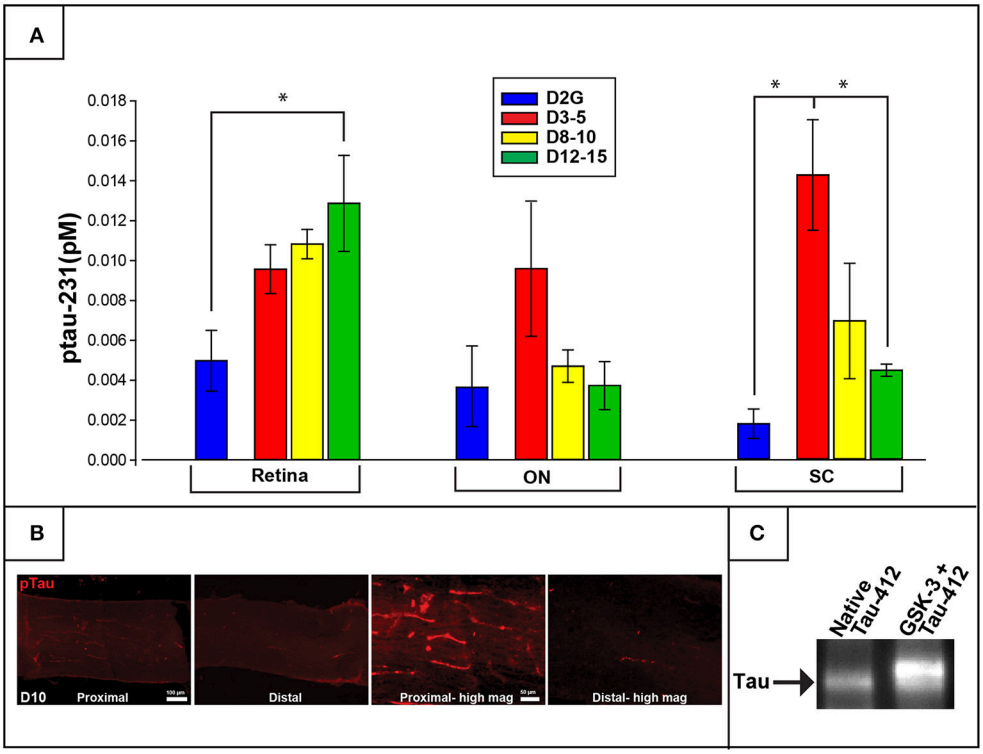

FIGURE 3 | Phosphorylated tau (ptau-231) is elevated early in the distal projection and is observed to translocate to the retina in pathologically-aged animals. (A) Multiplex quantification of ptau-231 in DBA/2J mice shows an age-dependent decrease of ptau in SC with an age-dependent increase in retinal ptau. In the SC, ptau-231 is significantly higher in the D3-5 group compared to D12-15 and D2G control group levels. In retina, however, D12-15 ptau-231 levels are significantly higher than D2G controls. Ptau levels in ON samples did not differ between groups. **(B)** Immunofluorescence for ptau-231 in 10-months. DBA/2J ON shows evidence of preferential accumulation of ptau-231 in the proximal portion compared to the distal portion of the nerve. **(C)** An example of co-immunoprecipitation data comparing native and hyperphosphorylated tau via reaction with GSK-3 suggests an increased affinity of phosphorylated tau for the retrograde motor component, dynactin-2. This is qualitatively illustrated by the increased optical density of Tau-5 (a marker for pan-tau) in the second lane representing hyperphosphorylated tau (GSK-3+Tau-412), compared to the first lane which contained only native tau. The tau band shown here corresponds to a molecular weight of approximately 43.5 kDa corresponding to the GSK-3 phosphorylation site, pS396/404. Asterisk indicates that groups are significantly different from bracketed comparison ($p < 0.05$). Error bars depict SEM.

DISCUSSION

Pathological phosphorylation and cleavage of cytoskeletal elements are commonly implicated in chronic neurodegenerative conditions, including glaucoma (Lee et al., 2000; Colucci-D'Amato et al., 2003; Knobloch and Mansuy, 2008; Chidlow et al., 2011). Specifically, roles for pNF-H, ptau, spectrin, β-tubulin, and the pathological protein $A\beta_{42}$ in the development, progression, and even classification and diagnosis of degenerative conditions have been prominent in both the clinical and basic research literature. However, the present experiments are the first to quantify this specific subset of proteins throughout the entire retinal projection of a glaucomatous mouse model; likewise, this study is the first to associate protein quantification with measures of axonal transport from the retina to its primary projection target in mouse, the SC. Our data (summarized in **Figure 6**) indicate that post-translational phosphorylation of neurofilament heavy-chain and tau occurs with age in DBA/2J mice. Spectrin breakdown in ON and SC precedes these effects, and early elevation of retinal $A\beta_{42}$ was evident in the youngest, pre-pathological age group of DBA/2J mice studied. Consequently, elevations in these proteins occur prior to anterograde transport loss in this well-characterized glaucoma model. When the temporal context of these molecular change are considered, it is plausible that early spectrin cleavage and $A\beta_{42}$ accumulation may perpetuate the sequence of degenerative events by facilitating aberrant cytoskeletal phosphorylation and thus, provoking disease progression (Dixit et al., 2008).

Microtubules are the substrate along which motor proteins carry cargo within axons. Therefore, disruption of microtubule organization inhibits axonal transport and, depending on the location and severity of the disruption, can trigger various destruction programs ranging from distal axonopathy to apoptosis (Cuchillo-Ibanez et al., 2008; Song et al., 2013; Zempel and Mandelkow, 2015). Relevant to our findings, abnormal microtubule distribution has been observed following laser coagulation-induced ocular hypertension in rats (Huang et al., 2011). Pharmacological disruption of microtubules with nocodazole treatment indicated that microtubule disruption is an early clinical event that occurs prior to decreased retinal

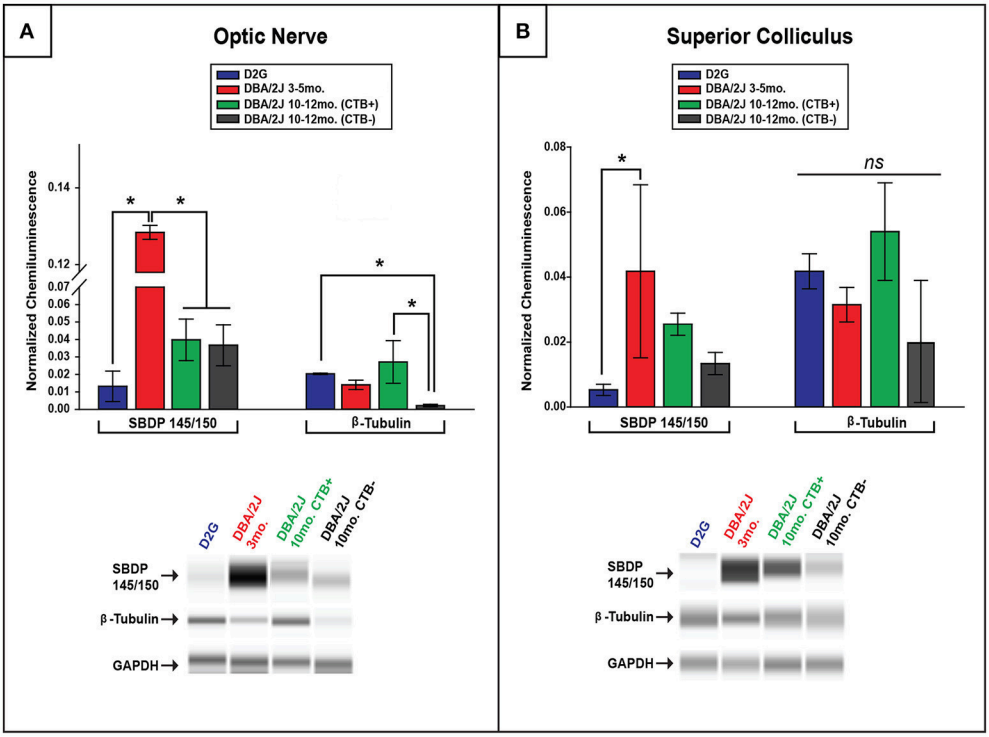

FIGURE 4 | Spectrin breakdown product (SBDP) 145/150 is elevated in young DBA/2J ON and SC while β-tubulin is decreased in a transport-dependent manner in pathologically-aged ON. (A) Chemiluminescence-based quantification using ProteinSimple Wes technology illustrates significantly higher levels of SBDP(145/150) within ON of D3-5 mice compared to all other groups, with no differences seen in pathologically-aged (10–12 months.) DBA/2J mice regardless of transport outcome. Bar graph (top) shows SBDP145/150 and β-tubulin normalized to GAPDH (a housekeeping gene marker), while corresponding examples of automated western output are shown below for ON. Importantly, a significant decrease in β-tubulin was observed in pathologically-aged ON associated with zero anterograde transport to the corresponding SC compared to controls and D10-12 mice with intact transport. **(B)** A significant elevation in SBDP chemiluminescence was observed in D3-5 SC compared to D2G controls **(B)**, with no differences in collicular β-tubulin elucidated. Bar graph (top) shows SBDP145/150 and β-tubulin normalized to GAPDH, while corresponding examples of automated western output are shown below for SC. (Refer back to **Figure 1** to see β-tubulin loss using immunofluorescence.) Error bars depict SEM. Asterisk indicates that groups are significantly different from bracketed comparison ($p < 0.05$)

nerve fiber thickness (Lim and Danias, 2012). Microtubules require a vast network of stabilizing, support, and adaptor proteins to maintain their functional and structured matrix (Ahlijanian et al., 2000; Roy et al., 2005). Neurofilaments, the most abundant component of the mature axonal cytoskeleton, aid in organization and stabilization of the microtubule matrix and other cytoskeletal elements. Phosphorylation of NF-H controls axon caliber (Petzold et al., 2008; Cooper et al., 2016), and hyper- or super-phosphorylation of neurofilament can slow its transport, leading it to accumulate and form aggregates that ultimately block transport (Nixon, 1994; Elder et al., 1998a,b; Julien and Mushynski, 1998; Jung and Shea, 1999, 2004), leading to eventual axon loss (Ackerley et al., 2003; Petzold et al., 2008; Lépinoux-Chambaud and Eyer, 2013). We showed that phosphorylated NF-H is significantly elevated in the SC of DBA/2J mice early (8–10 months) in the progression of glaucomatous pathology, decreasing only when glaucomatous pathology advances (12–15 months). Consequently, we also observed decreased β-tubulin in the ON (and to lesser extent in the SC) of transport-deficient 10–12 month DBA/2J projections compared to projections with intact transport—a finding that suggests loss of microtubule and cellular structure within the ON and SC as degeneration progresses (Schlamp et al., 2006; Crish et al., 2010; Adalbert and Coleman, 2012). Supporting this, our data showed increased pNF-H in the SC and retina of mice with transport deficits compared to mice with intact transport. Phosphorylation of neurofilaments decreases their affinity for tubulin, causing abnormal bundling and disorganization of the microtubule array (Buée et al., 2000; Jung et al., 2005; Zempel and Mandelkow, 2015). Therefore, elevation of pNF could be a driving force for transport loss.

Hyperphosphorylation of the microtubule-associated protein tau–a pathological hallmark of Alzheimer's disease (Iqbal et al., 2016)– promotes abnormal translocation and accumulation of tau in the soma and aberrant assembly of microtubules, driving axonal transport deficits and other neurodegenerative effects (Majid et al., 2014; Morfini et al., 2016). While tauopathy likely plays a mechanistic role in glaucoma, evidence of tau phosphorylation and translocation in a glaucoma model has only recently been uncovered (Chiasseu et al., 2016). The data from our study show: (1) an age-dependent increase in retinal ptau and (2) a large decrease in collicular ptau of glaucomatous

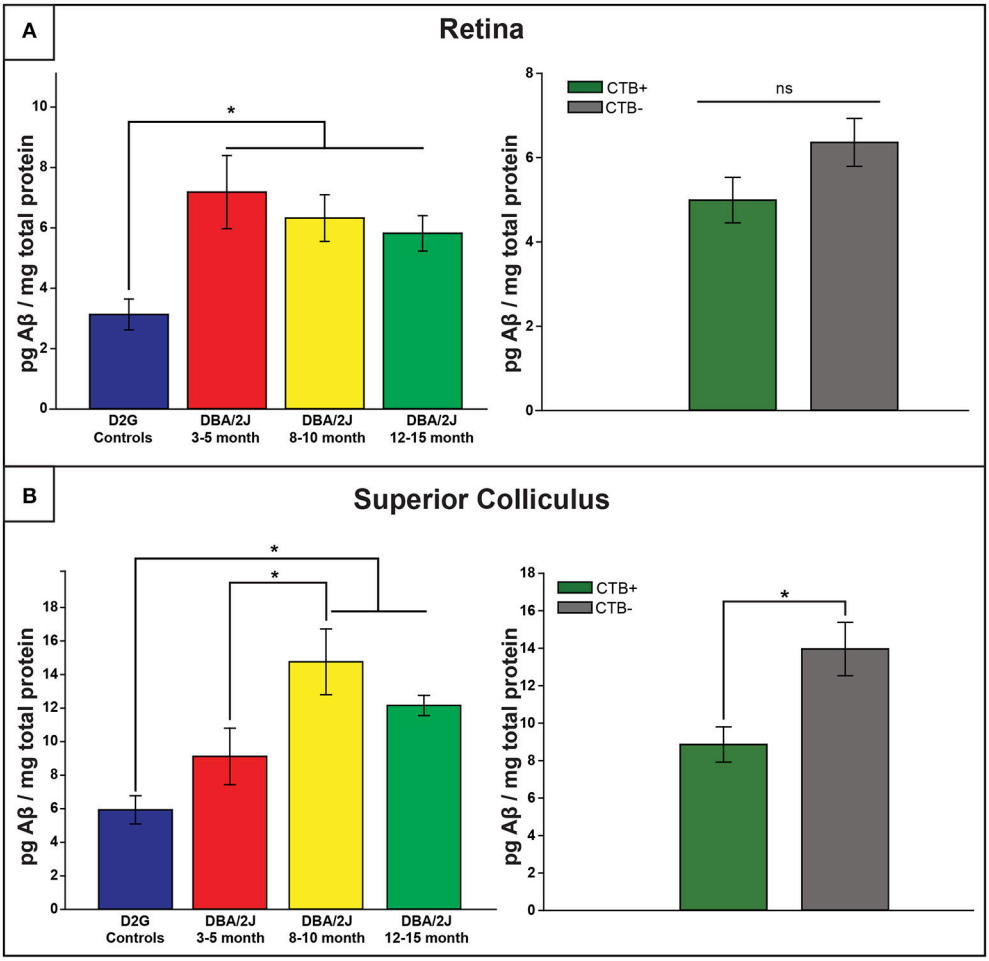

FIGURE 5 | Amyloid-β_{42} elevations provide an early retinal marker of pathology and are later observed in the distal projection. (A) Retinal Aβ_{42} was elevated in all DBA/2J age groups compared to controls (left), with no transport-dependent effects observed (right). **(B)** However, collicular elevations appeared later, with 8–10 and 12–15 month DBA/2J SC having significantly elevated levels compared to controls; a significant difference was also observed between 3–5 and 8–10 month DBA/2Js (left). Levels of Aβ_{42} were significantly elevated in SC lacking intact transport (CTB-) compared to transport-intact (CTB+) SC (right). Error bars indicate SEM. Asterisk indicates that groups are significantly different from bracketed comparison ($p < 0.05$).

DBA/2J animals. Supporting this, we found distal-to-proximal increases in ptau immunofluorescence in the ON of DBA/2J mice, indicating retrograde translocation of tau in glaucoma (Buée et al., 2000; Dixit et al., 2008). Additionally, we showed increased tau phosphorylation (at the threonine-231 residue) in the SC of our pre-pathological 3–5 months. DBA/2J mice—an early effect that preceded significant ptau accumulations in retina. These data suggest that tau translocation from the axon into the somatodendritic compartments occurs as tau becomes increasingly phosphorylated. While the mechanism of this translocation is unknown, it is possible that phosphorylation not only changes tau's affinity for microtubules (Johnson and Stoothoff, 2004) but also increases its affinity for the retrograde motor complex. Supporting this, we demonstrated that phosphorylation of tau increases its affinity for dynactin, a component of the retrograde motor complex that links the molecular motor dynein with its cargo (recall **Figure 3C**).

Calpain-mediated cleavage of α-II spectrin, has been implicated in secondary neurodegenerative processes (such as those resulting from traumatic brain injury; Yan and Jeromin, 2012) and serves as another indicator of axonal injury and pathology. Cleaved α-II spectrin has been found in varicosities and end bulb swellings (Uryu et al., 2007) and is shown to be upregulated in the retina of rodent glaucoma models with elevated IOP (Huang et al., 2010). Spectrin organizes the subaxolemmal actin scaffold that, among other functions, confers strength to axons (Xu et al., 2013), enabling it to resist mechanical stresses (Elson, 1988; Zhou et al., 1999; Jung et al., 2005; Xu et al., 2013). While we were unable to detect SBDP in any DBA/2J or control retina (in contrast to previous findings by Huang et al. (2010) who found elevated SBDP in an experimentally-induced ocular hypertension model), we did observe high levels of calpain-mediated spectrin breakdown product in the ON and SC of our pre-pathological, young DBA/2J mice. This result was

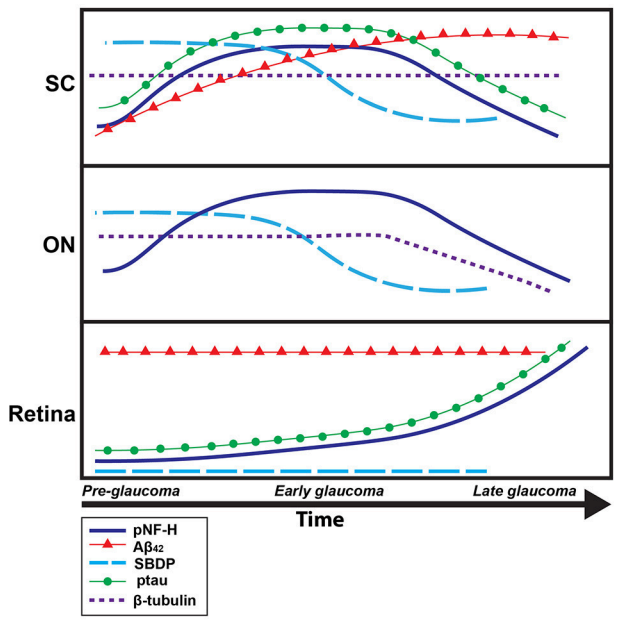

FIGURE 6 | Timeline summary of protein pathology within the DBA/2J retinal projection. A summary schematic of changes in protein levels over disease progression (pre-glaucomatous, early, and late glaucomatous ages), in the DBA/2J mouse model, for each tissue type analyzed (retina, ON, SC) is shown here. The x-axis corresponds to time while the y-axis corresponds to general protein levels. Each colored line corresponds to a specific protein: dark blue corresponds to pNF-H, red corresponds to $A\beta_{42}$, light blue corresponds to SBDP, green corresponds to ptau-231, dotted purple corresponds to β-tubulin. Increased/decreased slope of each line indicates increased/decreased concentrations of each specific protein over time.

somewhat unexpected, as elevated IOP, transport deficits, and axon loss are not typically present in DBA/2J at 3–5 months. Hence, pre-degenerative, post-translational modifications and breakdown of cytoskeletal elements in DBA/2J mice may make their RGC axons vulnerable to glaucomatous neurodegeneration once IOP increases at later ages (Inman et al., 2006).

Elevations in $A\beta_{42}$ fragments often accompany elevated SBDP and the pathological phosphorylation of tau and NF-H in neurodegeneration (Johnson et al., 2016). $A\beta_{42}$ protein is also implicated in axon transport deficits and axonopathy (Stokin et al., 2005; Chidlow et al., 2011), as well as in response to IOP elevation (Ito et al., 2012). We observed elevated levels of $A\beta_{42}$ in the retina of our youngest DBA/2J mice, suggesting this increase occurs prior to IOP elevation. Levels of $A\beta_{42}$ remained elevated in the retina throughout the stages of pathological progression in DBA/2J, and increased in the oldest DBA/2J age group SC. While $A\beta_{42}$ is not a cytoskeletal protein, it activates kinases such as GSK-3β which phosphorylate NF-H and tau (Muyllaert et al., 2008; Martin et al., 2011a,b), potentially conferring susceptibility to axon pathology.

The interplay between early, proximal elevations in Aβ and post-translational modification of cytoskeletal spectrin and neurofilament proteins may be partly explained by the calcium hypothesis of neurodegeneration (Chidlow et al., 2011; Crish and Calkins, 2011). Elevated intracellular calcium, partially promoted by Aβ-mediated increases in Ca^{2+} conductance (Kawahara and Kuroda, 2000) modulates subsequent calpain activation. Ca^{2+}-mediated calpain activation leads to specific cleavage of structural proteins such as neurofilament and spectrin (Crish and Calkins, 2011). This is supported by our observations of elevated calpain-mediated SBDP and $A\beta_{42}$ in young, pre-glaucomatous DBA/2J mice. As these pre-pathological mice do not exhibit elevated IOP at this early stage, these findings suggest that factors other than IOP may cause individuals to be predisposed to developing glaucoma (e.g., subtle changes in kinase activity, excitotoxic stress, or $A\beta_{42}$ load). Recent findings showing early increases in neuroinflammation and oxidative stress are germane here. Neuroinflammation is the earliest change reported in models of glaucoma, often occurring well before neurodegeneration (Wax and Tezel, 2009; Bosco et al., 2011; Howell et al., 2011; Wilson et al., 2015; Hines-Beard et al., 2016). Neuroinflammation can, directly or indirectly, increase the activity of a number of kinases responsible for the phosphorylation of NF and tau in chronic neurodegenerations (For example, CDK-5: Kitazawa et al., 2005; Weston and Davis, 2007; Noda et al., 2014). Oxidative stress is also seen in glaucoma and other neurodegenerations (Chrysostomou et al., 2013; Inman et al., 2013; Burté et al., 2014; Kim et al., 2015; Yang et al., 2016) and reactive oxygen species such as peroxynitrate activate kinases including GSK-3β and p38 that modify tau and other proteins (Zhang et al., 2006). In addition, accumulation of $A\beta_{42}$ and tau have been shown to lead to mitochondrial dysfunction and generation of reactive oxygen species (Luque-Contreras et al., 2014), effectively perpetuating the cycle of pathological phosphorylation and diminished axonal stability and function.

Conclusions

In conclusion, data from the DBA/2J model of glaucoma demonstrate that increased phosphorylation of cytoskeletal proteins such as neurofilament-heavy and tau occurs with age and pathology within the RGC projection. However, the relationship is non-monotonic and overall loss of axonal structure with advanced pathology contributes to decreases in protein concentration at late glaucomatous ages. Although the presumptive, initial stressor (elevated IOP) occurs proximally at the optic nerve head, early manifestations of pathologies can occur distally, as previously reported (Conforti et al., 2007; Crish et al., 2010; Crish and Calkins, 2011) and are not isolated to the eye and retina (Parrish, 2003; Ito et al., 2012). Additionally, our data describing early, pre-degenerative elevations in $A\beta_{42}$ and SBDP, have suggested that there are factors other than elevated IOP perpetuating glaucomatous neurodegeneration or predisposing RGC populations to respond adversely to high IOP later in life in the DBA/2J mouse.

These experiments provide new protein targets affected at pre- and early glaucomatous stages that may provide useful therapeutic tools for diagnosis or interventions that target more than IOP. Importantly, aberrant hyperphosphorylation of cytoskeletal elements, tau, and NF-H, occur prior to complete loss of anterograde transport and axon loss—supporting the idea that a therapeutic window exists in which subtle structural changes may be targeted to potentially prevent loss of function

or structure. This also suggests that activity of GSK-3β and other kinases that lead to hyperphosphorylation and protein translocation/mislocation, along with calpain-induced spectrin breakdown, are early events with clear mechanisms for inhibition. Elucidating the timeline and efficacy of drugs affecting these pathways, therefore, is a promising avenue for future research aimed at slowing, stopping, or reversing early pathology and the ultimate neurodegeneration that produces vision loss in glaucoma.

AUTHOR CONTRIBUTIONS

GW conducted all protein quantification assays, some immunofluorescence, and was involved in the design, analysis and interpretation of data as well as writing and revising the manuscript. MS assisted in sample collection, immunofluorescence and manuscript preparation. SC and DI conceptualized and designed the studies and assisted in the critical revision of the manuscript; CD assisted in immunofluorescent assays, analysis and interpretation of the data, as well as manuscript preparation and critically revising the manuscript.

FUNDING

This work was supported by a grant from the National Eye Institute (EY022358) to SC and by a Young Investigator Fellowship from Prevent Blindness Ohio to GW.

ACKNOWLEDGMENTS

We would like to acknowledge Dr. Werner Geldenhuys for his expertise and assistance in the co-immunoprecipitation experiments. We would also like to acknowledge Dr. Wendi Lambert for valuable discussion of the manuscript.

REFERENCES

Ackerley, S., Thornhill, P., Grierson, A. J., Brownlees, J., Anderton, B. H., Leigh, P. N., et al. (2003). Neurofilament heavy chain side arm phosphorylation regulates axonal transport of neurofilaments. *J. Cell Biol.* 161, 489–495. doi: 10.1083/jcb.200303138

Adalbert, R., and Coleman, M. P. (2012). Axon pathology in age-related neurodegenerative disorders. *Neuropathol. Appl. Neurobiol.* 39, 90–108. doi: 10.1111/j.1365-2990.2012.01308.x

Ahlijanian, M. K., Barrezueta, N. X., Williams, R. D., Jakowski, A., Kowsz, K. P., McCarthy, S., et al. (2000). Hyperphosphorylated tau and neurofilament and cytoskeletal disruptions in mice overexpressing human p25, an activator of cdk5. *Proc. Natl. Acad. Sci. U.S.A.* 97, 2910–2915. doi: 10.1073/pnas.040577797

Almasieh, M., Wilson, A. M., Morquette, B., Cueva Vargas, J. L., and Di Polo, A. (2012). The molecular basis of retinal ganglion cell death in glaucoma. *Prog. Retin. Eye Res.* 31, 152–181. doi: 10.1016/j.preteyeres.2011.11.002

Balaratnasingam, C., Morgan, W. H., Bass, L., Ye, L., McKnight, C., Cringle, S. J., et al. (2008). Elevated pressure induced astrocyte damage in the optic nerve. *Brain Res.* 1244, 142–154. doi: 10.1016/j.brainres.2008.09.044

Bosco, A., Steele, M. R., and Vetter, M. L. (2011). Early microglia activation in a mouse model of chronic glaucoma. *J. Comp. Neurol.* 519, 599–620. doi: 10.1002/cne.22516

Braak, E., Braak, H., and Mandelkow, E.-M. (1994). A sequence of cytoskeleton changes related to the formation of neurofibrillary tangles and neuropil threads. *Acta Neuropathol.* 87, 554–567.

Buckingham, B. P., Inman, D. M., Lambert, W., Oglesby, E., Calkins, D. J., Steele, M. R., et al. (2008). Progressive ganglion cell degeneration precedes neuronal loss in a mouse model of glaucoma. *J. Neurosci.* 28, 2735–2744. doi: 10.1523/JNEUROSCI.4443-07.2008

Buée, L., Bussière, T., Buée-Scherrer, V., Delacourte, A., and Hof, P. R. (2000). Tau protein isoforms, phosphorylation and role in neurodegenerative disorders11These authors contributed equally to this work. *Brain Res. Rev.* 33, 95–130. doi: 10.1016/S0165-0173(00)00019-9

Burroughs, S. L., Kaja, S., and Koulen, P. (2011). Quantification of deficits in spatial visual function of mouse models for glaucoma. *Invest. Ophthalmol. Vis. Sci.* 52, 3654–3659. doi: 10.1167/iovs.10-7106

Burté, F., Carelli, V., Chinnery, P. F., and Yu-Wai-Man, P. (2014). Disturbed mitochondrial dynamics and neurodegenerative disorders. *Nat. Rev. Neurol.* 11, 11–24. doi: 10.1038/nrneurol.2014.228

Chiasseu, M., Vargas, J. L. C., Destroismaisons, L., Velde, C. V., Leclerc, N., and Di Polo, A. (2016). Tau accumulation, altered phosphorylation, and missorting promote neurodegeneration in glaucoma. *J. Neurosci.* 36, 5785–5798. doi: 10.1523/jneurosci.3986-15.2016

Chidlow, G., Ebneter, A., Wood, J. P. M., and Casson, R. J. (2011). The optic nerve head is the site of axonal transport disruption, axonal cytoskeleton damage and putative axonal regeneration failure in a rat model of glaucoma. *Acta Neuropathol.* 121, 737–751. doi: 10.1007/s00401-011-0807-1

Chrysostomou, V., Rezania, F., Trounce, I. A., and Crowston, J. G. (2013). Oxidative stress and mitochondrial dysfunction in glaucoma. *Curr. Opin. Pharmacol.* 13, 12–15. doi: 10.1016/j.coph.2012.09.008

Coleman, M. (2005). Axon degeneration mechanisms: commonality amid diversity. *Nat. Rev. Neurosci.* 6, 889–898. doi: 10.1038/nrn1788

Colucci-D'Amato, L., Perrone-Capano, C., and di Porzio, U. (2003). Chronic activation of ERK and neurodegenerative diseases. *Bioessays* 25, 1085–1095. doi: 10.1002/bies.10355

Conforti, L., Adalbert, R., and Coleman, M. P. (2007). Neuronal death: where does the end begin? *Trends Neurosci.* 30, 159–166. doi: 10.1016/j.tins.2007.02.004

Cooper, M. L., Crish, S. D., Inman, D. M., Horner, P. J., and Calkins, D. J. (2016). Early astrocyte redistribution in the optic nerve precedes axonopathy in the DBA/2J mouse model of glaucoma. *Exp. Eye Res.* 150, 22–33. doi: 10.1016/j.exer.2015.11.016

Crish, S. D., and Calkins, D. J. (2011). Neurodegeneration in glaucoma: progression and calcium-dependent intracellular mechanisms. *Neuroscience* 176, 1–11. doi: 10.1016/j.neuroscience.2010.12.036

Crish, S. D., Dapper, J. D., MacNamee, S. E., Balaram, P., Sidorova, T. N., Lambert, W. S., et al. (2013). Failure of axonal transport induces a spatially coincident increase in astrocyte BDNF prior to synapse loss in a central target. *Neuroscience* 229, 55–70. doi: 10.1016/j.neuroscience.2012.10.069

Crish, S. D., Sappington, R. M., Inman, D. M., Horner, P. J., and Calkins, D. J. (2010). Distal axonopathy with structural persistence in glaucomatous neurodegeneration. *Proc. Natl. Acad. Sci. U.S.A.* 107, 5196–5201. doi: 10.1073/pnas.0913141107

Cuchillo-Ibanez, I., Seereeram, A., Byers, H. L., Leung, K.-Y., Ward, M. A., Anderton, B. H., et al. (2008). Phosphorylation of tau regulates its axonal transport by controlling its binding to kinesin. *FASEB J.* 22, 3186–3195. doi: 10.1096/fj.08-109181

Dengler-Crish, C. M., Smith, M. A., Inman, D. M., Wilson, G. N., Young, J. W., Crish, S. D., et al. (2014). Anterograde transport blockade precedes deficits in retrograde transport in the visual projection of the DBA/2J mouse model of glaucoma. *Front. Neurosci.* 8:290. doi: 10.3389/fnins.2014.00290

Dixit, R., Ross, J. L., Goldman, Y. E., and Holzbaur, E. L. F. (2008). Differential regulation of dynein and kinesin motor proteins by tau. *Science* 319, 1086–1089. doi: 10.1126/science.1152993

Elder, G. A., Friedrich, V. L. Jr, Bosco, P., Kang, C., Gourov, A., Tu, P.-H., et al. (1998a). Absence of the mid-sized neurofilament subunit decreases axonal

calibers, levels of light neurofilament (NF-L), and neurofilament content. *J. Cell Biol.* 141, 727–739. doi: 10.1083/jcb.141.3.727

Elder, G. A., Friedrich, V. L., Kang, C., Bosco, P., Gourov, A., Tu, P.-H., et al. (1998b). Requirement of heavy neurofilament subunit in the development of axons with large calibers. *J. Cell Biol.* 143, 195–205. doi: 10.1083/jcb.143.1.195

Elson, E. L. (1988). Cellular mechanics as an indicator of cytoskeletal structure and function. *Annu. Rev. Biophys. Biophys. Chem.* 17, 397–430. doi: 10.1146/annurev.bb.17.060188.002145

Fischer, L. R., Culver, D. G., Tennant, P., Davis, A. A., Wang, M., Castellano-Sanchez, A., et al. (2004). Amyotrophic lateral sclerosis is a distal axonopathy: evidence in mice and man. *Exp. Neurol.* 185, 232–240. doi: 10.1016/j.expneurol.2003.10.004

Haines, J. D., Inglese, M., and Casaccia, P. (2011). Axonal damage in multiple sclerosis. *Mt. Sinai J. Med.* 78, 231–243. doi: 10.1002/msj.20246

Hines-Beard, J., Bond, W. S., Backstrom, J. R., and Rex, T. S. (2016). Virus-mediated EpoR76E gene therapy preserves vision in a glaucoma model by modulating neuroinflammation and decreasing oxidative stress. *J. Neuroinflammation* 13, 39. doi: 10.1186/s12974-016-0499-5

Howell, G. R., Libby, R. T., Marchant, J. K., Wilson, L. A., Cosma, I. M., Smith, R. S., et al. (2007). Absence of glaucoma in DBA/2J mice homozygous for wild-type versions of *Gpnmb* and *Tyrp1*. *BMC Genet.* 8:45. doi: 10.1186/1471-2156-8-45

Howell, G. R., Macalinao, D. G., Sousa, G. L., Walden, M., Soto, I., Kneeland, S. C., et al. (2011). Molecular clustering identifies complement and endothelin induction as early events in a mouse model of glaucoma. *J. Clin. Invest.* 121, 1429–1444. doi: 10.1172/JCI44646

Huang, W., Fileta, J., Rawe, I., Qu, J., and Grosskreutz, C. L. (2010). Calpain activation in experimental glaucoma. *Invest. Ophthalmol. Vis. Sci.* 51, 3049–3054. doi: 10.1167/iovs.09-4364

Huang, X., Kong, W., Zhou, Y., and Gregori, G. (2011). Distortion of axonal cytoskeleton: an early sign of glaucomatous damage. *Invest. Ophthalmol. Vis. Sci.* 52, 2879–2888. doi: 10.1167/iovs.10-5929

Inman, D. M., Lambert, W. S., Calkins, D. J., and Horner, P. J. (2013). α-Lipoic acid antioxidant treatment limits glaucoma-related retinal ganglion cell death and dysfunction.pdf. *PLoS ONE* 8:e65389. doi: 10.1371/journal.pone.0065389

Inman, D. M., Sappington, R. M., Horner, P. J., and Calkins, D. J. (2006). Quantitative correlation of optic nerve pathology with ocular pressure and corneal thickness in the DBA/2 mouse model of glaucoma. *Invest. Ophthalmol. Vis. Sci.* 47, 986–996. doi: 10.1167/iovs.05-0925

Iqbal, K., Liu, F., and Gong, C.-X. (2016). Tau and neurodegenerative disease: the story so far. *Nat. Rev. Neurol.* 12, 15–27. doi: 10.1038/nrneurol.2015.225

Ito, Y., Shimazawa, M., Tsuruma, K., Mayama, C., Ishii, K., Onoe, H., et al. (2012). Induction of amyloid-β(1-42) in the retina and optic nerve head of chronic ocular hypertensive monkeys. *Mol. Vis.* 18, 2647–2657.

John, S. W., Smith, R. S., Savinova, O. V., Hawes, N. L., Chang, B., Turnbull, D., et al. (1998). Essential iris atrophy, pigment dispersion, and glaucoma in DBA/2J mice. *Invest. Ophthalmol. Vis. Sci.* 39, 951–962.

Johnson, G. V. W., and Stoothoff, W. H. (2004). Tau phosphorylation in neuronal cell function and dysfunction. *J. Cell Sci.* 117, 5721–5729. doi: 10.1242/jcs.01558

Johnson, V. E., Stewart, W., Weber, M. T., Cullen, D. K., Siman, R., and Smith, D. H. (2016). SNTF immunostaining reveals previously undetected axonal pathology in traumatic brain injury. *Acta Neuropathol.* 131, 115–135. doi: 10.1007/s00401-015-1506-0

Julien, J.-P., and Mushynski, W. E. (1998). Neurofilaments in Health and Disease. *Prog. Nucleic Acid Res. Mol. Biol.* 61, 1–23. doi: 10.1016/S0079-6603(08)60823-5

Jung, C., Lee, S., Ortiz, D., Zhu, Q., Julien, J.-P., and Shea, T. B. (2005). The high and middle molecular weight neurofilament subunits regulate the association of neurofilaments with kinesin: Inhibition by phosphorylation of the high molecular weight subunit. *Mol. Brain Res.* 141, 151–155. doi: 10.1016/j.molbrainres.2005.08.009

Jung, C., and Shea, T. B. (1999). Regulation of neurofilament axonal transport by phosphorylation in optic axons *in situ*. *Cell Motil. Cytoskeleton* 42, 230–240. doi: 10.1002/(SICI)1097-0169(1999)42:3<230::AID-CM6>3.0.CO;2-A

Jung, C., and Shea, T. B. (2004). Neurofilament subunits undergo more rapid translocation within retinas than in optic axons. *Mol. Brain Res.* 122, 188–192. doi: 10.1016/j.molbrainres.2003.10.008

Kang, J. H., Loomis, S. J., Wiggs, J. L., Willett, W. C., and Pasquale, L. R. (2014). A prospective study of folate, vitamin B_6, and vitamin B_{12} intake in relation to exfoliation glaucoma or suspected exfoliation glaucoma. *JAMA Ophthalmol.* 132, 549–559. doi: 10.1001/jamaophthalmol.2014.100

Kawahara, M., and Kuroda, Y. (2000). Molecular mechanism of neurodegeneration induced by Alzheimer's β-amyloid protein: channel formation and disruption of calcium homeostasis. *Brain Res. Bull.* 53, 389–397. doi: 10.1016/S0361-9230(00)00370-1

Kim, K.-Y., Perkins, G. A., Shim, M. S., Bushong, E., Alcasid, N., Ju, S., et al. (2015). DRP1 inhibition rescues retinal ganglion cells and their axons by preserving mitochondrial integrity in a mouse model of glaucoma. *Cell Death Dis.* 6, e1839. doi: 10.1038/cddis.2015.180

Kitazawa, M., Oddo, S., Yamasaki, T. R., Green, K. N., and LaFerla, F. M. (2005). Lipopolysaccharide-induced inflammation exacerbates tau pathology by a cyclin-dependent kinase 5-mediated pathway in a transgenic model of Alzheimer's disease. *J. Neurosci.* 25, 8843–8853. doi: 10.1523/JNEUROSCI.2868-05.2005

Knobloch, M., and Mansuy, I. M. (2008). Dendritic spine loss and synaptic alterations in Alzheimer's disease. *Mol. Neurobiol.* 37, 73–82. doi: 10.1007/s12035-008-8018-z

Köpke, E., Tung, Y. C., Shaikh, S., Alonso, A. C., Iqbal, K., and Grundke-Iqbal, I. (1993). Microtubule-associated protein tau: abnormal phosphorylation of a non-paired helical filament pool in Alzheimer disease. *J. Biol. Chem.* 268, 24374–24384.

Lee, M. S., Kwon, Y. T., Li, M., Peng, J., Friedlander, R. M., and Tsai, L. H. (2000). Neurotoxicity induces cleavage of p35 to p25 by calpain. *Nature* 405, 360–364. doi: 10.1038/35012636

Lépinoux-Chambaud, C., and Eyer, J. (2013). Review on intermediate filaments of the nervous system and their pathological alterations. *Histochem. Cell Biol.* 140, 13–22. doi: 10.1007/s00418-013-1101-1

Libby, R. T., Gould, D. B., Anderson, M. G., and John, S. W. (2005). Complex genetics of glaucoma susceptibility. *Annu. Rev. Genomics Hum. Genet.* 6, 15–44. doi: 10.1146/annurev.genom.6.080604.162209

Lim, H., and Danias, J. (2012). Effect of axonal micro-tubules on the morphology of retinal nerve fibers studied by second-harmonic generation. *J. Biomed. Opt.* 17:110502. doi: 10.1117/1.JBO.17.11.110502

Luque-Contreras, D., Carvajal, K., Toral-Rios, D., Franco-Bocanegra, D., and Campos-Peña, V. (2014). Oxidative stress and metabolic syndrome: cause or consequence of Alzheimer's disease? *Oxid. Med. Cell. Longev.* 2014:497802. doi: 10.1155/2014/497802

Majid, T., Ali, Y. O., Venkitaramani, D. V., Jang, M.-K., Lu, H.-C., and Pautler, R. G. (2014). *In vivo* axonal transport deficits in a mouse model of fronto-temporal dementia. *NeuroImage. Clin.* 4, 711–717. doi: 10.1016/j.nicl.2014.02.005

Martin, L., Latypova, X., and Terro, F. (2011a). Post-translational modifications of tau protein: implications for Alzheimer's disease. *Neurochem. Int.* 58, 458–471. doi: 10.1016/j.neuint.2010.12.023

Martin, L., Page, G., and Terro, F. (2011b). Tau phosphorylation and neuronal apoptosis induced by the blockade of PP2A preferentially involve GSK3β. *Neurochem. Int.* 59, 235–250. doi: 10.1016/j.neuint.2011.05.010

McKinnon, S. J. (2003). Glaucoma: ocular Alzheimer's disease? *Front. Biosci.* 8:s1140. doi: 10.2741/1172

McKinnon, S. J., Schlamp, C. L., and Nickells, R. W. (2009). Mouse models of retinal ganglion cell death and glaucoma. *Exp. Eye Res.* 88, 816–824. doi: 10.1016/j.exer.2008.12.002

Morfini, G. A., Burns, M., Binder, L. I., Kanaan, N. M., LaPointe, N., Bosco, D. A., et al. (2009). Axonal transport defects in neurodegenerative diseases. *J. Neurosci.* 29, 12776–12786. doi: 10.1523/JNEUROSCI.3463-09.2009

Morfini, G., Schmidt, N., Weissmann, C., Pigino, G., and Kins, S. (2016). Conventional kinesin: biochemical heterogeneity and functional implications in health and disease. *Brain Res. Bull.* 126, 347–353. doi: 10.1016/j.brainresbull.2016.06.009

Muyllaert, D., Kremer, A., Jaworski, T., Borghgraef, P., Devijver, H., Croes, S., et al. (2008). Glycogen synthase kinase-3b, or a link between amyloid and tau pathology? *Genes, Brain Behav.* 7, 57–66. doi: 10.1111/j.1601-183X.2007.00376.x

Nicolas, G., Fournier, C. M., Galand, C., Malbert-Colas, L., Bournier, O., Kroviarski, Y., et al. (2002). Tyrosine phosphorylation regulates alpha ii spectrin cleavage by calpain. *Mol. Cell. Biol.* 22, 3527–3536. doi: 10.1128/MCB.22.10.3527-3536.2002

Nixon, R. A. (1994). Phosphorylation on carboxyl terminus domains of neurofilament proteins in retinal ganglion cell neurons *in vivo*: influences on regional neurofilament accumulation, interneurofilament spacing, and axon caliber. *J. Cell Biol.* 126, 1031–1046. doi: 10.1083/jcb.126.4.1031

Noda, M., Takii, K., Parajuli, B., Kawanokuchi, J., Sonobe, Y., Takeuchi, H., et al. (2014). FGF-2 released from degenerating neurons exerts microglial-induced neuroprotection via FGFR3-ERK signaling pathway. *J. Neuroinflammation* 11:76. doi: 10.1186/1742-2094-11-76

Parrish, R. K. (2003). Reduction of intraocular pressure and glaucoma progression. *Evid. Based Eye Care* 4, 137–139. doi: 10.1097/00132578-200307000-00009

Petzold, A., Gveric, D., Groves, M., Schmierer, K., Grant, D., Chapman, M., et al. (2008). Phosphorylation and compactness of neurofilaments in multiple sclerosis: indicators of axonal pathology. *Exp. Neurol.* 213, 326–335. doi: 10.1016/j.expneurol.2008.06.008

Quigley, H. A. (1999). Neuronal death in glaucoma. *Prog. Retin. Eye Res.* 18, 39–57. doi: 10.1016/S1350-9462(98)00014-7

Roy, S., Zhang, B., Lee, V. M.-Y., and Trojanowski, J. Q. (2005). Axonal transport defects: a common theme in neurodegenerative diseases. *Acta Neuropathol.* 109, 5–13. doi: 10.1007/s00401-004-0952-x

Schlamp, C. L., Li, Y., Dietz, J. A., Janssen, K. T., and Nickells, R. W. (2006). Progressive ganglion cell loss and optic nerve degeneration in DBA/2J mice is variable and asymmetric. *BMC Neurosci.* 7:66. doi: 10.1186/1471-2202-7-66

Schultz, C., Koppers, D., Braak, E., and Braak, H. (1997). "Neurofibrillary degeneration in hypophysiotrophic nuclei of the aging human hypothalamus," in *Neuroendocrinology: Retrospect and Perspectives*, eds H. Kort and K. Usadel (Berlin; Heidelberg: Springer), 115–126.

Shea, T. B., and Chan, W. K.-H. (2008). Regulation of neurofilament dynamics by phosphorylation. *Eur. J. Neurosci.* 27, 1893–1901. doi: 10.1111/j.1460-9568.2008.06165.x

Song, Y., Kirkpatrick, L. L., Schilling, A. B., Helseth, D. L., Chabot, N., Keillor, J. W., et al. (2013). Transglutaminase and polyamination of tubulin: posttranslational modification for stabilizing axonal microtubules. *Neuron* 78, 109–123. doi: 10.1016/j.neuron.2013.01.036

Soto, I., Pease, M. E., Son, J. L., Shi, X., Quigley, H. A., and Marsh-Armstrong, N. (2011). Retinal ganglion cell loss in a rat ocular hypertension model is sectorial and involves early optic nerve axon loss. *Invest. Ophthalmol. Vis. Sci.* 52, 434–441. doi: 10.1167/iovs.10-5856

Stokin, G. B., Lillo, C., Falzone, T. L., Brusch, R. G., Rockenstein, E., Mount, S. L., et al. (2005). Axonopathy and transport deficits early in the pathogenesis of Alzheimer's disease. *Science* 307, 1282–1288. doi: 10.1126/science.1105681

Sunico, C. R., Domínguez, G., García-Verdugo, J. M., Osta, R., Montero, F., and Moreno-López, B. (2011). Reduction in the motoneuron inhibitory/excitatory synaptic ratio in an early-symptomatic mouse model of amyotrophic lateral sclerosis. *Brain Pathol.* 21, 1–15. doi: 10.1111/j.1750-3639.2010.00417.x

Tahzib, N. G., Ransom, N. L., Reitsamer, H. A., and McKinnon, S. J. (2004). Alpha-fodrin is cleaved by caspase-3 in a chronic ocular hypertensive (COH) rat model of glaucoma. *Brain Res. Bull.* 62, 491–495. doi: 10.1016/S0361-9230(03)00083-2

Tham, Y. -C., Li, X., Wong, T. Y., Quigley, H. A., Aung, T., and Cheng, C.-Y. (2014). Global prevalence of glaucoma and projections of glaucoma burden through 2040. *Ophthalmology* 121, 2081–2090. doi: 10.1016/j.ophtha.2014.05.013

Uryu, K., Chen, X.-H., Martinez, D., Browne, K. D., Johnson, V. E., Graham, D. I., et al. (2007). Multiple proteins implicated in neurodegenerative diseases accumulate in axons after brain trauma in humans. *Exp. Neurol.* 208, 185–192. doi: 10.1016/j.expneurol.2007.06.018

Wax, M. B., and Tezel, G. (2009). Immunoregulation of retinal ganglion cell fate in glaucoma. *Exp. Eye Res.* 88, 825–830. doi: 10.1016/j.exer.2009.02.005

Weston, C. R., and Davis, R. J. (2007). The JNK signal transduction pathway. *Curr. Opin. Cell Biol.* 19, 142–149. doi: 10.1016/j.ceb.2007.02.001

Wilson, G. N., Inman, D. M., Dengler-Crish, C. M., Smith, M. A., and Crish, S. D. (2015). Early pro-inflammatory cytokine elevations in the DBA/2J mouse model of glaucoma. *J. Neuroinflammation* 12:176. doi: 10.1186/s12974-015-0399-0

Wortman, J. C., Shrestha, U. M., Barry, D. M., Garcia, M. L., Gross, S. P., and Yu, C. C. (2014). Axonal transport: how high microtubule density can compensate for boundary effects in small-caliber axons. *Biophys. J.* 106, 813–823. doi: 10.1016/j.bpj.2013.12.047

Xu, K., Zhong, G., and Zhuang, X. (2013). Actin, spectrin, and associated proteins form a periodic cytoskeletal structure in axons. *Science* 339, 452–456. doi: 10.1126/science.1232251

Yan, X.-X., and Jeromin, A. (2012). Spectrin breakdown products (SBDPs) as potential biomarkers for neurodegenerative diseases. *Curr. Transl. Geriatr. Exp. Gerontol. Rep.* 1, 85–93. doi: 10.1007/s13670-012-0009-2

Yang, X., Hondur, G., and Tezel, G. (2016). Antioxidant treatment limits neuroinflammation in experimental glaucoma. *Invest. Ophthalmol. Vis. Sci.* 57, 2344–2354. doi: 10.1167/iovs.16-19153

Zempel, H., and Mandelkow, E.-M. (2015). Tau missorting and spastin-induced microtubule disruption in neurodegeneration: Alzheimer Disease and Hereditary Spastic Paraplegia. *Mol. Neurodegener.* 10, 68. doi: 10.1186/s13024-015-0064-1

Zhang, Y.-J., Xu, Y.-F., Liu, Y.-H., Yin, J., Li, H.-L., Wang, Q., et al. (2006). Peroxynitrite induces Alzheimer-like tau modifications and accumulation in rat brain and its underlying mechanisms. *FASEB J.* 20, 1431–1442. doi: 10.1096/fj.05-5223com

Zhou, L., Li, Y., and Yue, B. Y. (1999). Oxidative stress affects cytoskeletal structure and cell-matrix interactions in cells from an ocular tissue: the trabecular meshwork. *J. Cell. Physiol.* 180, 182–189.

Conflict of Interest Statement: The authors declare that the research was conducted in the absence of any commercial or financial relationships that could be construed as a potential conflict of interest.

frontiers in Neuroscience

REVIEW
published: 26 April 2017
doi: 10.3389/fnins.2017.00235

Shared and Differential Retinal Responses against Optic Nerve Injury and Ocular Hypertension

Manuel Vidal-Sanz, Caridad Galindo-Romero, Francisco J. Valiente-Soriano, Francisco M. Nadal-Nicolás, Arturo Ortin-Martinez, Giuseppe Rovere, Manuel Salinas-Navarro, Fernando Lucas-Ruiz, Maria C. Sanchez-Migallon, Paloma Sobrado-Calvo, Marcelino Aviles-Trigueros, María P. Villegas-Pérez and Marta Agudo-Barriuso*

Departamento de Oftalmología, Facultad de Medicina, Universidad de Murcia and Instituto Murciano de Investigación Biosanitaria Virgen de la Arrixaca, Murcia, Spain

OPEN ACCESS

Edited by:
Samuel David Crish, Northeast Ohio Medical University, USA

Reviewed by:
Glyn Chidlow, Royal Adelaide Hospital, Australia
Sudheendra N. R. Rao, University of Miami, USA

***Correspondence:**
Manuel Vidal-Sanz
manuel.vidal@um.es

Specialty section:
This article was submitted to Neurodegeneration, a section of the journal Frontiers in Neuroscience

Received: *02 March 2017*
Accepted: *07 April 2017*
Published: *26 April 2017*

Citation:
Vidal-Sanz M, Galindo-Romero C, Valiente-Soriano FJ, Nadal-Nicolás FM, Ortin-Martinez A, Rovere G, Salinas-Navarro M, Lucas-Ruiz F, Sanchez-Migallon MC, Sobrado-Calvo P, Aviles-Trigueros M, Villegas-Pérez MP and Agudo-Barriuso M (2017) Shared and Differential Retinal Responses against Optic Nerve Injury and Ocular Hypertension. Front. Neurosci. 11:235. doi: 10.3389/fnins.2017.00235

Glaucoma, one of the leading causes of blindness worldwide, affects primarily retinal ganglion cells (RGCs) and their axons. The pathophysiology of glaucoma is not fully understood, but it is currently believed that damage to RGC axons at the optic nerve head plays a major role. Rodent models to study glaucoma include those that mimic either ocular hypertension or optic nerve injury. Here we review the anatomical loss of the general population of RGCs (that express Brn3a; Brn3a$^+$RGCs) and of the intrinsically photosensitive RGCs (that express melanopsin; m$^+$RGCs) after chronic (LP-OHT) or acute (A-OHT) ocular hypertension and after complete intraorbital optic nerve transection (ONT) or crush (ONC). Our studies show that all of these insults trigger RGC death. Compared to Brn3a$^+$RGCs, m$^+$RGCs are more resilient to ONT, ONC, and A-OHT but not to LP-OHT. There are differences in the course of RGC loss both between these RGC types and among injuries. An important difference between the damage caused by ocular hypertension or optic nerve injury appears in the outer retina. Both axotomy and LP-OHT induce selective loss of RGCs but LP-OHT also induces a protracted loss of cone photoreceptors. This review outlines our current understanding of the anatomical changes occurring in rodent models of glaucoma and discusses the advantages of each one and their translational value.

Keywords: glaucoma, chronic ocular hypertension, acute ocular hypertension, axotomy, Brn3a retinal ganglion cells, melanopsin retinal ganglion cells, cone photoreceptors, retinal nerve fiber layer

INTRODUCTION

The mammalian retina is an extension of the central nervous system (CNS) specialized to capture environmental luminous information. Light is transduced into electrical signals by the photo pigments (opsins) expressed by rod and cone photoreceptors or by the intrinsically photosensitive retinal ganglion cells (ipRGCs). The rod and cone signals are further elaborated by intermediate neurons located in the outer and inner plexiform layers and reach their way out of the retina through the retinal ganglion cell (RGC) population. RGCs constitute approximately less than 3% of all retinal neurons but are the only ones whose axons exit the retina to convey luminous information to the retinorecipient target regions of the brain.

Luminous information serves three main purposes; allows a nocturnal perception of very dim lights, a colorful daylight perception of bright lights, and regulates a number of autonomous behaviors. The two first purposes are the basis of our conscious image-forming vision and this luminous information is carried out by the general population of RGCs, which express Brn3a. Light-triggered autonomous behaviors are carried out by the ipRGCs that express the photopigment melanopsin and are the basis for a number of non-image forming visual reflex behaviors (Hattar et al., 2002, 2003) such as the pupillary light reflex, the photoentrainment of circadian rhythms and photic suppression of melatonin (Lucas et al., 2014).

The retina has been a preferred extension of the adult mammalian CNS to study plasticity, regeneration and degeneration because of its accessibility for experimental manipulation and its well-known anatomy and physiology (Aguayo et al., 1987; Bray et al., 1987, 1991). The capacity of adult mammalian CNS neurons for axonal regeneration (Munz et al., 1985), re-innervation of their appropriate targets (Vidal-Sanz et al., 1991; Avilés-Trigueros et al., 2000), synapse formation (Vidal-Sanz et al., 1987, 1991; Keirstead et al., 1989) and recovery of simple visual behaviors (Sasaki et al., 1996; Whiteley et al., 1998; Vidal-Sanz et al., 2002) has been investigated in the adult rodent retina (Aguayo et al., 1987; Bray et al., 1987, 1991).

Rodent RGCs share their location in the innermost retinal layer of the retina with the displaced amacrine cells, a population that overlaps RGCs in soma size (Villegas-Pérez et al., 1988, 1993) and is even larger than the RGC population itself (Nadal-Nicolás et al., 2015a). This has obliged the utilization of specific labeling techniques to identify RGCs and distinguish them from the displaced amacrine cells (Vidal-Sanz et al., 2000), including the use of retrogradely transported neuronal tracers applied to their axons or targets (Thanos et al., 1987; Vidal-Sanz et al., 1987, 1988) and specific RGC markers. Morphological criteria such as soma and dendritic arborisation size and levels of stratification within the inner plexiform layer, as well as electrophysiological responses to light stimuli and target region of the brain, may render over 30 different types of RGCs in the healthy rodent retina (Sun et al., 2002a,b; Coombs et al., 2006; for review see: Sanes and Masland, 2015). Many of these attributes change after injury and thus cannot be used to identify damaged RGCs (for review see Tribble et al., 2014). Molecular markers for RGCs are scarce, most do not label the entire population of RGCs and are downregulated in response to retinal injury (Chidlow et al., 2005; Lönngren et al., 2006; Agudo et al., 2008), thus rendering their use unreliable to identify RGCs. At present, Brn3a and melanopsin are two well-known molecular markers that identify most of the adult rodent (rats and mice) RGCs that conduct respectively, information related to image-forming and nonimage-forming visual functions. We have recently described that in the rat Brn3a is expressed by approximately 96% of the RGCs while the remaining 4% which do not express Brn3a is composed of approximately one half of the ipsilaterally projecting RGCs (1.3%) and the melanopsin expressing RGCs (m^+RGCs) (2.6%) (Nadal-Nicolás et al., 2012, 2014; Galindo-Romero et al., 2013a; Valiente-Soriano et al., 2014). The differential expression of these two proteins, Brn3a and melanopsin, by the two functional types of RGCs makes double immunodetection a great tool to study in the same retinas the fate of these two distinct RGC populations upon injury and/or neuroprotection (Vidal-Sanz et al., 2015a,b; Agudo-Barriuso et al., 2016).

A progressive loss of RGCs and associated visual field deficits are a classic hallmark of the glaucomatous optic neuropathies (GON), a group of diseases that are the second leading cause of blindness in developed countries (Resnikoff et al., 2004). More recently, a number of additional features have been associated with GON, namely; characteristic defects in the nerve fiber layer, the optic disc and the optic nerve head (Quigley, 2011; Chauhan et al., 2014; Weinreb et al., 2014), as well as defects in the main subcortical and cortical visual targets (Yücel et al., 2003; Nucci et al., 2013). Moreover, other non-visually related areas of the cortex may also become affected (Frezzotti et al., 2014). In addition to RGCs, a number of reports have suggested that other non-RGC neurons are also affected in experimental or human GON retinas. Several studies have shown molecular, functional and structural changes in outer retinal layers (outer nuclear and outer segments) in humans (Nork et al., 2000; Barboni et al., 2011; Werner et al., 2011), non-human primates (Nork et al., 2000; Liu et al., 2014) and rodent models of glaucoma or ocular hypertension (OHT) (Mittag et al., 2000; Calkins, 2012; Fuchs et al., 2012; Pérez de Lara et al., 2014). These changes range from a diminution in the expression of opsins by photoreceptors to the severe loss of rods and cones with time (Ortín-Martínez et al., 2015).

The pathophysiology of GON is not fully understood, but much attention has been focussed on some of the most important risk factors and possible mechanisms; these include ocular hypertension, ischemia and axonal compression of the RGC axons within the initial segment of the optic nerve. Among the experimental rodent models of glaucoma there are two popular models that employ as a primary insult axotomy of the optic nerve or ocular hypertension.

The responses of RGCs to optic nerve injury have been studied extensively (Vidal-Sanz et al., 2000, 2007; Lindqvist et al., 2004; Jehle et al., 2008; Parrilla-Reverter et al., 2009a,b). Indeed, complete intraorbital optic nerve crush (ONC) or transection (ONT) are clean and reproducible models with relatively little inter-animal variability (Vidal-Sanz et al., 1987; Peinado-Ramón et al., 1996; Sobrado-Calvo et al., 2007; Parrilla-Reverter et al., 2009a; Sánchez-Migallón et al., 2011, 2016; Nadal-Nicolás et al., 2015a; Rovere et al., 2016a). Ocular hypertension tries to mimic one of the main risk factors of glaucoma and involves an increase of the intraocular pressure, but is a more complex model than axotomy and not as clean or reproducible (Salinas-Navarro et al., 2009c, 2010; Cuenca et al., 2010; Chidlow et al., 2011; Soto et al., 2011; Ortín-Martínez et al., 2015; Valiente-Soriano et al., 2015a,b; Rovere et al., 2016a). Recent studies have shown that m^+RGCs are particularly resistant to a number of acquired or induced retinal diseases (Cui et al., 2015; Vidal-Sanz et al., 2015b; Agudo-Barriuso et al., 2016; Rovere et al., 2016a); but their response to glaucoma or ocular hypertension-induced retinal degeneration has not yielded homogeneous results (Li et al., 2006; González-Fleitas et al., 2015; Valiente-Soriano et al., 2015a,b). However, a surmounting body of recent evidence points that m^+RGCs

are severely affected in human glaucomatous retinas (Obara et al., 2016) as well as in animal models of ocular hypertension (Valiente-Soriano et al., 2015a,b).

There are several ways to raise artificially the IOP in rodents (for review see, Morrison et al., 2011; Vidal-Sanz et al., 2012, 2015a). Here, we will focus on a chronic and an acute model of ocular hypertension; the laser photocoagulation of limbar and perilimbar tissues and the anterior chamber cannulation. The main difference between these two models resides on the net increase of the IOP and on its duration. The chronic model consists of laser photocauterizacion of the limbar and perilimbar tissues to induce ocular hypertension (LP-OHT) (Levkovitch-Verbin et al., 2002; WoldeMussie et al., 2002). In albino rats LP-OHT results in a significant increase of the IOP that is already evident by 12 h, peaks at 48 h and remains significantly elevated for the first week, declining slowly to reach normal values by 3 weeks (Schnebelen et al., 2009; Salinas-Navarro et al., 2010; Ortín-Martínez et al., 2015; Valiente-Soriano et al., 2015b). In albino and pigmented mice, IOP levels raise above control values during the first 5 days, returning to basal values by 7 days after LP (Salinas-Navarro et al., 2009c; Cuenca et al., 2010; Valiente-Soriano et al., 2015a). The acute model of ocular hypertension (A-OHT) consists of cannulation of the anterior chamber with a needle connected to a saline reservoir that is elevated to increase the IOP for a short period of time; for instance in our Lab we increased IOP to 76 ± 3 mm Hg for 75 min (Rovere et al., 2016a; Wang et al., 2017). The fellow (contralateral) eyes showed normal levels of IOP (9 ± 1 mm Hg) at all time intervals studied.

Here we review some recent studies in our Laboratory on rodent models of GON, namely intra-orbital optic nerve injury and acute or chronic induction of ocular hypertension. We have compared the effects of optic nerve injury or ocular hypertension on the innermost (RGCs and all cells in the RGC layer) and outer (L- and S-cones) retinal layers. We have used imaging and counting techniques developed in our Laboratory to identify, count, and map in the same entire retinal wholemounts: (i) the general population of RGCs (non-melanopsin expressing RGCs, identified with Brn3a, Brn3a$^+$RGCs); (ii) the population of intrinsically photosensitive RGCs (melanopsin expressing RGCs; m$^+$RGCs); (iii) the population of cells in the RGC layer (identified by DAPI nuclear counterstaining); (iv) the nerve fiber layer of the retina (identified with neurofibrillary antibodies), and; (v) the L- and S-cone photoreceptor populations (identified with L- and S-opsin antibodies).

RESULTS AND DISCUSSION

As we will see below, RGC damage in terms of quantitative and topographical loss differs between axotomy and OHT, as well as between Brn3a$^+$ and melanopsin$^+$RGCs. Furthermore, within each injury and RGC subtype, there are subtle differences among species and strain. Finally, neither insult causes the loss of non-RGC neurons in the ganglion cell layer (Ortín-Martínez et al., 2015; Nadal-Nicolás et al., 2015a) but ocular hypertension results in a secondary damage that reaches the outer retina (Ortín-Martínez et al., 2015).

Temporal Course of RGC Loss: Axotomy vs. OHT

To compare the time-course of RGC loss we gathered the results from our previously published work (**Figure 1**). We have estimated for each lesion, species and species strain the percentage of surviving Brn3a$^+$− and melanopsin$^+$RGCs at each time point, considering 100% the values in intact retinas (**Figure 1A**). All these values were obtained by quantifying the total number of RGCs identified in retinal whole-mounts. We performed an X,Y (time, survival) analysis using data in **Figure 1A**. We found that the loss of Brn3a$^+$RGCs adjusts well to either a segmental linear or to a linear regression (**Figure 1B**), providing a mathematical model to compare more easily the damage caused by each lesion in each species and strain. These adjustments are useful as well to predict the percentage of survival (or loss) at a given time post-lesion, or *vice versa*, and thus, to design experiments within a possible window for therapeutic intervention.

Brn3a$^+$RGCs: Axotomy vs. OHT

As shown in the regression analysis, axotomy triggers the linear loss of Brn3a$^+$RGCs in two sequential phases. During the first one, RGC death is abrupt and quick and lasts 7–12 days depending on the species, strain and the type of injury (**Figure 1B**, X_0 values, for example, the response is quicker in pigmented than in albino mice). In the albino rat, during the first phase approximately 80–95% of RGCs die, and this is followed by a second slower phase that lasts up to 450 (Nadal-Nicolás et al., 2015a) or 600 (Villegas-Pérez et al., 1993) days, the latest time points analyzed. During the second phase, there is a protracted loss of RGCs (Villegas-Pérez et al., 1993), so that by the latest time points analyzed after the lesion approximately 1–3% of RGCs survive (Villegas-Pérez et al., 1993; Nadal-Nicolás et al., 2015a).

LP-OHT resulted in progressive loss of RGCs as well as in a number of typical findings observed in a mouse model of inherited glaucoma, the DBA/2J mice (Schlamp et al., 2006; Crish et al., 2010; Calkins, 2012; Pérez de Lara et al., 2014). These include: loss of RGCs in pie-shaped sectors with their base toward the retinal periphery and their apex toward the optic disc; early damage to the RGC axons near the ON head, and survival of RGCs with their axonal transport altered (both orthograde and retrograde) (Salinas-Navarro et al., 2009c, 2010; Cuenca et al., 2010; Chidlow et al., 2011; Soto et al., 2011; Valiente-Soriano et al., 2015a,b). The course of RGC loss after LP-OHT or axotomy differs in two main points: (i) in albino rats and mice the first phase of RGC death is longer (X_0, 15–24 days) and less steep, and; (ii) RGC survival after LP-OHT is higher than after axotomy at the same time points. The main differences between rats and mice are that after the first phase of RGC death, LP-OHT does not cause a further loss in rats but it does in mice. However, we cannot discard that in mice RGC loss after LP-OHT stabilizes later than 30 days, the longest time analyzed in this species.

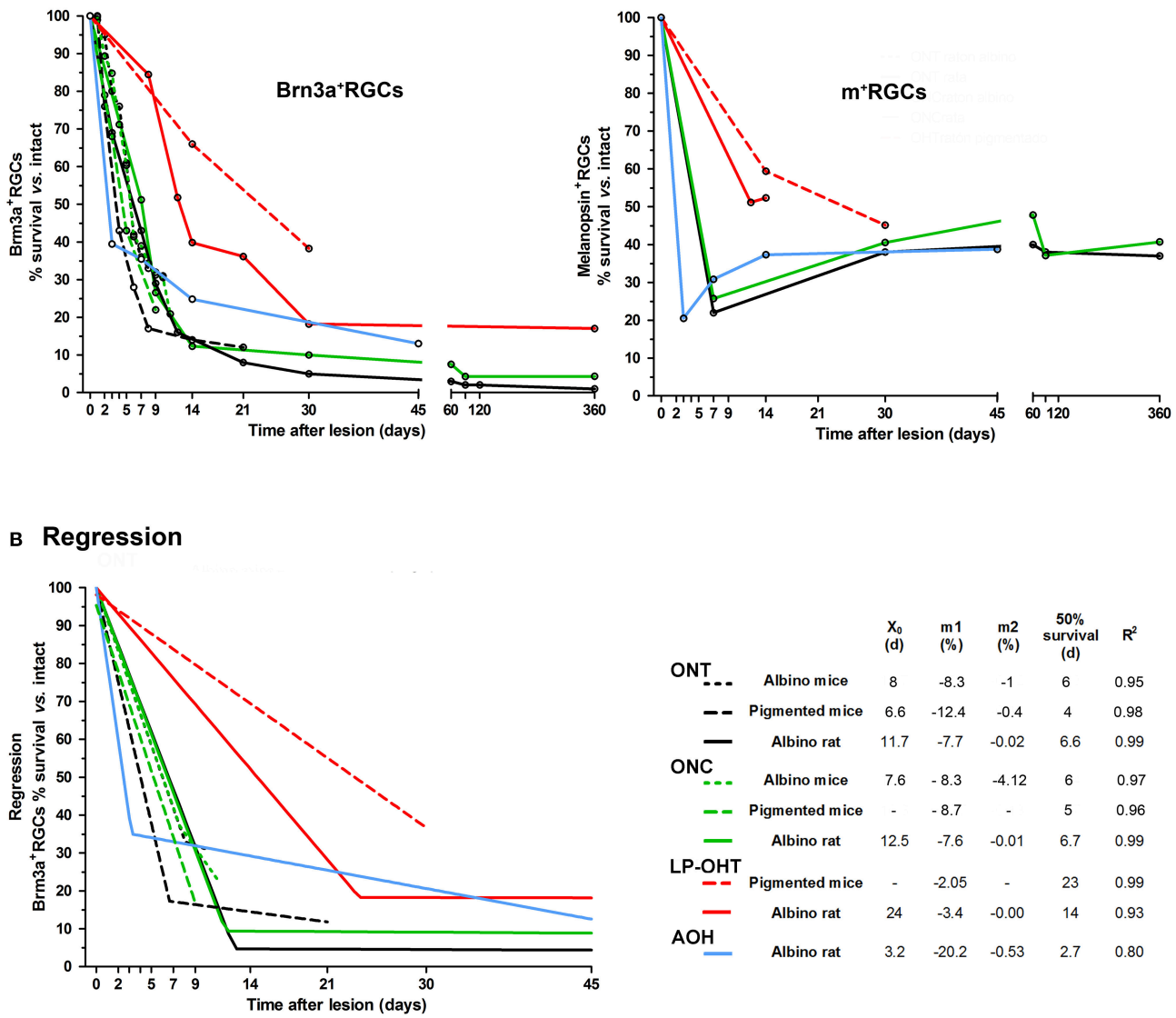

		X_0 (d)	m1 (%)	m2 (%)	50% survival (d)	R^2
ONT	Albino mice	8	-8.3	-1	6	0.95
	Pigmented mice	6.6	-12.4	-0.4	4	0.98
	Albino rat	11.7	-7.7	-0.02	6.6	0.99
ONC	Albino mice	7.6	- 8.3	-4.12	6	0.97
	Pigmented mice	-	- 8.7	-	5	0.96
	Albino rat	12.5	-7.6	-0.01	6.7	0.99
LP-OHT	Pigmented mice	-	-2.05	-	23	0.99
	Albino rat	24	-3.4	-0.00	14	0.93
AOH	Albino rat	3.2	-20.2	-0.53	2.7	0.80

FIGURE 1 | Temporal course of RGC loss after axotomy or ocular hypertension. (A) Graph showing the loss of Brn3a+RGCs (left) and melanopsin+RGCs (right) as percent of naive retinas vs. time post-lesion (days) after ONC, ONT, LP-OHT, or AOH in rats and mice. The open circles mark the time points of retinal analysis. Legend as in **(B). (B)** Graph showing the regression analysis of the loss of Brn3a+RGCs (percent of naive retinas, data in **(A)** vs. time post-lesion (days) after ONC, ONT, LP-OHT, or AOH in rats and mice. All courses adjust to either a segmental linear or to a linear regression. For ONT, ONC, and LP-OHT in rat the analysis was done with data points >45 days (see **A**) but the regression graph was cropped at 45 days for clarity. ONC, optic nerve crush at 0.5 mm from the optic head for mice, and 2 mm for rat. ONT: optic nerve transection at 0.5 mm from the optic nerve in both species. LP-OHT: ocular hypertension induced by laser-photocoagulation, in this model the increase of intra-ocular pressure lasts a week and rises on average up to 40 mmHg. AOH: acute ocular hypertension, induced by cannulating the anterior chamber, in this model the intra-ocular pressure was elevated to 76 mmHg for 75 min. X_0 indicates the day when the first linear phase of RGC loss changes to a second, slower, one. m1 and m2 are the slopes of the first and second linear phases, respectively and show the daily loss of RGCs (in percent). Fifty percent survival is the time (days) when, according to the mathematical analysis, half of the RGCs are lost. R^2 is the fitness of the regression. Albino mice: Swiss. Pigmented mice: C57/BL6. Albino rat: Sprague Dawley. These graphs were constructed using data from Salinas-Navarro et al. (2009c, 2010), Nadal-Nicolás et al. (2009, 2015a), Galindo-Romero et al. (2011, 2013b), Ortín-Martínez et al. (2015), Rovere et al. (2015, 2016a), Valiente-Soriano et al. (2015a,b), and Sánchez-Migallón et al. (2016).

The loss of Brn3a$^+$RGCs after A-OHT in rat also occurs in two phases. The first phase, in contrast with axotomy or LP-OHT, is very quick so that by day 3 approximately 65% Brn3a$^+$RGCs are lost (Rovere et al., 2016b). Thereafter RGC loss progressed further to 70% by 14 days and to 87% by 45 days, but, as it occurs after LP-OHT, their survival percentage is higher than after axotomy (e.g., 13% at 45 days vs. the 5% found after ONT).

Melanopsin$^+$ RGCs vs. Brn3a$^+$RGCs: Axotomy or A-OHT

When comparing the effects of axotomy or OHT on the survival of RGCs (**Figure 1A**) the first observation is a different survival ratio between Brn3a$^+$RGCs and m$^+$RGCs, both after axotomy or A-OHT. After axotomy, the number of Brn3a$^+$RGCs in rats and mice diminishes linearly during the first 2 weeks, when less than 20–25% of the RGC population survive (Galindo-Romero et al., 2011, 2013b; Nadal-Nicolás et al., 2015a; Sánchez-Migallón et al., 2016; Rovere et al., 2016a). Thereafter their loss is slow and continuous, for example, 90 days after axotomy the survival of Brn3a$^+$RGCs is approximately 5% (Nadal-Nicolás et al., 2015a). However, for rat m$^+$RGCs the scenario is quite different: during the first days after injury their numbers diminish significantly, even more than those of Brn3a$^+$RGCs, but later their survival is much higher (close to 40%) and moreover their numbers stabilize up to a year after axotomy (Nadal-Nicolás et al., 2015a). The lower number of rat m$^+$RGCs identified early after the injury is caused by a transient down-regulation of melanopsin expression triggered by axotomy or retrograde Fluorogold tracing (Nadal-Nicolás et al., 2015b; Agudo-Barriuso et al., 2016) which impairs their immunoidentification. Later, melanopsin expression gradually recovers and it becomes clear that rat m$^+$RGCs are more resilient than Brn3a$^+$RGCs to axotomy or A-OHT (Nadal-Nicolás et al., 2015a; Rovere et al., 2016a). Retinal injury results in the modification of the expression of many RGC genes (Chidlow et al., 2005; Lönngren et al., 2006; Agudo et al., 2008, 2009; Agudo-Barriuso et al., 2013), including the transient downregulation of melanopsin (Nadal-Nicolás et al., 2015b), but RGCs have been shown to express both melanopsin and Brn3a long time after injury (Sánchez-Migallón et al., 2011, 2016; Galindo-Romero et al., 2013a; Nadal-Nicolás et al., 2015a). Thus, it is important to have in mind that in rats, melanopsin is not a good marker of viability in short-term experiments, and therefore long time experiments are required to assess accurately the survival of the population of ipRGCs.

Finally, in rats more Brn3a$^+$RGCs survive after ONC than after ONT (Nadal-Nicolás et al., 2015a) probably because ONC is performed farther from the optic nerve head than ONT (Villegas-Pérez et al., 1993). However, the course of melanopsin down-regulation and m$^+$RGC loss to these same lesions is comparable (Nadal-Nicolás et al., 2015a). This suggests that for m$^+$RGCs, and in contrast to Brn3a$^+$RGCs, neither the type of axotomy nor the distance from the optic nerve head at which the injury is inflicted have an influence in their response.

Melanopsin$^+$RGCs vs. Brn3a$^+$RGCs: LP-OHT

In rats and pigmented mice, Brn3a$^+$RGCs and m$^+$RGCs respond similarly to LP-OHT, and at the time points analyzed we have not observed neither a recovery of melanopsin expression nor a higher survival of m$^+$RGCs than that of Brn3a$^+$RGCs (Valiente-Soriano et al., 2015a,b). However, we have not carried out experiments at times longer than 15 days (rat) or 1 month (mice) and thus we do not know whether there is a recovery of melanopsin expression with longer survival intervals after LP-OHT.

Topography of RGC Loss

To visualize the distribution of RGCs in control and injured retinas we have used isodensity or neighbor maps generated from our quantitative data. Isodensity maps depict the density of a given cell population on the retina using a color scale (Salinas-Navarro et al., 2009a,b), and are useful to determine the topological distribution of highly abundant cells such as Brn3a$^+$RGCs (Nadal-Nicolás et al., 2009, 2012) or cone photoreceptors (Ortín-Martínez et al., 2010, 2014). Neighbor maps illustrate the position of individual cells on the retina, the color assigned to each cell (dot) represents the number of cells around it (neighbors) in a given radius, and are useful to assess the topographic distribution of low abundance cells (i.e., m$^+$RGCs, Galindo-Romero et al., 2013a; Nadal-Nicolás et al., 2014; Valiente-Soriano et al., 2014).

The distribution of RGCs in intact (healthy) retinas is shown in **Figures 2A,B'**. In both species, the distribution of Brn3a$^+$RGC and m$^+$RGCs is complementary; Brn3a$^+$RGCs are more abundant in the medial-central retina and m$^+$RGCs in the periphery (Galindo-Romero et al., 2013a; Valiente-Soriano et al., 2014). Upon axotomy, the loss of Brn3a$^+$RGCs is diffuse (**Figures 2C–F**) and while m$^+$RGCs are lost across the whole retina, their population decreases predominantly in the dorsal retina (**Figures 2C'–F'**). Interestingly in rat the recovery of melanopsin expression that follows injury-induced downregulation of melanopsin occurs mainly in this area (compare panels C' and E').

Increasing the intraocular pressure, either by LP-OHT or A-OHT causes a sectorial or a patchy loss of Brn3a$^+$RGCs (**Figures 2G–J**). This pattern of RGC loss differs between both models, after LP-OHT surviving Brn3a$^+$RGCs are almost always found in pie-shaped sectors, with their widest part toward the retinal periphery and their vertex toward the optic disc, that are located predominantly in the ventral retina (Salinas-Navarro et al., 2009c, 2010; Valiente-Soriano et al., 2015a,b). A-OHT results in areas of low density of Brn3a$^+$RGCs, with a much less reproducible geographical pattern (Rovere et al., 2016a), that is reminiscent of the pattern observed after transient ischemia of the retina induced by selective ligature of the ophthalmic vessels (Lafuente López-Herrera et al., 2002).

For their part, m$^+$RGC loss after A-OHT or LP-OHT does not parallel the topography of Brn3a$^+$RGC loss (**Figures 2G'–J'**). Indeed, m$^+$RGCs loss is diffuse (Valiente-Soriano et al., 2015a,b; Rovere et al., 2016a) although more marked in the dorsal retina, as observed after axotomy. After A-OHT the recovery of melanopsin expression occurred, again, in the dorsal hemiretina (compare **Figures 2G'–I'**).

It is tempting to speculate that the different topography of Brn3a$^+$RGC loss reflects the nature of the injury itself (Vidal-Sanz et al., 2012, 2015a). Complete intraorbital ONC or ONT results in a diffuse loss throughout the retina with a marked absence of cells in areas or higher density, and this would be the result of lesioning the entire population of RGC axons within the ON head. Laser induced ocular hypertension results in a typical geographical pattern of pie-shaped sectors with their vertex toward the ON head (Salinas-Navarro et al., 2009c, 2010) that could be the result of damage to bundles of axons somewhere

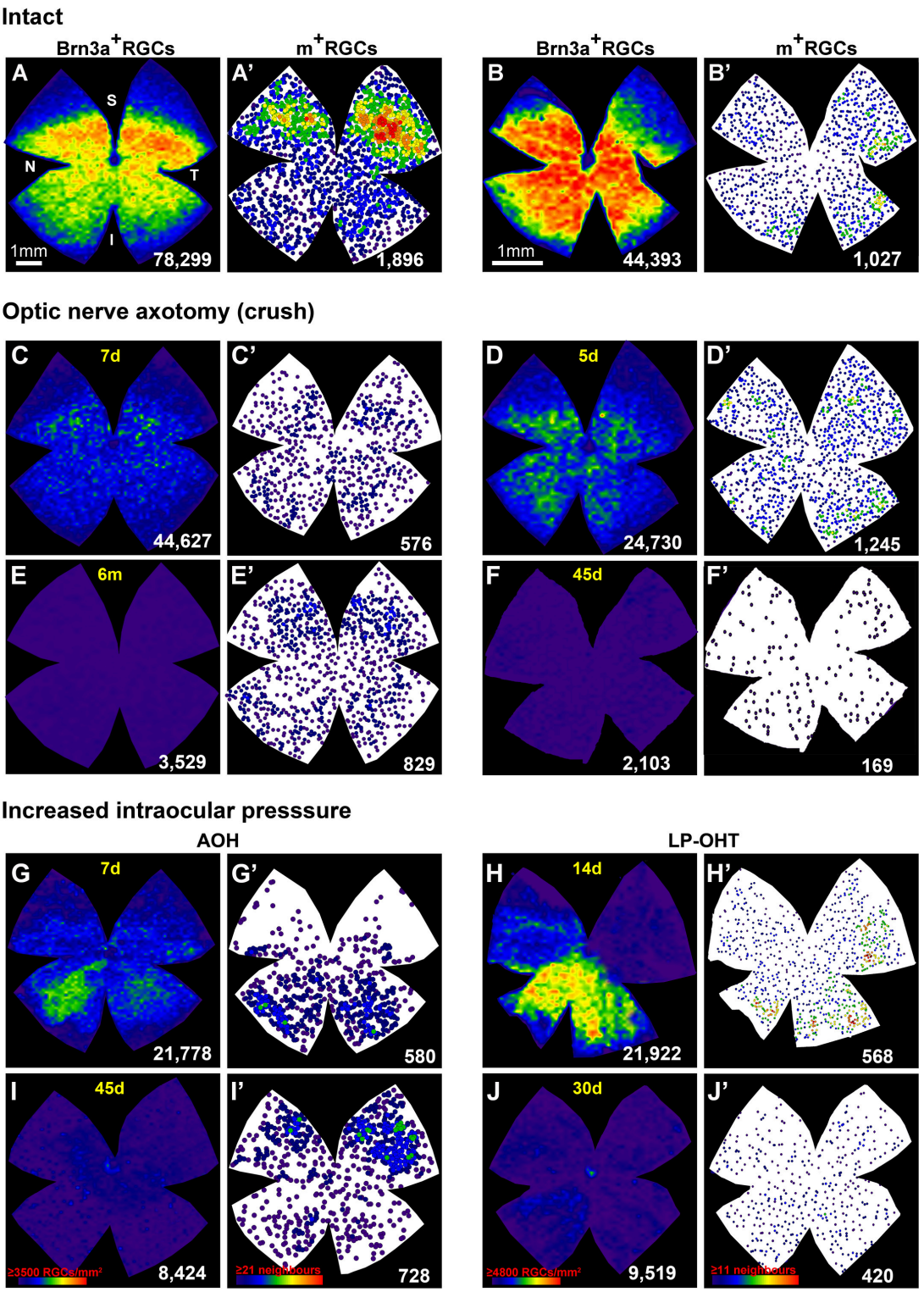

FIGURE 2 | Topography of RGC loss after axotomy or increased intraocular pressure. (A–J) isodensity maps showing the distribution of Brn3a+RGCs intact **(A,B)** or injured **(C–J)** retinas from rat **(A–I)** or mouse **(B–J)**. (**A'–J'**): neighbor maps showing the distribution of melanopsin+RGCs in the same retinas as (**A–J**). (**C–F**'): *(Continued)*

FIGURE 2 | Continued
axotomized retinas analyzed during the first phase of RGC death (**C,D**', 5 or 7 days) or long after the injury (**E,F'**, 45 days or 6 months). In both species axotomy causes a diffuse loss of both functional types of RGCs. Importantly, the survival percent of m+RGCs is higher than that of Brn3a+RGCs. In rat, shortly after the lesion **(C')** there are fewer m+RGCs than at 6 months **(E')** due to the transient downregulation of melanopsin (Nadal-Nicolás et al., 2015b). **(G–J')**: retinas analyzed after ocular hypertension (OHT) induced by either an acute increase of the intraocular pressure (**G,I**, 7 days and 45 days) or by laser photocogulation of the episcleral and perilimbar veins **(H,J**, 14 or 30 days). OHT causes a sectorial or patchy loss of Brn3a+RGCs and a diffuse loss of m+RGCs. As observed for axotomy, m+RGCs are more resilient than Brn3a+RGCs. Again, in rat melanopsin expression recovers partially with time post-AOH (**G**' vs. **I**'). Isodensity maps depict the density of RGCs with a color scale that goes from 0 RGCs/mm^2 (purple) to ≥3,500 (rat) or ≥4,800 (mouse) RGCs/mm^2 (red). In the neighbors maps each dot represents a m+RGC and its color the number of neighbors around it from purple (0–1 in mouse or 0–2 in rats) neighbors to red (≥11 rat, or ≥21 mouse) neighbors in a radius of 0.22 mm (rat) or 0.165 mm (mouse). Below each map is shown the total number of RGCs quantified in their corresponding retina. Bar scale for rat in **(A)** and for mouse in **(B)**. N, nasal; T, temporal; S, superior; I, inferior; d, days; m, months; A–OHT, acute ocular hypertension; LP–OHT, laser photocoagulation induced ocular hypertension. These original isodensity maps were constructed using data from Salinas-Navarro et al. (2009c, 2010), Nadal-Nicolás et al. (2009, 2015a), Galindo-Romero et al. (2011, 2013b), Ortín-Martínez et al. (2015), Rovere et al. (2015, 2016a), Valiente-Soriano et al. (2015a,b), and Sánchez-Migallón et al. (2016).

near the ON head, where they present their highest retinotopic arrangement (Guillery et al., 1995; Vidal-Sanz et al., 2012). Such a pattern of RGC loss is also observed for the very small proportion of Dogiel's RGCs that have their soma displaced to the inner nuclear layers (Nadal-Nicolás et al., 2015a). This particular pattern of retinal damage also appears reflected within the main retino-recipient areas of the brain. In rodents the vast majority of RGCs project to the contralateral superior colliculus (SC) (Salinas-Navarro et al., 2009a,b) and consequently ON axotomy results in complete SC denervation (Parrilla-Reverter et al., 2009a). LP-OHT results in a loss of synaptic terminals in concrete areas of the SC, reflecting their retinotopic distribution within the SC (Dekeyster et al., 2015; Valiente-Soriano et al., 2015a). AOH-induced RGC loss resulted in diffuse loss of Brn3a$^+$RGCs with some areas showing fewer RGCs, but without a consistent pattern that could compare to that induced by axotomy or LP-OHT. As abovementioned, such pattern of RGC loss observed after A-OHT resembled the patchy RGC loss observed after transient ischemia of the retina induced by selective ligature of the ophthalmic vessels (see **Figures 2**, **3** in Lafuente López-Herrera et al., 2002), suggesting a possible predominant ischemic nature of the insult inflicted to these retinas.

Retinal Nerve Fiber Layer

The progressive degeneration of the intra-retinal RGC axons (the retinal nerve fiber layer, RNFL) following optic nerve injury has been studied with classic (Leoz et al., 1914; Ramón y Cajal, 1914) and modern (Vidal-Sanz et al., 1987; Villegas-Pérez et al., 1988) neurofibrillary staining techniques. Studies in rodents, using quantitative and qualitative methods to identify RGCs and their intra-retinal axons, indicated that the loss of intra-retinal axons was only evident long after the vast majority of RGCs had already died; following ONT or ONC (Parrilla-Reverter et al., 2009b) and LP-OHT (Salinas-Navarro et al., 2009c, 2010). These results highlighted the problem of estimating RGC survival based on the appearance of the RNFL (Vidal-Sanz et al., 2012). More recently, we have examined and compared the *in vivo* and *ex vivo* appearance of the RNFL with the actual population of surviving RGCs and their topological distribution at different survival intervals ranging from 3 to 120 days after ONT. These studies showed a delayed disappearance of the intra-retinal RGC axons in relation to the loss of their RGC somata (Rovere et al., 2015). Such a disagreement between the time course of RGC loss and RFNL thinning (Chauhan et al., 2012; Choe et al., 2014; Munguba et al., 2014) may be clinically relevant because measurements of the RNFL thickness are often used as an indirect index of RGC survival in glaucoma. However, extrapolation of these data from rodent models to human diseases requires certain caution since optic nerve injury in rodents results in a very rapid loss of RGCs, while human's glaucomatous degeneration is a chronic long-term disease with a progressive but slow time-course progression. Such a slow rate of RGC death is important because clearance of RGC bodies and axons is performed by microglial cells, and it is possible that after an acute and massive insult, such as optic nerve crush or transection, the clearance of axonal debris by microglial cells is slower than the clearance of RGC somas. Moreover, in rodents, ON injury induces RFNL swelling (Abbott et al., 2014; Rovere et al., 2015) and this could mask the actual thickness of the RNFL. This RNFL swelling could be explained by an alteration of the axoplasmic transport (McKerracher et al., 1990; Pease et al., 2000), or by an inflammatory response that includes macro and microglial proliferation in the RNFL (Salvador-Silva et al., 2000; Sobrado-Calvo et al., 2007; Ramirez et al., 2010; De Hoz et al., 2013; Galindo-Romero et al., 2013b; Rojas et al., 2014). Indeed, a recent study has shown that administration of non-steroidal anti-inflammatory drugs results in a decrease of the RNFL swelling that follows ONT (Rovere et al., 2016b).

Responses of Non-RGC Neurons to Optic Nerve Axotomy or OHT

Ocular hypertension and ON injury induce primary damage to RGCs, this is a well-established observation documented by the decrease of RGCs that survive such injuries. Whether other neurons in the ganglion cell layer (GCL) are also affected by these injuries has been unknown for some time, with the idea in mind of a possible protracted transneuronal degeneration following massive RGC loss. Recently, it has been shown that complete intraorbital ONT or ONC does not affect the survival of displaced amacrine cells (Nadal-Nicolás et al., 2015a). Detailed examination of the GCL with RGC markers and displaced amacrine cell markers in retinas whose optic nerves had been completely crushed or cut showed no significant diminutions in the total numbers of displaced amacrine cells for up to 15 months after the lesion, whereas surviving RGCs amounted to approximately 1% of the original population (Nadal-Nicolás et al., 2015a). Similarly, the GCL was examined short and

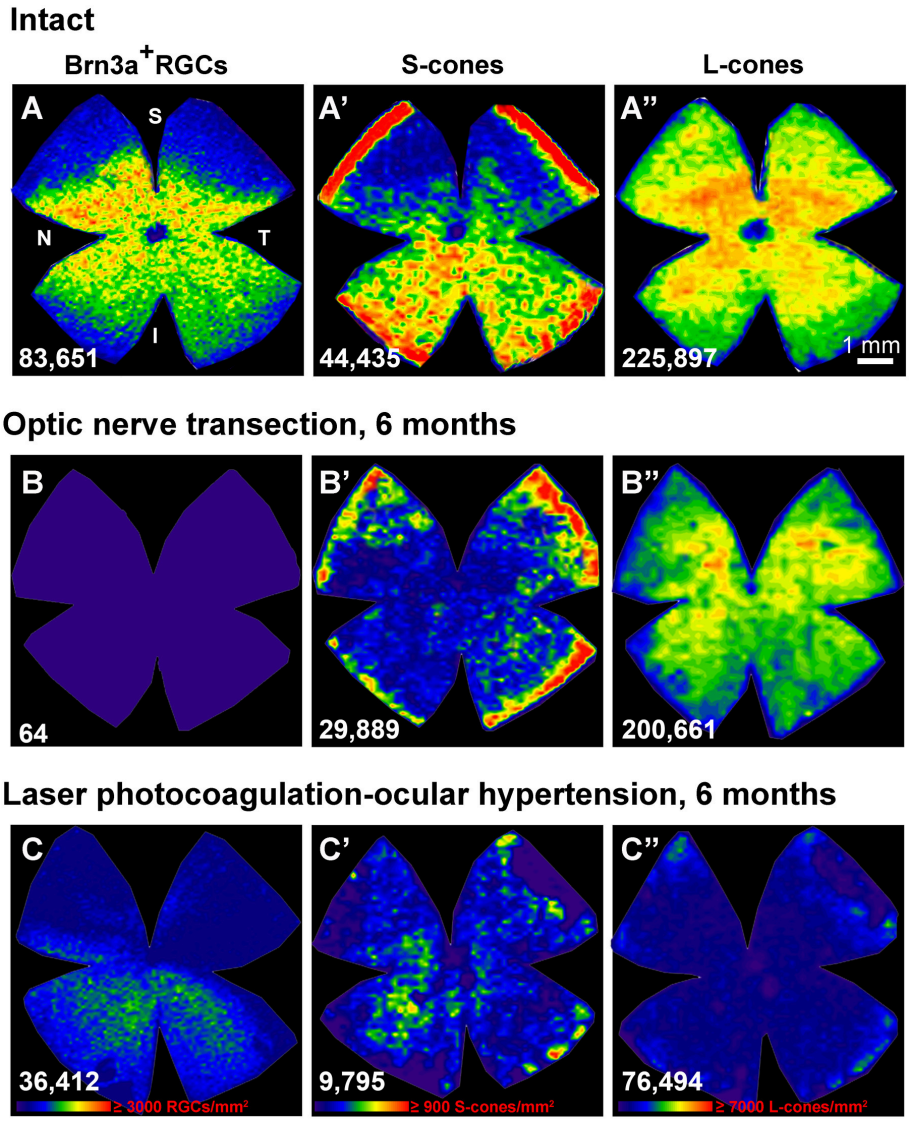

FIGURE 3 | Ocular hypertension but no optic nerve axotomy, causes the protracted loss of cone photoreceptors (A–C") : isodensity maps showing the topography of Brn3a+RGCs **(A–C)**, S-cones **(A'–C')** and L-cones **(A"–C")** in the same retina within each group. **(A–A")**: intact, **(B–B")**: 6 months after axotomy, **(C–C")**: 6 months ocular hypertension induced by laser photocoagulation. Isodensity color scale is found in **(C–C")** and goes from 0 cells/mm2 (purple) to ≥3,000 RGCs/mm^2, ≥900 S-cones/mm^2 or 7,000 L-cones/mm^2 (red). N, nasal; T, temporal; S, superior; I, inferior; d, days; These original isodensity maps were constructed using data from Ortín-Martínez et al. (2015).

long periods of time after the induction of OHT in adult rats (Ortín-Martínez et al., 2015) and mice (Valiente-Soriano et al., 2015a) to determine whether OHT resulted in specific loss of RGCs and not of other non-RGC neurons such as displaced amacrine cells. Retinas were immunolabelled with Brn3a to identify surviving RGCs and stained with DAPI to identify all nuclei present in the GCL. A topographic analysis of the GCL showed the typical pie-shaped sectors lacking Brn3a$^+$RGCs, but with normal numbers of DAPI$^+$ nuclei (see Figure 6 of Valiente-Soriano et al., 2015a; See Figures 3, 4 of Ortín-Martínez et al., 2015). These results documented that displaced amacrine cells did not die by OHT, as previously suggested (Jakobs et al., 2005; Kielczewski et al., 2005; Moon et al., 2005; Cone et al., 2010).

An additional long-standing controversy has been the issue of whether LP-OHT also induces damage to other neurons in the outer retinal layer (ORL) of the retina (Panda and Jonas, 1992; Kendell et al., 1995). Several studies in humans (Lei et al., 2008; Kanis et al., 2010; Choi et al., 2011; Werner et al., 2011), non-human primates (Nork, 2000; Nork et al., 2000; Liu et al., 2014) and rodent models of Glaucoma (Mittag et al., 2000; Heiduschka et al., 2010; Calkins, 2012; Fuchs et al., 2012; Fernández-Sánchez et al., 2014; Georgiou et al., 2014) suggested morphological and functional alterations of the ORL. Previous

studies from this Laboratory (Salinas-Navarro et al., 2009c; Cuenca et al., 2010; Vidal-Sanz et al., 2012) had also indicated alterations in the ORL. More recently, we have examined whether there was cone-photoreceptor loss in adult rats short and long time intervals after LP-OHT induction and after ONT (Ortín-Martínez et al., 2015; Vidal-Sanz et al., 2015a) using retrogradely transported tracers and molecular markers to identify surviving RGCs and specific opsin antibodies to identify L- and S-cone-photoreceptors. In agreement with the quantitative data shown earlier, by 6 months after ONT almost all Brn3a$^+$RGC have died, while the populations of L- and S-cone photoreceptors appears intact. This is in contrast to the situation observed after LP-OHT, the LP-OHT retinas showed approximately 70% RGC loss that was already apparent by 15 days but did not progress beyond 1 month and adopted the typical geographical pattern of pie-shaped sectors. In these retinas, the loss of L- and S-cones was first apparent by 1 month (35 and 20% loss, respectively) and progressed up to 6 months (80 and 65% loss, respectively). Moreover, there was a progressive downregulation of the rod-, L- and S-opsins to 60% of their normal values by 15 days and further decreases to less than 20% by 3 months after LP-OHT (see Figure 7 in Ortín-Martínez et al., 2015). Morphometrical analysis of paraffin-embedded cross-sections showed a significant reduction of the mean thickness of the outer nuclear layer (ONL) to approximately 2/3 of their normal values, and also a lack of cell nuclei in some areas of the ONL. Thus, indicating that in addition to L- and S-cone photoreceptors, rods had also degenerated (see Figure 8 in Ortín-Martínez et al., 2015). Overall, these data indicate that LP-OHT results in protracted degeneration of the outer retinal layers. The diffuse and patchy geographical pattern of L- and S-cones loss did not match the triangular pattern of RGC loss (Ortín-Martínez et al., 2015 and **Figure 3**). Because the retinal distribution of L- or S-cone loss does not parallel the sectorial loss of Brn3a$^+$RGCs, it is tempting to suggest that the mechanism(s) that trigger the protracted death of cones is not related with the death of RGCs, and thus it is unlikely that such a loss of L- or S-cone photoreceptors reflects trans-neuronal retrograde cell death. It is possible that LP-OHT causes an additional insult, probably related to choroid ischemia, responsible for the protracted loss of L- and S-cones. In summary, our studies indicate that following LP-OHT there is selective loss of RGCs in the ganglion cell layer, but with time there is also a protracted degeneration of the outer retinal layers that result in both S- and L-cone-photoreceptor loss (Ortín-Martínez et al., 2015; Vidal-Sanz et al., 2015a). Thus, photoreceptor loss may constitute and additional feature associated with ocular hypertension and this may have important implications for human GONs.

CONCLUDING REMARKS

Following ONC or ONT there is rapid loss of RGCs followed by a more protracted loss of RGCs (Villegas-Pérez et al., 1993; Nadal-Nicolás et al., 2015a). The minute proportion of surviving Brn3a$^+$RGCs contrasts with the much greater proportion of m$^+$RGCs that survives by 6 months after ONC or ONT (approximately 41 or 37%, respectively) or by 15 months after ONT (approximately 39%). Therefore two main different biological responses of m$^+$RGCs and Brn3a$^+$RGCs against optic nerve injury emerge: (i) m$^+$RGCs show a marked resilience against optic nerve axotomy reflected by the much smaller in magnitude amount of m$^+$RGCs loss. (ii) There is no protracted progression of m$^+$RGC loss beyond 1 month after injury as the population of m$^+$RGCs remains stable from 1 to 15 months after injury (Nadal-Nicolás et al., 2015a). Following A-OHT there is also progressive loss of RGCs; by 2 or 6 weeks, 25 or 13%, respectively, of the Brn3a$^+$RGC population survives in the retina. This is in contrast with the survival of m$^+$RGCs for the same periods (37 or 39%, respectively), indicating as well a special resilience of these neurons to A-OHT. Following LP-OHT there is also progressive loss of RGCs but the proportions of surviving m$^+$RGCs and Brn3a$^+$RGCs (at 12 or 14 days for the rat, and at 14 or 28 days for the mouse) were comparable suggesting that rat and mouse m$^+$RGCs do not show a special resilience against LP-OHT (Valiente-Soriano et al., 2015a,b). These results are in agreement with previous studies showing m$^+$RGC loss and non-image forming visual functional deficits in humans (Pérez-Rico et al., 2010; Kankipati et al., 2011; Nissen et al., 2014; Obara et al., 2016) as well as in animal models of glaucoma (Drouyer et al., 2008; De Zavalía et al., 2011; Zhang et al., 2013).

ONT or ONC results in diffuse RGC loss throughout the retinas with greater losses in areas of higher densities. LP-OHT resulted in characteristic pie-shaped sectors lacking RGCs, with a greater loss in the ventral retina. A-OHT results in rapid loss of RGCs and its topological distribution was reminiscent of the patchy loss observed after transient selective ligature of the ophthalmic vessels for 90 min (Lafuente López-Herrera et al., 2002), suggesting that A-OHT results in a predominant ischemic insult to these retinas (Rovere et al., 2016a).

LP-OHT or ONT result within the GCL of the retina, at the time intervals studied of 6 months after LP-OHT and 15 months after ONT, in selective loss of RGCs but not of other non-RGC neurons, such as displaced amacrine cells. However, long after LP-OHT there is progressive degeneration of the outer retinal layers as observed functionally (Cuenca et al., 2010) and structurally (Cuenca et al., 2010; Ortín-Martínez et al., 2015). It is possible that LP-OHT could inflict outer retinal damage, independent of the RGC-axonal damage that would evolve slowly with time into a progressive degeneration of the rod, L- and S-cone photoreceptor populations. Because in our LP-OHT studies, important elevations of the IOP were present during the first 2 weeks, it is possible that choroidal insufficiency could be a distinct pathological event in this model (Nork et al., 2014; Ortín-Martínez et al., 2015).

Finally, to study the progression of glaucomatous optic neuropathy, animal models of OHT resemble better the pathophysiology of human glaucoma; they mimic not only the optic nerve damage but also the possible choroid damage and/or ischemic insult which are thought to be the underlying insults of the disease. Indeed, chronic OHT models show the characteristic sectorial loss of RGCs and ON damage as well as the protracted degeneration of the outer retina observed in human patients (Nork, 2000; Choi et al., 2011; Werner et al., 2011). Acute

OHT models mimic an acute angle-closure glaucoma and may result in retinal ischemia leading to ON damage and RGC loss. These animal models of OHT show however, a high inter-animal variability and a poor correlation between the levels of IOP and the resulting damage, something that needs to be further investigated. On the other hand, optic nerve injury (axotomy) models are quite consistent in terms of topological, chronological and quantitative loss of RGCs. Thus, optic nerve crush or transection are quick and highly reproducible models for proof of concept assays to decipher injure-related molecular pathways and to test neuroprotective therapies.

AUTHOR CONTRIBUTIONS

All authors have reviewed and approved the final version of this manuscript. Conceptualized and designed the experiments: MVS, CGR, FV, FN, AO, GR, MSN, FL, MCS, PS, MAT, MPV, and MAB. Performed the experiments: CGR, FV, FN, AO, GR, MSN, FL, MCS, and PS. Data acquisition and analysis: CGR, FVS, FN, AO, GR, MSN, FL, and MCS. Data interpretation and manuscript drafting: MVS, CGR, FV, FN, AO, GR, MSN, FL, MCS, PS, MAT, MPV, and MAB. Contributed reagents/materials/analysis tools: MVS, MAT, MPV, and MAB.

FUNDING

Financial support for these studies was obtained from Fundación Séneca, Agencia de Ciencia y Tecnología Región de Murcia (19881/GERM/15), and the Spanish Ministry of Economy and Competitiveness, Instituto de Salud Carlos III, Fondo Europeo de Desarrollo Regional "Una Manera de Hacer Europa" (SAF2015-67643-P, PI16/00380; RD16/0008/0026, PI16/00031).

ACKNOWLEDGMENTS

We are grateful to our coworkers that have contributed to the various studies in the Laboratory of Experimental Ophthalmology over the years. The administrative assistance of Maria D. Soria Rodriguez and the technical expertise of Jose M. Bernal Garro is greatly acknowledged.

REFERENCES

Abbott, C. J., Choe, T. E., Lusardi, T. A., Burgoyne, C. F., Wang, L., and Fortune, B. (2014). Evaluation of retinal nerve fiber layer thickness and axonal transport 1 and 2 weeks after 8 hours of acute intraocular pressure elevation in rats. *Invest. Ophthalmol. Vis. Sci.* 55, 674–687. doi: 10.1167/iovs.13-12811

Aguayo, A. J., Vidal-Sanz, M., Villegas-Pérez, M. P., and Bray, G. M. (1987). Growth and connectivity of axotomized retinal neurons in adult rats with optic nerves substituted by PNS grafts linking the eye and the midbrain. *Ann. N. Y. Acad. Sci.* 495, 1–9. doi: 10.1111/j.1749-6632.1987.tb23661.x

Agudo, M., Pérez-Marín, M. C., Lönngren, U., Sobrado, P., Conesa, A., Cánovas, I., et al. (2008). Time course profiling of the retinal transcriptome after optic nerve transection and optic nerve crush. *Mol. Vis.* 14, 1050–1063.

Agudo, M., Pérez-Marín, M. C., Sobrado-Calvo, P., Lönngren, U., Salinas-Navarro, M., Cánovas, I., et al. (2009). Immediate upregulation of proteins belonging to different branches of the apoptotic cascade in the retina after optic nerve transection and optic nerve crush. *Invest. Ophthalmol. Vis. Sci.* 50, 424–431. doi: 10.1167/iovs.08-2404

Agudo-Barriuso, M., Lahoz, A., Nadal-Nicolás, F. M., Sobrado-Calvo, P., Piquer-Gil, M., Díaz-Llopis, M., et al. (2013). Metabolomic changes in the rat retina after optic nerve crush. *Invest. Ophthalmol. Vis. Sci.* 54, 4249–4259. doi: 10.1167/iovs.12-11451

Agudo-Barriuso, M., Nadal-Nicolás, F. M., Madeira, M. H., Rovere, G., Vidal-Villegas, B., and Vidal-Sanz, M. (2016). Melanopsin expression is an indicator of the well-being of melanopsin-expressing retinal ganglion cells but not of their viability. *Neural Regen. Res.* 11, 1243–1244. doi: 10.4103/1673-5374.189182

Avilés-Trigueros, M., Sauvé, Y., Lund, R. D., and Vidal-Sanz, M. (2000). Selective innervation of retinorecipient brainstem nuclei by retinal ganglion cell axons regenerating through peripheral nerve grafts in adult rats. *J. Neurosci.* 20, 361–374.

Barboni, M. T., Pangeni, G., Ventura, D. F., Horn, F., and Kremers, J. (2011). Heterochromatic flicker electroretinograms reflecting luminance and cone opponent activity in glaucoma patients. *Invest. Ophthalmol. Vis. Sci.* 52, 6757–6765. doi: 10.1167/iovs.11-7538

Bray, G. M., Vidal-Sanz, M., and Aguayo, A. J. (1987). Regeneration of axons from the central nervous system of adult rats. *Prog. Brain Res.* 71, 373–379. doi: 10.1016/S0079-6123(08)61838-5

Bray, G. M., Villegas-Pérez, M. P., Vidal-Sanz, M., Carter, D. A., and Aguayo, A. J. (1991). Neuronal and nonneuronal influences on retinal ganglion cell survival, axonal regrowth, and connectivety after axotomy. *Ann. N. Y. Acad. Sci.* 633, 214–228. doi: 10.1111/j.1749-6632.1991.tb15613.x

Calkins, D. J. (2012). Critical pathogenic events underlying progression of neurodegeneration in glaucoma. *Prog. Retin. Eye Res.* 31, 702–719. doi: 10.1016/j.preteyeres.2012.07.001

Chauhan, B. C., Malik, R., Shuba, L. M., Rafuse, P. E., Nicolela, M. T., and Artes, P. H. (2014). Rates of glaucomatous visual field change in a large clinical population. *Invest. Ophthalmol. Vis. Sci.* 55, 4135–4143. doi: 10.1167/iovs.14-14643

Chauhan, B. C., Stevens, K. T., Levesque, J. M., Nuschke, A. C., Sharpe, G. P., O'Leary, N., et al. (2012). Longitudinal *in vivo* imaging of retinal ganglion cells and retinal thickness changes following optic nerve injury in mice. *PLoS ONE* 7:e40352. doi: 10.1371/journal.pone.0040352

Chidlow, G., Casson, R., Sobrado-Calvo, P., Vidal-Sanz, M., and Osborne, N. N. (2005). Measurement of retinal injury in the rat after optic nerve transection: an RT-PCR study. *Mol. Vis.* 11, 387–396.

Chidlow, G., Ebneter, A., Wood, J. P., and Casson, R. J. (2011). The optic nerve head is the site of axonal transport disruption, axonal cytoskeleton damage and putative axonal regeneration failure in a rat model of glaucoma. *Acta Neuropathol.* 121, 737–751. doi: 10.1007/s00401-011-0807-1

Choe, T. E., Abbott, C. J., Piper, C., Wang, L., and Fortune, B. (2014). Comparison of longitudinal *in vivo* measurements of retinal nerve fiber layer thickness and retinal ganglion cell density after optic nerve transection in rat. *PLoS ONE* 9:e113011. doi: 10.1371/journal.pone.0113011

Choi, S. S., Zawadzki, R. J., Lim, M. C., Brandt, J. D., Keltner, J. L., Doble, N., et al. (2011). Evidence of outer retinal changes in glaucoma patients as revealed by ultrahigh-resolution *in vivo* retinal imaging. *Br. J. Ophthalmol.* 95, 131–141. doi: 10.1136/bjo.2010.183756

Cone, F. E., Gelman, S. E., Son, J. L., Pease, M. E., and Quigley, H. A. (2010). Differential susceptibility to experimental glaucoma among 3 mouse strains using bead and viscoelastic injection. *Exp. Eye Res.* 91, 415–424. doi: 10.1016/j.exer.2010.06.018

Coombs, J., Van der List, D., Wang, G. Y., and Chalupa, L. M. (2006). Morphological properties of mouse retinal ganglion cells. *Neuroscience* 140, 123–136. doi: 10.1016/j.neuroscience.2006.02.079

Crish, S. D., Sappington, R. M., Inman, D. M., Horner, P. J., and Calkins, D. J. (2010). Distal axonopathy with structural persistence in glaucomatous neurodegeneration. *Proc. Natl. Acad. Sci. U.S.A.* 107, 5196–5201. doi: 10.1073/pnas.0913141107

Cuenca, N., Pinilla, I., Fernández-Sánchez, L., Salinas-Navarro, M., Alarcón-Martínez, L., Avilés-Trigueros, M., et al. (2010). Changes in the inner and outer retinal layers after acute increase of the intraocular pressure in adult albino Swiss mice. *Exp. Eye Res.* 91, 273–285. doi: 10.1016/j.exer.2010.05.020

Cui, Q., Ren, C., Sollars, P. J., Pickard, G. E., and So, K. F. (2015). The injury resistant ability of melanopsin-expressing intrinsically photosensitive retinal ganglion cells. *Neuroscience* 284, 845–853. doi: 10.1016/j.neuroscience.2014.11.002

De Hoz, R., Gallego, B. I., Ramirez, A. I., Rojas, B., Salazar, J. J., Valiente-Soriano, F. J., et al. (2013). Rod-like microglia are restricted to eyes with laser-induced ocular hypertension but absent from the microglial changes in the contralateral untreated eye. *PLoS ONE* 8:e83733. doi: 10.1371/journal.pone.0083733

Dekeyster, E., Aerts, J., Valiente-Soriano, F. J., De Groef, L., Vreysen, S., Salinas-Navarro, M., et al. (2015). Ocular hypertension results in retinotopic alterations in the visual cortex of adult mice. *Curr. Eye Res.* 40, 1269–1283. doi: 10.3109/02713683.2014.990983

De Zavalía, N., Plano, S. A., Fernandez, D. C., Lanzani, M. F., Salido, E., Belforte, N., et al. (2011). Effect of experimental glaucoma on the non-image forming visual system. *J. Neurochem.* 117, 904–914. doi: 10.1111/j.1471-4159.2011.07260.x

Drouyer, E., Dkhissi-Benyahya, O., Chiquet, C., WoldeMussie, E., Ruiz, G., Wheeler, L. A., et al. (2008). Glaucoma alters the circadian timing system. *PLoS ONE* 3:e3931. doi: 10.1371/journal.pone.0003931

Fernández-Sánchez, L., Pérez De Sevilla Müller, L., Brecha, N., and Cuenca, N. (2014). Loss of outer retinal neurons and circuitry alterations in the DBA/2J mouse. *Investig. Ophthalmol. Vis. Sci.* 55, 6059–6072. doi: 10.1167/iovs.14-14421

Frezzotti, P., Giorgio, A., Motolese, I., De Leucio, A., Iester, M., Motolese, E., et al. (2014). Structural and functional brain changes beyond visual system in patients with advanced glaucoma. *PLoS ONE* 9:e105931. doi: 10.1371/journal.pone.0105931

Fuchs, M., Scholz, M., Sendelbeck, A., Atorf, J., Schlegel, C., Enz, R., et al. (2012). Rod photoreceptor ribbon synapses in DBA/2J mice show progressive age-related structural changes. *PLoS ONE* 7:e44645. doi: 10.1371/journal.pone.0044645

Galindo-Romero, C., Avilés-Trigueros, M., Jiménez-López, M., Valiente-Soriano, F. J., Salinas-Navarro, M., Nadal-Nicolás, F., et al. (2011). Axotomy-induced retinal ganglion cell death in adult mice: quantitative and topographic time course analyses. *Exp. Eye Res.* 92, 377–387. doi: 10.1016/j.exer.2011.02.008

Galindo-Romero, C., Jiménez-López, M., García-Ayuso, D., Salinas-Navarro, M., Nadal-Nicolás, F. M., Agudo-Barriuso, M., et al. (2013a). Number and spatial distribution of intrinsically photosensitive retinal ganglion cells in the adult albino rat. *Exp. Eye Res.* 108, 84–93. doi: 10.1016/j.exer.2012.12.010

Galindo-Romero, C., Valiente-Soriano, F. J., Jiménez-López, M., García-Ayuso, D., Villegas-Pérez, M. P., Vidal-Sanz, M., et al. (2013b). Effect of brain-derived neurotrophic factor on mouse axotomized retinal ganglion cells and phagocytic microglia. *Invest. Ophthalmol. Vis. Sci.* 54, 974–985. doi: 10.1167/iovs.12-11207

Georgiou, A. L., Guo, L., Cordeiro, F. M., and Salt, T. E. (2014). Electroretinogram and visual evoked potential assessment of retinal and central visual function in a rat ocular hypertension model of glaucoma. *Curr. Eye Res.* 39, 472–486. doi: 10.3109/02713683.2013.848902

González-Fleitas, M. F., Bordone, M., Rosenstein, R. E., and Dorfman, D. (2015). Effect of retinal ischemia on the non-image forming visual system. *Chronobiol. Int.* 32, 152–163. doi: 10.3109/07420528.2014.959526

Guillery, R. W., Mason, C. A., and Taylor, J. S. (1995). Developmental determinants at the mammalian optic chiasm. *J. Neurosci.* 15, 4727–4737.

Hattar, S., Liao, H. W., Takao, M., Berson, D. M., and Yau, K. W. (2002). Melanopsin-containing retinal ganglion cells: architecture, projections, and intrinsic photosensitivity. *Science* 295, 1065–1070. doi: 10.1126/science.1069609

Hattar, S., Lucas, R. J., Mrosovsky, N., Thompson, S., Douglas, R. H., Hankins, M. W., et al. (2003). Melanopsin and rod-cone photoreceptive systems account for all major accessory visual functions in mice. *Nature* 424, 76–81. doi: 10.1038/nature01761

Heiduschka, P., Julien, S., Schuettauf, F., and Schnichels, S. (2010). Loss of retinal function in aged DBA/2J mice e new insights into retinal neurodegeneration. *Exp. Eye Res.* 91, 779–783. doi: 10.1016/j.exer.2010.09.001

Jakobs, T. C., Libby, R. T., Ben, Y., John, S. W., and Masland, R. H. (2005). Retinal ganglion cell degeneration is topological but not cell type specific in DBA/2J mice. *J. Cell Biol.* 171, 313–325. doi: 10.1083/jcb.200506099

Jehle, T., Dimitriu, C., Auer, S., Knoth, R., Vidal-Sanz, M., Gozes, I., et al. (2008). The neuropeptide NAP provides neuroprotection against retinal ganglion cell damage after retinal ischemia and optic nerve crush. *Graefes Arch. Clin. Exp. Ophthalmol.* 246, 1255–1263. doi: 10.1007/s00417-007-0746-7

Kanis, M. J., Lemij, H. G., Berendschot, T. T., Van de Kraats, J., and Van Norren, D. (2010). Foveal cone photoreceptor involvement in primary open-angle glaucoma. *Graefes Arch. Clin. Exp. Ophthalmol.* 248, 999–1006. doi: 10.1007/s00417-010-1331-z

Kankipati, L., Girkin, C. A., and Gamlin, P. D. (2011). The post-illumination pupil response is reduced in glaucoma patients. *Invest. Ophthalmol. Vis. Sci.* 52, 2287–2292. doi: 10.1167/iovs.10-6023

Keirstead, S. A., Rasminsky, M., Fukuda, Y., Carter, D. A., Aguayo, A. J., and Vidal-Sanz, M. (1989). Electrophysiologic responses in hamster superior colliculus evoked by regenerating retinal axons. *Science* 246, 255–257. doi: 10.1126/science.2799387

Kendell, K. R., Quigley, H. A., Kerrigan, L. A., Pease, M. E., and Quigley, E. N. (1995). Primary open-angle glaucoma is not associated with photoreceptor loss. *Investig. Ophthalmol. Vis. Sci.* 36, 200–205.

Kielczewski, J. L., Pease, M. E., and Quigley, H. A. (2005). The effect of experimental glaucoma and optic nerve transection on amacrine cells in the rat retina. *Investig. Ophthalmol. Vis. Sci.* 46, 3188–3196. doi: 10.1167/iovs.05-0321

Lafuente López-Herrera, M. P., Mayor-Torroglosa, S., Miralles de Imperial, J., Villegas-Pérez, M. P., and Vidal-Sanz, M. (2002). Transient ischemia of the retina results in altered retrograde axoplasmic transport: neuroprotection with brimonidine. *Exp. Neurol.* 178, 243–258. doi: 10.1006/exnr.2002.8043

Lei, Y., Garrahan, N., Hermann, B., Becker, D. L., Hernandez, M. R., Boulton, M. E., et al. (2008). Quantification of retinal transneuronal degeneration in human glaucoma: a novel multiphoton-DAPI approach. *Investig. Ophthalmol. Vis. Sci.* 49, 1940–1945. doi: 10.1167/iovs.07-0735

Leoz, P., Ortin, G., and Arcuate, L. R. (1914). Procesos regenerativos del nervio óptico y retina, con ocasión de injertos nerviosos. *Trab. Lab. Invest. Biol.* 11, 239–254.

Levkovitch-Verbin, H., Quigley, H. A., Martin, K. R., Valenta, D., Baumrind, L. A., and Pease, M. E. (2002). Translimbal laser photocoagulation to the trabecular meshwork as a model of glaucoma in rats. *Invest. Ophthalmol. Vis. Sci.* 43, 402–410.

Li, R. S., Chen, B. Y., Tay, D. K., Chan, H. H., Pu, M. L., and So, K. F. (2006). Melanopsin-expressing retinal ganglion cells are more injury-resistant in a chronic ocular hypertension model. *Invest. Ophthalmol. Vis. Sci.* 47, 2951–2958. doi: 10.1167/iovs.05-1295

Lindqvist, N., Peinado-Ramón, P., Vidal-Sanz, M., and Hallböök, F. (2004). GDNF, Ret, GFRalpha1 and 2 in the adult rat retino-tectal system after optic nerve transection. *Exp. Neurol.* 187, 487–499. doi: 10.1016/j.expneurol.2004.02.002

Liu, K., Wang, N., Peng, X., Yang, D., Wang, C., and Zeng, H. (2014). Long-term effect of laser-induced ocular hypertension on the cone electroretinogram and central macular thickness in monkeys. *Photomed. Laser Surg.* 32, 371–378. doi: 10.1089/pho.2013.3693

Lönngren, U., Näpänkangas, U., Lafuente, M., Mayor, S., Lindqvist, N., Vidal-Sanz, M., et al. (2006). The growth factor response in ischemic rat retina and superior colliculus after brimonidine pre-treatment. *Brain Res. Bull.* 71, 208–218. doi: 10.1016/j.brainresbull.2006.09.005

Lucas, R. J., Peirson, S. N., Berson, D. M., Brown, T. M., Cooper, H. M., Czeisler, C. A., et al. (2014). Measuring and using light in the melanopsin age. *Trends Neurosci.* 37, 1–9. doi: 10.1016/j.tins.2013.10.004

McKerracher, L., Vidal-Sanz, M., Essagian, C., and Aguayo, A. J. (1990). Selective impairment of slow axonal transport after optic nerve injury in adult rats. *J. Neurosci.* 10, 2834–2841.

Mittag, T. W., Danias, J., Pohorenec, G., Yuan, H. M., Burakgazi, E., Chalmers-Redman, R., et al. (2000). Retinal damage after 3 to 4 months of elevated intraocular pressure in a rat glaucoma model. *Invest. Ophthalmol. Vis. Sci.* 41, 3451–3459.

Moon, J. I., Kim, I. B., Gwon, J. S., Park, M. H., Kang, T. H., Lim, E. J., et al. (2005). Changes in retinal neuronal populations in the DBA/2J mouse. *Cell Tissue Res.* 320, 51–59. doi: 10.1007/s00441-004-1062-8

Morrison, J. C., Cepurna Ying Guo, W. O., and Johnson, E. C. (2011). Pathophysiology of human glaucomatous optic nerve damage: insights from rodent models of glaucoma. *Exp. Eye Res.* 93, 156–164. doi: 10.1016/j.exer.2010.08.005

Munguba, G. C., Galeb, S., Liu, Y., Landy, D. C., Lam, D., Camp, A., et al. (2014). Nerve fiber layer thinning lags retinal ganglion cell density following crush axonopathy. *Invest. Ophthalmol. Vis. Sci.* 55, 6505–6513. doi: 10.1167/iovs.14-14525

Munz, M., Rasminsky, M., Aguayo, A. J., Vidal-Sanz, M., and Devor, M. G. (1985). Functional activity of rat brainstem neurons regenerating axons along peripheral nerve grafts. *Brain Res.* 340, 115–125. doi: 10.1016/0006-8993(85)90780-2

Nadal-Nicolás, F. M., Jiménez-López, M., Salinas-Navarro, M., Sobrado-Calvo, P., Alburquerque-Béjar, J. J., Vidal-Sanz, M., et al. (2012). Whole number, distribution and co-expression of brn3 transcription factors in retinal ganglion cells of adult albino and pigmented rats. *PLoS ONE* 7:e49830. doi: 10.1371/journal.pone.0049830

Nadal-Nicolás, F. M., Jiménez-López, M., Sobrado-Calvo, P., Nieto-López, L., Cánovas-Martínez, I., Salinas-Navarro, M., et al. (2009). Brn3a as a marker of retinal ganglion cells: qualitative and quantitative time course studies in naive and optic nerve-injured retinas. *Invest. Ophthalmol. Vis. Sci.* 50, 3860–3868. doi: 10.1167/iovs.08-3267

Nadal-Nicolás, F. M., Madeira, M. H., Salinas-Navarro, M., Jiménez-López, M., Galindo-Romero, C., Ortín-Martínez, A., et al. (2015b). Transient downregulation of melanopsin expression after retrograde tracing or optic nerve injury in adult rats. *Invest. Ophthalmol. Vis. Sci.* 56, 4309–4323. doi: 10.1167/iovs.15-16963

Nadal-Nicolás, F. M., Salinas-Navarro, M., Jiménez-López, M., Sobrado-Calvo, P., Villegas-Pérez, M. P., Vidal-Sanz, M., et al. (2014). Displaced retinal ganglion cells in albino and pigmented rats. *Front. Neuroanat.* 8:99. doi: 10.3389/fnana.2014.00099

Nadal-Nicolás, F. M., Sobrado-Calvo, P., Jiménez-López, M., and Vidal-Sanz, M. (2015a). Agudo-Barriuso, M. long-term effect of optic nerve axotomy on the retinal ganglion cell layer. *Invest. Ophthalmol. Vis. Sci.* 56, 6095–6112. doi: 10.1167/iovs.15-17195

Nissen, C., Sander, B., Milea, D., Kolko, M., Herbst, K., Hamard, P., et al. (2014). Monochromatic pupillometry in unilateral glaucoma discloses no adaptive changes subserved by the ipRGCs. *Front. Neurol.* 5:15. doi: 10.3389/fneur.2014.00015

Nork, T. M. (2000). Acquired color vision loss and a possible mechanism of ganglion cell death in glaucoma. *Trans. Am. Ophthalmol. Soc.* 98, 331–363.

Nork, T. M., Kim, C. B., Munsey, K. M., Dashek, R. J., and Hoeve, J. N. (2014). Regional choroidal blood flow and multifocal electroretinography in experimental glaucoma in rhesus macaques. *Invest. Ophthalmol. Vis. Sci.* 55, 7786–7798. doi: 10.1167/iovs.14-14527

Nork, T. M., Ver Hoeve, J. N., Poulsen, G. L., Nickells, R. W., Davis, M. D., Weber, A. J., et al. (2000). Swelling and loss of photoreceptors in chronic human and experimental glaucomas. *Arch. Ophthalmol.* 118, 235–245. doi: 10.1001/archopht.118.2.235

Nucci, C., Martucci, A., Cesareo, M., Mancino, R., Russo, R., Bagetta, G., et al. (2013). Brain involvement in glaucoma: advanced neuroimaging for understanding and monitoring a new target for therapy. *Curr. Opin. Pharmacol.* 13, 128–133. doi: 10.1016/j.coph.2012.08.004

Obara, E. A., Hannibal, J., Heegaard, S., and Fahrenkrug, J. (2016). Loss of melanopsin-expressing retinal ganglion cells in severely staged glaucoma patients. *Invest. Ophthalmol. Vis. Sci.* 57, 4661–4667. doi: 10.1167/iovs.16-19997

Ortín-Martínez, A., Jiménez-López, M., Nadal-Nicolás, F. M., Salinas-Navarro, M., Alarcón-Martínez, L., Sauvé, Y., et al. (2010). Automated quantification and topographical distribution of the whole population of S- and L-cones in adult albino and pigmented rats. *Invest. Ophthalmol. Vis. Sci.* 51, 3171–3183. doi: 10.1167/iovs.09-4861

Ortín-Martínez, A., Nadal-Nicolás, F. M., Jiménez-López, M., Alburquerque-Béjar, J. J., Nieto-López, L., García-Ayuso, D., et al. (2014). Number and distribution of mouse retinal cone photoreceptors: differences between an albino (Swiss) and a pigmented (C57/BL6) strain. *PLoS ONE* 9:e102392. doi: 10.1371/journal.pone.0102392

Ortín-Martínez, A., Salinas-Navarro, M., Nadal-Nicolás, F. M., Jiménez-López, M., Valiente-Soriano, F. J., García-Ayuso, D., et al. (2015). Laser-induced ocular hypertension in adult rats does not affect non-RGC neurons in the ganglion cell layer but results in protracted severe loss of cone-photoreceptors. *Exp. Eye Res.* 132, 17–33. doi: 10.1016/j.exer.2015.01.006

Panda, S., and Jonas, J. B. (1992). Decreased photoreceptor count in human eyes withsecondary angle-closure glaucoma. *Investig. Ophthalmol. Vis. Sci.* 33, 2532–2536.

Parrilla-Reverter, G., Agudo, M., Nadal-Nicolás, F., Alarcón-Martínez, L., Jiménez-López, M., Salinas-Navarro, M., et al. (2009b). Time-course of the retinal nerve fibre layer degeneration after complete intra-orbital optic nerve transection or crush: a comparative study. *Vision Res.* 49, 2808–2825. doi: 10.1016/j.visres.2009.08.020

Parrilla-Reverter, G., Agudo, M., Sobrado-Calvo, P., Salinas-Navarro, M., Villegas-Pérez, M. P., and Vidal-Sanz, M. (2009a). Effects of different neurotrophic factors on the survival of retinal ganglion cells after a complete intraorbital nerve crush injury: a quantitative *in vivo* study. *Exp. Eye Res.* 89, 32–41. doi: 10.1016/j.exer.2009.02.015

Pease, M. E., McKinnon, S. J., Quigley, H. A., Kerrigan-Baumrind, L. A., and Zack, D. J. (2000). Obstructed axonal transport of BDNF and its receptor TrkB in experimental glaucoma. *Invest. Ophthalmol. Vis. Sci.* 41, 764–774.

Peinado-Ramón, P., Salvador, M., Villegas-Pérez, M. P., and Vidal-Sanz, M. (1996). Effects of axotomy and intraocular administration of NT-4, NT-3, and brain-derived neurotrophic factor on the survival of adult rat retinal ganglion cells. A quantitative *in vivo* study. *Invest. Ophthalmol. Vis. Sci.* 37, 489–500.

Pérez de Lara, M. J., Santano, C., Guzmán-Aránguez, A., Valiente-Soriano, F. J., Avilés-Trigueros, M., Vidal-Sanz, M., et al. (2014). Assessment of inner retina dysfunction and progressive ganglion cell loss in a mouse model of glaucoma. *Exp. Eye Res.* 122, 40–49. doi: 10.1016/j.exer.2014.02.022

Pérez-Rico, C., de la Villa, P., Arribas-Gómez, I., and Blanco, R. (2010). Evaluation of functional integrity of the retinohypothalamic tract in advanced glaucoma using multifocal electroretinography and light-induced melatonin suppression. *Exp. Eye Res.* 91, 578–583. doi: 10.1016/j.exer.2010.07.012

Quigley, H. A. (2011). Glaucoma *Lancet* 377, 1367–1377. doi: 10.1016/S0140-6736(10)61423-7

Ramirez, A. I., Salazar, J. J., de Hoz, R., Rojas, B., Gallego, B. I., Salinas-Navarro, M., et al. (2010). Quantification of the effect of different levels of IOP in the astroglia of the rat retina ipsilateral and contralateral to experimental glaucoma. *Invest. Ophthalmol. Vis. Sci.* 51, 5690–5696. doi: 10.1167/iovs.10-5248

Ramón y Cajal, S. (1914). *Estudios sobre la degeneración y regeneración del sistema nervioso.* Madrid: Hijos de Nicolás Moya.

Resnikoff, S., Pascolini, D., Etya'ale, D., Kocur, I., Pararajasegaram, R., Pokharel, G. P., et al. (2004). Global data on visual impairment in the year 2002. *Bull. World Health Organ.* 82, 844–851.

Rojas, B., Gallego, B. I., Ramirez, A. I., Salazar, J. J., de Hoz, R., Valiente-Soriano, F. J., et al. (2014). Microglia in mouse retina contralateral to experimental glaucoma exhibit multiple signs of activation in all retinal layers. *J. Neuroinflammation* 11:133. doi: 10.1186/1742-2094-11-133

Rovere, G., Nadal-Nicolás, F. M., Agudo-Barriuso, M., Sobrado-Calvo, P., Nieto-López, L., Nucci, C., et al. (2015). Comparison of retinal nerve fiber layer thinning and retinal ganglion cell loss after optic nerve transection in adult albino rats. *Invest. Ophthalmol. Vis. Sci.* 56, 4487–4498. doi: 10.1167/iovs.15-17145

Rovere, G., Nadal-Nicolás, F. M., Sobrado-Calvo, P., García-Bernal, D., Villegas-Pérez, M. P., Vidal-Sanz, M., et al. (2016b). Topical treatment with bromfenac reduces retinal gliosis and inflammation after optic nerve crush. *Invest. Ophthalmol. Vis. Sci.* 57, 6098–6106. doi: 10.1167/iovs.16-20425

Rovere, G., Nadal-Nicolás, F. M., Wang, J., Bernal-Garro, J. M., García-Carrillo, N., Villegas-Pérez, M. P., et al. (2016a). Melanopsin-containing or non-melanopsin-containing retinal ganglion cells response to acute ocular hypertension with or without brain-derived neurotrophic factor neuroprotection. *Invest. Ophthalmol. Vis. Sci.* 57, 6652–6661. doi: 10.1167/iovs.16-20146

Salinas-Navarro, M., Alarcón-Martínez, L., Valiente-Soriano, F. J., Jiménez-López, M., Mayor-Torroglosa, S., Avilés-Trigueros, M., et al. (2010). Ocular hypertension impairs optic nerve axonal transport leading to

progressive retinal ganglion cell degeneration. *Exp. Eye Res.* 90, 168–183. doi: 10.1016/j.exer.2009.10.003

Salinas-Navarro, M., Alarcón-Martínez, L., Valiente-Soriano, F. J., Ortín-Martínez, A., Jiménez-López, M., Avilés-Trigueros, M., et al. (2009c). Functional and morphological effects of laser-induced ocular hypertension in retinas of adult albino Swiss mice. *Mol. Vis.* 15, 2578–98.

Salinas-Navarro, M., Jiménez-López, M., Valiente-Soriano, F. J., Alarcón-Martínez, L., Avilés-Trigueros, M., Mayor, S., et al. (2009b). Retinal ganglion cell population in adult albino and pigmented mice: a computerized analysis of the entire population and its spatial distribution. *Vision Res.* 49, 637–647. doi: 10.1016/j.visres.2009.01.010

Salinas-Navarro, M., Mayor-Torroglosa, S., Jiménez-López, M., Avilés-Trigueros, M., Holmes, T. M., Lund, R. D., et al. (2009a). A computerized analysis of the entire retinal ganglion cell population and its spatial distribution in adult rats. *Vision Res.* 49, 115–126. doi: 10.1016/j.visres.2008.09.029

Salvador-Silva, M., Vidal-Sanz, M., and Villegas-Perez, M. P. (2000). Microglial cells in the retina of Carassius auratus: effects of optic nerve crush. *J. Comp. Neurol.* 417, 431–447. doi: 10.1002/(SICI)1096-9861(20000221)417:4<431::AID-CNE4>3.0.CO;2-G

Sánchez-Migallón, M. C., Nadal-Nicolás, F. M., Jiménez-López, M., Sobrado-Calvo, P., Vidal-Sanz, M., and Agudo-Barriuso, M. (2011). Brain derived neurotrophic factor maintains Brn3a expression in axotomized rat retinal ganglion cells. *Exp. Eye Res.* 92, 260–267. doi: 10.1016/j.exer.2011.02.001

Sánchez-Migallón, M. C., Valiente-Soriano, F. J., Nadal-Nicolás, F. M., Vidal-Sanz, M., and Agudo-Barriuso, M. (2016). Apoptotic retinal ganglion cell death after optic nerve transection or crush in mice: delayed rgc loss with BDNF or a Caspase 3 inhibitor. *Invest. Ophthalmol. Vis. Sci.* 57, 81–93. doi: 10.1167/iovs.15-17841

Sanes, J. R., and Masland, R. H. (2015). The types of retinal ganglion cells: current status and implications for neuronal classification. *Annu. Rev. Neurosci.* 38, 221–246. doi: 10.1146/annurev-neuro-071714-034120

Sasaki, H., Coffey, P., Villegas-Perez, M. P., Vidal-Sanz, M., Young, M. J., Lund, R. D., et al. (1996). Light induced EEG desynchronization and behavioral arousal in rats with restored retinocollicular projection by peripheral nerve graft. *Neurosci. Lett.* 218, 45–48. doi: 10.1016/0304-3940(96)13121-9

Schlamp, C. L., Li, Y., Dietz, J. A., Janssen, K. T., and Nickells, R. W. (2006). Progressive ganglion cell loss and optic nerve degeneration in DBA/2J mice is variable and asymmetric. *BMC Neurosci.* 7:66. doi: 10.1186/1471-2202-7-66

Schnebelen, C., Pasquis, B., Salinas-Navarro, M., Joffre, C., Creuzot-Garcher, C. P., Vidal-Sanz, M., et al. (2009). A dietary combination of omega-3 and omega-6 polyunsaturated fatty acids is more efficient than single supplementations in the prevention of retinal damage induced by elevation of intraocular pressure in rats. *Graefes Arch. Clin. Exp. Ophthalmol.* 247, 1191–1203. doi: 10.1007/s00417-009-1094-6

Sobrado-Calvo, P., Vidal-Sanz, M., and Villegas-Perez, M. P. (2007). Rat retinal microglial cells under normal conditions, after optic nerve section, and after optic nerve section and intravitreal injection of trophic factors or macrophage inhibitory factor. *J. Comp. Neurol.* 501, 866–878. doi: 10.1002/cne.21279

Soto, I., Pease, M. E., Son, J. L., Shi, X., Quigley, H. A., and Marsh-Armstrong, N. (2011). Retinal ganglion cell loss in a rat ocular hypertension model is sectorial and involves early optic nerve axon loss. *Invest. Ophthalmol. Vis. Sci.* 52, 434–441. doi: 10.1167/iovs.10-5856

Sun, W., Li, N., and He, S. (2002a). Large-scale morphological survey of mouse retinal ganglion cells. *J. Comp. Neurol.* 451, 115–126. doi: 10.1002/cne.10323

Sun, W., Li, N., and He, S. (2002b). Large-scale morophological survey of rat retinal ganglion cells. *Vis. Neurosci.* 19, 483–493. doi: 10.1017/S0952523802194107

Thanos, S., Vidal-Sanz, M., and Aguayo, A. J. (1987). The use of rhodamine-B-isothiocyanate (RITC) as an anterograde and retrograde tracer in the adult rat visual system. *Brain Res.* 406, 317–321. doi: 10.1016/0006-8993(87)90799-2

Tribble, J. R., Cross, S. D., Samsel, P. A., Sengpie, F., and Morgan, J. E. (2014). A novel system for the classification of diseased retinal ganglion cells. *Vis. Neurosci.* 31, 373–380. doi: 10.1017/S0952523814000248

Valiente-Soriano, F. J., García-Ayuso, D., Ortín-Martínez, A., Jiménez-López, M., Galindo-Romero, C., Villegas-Pérez, M. P., et al. (2014). Distribution of melanopsin positive neurons in pigmented and albino mice: evidence for melanopsin interneurons in the mouse retina. *Front. Neuroanat.* 8:131. doi: 10.3389/fnana.2014.00131

Valiente-Soriano, F. J., Nadal-Nicolás, F. M., Salinas-Navarro, M., Jiménez-López, M., Bernal-Garro, J. M., Villegas-Pérez, M. P., et al. (2015b). BDNF rescues RGCs but not intrinsically photosensitive RGCs in ocular hypertensive albino rat retinas. *Invest. Ophthalmol. Vis. Sci.* 56, 1924–1936. doi: 10.1167/iovs.15-16454

Valiente-Soriano, F. J., Salinas-Navarro, M., Jiménez-López, M., Alarcón-Martínez, L., Ortín-Martínez, A., Bernal-Garro, J. M., et al. (2015a). Effects of ocular hypertension in the visual system of pigmented mice. *PLoS ONE* 10:e0121134. doi: 10.1371/journal.pone.0121134

Vidal-Sanz, M., Avilés-Trigueros, M., Whiteley, S. J., Sauvé, Y., and Lund, R. D. (2002). Reinnervation of the pretectum in adult rats by regenerated retinal ganglion cell axons: anatomical and functional studies. *Prog. Brain Res.* 137, 443–452. doi: 10.1016/S0079-6123(02)37035-3

Vidal-Sanz, M., Bray, G. M., and Aguayo, A. J. (1991). Regenerated synapses persist in the superior colliculus after the regrowth of retinal ganglion cell axons. *J. Neurocytol.* 20, 940–952. doi: 10.1007/BF01190471

Vidal-Sanz, M., Bray, G. M., Villegas-Pérez, M. P., Thanos, S., and Aguayo, A. J. (1987). Axonal regeneration and synapse formation in the superior colliculus by retinal ganglion cells in the adult rat. *J. Neurosci.* 7, 2894–2909.

Vidal-Sanz, M., De la Villa, P., Avilés-Trigueros, M., Mayor-Torroglosa, S., Salinas-Navarro, M., Alarcon-Martinez, L., et al. (2007). Neuroprotection of retinal ganglion cell function and their central nervous system targets. *Eye* 21, S42–S45. doi: 10.1038/sj.eye.6702888

Vidal-Sanz, M., Lafuente, M., Sobrado-Calvo, P., Selles-Navarro, I., Rodriguez, E., Mayor-Torroglosa, S., et al. (2000). Death and neuroprotection of retinal ganglion cells after different types of injury. *Neurotox. Res.* 2, 215–227. doi: 10.1007/BF03033795

Vidal-Sanz, M., Nadal-Nicolás, F. M., Valiente-Soriano, F. J., Agudo-Barriuso, M., and Villegas-Pérez, M. P. (2015b). Identifying specific RGC types may shed light on their idiosyncratic responses to neuroprotection. *Neural Regen. Res.* 10, 1228–1230. doi: 10.4103/1673-5374.162751

Vidal-Sanz, M., Salinas-Navarro, M., Nadal-Nicolás, F. M., Alarcón-Martínez, L., Valiente-Soriano, F. J., de Imperial, J. M., et al. (2012). Understanding glaucomatous damage: anatomical and functional data from ocular hypertensive rodent retinas. *Prog. Retin. Eye Res.* 31, 1–27. doi: 10.1016/j.preteyeres.2011.08.001

Vidal-Sanz, M., Valiente-Soriano, F. J., Ortín-Martínez, A., Nadal-Nicolás, F. M., Jiménez-López, M., Salinas-Navarro, M., et al. (2015a). Retinal neurodegeneration in experimental glaucoma. *Prog. Brain Res.* 220, 1–35. doi: 10.1016/bs.pbr.2015.04.008

Vidal-Sanz, M., Villegas-Pérez, M. P., Bray, G. M., and Aguayo, A. J. (1988). Persistent retrograde labeling of adult rat retinal ganglion cells with the carbocyanine dye diI. *Exp. Neurol.* 102, 92–101. doi: 10.1016/0014-4886(88)90081-7

Villegas-Pérez, M. P., Vidal-Sanz, M., Bray, G. M., and Aguayo, A. J. (1988). Influences of peripheral nerve grafts on the survival and regrowth of axotomized retinal ganglion cells in adult rats. *J. Neurosci.* 8, 265–280.

Villegas-Pérez, M. P., Vidal-Sanz, M., Rasminsky, M., Bray, G. M., and Aguayo, A. J. (1993). Rapid and protracted phases of retinal ganglion cell loss follow axotomy in the optic nerve of adult rats. *J. Neurobiol.* 24, 23–36. doi: 10.1002/neu.480240103

Wang, J., Valiente-Soriano, F. J., Nadal-Nicolás, F. M., Rovere, G., Chen, S., Huang, W., et al. (2017). MicroRNA regulation in an animal model of acute ocular hypertension. *Acta Ophthalmol.* 95, e10–e21. doi: 10.1111/aos.13227

Weinreb, R. N., Aung, T., and Medeiros, F. A. (2014). The pathophysiology and treatment of glaucoma: a review. *JAMA* 311, 1901–1911. doi: 10.1001/jama.2014.3192

Werner, J. S., Keltner, J. L., Zawadzki, R. J., and Choi, S. S. (2011). Outer retinal abnormalities associated with inner retinal pathology in nonglaucomatous and glaucomatous optic neuropathies. *Eye* 25, 279–289. doi: 10.1038/eye.2010.218

Whiteley, S. J., Sauvé, Y., Avilés-Trigueros, M., Vidal-Sanz, M., and Lund, R. D. (1998). Extent and duration of recovered pupillary light reflex following retinal ganglion cell axon regeneration through peripheral nerve grafts directed to the pretectum in adult rats. *Exp. Neurol.* 154, 560–572. doi: 10.1006/exnr.1998.6959

WoldeMussie, E., Yoles, E., Schwartz, M., Ruiz, G., and Wheeler, L. A. (2002). Neuroprotective effect of memantine in different retinal injury models in rats. *J. Glaucoma* 11, 474–480. doi: 10.1097/00061198-200212000-00003

Yücel, Y. H., Zhang, Q., Weinreb, R. N., Kaufman, P. L., and Gupta, N. (2003). Effects of retinal ganglion cell loss on magno-, parvo-, koniocellular pathways in the lateral geniculate nucleus and visual cortex in glaucoma. *Prog. Retin. Eye Res.* 22, 465–481. doi: 10.1016/S1350-9462(03)00026-0

Zhang, Q., Vuong, H., Huang, X., Wang, Y., Brecha, N. C., Pu, M., et al. (2013). Melanopsin-expressing retinal ganglion cell loss and behavioral analysis in the Thy1-CFP-DBA/2J mouse model of glaucoma. *Sci. China Life Sci.* 56, 720–730. doi: 10.1007/s11427-013-4493-1

Conflict of Interest Statement: The authors declare that the research was conducted in the absence of any commercial or financial relationships that could be construed as a potential conflict of interest.

Advantages of publishing in Frontiers

OPEN ACCESS
Articles are free to read for greatest visibility and readership

FAST PUBLICATION
Around 90 days from submission to decision

HIGH QUALITY PEER-REVIEW
Rigorous, collaborative, and constructive peer-review

TRANSPARENT PEER-REVIEW
Editors and reviewers acknowledged by name on published articles

Frontiers
Avenue du Tribunal-Fédéral 34
1005 Lausanne | Switzerland

Visit us: www.frontiersin.org
Contact us: info@frontiersin.org | +41 21 510 17 00

REPRODUCIBILITY OF RESEARCH
Support open data and methods to enhance research reproducibility

DIGITAL PUBLISHING
Articles designed for optimal readership across devices

FOLLOW US
@frontiersin

IMPACT METRICS
Advanced article metrics track visibility across digital media

EXTENSIVE PROMOTION
Marketing and promotion of impactful research

LOOP RESEARCH NETWORK
Our network increases your article's readership